Entry and the Kinetics of Emulsion Polymerisation

A thesis submitted in partial fulfilment of
the requirements for the Degree of

Doctor of Philosophy in Chemistry

at the
University of Canterbury
Christchurch
New Zealand

Kim Yao-Hua van Berkel
June 2004

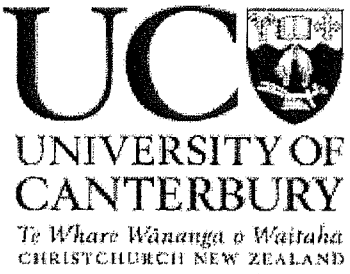

The real voyage of discovery consists not in seeking new landscapes, but in having new eyes.

– Marcel Proust (1871 – 1922)

Contents

Acknowledgements

Reflecting on several years of study, a long list of people to whom I am indebted for their contributions to this work soon emerges. Since an exhaustive set of acknowledgements may not sensibly be included here, the following highly condensed version must suffice.

Firstly, I am grateful to my supervisors for the instrumental and varied roles that they have assumed throughout the course of my studies; their guidance and friendship have been much appreciated. Greg Russell is thanked for the many contributions he has made to my development as a researcher over the past five years. Among other things, I am grateful for his patience, his considered and considerate approach as a scientist and a supervisor, and his dauntless (and sometimes unfathomable) confidence that I could get the job done. Bob Gilbert has made it possible for me to accomplish more in my Ph.D. than I ever would have anticipated. I thank him for his countless ideas, his endless enthusiasm and his boundless hospitality.

Without question, the quality of this research was greatly enhanced by the work of the technical staff at the University of Canterbury's Department of Chemistry. Those who must be particularly acknowledged for their toils (and good humour!) are Mike Pearce and Nick Oliver, who were responsible for the construction of a fine dilatometer, Rob McGregor and Dave MacDonald, who handled various glassware challenges and calamities, and Wayne Mackay, for his ability to offer useful advice on all manner of technical things. Bruce Clark is acknowledged for mass spectrometry analysis, and Manfred Ingerfeld (School of Biological Sciences, University of Canterbury) is thanked for his assistance with electron microscopy.

Thanks are extended to everyone at the University of Sydney's Key Centre for Polymer Colloids for their various contributions to this project and for making me welcome during my numerous visits to Sydney. Special mention must be made of David Sangster and Hank De Bruyn for their patient and valued tuition when I was learning the ropes of emulsion polymerisation experimentation, and after. I also wish to acknowledge the helpful scientific input and feedback offered by Brian Hawkett, Stuart Prescott and Dave Lamb over the course of this work.

There are a large number of people to whom I am much obliged for giving up their time to carry out various analyses for me, and for their enthusiasm in helping to decipher the results. To Jelica Strauch, Hollie Zondanos, Herbert Chiou and Shane Seabrook at the University of Sydney, and to Marie Squire, Cherry Chen and Martin Lee at the University of Canterbury, many thanks! Also deserving of note is Andrew Muscroft-Taylor who has tolerated a thousand inane questions about Organic Chemistry, has thrown many a frisbee with me, and has served to remind me just how many usable hours there are in a day.

My gratitude and deepest sympathies are offered to those who have had to put up with me on a daily basis for several years: my office-mates, Uma Adash and Greg Smith. Thanks to Uma for her companionship in the lab, to Greg for his various gems of computer wisdom, and to both for providing many sources of amusement and stress-relief over the years.

I wish to extend special thanks to Chris Ferguson for the many ways in which he has contributed to my Ph.D. – as a source of thoughtful advice, as a multi-purpose generator of useful experimental data (TEM, CHDF, PCS, HPPS, GPC), and as a friend. I am grateful to both Chris and Sarah for making me feel at home in Sydney, and for enduring my various culinary (mis)adventures.

Derek Caudwell and Michael McWhirter are thanked for their ongoing friendship, their various input into this work, and for consistently providing me with new perspectives (even if they are those of an engineer!).

Of course I also wish to acknowledge the generous financial contributions which have made this Ph.D. possible. The support of a New Zealand Foundation for Research Science and Technology Bright Future Scholarship is greatly appreciated, as is the support of a Shirtcliffe Fellowship. My many invaluable visits to Sydney were made possible by the P. A. Rolfe Scholarship Fund, to which I am extremely grateful. The support of the Australian Institute for Nuclear Science and Engineering, enabling γ-radiolysis work to be carried out, is also acknowledged.

Finally, it remains to express my gratitude to those nearest and dearest to me. My deepest thanks are extended to my family and Adrienne for their ongoing encouragement and support of my endeavours, and for always reminding me of what is important in life.

Abstract

An understanding of the process by which polymerising free radicals are created is of fundamental importance for any type of free radical polymerisation system. In the case of emulsion polymerisation this process is complicated by the fact that free radicals are usually generated in the aqueous phase, while the principal site of polymerisation is the interior of hydrophobic latex particles. This thesis details a study of the kinetics and mechanism for radical entry into latex particles in emulsion polymerisation.

A systematic investigation is carried out identifying the influences of initiator, monomer and particle surface type on the entry efficiency. Experimental entry efficiencies are obtained from a range of seeded styrene emulsion polymerisation systems at 50°C, employing potassium peroxodisulfate and 2,2′-azobis-(2-methylpropionamidine) dihydrochloride as initiators, and using latex particles stabilised by positive or negative surface charge. Changing either initiator or particle type is seen to affect the entry efficiency. Experimental results are able to be rationalised in terms of an existing theory for entry which suggests that entry occurs for persulfate-derived radicals after addition to two styrene monomer units, and for amidinium-derived radicals after addition to only one styrene monomer unit.

Entry efficiencies are also obtained from seeded experiments at 50°C using persulfate as initiator and methyl methacrylate as monomer, with considerably greater uncertainty arising in this case due to unexplained variations in the "acceleration" during Interval II of polymerisation. Comparison with entry theory for this system indicates that entry occurs for a persulfate-derived radical only after addition to at least 20 methyl methacrylate monomer units. Attempts to confirm this inferred value by analysis of aqueous-phase oligomers using mass spectrometry and gel-permeation chromatography are inconclusive.

In the hope of improving the accuracy with which entry rate data may be obtained from kinetic experiments the following investigations into more other aspects of emulsion polymerisation kinetics are carried out.

The contribution to entry from spontaneous polymerisation is measured for a wide range of styrene and methyl methacrylate systems and various mechanistic inferences are made. The

particle surface and aqueous phase are identified as likely loci for spontaneous radical generation.

The nature of chain stopping reactions in emulsion polymerisations of methyl methacrylate at 50°C are investigated through kinetic experiments and analysis of polymer molecular weight distributions. The radical chain length distribution is found to be approximately "transfer-controlled", and both kinetic data and molecular weight distributions are well described by current models for termination and the effects of column broadening in gel-permeation chromatography.

A new kinetic model for emulsion polymerisation is developed which extends the Smith-Ewart treatment to take account of all reactions of monomeric and aqueous-phase radicals. This new model treats exit and re-entry in terms of elementary physical and chemical processes, employing microscopic rate parameters and obviating the use of less meaningful parameters, such as k and α, which have traditionally been required for non-zero-one systems. The model is applied to the styrene and methyl methacrylate systems used in experimental work and confirms the accuracy of the entry data obtained using existing methods. However, no improvement in the fitting of methyl methacrylate acceleration data is obtained from using the new model with best estimates for all parameter values.

Finally, new approaches to modelling entry are proposed which may overcome the limitations posed by existing entry models. Most importantly, recommendations are made for including the kinetics of adsorption, desorption and entry of all aqueous radicals.

1. Introduction

1.1 The Study of Emulsion Polymerisation

Synthetic polymeric materials, in various forms, are undeniably of tremendous importance in modern times, pervading virtually all areas of human activity. One of the primary means for producing synthetic polymer on a commercial scale is by emulsion polymerisation, and this fact alone has long been sufficient to stimulate intensive research efforts in this field. Indeed, most of the significant advances made early on in the development of this technology were driven simply by the demand for polymeric commodities with various desired properties, and, in the absence of any comprehensive scientific basis, an empirical approach was frequently adopted.

Beyond its commercial significance as an important industrial process, emulsion polymerisation has emerged as an appealing and challenging area for purely scientific investigations in that it involves the complex interplay of different physical and chemical processes within a reaction medium that consists of a number of different phases. As a result of this complexity, the development of a detailed understanding of the underlying mechanisms of emulsion polymerisation through rigorous scientific endeavour has struggled to assume the pace set by the mostly empirical advances of industry. Nevertheless, over the past several decades a large body of scientific literature has begun to accumulate and the field of emulsion polymerisation research has progressed to the point where many of the fundamental processes are now understood at a molecular level (see, for example, the texts of Gilbert,[1] and Lovell and El-Aasser[2]).

The broad aim of the experimental and theoretical ventures presented in this thesis is to further the molecular level understanding of emulsion polymerisation, taking advantage of the solid foundation which has been established thus far. In general, the chosen setting for this work is latex particle growth in the presence of excess monomer, obviating the mechanistic complexities of new particle formation and polymerisation under conditions of varying monomer and polymer concentrations. Under such conditions the overall rate of polymerisation is determined solely by the relative rates at which free radicals are introduced

into and removed from the locus of polymerisation. Accordingly, careful measurement of the polymerisation rate enables the mechanisms of these radical-change processes to be probed. Amongst these, the mechanism for radical "entry" into latex particles will be singled out as a particular focus of this work. While numerous mechanistic theories abound for explaining the processes of emulsion polymerisation, it is often the case that the physical evidence required to verify or refute competing theories is lacking. The work presented here is intended to address this problem, presenting a range of new experimental kinetic data and interpreting these data in terms of existing theories, as well as developing and recommending new directions for future theoretical and experimental study.

Of course, despite best efforts here and elsewhere, there remains much that is imperfectly understood. However, it is apparent that the pursuit of a detailed mechanistic understanding of emulsion polymerisation continues to be not only a subject of considerable scientific interest, but also of ever-increasing importance in the production and optimisation of commercial polymer products. In view of these comments it is noted that the work of this thesis falls strictly into the category of "scientific interest", bearing no direct link with any particular commercial application. It is hoped, nonetheless, that the contribution made here will add to the overall progression of knowledge in this field and thus, in some small way, impact upon the ways in which emulsion polymerisation is practically applied.

1.2 A General Description of Emulsion Polymerisation

Before launching into detailed mechanistic considerations it is useful to present a brief overview of the emulsion polymerisation process. The process as it is described here is applicable in general terms to polymerisation in either the laboratory or industrial setting, despite the considerable difference in scale of the reactions and the complexity of the recipes used.

A typical *ab initio* polymerisation begins with the emulsification of monomer in water; the use of a relatively low water-solubility monomer results in the formation of an emulsion consisting of monomer droplets (with diameters of micron dimensions) dispersed throughout the aqueous phase. Also present in the emulsion may be surfactant (soap) molecules which partition themselves between the aqueous phase and interfacial regions such as the surface of a monomer droplet, where they act to stabilise the droplets against coalescence with one another. In the presence of sufficient added surfactant (*i.e.*, above the critical micelle

concentration in the aqueous phase, remembering that the actual concentration of surfactant is determined by the amount adsorbed onto particles) these molecules may form aggregates known as micelles, which may in turn accommodate a significant amount of monomer. Other reagents may also be added, such as co-monomer(s), a buffer to regulate the pH of the reaction medium, electrolytes to alter the ionic strength, or a chain transfer agent to influence the molecular weight of polymer produced (as explained in the following section).

The emulsion system is heated (or cooled) to the required reaction temperature and polymerisation begins with the introduction of some source of initiating free radicals in the water phase. This is commonly achieved using any of a variety of water-soluble compounds (*e.g.*, peroxy and azo compounds) whose thermal decomposition yields radical products at appropriate temperatures. Alternatively, initiation may be carried out using a water-soluble redox couple whose reaction generates radical species. Simply exposing the reaction medium to different types of radiation, for example UV- or γ-radiation, may also yield aqueous-phase radicals capable of initiating polymerisation.

Radicals derived from initiation in the aqueous phase may eventually give rise to the formation of long polymer chains. However, contrary to what the name suggests, the main locus of emulsion polymerisation is not inside the emulsified monomer droplets but in another discrete phase of small latex particles (with diameters in the range of a few hundred nanometres) formed in the early stages of polymerisation – a characteristic that was first identified by Harkins.[3] These particles contain many individual polymer chains and, once formed, will become swollen with monomer molecules. Additionally, surfactant molecules (if present) will adsorb to the particle surface, imparting colloidal stability. Eventually virtually all monomer present in the emulsion system will be converted to polymer, leaving a latex that consists only of polymeric particles dispersed throughout the water phase and stabilised by surfactant.

1.3 Fundamental Reactions in Free Radical Polymerisation

1.3.1 Initiation

As alluded to above, emulsion polymerisation is a form of free radical polymerisation, with monomer addition proceeding *via* a free radical active site. This process begins with the

generation of free radicals (in the aqueous phase), as illustrated below for the case of initiation by thermal decomposition of persulfate.

Scheme 1.1. Initiation by thermal decomposition of persulfate in the polymerisation of styrene.

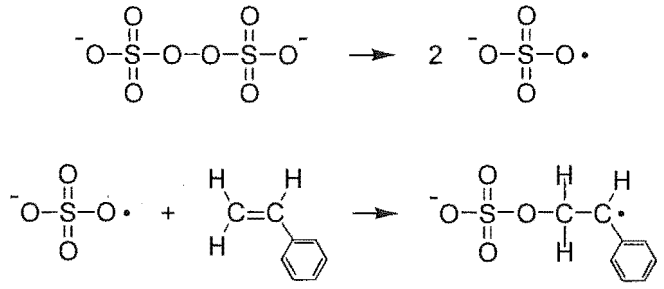

Here the peroxodisulfate dianion (commonly known as "persulfate") undergoes a thermally induced bond homolysis to produce two identical tetraoxidosulfate(•1–) primary radicals (commonly referred to simply as "sulfate" radicals). It is important to note, however, that the rate of initiation is not necessarily equal to the rate of primary radical generation, for these radicals may undergo geminate recombination or react with other species present. A true initiation event is therefore only deemed to occur when a primary radical adds to monomer to produce a growing radical -- illustrated with styrene in the second step in Scheme 1.1.

1.3.2 Propagation

The reaction responsible for radical addition to successive monomer units is called propagation. As illustrated in Scheme 1.2 for the case of a styrene polymerisation (with an oscillating line used to represent a polymeric chain), propagation gives rise to an increase in the degree of polymerisation of a growing radical, with the free radical active site being transferred to the newly attached monomer unit. As will be discussed in detail in later chapters, the rate coefficient for propagation may also be dependent on the chain length of the propagating radical.

Scheme 1.2. Propagation in the polymerisation of styrene.

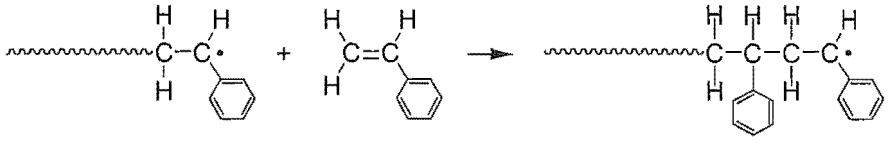

1.3.3 Termination

When the motion of two radical sites brings them into close proximity they may react to lose their radical activity. This reaction, known as termination, results in the generation of inert or "dead" polymer chains and may proceed *via* one or both of two mechanisms. Termination by combination, illustrated in Scheme 1.3, is where the two radicals react to form a single (bridging) bond, thus generating a single dead polymer chain whose degree of polymerisation is equal to the sum of those of the two reacting radicals.

Scheme 1.3. Termination by combination in the polymerisation of styrene.

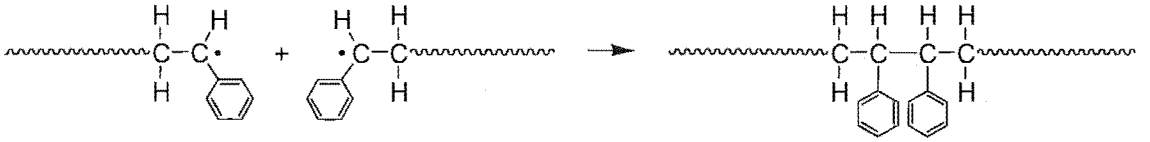

In a termination by disproportionation reaction (Scheme 1.4) one radical abstracts a hydrogen atom from the other. This results in the formation of two dead polymer chains that are equal in length to the reacting radicals. Additionally, one of the dead chains will be formed with an unsaturated end-group, while the other will be saturated.

Scheme 1.4. Termination by disproportionation in the polymerisation of methyl methacrylate.

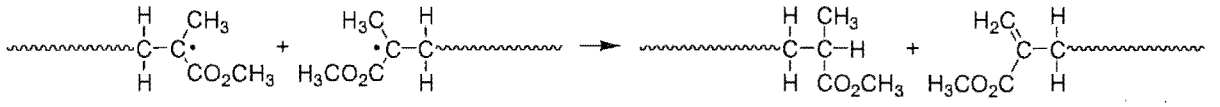

It is noted that the relative number of dead chains formed by combination events *versus* disproportionation events varies between different polymerisation systems (as will be further discussed in later chapters). For example, in styrene systems, termination is known to be almost entirely *via* the combination mechanism,[4] whereas in methyl methacrylate (MMA) systems, disproportionation predominates[5,6] (hence using these two monomers in Schemes 1.3 and 1.4 respectively).

1.3.4 Chain Transfer

Another important reaction in free radical polymerisation is chain transfer. Here a growing radical reacts by transferring its radical activity to another species, as exemplified in Scheme 1.5 for transfer to some generic chain transfer agent denoted A–X. In this case the radical

chain abstracts an atom to form a dead polymer chain and a new radical species derived from chain transfer agent (A•).

Scheme 1.5. Chain transfer to a generic chain transfer agent in the polymerisation of styrene.

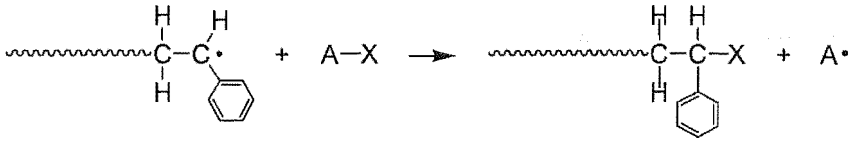

Normally X will be a hydrogen atom, as for example in thiols (R–SH, where R is an alkyl group). However sometimes X is not a hydrogen atom, *e.g.*, CCl_4 and CBr_4 function as chain transfer agents. Equally, chain transfer may be facilitated (according to various mechanisms) by a species already present in the system, such as monomer or polymer (in both cases a hydrogen atom is transferred).

Notably, while chain transfer results in the formation of a dead chain, no net radical loss occurs. Thus, assuming that the new radical generated by chain transfer undergoes propagation at a rate comparable to or faster than that of the original polymeric radical (and therefore this process does not act simply to retard or inhibit polymerisation), then addition of chain transfer agent constitutes a convenient means for influencing the molecular weight of dead polymer chains formed, with a higher occurrence of chain transfer leading to lower molecular weight polymer.

Another important class of chain transfer agents worthy of brief mention here are those that give rise to "reversible" chain transfer events. In the case of Reversible Addition Fragmentation chain Transfer (RAFT) a polymeric radical undergoes an addition reaction with a species such as a dithioester, losing its radical activity (becoming "dormant") and liberating another free radical species which may initiate polymerisation. Importantly, at a later stage another radical may undergo addition with the same dithioester to re-liberate the original dormant radical chain, which may then propagate further. This approach provides a means for maintaining a relatively low radical concentration in the polymerising system, thereby suppressing the loss of radicals by termination. In the ideal case, individual polymer chains are formed over unusually long timescales and systems with very narrow polydispersity result. Methods for applying the RAFT technique to emulsion polymerisation systems have recently been reported.[7-9]

1.4 Interfacial Processes in Emulsion Polymerisation

The reactions described in the previous section are common to all free radical polymerisation processes – albeit not necessarily employing the same reagents as above. In the case of emulsion polymerisation systems, initiation is restricted to the aqueous phase (assuming that a water-soluble initiator is used); however, propagation, termination and chain transfer occur to a greater or lesser extent in all phases: water, latex particles and monomer droplets. For a heterogeneous system of this sort it becomes additionally necessary to consider the physical and chemical processes occurring at the interfaces between different phases.

1.4.1 Latex Particle Formation

The formation of latex particles may be considered an interfacial process inasmuch as it *produces* interfacial area. There are two generally accepted mechanisms for particle formation: homogeneous nucleation and micellar entry.[1,2] Homogenous nucleation dominates particle formation in systems where the surfactant concentration is low (*i.e.*, below the critical micelle concentration). Under such conditions, initiating radicals generated in the aqueous phase will undergo propagation with aqueous monomer until an oligomer is formed which is sufficiently insoluble that it precipitates out of the water phase forming a new precursor particle. This precursor may subsequently swell with monomer and acquire surfactant, continuing to increase in size *via* propagation to become a true latex particle. Alternatively, at any stage precursor particles may undergo coagulation with one another or with established latex particles.

In the presence of excess surfactant (*i.e.*, above the critical micelle concentration), micellar nucleation is thought to usually be the dominant mode for particle formation. In this case initiating radicals either migrate into a micelle or form a micelle-like aggregate with surfactant molecules. Obviously this occurs at a lower degree of polymerisation than homogeneous nucleation. The monomer-swollen micellar interior then becomes the locus for rapid propagation, resulting in growth of the micellar precursor into a latex particle. Once again, coagulation of precursor particles may also occur prior to the formation of a true latex particle.

1.4.2 Monomer Diffusion

As stated earlier, the main locus of polymerisation is the latex particle interior – not the emulsified monomer droplets. In the presence of excess monomer the monomer droplets therefore serve merely as a reservoir of unreacted monomer. Clearly, the fact that emulsion polymerisation may be carried out to 100% conversion implies that there is effective diffusion of monomer from the droplets across the aqueous phase and into the particles. This diffusion is generally assumed to be sufficiently rapid on the timescale of other emulsion polymerisation processes that equilibrium conditions for the partitioning of monomer over all phases are maintained. However, it has been suggested that under conditions where the rate of consumption of monomer in the particles is extremely fast,[10] or where the monomer is highly insoluble in the aqueous phase,[11-13] the diffusion of monomer between phases may become rate-determining.

1.4.3 Radical Entry

Given that free-radicals are usually generated in the aqueous phase of an emulsion polymerisation, there must exist some mechanism by which these radicals migrate to the locus of polymerisation – the latex particle interior. While the supply of radicals is clearly crucial to a successful emulsion polymerisation, the present understanding of this process, known as radical "entry", is far from complete. It is generally accepted that entry of primary radicals furnished directly from a water-soluble initiator [such as the sulfate radical of Scheme 1.1] is highly unlikely, and that such radicals must first undergo some degree of propagation with monomer in the aqueous phase to form an oligomeric species that is sufficiently water-insoluble for entry to be a thermodynamically favourable occurrence. An important kinetic implication is thus that the possibility of termination of initiator-derived radicals in the aqueous phase prior to entry precludes the assumption that the rate of entry is equal to the rate of radical generation from initiator. Indeed, a discrepancy between these two rates has been observed in emulsion polymerisations of styrene.[14-17]

However, remaining somewhat controversial is the identification of the precise mechanism and rate-determining step(s) for entry. As is expounded shortly, a number of rival theories have been postulated; however, effective model discrimination has been hindered by the scarcity of quantitative experimental data for the entry process.

1.4.4 Radical Exit

It has been inferred from experiment that the transfer of radical activity from the particles back into the aqueous phase *via* radical "exit" is a non-negligible process in emulsion polymerisation.[1,14,18,19] The precise mechanism for this process is discussed in more detail below. However, assuming that there is an appreciable occurrence of chain transfer to monomer inside a particle (as will be clearly seen in later chapters), the possibility of exit follows intuitively, on the grounds that the monomeric *radical* species formed are of a very similar chemical nature to monomer *molecules* which, in turn, are known to readily undergo diffusion into the aqueous phase.

1.5 The Rate of Emulsion Polymerisation

In general terms the rate of polymerisation may be defined as the rate of disappearance of monomer as it is converted into polymer.

$$R_{pol} = -\frac{d[M]}{dt} = k_p [M] [R^\bullet] \qquad (1.1)$$

As shown in equation (1.1) this rate is related to the propagation rate coefficient, k_p, and the concentrations of both monomer, [M], and radicals, [R$^\bullet$], at the reaction locus. Given that the reaction locus in emulsion polymerisation is the interior of swollen latex particles, [M] = $[M]_p$, the intra-particle monomer concentration, and $[R^\bullet] = \bar{n}/(N_A V_s)$, where N_A is Avagadro's constant, V_s is the volume of a single swollen particle and $\bar{n}$ is defined as the average number of radicals per latex particle. Thus, substituting these quantities into equation (1.1) the value of R_{pol} may be obtained in units of moles of monomer converted per unit time per unit volume of the latex particle phase.

A more convenient way of expressing the rate of polymerisation in emulsion systems is given in equation (1.2). Here the rate is simply expressed as the total mass of monomer converted per unit time in the emulsion system, where $\hat{x}$ denotes conversion in grams. This expression follows from equation (1.1) by multiplying R_{pol} by the total volume of the particle phase: $V_s N_c V_w$, where N_c is the number concentration of particles in the aqueous phase and V_w the total aqueous phase volume, as well as by the molar mass of monomer, M_0.

$$\frac{d\hat{x}}{dt} = \frac{k_p [M]_p M_0 N_c V_w}{N_A} \bar{n} \tag{1.2}$$

Comparing the mass of converted monomer to the total mass of monomer added at the start of the reaction, m_M^{tot}, allows the fractional conversion, x, to be calculated. Thus, in some instances, where the analysis of fractional conversion data is preferred, the following slightly modified form of equation (1.2) is used:

$$\frac{dx}{dt} = \frac{k_p [M]_p M_0 N_c V_w}{m_M^{tot} N_A} \bar{n} \tag{1.3}$$

where dx/dt takes units of s^{-1}.

1.6 Interval Description of Emulsion Polymerisation

In light of the rate equations derived in the previous section it is convenient to describe the conditions in an emulsion polymerisation system at a given time in terms of one of three distinct states. Each of these "Intervals" of polymerisation is characterised by a different reaction environment and rate behaviour as described below.

1.6.1 Interval I

The first stage of an *ab initio* polymerisation inevitably involves the formation of latex particles, which may occur *via* either of the two mechanisms described earlier, depending on the precise reaction conditions. During this time the reaction medium will therefore contain precursor particles as well as newly formed latex particles and possibly also monomer droplets and monomer-swollen micelles. The total number of reaction loci (particles) increases throughout Interval I, corresponding to an increase in N_c and hence also polymerisation rate according to equation (1.2) or (1.3). This stage of polymerisation ceases when the concentration of particles formed is sufficiently high that all further radical species generated in the aqueous phase undergo particle entry before they are able to nucleate a particle themselves. Usually this corresponds to the time at which all micelles are stripped of their surfactant and monomer by growing latex particles.

1.6.2 Interval II

During Interval II, conditions are such that no new particle formation occurs – all new polymerising radicals undergo entry and N_c is constant – and sufficient monomer is present to saturate both particle and aqueous phases, with excess monomer present in the form of monomer droplets. An approximately constant saturated concentration of monomer, $[M]_p^{sat}$, is maintained at the reaction locus and a steady-state rate of polymerisation is attained. Particles grow in size as polymerised monomer is readily replaced by diffusion of monomer from the droplets.

1.6.3 Interval III

In the event that the amount of monomer present is insufficient to saturate the particle and aqueous phases, Interval III conditions are obtained. Here, the remaining monomer is partitioned between the particles and water and is gradually consumed by polymerisation, leading to a decrease in $[M]_p$ and thus a diminishing rate of polymerisation according to equation (1.2) or (1.3). Notably, however, the "Trommsdorff-Norrish effect" or "gel effect" may result in suppression of termination and hence in an increase in $\bar{n}$ which overrides the decrease of $[M]_p$ and results in an increase in rate towards high conversion.[20,21] Due to the greater density of polymer compared to monomer, Interval III of polymerisation is also accompanied by a contraction in the volume of monomer-swollen latex particles (except for rare systems in which the aqueous-phase concentration of monomer is very high).

Importantly, while a given polymerisation may proceed through all three Intervals described above, it is also possible to control conditions such that polymerisation involves only two or even one of these stages. For example, Interval I conditions may be avoided by conducting polymerisation in the presence of pre-formed, pre-swollen latex particles ("seed" particles). Thus, reaction may commence in Interval II with particle growth and eventually progress into Interval III when all excess monomer is consumed. Or, if no monomer droplets are initially present, both Intervals I and II may be absent; *i.e.*, Interval II or III conditions may be prescribed by the amount of added monomer. It should also be noted, however, that particle formation may well occur at any stage of a seeded polymerisation if the concentration of seed particles is insufficient to capture all new radical species formed – a phenomenon referred to as "secondary nucleation".

1.7 Kinetic Modelling of Emulsion Polymerisation

As is evident from equations (1.2) and (1.3), a key quantity in determining the rate of polymerisation is the average number of radicals per particle, $\bar{n}$. This value is, in turn, dictated by the relative rates of radical gain and loss in the particles and thus represents a window for insight into the mechanisms of these processes. The following provides a brief summary of some important existing kinetic methodologies used in modelling the value of $\bar{n}$ in emulsion polymerisation; these constitute essential background information and form a base for the modelling endeavours of the present study. Where necessary, these methodologies will be explicated in greater depth when they are implemented in later chapters.

1.7.1 The Model of Smith and Ewart

The founding quantitative kinetic treatment of emulsion polymerisation was the work of Smith and Ewart,[22] which culminated in the following well-known equation:

$$\frac{dN_n}{dt} = \rho N_{n-1} - [\rho + nk + n(n-1)c]N_n + (n+1)kN_{n+1} + (n+2)(n+1)cN_{n+2} \qquad (1.4)$$

The Smith-Ewart approach distinguishes latex particles on the basis of the number of propagating radicals they contain, with N_n being the number fraction of particles containing n radicals. It is noted that a commonly used index for such particle populations is i, however since i is used extensively throughout this thesis (including the present chapter) as notation for *radical chain length* we here adopt the index n to denote the *number of radicals per particle* in order to avoid any confusion.

As is evident from equation (1.4), the only processes that give rise to a change in the population of radicals in a particle are entry, exit and bimolecular termination, quantified by pseudo-first-order rate coefficients ρ, k and c respectively. Thus the infinite set of particle populations is interrelated; entry into an N_n-type particle results in the addition of a single radical to give an N_{n+1} particle, exit loss gives an N_{n-1} particle, and termination causes annihilation of two radicals forming an N_{n-2}-type particle.

Numerical solution of the set of coupled linear differential equations represented by equation (1.4) yields the population distribution for N_n and permits the average number of radicals per particle to be calculated as follows:

$$\bar{n} = \sum_{n=1}^{\infty} nN_n \tag{1.5}$$

Deficiencies in the Smith-Ewart approach have inevitably been revealed over time, a detailed exposition of which is undertaken in Chapter 8. Nevertheless, after fifty years the Smith-Ewart model remains an important foundation for kinetic studies.

1.7.2 Model for Exit

While Smith and Ewart made no distinction as to the types of radicals that may undergo exit from a particle, it is physically reasonable to suspect that this process is restricted to the radicals of greatest water solubility, *viz.*, monomeric radicals produced by intra-particle transfer to monomer reactions. This realisation was first made by Ugelstad *et al.*[23] and Nomura *et al.*[24] Clearly then, the process of radical exit is not just a phase transfer process, but entails a series of chemical and diffusive processes, and any predicted value for k must be based on model-dependent assumptions as to the nature of these processes.

Following the guiding principles of work presented elsewhere,[19,23-25] we therefore derive a value for k as follows. Assuming that monomeric radicals are the only radical species capable of desorbing from a latex particle, the exit process must begin with chain transfer to monomer inside a particle. In the present case the assumption is also made that the only possible fates for a monomeric radical in the particle phase are desorption or propagation (to form a dimeric radical incapable of desorption); it is supposed that termination with another radical is highly improbable, as will be reasonable when the value of $\bar{n}$ is relatively low. Further, we assume that diffusion of a monomeric radical within the interior of a latex particle is rapid and the rate-determining step for desorption is therefore diffusion of the radical away from the particle surface into the aqueous medium. This assumption is likely to be accurate under Interval II conditions of a typical emulsion polymerisation, although it is noted that under conditions of high weight fraction of polymer, and hence high viscosity inside a latex particle (such as late in Interval III of polymerisation), monomer diffusion may be slowed

significantly. In this event an alternative derivation that takes full account of intra-particle diffusion should be used.[24,26]

Given the above assumptions, the likelihood of transfer to monomer actually resulting in a true "exit" event is then determined by the probability of desorption and the value of k may be estimated as follows.

$$k = k_{tr}[M]_p \frac{k_{dM}}{k_{dM} + k_p^1[M]_p} \tag{1.6}$$

Here we assume that the rate coefficient for desorption of a monomeric radical is accurately approximated by that for a monomer molecule, k_{dM}. Additionally, k_{tr} is the rate coefficient for transfer to monomer and k_p^1 is the propagation rate coefficient for a monomeric radical.

The expression for k given above is seen to have two limiting forms. Firstly, in the event that the frequency of desorption is considerably greater than that of propagation, *i.e.*, $k_{dM} \gg k_p^1 [M]_p$, equation (1.6) simplifies to the following:

$$k = k_{tr}[M]_p \tag{1.7}$$

In this limit the rate coefficient for exit is simply equal to the frequency of transfer to monomer.

Alternatively, if one assumes that propagation is far more likely than desorption for a monomeric radical, *i.e.*, $k_p^1[M]_p \gg k_{dM}$, equation (1.6) takes its other limiting form:

$$k = \frac{k_{tr}\, k_{dM}}{k_p^1} \tag{1.8}$$

It is evident that the expression for k that is appropriate for use in modelling a given polymerisation system will depend on the precise reaction conditions for that system.

1.7.3 The Fate of Exited Radicals

Additionally, Ugelstad *et al.*[23] and Nomura *et al.*[24] were the first to acknowledge the fact that a radical that has undergone exit is not necessarily permanently lost, contrary to equation (1.4): the possibility exists for such radicals to encounter and re-enter another latex particle.

A simple way of handling this is to append to the value of ρ the flux of re-entrant radicals by employing a so-called "fate parameter", α, which represents in some way the fraction of exited radicals that undergo re-entry. The total flux of entering radicals is then given by:

$$\rho_{total} = \rho + \alpha k\bar{n} \qquad (1.9)$$

Here $k\bar{n}$ is the flux of exiting radicals and the fate parameter takes a value between $\alpha = 1$, corresponding to complete re-entry, and $\alpha = 0$, corresponding to complete aqueous-phase "homo-termination" of exited radicals (the latter being implicit in the original Smith-Ewart[22] work).

Extending the above approach Whang *et al.*[15] noted that exited radicals may also undergo "hetero-termination" with initiator-derived radicals. In the event that these initiator-derived radicals would otherwise have entered a latex particle, exit must cause a diminution of the flux of entering radicals. This observation gave rise to a new lower bound value of $\alpha = -1$ for the case of complete hetero-termination of this sort. Also, it revises the interpretation of $\alpha = 0$, which now just means that whatever radicals are lost by hetero-termination are exactly compensated for by re-entry. Importantly, coupling equation (1.9) with equation (1.4) for all $\alpha \neq 0$ introduces non-linearity to the set of equations, meaning that only numerical solution is possible.

While equation (1.9) is conceptually neat, it is only physically meaningful in the limits of $\alpha = 1$ and -1. Even more importantly, it is not a fundamental rate coefficient in that it actually represents the outcome of competing reactions, *i.e.*, it is a function of various *rates*. Thus it cannot rise above being an adjustable parameter, a flaw that will be addressed later in this work.

1.7.4 The "Pseudo-Bulk" Approximation

A number of analytic solutions have been derived which obviate the need for numerical solutions of the full set of Smith-Ewart equations under particular circumstances. The first of these likens the kinetics of an emulsion polymerisation system to those of a bulk system such that the evolution of $\bar{n}$ may be described by a single rate equation as follows:

$$\frac{d\bar{n}}{dt} = \left(\rho + \alpha k\bar{n}\right) - k\bar{n} - 2c\bar{n}^2$$

$$= \rho - (1-\alpha)k\bar{n} - 2c\bar{n}^2 \qquad (1.10)$$

Ballard *et al.* showed that this so-called "pseudo-bulk" equation provides an accurate approximation to the exact value of $\bar{n}$ [obtained *via* equation (1.4)] for conditions where either $\rho > c$ or $k > c$ is satisfied.[27] Under such conditions radicals are rapidly circulated among different latex particles and the separation, or "compartmentalisation", of radicals into distinct reaction loci may be neglected. This gives rise to so-called "Case 3" Smith-Ewart kinetics, with $\bar{n} > 0.5$,[10,27,28] although it is important to understand that systems with low $\bar{n}$ can also be pseudo-bulk in nature.

Once again, the effects of re-entry of exited radicals back into a latex particle are incorporated by way of the fate parameter, α, where $-1 \leq \alpha \leq 1$. It is essential to note that α is in general a complex function of $\bar{n}$, as shown by the various limiting forms in the next section.

1.7.5 The "Zero-One" Approximation

Another set of analytic solutions to the Smith-Ewart equations is applicable under conditions where the rate of intra-particle termination is relatively rapid, *i.e.*, $c \gg \rho$, k, and two radicals may not occupy a given latex particle for any significant length of time without undergoing termination. Thus radical entry into an occupied particle results in "pseudo-instantaneous" termination and at any time a particle may only contain either zero or one radical. Under such conditions a radical will propagate in isolation inside a latex particle until such time as either entry or exit occurs, thus there is a strong compartmentalisation effect. This situation is referred to as "Case 1" or "Case 2" of Smith-Ewart kinetics, with "Case 2" corresponding to the limiting value of $\bar{n} = 0.5$ given when $c \gg \rho \gg k$.

Under these circumstances no accuracy is lost in truncating the full set of Smith-Ewart equations to consider only the equations for N_0 and N_1. This approach, known as the "zero-one" approximation, was employed by Casey, Morrison *et al.*[1,19,25] to derive the following results.

General Case

The following three equations describe the time evolution of different latex particle types in the zero-one limit:

$$\frac{dN_0}{dt} = \rho\left(N_1 - N_0\right) + k_{dM}N_1^M \tag{1.11}$$

$$\frac{dN_1}{dt} = \rho N_0 - \rho N_1 - k_{tr}[M]_p N_1 + k_p^1[M]_p N_1^M \tag{1.12}$$

$$\frac{dN_1^M}{dt} = \rho_M N_0 - \rho N_1^M - k_{dM}N_1^M + k_{tr}[M]_p N_1 - k_p^1[M]_p N_1^M \tag{1.13}$$

Here N_0 denotes the fraction of all particles that are devoid of radicals. Particles occupied by a radical are further distinguished based on the nature of the radical: N_1 is the fraction of particles containing a single *polymeric* radical, while N_1^M denotes the fraction containing a single *monomeric* radical (formed by transfer to monomer). The rate coefficient for re-entry of exited monomeric radicals is specified as ρ_M (where 'M' here denotes 'monomeric radical'). An important point here is that equations (1.11) – (1.13) clearly do not contain the value of the overall rate coefficient for exit, k. Instead, the kinetics of exit are treated entirely in terms of the elementary processes of monomeric radicals, incorporating the rate coefficients for transfer to monomer, and monomeric radical propagation, desorption and re-entry.

Numerical solution of equations (1.11) – (1.13) may be carried out to obtain the value of $\bar{n}$, which, in the zero-one setting, is defined simply as the sum of radical-containing particle populations, $\bar{n} = N_1 + N_1^M$.

Casey, Morrison *et al.*[1,19,25] also showed that a series of analytic solutions for $\bar{n}$ may be obtained, based on the assumed fate of exited radicals, with each analytic form corresponding to a different physical limit. Further, for each analytic solution it is possible to identify a phenomenological value for the overall exit rate coefficient, k, in terms of various microscopic rate parameters (as is now shown).

Limit 1: Complete aqueous-phase termination of exited radicals

Here it is assumed that all exited radicals will encounter another radical whilst in the aqueous phase and undergo termination. Further kinetic distinction is then required depending on the nature of the aqueous-phase radical encountered.

- ***Limit 1a***

In the event that an exited radical encounters another exited radical in the aqueous phase, "homo-termination" ensues and the time evolution of $\bar{n}$ may be described by a single equation as follows:

$$\frac{d\bar{n}}{dt} = \rho(1-2\bar{n}) - k\bar{n} \qquad (1.14)$$

where $k = k_{tr}[M]_p \frac{k_{dM}}{k_{dM} + k_p^1[M]_p}$ [*cf.* equation (1.6)].

- ***Limit 1b***

In the case where an exited radical undergoes "hetero-termination" with an initiator-derived radical that would otherwise have undergone entry, the rate equation for $\bar{n}$ is slightly different:

$$\frac{d\bar{n}}{dt} = \rho(1-2\bar{n}) - k\bar{n} - k\bar{n}(1-2\bar{n}) \qquad (1.15)$$

where $k = k_{tr}[M]_p \frac{k_{dM}}{k_{dM} + k_p^1[M]_p}$ and the extra radical loss term accounts for the contribution to entry that the initiator-derived radical would have made, had it not terminated with an exited radical.

- ***Limit 1c***

In the zero-one case where exited radicals undergo hetero-termination in the aqueous phase but no significant diminishment in the rate of entry of initiator-derived radicals results – *i.e.*, in a system where the efficiency of radical entry is very low – the rate equation for $\bar{n}$ is identical in form to that of Limit 1a above [equation (1.14)].

Limit 2: Negligible aqueous-phase termination of exited radicals

In this alternative limit, all exited monomeric radicals survive in the aqueous phase sufficiently long that they eventually encounter a latex particle and undergo re-entry. In this

case different analytic forms are valid depending on the subsequent fate of the re-entrant radical.

- ***Limit 2a***

In Limit 2a re-entry of exited radicals is followed either by pseudo-instantaneous termination, if the particle is already occupied by a radical, or else by propagation to form a macro-radical that is incapable of re-exit; *i.e.*, it is assumed that $k_p^1[M]_p \gg k_{dM}$. The applicable rate equation is then:

$$\frac{d\bar{n}}{dt} = \rho(1-2\bar{n}) - 2k\bar{n}^2 \qquad (1.16)$$

where $k = \frac{k_{tr}\, k_{dM}}{k_p^1}$ [*cf.* equation (1.8)].

Importantly, it is the above limiting result which is used in this work for analysis of all styrene results.

- ***Limit 2b***

Alternatively, in the limit of rapid desorption, $k_{dM} \gg k_p^1[M]_p$, and the re-entrant monomeric radical is far more likely to re-exit a particle than it is to propagate therein. In this case all exited radicals are bound to continue to re-exit and re-enter latex particles until eventually an already occupied particle is entered and pseudo-instantaneous termination occurs. The rate equation for this limit is:

$$\frac{d\bar{n}}{dt} = \rho(1-2\bar{n}) - 2k\bar{n} \qquad (1.17)$$

where $k = k_{tr}[M]_p$ [*cf.* equation (1.7)].

1.7.6 Limitations of Approximate Solutions of the Smith-Ewart Equations

It is important to understand that the pseudo-bulk and zero-one kinetic treatments described above represent approximations to the general Smith-Ewart approach which are applicable under opposite limiting conditions: pseudo-bulk when radical compartmentalisation is negligible, and zero-one when intra-particle termination is pseudo-instantaneous and compartmentalisation is prevalent. Provided that appropriate conditions hold, these

approximate methods offer the advantage that accurate kinetic data (*i.e.*, values of $\bar{n}$) may be furnished from comparatively simple mathematical operations. Under "intermediate" conditions, where neither the pseudo-bulk nor zero-one simplifications may be employed, one may resort to (considerably more involved) numerical solution of the full Smith-Ewart equations [equation (1.4)]. Alternatively, a third approximate approach has been proposed by Lichti *et al.*[29] and recently further developed by Prescott *et al.*[9,30] wherein it is assumed that up to two radicals may co-exist in the same particle, but that entry of a third radical results in pseudo-instantaneous termination – the so-called "zero-one-two" model.

In any case, Prescott *et al.*[9,30] have recently determined that even under intermediate conditions, where neither the pseudo-bulk nor zero-one approximation is strictly admissible, the results obtained from whichever is the more accurate of these two approximations (under the particular conditions) will be in error by, at worst, 20 – 30%. While such an error may be unacceptable for data analysis in some emulsion polymerisation systems, an error of this magnitude is often within acceptable limits.

1.7.7 The Chain Length Dependence of Termination

An important consideration that has been omitted up until this point is the fact that under certain conditions various reactions in emulsion polymerisation are diffusion-controlled. In particular, the rapid rate of radical-radical annihilation means that diffusion of the two reacting radical sites is always the rate-determining step in termination reactions. Further, the motion of polymer molecules is dictated by their size (*i.e.*, degree of polymerisation). Thus, the diffusion control of termination entails a dependence of the termination rate coefficient on the chain lengths of the reacting radicals.

Drawing on the mathematical simplicity offered by the pseudo-bulk model, Russell *et al.*[31,32] formulated a model wherein values are specified for the second-order rate coefficient for termination, $k_t^{i,j}$, pertaining to the reaction of a pair of radicals of chain lengths i and j (in monomer units). Subsequently, an average value for the second-order termination rate coefficient in a given system, $\langle k_t \rangle$, may be obtained as a sum of the microscopic $k_t^{i,j}$ values, weighted according to the specific chain length distribution of polymerising radicals:

$$\langle k_t \rangle = \sum_{i=1}^{\infty} \sum_{j=1}^{\infty} k_t^{i,j} \frac{n_i}{\bar{n}} \frac{n_j}{\bar{n}} \tag{1.18}$$

Here n_i and n_j are the average number of radicals of degree of polymerisation i and j monomer units respectively per latex particle, and the average total number of radicals per particle $\bar{n}$ is simply the sum of n_i over all chain lengths i. $\langle k_t \rangle$ is then related to the pseudo-first-order rate coefficient for termination, c, appearing in equation (1.10) by $c = \langle k_t \rangle / (N_A V_s)$.

1.8 Entry in Emulsion Polymerisation

Having introduced existing theories for exit and termination, it remains to elaborate on the postulated mechanisms for the only other process affecting the intra-particle radical concentration: entry. Given that the mechanism for entry is a primary focus of the work of this thesis, a more thorough review is presented in this case.

1.8.1 Historical Models for Entry

In early studies of entry a number of competing mechanistic theories were put forward, each specifying different rate-determining steps for this process. The simplest "mechanism" for entry is the original assumption made by Smith and Ewart that all initiating radicals generated in the aqueous phase find their way into a latex particle. However, kinetic data for entry measured experimentally by Hawkett *et al.*,[14] Ballard *et al.*,[10] and Halnan *et al.*[33] showed that this simple assumption was not valid, with the rate of entry observed in many cases to be significantly less than that predicted solely from the rate of initiation.

More elaborate models for entry postulated in early years included the "diffusion control" model,[34-36] which assumes that diffusion of aqueous-phase radicals to the particle surface is the rate-controlling step for entry. Another theory supposes that displacement of surfactant from the particle surface is the rate-determining step.[37] It was also suggested that entry can be thought of as a colloidal interaction between a latex particle and an oligomeric aqueous-phase radical.[38]

The experimental study of Penboss *et al.*[39] aimed to discriminate between these models. Kinetic results obtained here from emulsion polymerisations of styrene with persulfate as initiator appeared to be consistent with either of two mechanisms: diffusion-controlled entry that is dependent on displacement of a surfactant molecule, or "colloidal entry". These authors expressed a preference for the latter mechanism, citing the observed[40] enhancement of the entry rate by the addition of an inert diluent (thought to promote colloidal interactions).

Adams *et al.*[17] went on to cast doubt over the inferences of Penboss *et al.* showing that variations in both surfactant coverage of particles and ionic strength in the aqueous phase gave rise to no appreciable change in the rate of entry for the styrene/persulfate system. Given that the surfactant displacement model for entry suggests a dependence on surfactant coverage, and entry by the colloidal mechanism should be affected by changes in electrostatic interactions with variation of surface charge and ionic environment, both these models for entry were apparently refuted. Furthermore, a measurement of the activation energy for entry made by Adams *et al.* was not consistent with that for the rate determining step(s) of any of the mechanisms postulated thus far.

1.8.2 The "Control by Aqueous-Phase Growth" Entry Model of Maxwell et al.

It was against the backdrop described above that the entry model of Maxwell, Morrison *et al.* emerged.[41] Noting the original suggestion made by Priest,[42] these authors postulated a mechanism that requires a water-soluble radical generated from initiator to add to aqueous monomer in order to effect successful transfer of radical activity from aqueous to particle phase. The key to this new model was the specification of a critical degree of polymerisation, z, in monomer units, at which initiator-derived radicals become surface-active and their only fate is irreversible entry into a latex particle. The rate of entry may then be equated to the rate of formation of "z-meric" radical species, which, in turn, is dictated entirely by the competing reactions for radicals in the aqueous phase: propagation and termination (and, in some rare cases, transfer[43]).

Thus, unlike earlier models which focussed on the radical-particle interaction step as the defining event for entry, the Maxwell-Morrison model asserts that the preceding aqueous-phase chemistry is of foremost importance; it is assumed that the processes of aqueous radical diffusion and adsorption onto latex particles are rapid, and the actual entry step itself is non-rate-determining. Furthermore, it is assumed that intra-particle processes occur subsequent to and independent of entry.

As an important aside, it is noted that all entry models must start with the model which now follows – it is just a matter of whether further (rate-determining) steps must be incorporated on top of the always-present kinetics now discussed.

The Maxwell-Morrison model is encapsulated in the following reaction scheme:

$$\text{initiator} \xrightarrow{fk_d} 2\,I^{\bullet} \tag{1.19}$$

$$I^{\bullet} + M \xrightarrow{k_{pl,w}} IM_1^{\bullet} \quad \text{(rapid)} \tag{1.20}$$

$$IM_i^{\bullet} + M \xrightarrow{k_{p,w}} IM_{i+1}^{\bullet}, \quad 1 \le i < z \tag{1.21}$$

$$IM_i^{\bullet} + T_w^{\bullet} \xrightarrow{2k_{t,w}} \text{inert products}, \quad 1 \le i < z \tag{1.22}$$

$$IM_z^{\bullet} \xrightarrow{\rho_{init}} \text{entry} \quad \text{(rapid)} \tag{1.23}$$

$I^{\bullet}$ is a primary free radical produced by initiation, illustrated here by thermal decomposition of initiator with overall rate coefficient fk_d, where k_d is the rate coefficient governing all decomposition events and f is the fraction of such events which actually give rise to propagating radicals. M is a monomer molecule, $IM_i^{\bullet}$ is an aqueous-phase radical derived from initiator and containing i monomer units, $T^{\bullet}$ is any aqueous-phase free radical species and $IM_z^{\bullet}$ is a surface-active radical bound to undergo entry. $k_{p,w}$ and $k_{t,w}$ are, respectively, the rate coefficients for aqueous propagation and termination, and ρ_{init} is the pseudo-first-order rate coefficient for entry of initiator-derived radicals.

Maxwell *et al.* assumed (based on experimental evidence[44-46]) that the initial propagation step, reaction (1.19) with rate coefficient $k_{pl,w}$, is so fast that it is not rate-determining. It is also important to note that reaction (1.23) does not imply that every encounter between a surface-active ($IM_z^{\bullet}$) radical and a particle results in a successful entry event. In fact the above model allows for an $IM_z^{\bullet}$ species to adsorb and desorb many times before undergoing true, irreversible "entry", defined here as propagation of an adsorbed radical into the particle interior. Thus, the model does not assume that *entry* and *adsorption* are equivalent (although they may be); it only assumes that essentially all $IM_z^{\bullet}$ species enter rather than undergoing any other *chemical* fate.

Based on reactions (1.19) – (1.23), Maxwell *et al.* wrote down the population balance equations which follow for aqueous radicals derived from initiator:

$$\frac{d[IM_1^\bullet]}{dt} = 2fk_d[I] - k_{p,w}[M]_w[IM_1^\bullet] - 2k_{t,w}[T_w^\bullet][IM_1^\bullet] \quad (1.24)$$

$$\frac{d[IM_i^\bullet]}{dt} = k_{p,w}[M]_w\left([IM_{i-1}^\bullet] - [IM_i^\bullet]\right) - 2k_{t,w}[T_w^\bullet][IM_i^\bullet], \quad 1 < i < z \quad (1.25)$$

$$\frac{d[IM_z^\bullet]}{dt} = k_{p,w}[M]_w[IM_{z-1}^\bullet] - \rho_{init}\frac{N_c}{N_A} \quad (1.26)$$

where [I] denotes the aqueous-phase concentration of initiator. It is noted that in the above radical balance equations the aqueous termination rate coefficient is defined such that each termination event (whether homo- or hetero-termination) may be written as claiming two radicals of interest. This approach is adopted for mathematical convenience, as explained in Appendix A.1.

The total concentration of aqueous-phase radicals $[T_w^\bullet]$ is then calculated as:

$$[T_w^\bullet] = \sum_{i=1}^{z-1}[IM_i^\bullet] \quad (1.27)$$

where equation (1.27) ignores the typically small contribution from exited radicals as well as the vanishingly small concentrations of $I^\bullet$ and $IM_z^\bullet$ radicals.

In their work Maxwell *et al.* acknowledged the resemblance that the above kinetic scheme bears to the earlier "HUFT" model for homogeneous nucleation due to Hansen and Ugelstad,[36] and Fitch and Tsai.[35] Indeed, those workers included a full treatment of the aqueous-phase radical reactions giving rise to oligomeric radicals capable of entry and particle formation. However their model was intended only for predicting rates of particle formation (as a process competing with entry), as opposed to rates of entry in the absence of new particle formation. Moreover, the HUFT model entails the potential for all aqueous radicals to undergo entry – free of the requirement for surface-activity imposed by Maxwell *et al.* Finally, a key development by Maxwell *et al.* was the use of a more appropriate value for $k_{t,w}$. Thus, while the two models bear similarities, each is fundamentally built upon a different physical basis.

Applying the steady-state approximation to equations (1.24) and (1.25) Maxwell *et al.* obtained:

$$[\mathrm{IM}_1^\bullet] = \frac{2fk_\mathrm{d}[\mathrm{I}]}{k_{\mathrm{p,w}}[\mathrm{M}]_\mathrm{w} + 2k_{\mathrm{t,w}}[\mathrm{T}_\mathrm{w}^\bullet]} \tag{1.28}$$

$$[\mathrm{IM}_i^\bullet] = \frac{k_{\mathrm{p,w}}[\mathrm{M}]_\mathrm{w}[\mathrm{IM}_{i-1}^\bullet]}{k_{\mathrm{p,w}}[\mathrm{M}]_\mathrm{w} + 2k_{\mathrm{t,w}}[\mathrm{T}_\mathrm{w}^\bullet]}$$

$$= [\mathrm{IM}_1^\bullet]\left(\frac{k_{\mathrm{p,w}}[\mathrm{M}]_\mathrm{w}}{k_{\mathrm{p,w}}[\mathrm{M}]_\mathrm{w} + 2k_{\mathrm{t,w}}[\mathrm{T}_\mathrm{w}^\bullet]}\right)^{i-1}, \quad 1 < i < z \tag{1.29}$$

$$\rho_\mathrm{init} = k_{\mathrm{p,w}}[\mathrm{M}]_\mathrm{w}[\mathrm{IM}_{z-1}^\bullet]\frac{N_\mathrm{A}}{N_\mathrm{c}} \tag{1.30}$$

Equations (1.27) – (1.30) may be solved iteratively (in the simplest instance, using a spreadsheet or simple computer program) to yield the concentrations of all initiator-derived aqueous radicals and hence the value of ρ_init.

Maxwell *et al.*[41] also developed an analytic form for ρ_init based on the following approximation for the total aqueous radical concentration:

$$[\mathrm{T}_\mathrm{w}^\bullet] = \left(\frac{fk_\mathrm{d}[\mathrm{I}]}{k_{\mathrm{t,w}}}\right)^{\frac{1}{2}} \tag{1.31}$$

Substituting equations (1.28), (1.29) and (1.31) into equation (1.30) gives:

$$\rho_\mathrm{init} = \frac{2fk_\mathrm{d}[\mathrm{I}]N_\mathrm{A}}{N_\mathrm{c}}\left\{\frac{2\sqrt{fk_\mathrm{d}[\mathrm{I}]\,k_{\mathrm{t,w}}}}{k_{\mathrm{p,w}}[\mathrm{M}]_\mathrm{w}} + 1\right\}^{1-z} \tag{1.32}$$

where $[\mathrm{M}]_\mathrm{w}$ is the aqueous-phase monomer concentration.

While equation (1.31) is only strictly valid in the physical limit where a negligible fraction of radicals undergo entry, in Chapter 8 it will be shown that, in practice, this approximation leads to good agreement between numerical and analytic results over a wide range of conditions.

The Maxwell-Morrison model identifies entry as one of only two modes for aqueous-phase radical loss, the other being bimolecular termination [reaction (1.22)]. The rate of entry is thus determined by the probability that an initiator-derived radical will propagate to length z without terminating. In the case where $z = 1$, an entering species is formed after just the initial (rapid) propagation step and there is no possibility of aqueous-phase termination; thus

entry is 100% successful and $\rho_{init} \propto [I]$ as seen in equation (1.32). For $z \geq 2$, radicals reside for longer in the aqueous phase, increasing the probability of termination before an entering species is formed. Any value of ρ_{init} may therefore be related to $\rho_{100\%}$, the value corresponding to entry of all radicals, by an "entry efficiency" factor f_{entry} (not to be confused with the symbol f denoting "initiator efficiency"):

$$f_{entry} = \frac{\rho_{init}}{\rho_{100\%}} = \rho_{init} \frac{N_c}{2fk_d[I]N_A} \tag{1.33}$$

Comparing equations (1.32) and (1.33), the following analytic approximation for f_{entry} is trivially obtained from the Maxwell-Morrison entry model:

$$f_{entry} = \left\{ \frac{2\sqrt{fk_d[I]\, k_{t,w}}}{k_{p,w}[M]_w} + 1 \right\}^{1-z} \tag{1.34}$$

It is noted that while the analytic forms for ρ_{init} and f_{entry} rely on the approximate value for $[T^{\bullet}_w]$ in equation (1.31), derived assuming limited entry of radicals, equations (1.32) and (1.34) are also accurate in the high entry efficiency case of $z = 1$. This seemingly contradictory result arises from the fact that when $z = 1$ there is no incidence of termination; hence the error associated with the approximate value for $[T^{\bullet}_w]$ is inconsequential.

Importantly, equation (1.34) specifies that the entry efficiency is independent of the latex particle concentration, N_c – consistent with the assumption that, for a radical of length z, entry occurs far more rapidly than any other aqueous-phase process (*i.e.*, propagation or termination). Maxwell *et al.* justified this assumption by comparison of the frequency for entry with those for other processes. Indeed, it may be shown that at typical particle concentrations for emulsion polymerisation (*i.e.*, N_c of the order of $10^{15} - 10^{17}$ dm^{-3}) the frequency of entry is several orders of magnitude higher than that of either propagation or termination. Thus all aqueous radicals reaching degree of polymerisation z will enter (rather than propagating or terminating) and f_{entry} will be insensitive to changes in particle concentration under typical conditions (as are used in the present work). Only at considerably lower than typical particle concentrations, *i.e.*, $N_c \sim 10^{13}$ dm^{-3}, would the entry efficiency be expected to show any significant dependence on N_c, due to appreciable propagation and termination of z-meric radicals. A more detailed discussion than that given here may be found in the original work of Maxwell *et al.*[41]

The validity of the Maxwell-Morrison model was demonstrated by comparison with the best kinetic data available at the time of its inception: a series of studies of entry in the emulsion polymerisation of styrene using persulfate as initiator.[14,15,17,47] Treating the integer z as the sole independent variable, Maxwell et al. found excellent accord between model and experiment (for this particular system). Further, the obtained value of $z = 2 - 3$ could be justified on the basis of thermodynamic considerations of the entering species.

1.8.3 Recent Investigations of Entry

In the decade since Maxwell *et al.* published their theory it has gained reasonable acceptance. A number of experimental investigations into the entry process have also subsequently appeared in the literature over this time period.

One approach has been characterisation of the oligomeric species generated in the aqueous phase during an emulsion polymerisation in order to gain insight into events related to entry. Morrison *et al.*[48] used isotachophoresis to study the oligomeric species produced in emulsion polymerisations of styrene initiated by potassium persulfate. While the data showed good qualitative agreement with the theoretical predictions of Maxwell *et al.*,[41] (*i.e.*, that z is of order 2 – 3 for the styrene/persulfate system) they relied on comparisons with model compounds designed to be analogous to oligomers formed in emulsion polymerisation, and were thus rather indirect results.

Poehlein and co-workers employed a range of more direct spectroscopic techniques for the characterisation of oligomers formed in seeded and unseeded emulsion polymerisations. This work included analysis of aqueous-phase oligomers in emulsion copolymerisation systems,[49,50] as well as an intra-particle inhibition method for isolating oligomers produced in vinyl acetate emulsion polymerisations.[51] While these results appear to be in line with the predictions of Maxwell *et al.*, the data presented in this case (in particular mass spectra) are by no means indisputable supporting evidence.

The most definitive analysis of aqueous oligomers presented thus far is that of Thomson *et al.*[52] who used matrix-assisted laser desorption/ionization time-of-flight (MALDI-TOF) mass spectrometry to deduce the nature of oligomers from *ab initio* (unseeded) surfactant-free emulsion polymerisations of MMA with persulfate as initiator. They observed MMA oligomers ranging in length from 2 to 14 monomer units in these systems, with the average

degree of polymerisation in the range of 6 – 9, suggesting that entry in these systems is by radicals of significantly greater length than in equivalent styrene systems.

Marestin *et al.*[53] also investigated entry in MMA polymerisations. These workers used a novel radical trapping method which involved grafting free radical amino-TEMPO (4-amino-2,2,6,6-tetramethyl-1-piperidinyloxy) groups onto the surface of latex particles. Entering oligomeric radicals from the aqueous phase were trapped by the TEMPO groups and analysis of the resulting polymer using both IR spectroscopy and GPC revealed the average composition of the entrant oligomeric species to be approximately 5 – in line with the results of Thomson *et al.* In addition, these workers estimated the rate of entry from the observed decay in the ESR signal from the nitroxide free radicals over time. Notably, these results suggested an entry efficiency of 30 – 40% (*i.e.*, well below 100%) for this system.

Tauer and Deckwer[54] have reported results obtained from analysis of the polymer formed in persulfate-initiated emulsion polymerisations of styrene, under conditions of very low monomer concentration and relatively low pH, using MALDI-TOF mass spectrometry. These authors identified the possibility of a range of polymer chain end-groups, suggesting the presence of SO_4^-, H, OH and COO^- (carboxylate) groups, and concluding that under such conditions initiation in these systems is not only by sulfate radicals generated directly from persulfate (as expected) but also by a range of species formed *via* radical side-reactions. It was further claimed that these results indicate that radical surface-activity is not required for entry (contrary to the postulate of the Maxwell-Morrison model). However, when considering the suggestions of these authors, it should be noted that the presence of different end-groups does not, in itself, refute the notion that entrant radicals must be surface-active. It simply suggests that the overall value of z inferred for such a system is likely to reflect a range of z values corresponding to the different initiating radicals. Moreover, the presence of end-groups other than those derived from initiator in "dead" polymer chains at the end of a polymerisation is not conclusive evidence for initiation by other radical species; these end-groups could equally result from reactions (such as chain transfer, disproportionation or hydrolysis) occurring after particle nucleation/entry, or indeed, after termination of polymeric radicals – especially under the low pH conditions used in these particular experiments.

Morrison *et al.*[1,55,56] investigated the suggestion that the (non-rate-determining) entry step is diffusion-controlled by way of so-called "competitive growth" experiments. These authors showed that in the case of a bimodal size distribution of seed latex particles the rate

coefficient for entry varies with particle radius approximately as expected for a diffusion-controlled process. Moreover, Coen *et al.* have shown[57] for the styrene/persulfate system, using electrostatically stabilised latex particles, that the rate coefficient for entry of initiator-derived radicals is apparently independent of particle size (within experimental uncertainty), consistent with the suggestion by Maxwell *et al.*[41] that the diffusion-controlled entry step in such systems is also sufficiently rapid to be non-rate-determining.

Another kinetic study of note is that of Colombié *et al.*,[58] where entry rate data were obtained for seeded polymerisations of styrene using reaction calorimetry. These data showed that changing the nature of the particle surface, through the use of varying amounts of anionic and nonionic surfactant, had no significant effect on the value of the entry rate coefficient.

Leemans *et al.*[59] also investigated the kinetic effects of different surfactants in *ab initio* emulsion polymerisations of MMA employing various block polyelectrolytes as adsorbed electrosteric stabilisers. In this case the experimental results suggest that the precise nature of the polyelectrolyte used, *i.e.*, charge and molecular weight, has a significant impact on the rate of polymerisation observed.

Coen *et al.*[57] and Vorwerg *et al.*[60] examined the effects of electrosteric stabiliser on the kinetics of styrene emulsion polymerisations. In these studies the stabiliser, poly(acrylic acid), was copolymerised onto pre-formed polystyrene particles and the resulting latex was used in seeded polymerisations. Data obtained indicate that the rate coefficient for entry is reduced in the presence of extensive electrosteric stabiliser.

1.9 Motivation for the Present Study and Statement of Aims

It might be hoped that some new understanding of the mechanism for entry, and hence also the validity of the Maxwell-Morrison model, could be obtained through careful inspection of the accumulated results of existing experimental studies. However, it is apparent from the brief literature review presented above that the number of such studies that provide quantitative insight into the entry process is somewhat limited. In fact the only systematic study of the variation of ρ is the original work of Hawkett *et al.*,[14] which was for one type of latex (anionically stabilised) of one polymer (polystyrene) with one initiator (KPS). This is clearly a very limited data set. Other published studies have employed a variety of different experimental techniques and interpretive approaches, and are generally limited to specific

polymerisation systems and/or reaction conditions, making it difficult to assure meaningful comparisons between different studies; moreover, very few studies have actually measured ρ. A major aim of this study is to generate ρ values, and further, to do so for a wider range of conditions than Hawkett *et al.*[14] did.

Importantly, most of the above investigations may be broadly categorised into one of the following key areas:

- Examining the influence of the initiator on entry
- Examining the influence of the monomer on entry
- Examining the influence of the particle surface on entry

In the context of the Maxwell-Morrison entry model the importance of the initiator type to the entry process is evident in that it is the initiator-derived radical that lends hydrophilic character to the oligomeric aqueous-phase radical formed. Thus, a more hydrophilic initiating radical will need to add to a greater number of (hydrophobic) monomer units in order to form a surface-active species capable of undergoing entry, and the value of z will be higher.

Clearly though, the nature of the monomer also has a strong influence on entry: the more hydrophilic the monomer, the more propagation steps that will be required to form a surface-active radical for entry, *i.e.*, z will be higher. Additionally, the rate of propagation, as governed by the monomer's water-solubility and propagation rate coefficient, will critically determine the rate at which entering species are formed.

The results of Leemans *et al.*,[59] Coen *et al.*[57] and Vorwerg *et al.*[60] above suggest that the nature of the particle surface may also play an important role in the entry process. Notably, any such effect is at variance with the essence of the Maxwell-Morrison entry model which contends that the rate of entry is determined solely by aqueous-phase reactions and thus independent of particle surface effects; the particle surface is regarded merely as a hydrophobic interface for radicals to adsorb onto.

The principal aim of the present project is to provide the first systematic study incorporating all of the key influences on entry identified above: properties of initiator, monomer and particle surface. In the first instance, the results obtained here will serve to extend the range of quantitative kinetic data available for entry in emulsion polymerisation systems.

Interpretation of these new results, together with any relevant literature findings, will then provide useful new insights into which factors are most crucial to defining the entry process at the molecular level. This systematic investigation will also permit the accuracy of the existing mechanistic understanding of entry – the Maxwell-Morrison model – to be assessed more thoroughly than in any previous study. It is of interest to ascertain whether or not this model provides a satisfactory explanation for entry data procured over a wide range of experimental conditions. Importantly, the data sought here are also such that they are capable of refuting the fundamental postulates of the Maxwell-Morrison entry model. In this way it may be possible to identify specific limitations of the model and, where necessary, to recommend alternative approaches.

1.10 Thesis Outline

This thesis begins, in Chapter 2, with a detailed explanation of the experimental techniques used most frequently through the course of this work. Included are the procedures followed for preparation and characterisation of latexes for use in seeded polymerisation, and methods for determining the key type of datum for kinetic analyses performed here: the conversion of monomer into polymer.

Chapter 3 describes experimental investigations of entry in the seeded emulsion polymerisation of styrene. Kinetic data are obtained from polymerisation systems employing different combinations of initiator and seed latex, and analysis reveals the consequences for entry of changing either the nature of the initiating radicals or the type of particle surface charge. An explanation for the observed results is sought from comparison with predictions of the Maxwell-Morrison model.

An account of kinetic investigations using seeded MMA emulsion systems is presented in Chapter 4. A variety of kinetic treatments are utilised to obtain entry data for these systems. Comparison with the results of Chapter 3 for styrene systems provides insights into the influence of monomer in the entry process, and once again results are interpreted in terms of the Maxwell-Morrison model.

As mentioned earlier, an alternative means for eliciting information on entry is the analysis of aqueous-phase oligomers formed in emulsion polymerisation. In Chapter 5 this approach is used to attempt to clarify the nature of entering radicals formed in MMA/persulfate systems.

It will be seen that the investigation of entry kinetics in the MMA systems of Chapter 4 demands an accurate account of the kinetics of radical loss by exit and bimolecular termination. In Chapter 6 these processes are examined in detail using two approaches: analysis of kinetic data from experiments initiated by chemical and γ-radiolytic means, and analysis of molecular weight data obtained from gel-permeation chromatography. Measured values of the rate coefficients for transfer to monomer (a prerequisite for radical exit) and termination are reconciled in terms of simulated results based on the best current models for these chain stopping reactions.

An important but poorly understood phenomenon in emulsion polymerisation is the radical entry process giving rise to polymerisation in the absence of any intentionally added radical source – termed "spontaneous polymerisation". As shown in Chapters 3, 4 and 6 the kinetic effects of spontaneous polymerisation become especially significant under conditions where the entry rate is low, such as during a γ-relaxation or polymerisation with low initiator concentration. In Chapter 7 all kinetic results for spontaneous polymerisation in styrene and MMA emulsion systems acquired over the course of this project are collated. These results are interpreted in terms of the (limited) existing theories for spontaneous polymerisation and new mechanistic inferences are drawn.

Chapter 8 begins with a discussion of the deficiencies in the pioneering kinetic treatment for emulsion polymerisation formulated by Smith and Ewart. A new modelling methodology is developed which extends the Smith-Ewart approach to include all reactions of monomeric and aqueous-phase radicals. This new model is compared to existing kinetic models by way of exemplary numerical solutions for styrene, MMA and butyl methacrylate systems, and the specific benefits offered by the new model are made clear.

Over the course of this work various limitations of the Maxwell-Morrison entry model are identified. In Chapter 9 are postulated a number of theoretical advances on this entry model intended to address specific limitations, thus providing a basis from which future entry modelling efforts may proceed.

The final chapter of this thesis, Chapter 10, assembles the key findings of the work carried out here, summarising the new insights gained into the kinetics and mechanism of entry (and emulsion polymerisation in general), and highlighting directions for future work prompted by the results contained in this thesis.

1.11 A Note on the Structure of this Thesis

As far as is reasonably possible this thesis has been written in such a form that the reader may approach each chapter independently, *i.e.*, in the manner of a collection of smaller separate publications. It is hoped that this structure adds clarity and makes specific sections of work more easily accessible to the reader. Of course, it is impossible – and indeed would be negligent – to forsake all references between different chapters. Moreover, some chapters are seen to be strongly interrelated, *e.g.*, Chapters 4, 5 and 6 which collectively deal with the kinetics of MMA emulsion systems. As such, it is additionally hoped that the chosen structure does not excessively compromise the form expected of a literary work of this type.

It is acknowledged that this choice of structure inevitably leads to a certain amount of repetition of material, especially with regard to background information and the presentation of mathematical expressions. However, it is hoped that the careful consideration given to this issue has resulted in a final product that is not overly taxing on the reader.

1.12 References

(1) Gilbert, R. G. *Emulsion Polymerization: A Mechanistic Approach*; Academic: London, 1995.

(2) Lovell, P. A.; El-Aasser, M. S. *Emulsion Polymerization and Emulsion Polymers*; Lovell, P. A.; El-Aasser, M. S., Ed.; Wiley: New York, 1997.

(3) Harkins, W. D. *J. Am. Chem. Soc.* **1947**, *69*, 1428.

(4) Moad, G.; Solomon, D. H. *The Chemistry of Free Radical Polymerization*; Pergamon: Oxford, 1995.

(5) Zammit, M. D.; Davis, T. P.; Haddleton, D. M. *Macromolecules* **1996**, *29*, 492.

(6) Zammit, M. D.; Davis, T. P.; Haddleton, D. M.; Suddaby, K. G. *Macromolecules* **1997**, *30*, 1915.

(7) Prescott, S. W.; Ballard, M. J.; Rizzardo, E.; Gilbert, R. G. *Macromolecules* **2002**, *35*, 5417.

(8) Ferguson, C. J.; Hughes, R. J.; Pham, B. T. T.; Hawkett, B. S.; Gilbert, R. G.; Serelis, A. K.; Such, C. H. *Macromolecules* **2002**, *35*, 9243.

(9) Prescott, S. W., 2003, Ph.D. Thesis, University of Sydney.

(10) Ballard, M. J.; Napper, D. H.; Gilbert, R. G. *J. Polym. Sci., Polym. Chem. Edn.* **1984**, *22*, 3225.

(11) Rimmer, S.; Tattersall, P. *Polymer* **1999**, *40*, 5729.

(12) Leyrer, R. J.; Machtle, W. *Macromol. Chem. Phys.* **2000**, *201*, 1235.

(13) Lau, W. *Macromol. Symp.* **2002**, *182*, 283.

(14) Hawkett, B. S.; Napper, D. H.; Gilbert, R. G. *J. Chem. Soc. Faraday Trans. 1* **1980**, *76*, 1323.

(15) Whang, B. C. Y.; Napper, D. H.; Ballard, M. J.; Gilbert, R. G.; Lichti, G. *J. Chem. Soc. Faraday Trans. 1* **1982**, *78*, 1117.

(16) Penboss, I. A.; Napper, D. H.; Gilbert, R. G. *J. Chem. Soc. Faraday Trans. 1* **1983**, *79*, 1257.

(17) Adams, M. E.; Trau, M.; Gilbert, R. G.; Napper, D. H.; Sangster, D. F. *Aust. J. Chem.* **1988**, *41*, 1799.

(18) Lacík, I.; Casey, B. S.; Sangster, D. F.; Gilbert, R. G.; Napper, D. H. *Macromolecules* **1992**, *25*, 4065.

(19) Morrison, B. R.; Casey, B. S.; Lacík, I.; Leslie, G. L.; Sangster, D. F.; Gilbert, R. G.; Napper, D. H. *J. Polym. Sci. A: Polym. Chem.* **1994**, *32*, 631.

(20) Norrish, R. G. W.; Smith, R. R. *Nature* **1942**, *150*, 336.

(21) Trommsdorff, E.; Kohle, E.; Lagally, P. *Makromol. Chem.* **1948**, *1*, 169.

(22) Smith, W. V.; Ewart, R. H. *J. Chem. Phys.* **1948**, *16*, 592.

(23) Ugelstad, J.; Hansen, F. K. *Rubber Chem. Technol.* **1976**, *49*, 536.

(24) Harada, M.; Nomura, M.; Eguchi, W.; Nagata, S. *J. Chem. Eng. Japan* **1971**, *4*, 54.

(25) Casey, B. S.; Morrison, B. R.; Maxwell, I. A.; Gilbert, R. G.; Napper, D. H. *J. Polym. Sci. A: Polym. Chem.* **1994**, *32*, 605.

(26) Asua, J. M. *Macromolecules* **2003**, *36*, 6245.

(27) Ballard, M. J.; Gilbert, R. G.; Napper, D. H. *J. Polym. Sci., Polym. Letters Edn.* **1981**, *19*, 533.

(28) Adams, M. E.; Russell, G. T.; Casey, B. S.; Gilbert, R. G.; Napper, D. H.; Sangster, D. F. *Macromolecules* **1990**, *23*, 4624.

(29) Lichti, G.; Gilbert, R. G.; Napper, D. H. *J. Polym. Sci. A.* **1980**, *18*, 1297.

(30) Prescott, S. W.; Ballard, M. J.; Gilbert, R. G. *J. Polym. Sci. Part A Polym. Chem.* **submitted**.

(31) Russell, G. T.; Gilbert, R. G.; Napper, D. H. *Macromolecules* **1992**, *25*, 2459.

(32) Russell, G. T.; Gilbert, R. G.; Napper, D. H. *Macromolecules* **1993**, *26*, 3538.

(33) Halnan, L. F.; Napper, D. H.; Gilbert, R. G. *J. Chem. Soc. Faraday Trans. 1* **1984**, *80*, 2851.

(34) Vanderhoff, J. W., in *Vinyl Polymerization*; Ham, G., Ed.; Marcel Dekker: New York, 1969; Vol. 7 part 2.

(35) Fitch, R. M.; Tsai, C. H., in *Polymer Colloids*; Fitch, R. M., Ed.; Plenum: New York, 1971, p 73.

(36) Hansen, F. K.; Ugelstad, J., in *Emulsion Polymerization*; Piirma, I., Ed.; Academic: New York, 1982.

(37) Yeliseyeva, V. I., in *Emulsion Polymerization*; Piirma, I., Ed.; Academic: New York, 1982.

(38) Ottewill, R. O., in *Emulsion Polymerization*; Piirma, I., Ed.; Academic: New York, 1982.

(39) Penboss, I. A.; Gilbert, R. G.; Napper, D. H. *J. Chem. Soc. Faraday Trans. 1* **1986**, *82*, 2247.

(40) Lichti, G.; Sangster, D. F.; Whang, B. C. Y.; Napper, D. H.; Gilbert, R. G. *J. Chem. Soc., Faraday Trans. 1* **1984**, *80*, 2911.

(41) Maxwell, I. A.; Morrison, B. R.; Napper, D. H.; Gilbert, R. G. *Macromolecules* **1991**, *24*, 1629.

(42) Priest, W. J. *J. Phys. Chem.* **1952**, *56*, 1077.

(43) De Bruyn, H.; Gilbert, R. G. *Polymer* **2001**, *42*, 7999.

(44) McAskill, N. A.; Sangster, D. F. *Aust. J. Chem.* **1979**, *32*, 2611.

(45) McAskill, N. A.; Sangster, D. F. *Aust. J. Chem.* **1984**, *37*, 2137.

(46) Maruthamuthu, P. *Makromol. Chem., Rapid. Commun.* **1980**, *1*, 23.

(47) Leslie, G. L.; Gilbert, R. G.; Napper, D. H. *Aust. J. Chem.* **1992**, *45*, 2057.

(48) Morrison, B. R.; Maxwell, I. A.; Napper, D. H.; Gilbert, R. G.; Ammerdorffer, J. L.; German, A. L. *J. Polym. Sci., Polym. Chem. Edn.* **1993**, *31*, 467.

(49) Wang, S.-T.; Poehlein, G. W. *J. Appl. Polym. Sci.* **1993**, *50*, 2173.

(50) Wang, S.-H.; Poehlein, G. W. *J. Appl. Polym. Sci.* **1994**, *51*, 593.

(51) Kshirsagar, R. S.; Poehlein, G. W. *J. Appl. Polymer Sci.* **1994**, *54*, 909.

(52) Thomson, B.; Wang, Z.; Paine, A.; Lajoie, G.; Rudin, A. *J. Polym. Sci. Part A - Polymer Chem.* **1995**, *33*, 2297.

(53) Marestin, C.; Guyot, A.; Claverie, J. *Macromolecules* **1998**, *31*, 1686.

(54) Tauer, K.; Deckwer, N. *Acta Polymerica* **1998**, *49*, 411.

(55) Morrison, B. R.; Maxwell, I. A.; Gilbert, R. G.; Napper, D. H., in *ACS Symp. Series - Polymer Latexes - Preparation, Characterization and Applications*; Daniels, E. S., Sudol, E. D. and El-Aasser, M., Ed.; American Chemical Society: Washington D.C., 1992; Vol. 492, p 28.

(56) Casey, B. S.; Morrison, B. R.; Gilbert, R. G. *Prog. Polym. Sci.* **1993**, *18*, 1041.

(57) Coen, E.; Lyons, R. A.; Gilbert, R. G. *Macromolecules* **1996**, *29*, 5128.

(58) Colombie, D.; Sudol, E. D.; El-Aasser, M. S. *Macromolecules* **2000**, *33*, 4347.

(59) Leemans, L.; Jerome, R.; Teyssie, P. *Macromolecules* **1998**, *31*, 5565.

(60) Vorwerg, L.; Gilbert, R. G. *Macromolecules* **2000**, *33*, 6693.

2. Experimental Methods

2.1 Introduction

A wide range of experimental techniques were employed during the course of these investigations. In keeping with the general structure of this thesis, specific information relating to each of these is provided, as appropriate, in subsequent chapters; however, a more detailed discussion of some frequently used (*i.e.*, the most important) experimental methods is now undertaken.

2.2 Seeded Emulsion Polymerisation

Most experimental work carried out over the course of this project involved emulsion polymerisation in the presence of a known concentration of pre-formed latex particles – seeded polymerisation. In such experiments it may be accurately assumed (at least for the relatively low water-solubility monomers typically used in emulsion polymerisation) that all polymerisation occurs in the interior of the seed particles. For interpretation of the data it is necessary to establish that the number of latex particles neither increases, by way of new particle formation, nor decreases, *via* coagulation.

In the context of kinetic studies, this approach affords a considerable degree of control. For seeded experiments the particle concentration, N_c, appearing in equations (1.2) and (1.3) of Chapter 1 is pre-determined. Given that the rate coefficient for propagation, k_p, may be measured independently (*e.g.*, using pulsed-laser polymerisation[1,2]), that the total mass of added monomer, m_M^{tot}, is dictated by the known mass added, and that the value of $[M]_p$ may be determined using methods described shortly, it is possible to infer the average number of radicals per particle, $\bar{n}$, directly from the rate of seeded polymerisation.

2.3 Seed Latex Preparation

As just explained, it is first necessary to have a seed latex in order to carry out seeded emulsion polymerisation. The preparation of seed latexes is now detailed.

2.3.1 Latex Synthesis

Full details of reagents used in the synthesis of seed latexes, as well as specific reaction conditions, are given in Chapters 3 and 4. The general procedure for synthesis of seed latexes was as follows.

Seed latex synthesis was conducted using a 1 dm^3 glass and stainless steel walled reactor whose design has been described in detail elsewhere.[3] Temperature control was provided by a glass water-jacket and stirring by means of an overhead stirrer with a pitched blade impellor.

Water containing dissolved surfactant and (in some cases) buffer was added to the reactor and heated to the desired reaction temperature with stirring. Monomer was then added with sufficient stirring to form an emulsion and the reactor allowed to return to the required temperature. Finally, initiator, dissolved in a small amount of water, was added and the reactor sealed for the allotted reaction time. A positive pressure of nitrogen gas inside the reactor prevented any oxygen from leaking in during the polymerisation.

At the completion of polymerisation the seed latex was filtered through glass wool to remove any coagulum that may have formed and final conversion of monomer into polymer was determined by gravimetry.

2.3.2 Dialysis

In a seeded polymerisation it is crucial that the concentrations of all reagents are accurately known, and the presence of unknown quantities of residual species (other than latex particles) in the seed latex may well have a significant influence on the kinetics of seeded polymerisation. The presence of excess surfactant, for example, could give rise to formation of micelles and thus facilitate secondary nucleation, and the presence of unreacted initiator could lead to a higher than expected flux of initiating free radicals. In order to minimise any such effects, the seed latexes used in the present study were subjected to a thorough dialysis regime.

Here the latex was placed inside a narrow cellulose acetate tube (with ends tied securely to prevent any latex from leaking out) which was then immersed in a large volume of distilled water (approximately 20 times the volume of latex). Over time, the concentration gradient across the wall of the tube causes migration of small species, including residual surfactant,

initiator, buffer, monomer and aqueous oligomer, from the latex into the distilled water, while the much larger latex particles are confined within the dialysis tube. Dialysis was continued, with the distilled water being replaced up to several times per day, until conductivity measurements of the water phase were seen to converge to a constant (low) value close to that of the distilled water.

2.4 Latex Particle Size Analysis

Various techniques were employed for the determination of latex particle size during the course of this work. An accurate measure of particle diameter is not only important for identifying the size dependence of various quantities, but also crucially determines the calculated latex particle volume and thus the accuracy of the value of N_c associated with a given starting mass of polymer in seeded experiments; this in turn is used to determine $\overline{n}$ from the observed rate in subsequent seeded emulsion polymerisation, and accurate $\overline{n}$ values are essential for determining rate coefficients for entry, *etc.* Furthermore, it is implicitly assumed that the latex particles are of uniform size (this assumption is implicit in the analysis of $\overline{n}$ values, because such analysis assumes that all particles have the same rate coefficient values, some of which are known to depend on particle size). Thus, determination of the actual particle size distribution and polydispersity of the seed latex provides some indication as to the accuracy of this assumption.

2.4.1 Transmission Electron Microscopy

Transmission electron microscopy (TEM) is a widely used technique for measuring the average particle diameter and, importantly, the full particle size distribution (PSD) for a latex. For this project TEM was carried out at the University of Sydney's Key Centre for Microscopy and Microanalysis using either a Philips CM12 or a Philips CM120 Biofilter microscope. TEM was also carried out at the University of Canterbury using either the JEOL JEM-1200 EX microscope in the Department of Plant and Microbial Sciences, or the Hitachi H600 in the Mechanical Engineering Department.

Samples for TEM were prepared as follows. First a support film of Pioloform™ [poly(vinyl butaryl)] was deposited on the bare TEM grid, and a thin carbon coating applied to impart strength and improved conductivity. The latex sample was diluted with water (Milli-Q) to a polymer content of ~ 0.1 % by weight and, if necessary, polystyrene standard latex particles

of known diameter and narrow polydispersity were added for reference. A drop of diluted latex was then placed on the grid and dried overnight at room temperature before inspection by TEM.

Analysis of images obtained from electron microscopy was carried out using either Zeiss KS 400 or Scion Image for Windows image analysis software. Due to the uncertainty associated with the precise magnification in TEM, accurate determination of PSDs for sample latexes was obtained by comparison with polystyrene latex particle standards. Here a reference scale was established by measuring the diameter of ~ 100 standard particles, and the PSD for the sample latex determined from measuring the diameter of 500 – 1000 sample particles.

TEM is a characterisation technique well suited to hard polymers (such as polystyrene) which are resilient to the conditions of the electron beam. As explained in Chapter 4, in the case of polymers that are prone to deformation under such conditions special measures may be required to obtain accurate particle size data.

2.4.2 Capillary Hydrodynamic Fractionation

Another particle sizing method employed in this work was capillary hydrodynamic fractionation (CHDF). This technique identifies latex particles of different sizes on the basis of their elution time through a length of narrow capillary tubing, with larger particles eluting more quickly than smaller particles.

All CHDF analyses were carried out at the University of Sydney's Key Centre for Polymer Colloids using a MATEC Applied Sciences CHDF-1100 fitted with a C570 high sensitivity column and employing GR500™ eluent at a flow rate of 1.40 mL min^{-1}. Particle size calibration was performed using polystyrene particle standards.

In principle, the fractionation provided by CHDF enables not only the average particle diameter, but also the particle size distribution and thus the polydispersity for a sample latex to be determined. Notably, it was found in this work that while the average diameter obtained from CHDF was generally in good agreement with that from TEM, the polydispersity index (ratio of weight-average to number-average particle diameter) measured by CHDF was consistently higher than that from TEM by up to ~ 10%. In light of this, only the polydispersities measured by TEM – thought to be most accurate – are quoted in this thesis.

2.4.3 Dynamic Light Scattering

Measurements of particle size using two different dynamic light scattering techniques were also carried out at the University of Sydney's Key Centre for Polymer Colloids for comparison with TEM and CHDF analyses. While these methods provide useful estimates of the average particle diameter for a latex, they do not accurately determine the exact distribution of particle sizes.

Photon correlation spectroscopy (PCS) determines average particle size on the basis of diffusion coefficients measured from light scattered by moving particles. PCS measurements were conducted using a Brookhaven instrument consisting of a BI-200SM Version 2 goniometer with a 633 nm 35 mW He-Ne laser, BI-APD avalanche photodiode detector, and PC1 B1-9000AT EN correlator.

Particle sizes were also measured using a Malvern High Performance Particle Sizer (HPPS) instrument, with the principle difference between HPPS and PCS being the angle at which the intensity of scattered light is measured. PCS typically measures light scattered at 90° while HPPS measures the intensity of back-scattered light (*i.e.*, at a very small angle from the incident beam).

2.5 Determining the Intra-Particle Monomer Concentration

An important quantity in the analysis of kinetic data obtained from seeded emulsion polymerisations is the concentration of monomer at the locus of polymerisation, *viz.*, inside monomer-swollen latex particles. In the simplest instance it may be possible to prescribe the intra-particle monomer concentration, denoted $[M]_p$, by adding a known amount of monomer and assuming that all added monomer is located inside the latex particles (as will be the case for seeded polymerisations commencing in Interval III using a monomer of negligible water solubility). However, the extent to which a latex particle will swell with monomer is limited by the complex thermodynamic balance between a particle's surface free energy (which increases with increasing particle size) and the free energy of mixing of monomer and polymer in the particle interior (which decreases with increasing particle size).[4] As a particle swells with monomer a thermodynamic equilibrium is eventually attained such that no further added monomer will be accommodated by the latex particles – the particles are saturated. In this event any excess monomer will be contained in monomer droplets dispersed in the

aqueous phase (as is the case for seeded polymerisations starting in Interval II). Thus, it becomes important to establish the saturated-particle monomer concentration, $[M]_p^{sat}$. Given that the thermodynamic balance determining this concentration is likely to be affected by, *e.g.*, variations in unswollen particle diameter and surface characteristics between different latexes, it is best practice to measure this value for each seed latex individually.

2.5.1 Static Swelling Method

While various methods are available for determining $[M]_p^{sat}$ for a latex, the one used most extensively in this work was the so-called "static swelling" method.[5-7] Here a seeded emulsion system was prepared in a similar way to that for a seeded kinetic run (described shortly). A dilatometer vessel was charged with seed latex particles, surfactant, water and a small amount of inhibitor (*e.g.*, 0.01 g of hydroquinone, to prevent any polymerisation occurring during the measurement), as well as sufficient monomer to saturate both latex particle and aqueous phases and provide a small excess of the order of one gram of monomer. The mixture was stirred overnight to saturate particles and water with monomer at room temperature. The mixture was then heated to the required temperature and stirred for a further 60 minutes to ensure complete saturation before stirring was stopped and the mixture left to separate into two immiscible (monomer and aqueous) layers. After a further 60 minutes a narrow capillary tube, of known bore diameter, was attached to the dilatometer vessel and the excess monomer which had separated from the aqueous phase was carefully displaced into the capillary by addition of a small amount of water. The length of separated monomer in the capillary was measured precisely using a dilatometry "tracker" instrument (described further below) and the exact mass of excess monomer calculated (using the density of monomer). By allowing for the small amount of monomer dissolved in the aqueous phase it was thus possible to infer the value of $[M]_p^{sat}$ from total monomer added by mass balance.

$$m_M^p = m_M^{tot} - m_M^{excess} - [M]_w^{sat} V_w M_0 \tag{2.1}$$

$$[M]_p^{sat} = \frac{m_M^p / M_0}{\frac{m_M^p}{d_M} + \frac{m_p^{seed}}{d_p}} \tag{2.2}$$

Here m_M^p = mass of monomer in the swollen latex particles, m_M^{tot} = total mass of added monomer, m_M^{excess} = mass of excess monomer measured, $[M]_w^{sat}$ = saturated concentration of

monomer in water (which must first be measured), V_w = volume of the aqueous phase of the emulsion, and M_0 = molar mass of monomer. m_p^{seed} is the mass of polymer in the latex particles, d_p the density of polymer, and d_M the density of monomer. Preferably, values of d_M and d_p measured for solutions of polymer in monomer should be used. In the absence of such data, densities of pure monomer and polymer may be used; however, it is noted that this approach implicitly assumes ideal mixing of monomer and polymer inside a latex particle.

2.5.2 Kinetic Method

An alternative method determines the value of $[M]_p^{sat}$ directly from kinetic data measured for a seeded polymerisation. This method, variants of which have been used to measure $[M]_p^{sat}$ for a range of systems,[6,8-10] relies on the fact that the rate of polymerisation, dx/dt, is directly proportional to the value of $[M]_p$, as shown in equations (1.2) and (1.3) of Chapter 1. During Interval II the value of $[M]_p$ remains constant at its saturation value, sustained by the supply of monomer in the monomer droplets. Thus, provided that k_p, N_c and $\bar{n}$ remain relatively constant through Interval II, so too will the polymerisation rate.

However, when the system enters Interval III, and no monomer droplets remain, the value of $[M]_p$ gradually declines. The fractional conversion corresponding to the transition from Interval II to III, denoted x_{trans}, is then identifiable as the first point at which dx/dt is seen to decrease from its constant Interval II value. The value of $[M]_p^{sat}$ may be calculated from the value of x_{trans} as follows:[7]

$$[M]_p^{sat} = (1 - x_{trans}) \frac{m_M^{tot} / M_0}{\frac{m_M^{tot}}{d_M} + \frac{m_p^{seed}}{d_p} + x_{trans} m_M^{tot}\left(\frac{1}{d_p} - \frac{1}{d_M}\right)} \qquad (2.3)$$

The reproducibility of the value of $[M]_p^{sat}$ so obtained may be tested by repeating the above procedure with different initial amounts of added monomer.

Notably, this method is best suited to measuring $[M]_p^{sat}$ for systems where the value of $\bar{n}$ is approximately constant over Interval II. For systems wherein Interval II $\bar{n}$ varies significantly (as will be seen for MMA in Chapter 4) the value of x_{trans} is more difficult to identify from rate data and the static swelling method is therefore preferable.

The kinetic method described above is illustrated in Figure 2.1 for a seeded emulsion polymerisation of styrene at 50°C using persulfate as initiator (the system KPS/AN01 of Chapter 3). After an initial approach to steady-state the polymerisation rate is seen to remain constant during Interval II until a time of 35 min, corresponding to $x_{trans} = 0.24$, when the rate begins to gradually decrease into Interval III (with the increase in dx/dt observed after ~ 90 min indicating the onset of a gel effect). Also shown in Figure 2.1 is the time evolution of $[M]_p$ as calculated using the value of $[M]_p^{sat} = 5.43$ M measured for this particular seed latex by the static swelling method. As is evident from the results presented, the value of $[M]_p^{sat} = 5.29$ M inferred using the kinetic method is in good accord with that from static swelling.

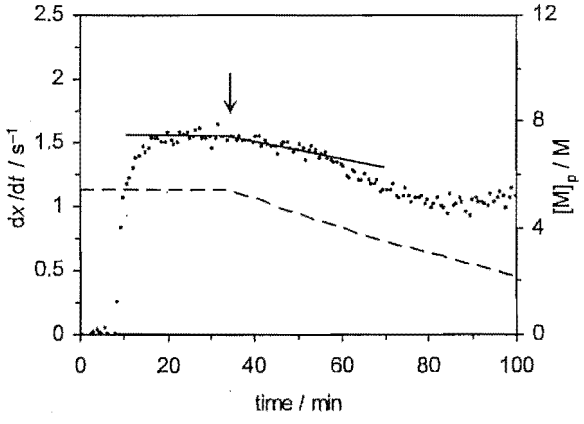

Figure 2.1. Rate of polymerisation, dx/dt (circles), and intra-particle monomer concentration, $[M]_p$ (dashed line), calculated using $[M]_p^{sat}$ from static swelling), as functions of conversion for a persulfate initiated seeded emulsion polymerisation of styrene at 50°C; arrow indicates estimated point of transition from Interval II to III; solid lines superimposed as a visual guide.

While values of $[M]_p^{sat}$ determined for styrene seed latexes from a number of experiments using the kinetic method were generally found to agree reasonably well with static swelling results, the former were subject to a significant degree of experimental scatter, associated with the need to precisely identify the Interval II to III transition point from relatively noisy rate data (as is evident from the results presented in Figure 2.1). Thus, throughout this work only values of $[M]_p^{sat}$ measured using the static swelling method will be presented and adopted for use in kinetic analyses.

2.6 Dilatometry

The principal technique used to obtain experimental kinetic data throughout this work was dilatometry. Dilatometry makes use of the fact that the density of polymer is greater than that of monomer, and hence that polymerisation gives rise to a measurable volume contraction of the reaction medium. Careful monitoring of this volume contraction yields data from which the cumulative conversion of monomer into polymer may be accurately inferred. While this technique is highly sensitive to interference from any non-polymerisation sources of volume change in the system, of particular appeal is the fact that this procedure is non-invasive – requiring no sampling of the reaction medium – and may be automated, permitting data to be collected in an effectively continuous manner (*cf.* other methods such as gravimetry below).

Most of the kinetic experiments for this work were carried out using a custom-designed dilatometry instrument constructed at the University of Canterbury, a brief description of which is now provided. It is noted that a number of experiments conducted at the Key Centre for Polymer Colloids of the University of Sydney and at the facilities of the Australian Nuclear Science and Technology Organisation employed a dilatometry apparatus very similar in design and operation to that at the University of Canterbury.

2.6.1 Dilatometer Design and Operation

The key features of the University of Canterbury dilatometer are illustrated schematically in Figure 2.2. The reaction medium is contained in a glass vessel of volume 60 cm^3, outfitted with a glass water-jacket. Temperature control is achieved by a continuous flow of heated water through the glass jacket provided by a water heater/circulator unit, and stirring of the reaction medium is afforded by a magnetic stirrer and stirring bar placed inside the reaction vessel. A long narrow glass capillary tube is attached to the top of the reaction vessel by a small ground-glass joint. The tube is held in place vertically by two rigid arms protruding from a stainless steel rod, which is in turn anchored to a large metal base-plate.

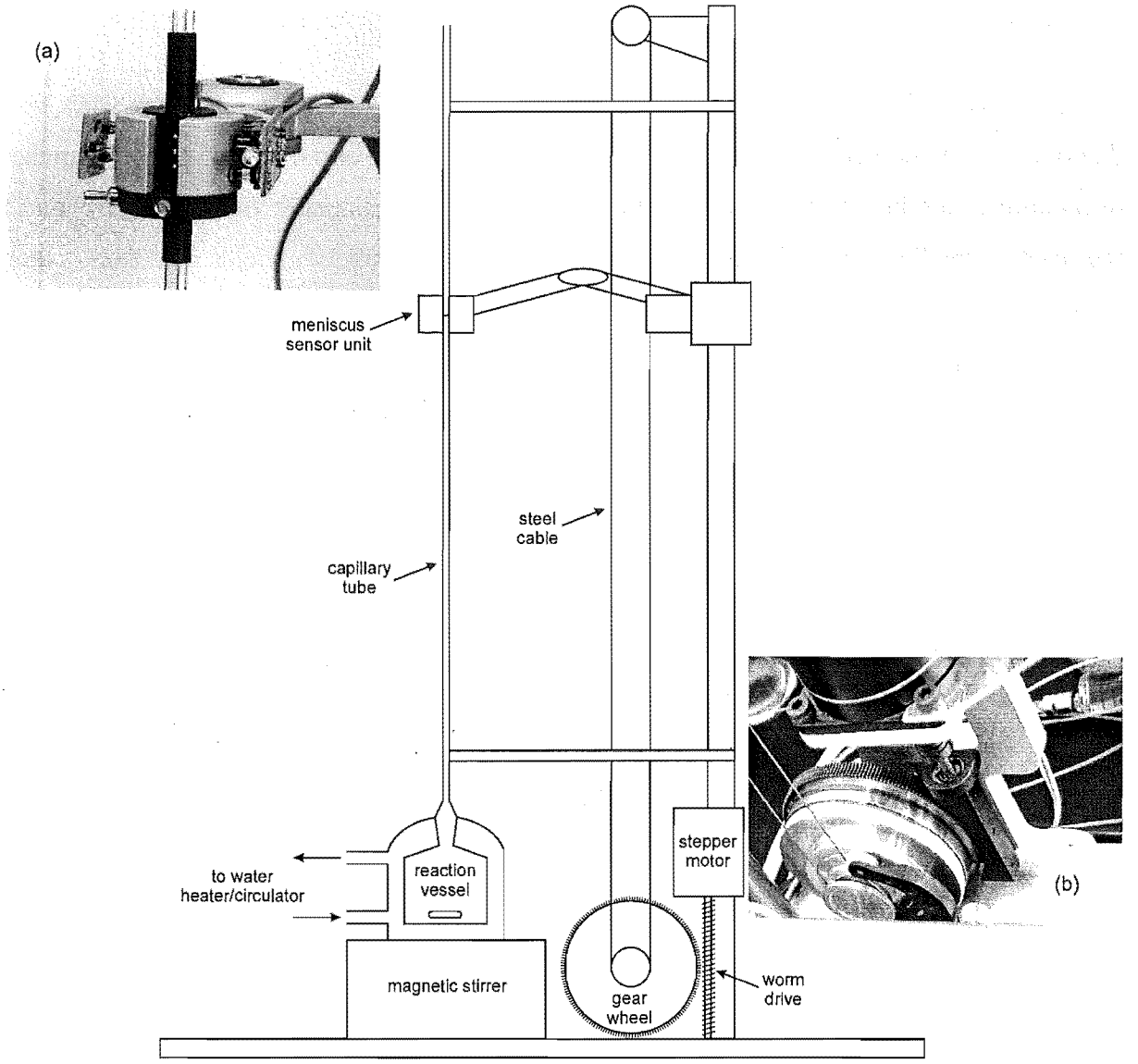

Figure 2.2. Schematic diagram of University of Canterbury dilatometry instrument; inset **(a)** is a photograph of the meniscus sensor unit; inset **(b)** is a photograph of the stepper motor/worm-drive/gear wheel/drive pulley assembly.

Also mounted to this stainless steel rod is the meniscus sensor unit responsible for monitoring the change in meniscus height in the capillary tube over time. This sensor unit is positioned around the capillary tube and connected to the steel rod by a (horizontally) flexible metal arm which glides up and down the rod on metal ball bearings. The height of the arm is controlled by a stainless steel cable that extends between two pulleys located at the top and bottom of the steel rod. The bottom pulley, or "drive pulley", is attached to a gear wheel which is rotated by a worm-drive under the precise control of a stepper motor. In this way, a given revolution of the stepper motor is translated into a precise length of vertical travel by the arm and sensor unit. The length of vertical travel corresponding to a single step of the stepper motor is

known as the "step length" and is determined by the drive pulley diameter, the worm-drive inclination, and specifications of the motor and gear wheel. The present setup, employing a stepper motor with step angle 0.9° (giving 400 steps per full revolution) and a gear wheel salvaged from an X-ray diffractometer, permits a resolution of order 0.5 microns per step in meniscus height measurements (this degree of precision being approximately 5 times better than that of the dilatometry instruments at the University of Sydney or Australian Nuclear Science and Technology Organisation).

The meniscus sensor unit houses a series of three light-emitting diodes which each direct a narrow beam of light through the glass capillary tube to a phototransistor. While all three beams may be employed for calibration purposes, only one light beam is actually required for tracking the meniscus height. The principal of meniscus detection is that the refractive index of dodecane (~ 1.4, the meniscus liquid) is closer to that of glass (~ 1.5) than is that of air (~ 1.0). Thus, when the sensor is below the meniscus level, the beam of light passing through the dodecane-filled section of capillary tube is refracted to a lesser extent (and the receiving phototransistor registers a higher light intensity) than when the sensor is above the meniscus. The meniscus level is then defined as the point at which the intensity of light passing through the capillary is the average of the intensities transmitted above and below meniscus.

Automated tracking of the meniscus height is controlled by a computer connected to both the sensor unit and the stepper motor, and consists of readings taken at regular, controllable time intervals (typically of the order of 10 – 60 seconds). At the time of a given reading the meniscus sensor unit determines whether it is positioned above, below or at the meniscus by the measured intensity of light transmitted through the capillary tube. If the sensor is above the meniscus (as will be the case if contraction has occurred during the preceding time interval) a signal is sent to the stepper motor and the sensor unit is moved downwards until the meniscus is detected. Alternatively, if the sensor unit is initially below the meniscus (*e.g.*, in the case of thermal expansion or bubble formation), the unit moves upwards to locate the meniscus. The reading time and new meniscus height are logged by the computer and the sensor unit then remains stationary until the next height reading is required.

2.6.2 *Calibration*

The volume of the dilatometer reaction vessel (with magnetic stirring bar present) was determined from the measured weight difference of the vessel when empty and when filled with distilled water.

The bore radius of the glass capillary tube was determined as follows. A syringe was attached and used to draw a bead of mercury (triply distilled) of length ~ 10 cm into the tube. The length of this bead, l_{Hg}, was accurately measured using a Vernier calliper, and the volume of mercury, V_{Hg}, determined from its measured weight and known density[11] at the relevant temperature. The bore radius of the tube was then calculated as:

$$r_{cap} = \left(\frac{V_{Hg}}{\pi \, l_{Hg}} \right)^{\frac{1}{2}} \tag{2.4}$$

The consistency of the capillary bore radius was confirmed by repeating the above measurement at different points along the length of the tube.

The precise step length of the dilatometry tracker setup (~ 0.5 microns) was calibrated prior to each kinetic experiment by measurement (in steps) of a stainless steel rod of known length (10 cm).

The intensity of light transmitted through the capillary tube by the meniscus sensor unit which corresponds to the meniscus location was determined by separately measuring the transmitted intensities above and below the meniscus and averaging these values. This calibration was carried out prior to each experiment.

2.6.3 *Experimental Procedure*

For kinetic experiments the dilatometer vessel was charged with seed latex particles, monomer and surfactant as necessary and filled almost completely with water, leaving a small volume (< 5 cm^3) to accommodate thermal expansion and addition of initiator solution. The glass-stoppered vessel was then stirred overnight at room temperature to swell the particles with monomer. Prior to the commencement of polymerisation the reaction medium was thoroughly degassed to prevent the liberation of dissolved gases, and thus the formation of bubbles, during the course of the experiment. A simple and effective method for degassing

was found to be the following. A rubber septum was connected to the top of the dilatometer vessel *via* a piece of glassware consisting of a ground-glass joint and a vacuum tap. When the tap was closed the septum was completely isolated from the reaction medium; however, opening the tap briefly, the pressure in the dilatometer vessel could be reduced by extracting some of the headspace gases using a large syringe and a needle passed through the septum. In this way, the loss of monomer due to swelling of the rubber septum or the application of extended periods of vacuum was avoided. The reaction mixture was heated to 10°C above the reaction temperature and degassed by repeating the above procedure several times over a period of 20 – 30 minutes. Over this time the appearance of many small bubbles at the surface of the reaction mixture indicated the effective removal of dissolved gases, and towards the end of the degassing period it usually became possible to induce boiling of the reaction mixture using the syringe.

It is worth noting that the degassing procedures developed in this work proved to be extremely successful, with longest induction times for chemically initiated experiments being of the order of one hour (for lowest initiator concentrations), and even in the case of experiments with no added initiator the induction time was consistently only five hours or less. This is a valuable improvement in experimental procedure as lengthy and highly variable induction times are traditionally a bugbear of experimental work in this area.

After degassing, the temperature was lowered to the reaction temperature for a period of at least 15 – 20 minutes to ensure full thermal equilibration. The degassing glassware was removed and replaced by the glass capillary tube, with stirring halted during this time to limit the introduction of new dissolved gases. At this stage initiator was added in the form of a small volume (1 – 3 cm^3) of aqueous solution injected below the surface of the reaction medium using a syringe and needle. Additional water – degassed using a vacuum pump and heated to the reaction temperature – was then added to the dilatometer vessel by way of a syringe and a length of narrow polyethylene tubing threaded through the glass capillary tube. The added water expanded the reaction mixture into the capillary tube; however, particular care was taken to ensure that a small volume of monomer collected at the base of the capillary tube in the region of the ground-glass joint. This monomer layer served to trap any large monomer droplets which were not adequately dispersed by the stirrer and thus floated to the top of the reaction medium. In the absence of such a layer it was not uncommon to witness a substantial amount of monomer (in the form of large droplets) rising up the capillary tube to

collect at the top and remain unreacted. Importantly, the presence of the separated monomer layer at the base of the capillary did not give rise to any sort of starved-feed effect as this layer was deliberately positioned in such a way that it was significantly agitated by the action of the stirrer. Thus, the monomer layer was continuously replenished and depleted as monomer droplets collected and were re-dispersed. As monomer in the dispersed phase was consumed it was replaced by new droplets liberated from the monomer layer by stirring, until eventually the monomer layer disappeared completely. Using this approach no monomer was left isolated from the reaction medium.

It is noted that the problem of inadequately emulsified monomer stems from the less than optimal stirring conditions provided by a magnetic stirring bar, even under the most vigorous stirring regime possible. This situation was found (through trial and error) to be somewhat improved by constructing a dilatometer vessel whose diameter was slightly greater than its height. It is suggested that stirring characteristics might be improved by the addition of baffles to the vessel walls (in the form of a series of vertical indentations in the glass), possibly obviating the need for a layer of separated monomer. However, this notion remains to be investigated.

Degassed water was added above the monomer layer to fill the length of glass capillary tubing, and finally a small layer (1 – 5 cm) of dodecane was placed atop the water. The purpose of the dodecane was to provide a uniform meniscus that moves smoothly down the capillary, with the rate of descent of a water meniscus being comparatively irreproducible due to the higher surface tension of water.

Finally, the meniscus tracking software was started and the tracker commenced taking height readings at (specified) regular time intervals as described above.

2.6.4 Some Cautionary Notes for Dilatometry

In addition to the possibility of monomer loss *via* droplets rising up the capillary tube (described above), there are a number of other potential problem areas for dilatometry; these are now briefly discussed.

Any process other than polymerisation which causes a change in the volume of the reaction medium will clearly be a source of error. The simplest such process is thermal expansion or contraction as a result of inconsistent temperature control. Thus it is important to employ a

water heater/circulator that controls temperature accurately (*e.g.*, with a drift of less than ± 0.1°C), and which circulates the water at a consistent rate and sufficiently rapidly to prevent significant heat loss through the water-jacket and connecting hoses.

Another source of error is the formation of bubbles, which is, in turn, generally the result of inadequate degassing of the reaction medium prior to polymerisation. Under such conditions it is possible that a bubble may form simply from the spontaneous liberation of dissolved gases. However, a more likely scenario for bubble formation is the presence of a gas-evolving species such as an azo-initiator, from which the total evolved nitrogen concentration will increase with time according to $[N_2] = [I]_0\{1 - \exp(-k_d t)\}$ (where t is time, $[I]_0$ is the starting concentration of initiator and k_d the first-order rate coefficient for its decomposition), or a buffer such as sodium hydrogen carbonate which may generate a significant concentration of carbon dioxide gas. Initially, any such gases will be dissolved in the reaction medium; however eventually sufficient gas may be evolved to completely saturate the medium and lead to nucleation of a bubble. Assuming that such gas-evolving species may not be substituted by alternative reagents (*e.g.*, an initiator such as KPS or a buffer such as sodium acetate), the likelihood of bubble formation may be minimised only by particularly stringent degassing efforts, with the hope that all evolved gases will remain dissolved in the reaction medium.

Bubble formation may also occur in the absence of gas-evolving reagents simply as a result of conversion of monomer to polymer. Given that gases are considerably more soluble in monomer than in polymer, upon polymerisation the excess gas dissolved in the monomer must be accommodated elsewhere in the reaction medium. In the case of experiments with particularly large amounts of added monomer the gas yielded in this way may be sufficient to saturate the reaction medium and cause a bubble to be nucleated.

A further means for bubble formation that is relevant at high temperatures is boiling of the reaction mixture. For MMA emulsion systems at temperatures in excess of 80°C it was observed in this work that the generation of low pressure regions (known as "cavitation") behind the spinning bar may be sufficient to induce boiling of the emulsion, producing bubbles of gaseous water and/or monomer. This effect is seen to be diminished by employing a reduced rate of stirring; however this measure may also result in inadequate emulsification in the system.

It is noted that the presence of a bubble in the reaction vessel prior to the start of a dilatometry run may not be ruinous to the kinetic data obtained, *provided* that this bubble remains inside the vessel throughout the experiment, that its volume remains constant, and that no further bubbles are formed. Generally, however, it is preferable to remove any bubbles present before the commencement of polymerisation as the above criteria may be difficult to ascertain. Moreover, since gases are more compressible than liquids, stirring has been observed to cause fluctuations in a bubble's shape and volume resulting in considerable instability in the meniscus and noisy dilatometry data.

In general it is clear that bubbles are a bane in dilatometry and that the possibility of their formation is one of the major difficulties associated with this technique, which otherwise is very well suited to emulsion polymerisation.

Another detrimental source of volume change inside the reaction vessel is leakage of the reaction mixture through the ground-glass joint. This decrease in volume exaggerates the decline in meniscus height, causing an artificially high rate of polymerisation to be inferred. Clearly, leakage from the vessel is readily identifiable and may be avoided simply by ensuring the glass joint is well-secured.

Another possible source of dilatometry error is the presence of small droplets attached to the inner surface of the capillary tube. Such droplets are capable of refracting the light beam of the meniscus sensor unit to give a transmitted intensity that corresponds to that of the meniscus. In such cases the sensor unit will cease to follow the descending meniscus and instead remain stationary at the height of the droplet for all future readings. This problem may be avoided by ensuring that the dodecane layer is free of small water droplets attached to the capillary wall and, similarly, that no monomer droplets are present on the capillary wall in the water layer.

2.6.5 Data Analysis

While dilatometry is based on measurement of the overall volume change of the reaction medium, the dilatometry tracker instrument itself monitors only the change in meniscus *height*, Δh_{dil}, as a function of time. Provided that the meniscus level remains within the capillary tube (whose bore radius has been calibrated as described above) the change in volume, ΔV_{dil}, is trivially related to the height change as follows:

$$\Delta V_{dil} = \pi r_{cap}^{2} \Delta h_{dil} \tag{2.5}$$

The convention used here is a *positive* value of Δh_{dil}, and hence also ΔV_{dil}, is associated with *downward* movement of the meniscus. This accounts for the fact that the volume *contraction* measured by dilatometry is used to infer the extent of *increasing* conversion of monomer into polymer with time.

Once the reaction medium has attained a thermal equilibrium, any contraction (or expansion) can only be the result of chemical change within the system. Under circumstances where it is safe to assume ideal mixing of monomer and water (*i.e.*, that monomer has the same specific volume in water as in an organic phase), or, alternatively, if the amount of monomer dissolved in the aqueous phase is negligible (*e.g.*, for a monomer with very low water solubility such as styrene), the measured contraction is simply due to the decrease in volume as monomer is converted into (denser) polymer. As such, the fractional conversion, x, may be calculated directly from the cumulative volume contraction as follows:

$$x = \frac{\hat{x}}{m_M^{tot}} = \frac{\Delta V_{dil}}{m_M^{tot}\left(\frac{1}{d_M} + \frac{1}{d_p}\right)} \tag{2.6}$$

where $\hat{x}$ is mass conversion. Once again, values of d_M and d_p measured for solutions of polymer in monomer are preferable; the use of pure monomer and polymer densities implicitly assumes ideal mixing inside a latex particle. Note that two different ideal mixing assumptions have been made here, as indicated – the two should not be confused.

In the case of monomers that are appreciably soluble in water, such as methyl methacrylate (MMA) and vinyl acetate, the non-ideal mixing of monomer and water may not always be neglected and the following iterative approach[5] is required to calculate conversion for such systems. First, an initial value of conversion is calculated from ΔV_{dil} according to equation (2.6) (assuming ideal mixing of monomer and water). The mass of monomer in the swollen latex particles is then calculated by mass balance using the total mass of added monomer and the mass of monomer in the aqueous phase, m_M^w, as follows:

$$m_M^w = [M]_w V_w M_0 \tag{2.7}$$

$$m_M^p = m_M^{tot} - \hat{x} - m_M^w = m_M^{tot}(1-x) - m_M^w \tag{2.8}$$

where $[M]_w$ is the concentration of aqueous monomer. For the first iteration, m_M^w takes the saturated value of $m_M^w = [M]_w^{sat} V_w M_0$.

A value for the intra-particle monomer concentration is then calculated as follows:

$$[M]_p = \frac{m_M^p / M_0}{\frac{m_M^p}{d_M} + \left(\frac{m_p^{seed} + \hat{x}}{d_p}\right)} = \frac{m_M^p / M_0}{\frac{m_M^p}{d_M} + \left(\frac{m_p^{seed} + x\, m_M^{tot}}{d_p}\right)} \tag{2.9}$$

If the value of $[M]_p$ so obtained is equal to or greater than the value of $[M]_p^{sat}$ then both the intra-particle and aqueous monomer concentrations take their saturated values (*i.e.*, Interval II conditions hold). In this case the amount of monomer in the aqueous phase has not changed and so the only cause of volume contraction is the conversion of monomer into polymer. It is therefore accurate to use the original value for conversion calculated using equation (2.6).

However, if the value of $[M]_p$ obtained above is less than $[M]_p^{sat}$, there is insufficient monomer present to saturate the particle and aqueous phases (*i.e.*, Interval III conditions hold). A new value for $[M]_w$ is then calculated using the following empirical relation, due to Ballard *et al.*:[5]

$$\frac{[M]_w}{[M]_w^{sat}} = \left(\frac{[M]_p}{[M]_p^{sat}}\right)^{0.6} \tag{2.10}$$

and m_M^w is recalculated according to equation (2.7). These values are used to obtain an improved value for x.

$$x = \frac{\hat{x}}{m_M^{tot}} = \frac{\Delta V_{dil} + \left(m_{M,init}^w - m_M^w\right)\left(\frac{1}{d_M} - \frac{1}{d_{M,w}}\right)}{m_M^{tot}\left(\frac{1}{d_M} - \frac{1}{d_p}\right)} \tag{2.11}$$

The need for this procedure is because during Interval III the volume contraction is affected not only by conversion of monomer into polymer but also by the migration of some monomer from the aqueous phase (where monomer mixes non-ideally with water) into the particles (where mixing is assumed to be ideal) as required to swell the newly formed polymer. The second term in the numerator of equation (2.11) accounts for this effect. Here $d_{M,w}$ is the density of monomer in water and $m_{M,init}^w$ is the total mass of monomer dissolved in the aqueous phase at the commencement of the polymerisation. The improved values of conversion and

m_M^w are then returned to equation (2.8) as starting values for the next iteration, and the process repeated until convergence in the value of x is achieved.

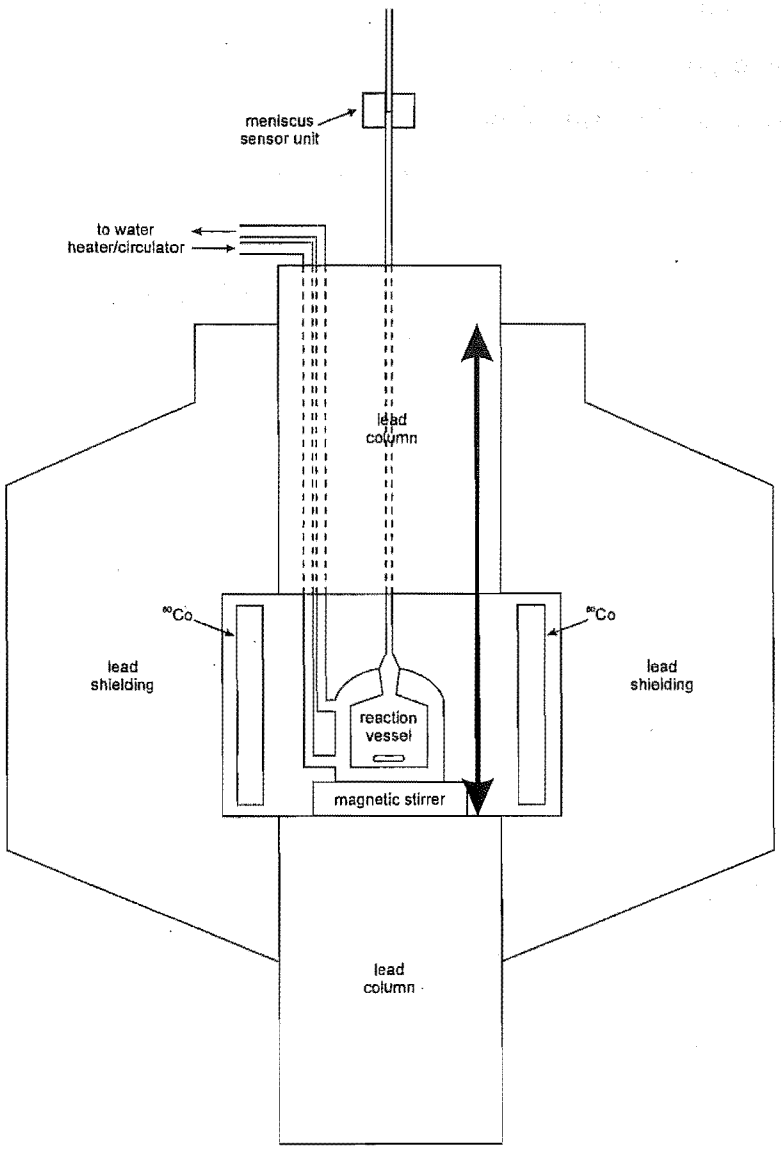

Figure 2.3. Schematic diagram of dilatometry instrument for γ-radiolysis experiments at Australian Nuclear Science and Technology Organisation.

2.7 γ-Radiolysis Experiments

Dilatometry was used to measure conversion in kinetic experiments involving γ-radiolysis as a source of initiating radicals. Here the experimental setup was very similar to that shown in Figure 2.2 but with slight modifications allowing the reaction vessel to be exposed to the γ-source. As shown in Figure 2.3, the dilatometer vessel was positioned in a small cavity between two large columns of lead (as shielding from the γ-radiation) above and below it. A

large ring of further lead shielding surrounded the in-source reaction cavity and housed rods of ^{60}Co – the source of γ-radiation. The lead columns were controlled by a motor which allowed the cavity containing the dilatometer vessel to be lowered, exposing the reaction medium to the γ-source, or raised, shielding the vessel from the source (the lead columns also moving up and down at the same time). The capillary tube was threaded through the uppermost lead column enabling the vessel and capillary to be filled in the usual way, and allowing the meniscus height to be monitored by the sensor unit. Temperature control was provided by heated water, supplied to the vessel's water jacket *via* connecting hoses threaded through the lead column; stirring was provided by a magnetic stirrer placed inside the cavity; and degassing was carried out exactly as previously described.

2.8 Gravimetry

Another technique used for determination of conversion was gravimetry. The procedure used here was to weigh a small aluminium dish before and after the addition of a few millilitres of latex. The dish was placed in a 60°C oven overnight, allowing the more volatile components of the latex (*e.g.*, monomer, water) to be dried off. The dish was then cooled and re-weighed to determine the total mass of solid residue, and the known masses of any non-volatile ingredients subtracted to give the mass of polymer present. Comparison of this value with the initial masses of monomer and seed polymer enabled the final conversion to be calculated.

While this method is less suitable than dilatometry for measuring conversion as a function of time, it was used routinely as a means for determining the polymer content of seed latexes, as well as for verifying the conversion at the end of a kinetic run as determined by dilatometry. Typically, final conversion values from dilatometry and gravimetry agreed to within 5%. Any significant discrepancy between gravimetric and dilatometric final conversion values could indicate a leaking vessel, bubble formation, or the occurrence of significant polymerisation prior to the commencement of meniscus height tracking. It is important to be aware, however, that the gravimetric measurement of final conversion is prone to error in the event of significant coagulation on the surfaces of the vessel and stirring bar, with the removal of polymer by coagulation potentially resulting in an artificially low value for final conversion. Also there can be problems if the monomer is relatively non-volatile, and/or can be trapped within the film that is formed as the latex dries. An important point here is that, all going well, dilatometry provides a much more accurate value of final conversion than gravimetry

for emulsion polymerisation; consequently, undue emphasis should not be placed on gravimetry results for these systems.

2.9 References

(1) Buback, M.; Gilbert, R. G.; Hutchinson, R. A.; Klumperman, B.; Kuchta, F.-D.; Manders, B. G.; O'Driscoll, K. F.; Russell, G. T.; Schweer, J. *Macromol. Chem. Phys.* **1995**, *196*, 3267.

(2) Beuermann, S.; Buback, M.; Gilbert, R. G.; Hutchinson, R. A.; Klumperman, B.; Olaj, F. O.; Russell, G. T.; Schweer, J. *Macromol. Chem. Phys.* **1997**, *198*, 1545.

(3) Ferguson, C. F., 2000, Ph.D. Thesis, University of Canterbury.

(4) Morton, M.; Kaizerman, S.; Altier, M. W. *J. Colloid Sci.* **1954**, *9*, 300.

(5) Ballard, M. J.; Napper, D. H.; Gilbert, R. G. *J. Polym. Sci., Polym. Chem. Edn.* **1984**, *22*, 3225.

(6) Halnan, L. F.; Napper, D. H.; Gilbert, R. G. *J. Chem. Soc. Faraday Trans. 1* **1984**, *80*, 2851.

(7) Gilbert, R. G. *Emulsion Polymerization: A Mechanistic Approach*; Academic: London, 1995.

(8) Hawkett, B. S.; Napper, D. H.; Gilbert, R. G. *J. Chem. Soc. Faraday Trans. 1* **1980**, *76*, 1323.

(9) Penboss, I. A.; Gilbert, R. G.; Napper, D. H. *J. Chem. Soc. Faraday Trans. 1* **1986**, *82*, 2247.

(10) Maxwell, I. A.; Napper, D. H.; Gilbert, R. G. *J. Chem. Soc., Faraday Trans. 1* **1987**, *83*, 1449.

(11) Lide, D. R. *CRC Handbook of Chemistry and Physics*; 82nd ed.; Lide, D. R., Ed.; CRC Press, 2001.

3. Entry in the Emulsion Polymerisation of Styrene – A Monomer of Low Water-Solubility[†]

3.1 Introduction

Styrene is a widely studied monomer in emulsion polymerisation (and in free radical polymerisation in general) and, consequently, established values are available for many of the rate parameters pertaining to styrene emulsion systems. These systems are therefore well-suited to kinetic investigations, and Chapter 1 outlined a number of studies of entry kinetics in styrene systems which adopted a range of different experimental approaches. The principal aim of this Chapter is to obtain new quantitative kinetic data for entry in the emulsion polymerisation of styrene, under various conditions, and to assess whether the current mechanistic understanding of entry satisfactorily accounts for these data.

In comparison to some of the more elaborate experimental systems described in Chapter 1 (incorporating radical trapping agents and electrosteric stabilisers) the systems elected for study here are somewhat simpler. The motivation for this is the fact that the Maxwell-Morrison[1] entry model was originally validated on the basis of results from just one type of polymerisation system, *viz.* polymerisation of styrene using anionically stabilised latex particles with potassium persulfate as initiator. It is suggested that considerable scope exists for useful experimentation using variants of this "simple" system to test the entry model, in the absence of the added effects of radical traps and electrostatic stabilisers. An improved understanding of entry in simple emulsion systems is, of course, also of fundamental importance in exploring more complex systems.

In this work we seek to obtain kinetic data from four variants on the simple emulsion polymerisation system described above. Two different initiators will be employed: potassium persulfate (or KPS), the anionic initiator mentioned above which has been widely used in

[†] Most of the work in this chapter has appeared in the following publication: van Berkel, K. Y.; Russell, G. T.; Gilbert, R. G. *Macromolecules* **2003**, *36*, 3921. The substantially new work is that of section 3.4.9.

kinetic work of this sort, and 2,2′-azobis-(2-methylpropionamidine) dihydrochloride (hereafter referred to as V-50), a cationic azo-initiator that has also found extensive application in emulsion polymerisation for some time,[2,3] with structure given in Scheme 3.1. Similarly, two different latex types will be used, one anionically stabilised (with negatively charged groups adsorbed or anchored to the particle surface), the other cationically stabilised. Well-established methods described in Chapter 1 and elsewhere[4] will be used to extract entry rate data for four systems spanning the four different combinations of initiators and latex types.

Scheme 3.1. Chemical structure of 2,2′-azobis-(2-methylpropionamidine) dihydrochloride, or V-50.

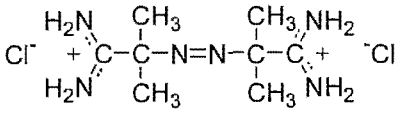

It is noted that similar experimental studies to this one have been undertaken previously. Marestin *et al.* compared kinetic data from their spin-trap/ESR experiments for MMA with KPS and V-50 as initiators, finding that these two initiators gave similar values for the entry rate coefficient under the conditions used.[5] It is noted, however, that when differences in particle concentrations and initiator decomposition rates between these experiments are taken into account, similarity in the value of the entry rate coefficient may not necessarily be indicative of an identical mechanism for entry. Reasons for this will become clear later in the present paper.

Leemans *et al.* proposed[6] that charge interactions between block polyelectrolyte surfactants and entrant radicals gave rise to differences in the rate of MMA emulsion polymerisation. In the absence of any knowledge of the actual rates of particle *entry* and *exit* it seems difficult to unambiguously attribute the observed rate disparity to an entry effect. Moreover, it is suggested that the possibility of differences in the rates of initiator decomposition and particle formation in their *ab initio* (unseeded) polymerisations might further complicate the interpretation of these results.

Finally, Penboss *et al.*[7] studied entry in the seeded emulsion polymerisation of styrene using three different initiators, namely the anionic and cationic initiators intended for the present study as well as the Fe^{2+}/H_2O_2 redox initiator system (which generates neutral radicals). These workers reported minimal effect of changing initiator type on the value of the entry rate

coefficient. However, these results were obtained using an earlier kinetic scheme for emulsion polymerisation; moreover, the raw data span a relatively narrow range of initiator and particle concentrations and cannot be unambiguously re-processed to permit accurate model discrimination.

3.2 Background Considerations

3.2.1 The "Control by Aqueous-Phase Growth" (Maxwell-Morrison) Model for Entry

The entry model of Maxwell *et al.*,[1] discussed in detail in Chapter 1, plays an important part in the kinetic analyses of the present Chapter. The key elements of this model are now briefly recalled.

The Maxwell-Morrison model's fundamental criterion for entry is that a free radical generated in the aqueous phase must propagate to reach some critical degree of polymerisation, z (in monomer units), at which point it becomes a surface-active species and undergoes rapid irreversible entry into a latex particle. Thus, the model postulates that the kinetics of entry are governed entirely by the aqueous-phase chemistry leading to the formation of "z-meric" radicals, as described in the following reaction scheme:

$$\text{initiator} \xrightarrow{fk_d} 2\,\text{I}^\bullet \tag{3.1}$$

$$\text{I}^\bullet + \text{M} \xrightarrow{k_{p1,w}} \text{IM}_1^\bullet \quad \text{(rapid)} \tag{3.2}$$

$$\text{IM}_i^\bullet + \text{M} \xrightarrow{k_{p,w}} \text{IM}_{i+1}^\bullet, \quad 1 \le i < z \tag{3.3}$$

$$\text{IM}_i^\bullet + \text{T}_w^\bullet \xrightarrow{2k_{t,w}} \text{inert products}, \quad 1 \le i < z \tag{3.4}$$

$$\text{IM}_z^\bullet \xrightarrow{\rho_{init}} \text{entry} \quad \text{(rapid)} \tag{3.5}$$

where $\text{I}^\bullet$ is a primary free radical produced by initiation (illustrated here by thermal decomposition of initiator with overall rate coefficient fk_d), M is a monomer molecule, $\text{IM}_i^\bullet$ is an aqueous-phase radical derived from initiator and containing i monomer units, $\text{T}^\bullet$ is any

aqueous-phase free radical species, $IM_z^\bullet$ is a surface-active radical bound to undergo entry and ρ_{init} is the pseudo-first-order rate coefficient for entry of radicals derived from initiator.

In what follows it is assumed (based on experimental evidence[8-10]) that the initial propagation step, reaction (3.2), is so fast that it is not rate-determining.

Maxwell *et al.* demonstrated that an exact value for ρ_{init} may be obtained from numerical solution of the steady-state form of the full set of rate equations pertaining to the above reaction scheme, while a reasonable approximation is provided by the following analytic solution:

$$\rho_{init} = \frac{2fk_d[I]N_A}{N_c}\left\{\frac{2\sqrt{fk_d[I]\,k_{t,w}}}{k_{p,w}[M]_w} + 1\right\}^{1-z} \tag{3.6}$$

where [I] is the aqueous initiator concentration, N_A is Avogadro's constant, N_c is the number concentration of latex particles in the aqueous phase and $[M]_w$ the concentration of aqueous monomer.

The value of ρ_{init} is related to $\rho_{100\%}$, the value corresponding 100% radical entry, by the "entry efficiency" factor f_{entry}:

$$f_{entry} = \frac{\rho_{init}}{\rho_{100\%}} = \rho_{init}\frac{N_c}{2fk_d[I]N_A} \tag{3.7}$$

Equation (3.7) may therefore be used to obtain f_{entry} from experimental values of ρ_{init}, provided that the values of fk_d, [I] and N_c are known. Comparison of equations (3.6) and (3.7) also gives an analytic form for f_{entry} according to Maxwell *et al.*

$$f_{entry} = \left\{\frac{2\sqrt{fk_d[I]\,k_{t,w}}}{k_{p,w}[M]_w} + 1\right\}^{1-z} \tag{3.8}$$

3.2.2 Comparing Entry Data From Different Systems

In this study it will be of interest to compare entry data from different systems. An important consideration here is the sensitivity of ρ_{init} to N_c. Since ρ_{init} is the entry rate per particle, it follows that for two systems with the same total flux of entering radicals, ρ_{init} must decrease

as N_c is increased, as in equation (3.6). Therefore, a valid comparison of ρ_{init} values from different systems must take into account any difference in N_c. This is achieved by comparing values of f_{entry} rather than ρ_{init}, as the entry efficiency is independent of the particle concentration [equation (3.8)]. A further factor is that the entry rate and efficiency are governed by the aqueous-phase radical flux, which is dependent not only on [I] but also on fk_d [see equations (3.6) – (3.8)]. This means that for systems with different initiators, meaningful comparison of entry rate data is only possible if the difference in fk_d is taken into account. This may be achieved by comparing data at equal values of initiator radical flux, $2fk_d[I]$, as opposed to equal initiator concentration. All experimental data will be presented in this new and more mechanistically discerning way in this Chapter. A *caveat* is that k_d may vary, *e.g.*, because of radical-induced initiator decomposition.[11]

3.2.3 Measurement of Entry Rate Coefficients

In practice, the only kinetic data that can be readily and accurately measured comprise the overall rate of conversion of monomer into polymer. In this case it is most convenient to quantify this rate in terms of the rate of fractional conversion, x, given by (see Chapter 1):

$$\frac{dx}{dt} = \frac{k_p [M]_p M_0 N_c V_w}{m_M^{tot} N_A} \bar{n} \qquad (3.9)$$

where k_p is the intra-particle propagation rate coefficient, $[M]_p$ is the monomer concentration in the particle phase, M_0 is the molar mass of monomer, m_M^{tot} is the total mass of added monomer, V_w the volume of aqueous phase, and $\bar{n}$ the average number of radicals per latex particle. The value of $\bar{n}$ is determined by all processes that introduce and remove radicals to and from a latex particle. This includes entry of radicals from the aqueous phase, radical exit from a particle, and bimolecular termination inside a particle. If the particle diameter is sufficiently small (*e.g.*, < 100 nm for styrene or < 30 nm for butyl acrylate[12] at 50°C, the actual value depending on monomer concentration and other quantities), the rate of termination between two radicals in the same particle is so rapid that this reaction is not rate-determining – so-called "zero-one" conditions. For zero-one systems, $\bar{n}$ is determined only by the rate coefficients of radical entry and exit, and accurate data for $\bar{n}$ may therefore be used to infer these. The value of $\bar{n}$ is obtained from the observed polymerisation rate via equation (3.9) (using accurate values of $[M]_p$ and N_c) and is best obtained in a seeded emulsion

polymerisation in the absence of secondary nucleation. For most monomers (including styrene) it is likely that all radicals which have exited will re-enter a particle, and the applicable zero-one rate equation in the case of styrene has therefore been established[4,13,14] as that of "Limit 2a" kinetics [see equation (1.16) in Chapter 1]:

$$\frac{d\bar{n}}{dt} = \rho(1 - 2\bar{n}) - 2k\bar{n}^2 \qquad (3.10)$$

where k is the rate coefficient for exit. The value of the entry rate coefficient may then be inferred from a system in which $\bar{n}$ varies significantly with time by matching this time evolution to the solution of equation (3.10). Alternatively, if k is known, one can use the steady-state form of equation (3.10):

$$\rho = 2k\frac{\bar{n}_{SS}^{\,2}}{1 - 2\bar{n}_{SS}} \qquad (3.11)$$

where $\bar{n}_{SS}$ is the steady-state value of $\bar{n}$.

A value for k may be obtained from careful interpretation of the rate data obtained early in the polymerisation, before a steady-state is attained.[15] However, this method is susceptible to error because of retardation by oxygen.[16] An alternative technique involves the use of γ-radiation as an intermittent source of initiating radicals,[17] by exposing the emulsion system to γ-radiation until a steady-state "in-source" polymerisation rate is established. Initiation is then halted by removal from the γ-source. The rate of polymerisation slows from the in-source rate to a lower "out-of-source" rate. By fitting an integrated form of equation (3.10) to this "γ-relaxation" rate data, a value for k may be determined,[4,18] free of any retardation effects. While the use of γ-radiolysis in this experimental fashion may be traced back at least 40 years,[19] these pioneering efforts were oblivious of the complexities of emulsion polymerisation kinetics, and thus the data were not analysed to obtain entry or exit rate coefficients.

The out-of-source polymerisation rate in the γ-relaxation experiments is usually non-zero[17] (note that this is a genuine phenomenon – even if given more time to relax, the system will not reach a zero rate). The origin of this so-called "spontaneous polymerisation" is not fully understood for most emulsion systems,[20,21] in which it is often more significant than in the equivalent bulk systems. The value of ρ which is obtained, along with k, from fitting of γ-

relaxation data (see above) will be denoted ρ_{spont}. This is the component of entry from "spontaneously-generated" radicals. An important kinetic implication here is that the value of ρ obtained [using equation (3.11)] from chemically initiated experiments clearly must incorporate the contribution ρ_{spont} in addition to entry of radicals derived from initiator, the quantity of primary interest here:

$$\rho = \rho_{init} + \rho_{spont} \tag{3.12}$$

An alternative way of determining ρ_{spont} is to measure the value of $\bar{n}_{SS}$ for a seeded emulsion polymerisation in the absence of any added initiator, and then calculate ρ_{spont} from equation (3.11) using the value for k established from γ-relaxation. Both these methods for determining ρ_{spont} will be used in this work.

It is emphasised that values of the ρ_{init} and f_{entry} determined in this way from experimental data and using equations (3.9) – (3.12) and (3.7) respectively are values obtained from rate data with minimal model-based assumptions and are totally independent of the entry model of Maxwell *et al.* described by reactions (3.1) – (3.6).

3.3 Experimental Details

3.3.1 Synthesis of Seed Latexes

Three electrostatically stabilised polystyrene latexes were prepared for use in seeded experiments; details of these latexes are given in Table 3.1. Latex AN04 was a duplicate of AN01 prepared according to the same recipe. All three latexes were used in γ-relaxation experiments (discussed shortly); however, only AN01 and CAT02 were employed extensively for chemically initiated experiments.

Table 3.1. Seed latex preparation and characteristics.

ingredient	seed latexes AN01 and AN04	seed latex CAT02
water (Milli-Q) / g	600	600
styrene / g	92.0	90.0
surfactant / g	11.8 (Aerosol MA-80)	4.57 (DTAB)
NaHCO3 / g	1.25	–
polystyrene / g	0.920	0.910
initiator / g	1.30 (KPS)	0.288 (V-50)
temperature	90°C	90°C
reaction time	24 h	4 h
number-average unswollen particle diameter / nm		
TEM (polydispersity†)	64 (1.02)	63 (1.06)
CHDF	57	54
PCS‡	63	70
value used for kinetic analysis	64	63

† Ratio of weight-average to number-average particle diameter

‡ PCS average $= \sqrt{(8^{th}\text{ moment})/(6^{th}\text{ moment})}$

Styrene (Huntsman, stabilised with 4-methoxyphenol inhibitor) was first passed through a column of basic alumina and then distilled under reduced pressure (first and last 10% discarded), before being stored at 0°C for no longer than two weeks before use. Aerosol MA-80 (sodium di(1,3-dimethylbutyl)sulfosuccinate, 80% solution in isopropanol and water, Cytec), dodecyltrimethylammonium bromide (DTAB, Aldrich), sodium hydrogencarbonate and potassium persulfate (KPS) (both BDH AnalaR grade) were used

without further purification in the seed synthesis. 2,2′-Azobis-(2-methylpropion-amidine) dihydrochloride (V-50, Aldrich) was recrystallised from water/acetone (50% w/w) prior to use.

For synthesis of seed latexes, a 1 dm^3 glass reactor was charged with water, surfactant and buffer, and the solution heated to 90°C. A small amount (30 cm^3) of water was retained to dissolve initiator. A trace amount of bulk polystyrene was dissolved in styrene monomer immediately prior to use (a technique thought to improve the efficiency of radical capture in the early stages of polymerisation,[22-24] thereby serving to lower the polydispersity of the latex particle size distribution). The polymer/monomer solution was added to the reactor and emulsified by stirring at 450 rpm, and finally initiator was added. The reaction was left to proceed for the specified time with final conversion (gravimetry) of ≈ 100%.

Seed latexes were dialysed against distilled water (changed daily) for eight days, over which time conductivity measurements were seen to converge to a constant value. The dialysed latexes were filtered through glass wool to remove any traces of coagulum. Particle size distributions were measured by transmission electron microscopy (TEM), and average size by both capillary hydrodynamic fractionation (CHDF) and photon correlation spectroscopy (PCS) for comparison; results are presented in Table 3.1. These three methods are in relatively good agreement. As TEM is considered the most accurate method of these three for particle sizing, the sizes obtained using TEM were adopted as the values for all kinetic data analysis.

3.3.2 Kinetic Experiments

All kinetic experiments were seeded emulsion polymerisations of styrene commencing in Interval II (in the presence of monomer droplets), so that $[M]_p$ remains essentially constant. The details of the composition of typical polymerisations are given in Table 3.2. For kinetic runs, KPS was recrystallised from water and V-50 from water/acetone (50% w/w). The rate of polymerisation was measured by automated dilatometry using the methods described in Chapter 2, with the densities of monomer and polymer respectively taken as $d_M = 0.878$ g cm^{-3} and $d_p = 1.044$ g cm^{-3} at 50°C.[25] Final conversions from dilatometry were verified by gravimetry. A water-jacketed 60 cm^3 dilatometer vessel was charged with seed polymer, styrene, surfactant and water (Milli-Q), and stirred overnight to swell seed latex particles with monomer. The reaction mixture was then overheated to 60°C and degassed under reduced

pressure in order to prevent the formation of any bubbles inside the vessel during the course of a kinetic run (which would make it impossible to measure rate data accurately by dilatometry). For experiments using V-50, particular care was required to ensure that degassing was adequate, as the evolution of N_2 from the decomposition of this initiator increases the chance of bubble formation. After sufficient thermal equilibration time at 50°C the reaction mixture was stirred vigorously to ensure monomer emulsification. Finally, initiator was added (or, in the case of γ-radiolysis experiments, the system was exposed to the γ-source). At the end of the polymerisation a small amount of hydroquinone was added to quench the reaction. Latexes were inspected by TEM and experiments used for kinetic analysis only if negligible secondary nucleation occurred (a discussion of the kinetic effects of secondary nucleation and acceptable limits is presented in Appendix A.2).

Table 3.2. Details of seeded emulsion polymerisations.

seed latex	AN01		AN04		CAT02/CATH03
N_c / dm^{-3}	7.5×10^{16}	1.6×10^{17}	2.4×10^{17}	N_c / dm^{-3}	1.0×10^{17}
seed polymer / g	0.60	1.20	1.05	seed polymer / g	0.75
styrene / g	2.00	4.00	3.40	styrene / g	3.00
AMA-80 / g	0.040	0.080	0.070	DTAB / g	0.090
KPS or V-50 / g	0.00005 – 0.02		–	KPS or V-50 / g	0.00005 – 0.02

3.3.3 *Measurement of* $[M]_p^{sat}$

It was necessary to measure the saturated particle monomer concentration, $[M]_p^{sat}$, for each latex individually, as this quantity is affected by particle size and surface characteristics. This was done using the "static swelling" method, details of which have been given in Chapter 2 and elsewhere.[4,26,27] In each case the value of $[M]_p^{sat}$ was determined at 50°C (the temperature used in kinetic experiments). The results for all seed latexes are presented in Table 3.3.

Table 3.3. Results of static swelling measurements, spontaneous polymerisation and γ-relaxation experiments for all seed latexes at 50°C.

seed latex	$[M]_p^{sat}$ / M	$\bar{n}_{SS}$ spontaneous polymerisation†	dose rate / Gy h^{-1}	k / 10^{-2} s^{-1}	k_{theor} / 10^{-2} s^{-1}	ρ_{spont}† / 10^{-4} s^{-1}
AN01	5.4	0.063	188	1.2 ± 0.2	1.4	1.1 ± 0.2
CAT02	6.1	0.30	165	1.0 ± 0.6	1.4	40 ± 20
CATH03	5.7	0.036	158	0.9 ± 0.1	1.4	0.25 ± 0.04
AN04	5.3	0.11‡	165	0.75 ± 0.1	1.4	1.5 ± 0.3‡

† From steady-state spontaneous polymerisation (in good agreement with γ-relaxation) unless otherwise specified

‡ From γ-relaxation only

3.4 Results and Discussion

3.4.1 Spontaneous Polymerisation

Also presented in Table 3.3 are the values of $\bar{n}_{SS}$ observed in emulsion polymerisations carried out with no added initiator, *i.e.*, where the only source of initiation was spontaneously-generated radicals. The rate of spontaneous polymerisation for the anionically stabilised latex AN01 was typical of values reported for styrene emulsion polymerisation. However, an unusually high (and reproducible) rate was observed for the cationic latex CAT02, giving a value of $\bar{n}_{SS}$ approximately five times larger than that for the anionic latex. Mechanistically this high value for $\bar{n}_{SS}$ may be explained by either a higher entry spontaneous rate coefficient (ρ_{spont}) or a lower exit rate coefficient (k) in the cationic latex, or a combination of both these effects. γ-relaxation experiments (presented in Table 3.3 and discussed in detail later) revealed that k for CAT02 was comparable to that of the anionic latex, indicating that the rate enhancement for spontaneous polymerisation was an entry-related phenomenon. As this is a spectacular effect – $\bar{n}_{SS} \approx 0.3$ for a zero-one system without use of any initiator! – it is worth discussing.

One possible explanation for this high spontaneous entry rate is generation of radicals from a reaction involving residual amine and peroxide species from the seed latex. Various amine products are known to form as products of V-50 radical recombination reactions.[28] Possible processes are:

$$IM_i^{\bullet} + O_2 \xrightarrow{k_{O_2}} IM_iOO^{\bullet} \quad (3.13)$$

$$IM_iOO^{\bullet} + M \xrightarrow{k_{p,O^{\bullet}}} IM_iOOM^{\bullet} \quad (3.14)$$

$$IM_iOO^{\bullet} + T^{\bullet} \xrightarrow{k_{t,O^{\bullet}}} IM_iOOT \text{ (combination)} \quad (3.15)$$

$$IM_iOO^{\bullet} + T^{\bullet} \xrightarrow{k_{t,O^{\bullet}}} IM_iOOH + T \text{ (disproportionation)} \quad (3.16)$$

Peroxide species may be formed by the incorporation of oxygen into polymer chains. Oxygen is a very effective radical scavenger, reacting rapidly with carbon-centered radicals according to reaction (3.13), with $k_{O_2} > 10^9$ M^{-1} s^{-1}, to yield a relatively stable peroxyl radical.[29,30] Peroxyl radical addition to monomer [reaction (3.14)] is much slower, with $k_{p,O^{\bullet}} = 41$ M^{-1} s^{-1} for styrene;[31] nevertheless, successful copolymerisation of oxygen and styrene has been reported under certain exceptional conditions.[32,33] However, given that $k_{t,O^{\bullet}}$ in reactions (3.15) and (3.16) is likely to be $10^9 - 10^{10}$ M^{-1} s^{-1} for emulsion polymerisation, peroxyl radicals are far more likely to undergo termination than copolymerisation. Thus, the presence of oxygen enhances the overall rate of radical loss and is responsible for appreciable periods of inhibition and/or retardation commonly seen in the early stages of polymerisation.[16] equations (3.13) – (3.16) show that any oxygen present at the commencement of polymerisation will eventually be incorporated into a polymer chain giving a peroxide functionality. The potential for radicals to be formed from thermal homolysis of polymeric peroxides is recognised;[34] however it appears that this is only likely to occur significantly at temperatures in excess of 100°C. [35,36] Importantly, the presence of various amines has been seen to significantly accelerate peroxide reactions.[35,37]

It is of interest to consider the potential for polymeric peroxide formation in the emulsion polymerisation systems used in the present work. The solubility of oxygen in water is approximately 1 mM.[38] While no comparable value was found for the solubility of oxygen in

styrene, it may be expected to be similar to that reported for toluene: 9 mM.[39] Since no effort was made to deoxygenate either water or monomer in the synthesis of seed latexes, it is reasonable to estimate that the overall concentration of oxygen at the commencement of polymerisation is ~ 10^{-3} M. In light of the discussion above, this may be expected to yield approximately 10^{-3} M of peroxide functionalities during the polymerisation. These peroxide groups would most likely be located mainly in small oligomeric species in the aqueous phase given that any radical that reacts with oxygen to form a peroxyl radical is far more likely to undergo termination than to propagate further to form an entering species, and termination of two non-surface-active radical species will give non-surface-active products. A large proportion of the peroxide-containing oligomers may be expected to be removed from the seed latex during dialysis; however dialysis is unlikely to remove all traces of oligomer. Therefore it is not unreasonable to expect the presence of some polymeric peroxides in the seed latexes.

Thermal decomposition of any such polymeric peroxides is expected to have little effect on the kinetic experiments, since these were at 50°C (although it has been established[21] that these can be a major source of spontaneously-generated radicals at this temperature in the emulsion polymerisation of chlorobutadiene). It is conceivable, however, that an induced decomposition process might provide a significant source of initiating radicals. Induced decomposition of peroxides by residual amine species present in the aqueous phase of the cationic latex CAT02 thus provides one possible explanation for the unusually high rate of spontaneous polymerisation observed for this latex. It is proposed here that radicals are formed via a redox mechanism similar to that described for other amine/peroxide redox couples,[34] as shown in Scheme 3.2.

Scheme 3.2. Amine-induced decomposition of polymeric peroxide.

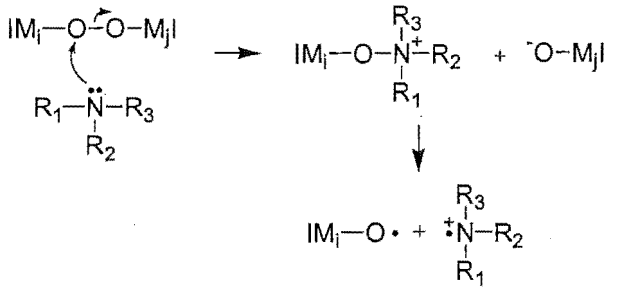

The much lower rate of spontaneous polymerisation seen in the case of the anionic latex AN01 is consistent with the proposed mechanism in that the synthesis of latex AN01 did not involve any reagents with amine functionality (although polymeric peroxides will still form).

Latex CAT02 was deemed unsuitable for kinetic experiments as entry of spontaneously-generated radicals would dominate all entry events even in the presence of added chemical initiator, thereby introducing unacceptable uncertainty to any values of ρ_{init} obtained. However, it was found that extended heat-treatment of the latex had a profound effect on the rate of spontaneous polymerisation. Latex CAT02 was deoxygenated by sparging with argon and was then heated to 90°C for 4 days. The value of $\overline{n}_{SS}$ for spontaneous polymerisation of the heat-treated latex (labeled CATH03) was reduced to less than 20% that of the original latex, as shown in Table 3.3 making latex CATH03 suitable for kinetic experiments to accurately measure ρ_{init}.

The effect of heat-treatment may be interpreted in terms of the mechanism proposed above for spontaneous polymerisation in latex CAT02. It is suggested that heating to 90°C results in accelerated decomposition of polymeric peroxides via the reaction in Scheme 3.2, and as well the simple thermal decomposition process is likely to be more significant at this higher temperature. Four days is sufficient time to cause extensive decay of the polymeric peroxides postulated to be present.

It is important also to consider other possible effects of heat-treatment on the latex. In particular it is recognised that the amidinium functionality of V-50 derived species is susceptible to hydrolysis under such conditions, as shown in Scheme 3.3. V-50 chain end-groups anchored at the latex particle surface provide stabilising cationic surface charge. Thus hydrolysis of the amidinium functionality at these sites will result in a lowering of the particle surface charge. However, also contributing to the surface charge is cationic DTAB surfactant added to the seed latex for kinetic experiments. This surfactant is present at the particle surface in considerable excess of the V-50 end-groups (approximately 10 – 20 times by molar ratio), and thus it is unlikely that even extensive hydrolysis of V-50 end groups during the heat treatment would have any significant effect on the overall surface charge of the cationic latex during a seeded experiment.

Scheme 3.3. Hydrolysis of polymer amidinium functionality.

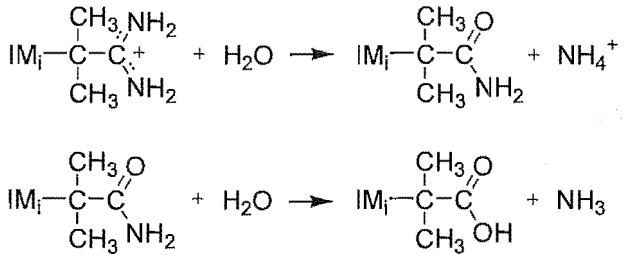

3.4.2 γ-relaxation Experiments

γ-relaxation experiments were carried out for all three seed latexes, AN01, CAT02, CATH03. Typical data (time dependence of conversion and $\bar{n}$) from such an experiment are shown in Figure 3.1. Conditions used and kinetic data obtained are given in Table 3.3. The data were analysed as outlined above to obtain k and ρ_{spont}. Multiple γ exposures and relaxations were conducted and the results presented here are average values, along with uncertainties estimated from the scatter in experimental data.

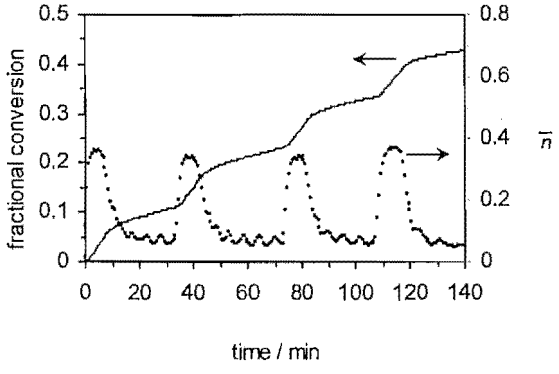

Figure 3.1. Conversion (line) and $\bar{n}$ (circles) as functions of time for a γ-relaxation run at 50°C using cationic latex CATH03 and γ-radiolysis dose rate of 158 Gy h^{-1}. Values of k and ρ_{spont} were obtained from data fitting of the γ-relaxation regions 7 – 34 min, 42 – 74 min, 82 – 108 min and 117 – 145 min.

Table 3.3 also shows the theoretical value for the exit rate coefficient, k_{theor}, as calculated for the case of Limit 2a kinetics (see Chapter 1 and elsewhere[4,13,14,40,41]). Here radical exit from a particle involves transfer to monomer followed by desorption of the monomeric radical, M•, into the aqueous phase. Alternatively, M• may undergo propagation before desorption can occur, in which case an exit event is not completed. One then has:

$$k_{theor} = \frac{k_{tr}\, k_{dM}}{k_p^1} = \frac{3D_w[M]_w}{r_s^2[M]_p}\frac{k_{tr}}{k_p^1} \qquad (3.17)$$

Here the rate coefficient for desorption of M$^\bullet$ is assumed to be the same as that of a monomer molecule, k_{dM}, a derivation for which is available in the literature[4,41] as well as in Appendix A.5 of this thesis. D_w = monomeric diffusion coefficient in water, k_{tr} = rate coefficient for transfer to monomer, k_p^1 = rate coefficient for propagation of a monomeric radical and r_s = radius of the swollen latex particle. The following literature values for styrene at 50°C were used in calculations: $D_w = 1.5 \times 10^{-9}$ m^2 s^{-1},[42] $[M]_w^{sat} = 4.3 \times 10^{-3}$ M,[43] $k_{tr} = 9.3 \times 10^{-3}$ M^{-1} s^{-1},[44] $k_p^1 = 4\, k_p = 1.0 \times 10^3$ M^{-1} s^{-1}.[4]

The results in Table 3.3 provide good support for the exit model described. The observed similarity in experimental k values obtained for the four seed latexes is as predicted given that all four latexes are of very similar particle size.

The values of $\bar{n}_{SS}$ and ρ_{spont} presented in Table 3.3 are those obtained from kinetic runs in the absence of any added initiator as described earlier (except in the case of AN04, where no steady-state run was carried out). Importantly, these values of $\bar{n}_{SS}$ and ρ_{spont} agree closely with those obtained from γ-relaxation (not shown, except for AN04). The values of ρ_{spont} yielded by the former method are those adopted for use in equation (3.12) in all kinetic analysis. This is for two reasons: (1) The steady-state spontaneous polymerisations afford greater precision, and (2) experiments wherein the system is never exposed to γ-radiation should more faithfully reproduce the contribution from spontaneous polymerisation present in chemical runs.

Also evident in Table 3.3 is the considerably larger value of ρ_{spont} obtained for latex CAT02 compared to the other two latexes. This is thought to be due to an additional source of initiating radicals present only in CAT02, as discussed above.

The uncertainties associated with the values of k and ρ_{spont} for latex CAT02 are somewhat greater than for the other two latexes. This is because the γ-relaxation method relies on accurate fitting of rate data obtained during the period where the rate of polymerisation decays from its in-source steady-state value to a lower out-of-source value (typically this

takes up to 30 minutes). In the case of latex CAT02 the high out-of-source (spontaneous) rate meant that the second-order loss process tends to be masked [see equation (3.10)].[45]

It is also worth noting that at low initiator concentrations ρ_{spont} may constitute up to 20% of the total entry rate coefficient (see values in the following subsection). Taking accurate account of spontaneous entry is thus critical to obtaining accurate entry rate data under such conditions.

3.4.3 Chemically Initiated Experiments

Polymerisation rate data from kinetic experiments with added chemical initiator, exemplified in Figure 3.2, were analysed using equations (3.7) and (3.9) – (3.12). This involved using data presented in Table 3.3 as well as the following literature values appropriate for styrene emulsion polymerisation at 50°C: fk_d(KPS) = 1.1 × 10^{-6} s^{-1},[46] fk_d(V-50) = 4.8 × 10^{-6} s^{-1},[28,47] k_p(styrene) = 2.6 × 10^2 M^{-1} s^{-1}.[48] Note in Figure 3.2 that $\bar{n}$ is seen to increase above 0.5 after the system has entered Interval III (60 minutes into the polymerisation). It is well understood that this observed departure from zero-one conditions is a consequence of slower termination.[4] In order to ensure that the zero-one kinetic treatment used here was valid, data analysis was restricted to Interval II of polymerisation (in the case of Figure 3.2 only the first 23 min of polymerisation) when the termination rate is sufficiently high (in these experiments) that zero-one conditions prevail.

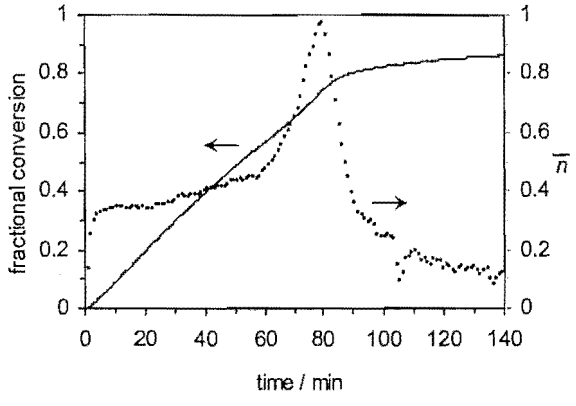

Figure 3.2. Conversion (line) and $\bar{n}$ (circles) as functions of time for a chemically-initiated run at 50°C using anionic seed latex AN01 and [KPS] = 1.5 mM. The value of $\bar{n}_{SS}$ is taken from the region 6 – 23 min.

Four polymerisation systems were examined: the four pairings possible from use of either KPS (anionic) or V-50 (cationic) as initiator and either AN01 (anionic) or CATH03 (cationic) as latex. The following labels specify the pairings: KPS/AN01, V-50/CATH03, KPS/CATH03, V-50/AN01. Detailed numerical results for each of these systems are tabulated in Appendix A.3; in what follows results will only be graphically presented.

3.4.4 KPS/AN01

Entry data were obtained using an anionically stablised latex with KPS as (anionic) initiator to provide a comparison with previous results[7,15,49,50] and to establish a benchmark for subsequent experiments. Comparison is made with earlier extensive data obtained by Hawkett *et al.*[15] for the same type of system, re-analysed by fitting to equation (3.10) (second-order loss, which is a better model for such data than the first-order loss assumed in the pioneering paper of Hawkett *et al.*). For this purpose, the value of k was obtained by re-analysing the γ-relaxation data obtained by Lansdowne *et al.*[17] on the same latex.

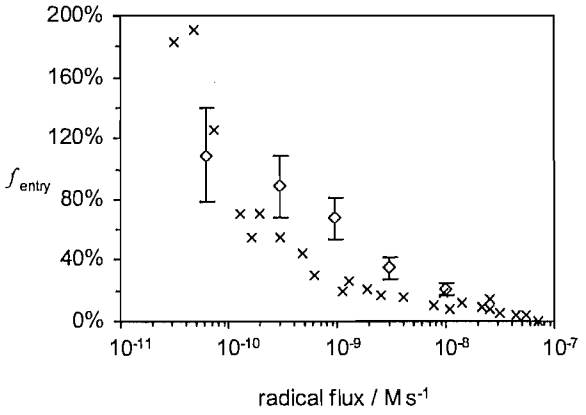

Figure 3.3. f_{entry} obtained for polymerisation system KPS/AN01 (diamonds) at 50°C, presented together with data reprocessed from references[17] and[15] (crosses) as a function of radical flux.

Figure 3.3 gives values of f_{entry} for the system KPS/AN01 presented along with estimated experimental uncertainties arising mainly from the values for ρ_{spont} and k. These data show acceptable agreement with the re-processed data of Hawkett *et al.* One has the expected trend of decreasing entry efficiency with increasing radical flux, although in most cases the efficiencies obtained in the present work are somewhat higher than those previously published. Also of note are f_{entry} values apparently greater than 100% for radical flux less than 1×10^{-11} M s^{-1} (or [KPS] < 5×10^{-5} M) in both sets of data. This is not to suggest that the

flux of initiating radicals is being supplemented by some unknown radical source, but is more likely the result of uncertainty in one or more of the values used to calculate f_{entry} in equation (3.7), possibly the initiator decomposition rate coefficient, fk_d, a quantity which is sensitive to the precise experimental conditions.[46] It is also possible that ρ_{spont} may vary with radical flux, and thus that an incorrect value of ρ_{spont} – to which ρ_{init} is highly sensitive at low radical flux – has been used.

3.4.5 V-50/CATH03

f_{entry} data obtained for this system are presented in Figure 3.4 and reveal a high entry efficiency that shows no consistent variation with changing radical flux [an approximately constant f_{entry} means an entry rate coefficient that shows a linear increase with initiator concentration, as implicit in equation (3.6)]. Experiments were attempted at higher initiator concentration, but the high rate of evolution of nitrogen gas from V-50 decomposition under such conditions resulted in bubble formation early in the polymerisation, making accurate dilatometric measurement of the polymerisation rate impossible.

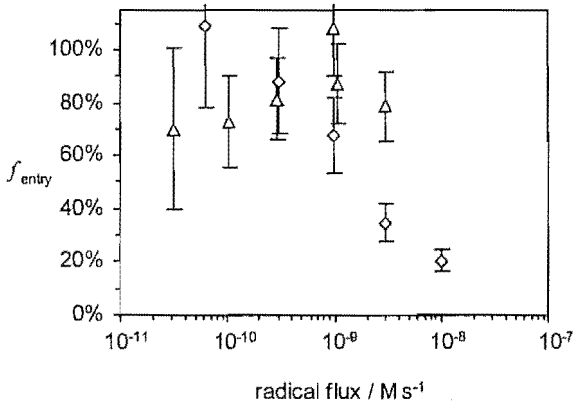

Figure 3.4. f_{entry} as a function of radical flux for polymerisation systems KPS/AN01 (diamonds) and V-50/CATH03 (triangles) at 50°C.

Comparing the f_{entry} data from system V-50/CATH03 with those from KPS/AN01 in Figure 3.4 shows the effect of changing from a polymerisation system where both entering species and particle surface are anionically charged to one in which both are cationically charged. It is clear that the trend with increasing initiator radical flux is not the same in both cases. This may be the result of an inherent difference in entry in anionic versus cationic systems, although it seems unlikely that this difference is related to any charge interaction, given that

entry in both these systems involves the interaction of entering species and latex particles of like charge. The difference may be more specifically related to changing either the initiator type or the latex type. In order to more explicitly determine the nature of this entry effect, and indeed the existence of any significant charge effect, we next consider the results of the two systems which combine oppositely charged initiators and latex particles.

3.4.6 KPS/CATH03

f_{entry} data obtained for this system, incorporating anionic initiator and cationic latex particles, are presented in Figure 3.5. The trend seen for this system is very similar to that seen in the other KPS system (KPS/AN01), with f_{entry} decreasing as the initiator concentration is increased. As before, apparent values of f_{entry} in excess of 100% were obtained; in this case a value of 318% lies well outside the limits of any reasonable experimental uncertainty. These data (with the highest result omitted in the interests of scale) are presented along with those from KPS/AN01 in Figure 3.5. These two data sets are very close, suggesting that the common element between these two systems, the initiator type (KPS), is of central importance in defining the nature of the entry process: changing the nature of the particle surface charge has little or no effect on entry, completely consistent with the entry model of Maxwell *et al.* Equally, it seems that there is little effect from any charge-charge interaction between entering species and particle surface, since changing from like to unlike charges has no clear impact on the values of f_{entry} obtained. These findings are fully consistent with the entry model of Maxwell *et al.*[1] but they are difficult to reconcile with suggestions that the entry rate is controlled by diffusion to the particle surface,[51-53] by surfactant displacement[54] or by colloidal interactions.[55]

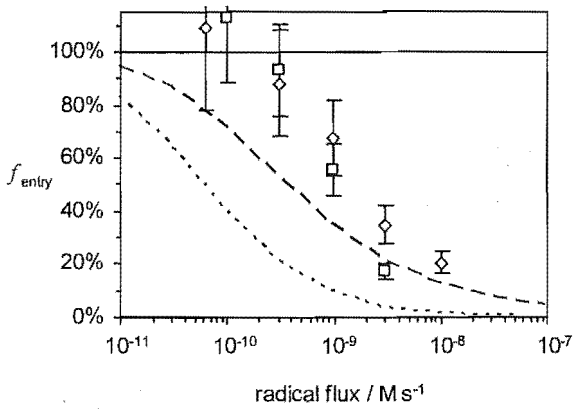

Figure 3.5. f_{entry} as a function of radical flux for entry of anionic initiator into anionic and cationic latex. Points: experimental; KPS/AN01 (diamonds) and KPS/CATH03 (squares). Lines: modelled values calculated using Maxwell *et al.* model with $z = 1$ (————), $z = 2$ (— — — —), or $z = 3$ (– – – –); parameter values as in text.

3.4.7 V-50/AN01

The final system to be considered is that in which V-50 was used as initiator in combination with the anionic latex AN01. The entry efficiency data obtained here are shown in Figure 3.6. Experiments carried out with V-50 concentration in excess of 10^{-3} M resulted in rapid coagulation of the seed latex (as the electrostatic repulsion between like-charged particles is diminished by the high concentration of ions in the aqueous phase) and provided no usable rate data. Also, the rate of entry observed in experiments with V-50 concentration 4×10^{-7} M was approximately the same as that in the absence of any added initiator, and therefore no experiments were undertaken at lower initiator concentration than this.

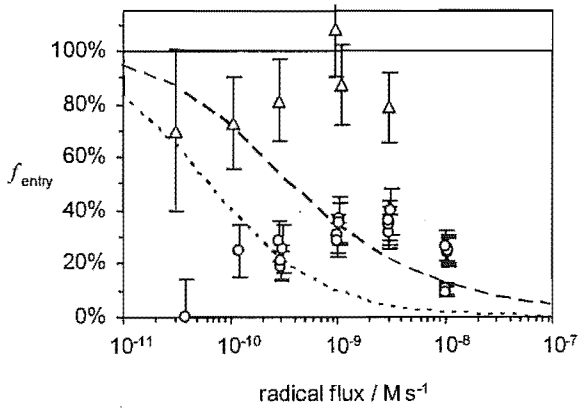

Figure 3.6. f_{entry} as a function of radical flux for entry of cationic initiator into cationic and anionic particles. Points: experimental; V-50/CATH03 (triangles) and V-50/AN01 (circles). Lines: modelled values calculated using Maxwell *et al.* model with $z = 1$ (————), $z = 2$ (— — — —), or $z = 3$ (– – – –); parameter values as in text.

Entry efficiencies for this system are low and, as for the other V-50 initiated system V-50/CATH03, are relatively invariant with initiator concentration, generally falling in the range 0.2 – 0.4. These somewhat unusual results prompted more exhaustive experimental investigations to ensure that these low efficiencies were indeed reproducible, as was indeed found to be the case. Also, in an attempt to elicit more information about entry in this system, experiments were carried out at two different particle concentrations. Notably, changing the particle concentration appears to have no significant effect on f_{entry} (as indeed is predicted by the model – a point discussed earlier in the text).

The results from the systems discussed above suggest that of the variables considered in this study, initiator type may be of most importance in defining the entry process. Figure 3.6 compares results from V-50/AN01 (cationic entry into anionic latex) with those from V-50/CATH03 (cationic entry into cationic latex). Unlike the results seen for the KPS systems, there is clearly a discrepancy between entry data obtained from the two V-50 systems. Changing from cationically to anionically stablised latex particles results in a consistent and general decrease in entry efficiency. Possible reasons for this will shortly be discussed.

As well as the obvious difference between these two data sets, a similarity is also noted: in both cases f_{entry} is relatively invariant with changing initiator concentration. This observation will be seen to be significant in the light of the modelling results presented below.

3.4.8 Modelling Entry

The experimental data for all four polymerisation systems above are now interpreted in terms of the entry model of Maxwell *et al.*[1] It is important to note that this entry model is applied only to entry of radicals derived from (chemical) initiator and is not used to model the processes of exit or re-entry: radicals which re-enter after exiting, which arise from transfer within a latex particle, are chemically quite distinct from those derived directly from aqueous-phase initiator. Exit and re-entry involve species which are chemically different to initiator-derived radicals and hence must be treated using different methods, as touched upon earlier in the text [equation (3.10) for re-entry and equation (3.17) for exit].

Here we employ the population balance equations for initiator-derived aqueous-phase radicals given in Chapter 1 as equations (1.24) – (1.26), solving these equations numerically to obtain model values for ρ_{init}, and hence f_{entry}, under the same conditions used in experiments. It is noted that the analytic form for f_{entry} given in equation (3.8) may also be used, however this solution relies on the approximation that $2fk_d[I] \approx 2k_{t,w}[T^\bullet_w]$ and is thus only strictly accurate under conditions of low entry efficiency.

Parameter values for in model calculations were as stated above, along with $k_{t,w} = 3.5 \times 10^9$ M^{-1} s^{-1},[1] letting z range from 1 to 3; results are shown in Figures 3.5 and 3.6. Maxwell *et al.*[1] noted that the model may be improved with a chain length dependent $k_{p,w}$, thus allowing for slightly higher propagation rate coefficients for very short (*i.e.*, 1-meric or 2-meric) radicals. This modification[4] provides some improvement in the fitting of experimental data from KPS-initiated styrene polymerisations, but the fit with chain length independent $k_{p,w}$ was satisfactory for the present work.

Figure 3.5 shows that the experimental data for both KPS systems are fitted reasonably well by the model with $z \approx 2$. These results are in good agreement with the value of z between 2 and 3 put forward by Maxwell *et al.* for the corresponding system.

Figure 3.6 compares model with experiment for both V-50 systems. The interpretation of these results is more ambiguous than for KPS. In the case of the V-50/CATH03 system, the model seems to give the closest fit with $z = 1$. Although the experimental results are generally less than the model prediction of 100%, it is clear that efficiencies are very high and that f_{entry} is relatively invariant with changing radical flux. This is as expected for $z = 1$ where an

entering species is formed after only the first (rapid) propagation event and there is thus no possibility of termination. If the radical takes any longer to become ready to enter, then f_{entry} must decrease as initiator concentration increases, but this is not observed for either V-50 system.

On the basis of the model of Maxwell *et al.* and results for the KPS systems, one would expect that changing from cationic to anionic latex particles while keeping the same initiator should have no effect on entry rates. However this is not the case for the V-50/AN01 system. The fact that f_{entry} is relatively invariant with radical flux for this system is certainly in line with a value of $z = 1$, but the much lower entry efficiencies obtained suggest that the value of $z = 2$ used in the entry model of Maxwell *et al.* for styrene/persulfate systems does not provide a complete explanation for this system.

Alternative entry mechanisms may be suggested to explain this anomaly. One may be charge-charge interactions between initiator and particles. However, not only do KPS results indicate that no such effect exists, but the V-50 results are qualitatively inconsistent with this suggestion: one would expect higher entry rates for the situation of positive initiator and negative particle surface, but the opposite is observed. A more likely explanation is as follows. The apparent difference in z for KPS ($z = 2$) and V-50 ($z = 1$) suggests that V-50 is inherently more surface-active than KPS. As a result V-50 may be more susceptible to interaction with the particle surface: a significant proportion of V-50 initiator may be adsorbed onto the particle surface. This would entail different mechanisms for initiation and entry compared to those for initiation strictly in the aqueous phase. One can imagine that more V-50 might be absorbed onto the negatively charged surface, and that the resulting surface-phase initiation may have a lower fk_d than in the aqueous phase, *e.g.*, a lower f due to the close proximity of radicals on the surface, or a lower k_d due to the less polar environment. This suggestion is speculative, and requires further investigation. What is clear is that some surface activity of V-50 makes it easy to justify that its f_{entry} values are relatively independent of initiator concentration: wherever effective initiation occurs, the resulting radicals very quickly enter latex particles and start polymerising.

3.4.9 Investigating Initiator Decomposition Using Added Inhibitor

In an effort to establish whether the low entry efficiency observed in the V-50/AN01 system may stem from the rate of generation of initiating radicals depending on the nature of the seed

particles, the following experimental methodology was employed. Seeded styrene emulsion polymerisations using V-50 as initiator in the AN01 system were carried out in the usual way, except that hydroquinone (HQ, recrystallised from water) was added at the start of the polymerisation, immediately prior to initiator. Any subsequent inhibition period and polymerisation were monitored by dilatometry.

In the absence of inhibition due to any other species (*e.g.*, dissolved oxygen) the length of the inhibition period, t_{inhib}, is related to the initial concentrations of initiator, $[I]_0$, and hydroquinone, $[HQ]_0$, according to equation (3.18).

$$[HQ]_0 n_{term} = 2f[I]_0 \left\{1 - \exp(-k_d t_{inhib})\right\} \quad (3.18)$$

Here k_d is the first-order rate coefficient for initiator decomposition, and as such $[I]_0\exp(-k_d t_{inhib})$ gives the concentration of initiator molecules that remain undecomposed at the end of the inhibition period. Assuming that each initiator decomposition event gives rise to two primary radicals, and that f (the "initiator efficiency") is the fraction of these radicals that is not lost to geminate recombination and any other possible side reactions, then the right-hand-side of equation (3.18) quantifies the cumulative concentration of aqueous radicals formed over the inhibition period that react with aqueous inhibitor (assuming that inhibition is complete). The left-hand-side of equation (3.18) expresses this same quantity in terms of the concentration of added inhibitor and the number of radicals claimed by termination with a single inhibitor molecule, n_{term}. In the case of hydroquinone the value of n_{term} is not known precisely. However, assuming that n_{term} is constant for reaction with a particular type of initiating radical, it should be possible to at least semi-quantitatively compare the results obtained for the same initiator with different *seed latexes* (as is of interest here).

It is important to note that t_{inhib} in equation (3.18) was measured from the time at which initiator was added ($t = 0$). In practice, however, a delay period of up to 5 min elapsed between the addition of initiator and the commencement of dilatometric monitoring – the time required to attach the glass capillary tube to the dilatometer vessel and fill it with degassed water and dodecane (see Chapter 2 for details). Importantly, gravimetric measurement of conversion confirmed that negligible polymerisation occurs during this period. Moreover, in the case of experiments where an appreciable period of zero rate was observed after the commencement of dilatometric readings (*i.e.*, when $t_{inhib} \gg 5$ min), this delay had no effect on

the measured value of t_{inhib}. However, in experiments where the inhibition time was shorter than ~ 5 min this approach clearly could not yield an accurate measurement of t_{inhib}.

It was also important here that any inhibition due to residual dissolved oxygen be insignificant compared to that of the added hydroquinone. The concentration of initiator used here (1 mM) was sufficiently high that earlier experiments, with no added inhibitor, exhibited no appreciable inhibition period (*i.e.*, $t_{inhib} < 5$ min) due to oxygen.

The results obtained from experiments using both V-50 systems are presented in Table 3.4. It is clear that for the V-50/CATH03 system the addition of hydroquinone gives rise to a measurable and reproducible inhibition period. Notably, the value of $\bar{n}_{SS}$ measured subsequent to this inhibition agrees well with that observed previously in the absence of hydroquinone. Assuming values of $f = 0.6$[47] and $k_d = 8.0 \times 10^{-6}$ s^{-1}[28] for V-50 at 50°C in equation (3.18), a value for n_{term} of 2.4 – 3.0 is inferred for hydroquinone. Such a value is physically reasonable considering that a possible product of radical reaction with hydroquinone is quinone, which may itself give rise to further radical termination reactions, providing the potential for loss of up to four radicals per hydroquinone molecule.[34]

Table 3.4. Results of added inhibitor experiments using V-50 as initiator.

seed latex	$[V\text{-}50]_0$ / M	$[HQ]_0$ / M	t_{inhib} / min	n_{term}	$\bar{n}_{SS}$	$\bar{n}_{SS}$ ($[HQ]_0 = 0$ M)†
CATH03	1×10^{-3}	5×10^{-6}	26	3.0	0.39	0.40
CATH03	1×10^{-3}	1×10^{-5}	42, 43	2.4	0.39	0.40
AN01	1×10^{-3}	1×10^{-5}	< 5, < 5	–	0.32	0.35

† Average $\bar{n}_{SS}$ measured from experiments with no added inhibitor described earlier.

In contrast, for experiments where hydroquinone was added to the V-50/AN01 system it was found that polymerisation was already underway when dilatometric monitoring began. In these cases we may only conclude that the inhibition period is between 0 and 5 minutes.

However, it is clear that the inhibition period for the anionic latex is far shorter than that for the cationic latex.

Given that hydroquinone is a water-soluble inhibitor, these results appear to refute the possibility that the low entry efficiency observed for the V-50/AN01 system is simply the result of a diminished rate of aqueous-phase decomposition of V-50. If this were the case one would expect to observe a relatively longer inhibition period for the low entry efficiency system; the opposite is seen here.

Notably, these results are consistent with the earlier postulate that the particle surface may be a significant or perhaps even dominant locus for V-50 radical generation. In this event V-50 would not behave as a "normal" aqueous-phase initiator and the entry process would be governed by different processes (such as V-50 adsorption/desorption kinetics and rates of decomposition and termination on the particle surface) and may well be independent of the effects of an inhibitor added to the aqueous-phase. It is also of note that the value of $\bar{n}_{SS}$ for this system is approximately unaffected by the presence of a significant concentration of aqueous inhibitor.

Further experiments were carried out as above using KPS as initiator, instead of V-50. The intention here was to determine whether the effect of added hydroquinone on KPS systems was in line with expectations based on V-50 results. Here one may be relatively confident that KPS will act as a "normal" aqueous-phase initiator regardless of latex particle type, and therefore that hydroquinone will have a consistent effect on both the KPS/CATH03 and KPS/AN01 systems.

Table 3.5. Results of added inhibitor experiments using KPS as initiator.

seed latex	$[KPS]_0$ / M	$[HQ]_0$ / M	t_{inhib} / min	n_{term}	$\bar{n}_{SS}$	$\bar{n}_{SS}$ ($[HQ]_0 = 0$ M)†
CATH03	1.5×10^{-3}	5×10^{-6}	19	0.7	0.25	0.28
AN01	1.5×10^{-3}	5×10^{-6}	10	0.3	0.29	0.34

† Average $\bar{n}_{SS}$ measured from experiments with no added inhibitor described earlier.

The results presented in Table 3.5 show that appreciable and roughly comparable (although by no means identical) inhibition periods were observed for both KPS systems in the presence of the same concentration of aqueous inhibitor, confirming that radical generation from KPS is not subject to the unusual effect observed for V-50. However, it is clear from the very low value of $n_{term} = 0.3 - 0.7$ inferred here [assuming values of $f = 1.0$ and $k_d = 1.1 \times 10^{-6}$ s^{-1} for KPS at 50°C[46] in equation (3.18)] that the inhibitory effect of hydroquinone is far weaker for radicals generated from KPS than for V-50 radicals. Assuming that the model of equation (3.18) is valid, these results may reflect an inherently lower reactivity of hydroquinone with oxygen-centred (KPS) radicals compared with carbon-centred (V-50) radicals; however, no evidence for this was encountered in the literature. Another possible explanation here is an enhanced decomposition rate coefficient for KPS in the presence of hydroquinone, as reported by Santos *et al.*[56] (admittedly for conditions of much higher [HQ] than used here). These authors proposed that hydroquinone is able to penetrate the solvent cage surrounding a persulfate molecule and act as a proton donor which accelerates the decomposition process. An estimate of the k_d enhancement required to explain the short inhibition times observed for KPS here may be obtained by assuming a best estimate for n_{term} of 2.4 – 3.0 (as found in V-50 experiments). Using equation (3.18) with $[KPS]_0 = 1.5 \times 10^{-3}$ M and $[HQ]_0 = 5 \times 10^{-6}$ M, a measured value of $t_{inhib} = 10$ min (Table 3.5) then suggests that $k_d = 7.5 \times 10^{-6}$ s^{-1} – approximately 7 times the literature value of 1.1×10^{-6} s^{-1}.[46] This is comparable to the ~ 8-fold enhancement reported by Santos *et al.*

Given the uncertainty in the mechanism of inhibition by hydroquinone described above, and variation in the apparent value of n_{term} for different radical types, additional experiments were attempted using Fremy's salt (potassium nitrosodisulfonate) as an aqueous-phase inhibitor. It was hoped that inhibition by this nitroxide monoradical species would follow a simple one-to-one stoichiometry with initiating radicals, and thus yield less ambiguous kinetic results than those of hydroquinone. However, the highly reactive nature of Fremy's salt makes it difficult to obtain reliable kinetic results,[45] and despite various careful attempts at adding Fremy's salt either in freshly prepared solution or solid form (following the recommendations of Lacík *et al.*), no reproducible inhibition effect was obtained using this inhibitor. It must be mentioned that Fremy's salt is not an easy reagent to work with in this regard, and results from one-off experiments with it should not be assumed to be reliable.

In summary, although no definite results have come from these experiments, the V-50/AN01 results here are at least consistent with the suggestion that initiation might be largely particle surface-based in this system. This is an important finding, and has made these experiments worthwhile.

3.4.10 Understanding z Values

Maxwell *et al.* rationalised the value of $z = 2$ for styrene polymerisation with KPS as initiator using thermodynamic considerations: an aqueous-phase radical incorporating an initiator end-group and two monomer units is sufficiently surface-active to adsorb strongly to (or go inside) a latex particle. These authors considered the driving forces associated with such an adsorption process. Firstly they estimated the hydrophobic free energy of adsorption ΔG_{hyd} for a styrene molecule by considering its different components. They similarly estimated (from surfactant micellisation data) the value of ΔG_{hyd} required to render a polar SO_4^- group surface-active. Comparison of these two values enabled an estimate to be made for the minimum number of styrene units required to yield a surface-active oligomeric KPS-styrene radical. This method was generalised to provide estimates for z for any monomer with KPS as initiator using equation (3.19) (where the integer function "int" reduces to the next lowest integer value):

$$z(\mathrm{KPS}) = 1 + \mathrm{int}\left\{\frac{-23\ \mathrm{kJ\ mol^{-1}}}{RT\ \ln([\mathrm{M}]_w/\mathrm{mol\ dm^{-3}})}\right\} \qquad (3.19)$$

Equation (3.19) gives a value of $z = 2$ for styrene.

Scheme 3.4. Structure of oligomeric styrene entering species derived **(a)** from KPS and **(b)** from V-50.

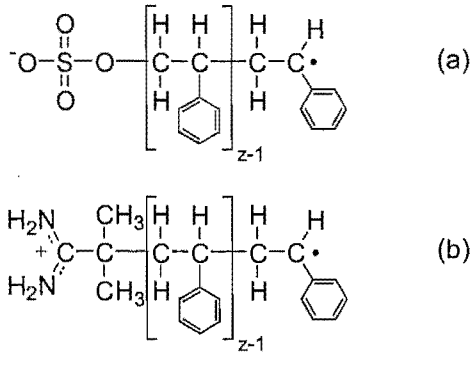

Entering species derived from KPS and V-50 are shown in Scheme 3.4. Both entering species include a polar end-group, but for V-50 there is a non-polar $C(CH_3)_2$ component also present.

It is suggested that this non-polar functionality may best be considered as part of the hydrophobic portion of the entering species, along with the z styrene monomeric units incorporated. Assuming that the hydrophilic character of the polar $C(NH_2)_2^+$ group from V-50 is approximately the same as that of SO_4^- (in the absence of any better estimate), then due to the presence of the non-polar functionality in the V-50 end-group one expects that fewer hydrophobic monomer units are needed to form a surface-active entering species (*i.e.*, z is lower for V-50).

It remains to determine whether or not this effect is sufficient to justify a difference in z of one monomer unit as has been suggested. An estimate may be made based on the reasoning of Maxwell *et al.* In calculating the value for ΔG_{hyd} of 23 kJ mol^{-1} required for KPS, these workers assumed a value of approximately 3 kJ mol^{-1} for ΔG_{hyd} corresponding to a single CH_2 group. Such a contribution from each of the three carbon atoms in the non-polar part of the V-50 end-group to the total hydrophobic free energy of the oligomer would result in a reduction from the 23 kJ mol^{-1} associated with KPS to approximately 14 kJ mol^{-1} for V-50. Thus, a modification of equation (3.19) may be formulated to estimate z for any monomer with V-50 as initiator:

$$z(\text{V-50}) = 1 + \text{int}\left\{\frac{-14 \text{ kJ mol}^{-1}}{RT \ln([\text{M}]_w/\text{mol dm}^{-3})}\right\} \qquad (3.20)$$

which yields $z = 1$ for styrene and V-50, in accord with deductions from experimental data. In view of this, the only unexplained aspect of all our entry data is that fk_d seems to be lower than expected in the V-50/anionic seed system, as discussed above.

3.5 Conclusions

Kinetic data for radical entry in the emulsion polymerisation of styrene have been obtained for four different systems, incorporating an anionic and a cationic initiator (persulfate and V-50) into both anionically- and cationically-charged latexes. Presenting data in the form of f_{entry} as a function of radical flux permits direct comparison, independent of any effects from differences in the rate of initiation and particle concentration between polymerisation systems.

Data for an anionic initiator with anionic latex showed acceptable agreement with previously published data for a similar system.[15] Moreover, changing the nature of the latex particle

surface charge had a minimal effect on the entry efficiency, suggesting that charge interactions between the particle surface and entering radicals have little or no impact on the entry process, consistent with the entry model of Maxwell *et al.*[1] However, changing the initiator charge had a significant effect on the initiator efficiency: the anionic initiator had decreasing entry efficiency with increasing radical flux, whereas the cationic initiator had efficiencies that were relatively invariant with changing radical flux. These results demonstrate the importance of the nature of the initiator (in the sense of the initiating radicals it gives rise to) in defining the mechanism for entry in emulsion polymerisation.

Experimental results were also compared with results calculated using the entry model of Maxwell *et al.* under the same conditions. The model assumes that aqueous-phase chemistry alone determines the rate of entry, and gives excellent accord with experiments where KPS was the initiator with $z = 2$, *i.e.*, a primary KPS radical must undergo two propagation events before a species capable of entry is formed, the first being rapid. This value of z is in accord with predictions made by the same authors on the basis of thermodynamic considerations. Where V-50 was used, comparison with model results is somewhat more ambiguous. Entry efficiency for this cationic initiator is high. A value for $z = 1$ (*i.e.*, virtually every radical enters a particle without aqueous-phase termination) appears most likely, although further experiments may be required to verify this. This value for z may be understood using thermodynamic reasoning similar to that given by Maxwell *et al.* for the peroxide initiator.

The results refute alternative models in the literature[51-55] that entry may be controlled by double-layer (colloidal) interactions, surfactant displacement or diffusion control.

Finally, it was also observed that the cationically-charged latex had a very high rate of spontaneous initiation, which may be rationalised in terms of radical chemistry arising from the presence of amidino species in combination with peroxidic functionalities.

3.6 References

(1) Maxwell, I. A.; Morrison, B. R.; Napper, D. H.; Gilbert, R. G. *Macromolecules* **1991**, *24*, 1629.

(2) Sakota, K.; Okaya, T. *J. Appl. Poly. Sci.* **1976**, *20*, 1725.

(3) Goodwin, J. W.; Ottewill, R. H.; Pelton, R. *Colloid Polym. Sci.* **1979**, *257*, 61.

(4) Gilbert, R. G. *Emulsion Polymerization: A Mechanistic Approach*; Academic: London, 1995.

(5) Marestin, C.; Guyot, A.; Claverie, J. *Macromolecules* **1998**, *31*, 1686.

(6) Leemans, L.; Jerome, R.; Teyssie, P. *Macromolecules* **1998**, *31*, 5565.

(7) Penboss, I. A.; Napper, D. H.; Gilbert, R. G. *J. Chem. Soc. Faraday Trans. 1* **1983**, *79*, 1257.

(8) McAskill, N. A.; Sangster, D. F. *Aust. J. Chem.* **1979**, *32*, 2611.

(9) McAskill, N. A.; Sangster, D. F. *Aust. J. Chem.* **1984**, *37*, 2137.

(10) Maruthamuthu, P. *Makromol. Chem., Rapid. Commun.* **1980**, *1*, 23.

(11) Howard, J. A.; Patai, S., in *The Chemistry of Peroxides*; Wiley: Chichester, 1983, p 235.

(12) Maeder, S.; Gilbert, R. G. *Macromolecules* **1998**, *31*, 4410.

(13) Casey, B. S.; Morrison, B. R.; Maxwell, I. A.; Gilbert, R. G.; Napper, D. H. *J. Polym. Sci. A: Polym. Chem.* **1994**, *32*, 605.

(14) Morrison, B. R.; Casey, B. S.; Lacík, I.; Leslie, G. L.; Sangster, D. F.; Gilbert, R. G.; Napper, D. H. *J. Polym. Sci. A: Polym. Chem.* **1994**, *32*, 631.

(15) Hawkett, B. S.; Napper, D. H.; Gilbert, R. G. *J. Chem. Soc. Faraday Trans. 1* **1980**, *76*, 1323.

(16) De Bruyn, H.; Hawkett, B. S.; Gilbert, R. G. *Polymer* **2000**, *41*, 8633.

(17) Lansdowne, S. W.; Gilbert, R. G.; Napper, D. H.; Sangster, D. F. *J. Chem. Soc. Faraday Trans. 1* **1980**, *76*, 1344.

(18) Casey, B. S.; Morrison, B. R.; Gilbert, R. G. *Prog. Polym. Sci.* **1993**, *18*, 1041.

(19) Hummel, D.; Ley, G.; Schneider, C. *Advan. Chem. Ser.* **1962**, *34*, 60.

(20) Hawkett, B. S., 1980, Ph.D. Thesis, University of Sydney.

(21) Christie, D. I.; Gilbert, R. G.; Congalidis, J. P.; Richards, J. R.; McMinn, J. H. *Macromolecules* **2001**, *34*, 5158.

(22) Miller, C. M.; Sudol, E. D.; Silebi, C. A.; El-Aasser, M. S. *Macromolecules* **1995**, *28*, 2754.

(23) Miller, C. M.; Sudol, E. D.; Silebi, C. A.; El-Aasser, M. S. *Macromolecules* **1995**, *28*, 2765.

(24) Miller, C. M.; Sudol, E. D.; Silebi, C. A.; El-Aasser, M. S. *Macromolecules* **1995**, *28*, 2772.

(25) Patnode, W. P.; Scheiber, W. J. *J. Am. Chem. Soc.* **1939**, *61*, 3449.

(26) Ballard, M. J.; Napper, D. H.; Gilbert, R. G. *J. Polym. Sci., Polym. Chem. Edn.* **1984**, *22*, 3225.

(27) Halnan, L. F.; Napper, D. H.; Gilbert, R. G. *J. Chem. Soc. Faraday Trans. 1* **1984**, *80*, 2851.

(28) Dougherty, T. J. *J. Am. Chem. Soc.* **1961**, *83*, 4849.

(29) Maillard, B.; Ingold, K. U.; Scaiano, J. C. *J. Am. Chem. Soc.* **1983**, *105*, 5095.

(30) Neta, P.; Huie, R. E.; Ross, A. B. *J. Phys. Chem. Ref. Data* **1990**, *19*, 413.

(31) Patai, S. *The Chemistry of Peroxides*; Patai, S., Ed.; Wiley: Chichester, 1983.

(32) Bovey, F. A.; Kolthoff, I. M. *J. Am. Chem. Soc.* **1947**, *69*, 2143.

(33) Miller, A. A.; Mayo, F. R. *J. Am. Chem. Soc.* **1956**, *78*, 1017.

(34) Moad, G.; Solomon, D. H. *The Chemistry of Free Radical Polymerization*; Pergamon: Oxford, 1995.

(35) Mayo, F. R.; Miller, A. A. *J. Am. Chem. Soc.* **1956**, *78*, 1023.

(36) Bhanu, V. A.; Kishore, K. *Chem. Rev.* **1991**, *91*, 99.

(37) Mukundan, T.; Bhanu, V. A.; Kishore, K. *J. Chem. Soc., Chem. Commun.* **1989**, 780.

(38) Lide, D. R. *CRC Handbook of Chemistry and Physics*; 82nd ed.; Lide, D. R., Ed.; CRC Press, 2001.

(39) Field, L. R.; Wilhelm, E.; Battino, R. *J. Chem. Thermodynamics* **1974**, *6*, 237.

(40) Harada, M.; Nomura, M.; Eguchi, W.; Nagata, S. *J. Chem. Eng. Japan* **1971**, *4*, 54.

(41) Ugelstad, J.; Hansen, F. K. *Rubber Chem. Technol.* **1976**, *49*, 536.

(42) Wilke, C. R.; Chang, P. *A.I.Ch.E. J.* **1955**, *1*, 264.

(43) Lane, W. H. *Ind. Eng. Chem.* **1946**, *18*, 295.

(44) Tobolsky, A. V.; Offenbach, J. *J. Polym. Sci.* **1955**, *16*, 311.

(45) Lacík, I.; Casey, B. S.; Sangster, D. F.; Gilbert, R. G.; Napper, D. H. *Macromolecules* **1992**, *25*, 4065.

(46) Behrman, E. J.; Edwards, J. O. *Rev. Inorg. Chem.* **1980**, *2*, 179.

(47) Hammond, G. S.; Neuman, R. C., Jr. *J. Am. Chem. Soc.* **1963**, *85*, 1501.

(48) Buback, M.; Gilbert, R. G.; Hutchinson, R. A.; Klumperman, B.; Kuchta, F.-D.; Manders, B. G.; O'Driscoll, K. F.; Russell, G. T.; Schweer, J. *Macromol. Chem. Phys.* **1995**, *196*, 3267.

(49) Whang, B. C. Y.; Napper, D. H.; Ballard, M. J.; Gilbert, R. G.; Lichti, G. *J. Chem. Soc. Faraday Trans. 1* **1982**, *78*, 1117.

(50) Adams, M. E.; Trau, M.; Gilbert, R. G.; Napper, D. H.; Sangster, D. F. *Aust. J. Chem.* **1988**, *41*, 1799.

(51) Vanderhoff, J. W., in *Vinyl Polymerization*; Ham, G., Ed.; Marcel Dekker: New York, 1969; Vol. 7 part 2.

(52) Fitch, R. M.; Tsai, C. H., in *Polymer Colloids*; Fitch, R. M., Ed.; Plenum: New York, 1971, p 73.

(53) Hansen, F. K.; Ugelstad, J., in *Emulsion Polymerization*; Piirma, I., Ed.; Academic: New York, 1982.

(54) Yeliseyeva, V. I., in *Emulsion Polymerization*; Piirma, I., Ed.; Academic: New York, 1982.

(55) Ottewill, R. O., in *Emulsion Polymerization*; Piirma, I., Ed.; Academic: New York, 1982.

(56) Santos, A. M.; Vindevoghel, P.; Graillat, C.; Guyot, A.; Guillot, J. *J. Polym. Sci., Part A: Polym. Chem.* **1996**, *34*, 1271.

4. Entry in the Emulsion Polymerisation of Methyl Methacrylate – A Monomer of Moderate Water-Solubility

4.1 Introduction

Having established the effects of initiator and particle surface charge on the entry process for styrene systems, it is next of interest to investigate the influence of monomer. Extensive investigation of the emulsion polymerisation of styrene has revealed a relatively low value of z, reflecting the low water solubility of this monomer – a water-soluble radical derived from initiator need only acquire one or two styrene monomer units before a surface-active radical is formed and entry rapidly ensues.

It is therefore appropriate to select a more hydrophilic (and thus higher z value) monomer for investigation here. The monomer chosen is methyl methacrylate, whose (saturation) water solubility (0.15 M at 50°C[1]) is considerably greater than that of styrene (0.0043 M at 50°C[2]). This monomer is also deemed favourable for this work due to the fact that, like styrene, it is one of the most thoroughly studied monomers for free-radical polymerisation and therefore reliable values are available for many of the other parameters required for data analysis.

The emulsion polymerisation of methyl methacrylate (MMA) has been the subject of various types of study for several decades and, in particular, a number of quantitative investigations relevant to the process of entry have emerged in recent years. The findings of Wang *et al.*,[3] Thomson *et al.*,[4] Marestin *et al.*[5] and Leemans *et al.*[6] were briefly discussed in Chapters 1 and 3. Of particular interest amongst these works are the results of Thomson *et al.*,[4] who isolated oligomeric species remaining in the aqueous phase after surfactant-free emulsion polymerisations of MMA and analysed these using MALDI-TOF mass spectrometry and gel-permeation chromatography (GPC). The observation by these workers of oligomers with sizes ranging from 2 – 14 monomer units is immediately suggestive of a significantly higher value of z for MMA/persulfate compared to styrene/persulfate, considering that even if a significant proportion of these species were formed by combination reactions (unlikely for MMA[7,8]), there must still be significant formation of radicals at least ~ 7 monomer units in length.

Also of relevance here are the findings of Marestin *et al.*,[5] who used surface-bound free radical amino-TEMPO groups to trap oligomeric radicals arriving at the surface of latex particles in seeded emulsion polymerisations of MMA. The trapped oligomers were analysed using IR spectroscopy and GPC, and their average composition determined to be approximately 5 monomer units. Marestin *et al.* took these results as direct evidence for a value of $z \approx 5$ for MMA; however it is noted that the high concentration of amino-TEMPO groups at the particle surface (~ 9700 per particle[5]), combined with the rapidity of radical-radical reactions, may well have resulted in significant trapping of oligomeric radicals of chain lengths less than z, *i.e.*, radicals that would ordinarily adsorb only temporarily to the particle surface before rapidly desorbing again. Thus, the oligomers isolated under these non-polymerising conditions may not accurately reflect the "entrant" radicals in a true emulsion polymerisation system. Further, an *average* length of 5 implies a significant contribution from species that are longer than 5 in length, *i.e.*, a value of z greater than 5.

The study which has provided the most significant quantitative insight into the emulsion polymerisation kinetics of MMA to date is the now relatively old work of Ballard *et al.*[1] This extensive study furnished unique values for a range of the rate coefficients in this system as well as numerous mechanistic deductions which form the basis for the kinetic investigations embarked upon in the present chapter. A detailed discussion of the findings of Ballard *et al.* is presented shortly.

The aim of this section of work is to build on the current understanding of the kinetics and mechanism of the emulsion polymerisation of MMA, with the specific goal of obtaining accurate values for the entry rate coefficient and entry efficiency for initiator-derived radicals in this system, something Ballard *et al.*[1] did not really do (they were not confident in the quantitative accuracy of some data that they obtained). As well as being of interest in themselves, comparison of these results with data already presented for styrene will shed light on the effects of monomer on the entry process. Importantly, this data will also serve to test the accuracy with which the Maxwell-Morrison model predicts the influence of monomer properties (*e.g.*, k_p, $[M]_w$) on the values of these entry rate parameters, both in their own right and for one monomer relative to another.

4.2 Background Considerations

4.2.1 The "Control by Aqueous-Phase Growth" (Maxwell-Morrison) Model for Entry

For ease of reference the reaction scheme derived from the hypothesised entry model of Maxwell *et al.*[9] is once again presented below.

$$\text{initiator} \xrightarrow{fk_d} 2\,\text{I}^\bullet \tag{4.1}$$

$$\text{I}^\bullet + \text{M} \xrightarrow{k_{p\text{I,w}}} \text{IM}_1^\bullet \quad \text{(rapid)} \tag{4.2}$$

$$\text{IM}_i^\bullet + \text{M} \xrightarrow{k_{p,w}} \text{IM}_{i+1}^\bullet, \quad 1 \le i < z \tag{4.3}$$

$$\text{IM}_i^\bullet + \text{T}_w^\bullet \xrightarrow{2k_{t,w}} \text{inert products}, \quad 1 \le i < z \tag{4.4}$$

$$\text{IM}_z^\bullet \xrightarrow{\rho_{init}} \text{entry} \quad \text{(rapid)} \tag{4.5}$$

Closely associated with this model is the analytic solution for the entry rate coefficient, ρ_{init}, derived by Maxwell *et al.*

$$\rho_{init} = \frac{2fk_d[\text{I}]N_A}{N_c}\left\{\frac{2\sqrt{fk_d[\text{I}]\,k_{t,w}}}{k_{p,w}[\text{M}]_w} + 1\right\}^{1-z} \tag{4.6}$$

It is also recalled that the fraction of all radicals generated from initiator that undergo entry – the "entry efficiency" – is defined as:

$$f_{entry} = \frac{\rho_{init}}{\rho_{100\%}} = \rho_{init}\frac{N_c}{2fk_d[\text{I}]N_A} \tag{4.7}$$

4.2.2 Measurement of Entry Rate Coefficients

As mentioned previously, rate parameters for entry may not be measured directly using dilatometry and, instead, are inferred from the accurate measurement of the conversion of monomer into polymer over time, which dilatometry does provide. In the present case, the most convenient form of such data will be seen to be in terms of conversion in grams, $\hat{x}$, with

the rate of polymerisation expressed as $d\hat{x}/dt$ (in grams per second). This rate is related directly to the average number of radicals inside a latex particle, denoted $\bar{n}$, as follows (see Chapter 1):

$$\frac{d\hat{x}}{dt} = \frac{k_p [M]_p M_0 N_c V_w}{N_A} \bar{n} \tag{4.8}$$

Since the magnitude of $\bar{n}$ is directly influenced by the occurrence of radical entry (*inter alia*), this value is key to unravelling the kinetics of the entry process. Importantly, unlike the styrene systems of the previous chapter, MMA emulsion systems have been shown not to obey zero-one kinetics under typical experimental conditions (as discussed below: the rate of termination is not sufficiently fast to guarantee pseudo-instantaneous termination upon radical entry into an occupied particle). Thus, in this case it is not possible to draw on the considerable understanding which has been developed for zero-one systems.

The procedure for obtaining ρ in the case of non-zero-one systems is less established and, as will be seen through the course of this chapter, a variety of approaches may be required. Nevertheless, the general strategy remains similar to the zero-one case: in order to isolate the value of ρ from the measured value of $\bar{n}$ it is necessary to determine values for the kinetic parameters k and c pertaining to the radical loss processes of exit and bimolecular termination respectively. Once again "γ-relaxation" experiments are employed as a useful means for studying the non-steady-state kinetics associated with rapid changes in the rate of initiation. As outlined already, in these experiments the emulsion system is exposed to γ-radiation until a steady-state polymerisation rate is established and initiation is then halted by removal from the γ-source, causing the rate of polymerisation to slow from the "in-source" rate to a lower "out-of-source" rate. The precise nature of the decay in polymerisation rate is largely determined by the radical loss kinetics; hence the values of k and/or c may be obtained by careful analysis of the γ-relaxation data.

Notably, as was observed for the styrene systems of the previous chapter, it will be seen that the out-of-source rate of polymerisation in MMA systems is also non-zero. Thus it is necessary to account for the contribution to the entry rate coefficient arising from entry of spontaneously-generated radicals, ρ_{spont}.

$$\rho = \rho_{init} + \rho_{spont} \tag{4.9}$$

In the absence of a detailed understanding of the mechanism for spontaneous polymerisation (*i.e.*, where the culprit radicals are generated and what reactions they may undergo), we once again assume that the two entry processes quantified by ρ_{init} and ρ_{spont} occur independently of one another, as indicated by equation (4.9), and thus that there is no interaction between initiator-derived and spontaneously-generated radicals in the aqueous phase. Obviously this assumption cannot be rigorous; however equation (4.9) is still justifiable in that there is only a small range of conditions in which both ρ_{init} and ρ_{spont} are comparable in magnitude. Otherwise one contribution is much larger than the other, in which event equation (4.9) should be reasonably accurate.

4.2.3 The Work of Ballard et al.

As mentioned above, the extensive and detailed work of Ballard *et al.*[1] on the emulsion polymerisation of MMA provides a starting point for the present study. Therefore, it is pertinent at this stage to summarise several key results from this early work which will be seen to be of particular importance through the course of the current investigation.

1. "Pseudo-bulk" kinetics in MMA emulsion polymerisations.

Based on a detailed analysis of data from systems with chemical (persulfate) initiator as well as systems using γ-radiolysis as the radical source, Ballard *et al.* concluded that under a wide range of conditions the emulsion polymerisation of MMA is well described by kinetics akin to those for a bulk polymerisation system. Here the time evolution of the average number of radicals inside a particle, $\bar{n}$, may be described as follows:

$$\frac{d\bar{n}}{dt} = \rho - (1-\alpha)k\bar{n} - 2c\bar{n}^2$$
$$= \left(\rho + \alpha k\bar{n}\right) - k\bar{n} - 2c\bar{n}^2 \qquad (4.10)$$

where ρ, k and c are respectively the pseudo-first-order rate coefficients for radical entry, exit and termination. The value of c is, in turn, related to the second-order rate coefficient for bimolecular termination (averaged over all chain lengths), $\langle k_t \rangle$, through the volume of a swollen latex particle, V_s, as follows.

$$c = \frac{\langle k_t \rangle}{N_A V_s} \qquad (4.11)$$

As described in Chapter 1, the "pseudo-bulk" equation, (4.10), is an approximation to the exact solution of the well-known Smith-Ewart equations for emulsion polymerisation kinetics[10] and has the advantage that it may be solved relatively simply using a steady-state approximation to give model values for $\bar{n}$ under various conditions. Ballard *et al.* showed that, ignoring any effects of chain length dependent termination rate coefficients, this approximation is accurate under conditions where either $\rho > c$ or $k > c$ is satisfied.[11] The effects of re-entry of exited radicals back into a latex particle were also incorporated by way of the so-called "fate parameter", α – intended to encapsulate the net effect of exited radicals on the value of $\bar{n}$, with $\alpha = 1$ corresponding to re-entry of all exited radicals and $\alpha = -1$ corresponding to complete "hetero-termination" of exited radicals (*i.e.*, cross-termination between an exited radical and an initiator-derived radical) in the aqueous phase. The second form of equation (4.10) makes clear how α gives these limiting cases.

Importantly, these workers showed that under conditions of low aqueous-phase radical flux – *e.g.* during the "out-of-source" period of a γ-relaxation experiment – the value of α is essentially 1 (complete re-entry), as would intuitively be expected: the concentration of aqueous radicals is too low to give rise to significant termination of exited radicals. In this case radical exit has a negligible overall effect on the value of $\bar{n}$ and equation (4.10) is simplified to the following form.

$$\frac{d\bar{n}}{dt} = \rho - 2c\bar{n}^2 \qquad (4.12)$$

The steady-state value for $\bar{n}$ is then trivially obtained from equation (4.12) as

$$\bar{n} = \left(\frac{\rho}{2c}\right)^{\frac{1}{2}} = \left(\frac{\rho N_A V_s}{2\langle k_t \rangle}\right)^{\frac{1}{2}} \qquad (4.13)$$

where the value of c has also been substituted according to equation (4.11).

2. Interval II behaviour of MMA emulsion polymerisations.

A changing rate of polymerisation is to be expected under some (non-steady-state) emulsion polymerisation conditions, such as at high conversion when the rate of termination is changing rapidly as a result of the "gel effect". However, one might expect a constant rate during Interval II of polymerisation, given the provisions of constant

particle number and constant monomer concentration. Interestingly, for MMA this is not the case and the rate of polymerisation is found to increase throughout this period of the polymerisation. Ballard *et al.* ascribed this increase in Interval II rate to an increase in the average number of radicals per particle. Specifically, it was noted that, on the basis of equation (4.13) above, in the case of a pseudo-bulk system with $\alpha = 1$ the steady-state value of $\bar{n}$ would not be expected to remain constant during Interval II at all, but should instead increase as the particle volume increases with conversion. It is noted that this increase in radical *number* (and hence rate) is a direct result of the radical *concentration* inside the particles remaining constant while the volume of a latex particle (the effective reaction volume) increases over the course of Interval II.

It is important to note that a changing value of $\bar{n}$ does not necessarily imply the absence of steady-state conditions; indeed, if such were the case equation (4.13) would be invalid. The existence of steady-state conditions ultimately depends on the rate at which $\bar{n}$ is changing with time. During Interval II the increase in $\bar{n}$ with changing volume is relatively slow and consequently the rapid exchange of radicals between particles by entry and exit events is sufficient to maintain a steady-state value for $\bar{n}$, *i.e.*, during Interval II the value of $\bar{n}$ changes gradually. Importantly, this volume effect on $\bar{n}$ is a general effect in emulsion polymerisation, and will be operative in any system where intra-particle termination is rate-determining. It is surprising that MMA is the only emulsion polymerisation system which has been studied with sufficient rigour to observe this effect.

3. Low entry efficiency for initiator-derived aqueous-phase radicals.

Comparing their measured values for the entry rate coefficient to the flux of radicals from initiator, Ballard *et al.* also concluded that the efficiency of entry was generally well below 100% for this system, falling in the range 20 – 50%. The relevance of this result will become clear over the course of this chapter.

4.3 Experimental Details

4.3.1 Synthesis of Seed Latex

Methyl methacrylate (Mitsubishi Rayon, stabilised with 4-methoxyphenol inhibitor) was passed through a column of basic alumina and distilled under reduced pressure (first and last

10% discarded) to remove inhibitor. The purified monomer was stored at 0°C for no longer than two weeks before use. Aerosol MA-80 (AMA-80, sodium di(1,3-dimethylbutyl)sulfosuccinate, 80% solution in isopropanol and water, Cytec) and sodium hydrogencarbonate (BDH AnalaR grade) were used without further purification. Potassium persulfate (KPS) (BDH AnalaR grade) was recrystallised from water before use.

Table 4.1. Seed latex MMA06 preparation and characteristics.

ingredient	amount
water (Milli-Q)	750 g
MMA	190 g
AMA-80	20.0 g
$NaHCO_3$	1.00 g
KPS	3.01 g
particle sizing method	number-average unswollen particle diameter / nm
CHDF	85
HPPS	99
TEM (polydispersity)†	88 (1.02)
value used for kinetic analysis	85

† TEM results obtained from carbon-coated latex sample; polydispersity calculated as ratio of weight-average to number-average particle diameter

Synthesis of seed latex was based on a recipe of Ballard *et al.* (his seed latex SL03[1]) and details are given in Table 4.1. A 1 dm^3 glass reactor was charged with water, surfactant (AMA-80) and buffer ($NaHCO_3$), and the solution heated to 60°C. A small amount (50 cm^3) of water was retained to dissolve initiator. Monomer was added to the reactor and emulsified by stirring at 450 rpm, and finally initiator was added. The reaction was left to proceed for 3

hours before the temperature was raised to 80°C and the reactor vessel opened. The reaction was then left to proceed for a further 12 hours in order for any residual monomer either to be polymerised or to be evaporated, and any residual initiator to be decomposed.

The seed latex produced, labelled MMA06, was dialysed against distilled water (changed three times daily) for ten days, over which time conductivity measurements were seen to converge to a constant value. The dialysed latex was filtered through glass wool to remove any traces of coagulum. Particle size distributions were measured by capillary hydrodynamic fractionation (CHDF, Matec) and dynamic light scattering (HPPS, Malvern) for comparison. Another method commonly used for particle size determination, transmission electron microscopy (TEM), was complicated in this case by the fact that poly(methyl methacrylate) latex particles are prone to softening/deformation and aggregation (distortion of spherical shape and fusing together of separate particles) under the electron beam and it is difficult to obtain an accurate measure of particle size. Two approaches were used in an attempt to overcome this problem:

1. The deposition of a thin (< 5 nm) layer of gold on the surface of the latex sample for TEM (a technique known as "gold sputtering").

2. The deposition of a thin (< 5 nm) layer of carbon on the surface of the latex sample for TEM ("carbon sputtering").

The aim of both these coating processes was to aid in dissipating the electrons received by the polymer under the microscope beam and thus reduce the damaging effects of heat on the particles. However, the first approach above was found to be unsuitable in that the gold sputtering process itself led to extensive deformation of the particles. The carbon sputtering technique was found to be far more successful. Some particle deformation from the coating process was evident; however the coated particles appeared very stable under the electron beam and retained their original size and shape well enough for a reasonable estimate of particle size to be made.

Results from all particle sizing methods used are presented in Table 4.1. In this case, the particle diameter measured by CHDF is adopted for use in all kinetic analyses given the uncertainty in the TEM value arising from particle deformation. It is notable however, that the results from all three particle sizing methods employed are in reasonable agreement. It is also noted that the diameter measured here is somewhat larger than that reported by Ballard *et*

al., 74 nm (measured by both TEM and ultracentrifugation), for latex SL03 – synthesised according to the same procedure. An obvious source for such discrepancy is an error in size calibration in the present case and/or by Ballard *et al.* Another explanation may be subtle differences in reaction conditions, one possible example being reactor design and another being the precise nature of the small rise in temperature often observed in the early stages of polymerisation – which may impact on the particle formation process. In the present case a small degree of control over this "exotherm" was afforded by the reactor temperature control regime. The same cannot be assumed for the case of Ballard *et al.*

4.3.2 Values of $[M]_p^{sat}$ *and* $[M]_w^{sat}$

Analysis of the kinetic data from seeded polymerisations requires a knowledge of the values of the intra-particle monomer concentration for particles saturated with monomer, denoted $[M]_p^{sat}$, as well as the concentration of monomer in saturated aqueous solution, $[M]_w^{sat}$.

In the case of $[M]_p^{sat}$ it is necessary to carry out a measurement for the particular seed latex used, as this quantity is affected by particle size and surface characteristics. A value for $[M]_p^{sat}$ of 6.9 M was measured at 50°C (the temperature used for kinetic experiments) for seed latex MMA06 using the "static swelling" method, details of which are given in Chapter 2 and elsewhere.[1,12,13] This value is close to the value of 6.6 M used by Ballar *et al.*[1]

The value of $[M]_w^{sat}$ at 50°C measured by Ballard *et al.*[1] of 0.15 M was adopted for the kinetic analyses performed here. No re-measurement was carried out in this case as the water-solubility of monomer is likely to be relatively insensitive to the precise reaction conditions in a typical seeded experiment of the sort conducted here. These authors also determined that the unsaturated aqueous monomer concentration, $[M]_w$, obeys the following empirical relation:

$$\frac{[M]_w}{[M]_w^{sat}} = \left(\frac{[M]_p}{[M]_p^{sat}}\right)^{0.6} \tag{4.14}$$

Therefore, the value of $[M]_w$ may be obtained at any time from the values of $[M]_p^{sat}$ and $[M]_w^{sat}$ (given above) and the known monomer concentration inside the (unsaturated) latex particles, $[M]_p$.

4.3.3 Kinetic Experiments

All kinetic experiments were seeded emulsion polymerisations of MMA at 50°C commencing in Interval II (in the presence of monomer droplets), so that $[M]_p$ remained essentially constant. The details of the composition of typical polymerisations are given in Table 4.2. The rate of polymerisation was measured by automated dilatometry using the methods described in Chapter 2 with the densities of monomer and polymer at 50°C respectively taken as d_M = 0.909 g cm^{-3} and d_p = 1.226 g cm^{-3},[14] the latter being the density of polymer in a monomer solution (applicable to monomer-swollen latex particles). The density of monomer dissolved in water at 50°C was measured experimentally (see Chapter 6 for details) as 0.981 g cm^{-3} and final dilatometric conversions were verified by gravimetry. A water-jacketed dilatometer vessel (of volume 60 cm^3 for chemically initiated runs, or 30 cm^3 for γ-radiolysis) was charged with seed polymer, methyl methacrylate, AMA-80 and water (Milli-Q), and stirred overnight to swell seed latex particles with monomer. The reaction mixture was then overheated to 60°C and degassed under reduced pressure in order to prevent the formation of any bubbles inside the vessel during the course of a kinetic run (which would make it impossible to measure rate data accurately by dilatometry). After sufficient thermal equilibration time at 50°C the reaction mixture was stirred vigorously to ensure monomer emulsification. Finally, initiator was added or, in the case of γ-radiolysis experiments, the system was exposed to the γ-source. At the end of the polymerisation a small amount of hydroquinone was added to quench the reaction. Since the kinetic analysis of these seeded emulsion polymerisations relies on the absence of new particle formation, latexes were inspected for evidence of new particle formation by TEM. In this case, since it was necessary only to ensure the absence of a significant secondary particle population, and highly accurate particle size determination was not required, carbon sputtering of latex samples was not carried out.

It is noted that the composition of the reaction mixture (*i.e.*, seed polymer, monomer, surfactant) used in γ-radiolysis experiments was quite similar to that used for chemically initiated runs, despite the fact that the volume of the reaction vessel was significantly less in the γ-radiolysis case. This composition was required in order to provide sufficient monomer for an accurately measurable volume contraction, and thus accurate kinetic data, to be obtained.

Table 4.2. Details of seeded emulsion polymerisations.

	chemically initiated experiments	γ-radiolysis experiments
N_c / dm^{-3}	4.3×10^{16}	1.0×10^{17}
seed (MMA06) polymer / g	0.89	0.92
MMA / g	5.25	4.80
AMA-80 / g	0.031	0.033
KPS / g	0.004 – 0.05	–
γ-radiolysis dose rate / Gy h^{-1}	–	146

4.4 Theory: the "Acceleration" During Interval II

As mentioned above, the steady-state period of Interval II of an emulsion polymerisation of MMA is characterised by a gradual increase in the value of $\bar{n}$ with conversion. This is illustrated schematically in Figure 4.1.

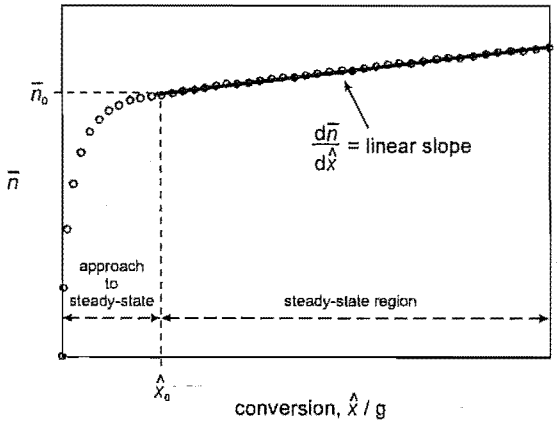

Figure 4.1. Schematic plot of experimental $\bar{n}$ data (circles) from Interval II of the emulsion polymerisation of MMA showing approach to steady-state and steady-state region, with linear fit (solid line) used to calculate value of $\bar{a}$.

In their work Ballard *et al.* established a method for quantifying this evolution of $\bar{n}$ during the steady-state period and defined an "acceleration" parameter, $\bar{a}$, as follows:

$$\bar{a} = \frac{\dfrac{d\bar{n}}{d\hat{x}} m_p^0}{\bar{n}_0} \qquad (4.15)$$

Here $d\bar{n}/d\hat{x}$ is the average rate of change of $\bar{n}$ with conversion over the steady-state period of Interval II (*i.e.*, neglecting the period of approach to steady-state shown in Figure 4.1), obtained from the slope of a linear fit to the $\bar{n}(\hat{x})$ data during this time. $\bar{n}_0$ and m_p^0 are, respectively, the value of $\bar{n}$ and total mass of polymer present at the start of the steady-state period (as opposed to being $t = 0$ values). Using m_p^{seed} to denote the mass of seed polymer initially added and $\hat{x}_0$ to denote the value of conversion at the start of the steady-state period (see Figure 4.1), m_p^0 is then calculated as

$$m_p^0 = m_p^{seed} + \hat{x}_0 \qquad (4.16)$$

Ballard *et al.* used equation (4.13) to derive a theoretical value for the "acceleration" based on the assumption that the rate increase is related to the increase in latex particle volume during the steady-state period. This derivation (a full and more precise version of which is given in Appendix A.4) gives the following exact form for $\bar{n}$ as a function of conversion:

$$\bar{n} = \bar{n}_0 \left(1 + \frac{\hat{x} - \hat{x}_0}{m_p^0} \right)^{\frac{1}{2}} \qquad (4.17)$$

It is noted that the value of $(\hat{x} - \hat{x}_0)$ appearing in equation (4.17) and elsewhere corresponds to the mass of monomer converted into polymer *only* during the steady-state period; thus at the start of this period $\hat{x} = \hat{x}_0$ and $(\hat{x} - \hat{x}_0) = 0$. According to equation (4.13), $\bar{n}_0 = \left(\dfrac{\rho N_A V_s^0}{2 \langle k_t \rangle} \right)^{\frac{1}{2}}$, where V_s^0 is the volume of a swollen latex particle at the start of the steady-state period. Equation (4.17) is then approximated by a truncated Taylor-series in $(\hat{x} - \hat{x}_0)$, neglecting second and higher order terms to give the following approximate expression for $\bar{n}$:

$$\bar{n} = \bar{n}_0 + \frac{\bar{n}_0}{2\, m_p^0}(\hat{x} - \hat{x}_0) \tag{4.18}$$

From this linear approximation, the value of $\bar{a}$ may be calculated using equation (4.15).

$$\bar{a} = \frac{\dfrac{d\bar{n}}{d\hat{x}} m_p^0}{\bar{n}_0} = \frac{\left(\dfrac{\bar{n}_0}{2\, m_p^0}\right) m_p^0}{\bar{n}_0} = \frac{1}{2} \tag{4.19}$$

The theoretical value for $\bar{a}$ derived by Ballard *et al.* is therefore 0.5, as shown in equation (4.19). It is worth noting that this constant value for $\bar{a}$ predicts that the measured acceleration in Interval II, as defined in equation (4.15), should be independent of the particular experimental conditions, such as temperature, initiator concentration and particle number.

It is important to note that the sub- or super-script 0 (*e.g.*, as in $\bar{n}_0$) is used throughout this work to denote the specific value of a quantity *at the start of the Interval II steady-state period* and should not be confused with the specific value at the start of the experiment (*i.e.*, at zero time) or at zero conversion, either of which may not necessarily coincide with the start of the steady-state period. As an aside it is noted, however, that the mathematical framework developed above for the acceleration may equally be applied if, for instance, the values denoted sub- or superscript 0 are *all* re-defined as the specific values at zero conversion (*i.e.*, such that $\hat{x}_0 = 0$ and $m_p^0 = m_p^{seed}$) – with the important requirement that the value of $\bar{n}_0$ be determined by extrapolation to zero conversion of the linear fit to $\bar{n}$. In this work the former interpretation is preferred as it avoids such an extrapolation.

In terms of the present study, it was initially of interest to check the accuracy of the approximations leading to the theoretical value of $\bar{a} = 0.5$ derived by Ballard *et al.* In order to do this the value of $\bar{n}$ was calculated as a function of conversion for the steady-state period using both the non-linear, "exact" method of equation (4.17), as well as the linear, "approximate" method of Ballard *et al.* [equation (4.18)], in both cases $\bar{n}_0$ being evaluated according to equation (4.15). The following representative parameter values for the system presently under investigation were used: $\hat{x}$ up to 0.7 g, $m_p^0 = 0.85$ g, $V_s^0 = 1.3 \times 10^{-18}$ dm^3, $\rho =$ 0.01 s^{-1}, $\langle k_t \rangle = 1.9 \times 10^4$ M^{-1} s^{-1}. These model calculations were used only to predict the steady-state evolution of $\bar{n}$; thus the approach to steady-state was omitted. The calculated data are presented in Figure 4.2.

Being non-linear, the exact modelled $\overline{n}$ data were least-squares fitted to a straight line and the slope of the line used to calculate a value for $\overline{a}$ according to equation (4.15). As is evident from Figure 4.2, the data calculated using the exact method exhibit a slightly lower average (linearised) acceleration, with $\overline{a}_{\text{exact}} = 0.42$, than the approximate method of Ballard *et al.*, with $\overline{a}_{\text{approx}} = 0.5$.

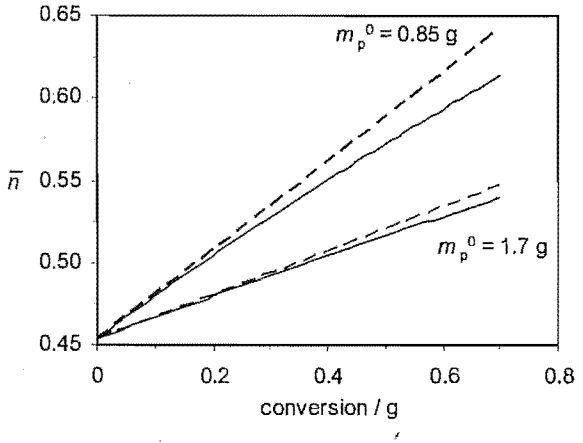

Figure 4.2. Theoretical evolution of $\overline{n}$ with conversion calculated using parameter values given in text and m_p^0 = 0.85 g or 1.70 g; exact method (solid line) from equation (4.17) and approximate method (dashed line) from equation (4.18).

In order to establish the effect of changing conditions on the modelled value of $\overline{a}$, the calculations described above were repeated assuming double the starting mass of polymer: m_p^0 = 1.70 g. The results, also shown in Figure 4.2 once again reveal a lower acceleration for the $\overline{n}$ data modelled using the exact approach compared to that of the approximate data, with values of $\overline{a}_{\text{exact}} = 0.46$ and $\overline{a}_{\text{approx}} = 0.5$.

Additionally, the effect of fitting different conversion ranges on the value of $\overline{a}$ was determined for the data modelled with $m_p^0 = 0.85$ g. Applying a linear fit only over the range $0 \leq \hat{x} \leq 0.35$ g led to a value of $\overline{a}_{\text{exact}} = 0.46$, somewhat greater than the value of $\overline{a}_{\text{exact}} = 0.42$ obtained from fitting the conversion range $0 \leq \hat{x} \leq 0.7$ g earlier. Of course, the value of $\overline{a}_{\text{approx}}$ = 0.5 always remains unchanged. It is also worth noting that the effect on $\overline{a}_{\text{exact}}$ of doubling m_p^0 is equivalent to halving the range of steady-state conversion fitted.

The small but significant differences in $\overline{a}_{\text{exact}}$ observed above highlight the fact that the value of $\overline{a}$ predicted by theory is indeed sensitive to the values of certain parameters – in particular,

the mass of polymer at the start of the steady-state period, m_p^0, and the range of conversion to be considered. It is seen that the approximate, "truncated Taylor-series" method of Ballard *et al.* lacks this sensitivity, predicting a constant value for $\bar{a}$ under *all* conditions and introducing a possible source of error. For this reason, unless otherwise stated, the theoretical value of the acceleration will always be calculated using the exact method described above, applied over the full steady-state conversion range of Interval II. In addition, it is equally important to note here that a range of calculations of $\bar{a}_{exact}$ as above using different values of ρ and $\langle k_t \rangle$ resulted in the same value of $\bar{a}_{exact}$ = 0.42 in every case (for m_p^0 = 0.85 g fitted over 0.7 g of conversion), thus revealing that the value of $\bar{a}$ is *independent* of the magnitude of these rate parameters, provided that the values of ρ and $\langle k_t \rangle$ are constant with conversion (which is reasonable for Interval II at 50°C, under which conditions w_p, the weight fraction of polymer in the particles, is constant and [KPS] decreases slowly – hence relatively constant $\langle k_t \rangle$ and ρ respectively).

4.5 Results

4.5.1 γ-relaxation Experiments

Duplicate seeded γ-relaxation experiments (G31 and G32) were carried out at 50°C as described earlier, with conversion as a function of time determined dilatometrically and $\bar{n}$ calculated using equation (4.8). The literature value of k_p = 649 M^{-1} s^{-1} for MMA at 50°C[15] was used here and in all subsequent kinetic analyses. The principal aim of these experiments was to unambiguously determine the value of the effective (pseudo-first-order) termination rate coefficient, c, and hence also the closely related intra-particle bimolecular termination rate coefficient, $\langle k_t \rangle$.

Presented in Figure 4.3 are typical data from an experiment in which two γ-relaxations were performed during the same polymerisation. It is worth noting that early in Interval II (from 0 – 8 min), when the system was exposed to a constant dose of γ-radiation, the "in-source" value of $\bar{n}$ was seen not to be constant but gradually increasing with time, with fitting of the steady-state region yielding a value of $\bar{a}$ = 0.32 (for run G32 with m_p^0 = 0.96 g and conversion up to 0.6 g). This is consistent with the Ballard *et al.* explanation for the acceleration,

described above, which should apply irrespective of the method of radical generation used (*i.e.*, whether a chemical or radiolytic radical source is used).

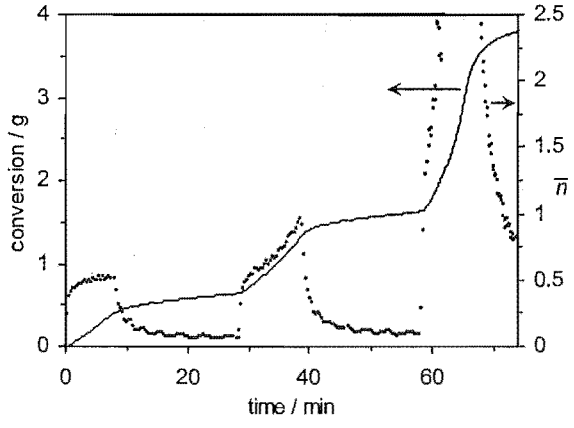

Figure 4.3. Conversion (line) and $\bar{n}$ (points) as functions of time for a γ-relaxation experiment at 50°C with γ-radiolysis dose rate of 146 Gy h^{-1} (run G32). Interval II period of polymerisation from 0 – 30 min.

The γ-radiolysis polymerisation data were fitted using the applicable form of the pseudo-bulk equation with $\alpha = 1$, equation (4.12). Integrating this equation together with equation (4.8) gives the following solutions for $\bar{n}$ and $\hat{x}$ as functions of time.

$$\bar{n} = \bar{n}_f \frac{Q \exp(2\delta t) - 1}{Q \exp(2\delta t) + 1} \tag{4.20}$$

$$\hat{x} = \frac{k_p [M]_p M_0 N_c V_w}{2 N_A c} \left[\ln\left|Q \exp(\delta t) + \exp(-\delta t)\right| - \ln\left|Q + 1\right| \right] \tag{4.21}$$

Here $Q = \frac{\bar{n}_f + \bar{n}_i}{\bar{n}_f - \bar{n}_i}$, $\delta = 2\, c\, \bar{n}_f$, and $\bar{n}_f = \left(\frac{\rho}{2\, c}\right)^{\frac{1}{2}}$. $\bar{n}_i$ and $\bar{n}_f$ denote the initial and final steady-state values of $\bar{n}$ respectively.

It is noted that these results have been presented elsewhere,[1] but without the modulus functions in equation (4.21) and, consequently, in a form that is only applicable to the approach to the in-source steady-state during an insertion into a γ-source. The form given above (including moduli) is, however, a general result applicable to the kinetics of both a γ-insertion or γ-relaxation, and (if so desired) also to the approach to steady-state for a chemically initiated polymerisation.

In the γ-relaxation case the system begins in its in-source steady-state (with $\overline{n}_i > 0$) and decays to the out-of-source steady-state, where only spontaneous polymerisation occurs. Therefore the value of ρ obtained from fitting corresponds to that from entry of spontaneously-generated radicals only, ρ_{spont}, and the final value of $\overline{n}$ is that associated with spontaneous polymerisation, $\overline{n}_{spont}$.

Values for ρ_{spont} and c were obtained by non-linear least-squares fitting of equation (4.21) to the experimental conversion-time data obtained immediately after removal of the system from the γ-source. It was found that equation (4.21) gave a precise fit to the data, suggesting that the underlying kinetic model is appropriate. The value of $\langle k_t \rangle$ was then calculated from c. These average values are presented in Table 4.3 along with experimental uncertainties estimated from the two measurements. Alternatively, equation (4.20) could have been fitted to the experimental $\overline{n}$ data; however a disadvantage of this approach is that these first-derivative data typically bear a greater degree of scatter. It is noted that equations (4.20) and (4.21) assume a constant value of $[M]_p$. Furthermore, termination is thought to be a diffusion-controlled reaction, hence the values of $\langle k_t \rangle$ and c will be affected, *inter alia*, by the viscosity of the latex particle interior and therefore sensitive to changes in the weight fraction of polymer (w_p) inside the particles. As such, the only data used for analysis of radical loss kinetics were those from the first relaxation in each experiment, commencing in Interval II where the values of both $[M]_p$ (6.9 M) and w_p (0.30) are approximately constant due to the presence of excess monomer.

Table 4.3. Results obtained from fitting of kinetic data for γ-relaxation of MMA at 50°C.

c / s^{-1}	$\langle k_t \rangle^{\dagger}$ / M^{-1} s^{-1}	$\overline{n}_{spont}$	ρ_{spont} / s^{-1}
$(2.4 \pm 0.1) \times 10^{-2}$	$(1.9 \pm 0.1) \times 10^{4}$	0.074 ± 0.007	$(1.5 \pm 0.1) \times 10^{-4}$

† Value of $\langle k_t \rangle$ calculated according to equation (4.11) using tabulated value of c and swollen particle volume at the start of the steady-state period, $V_s^0 = 1.3 \times 10^{-18}$ dm^{-3}.

4.5.2 *Chemically Initiated Experiments*

Polymerisation rate data were obtained using dilatometry from chemically initiated (KPS) seeded emulsion polymerisations of MMA at 50°C over a range of initiator concentrations. As has been observed previously,[1] a feature of these data was the absence of a constant rate of polymerisation during Interval II of polymerisation. This is exemplified by Figure 4.4, wherein the average number of radicals per particle, $\bar{n}$, has been calculated from the rate according to equation (4.8) and plotted as a function of time.

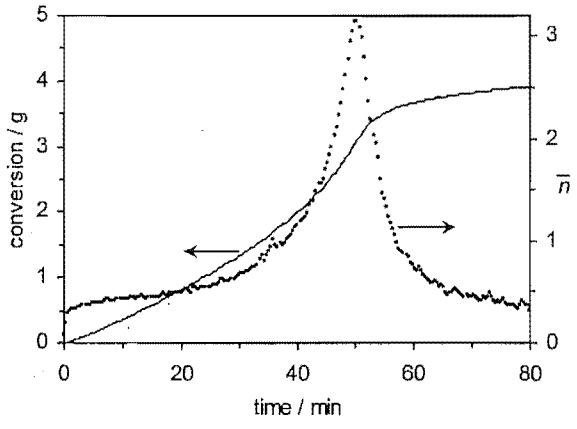

Figure 4.4. Conversion (line) and $\bar{n}$ (points) as functions of time for a chemically initiated seeded emulsion polymerisation of MMA at 50°C with [KPS] = 1 mM (run C50). Interval II period of polymerisation from 0 – 17 min.

Although a constant value of $\bar{n}$ is never attained, it is apparent that after an initial rapid increase (a consequence of all particles being devoid of radicals at the start of a seeded polymerisation), $\bar{n}$ is seen to increase relatively slowly with increasing time (and conversion) over the course of Interval II.

As discussed above, the existing theory accounts for this acceleration behaviour in terms of the particle volume dependence of the value of $\bar{n}$ through Interval II, and Ballard *et al.* put forward values of the acceleration measured experimentally as evidence in support of this hypothesis. A selection of their results is presented in Figure 4.5, along with the ("exact") value of $\bar{a} = 0.42$ calculated earlier from theory with $m_p^0 = 0.85$ g and $\hat{x} \leq 0.7$ g (consistent with the conditions used in the present chemically initiated experiments). Conveniently, this theoretical value of $\bar{a} = 0.42$ was also found from model calculations to be approximately applicable to the experimental conditions of Ballard *et al.*[1] (*viz.*, $m_p^0 \approx 1.8$ g and conversion up

to ~ 1.3 g). Despite a significant degree of scatter in these experimental results it is clear that at low initiator concentration the value of $\bar{a}$ is close to the predicted result. However, several values of $\bar{a}$ well above 0.5 were obtained at higher initiator concentrations. According to Ballard *et al.* this deviation from the theoretical value may be explained in terms of a so-called "monomer starvation" effect. They suggested that at high initiator concentrations the rate of monomer consumption inside the latex particles might exceed the rate at which monomer is replenished by diffusion from monomer droplets in the aqueous phase. Under these non-equilibrium conditions the polymer concentration in the particles gradually increases, leading to a reduction in the (diffusion-controlled) rate of termination and hence an enhanced rate of increase in $\bar{n}$.

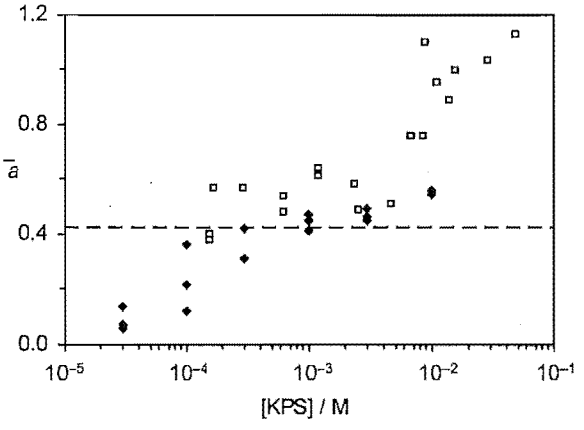

Figure 4.5. $\bar{a}$ as a function of initiator (KPS) concentration from chemically initiated runs at 50°C. Experimental data from both the present study (filled diamonds) as well as from Ballard *et al.*[1] (empty squares) are shown along with the exact value for the acceleration from theory of $\bar{a} = 0.42$ (dashed line).

In order to further test the conclusions of Ballard *et al.*, the acceleration was measured for all the experiments in the present study in the same way as the earlier work, using a linear fit to the value of $\bar{n}$ over the entire steady-state region of Interval II (as illustrated in Figure 4.6), and calculating $\bar{a}$ according to equation (4.15). The results are presented graphically in Figure 4.5, and the values for both $\bar{a}$ and $\bar{n}_0$ obtained from each experiment are also given in Table 4.4.

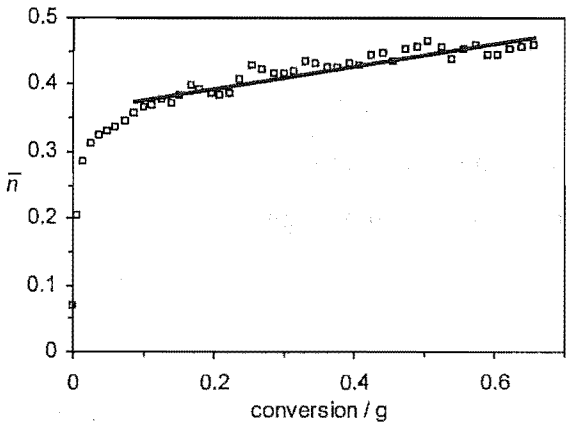

Figure 4.6. $\bar{n}$ as a function of conversion for Interval II of a chemically initiated seeded emulsion polymerisation of MMA at 50°C with [KPS] = 1 mM (run C50); experimental data (squares) and linear fit to steady-state region (line). Fitting gives $\bar{n}_0 = 0.376$ and $\bar{a} = 0.41$.

While the values of $\bar{a}$ measured from experiment in the present study appear to show excellent agreement with the theoretical value of $\bar{a}$ = 0.42 at intermediate initiator concentrations (remember that $\bar{a}$ is essentially a scond derivative of the experimental data, so it cannot be expected to be precisely 0.42), there appears to be a general trend of increasing acceleration with increasing initiator concentration. At the highest initiator concentration used in the present experiments, 10 mM, the measured acceleration is slightly above the theoretical value, while at the lowest initiator concentration of 0.03 mM the acceleration is well below the theoretical value. In line with this trend was the finding that in experiments with no added initiator (so-called spontaneous polymerisation) the acceleration was negligible (within experimental error), as detailed in Table 4.4.

Comparing the experimental data from the earlier work of Ballard *et al.* with that of the present study, it is interesting to note that although there is scatter in both sets of results (there is appreciably less in the present work due to the more precise dilatometric procedures), all data appear to follow a consistent trend of increasing acceleration with increasing initiator concentration; reasonable accord with the (constant) theoretical acceleration value is only seen in the region of intermediate initiator concentration (*ca.* 1 mM).

Table 4.4. Results obtained from kinetic experiments using chemical initiator (KPS), with ρ calculated from equation (4.22) using values of $\bar{n}$ and c at the start of the steady-state period.

Run	[KPS] / 10^{-3} M	$\bar{n}_0$	$\bar{a}$	ρ_0 / 10^{-4} s^{-1}
C80	0	0.070	0.025	2.3
C88	0	0.10	–0.070	4.9
C54	0.030	0.11	0.14	5.8
C61	0.030	0.13	0.073	8.0
C101	0.030	0.14	0.061	8.7
C52	0.10	0.17	0.36	14
C68	0.10	0.17	0.13	13
C102	0.10	0.19	0.22	16
C69	0.30	0.26	0.42	29
C62	0.30	0.27	0.32	32
C73	1.0	0.33	0.47	50
C67	1.0	0.34	0.45	52
C66	1.0	0.35	0.47	54
C50	1.0	0.38	0.41	62
C72	3.0	0.45	0.49	92
C55	3.0	0.45	0.46	89
C70	3.0	0.46	0.45	98
C56	9.9	0.55	0.56	138
C58	9.9	0.58	0.55	152

The above results for the acceleration immediately bring into question the simple approach of treating data from chemically initiated experiments using the pseudo-bulk equation with α = 1. Nevertheless, it is instructive at this stage to complete the analysis by calculating values

for ρ using the steady-state solution to equation (4.12). Rearranging equation (4.13), ρ may be calculated as follows,

$$\rho = 2\,c\,\bar{n}^2 \qquad (4.22)$$

Hence, for each experiment the value of $\bar{n}_0$ was used together with the associated value of c_0 at the start of the steady-state period to calculate a value, ρ_0. Results are presented in Table 4.4.

4.6 Development of Data Analysis

As a first approximation, it has been assumed that the polymerisation kinetics are fully described by equation (4.12), the pseudo-bulk equation with $\alpha = 1$, leading to the results presented in Tables 4.3 and 4.4. While this kinetic treatment is known to be adequate for the case of a γ-relaxation experiment,[1] no such assurance exists for the case of chemical initiation. Indeed, the data presented above for the acceleration suggest that this approach does not fully account for the data and, ultimately, cast uncertainty on the values of ρ presented in Table 4.4. The degree of this uncertainty is illustrated for one experiment in Figure 4.7, where ρ has once again been calculated using equation (4.22). However, in this case ρ was calculated as a function of conversion over all of Interval II using the measured values of $\bar{n}$ and the volume dependent value of c [from equation (4.11)] at each point, a process which automatically (and exactly) accounts for the acceleration in rate due to increasing particle volume.

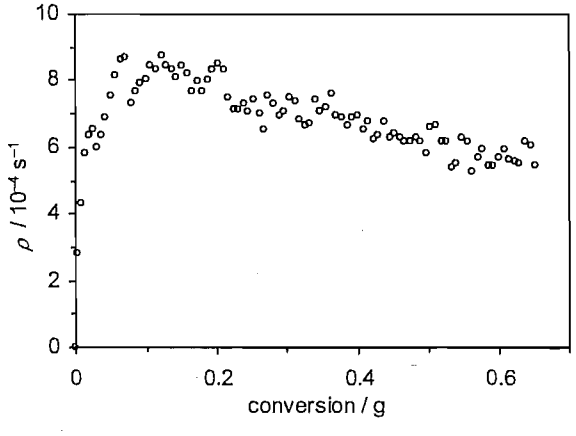

Figure 4.7. ρ obtained as a function of conversion from Interval II of a chemically initiated seeded emulsion polymerisation of MMA at 50°C with [KPS] = 0.03 mM (run C101) according to the pseudo-bulk equation with $\alpha = 1$ [equation (4.22)].

Implicit in the kinetic treatment used thus far is the assumption of constant ρ during Interval II. However, Figure 4.7 clearly shows a decrease of 30 – 40% in the value of ρ over Interval II in this case. It is apparent that the only experiments for which the value of ρ obtained will be constant over Interval II are those where the acceleration matches the theoretical value, *i.e.*, experiments with [KPS] ~ 10^{-3}. Also, the value of ρ calculated in Table 4.4 from the values of $\bar{n}$ and c at the start of the steady-state period will, in fact, be an upper bound for ρ at low initiator concentration, and a lower bound at high initiator concentration.

Having identified the limitations of the approach of using the pseudo-bulk equation with $\alpha = 1$, an improved kinetic treatment is now sought. The procedure here focuses on the observed trend in $\bar{a}$ as a function of initiator concentration (see Figure 4.5). The fundamental reasoning is that *any kinetic theory that predicts values of $\bar{a}$ in closer accord with these results may similarly be assumed to provide more reliable values for ρ.*

Considering the experimental acceleration data in Figure 4.5, it is possible that the values of $\bar{a}$ measured to be slightly above the theoretical value of 0.42 in the present study may be reconciled in terms of a small effect from "monomer starvation" at high initiator concentrations – following the original postulate of Ballard *et al.* That said, this explanation is unsatisfactory in that it is impossible to quantify, *i.e.*, one has to accept on faith that it quantitatively explains the data. More difficult to explain, however, are the low accelerations measured at low initiator concentrations. In the following sections we detail the methodology and results of several different attempts to account for this trend.

4.6.1 Pseudo-Bulk Equation with $\alpha = 1$, Variations in Parameter Values

As a starting point, we examine the parameters in equation (4.17) that affect the evolution of $\bar{n}$ and attempt to rationalise the observed variation in $\bar{a}$ in terms of an unacknowledged deviation in the value of one or more of these parameters.

a. Entry rate coefficient. Given that the value of ρ is assumed to be constant throughout the steady-state period, a lower than expected acceleration could reflect a real decrease in the value of ρ that is not currently accounted for (*e.g.* of the form illustrated in Figure 4.7).

Since the value of ρ_{init}, and hence ρ, is critically related to the initiator concentration, one possible explanation is a decrease in initiator concentration over time. Such an effect

would also be consistent with the fact that the experiments at lowest initiator concentration (0.03 mM), exhibiting the lowest acceleration, have a steady-state period of much longer duration (~ 60 minutes) than the higher initiator concentration experiments (*e.g.*, [KPS] = 10 mM where the steady-state period lasts only ~ 10 minutes). However, this explanation is unlikely since the first-order rate coefficient for decomposition of KPS at 50°C is 1.1×10^{-6} s^{-1},[16] giving a decrease in initiator concentration of less than 0.5% over 60 minutes. However, in the event that some other reaction was also consuming initiator, for example induced decomposition (as is seen in the case of vinyl acetate polymerisations[17]), the above suggestion might not be ruled out. Of course, this initiator consumption idea can only explain a reduction in $\bar{a}$, not an increase, and it would be highly coincidental that at just the initiator concentration at which this effect stopped operating, a different effect which causes the opposite behaviour, *i.e.*, increased $\bar{a}$, started (see Figure 4.5).

Another possible explanation may lie in the nature of entry from spontaneously-generated radicals and the dependence of this phenomenon on time and/or conversion. Since equation (4.9) assumes constant ρ_{spont}, a decrease in this value over the course of Interval II would undoubtedly result in a lower than expected value of $\bar{a}$. It is recalled that $\bar{a}$ is approximately zero for experiments with no added initiator, *i.e.*, $\bar{n}$ is constant over Interval II in this case. Assuming for now that $\langle k_t \rangle$ is invariant, equation (4.13) then requires a constant value of the product ρV_s. One may therefore postulate that ρ_{spont} is a volume dependent quantity which decreases over the Interval II steady-state period from some starting value, ρ^0_{spont}, according to $\rho_{spont} = \rho^0_{spont} V^0_s / V_s$. In order to estimate the effect on the acceleration, this new expression for ρ_{spont} may be combined with equations (4.9) and (4.13) to calculate model data for $\bar{n}$ as a function of conversion, and hence the value of $\bar{a}$, under a range of conditions. Here we use the same representative parameter values as earlier: $\hat{x}$ up to 0.7 g, $m^0_p = 0.85$ g, $V^0_s = 1.3 \times 10^{-18}$ dm^3, $\langle k_t \rangle = 1.9 \times 10^4$ M^{-1} s^{-1}. The value of ρ^0_{spont} is set to 6×10^{-4} s^{-1} and ρ_{init} is varied over the range 1×10^{-5} to 3×10^{-2} s^{-1}. The model values of $\bar{a}$ obtained are presented as a function of $\bar{n}_0$ in Figure 4.8, together with the values of $\bar{a}$ measured experimentally (shown for comparison).

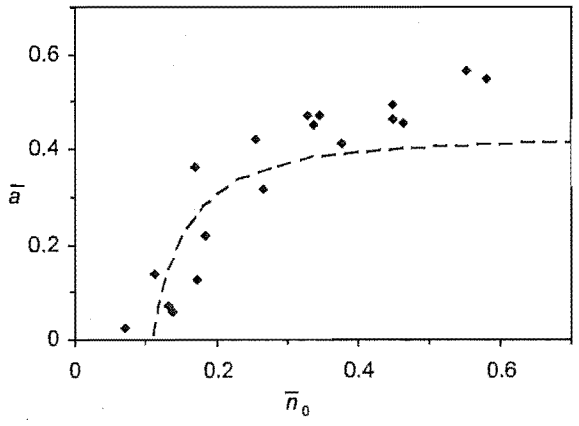

Figure 4.8. Model values of $\bar{a}$ (dashed line) presented as a function of $\bar{n}_0$, illustrating the possible effects of a volume dependent value of ρ_{spont} on the acceleration (parameter values given in text); experimental $\bar{a}$ data (diamonds) also presented for comparison.

Clearly, the volume dependent value of ρ_{spont} causes a significant reduction in modelled $\bar{a}$ towards low ρ (and low $\bar{n}_0$). Moreover, it is seen that using a physically plausible value for ρ^0_{spont} these simple calculations are able to provide excellent accord with experimental data.

Unfortunately, while these simple model results may appear encouraging it is emphasised that the explanation for low measured $\bar{a}$ values postulated above can ultimately be verified only by a detailed understanding of spontaneous polymerisation, which is beyond the scope of this investigation. Moreover, it is difficult to conceive of any physical explanation for an inverse dependence of ρ_{spont} on particle volume. One possibility is the gradual exhaustion of the (unknown) source of spontaneous radicals; however, in this event it would be highly coincidental that the effect is so well described by a $1/V_s$ dependence.

b. Bimolecular termination rate coefficient. Given that the value of $\langle k_t \rangle$ is also assumed to be constant during the steady-state period, a lower than expected acceleration could reflect a gradual increase in the value of $\langle k_t \rangle$. This explanation gains impetus when it is considered that the value of $\langle k_t \rangle$ is now understood to be dependent on the chain length distribution of the radicals in the system.[18,19] In the present case, one might expect the increase in the value of $\bar{n}$ to be accompanied by a general shift of this distribution towards short radical chain lengths, resulting in an increase in the value of $\langle k_t \rangle$. While this

suggested explanation is consistent with the data, it will presently be shown that the true effect of chain length dependent termination is somewhat different to that predicted above, and moreover the magnitude of this effect alone is likely to be far too small to account for the $\bar{a}$ values measured. Further, this idea also cannot explain why some $\bar{a}$ are greater than expected.

c. Swollen particle volume. A lower than expected acceleration could equally be due to a change in the value of V_s that has not been accounted for. For example, we assume that the monomer concentration inside the particles remains constant throughout the experiment at the value used to calculate the swollen volume at the start of the steady-state period (according to $V_s^0 = \frac{d_M}{d_M - [M]_p M_0} \frac{m_p^0}{d_p}$). If the value of $[M]_p$ was to decrease slightly as the latex particles increase in size during the steady-state period, the associated effect on the swollen particle volume may be sufficient to explain the low acceleration observed in some cases. However, this explanation opens a can of worms, because if $[M]_p$ is changing then the calculated $\bar{n}$ values are incorrect, meaning that $\bar{a}$ is, in fact, not as it seems. Further, this explanation alone cannot explain all the data since the change in particle size is the same in all the experiments. Thus any effect on acceleration from a change in $[M]_p$ (and hence V_s) should affect all experiments equally and does not allow for the variation in $\bar{a}$ with changing initiator concentration. Finally, it is noted that the Morton equation[20] predicts $[M]_p$ to increase with increasing particle size – not decrease as has been speculated here. Nonetheless this raises an interesting question: how would kinetics (deduced assuming constant $[M]_p$, swollen volume, *etc.*) be affected if $[M]_p$ actually increases during Interval II?

While some degree of explanation for the unexpected trend in experimental $\bar{a}$ values may be afforded by one or more of the above effects, it is difficult to attest which (if any) of these could provide a comprehensive account of the data. We therefore next consider the possibility that one or more of the fundamental kinetic assumptions leading to equation (4.12) is erroneous. Specifically we will examine the effects of: incomplete re-entry of exited radicals, chain length dependence of intra-particle termination reactions, and compartmentalisation of radicals into distinct latex particles.

4.6.2 Pseudo-Bulk Equation, Departure from $\alpha = 1$

While the pseudo-bulk equation with $\alpha = 1$, and hence the assumption of complete re-entry of exited radicals, is likely to be applicable to the case of a γ-relaxation experiment, it is questionable whether this assumption is accurate in the case of chemically initiated experiments. Here it is necessary to consider the fact that increasing initiator concentration gives rise to a higher aqueous-phase radical flux, and thus an increased probability of aqueous-phase termination of an exited radical. Any such significant termination will result in a value of α less than one. This would not appear to present any great problem in that one may simply resort to solving the full pseudo-bulk equation, (4.10), which incorporates α. However, in practice this approach suffers two limitations which bear discussion.

Firstly, equation (4.10) includes four kinetic parameters: ρ, c, k and α. Of these only the value of c has been determined independently by γ-relaxation experiments, leaving three parameters unknown. Experimental data in this case comprise the evolution of $\overline{n}$ as a function of conversion from chemically initiated experiments, effectively providing values for two observables: the overall magnitude of $\overline{n}$ and its rate of increase with conversion, *i.e.*, the acceleration, $\overline{a}$. Thus it is possible to determine the values of, at most, two out of ρ, k and α. In fact, unique determination of all 3 is impossible anyway, for the form of equation (4.10) only allows determination of ρ and the coupled term $(1 - \alpha)k$. Since the value of the exit rate coefficient, k, may be estimated from existing theories[21-24] (at least to within a factor of 4), it is then most logical to extract a value for α based on a calculated value for k. However, the authenticity of these "experimental" α values depends entirely on the accuracy of the exit model used.

Secondly, it is apparent that the parameter α, while being easy to wield, represents a complex encapsulation of several microscopic kinetic events, including adsorption, desorption and aqueous-phase propagation and termination. Furthermore, except in the cases of the limiting values of α (1 and –1), this parameter must itself be a function of the aqueous-phase radical concentration, and hence also of $\overline{n}$, thus introducing a non-linearity to equation (4.10). However, the existing kinetic treatment offers no straightforward means for relating the value of α to microscopic rate coefficients or the value of $\overline{n}$. Further, in any one experiment the change in $\overline{n}$ is small, so it is reasonable to assume that α should be constant for a given experiment, even if it changes from one experiment to another. However, what this really

emphasises is that for values other than 1 and –1, α lacks rigorous physical meaning, and in this sense is an unsatisfactory parameter.

Table 4.5. Results obtained from non-linear least-squares fitting of equation (4.10) to data from kinetic experiments using chemical initiator (KPS) with c from equation (4.11); α calculated using k from equation (4.25).

Run	[KPS] / 10^{-3} M	$\bar{a}_{expt}$†	$\bar{a}_{fitted}$	$(1-\alpha)k$ / 10^{-3} s^{-1}	ρ / 10^{-4} s^{-1}	α
C54	0.030	0.14	0.15	14	22	0.945
C61	0.030	0.073	0.084	35	54	0.864
C101	0.030	0.061	0.065	49	77	0.807
C52	0.10	0.36	0.37	2.0	17	0.992
C68	0.10	0.13	0.14	24	54	0.908
C102	0.10	0.22	0.22	12	37	0.955
C69	0.30	0.42	0.42	0.61	30	0.998
C62	0.30	0.32	0.32	6.6	49	0.974
C73	1.0	0.47	0.43	0	50	1.000
C67	1.0	0.45	0.43	0	52	1.000
C66	1.0	0.47	0.44	0	55	1.000
C50	1.0	0.41	0.42	1.2	66	0.995
C72	3.0	0.49	0.43	0	94	1.000
C55	3.0	0.46	0.44	0	90	1.000
C70	3.0	0.45	0.43	0	98	1.000
C56	9.9	0.56	0.44	0	147	1.000
C58	9.9	0.55	0.44	0	160	1.000

† Values of $\bar{a}_{expt}$ taken from Table 4.4.

In view of these facts it is unwise to overestimate the worth of α as a true kinetic parameter. However, cautious use of equation (4.10) may provide useful insights into how generally applicable the pseudo-bulk equation is.

The steady-state solution to equation (4.10), a quadratic equation in $\bar{n}$, was non-linear least-squares fitted to the data for $\bar{n}$ as a function of conversion from each chemically initiated experiment, with ρ and $(1 - \alpha)k$ as adjustable fitting parameters. The value of $c(\hat{x})$ was predetermined in each case using the data in Table 4.3 and the volume dependence of equation (4.11). The values of ρ and $(1 - \alpha)k$ obtained in each case are presented in Table 4.5.

Also presented in Table 4.5 are the values of $\bar{a}$ calculated in each case from data fitting using the method of equation (4.15) as earlier. Comparing the values of $\bar{a}_{\text{fitted}}$ with $\bar{a}_{\text{expt}}$ (the experimental data of Table 4.4) it is evident that if the value of α is allowed to vary from unity it is possible to accurately model the low accelerations observed at low [KPS]. However, it is noted that the values of $\bar{a}_{\text{fitted}}$ obtained at highest [KPS] show poorer agreement with $\bar{a}_{\text{expt}}$, corresponding to a comparatively poor fit to the steady-state $\bar{n}(\hat{x})$ data [also see Figures 4.11 (a) and (b) presented shortly].

The allowance for $\alpha < 1$ also means that, unlike the earlier analysis, the value of ρ obtained from fitting at low [KPS] is not subject to any systematic variation with conversion, as is illustrated in Figure 4.9 for the same experiment (run C101) as earlier.

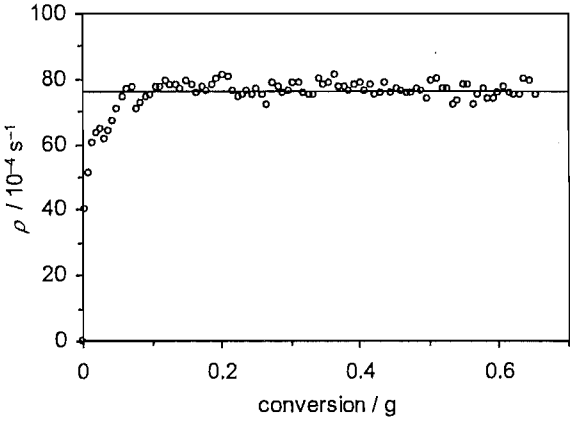

Figure 4.9. ρ obtained as a function of conversion from Interval II of a chemically initiated seeded emulsion polymerisation of MMA at 50°C with [KPS] = 0.03 mM (run C101) according to the equation (4.23) with (1 –

$\alpha)k = 5.1 \times 10^{-2}$ s^{-1} (circles); the value of $\rho = 7.6 \times 10^{-3}$ s^{-1} obtained from least-squares fitting is also presented (line).

Here ρ is evaluated according to equation (4.23) [obtained from the steady-state solution to equation (4.10)] using the values of ρ and $(1 - \alpha)k$ from data fitting together with experimental $\bar{n}$ data and c from γ-relaxation.

$$\rho = (1 - \alpha)k\bar{n} - 2c\bar{n}^2 \tag{4.23}$$

It is evident that the value of ρ calculated in this way is relatively constant and in good accord with the value from least-squares fitting over all of Interval II. However, it should also be realised that in the case of low [KPS], a relatively high value of the $(1 - \alpha)k$ term in equation (4.23) – corresponding to a high incidence of radical loss by exit – is required to obtain good fit to experimental data. This gives rise to a considerable increase in the value of ρ at low [KPS] compared with earlier fitting with $\alpha = 1$ (*e.g.*, compare Figures 4.7 and 4.9).

Interpreting $(1 - \alpha)k$ values

As intimated above, the value of $(1 - \alpha)k$ from each experiment may yield a value for the parameter α if a suitable means is known for estimating k. As described in Chapter 1, a simple derivation assuming that exit is by monomeric radicals with diffusion away from the particle as the rate-determining step gives the following expression for k (equation 1.6 of Chapter 1):

$$k = k_{tr}[M]_p \frac{k_{dM}}{k_{dM} + k_p^1[M]_p} \tag{4.24}$$

where k_{dM} = rate coefficient for monomer desorption, k_{tr} = rate coefficient for transfer to monomer, and k_p^1 = propagation rate coefficient for a monomeric radical.

The above expression was also shown to give two limiting forms for k. When the frequency of desorption is much greater than that of propagation ($k_{dM} \gg k_p^1[M]_p$):

$$k = k_{tr}[M]_p \tag{4.25}$$

Alternatively, if propagation is much more likely than desorption ($k_p^1[M]_p \gg k_{dM}$), equation (4.24) gives:

$$k = \frac{k_{tr}\, k_{dM}}{k_p^1} \tag{4.26}$$

Having established two limits for the value of k, it is necessary to consider which of these is best applied to the present system. The value of k_{dM} may be calculated according to equation (4.27), derivations for which are available in the literature[12,21] and in Appendix A.5.

$$k_{dM} = \frac{3D_w[M]_w}{r_s^{\,2}[M]_p} \tag{4.27}$$

Values of k_{dM} calculated as a function of swollen particle radius, with the diffusion coefficient for monomer in water, $D_w = 1.7 \times 10^{-9}$ m^2 s^{-1},[25] $[M]_w = 0.15$ M,[1] and the measured value of $[M]_p = 6.9$ M, are presented in Figure 4.10. Also presented are limiting values for $k_p^1[M]_p$ calculated using literature data for k_p^1. There exists both theoretical[26] and experimental evidence[12,27,28] to suggest that the value of k_p^1 is significantly greater than the long chain value of k_p – perhaps even in the order of $k_p^1 \approx 15\ k_p$.[26,28] Consequently, in Figure 4.10 two values of $k_p^1[M]_p$ are presented: one a lower bound obtained using $k_p^1 = k_p$, the other an upper bound obtained using $k_p^1 = 15\ k_p$.[26,28]

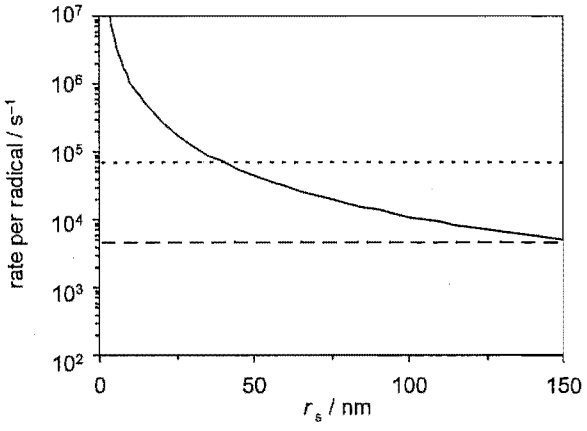

Figure 4.10. Rates of desorption and propagation calculated per radical for monomeric radicals inside an MMA latex particle and presented as a function of swollen particle radius; k_{dM} represented as (———), $k_p^1[M]_p = k_p[M]_p$ represented as (– – – –), $k_p^1[M]_p = 15\ k_p[M]_p$ represented as (- - - - -).

For the present system the swollen particle radius is approximately 68 nm. Therefore, from Figure 4.10 it is apparent that taking the lower bound value for k_p^1 gives desorption as the most likely fate of a monomeric radical, whereas if k_p^1 takes its upper bound value propagation is the more probable fate. Given a degree of uncertainty in the value of k_p^1 it becomes necessary to consider both these limits, and hence to calculate k using both equations (4.25) and (4.26).

Values of α calculated for each experiment using the value of $(1 - \alpha)k$ from fitting together with k from equation (4.25), are presented in Table 4.5. Here the value $k_{tr} = 5.7 \times 10^{-5}\ k_p = 3.7 \times 10^{-2}\ M^{-1}\ s^{-1}$ was used for the rate coefficient for transfer to monomer in calculating k. This value, reported for the emulsion polymerisation of MMA at 50°C,[29] is thought to be more suitable for the present study than lower values reported for bulk polymerisations,[30] given that emulsion polymerisation systems consist of a mixture of ingredients and the presence of trace amounts of "adventitious impurities" capable of acting as chain transfer agents may not be ruled out.

The values of α obtained above appear to be physically reasonable and, moreover, they show a general trend, increasing with initiator concentration until $\alpha = 1$ is reached. However, the physical interpretation of this data is somewhat problematic. The values of $\alpha < 1$ at lowest [KPS] indicate that re-entry of exited radicals is less than 100% due to aqueous-phase termination, whereas at higher [KPS], $\alpha = 1$ suggests that re-entry is complete under these conditions. This trend is contrary to what one might expect, given that an increase in initiator concentration raises the aqueous radical concentration and hence also the probability of aqueous-phase termination.

It remains to consider the other limiting case for k represented by equation (4.26), and the values of ρ and α obtained when this form is used. Here it is noted that the value of k_{dM} given by equation (4.27) shows a dependence on particle radius. The values of both k_{dM} and k must therefore change with conversion, which will in turn affect the evolution of $\bar{n}$ (*i.e.*, the acceleration) during Interval II. As a result of this complication re-fitting of the data from each experiment using the following procedure was necessary. The steady-state solution to equation (4.10) was once again non-linear least-squares fitted to the experimental data for $\bar{n}(\hat{x})$, this time with ρ and α as the only adjustable parameters. The value of c was calculated according to the volume dependence of equation (4.11) and the value of k was calculated as a

function of conversion according to equations (4.26) and (4.27), with $k_p^1 = 15$ $k_p = 9742$ M^{-1} s^{-1} and other parameter values as quoted above in the text and Table 4.3. The results obtained for each experiment are presented in Table 4.6.

Table 4.6. Results obtained from non-linear least-squares fitting of equation (4.10) to data from kinetic experiments using chemical initiator (KPS) with c from equation (4.11) and k from equations (4.26) and (4.27).

Run	[KPS] / 10^{-3} M	$\bar{a}_{expt}$†	$\bar{a}_{fitted}$	ρ / 10^{-4} s^{-1}	α
C54	0.030	0.14	0.44	4.9	1.000
C61	0.030	0.073	0.43	6.5	1.000
C101	0.030	0.061	0.43	6.9	1.000
C52	0.10	0.36	0.43	13	1.000
C68	0.10	0.13	0.43	11	1.000
C102	0.10	0.22	0.43	14	1.000
C69	0.30	0.42	0.44	28	1.000
C62	0.30	0.32	0.43	30	1.000
C73	1.0	0.47	0.48	90	0.857
C67	1.0	0.45	0.46	73	0.926
C66	1.0	0.47	0.48	91	0.873
C50	1.0	0.41	0.44	61	1.000
C72	3.0	0.49	0.50	217	0.674
C55	3.0	0.46	0.46	122	0.913
C70	3.0	0.45	0.46	137	0.900
C56	9.9	0.56	0.57	1064	–0.942
C58	9.9	0.55	0.56	928	–0.557

Comparing the values of $\bar{a}_{fitted}$ and $\bar{a}_{expt}$ in Table 4.6 it is evident that, contrary to the earlier limiting case, when some radical loss *via* exit is introduced with the radius dependent value of

k from equation (4.26) it is possible to accurately model the accelerations observed for experiments with [KPS] ≥ 1 mM; however the experimental values of $\bar{a}$ at low initiator concentration are not accounted for. Interestingly, this indicates that the combination of the radius dependent second-order (in $\bar{n}$) termination process with the radius dependent first-order exit loss process must in fact give rise to a higher limiting acceleration than that due to loss by termination alone.

As before the α values obtained from fitting are reasonable and follow a consistent trend; however in this case the physical interpretation is somewhat clearer. The value of $\alpha = 1$ obtained for experiments with [KPS] ≤ 3 mM indicates complete re-entry of all exited radicals and is consistent with the aqueous-phase radical concentration being relatively low. Towards higher [KPS] the value of α is seen to decrease below one. This is consistent with there being less than 100% re-entry of exited radicals due to some termination occurring at higher aqueous phase radical concentrations. The values of $\alpha < 0$ obtained from fitting of the highest [KPS] experiments are consistent with (and indeed only possible if there is) significant hetero-termination between exited monomeric radicals and initiator-derived radicals in the aqueous phase.

However, it should be reiterated that in several cases experimental acceleration values of $\bar{a} <$ 0.42 were not accurately reproduced by the fitted results, even with $\alpha = 1$, reflecting comparatively poor fitting of steady-state $\bar{n}(\hat{x})$ data obtained at low [KPS]. A less adequate data fit of this sort is illustrated as the dashed line in Figure 4.11 (a), and may be compared with a good data fit obtained at high [KPS] in Figure 4.11 (b) (also a dashed line).

Also shown in Figures 4.11 (a) and (b) are exemplary data fits (solid lines) for the same experiments using the earlier fitting approach which assumed radius independent k. It is recalled in that case that the data fit obtained was best at low [KPS] and comparatively poor at high [KPS].

Finally, it is also worth noting that all existing information[26-28,31] on chain length dependent propagation suggests that $k_p^1 = 15\ k_p$ is much more likely for MMA than $k_p^1 = k_p$, *i.e.*, that the second exit limit used here is more likely.

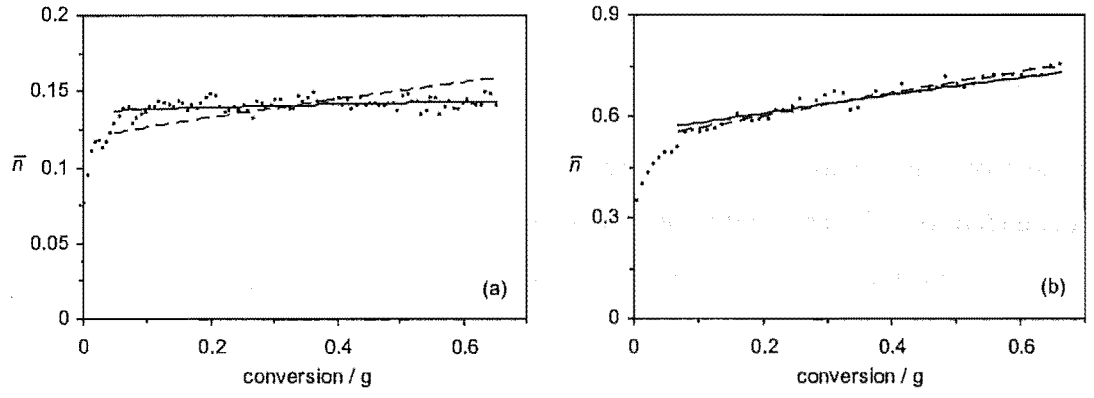

Figure 4.11. Exemplary non-linear fitting of equation (4.10) to data from kinetic experiments (points) using chemical initiator (KPS), assuming either radius independent k (———), or k as given by equations (4.26) and (4.27) (– – – –); **(a)** experiment with [KPS] = 0.03 mM (run C101); **(b)** experiment with [KPS] = 10 mM (run C56).

Summarising the results obtained in this section, it is clear that allowing α to take values less than one in pseudo-bulk modelling provides significant improvement to the fitting of experimental acceleration data in several cases and is therefore a useful first step in our analysis. However, it is seen that the exact nature of this improvement is strongly dependent on the assumed model for exit and, moreover, no particular model affords a comprehensive improvement to data fitting for all experiments. Finally, it is noted that while results obtained with varying α are certainly of interest in terms of a pure data fitting exercise, this approach is severely limited with regard to the goal of advancing the mechanistic understanding of this system. Since α cannot be interpreted in terms of microscopic rate coefficients and concentrations of reacting species, it is not possible to infer any definitive physical meaning from trends observed in the values of α or $(1 - \alpha)k$.

4.6.3 Chain Length Dependent Termination

Negligible reaction of exited radicals in the aqueous-phase

Up until this point it has been assumed that the rate coefficients for all radical reactions are independent of the degree of polymerisation of the reacting radical(s). However, this convenient assumption is unlikely to be accurate in all cases. In particular, the rate of the termination reaction involving two radical chains is determined by the rate at which these radicals diffuse through the reaction medium; since radical diffusion rates are related to the degree of polymerisation, so must the rate of termination be. The aim of this section is

therefore to determine the effect that this assumption of chain length independent termination has on the analysis of kinetic data from the present study.

Here the approach is to carry out modelling based on a kinetic scheme that incorporates chain length dependent (CLD) termination and compare the results obtained with those from chain length independent (CLI) modelling, within the confines of the pseudo-bulk equation, (4.10). A methodology for modelling polymerisation kinetics with chain length dependent termination has been established by Russell *et al.*[18,19] This model finds its origins in the pseudo-bulk model, but is a significantly more complete treatment, a fundamental point of difference being the value of the termination rate coefficient, $\langle k_t \rangle$, defined as an average over all chain lengths as follows:

$$\langle k_t \rangle = \sum_{i=1}^{\infty} \sum_{j=1}^{\infty} k_t^{i,j} \frac{n_i}{\bar{n}} \frac{n_j}{\bar{n}} \tag{4.28}$$

Here n_i and n_j are the average number of radicals of degree of polymerisation i and j respectively per latex particle, and $\bar{n}$ is the average total number of radicals per particle (*i.e.*, the sum of n_i over all chain lengths i). The rate coefficient $k_t^{i,j}$ is defined as the microscopic rate coefficient for a particular termination reaction between a pair of radicals of chain lengths i and of j, thus allowing for the possibility of chain length dependent termination.

The pseudo-bulk modelling presented thus far, assuming chain length independent termination, may be manifested mathematically by stipulating a constant value for $k_t^{i,j}$ in equation (4.28), and thus a value of $\langle k_t \rangle$ that is unresponsive to the particular values of n_i and n_j. If we now consider the case where $k_t^{i,j}$ varies with i and j, the value of $\langle k_t \rangle$ may only be calculated from a detailed knowledge of the values of $k_t^{i,j}$ and all n_i. Since termination is diffusion-controlled, in the present case an expression for $k_t^{i,j}$ may be derived using the Smoluchowski equation, which gives,

$$k_t^{i,j} = 2\pi\sigma p_{spin}(D_i + D_j)N_A \tag{4.29}$$

where σ is the interaction radius for radical-radical reaction, p_{spin} is the probability of radical reaction based on spin alignments, and D_i and D_j are the diffusion coefficients for radicals of chain length i and j respectively (see Appendix A.1 for further details regarding the definition of termination rate coefficients). The value of D_i may be related back to the monomeric

diffusion coefficient, D_1, using an appropriate scaling law: $D_i = D_1 i^{-e}$. Here the exponent e is introduced to describe the precise nature of the chain length dependence of the diffusion coefficient and may be estimated from experimental diffusion data measured by pulsed-field-gradient NMR.[32] We next define the rate coefficient for termination between a pair of monomeric radicals as: $k_t^{1,1} = 2\pi\sigma\rho_{spin}(D_1+D_1)N_A$. Rearrangement of equation (4.29) then gives the following so-called "diffusion mean" expression for $k_t^{i,j}$.

$$k_t^{i,j} = \tfrac{1}{2} k_t^{1,1}\left(i^{-e} + j^{-e}\right) \tag{4.30}$$

Rate equations may also be formulated to describe the evolution of radical concentrations for all chain lengths as follows:

$$\frac{dn_1}{dt} = \rho + k_{tr}[M]_p \sum_{j=2}^{\infty} n_j - k_p^1[M]_p n_1 - 2n_1 \sum_{j=1}^{\infty} c^{1,j} n_j \tag{4.31}$$

$$\frac{dn_2}{dt} = k_p^1[M]_p n_1 - k_p[M]_p n_2 - k_{tr}[M]_p n_2 - 2n_2 \sum_{j=1}^{\infty} c^{2,j} n_j \tag{4.32}$$

$$\frac{dn_i}{dt} = k_p[M]_p\left(n_{i-1} - n_i\right) - k_{tr}[M]_p n_i - 2n_i \sum_{j=1}^{\infty} c^{i,j} n_j, \quad \text{for } i > 2 \tag{4.33}$$

where $c^{i,j} = \dfrac{k_t^{i,j}}{N_A V_s}$ and the following assumptions have been adopted. Firstly, for simplicity it is assumed that entry is by monomeric radicals (*i.e.*, entry contributes only to the value of n_1). Further, we assume that entry-derived monomeric radicals behave identically to monomeric radicals produced by transfer to monomer. It is noted that more complex treatments which avoid both the above assumptions may be used instead, but the changes entailed will affect only a small number of radical populations and are thus unlikely to cause any significant deviation from the results here. It is also assumed that only monomeric radicals may undergo exit, and, in the present instance, that all exited radicals re-enter a latex particle; *i.e.*, $\alpha = 1$ is assumed, hence there are no exit and re-entry terms in equation (4.31). This is not to say that $\alpha = 1$, but it is legitimate to assume this for the exercise of testing the effect of introducing chain length dependent termination, which is the aim here. Finally, the radical number is calculated according to:

$$\bar{n} = \sum_{i=1}^{\infty} n_i \tag{4.34}$$

The radical chain length distribution, and hence the values of $\bar{n}$ and $\langle k_t \rangle$, may thus be obtained from numerical solution of the population balance differential equations (4.31) – (4.33). Here we use the "truncated coarse-graining" method of Russell *et al.*, a detailed explanation of which can be found in the original publications by these authors.[18,19,33] This approach is now applied to the simulation of seeded emulsion polymerisations of MMA at 50°C. The parameter values used in these simulations are detailed in Table 4.7.

Table 4.7. Details of simulations using the pseudo-bulk model with chain length dependent termination and complete re-entry of exited radicals.

Simulation parameter	Value/Range	Reference
$\hat{x}$ / g	0 – 0.7	–
m_p^{seed} / g	0.85	–
r_u^{seed} / nm	42.5	–
$[M]_p$ / M	6.9	–
k_p / M^{-1} s^{-1}	649	15
k_p^1 / k_p	15	27,28
k_{tr} / M^{-1} s^{-1}	3.7×10^{-2}	29
e	1.26	32,34
a / Å	6.9	35
ρ / s^{-1}	$10^{-5} - 10^{-1}$	–
$k_t^{1,1}$ / M^{-1} s^{-1}	9.8×10^7	–

These values were chosen to be representative of the emulsion polymerisation conditions used in the experimental part of this study, hence the conversion range 0 g ≤ $\hat{x}$ ≤ 0.7 g is used,

along with values of $m_p^{seed} = 0.85$ g and the radius of an unswollen seed particle, $r_u^{seed} = 42.5$ nm. The value of the chain length dependence exponent e is estimated from the empirical "universal" scaling law of Griffiths *et al.*,[32] and is appropriate for the particular weight fraction of polymer, $w_p = 0.30$, during Interval II of the kinetic experiments. A literature value[35] is used for the parameter a which is required to calculate the rate coefficient for "reaction diffusion". This process, described by equation (4.35) and explained in detail below, is included in all calculations carried out here. The range of ρ values was chosen based on the results obtained in the preceding sections and is thought to more than span the range necessary for fitting of the present experimental data. Finally, the value of $k_t^{1,1}$ in Table 4.7 was adjusted to give an overall value of $\langle k_t \rangle$ of approximately 1.9×10^4 M^{-1} s^{-1} – equal to that obtained independently from γ-relaxation experiments – in the case of the simulation with the (lowest) value of $\rho = 1 \times 10^{-5}$ s^{-1}. Effectively this means that the product $\sigma p_{spin} D_1$ is treated as an adjustable parameter, although it will be seen in Chapter 6 that the obtained value for this factor is in reasonable accord with best estimates for these values. All in all, this procedure provides a benchmark for assessing the effects of chain length dependent termination on the values of $\langle k_t \rangle$ and $\overline{n}$.

In addition to the above simulations using chain length dependent termination, in each case the value of $\overline{n}$ was also calculated for identical conditions using equation (4.13): the steady-state solution to the pseudo-bulk equation with $\alpha = 1$. Here a constant value of $\langle k_t \rangle = 1.9 \times 10^4$ M^{-1} s^{-1} was always used, thus providing results with chain length *independent* termination for comparison.

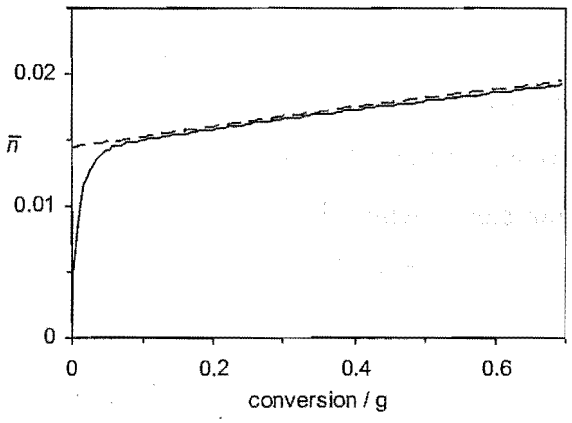

Figure 4.12. Simulated data for $\bar{n}$ as a function of Interval II conversion for MMA at 50°C with $\rho = 10^{-5}$ s^{-1} obtained using both the chain length dependent termination model (solid line) and chain length independent model (dashed line).

In Figure 4.12 we present results from simulations using the CLD and CLI termination models for simulations with $\rho = 1 \times 10^{-5}$ s^{-1}. It is evident that there is some discrepancy between the values of $\bar{n}$ in each case: the CLD model data show a rapid transient in $\bar{n}$ initially followed by a steady increase over the remainder of Interval II; the steady-state CLI model data of course exhibit no rapid transient in $\bar{n}$ and the steady-state value of $\bar{n}$ is always slightly greater than that from the CLD model. Noting that in the above simulations the value of $\langle k_t \rangle$ from the CLD model is 1.9×10^4 M^{-1} s^{-1} (*i.e.*, equal to that specified for simulations with CLI termination), and moreover that the CLD value of $\langle k_t \rangle$ is found in this case to be approximately constant with conversion over Interval II, the observed discrepancy in the results of Figure 4.12 cannot be due to some effect of CLD termination and is therefore attributed to the steady-state approximation that is invoked in the CLI modelling method; given that the steady-state assumption of $d\bar{n}/dt = 0$ does not *strictly* hold due to the change in $\bar{n}$ with particle volume, there must then be some (small) error associated with this approximation – the extent of this error is revealed by comparison with the full time-dependent solution given by the CLD method. That this error has been shown to be negligible is obviously pleasing.

Importantly, it is found that while the steady-state approximation gives a small error in the magnitude of $\bar{n}$, this has a negligible effect on the measured acceleration. Here $\bar{a}$ is measured in both cases from a linear fit to $\bar{n}$ data in the range $0.1 \leq \hat{x} \leq 0.7$ (in order to avoid the initial transient in $\bar{n}$) and the value $\bar{a} = 0.44$ is obtained from both models. Since it is the variation in

$\overline{a}$ with initiator concentration (and hence ρ) that is of primary interest in the present investigations, it is thus concluded that any error arising from the steady-state approximation may be safely neglected here. It is also observed that the above value of $\overline{a}$ is slightly higher than the value of $\overline{a} = 0.42$ quoted in section 4.4 for the CLI model with identical parameter values to those used here. This difference reflects the fact that the earlier value of $\overline{a}$ was measured over the larger conversion range of $0 \leq \hat{x} \leq 0.7$ and hence there is a small difference in the value of m_p^0 used in equation (4.15).

Also important from Figure 4.12 is the finding that CLD termination has a negligible effect on $\overline{a}$. Earlier it was speculated that as $\overline{n}$ increases during Interval II, this might change the n_i distribution, thus the value of $\langle k_t \rangle$, and thus the acceleration. Insofar as this occurs, it must be negligible in effect.

At this point we note that there exists some degree of flexibility in terms of the CLD modelling described above. Specifically, the following matters must be addressed:

(1) In Table 4.7 we specify a single value of the scaling law exponent, $e = 1.26$, implicitly assuming that this chain length dependence of the radical diffusion coefficients is applicable in all cases. A more sophisticated approach[18,19] would take into account the possibility that this scaling coefficient varies somewhat with both weight fraction of polymer, w_p, and radical chain length. Noting that all polymerisations in the present study were conducted in Interval II (and therefore with constant w_p), the first of these extensions is clearly redundant. In order to assess the consequences of our assumption that e is independent of chain length, each simulation was repeated using an alternative scaling law. Here the value $e = 1.26$ was applied only to scaling of diffusion coefficients for radicals up to degree of polymerisation 10. This value is expected to be accurate for this range (at least), given that the empirical scaling law of Griffiths *et al.*[32] was derived from diffusion data for oligomers from monomeric to decameric in length. For radicals of degree of polymerisation greater than 10 the value $e = 2.00$ was used, corresponding to the well-known scaling law for diffusion by reptative motion,[36] and resulting in much slower diffusion of long radicals than in the previous simulations.

(2) In addition to the type of diffusion discussed above which describes only the translational or "centre-of-mass" motion of a radical chain, a contribution to D_i is also widely

recognised from "reaction diffusion" (or "residual diffusion"). This term describes the movement of the free-radical site of a growing chain due to its propagative addition to successive monomer units (in the manner of a "random walk"), and becomes most important at high w_p where centre-of-mass diffusion is slowed considerably. The rate coefficient for reaction diffusion, D_{rd}, may be calculated as follows,[35]

$$D_{rd} = \tfrac{1}{6} k_p [M]_p a^2 \qquad (4.35)$$

where a is the root-mean-square end-to-end distance per square root of the number of monomer units in a polymer chain. The contribution from reaction diffusion D_{rd} may then be added to the centre-of-mass value of D_i given by equation (4.29). In order to determine the significance of reaction diffusion to the results at hand, simulations were conducted with and without the addition of the contribution to diffusion from D_{rd}.

(3) As described in section 4.6.2, there exists considerable uncertainty in the value of k_p^1. In order to specify a value for the purpose of CLD modelling simulations we adopt in Table 4.7 the value of $k_p^1 = 15\ k_p$ which is likely to be an upper bound for k_p^1 as described earlier. In order to ascertain the possible effects on modelling results of uncertainty in this value, simulations were also repeated using the lower bound value of $k_p^1 = k_p$.

The results obtained from the range of simulations carried out as part of (1) – (3) above showed that the value of $\langle k_t \rangle$ and hence also the value of $\overline{n}$ during Interval II, as modelled with CLD termination, show some degree of sensitivity to each of the modelling variations applied. It is therefore emphasised that application of this model to detailed fitting of $\overline{n}$ data from experiment should be accompanied by specific details regarding each of the above considerations. However, despite the disparity between the values of $\overline{n}$ obtained using different modelling variants, it was discovered that the value of $\overline{a}$ measured in each case from $\overline{n}$ over Interval II is the same for a given value of ρ. Since it is the variation of $\overline{a}$ with initiator concentration (or equivalently with ρ) that is of foremost interest here, we may confidently conclude that the aspects of the modelling described in (1) – (3) above introduce no significant uncertainty to subsequent discussion.

The values of $\overline{a}$ measured for each of five CLD model simulations using the parameter values quoted in Table 4.7, and spanning the specified range of ρ values, are presented in Figure

4.13. Also presented is the (constant) value of $\overline{a} = 0.44$ obtained in each case from the results of CLI modelling with $\langle k_t \rangle = 1.9 \times 10^4$ M^{-1} s^{-1}.

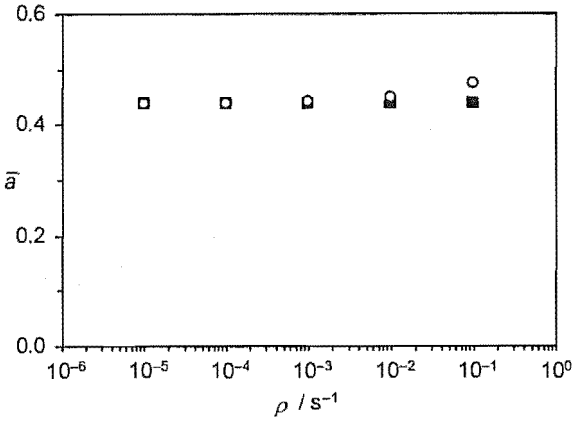

Figure 4.13. $\overline{a}$ calculated from model data simulated using the CLD termination model (open circles) and the CLI termination model (filled squares), presented as a function of ρ.

The values of $\overline{a}$ obtained from modelling with CLD and CLI termination are seen to be equal only at lowest ρ, the value from CLD modelling increasing with increasing ρ. The explanation for this effect must lie in the effect of CLD termination on the value of $\langle k_t \rangle$. Furthermore, as remarked in section 4.4 a change in the overall magnitude of $\langle k_t \rangle$ as the value of ρ is changed for each simulation does not introduce any change in $\overline{a}$; so the change observed in $\overline{a}$ must be due to CLD termination changing the value of $\langle k_t \rangle$ *with conversion* over Interval II. Indeed, inspection of the CLD model data reveals that the value of CLD $\langle k_t \rangle$ decreases during Interval II by almost 4 % for the simulation with $\rho = 10^{-1}$ s^{-1}, where the value of $\overline{a}$ is also greatest. The decrease in $\langle k_t \rangle$ must reflect a shift in the radical chain length distribution towards longer chain lengths (for which $k_t^{i,j}$ values are relatively low) with increasing conversion. This shift is readily explained when it is noted that the only rate parameters in equations (4.31) – (4.33) exhibiting a conversion dependence are the microscopic radical loss coefficients, $c^{i,j}$, which decrease as the particle volume increases with conversion. As the values of $c^{i,j}$ decrease, radical loss by termination becomes relatively less prevalent as compared to loss by chain transfer and as such the radical chain length distribution changes to more closely resemble that of the "transfer limit", where all radical loss is *via* transfer. It is noted that this result is unexpected, for the expectation was that as $\overline{n}$

increases with conversion, $\langle k_t \rangle$ would increase, but in fact simulations show that the opposite occurs.

As seen in Figure 4.13 the extent of the volume effect described above on the radical chain length distribution, and hence on the value of $\overline{a}$, lessens with decreasing ρ. This is because a lower entry rate coefficient necessarily means a lower total number of radicals per particle, $\overline{n}$, and an overall decrease in the frequency of termination. The radical chain length distribution therefore moves closer to the transfer limit with decreasing ρ, and in the present case this limit is seen to be reached when $\rho \approx 10^{-4}$ s^{-1}. Under transfer-controlled conditions, values of n_i are independent of variation in $\overline{n}$, thus the volume effect responsible for the variation in CLD $\langle k_t \rangle$ above becomes negligible and the value of $\overline{a}$ converges to the value given by modelling with CLI termination.

Significantly, the results from CLD modelling presented in Figure 4.13 reveal a trend of increasing $\overline{a}$ with increasing ρ (and hence with increasing initiator concentration) – a trend that is not observed when termination is assumed to be chain length *independent*. This trend is in accord with that seen in experimental $\overline{a}$ data and suggests that CLD termination may provide some explanation for the experimental acceleration results. However, the magnitude of the trend is far smaller than is seen in experiment. Further, it must be reiterated that the value of $\overline{a}$ from CLD modelling is seen to converge to the value from CLI modelling at low ρ, obtained with high initiator concentration, where $\overline{a} > 0.4$. Thus, no explanation is revealed for experimental data at low initiator concentrations.

Incorporating aqueous-phase reactions of exited radicals

The simulations carried out above using the pseudo-bulk model with CLD termination, and assuming complete re-entry of exited radicals, were unable to reproduce the low accelerations observed experimentally. In section 4.6.2 it was shown for the case of pseudo-bulk modelling with CLI termination that when the assumption of complete re-entry was removed (by permitting $\alpha < 1$) it was possible at least to accurately fit the data for these low accelerations, even if a detailed understanding of the underlying kinetics remained elusive. In light of this, the approach of the present section is to modify the CLD termination pseudo-bulk model analogously, allowing for incomplete re-entry of exited radicals. However, unlike the earlier work where this could be achieved only through variation of the fate parameter, α, in this

section we undertake a more thorough kinetic treatment of the aqueous-phase reactions of exited radicals.

Here it is assumed that an exited radical (in the aqueous phase), denoted $M_w^\bullet$ and of course generated by desorption of a monomeric radical from a particle, may only subsequently react by aqueous-phase termination, propagation or re-entry into a particle. Further, it is assumed that aqueous-phase propagation of an exited radical produces a dimeric radical that undergoes instantaneous re-entry into a particle. This assumption is intended to reflect the fact that exit-derived radicals contain no initiator end-group and their water-solubility is therefore expected to decrease dramatically with addition to monomer.[23] This leads to the following rate equation:

$$\frac{d[M_w^\bullet]}{dt} = k_{dM} n_1 \frac{N_c}{N_A} - k_{p,w}^M [M]_w [M_w^\bullet] - 2k_{t,w}[T_w^\bullet][M_w^\bullet] - k_{re}\frac{V_w}{V_r}\frac{N_c}{N_A}[M_w^\bullet] \qquad (4.36)$$

where $k_{p,w}^M$ is the rate coefficient for aqueous-phase propagation of an exited monomeric radical, k_{re} is the re-entry rate coefficient and V_r is the total reactor volume. A volume correction is applied to the re-entry term in equation (4.36) [and later in equation (4.42)]: since the interior of a latex particle is not included as part of the aqueous phase k_{re} must strictly be defined in terms of the total reactor volume and thus multiplied by the ratio V_w/V_r in order to give consistency with the particle (N_c) and radical ($[M_w^\bullet]$) concentrations defined in terms of the aqueous-phase volume.[37]

Clearly, some means is required for estimating the total aqueous-phase radical concentration, $[T_w^\bullet]$. Here we draw on equations (4.1) – (4.5), which yield the following population balances:

$$\frac{d[IM_1^\bullet]}{dt} = 2fk_d[I] - k_{p,w}[M]_w[IM_1^\bullet] - 2k_{t,w}[T_w^\bullet][IM_1^\bullet] \qquad (4.37)$$

$$\frac{d[IM_i^\bullet]}{dt} = k_{p,w}[M]_w\left([IM_{i-1}^\bullet] - [IM_i^\bullet]\right) - 2k_{t,w}[T_w^\bullet][IM_i^\bullet], \quad 1 < i < z \qquad (4.38)$$

$$\frac{d[IM_z^\bullet]}{dt} = k_{p,w}[M]_w[IM_{z-1}^\bullet] - \rho_{init}\frac{N_c}{N_A} \qquad (4.39)$$

Now, $[T_w^\bullet]$ may be calculated as a sum over all aqueous radical species.

$$[T_w^\bullet] = [M_w^\bullet] + \sum_{i=1}^{z-1} [IM_i^\bullet] \tag{4.40}$$

Having adopted the above equations to describe the aqueous-phase radical concentrations it is necessary also to specify the degree of polymerisation, z, for entry of initiator-derived radicals. The rate coefficient for entry may then be calculated from the concentration of $(z-1)$-mers as follows,

$$\rho_{init} = k_{p,w}[M]_w[IM_{z-1}^\bullet]\frac{N_A}{N_c} \tag{4.41}$$

Finally, in order to account for the fact that entry is no longer restricted to monomeric radicals and in order to introduce all these new kinetic processes, population balance equations (4.31) – (4.33) for intra-particle radicals must be modified slightly to the following:

$$\frac{dn_1}{dt} = \rho\delta_{1,z} + k_{re}\frac{V_w}{V_r}[M_w^\bullet] + k_{tr}[M]_p\sum_{j=2}^{\infty} n_j - k_{dM}n_1 - k_p^1[M]_p n_1 - 2n_1\sum_{j=1}^{\infty} c^{1,j}n_j \tag{4.42}$$

$$\frac{dn_2}{dt} = \rho\delta_{2,z} + k_{p,w}^M[M]_w[M_w^\bullet]\frac{N_A}{N_c} + k_p^1[M]_p n_1 - k_p[M]_p n_2 - k_{tr}[M]_p n_2 - 2n_2\sum_{j=1}^{\infty} c^{2,j}n_j \tag{4.43}$$

$$\frac{dn_i}{dt} = \rho\delta_{i,z} + k_p[M]_p(n_{i-1} - n_i) - k_{tr}[M]_p n_i - 2n_i\sum_{j=1}^{\infty} c^{i,j}n_j, \quad \text{for } i > 2 \tag{4.44}$$

Here $\delta_{i,z}$ is the Kronecker δ (defined as $\delta_{i,j} = 1$, $i = j$; $\delta_{i,j} = 0$, $i \neq j$) and entry of spontaneously generated radicals is neglected (for simplicity) so that $\rho = \rho_{init}$.

Thus, equations (4.36) – (4.44) above, together with equations (4.28), (4.30) and (4.34) from the previous section, form the complete set of rate equations required for pseudo-bulk modelling with CLD termination and a detailed account of aqueous-phase radical reactions. Equations (4.42) – (4.44) were solved using the same numerical methods as earlier[18,19] to obtain the intra-particle chain length distribution as well as all aqueous radical concentrations, and hence also the values of $\overline{n}$ and $\langle k_t \rangle$, over the course of Interval II of polymerisation, while the aqueous radical concentrations were calculated as now explained.

At this point it is timely to make reference to an earlier work[37] that also incorporated microscopic aqueous-phase kinetics into the CLD termination pseudo-bulk scheme, and which provided much guidance for the present effort. That formulation differed from the one developed here primarily in that it did not allow for the presence of initiator-derived radicals; such was unnecessary as the intent was only to model the out-of-source period of γ-relaxation experiments. Of particular import to the present treatment is the earlier finding that it was prohibitively impractical, in computational terms, to solve the population balance differential equations for aqueous-phase radicals simultaneously with those for intra-particle radicals. Therefore, the alternative approach used was to solve the aqueous-phase radical concentrations in the steady-state. This was justified by the fact that the intra-particle populations change sufficiently slowly with time, compared with the relatively short timescale of aqueous-phase reactions, that the steady-state values for the aqueous-phase radical concentrations will rapidly adjust to any such changes. Accordingly, we apply the steady-state approximation to the equations for aqueous radicals, (4.36) – (4.38), to obtain the following equations which may be solved in their place.

$$[\mathrm{M}_{\mathrm{w}}^{\bullet}] = \frac{k_{\mathrm{dM}} n_1 \dfrac{N_{\mathrm{c}}}{N_{\mathrm{A}}}}{k_{\mathrm{p,w}}^{\mathrm{M}}[\mathrm{M}]_{\mathrm{w}} + 2k_{\mathrm{t,w}}[\mathrm{T}_{\mathrm{w}}^{\bullet}] + k_{\mathrm{re}} \dfrac{N_{\mathrm{c}}}{N_{\mathrm{A}}} \dfrac{V_{\mathrm{w}}}{V_{\mathrm{r}}}} \tag{4.45}$$

$$[\mathrm{IM}_1^{\bullet}] = \frac{2fk_{\mathrm{d}}[\mathrm{I}]}{k_{\mathrm{p,w}}[\mathrm{M}]_{\mathrm{w}} + 2k_{\mathrm{t,w}}[\mathrm{T}_{\mathrm{w}}^{\bullet}]} \tag{4.46}$$

$$[\mathrm{IM}_i^{\bullet}] = \frac{k_{\mathrm{p,w}}[\mathrm{M}]_{\mathrm{w}}[\mathrm{IM}_{i-1}^{\bullet}]}{k_{\mathrm{p,w}}[\mathrm{M}]_{\mathrm{w}} + 2k_{\mathrm{t,w}}[\mathrm{T}_{\mathrm{w}}^{\bullet}]}, \quad 1 < i < z \tag{4.47}$$

At each call of the differential equation solving routine, the above equations were solved iteratively, using $[\mathrm{M}_{\mathrm{w}}^{\bullet}] = [\mathrm{IM}_i^{\bullet}] = 0$ M and $[\mathrm{T}_{\mathrm{w}}^{\bullet}] = \sqrt{fk_{\mathrm{d}}[\mathrm{I}]/k_{\mathrm{t,w}}}$ as starting approximations.

The parameter values chosen for simulations using the above kinetic treatment are appropriate for the emulsion polymerisation of MMA at 50°C and are consistent with the simulations of the previous section, along with several additions. $\hat{x}$, $m_{\mathrm{p}}^{\mathrm{seed}}$, $r_{\mathrm{u}}^{\mathrm{seed}}$, $[\mathrm{M}]_{\mathrm{p}}$, k_{p}, k_{tr}, e, a and $k_{\mathrm{t}}^{1,1}$ are as already given in Table 4.7. The value for $k_{\mathrm{t,w}} = 3.7 \times 10^9$ M^{-1} s^{-1} is the same as that adopted by Maxwell *et al.*[9] (note the "factor of 2 definition" used here) who in turn cited the experimental findings of Dainton *et al.*[38,39] from reactions of small acrylonitrile radicals in

aqueous solution. In the absence of any better estimate, $k_{p,w}^{M}$ and $k_{p,w}$ are assigned the bulk value of k_p from Table 4.7. Of course this is inconsistent with $k_p^1 = 15\ k_p$, but putting $k_{p,w}^{M} = 15\ k_p$ will only decrease aqueous-phase residence times, and thus reduce any kinetic effects of desorption. So by putting $k_{p,w}^{M} = k_p$ we maximise the possibility of any aqueous phase effects. This will be further discussed later in this chapter. The reactor volume is set equal to that of the dilatometer vessel used in chemically-initiated experiments (60 cm^3), and the aqueous-phase volume is calculated by subtracting the volumes of monomer and polymer. The range of initiator (KPS) concentrations used is $10^{-5} - 10^{-2}$ M, and the literature value of $fk_d = 1.1 \times 10^{-6}\ s^{-1}$ for KPS at 50°C[16] is used here (and in all subsequent kinetic analyses). The rate coefficient for desorption of monomeric radicals, k_{dM}, is calculated according to equation (4.27), and the value of k_{re} may be estimated from the Smoluchowski equation:

$$k_{re,coll} = 4\pi D_w r_s N_A \qquad (4.48)$$

Here the value of $k_{re,coll}$ represents an upper bound for the value of k_{re} by assuming that the re-entry process is limited only by diffusion, *i.e.*, every collisional encounter between an aqueous monomeric radical and a latex particle results in a successful re-entry event. Equation (4.48) approximates the aqueous diffusion coefficient for a monomeric radical as being the same as for monomer (D_w), and reasonably assumes, for mutual aqueous diffusion of a particle and a monomeric radical, that $D_{part} + D_w \approx D_w$, where D_{part} is the aqueous diffusion coefficient for a particle. Further, it is assumed that $r_s + r_M \approx r_s$, where r_M is the radius of an aqueous monomeric radical. The latter two of these assumptions follow from a particle being much more massive than a monomeric radical. Finally, the values of remaining rate parameters, which vary for different simulations, are as specified in Table 4.8.

As before, simulations with CLD termination are accompanied by CLI modelling using equation (4.13), with a constant value of $\langle k_t \rangle = 1.9 \times 10^4\ M^{-1}\ s^{-1}$, for comparison.

Table 4.8. Details of simulations with chain length dependent termination.

Simulation	(a)	(b)	(c)	(d)	(e)
Simulation parameter			Value		
k_p^1 / k_p	15	15	1	15	15
$k_{re} / k_{re,coll}$	1	1	1	10^{-6}	10^{-6}
$k_{p,w}^M / k_{p,w}$	1	1	1	1	10^{-2}
z	1	20	20	20	20

A range of simulations were carried out under various conditions, a selection of which is detailed in Table 4.8 and labelled (a) – (e). Results from each of these simulations are presented in the corresponding Figures 4.14 (a) – (e). As in the previous section, results are presented in the form of $\bar{a}$ as a function of ρ, since it is the variation in $\bar{a}$ that is of key significance in the present investigation. In this case ρ is calculated for each simulation from the full set of rate equations for aqueous-phase species given above. It is variation of the initiator concentration, [KPS], from 10^{-6} to 10^{-2} M in decade intervals, that gives rise (indirectly) to the variation of ρ in each set of simulations here.

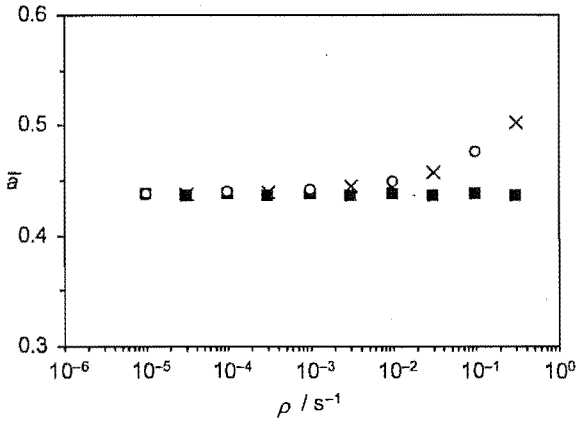

Figure 4.14. (a) $\bar{a}$ calculated from simulations using the CLD termination model with complete re-entry (open circles), the CLD termination model with complete aqueous-phase kinetics (crosses), and the CLI termination model (filled squares).

In Figure 4.14 (a) we first compare the results from simulation (a) of Table 4.8 with those obtained already using the CLD termination model of the previous section, which assumes complete re-entry of exited radicals. It is evident that the value of $\bar{a}$ shows exactly the same variation with changing ρ in both cases; the inclusion of full aqueous-phase kinetics makes no significant difference under these conditions. This result is perhaps not unexpected given that a value of $z = 1$ was used in parameter set (a) (consistent with the assumptions used in the earlier simulations) and the concentration of initiator-derived radicals in the aqueous-phase is thus likely to be vanishingly small, leaving homo-termination as the only avenue for loss of exited monomeric radicals. We therefore next examine the effect of having a higher value of z and, accordingly, an appreciable concentration of initiator-derived radicals in the aqueous phase.

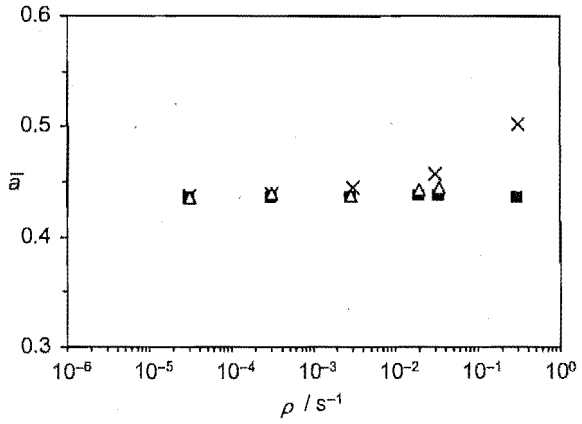

Figure 4.14. (b) $\bar{a}$ calculated from simulations using the CLD termination model with complete aqueous-phase kinetics: $z = 1$ (crosses), $z = 20$ (open diamonds); and the CLI termination model (filled squares).

Figure 4.14 (b) presents the results obtained using parameter sets (a) and (b) of Table 4.8, the only difference between these two sets of simulations being the chain length for entering species: $z = 1$ and $z = 20$ respectively. The latter value was chosen as a deliberately generous estimate of this quantity (given that an estimate of $z = 5$ for MMA has been postulated on thermodynamic grounds,[9] as will be discussed later) in order to maximise the effects of aqueous-phase termination. It is noted that the discrepancy between ρ values obtained in each case for identical values of [KPS], evident as the misalignment of the two data sets, is a direct consequence of the difference in z.

Increasing the value of z is seen to have a significant effect on the values of $\bar{a}$ obtained from simulations. While the overall trend in $\bar{a}$ remains similar to that seen in previous CLD

modelling, the values of $\bar{a}$ at highest ρ and [KPS] with $z = 20$ are somewhat lower than the comparable data obtained with $z = 1$ (although still not falling below the values from CLI modelling). Given that a value of $z = 20$ gives rise to a considerable increase in the concentration of aqueous-phase radicals, the first inclination may be to presume that this effect is due to increased hetero-termination of exited radicals at high [KPS]. However, in section 4.6.2 is was shown that such aqueous termination (alone) should have the opposite effect of *increasing* the value of $\bar{a}$. In this case a more likely explanation is thought to be the following. Increasing the value of z from 1 to 20 means that entry now supplies radicals of significantly longer chain length to the particles, causing a shift in the n_i distribution towards longer chain lengths (and relatively lower values of $k_t^{i,j}$) and thus an overall decrease in the frequency of termination. This new radical distribution will be closer to that of the transfer limit and consequently the volume effect responsible for the variation in CLD $\langle k_t \rangle$, and hence $\bar{a}$, will have less impact than in earlier simulations with comparable ρ but $z = 1$. Whether or not this is the true the explanation here, one thing that is clear from these simulations is that the interpretation of the kinetic effects from changing even a single parameter value (such as z) is not always straightforward.

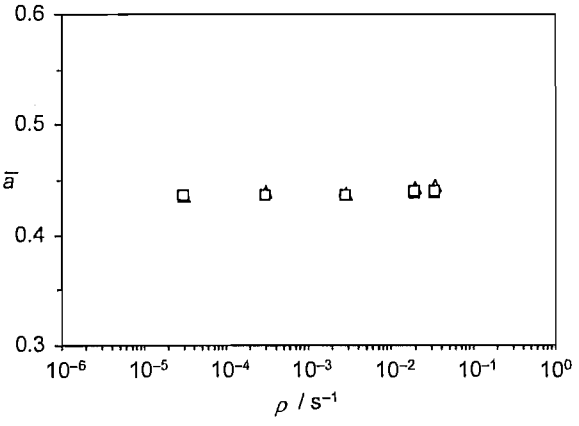

Figure 4.14. (c) $\bar{a}$ calculated from simulations using the CLD termination model with complete aqueous-phase kinetics: $k_p^1/k_p = 15$ (open triangles), $k_p^1/k_p = 1$ (open squares); and the CLI termination model (filled squares).

Once again it is also necessary to acknowledge the uncertainty in the value of k_p^1. In simulations (a) and (b) above a value of $k_p^1 = 15\ k_p$ (*i.e.*, the upper bound value) was adopted. In Figure 4.14 (c) are presented the results from simulation (b), together with $\bar{a}$ data from simulations where the lower bound value of $k_p^1 = k_p$ is assumed. The effect of this change on

the values of $\bar{a}$ obtained is virtually negligible. Notably, analogous simulations conducted for the case with $z = 1$ lead to the same conclusion. It is evident that the acceleration during Interval II is far less sensitive to the precise value of k_p^1 than it is to the aqueous-phase conditions affecting the reactions of exited radicals.

The above simulations would appear to indicate that the variation of $\bar{a}$ with ρ and [KPS] in pseudo-bulk modelling with CLD termination is affected to a relatively small extent by the inclusion of a complete aqueous-phase kinetic scheme. A corollary of this is that the preceding modelling, with its simplifying assumption of complete re-entry of all exited monomeric radicals, is likely to be acceptably accurate, at least for the case of Interval II of MMA emulsion polymerisations at 50°C. This inference is now briefly examined through a consideration of the aqueous-phase reactions of exited radicals.

Aqueous-phase reactions of exited radicals

The reaction rate per exited radical (*i.e.*, the reaction frequency for an exited radical) for each of re-entry (R_{re}), aqueous-phase propagation ($R_{p,w}$), and termination ($R_{t,w}$) may be calculated as follows:

$$R_{re} = k_{re}\frac{N_c}{N_A}\frac{V_w}{V_r} \tag{4.49a}$$

$$R_{p,w} = k_{p,w}^{M}[M]_w \tag{4.49b}$$

$$R_{t,w} = 2k_{t,w}[T_w^\bullet] \tag{4.49c}$$

For the purposes of the current exercise, it is assumed that $k_{p,w}^{M} = k_{p,w} = 649$ M^{-1} s^{-1}, $[M]_w = 0.15$ M, $k_{t,w} = 3.7 \times 10^9$ M^{-1} s^{-1}, $N_c = 4.3 \times 10^{16}$ dm^{-3}, and $V_w/V_r \approx 1$ (a simplification that incurs only a relatively small error). Equation (4.48), with $D_w = 1.7 \times 10^{-9}$ m^2 s^{-1} and $r_s = 68$ nm, gives a value for $k_{re,coll}$ of 8.7×10^{11} M^{-1} s^{-1}. The following reaction rates are then calculated for re-entry and propagation: $R_{re} = 6.2 \times 10^4$ s^{-1} and $R_{p,w} = 97$ s^{-1}; already we see that re-entry is more probable than propagation. It also follows that in order for aqueous-phase termination to compete with re-entry, *i.e.*, $R_{t,w} \approx R_{re}$, we require conditions such that $[T_w^\bullet] \approx 8 \times 10^{-6}$ M. Such aqueous-phase conditions are certainly unlikely in the present setting, where the total concentration of initiator is only in the range of $10^{-6} - 10^{-2}$ M. Also,

one sees that using $k_{p,w}^{M} = 15\ k_p$ will change nothing (it will only give rise to a slight increase in re-entry by propagation, and thus even further reduce the likelihood of aqueous-phase loss of exited radicals).

However, it must be acknowledged that the value of R_{re} above is based on the diffusion-limited value of k_{re}, and that if, in actuality, there was a barrier to re-entry (*e.g.*, the result of a particle-radical interaction of some sort) this value may well be substantially lower. We therefore also consider the case where $k_{re} \ll k_{re,coll}$, such that $R_{re} \ll R_{p,w}$. Recognising that aqueous-phase propagation of an exited radical ultimately results in re-entry (albeit by a different mechanism to that represented by k_{re}), we now require $R_{t,w} \approx R_{p,w}$ in order for any appreciable termination of exited radicals to occur; *i.e.*, the total aqueous radical concentration must be of order $[T_w^{\bullet}] \approx 10^{-8}$ M. Given that the value of $[T_w^{\bullet}]$ generated in the simulations above was found to be, at most, of order 10^{-9} M (obtained in simulations with $z = 20$ and [KPS] = 10 mM), the prospect of termination of exited radicals in the aqueous phase appears highly improbable. Moreover (re-iterating an earlier point) increasing $k_{p,w}^{M}$ above k_p will only make such termination even more improbable.

While the above exercise admittedly rests on a number of estimations, it nevertheless provides support for (and aids in the interpretation of) the results observed from the simulations in this section.

In light of the predictions gleaned from the above calculations, two further sets of simulations are of interest. The first of these employs the value of $k_{re} = 10^{-6}\ k_{re,coll}$, as listed in Table 4.8 (d), and gives rise to conditions of $R_{p,w} > R_{re}, R_{t,w}$. The second uses the same value for k_{re} together with the value of $k_{p,w}^{M} = 10^{-2}\ k_{p,w}$, as in Table 4.8 (e), which gives conditions of $R_{t,w} \approx R_{p,w} > R_{re}$. Of course, $k_{p,w}^{M} = 10^{-2}\ k_{p,w}$ is (almost certainly) non-physical, but it is worthwhile to do this "experiment" to see what its effect would be.

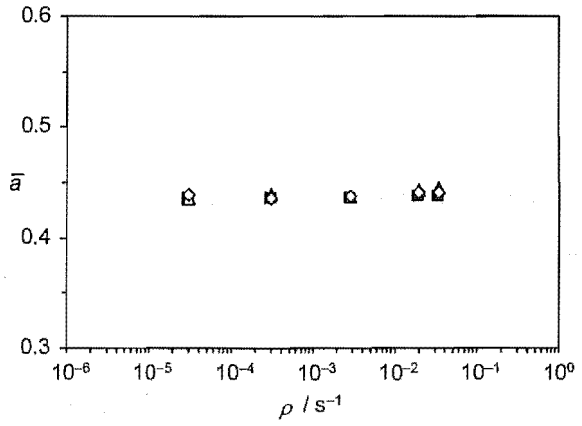

Figure 4.14. (d) $\bar{a}$ calculated from simulations using the CLD termination model with complete aqueous-phase kinetics: $k_{re}/k_{re,coll} = 1$ (open triangles), $k_{re}/k_{re,coll} = 10^{-6}$ (open diamonds); and the CLI termination model (filled squares).

Presented in Figure 4.14 (d) are the values of $\bar{a}$ as a function of ρ calculated from simulation set (d). Under these conditions, exited monomeric radicals react predominantly by propagation and subsequent dimeric re-entry. Also presented are the results from previous simulations (b) where monomeric re-entry dominated. Comparison of these two data sets reveals no significant differences in terms of the variation of $\bar{a}$ with ρ and [KPS], indicating that the nature of the acceleration during Interval II is not sensitive to which of the two different mechanisms for re-entry is operative, so long as re-entry prevails.

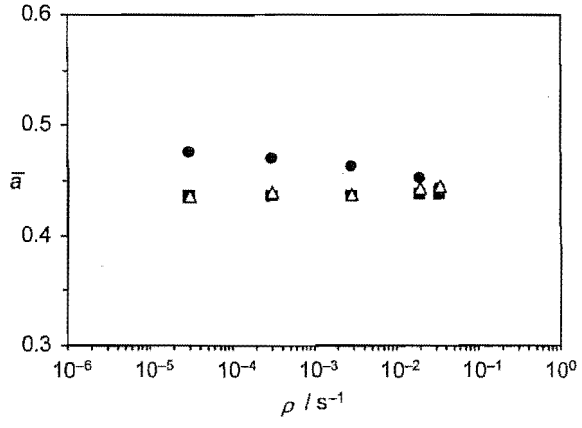

Figure 4.14. (e) $\bar{a}$ calculated from simulations using the CLD termination model with complete aqueous-phase kinetics: $k^{M}_{p,w}/k_{p,w} = 1$ (open triangles), $k^{M}_{p,w}/k_{p,w} = 10^{-2}$ (filled circles); and the CLI termination model (filled squares).

Figure 4.14 (e) contains the values of $\bar{a}$ as a function of ρ calculated from simulation set (e), under conditions where (due to the low values used for k_{re} and $k_{p,w}^{M}$) monomeric radical re-entry of exited radicals is negligible and both the processes of propagation/dimeric re-entry and aqueous-phase termination occur at comparable rates over the relevant range of [KPS]. Included once again for comparison are the results from simulation set (b). In this case a significant difference in the variation of $\bar{a}$ with ρ and [KPS] is observed between the two data sets. It is evident that the incidence of significant aqueous-phase termination results in an appreciable enhancement in the acceleration, particularly at low [KPS]. This effect, it is believed, is due to the fact that radius dependent k operating alone (*i.e.*, with $c = 0$) actually gives rise to $\bar{a} \approx 0.67$ (results not presented in this work), which is higher than the value of $\bar{a}$ due to radius dependent c alone. As ρ increases the system will naturally move from one of these limits to the other; it is believed that this is the explanation for the variation in $\bar{a}$ observed in Figure 4.14 (e). In any event, what is most significant here is that even under the relatively extreme conditions prescribed in the above simulations, in no case is the value of $\bar{a}$ seen to fall below the figure given by CLI modelling under equivalent conditions.

Summarising the results obtained above from CLD modelling with complete aqueous-phase kinetics, it is seen that the results here are not dissimilar to those obtained from the earlier CLD modelling, with complete re-entry, in that both approaches offer the possibility of some variation in $\bar{a}$ with [KPS]. Moreover, in most cases the observed variation was a slight increase in $\bar{a}$ with increasing [KPS], consistent with the trend seen in experimental acceleration data. However, while it is certainly possible that the effects of CLD termination (with or without aqueous-phase kinetics) contribute to the trend in experimental $\bar{a}$ data, this cannot be the full explanation. Not only is the variation in $\bar{a}$ seen in CLD modelling of a much smaller magnitude than that of experiment, but even more crucially not a single simulation furnished a value of $\bar{a}$ that was significantly less than the value given by CLI pseudo-bulk modelling (*i.e.*, approximately 0.44). Consequently, the CLD termination methodology employed in this section is unable to improve the quantitative account of the majority of experimental results (with $\bar{a} < 0.44$) beyond that already given by CLI procedures.

A very important finding is that best estimates of k_{re} and $k_{p,w}^{M}$ result in very limited aqueous-phase termination of exited radicals, even at high initiator concentrations. Further, clearly this finding is general, because there is nothing MMA-specific about the value of $k_{re,coll}$. This

suggests that emulsion polymerisation kinetics will essentially always be $\alpha = 1$, with exit only bringing radical loss insofar as it brings a radical into contact with a radical in another particle, where in its original particle it would have no such contact, *i.e.*, compartmentalisation effects.

4.6.4 Compartmentalisation

All modelling approaches used so far, with either CLI or CLD termination, have been based fundamentally on the tenets of the pseudo-bulk model. Thus, underlying all the above results is the assumption that radicals are circulated amongst all polymerisation loci (latex particles) sufficiently rapidly that the "compartmentalisation" of radicals into distinct particles need not be acknowledged. As stated earlier, this situation is a limiting case of the more general kinetic model of Smith and Ewart,[10] and only holds for the situation where $\rho > c$ and/or $k > c$. Ballard *et al.* made clear in their work[1,29] that under conditions where the pseudo-bulk approximation is not accurate (*i.e.*, in the event that ρ, $k < c$) the value of $\overline{a}$ falls below that calculated from the conversion-dependence of $\overline{n}$ in equation (4.17). However, they were not so much concerned with elucidating the precise kinetic effects of compartmentalisation as they were with knowing the limitations for use of the pseudo-bulk approximation. This effect is however of particular interest in the context of the present study in that compartmentalisation represents a possible explanation for the low values of $\overline{a}$ observed experimentally. Therefore, in this section we examine the effects of compartmentalisation on modelling of experimental data for the MMA system at 50°C through the use of the Smith-Ewart equation.

The well-known kinetic equation due to Smith and Ewart is recalled from Chapter 1 as:

$$\frac{dN_n}{dt} = \rho N_{n-1} - [\rho + nk + n(n-1)c]N_n + (n+1)kN_{n+1} + (n+2)(n+1)cN_{n+2} \qquad (4.50)$$

Here latex particles are distinguished by the number of propagating radicals they contain, with N_n being the number fraction of particles containing n radicals, which is related to the fractions containing $(n-1)$, $(n+1)$ and $(n+2)$ radicals *via* the rate coefficients for entry, exit and termination as shown. The average number of radicals per particle is then calculated in terms of N_n as follows:

$$\overline{n} = \sum_{n=1}^{\infty} nN_n \tag{4.51}$$

The original formulation by Smith and Ewart simply assumed that all intra-particle radicals undergo exit at the rate stipulated by the rate coefficient k, and that this exit is inevitably followed by termination in the aqueous phase. However, given the subsequent realisations that (1) exit is due only to desorption of radicals produced by transfer to monomer, and (2) aqueous-phase termination of exited radicals is not guaranteed, the contemporary implementation and interpretation of the Smith-Ewart model is somewhat different, as will shortly be seen.

It should also be noted that the value of c in equation (4.50) is assumed to be independent of chain length. Of course, ideally the Smith-Ewart treatment could be combined with the CLD termination kinetic scheme of the previous section, however the mathematical problem of solving the very large set of equations associated with such a kinetic approach remains intractable at present.[40] In any case, from the results obtained in the previous section using CLD termination modelling it is evident that for the conditions under most scrutiny here (*viz.*, MMA at 50°C with low initiator concentration) CLD termination is unlikely to have any profound effect on the quantity of direct interest: the acceleration, $\overline{a}$. In other words, the *trends* predicted by the Smith-Ewart equations are not significantly affected by using a constant c rather than a chain-length-averaged value which can change (in principle) as $\overline{n}$ changes.

Re-entry followed by propagation

It will be assumed throughout this investigation that all exited monomeric radicals re-enter a latex particle; given the estimates made using equations (4.49) in the previous section, this seems by far the most likely scenario for the present system. Initially, we further assume that every re-entrant radical rapidly propagates to form a macro-radical incapable of exit, *i.e.*, we assume that $k_p^1[M]_p \gg k_{dM}$. It is therefore necessary to augment the rate coefficient for entry appropriately to account for the flux of re-entering radicals. This is accomplished (in a similar way to Ballard *et al.*[11]) by defining a new rate coefficient for *total* radical entry as follows:

$$\rho_{total} = \rho + k\overline{n} \tag{4.52}$$

Re-entry is now specifically accounted for in equation (4.50) by replacing ρ with ρ_{total}. Equation (4.52) on its own only assumes no aqueous-phase termination of exited free radicals. However, using this expression in equation (4.50) also assumes that the fate of a re-entering radical is unrelated to the number of radicals in the re-entered particle. In other words, it assumes that a re-entrant radical stays in the first particle it enters, as claimed above. This is a subtle but important point.

Replacing ρ with ρ_{total} in equation (4.50) it is also clear that ρ_{total} is now coupled to the particle populations, N_n, through the value of $\bar{n}$. For a given set of ρ, k and c values the value of $\bar{n}$ may thus be calculated according to equations (4.50) – (4.52). An efficient means for finding the *steady-state* solution of this set of coupled equations is the so-called "recursive-closure" method.[11] Calculating the evolution of $\bar{n}(\hat{x})$ during Interval II, as c changes with increasing conversion, then allows a model value of $\bar{a}$ to be obtained using equation (4.15).

To illustrate the effects of compartmentalisation, the value of $\bar{a}$ is first calculated from the results of a range of model calculations using the above method and the "standard" parameter values of $m_p^{seed} = 0.85$, $r_u^{seed} = 42.5$ nm, $[M]_p = 6.9$ M, and $0 \leq \hat{x} \leq 0.7$. Figure 4.15 is a surface plot of $\bar{a}$ as a function of the values of both ρ/c and k/c (noting that only the *relative* values of ρ and k are of importance in calculations). The values of ρ/c and k/c refer to the values at the start of the steady-state period of Interval II (since c changes with conversion during a given simulation).

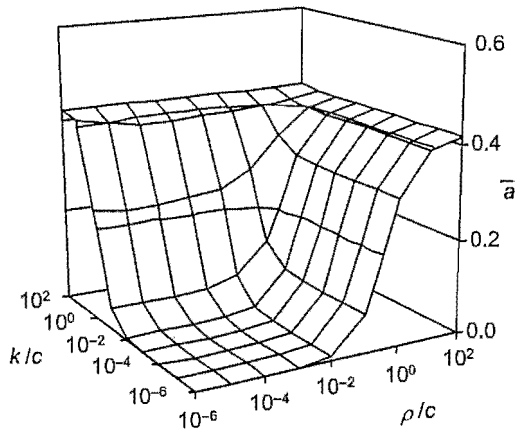

Figure 4.15. $\bar{a}$ calculated from model $\bar{n}$ data generated for a range of both ρ/c and k/c values using the Smith-Ewart model and assuming propagation of re-entrant radicals.

Here we observe that when at least one of $\rho/c > 1$ or $k/c > 1$ holds, $\bar{a}$ takes the pseudo-bulk value of approximately 0.42. However, the emphasis of this plot is the region of ρ/c, $k/c < 1$ where $\bar{a}$ is seen to decrease markedly. This effect is the result of compartmentalisation; as c becomes comparatively large, termination kinetics become non-rate-determining and the rate of radical loss is dictated primarily by the rate of exit from the particles. This corresponds to the so-called "zero-one" kinetic limit[12] where entry or re-entry into any particle already containing a growing radical results in "pseudo-instantaneous" termination, and consequently no particle can be occupied by more than one radical at any given time. Mathematically, the zero-one limit may be expressed by the closure condition that entry into an N_1 particle gives an N_0 particle. The set of equations (4.50) then becomes truncated so that no populations other than N_0 and N_1 need be considered.

$$\frac{dN_0}{dt} = \rho_{total}N_1 - \rho_{total}N_0 \tag{4.53}$$

$$\frac{dN_1}{dt} = \rho_{total}N_0 - (\rho_{total} + k)N_1 \tag{4.54}$$

Realising further that in the zero-one case $N_1 = \bar{n}$ and $N_0 = (1 - \bar{n})$, and that ρ_{total} includes the contribution from re-entry [equation (4.52)], the following time-evolution of $\bar{n}$ follows from equation (4.54).

$$\frac{d\bar{n}}{dt} = \rho(1 - 2\bar{n}) - 2k\bar{n}^2 \tag{4.55}$$

Here the exit loss term is second-order in $\bar{n}$ since both the rate of formation of exiting radicals, as well as the probability of entry into an occupied (N_1) particle, depend on $\bar{n}$. This corresponds to the so-called zero-one "Limit 2a" of Chapter 1.

The value of $\bar{a}$ reflects the conversion dependence, or more accurately the particle radius dependence, of the radical loss processes that are operative. Therefore if, as in this case, the value of k is assumed to be constant with particle radius (discussed further below), then at sufficiently low ρ/c and k/c ($\sim 10^{-2}$ according to Figure 4.15) the zero-one approximation leading to equation (4.55) becomes accurate and the limiting value of $\bar{a} = 0$ is obtained.

It is therefore possible that the low acceleration data from experiment may be explained by the present system lying somewhere between the pseudo-bulk and zero-one kinetic limits; *i.e.*, the effects of compartmentalisation are non-negligible and vary with the experimental conditions. The approach used here for fitting of experimental data from chemically initiated experiments is as follows. Firstly, the conversion dependent value of c is calculated using equation (4.11) and the value of $\langle k_t \rangle$ from γ-relaxation experiments. ρ and k are treated as the only adjustable fitting parameters and for a given pair of these values $\bar{n}$ is calculated as a function of Interval II conversion from equations (4.50) – (4.52) as described above. Comparison of the modelled $\bar{n}$ data with Interval II $\bar{n}$ data from experiment enables the calculation of the sum of squared residuals and the process is repeated over an increasing range of ρ and k values until the value of this sum is minimised. The specific pair of ρ and k values giving the best fit to the experimental $\bar{n}$ data may thus be isolated, together with a two-dimensional joint confidence interval (JCI)[41] indicating a particular level of statistical uncertainty associated with each value (in this case the JCI corresponding to the 95% confidence limit was used). The results obtained from fitting of experimental data are shown in Figure 4.17.

At this point we return momentarily to the assumption made earlier that $k_p^1[M]_p \gg k_{dM}$, and hence that re-entrant monomeric radicals are bound to undergo propagation inside a particle before they are able to desorb (or "re-exit") back into the aqueous phase. In section 4.6.2 it was shown that under such conditions the appropriate expression for k is that of equation (4.26). Clearly then, k should not be radius independent but should scale as $1/r_s^2$. The effect of a radius dependent k on the value of $\bar{a}$ must therefore also be considered. As before, it is instructive to first construct a plot of model values of $\bar{a}$ before launching into full fitting of experimental data. In Figure 4.16 are presented values of $\bar{a}$ calculated using the same parameter values as for Figure 4.15 but taking into account the decrease in k during Interval II described by equation (4.26). Thus k/c now refers to both the values of *k and c* at the start of the steady-state period (both of which now change with conversion). It is evident that the radius dependence of k gives rise to an enhancement of the acceleration (as expected from earlier work – see Table 4.6) under conditions such that both $k/c < 1$ and $k > \rho$, with the value of $\bar{a}$ tending towards a plateau at approximately 0.25. Also noteworthy is the observation that $\bar{a}$ is still seen to decrease towards zero when both $\rho/c \ll 1$ and $\rho \gg k$. This rather subtle effect is explained by the fact that when termination is rapid and non-rate-determining (in the

zero-one limit) and the frequency of entry events far exceeds that of exit events, the dominant mode of radical loss is *via* entry of an initiator-derived radical into a particle that already contains a growing radical, resulting in rapid termination; *i.e.*, the $(-2\rho\overline{n})$ term in equation (4.55) becomes the dominant radical loss term. Since ρ is independent of particle radius the value of $\overline{a}$ tends towards zero under these circumstances.

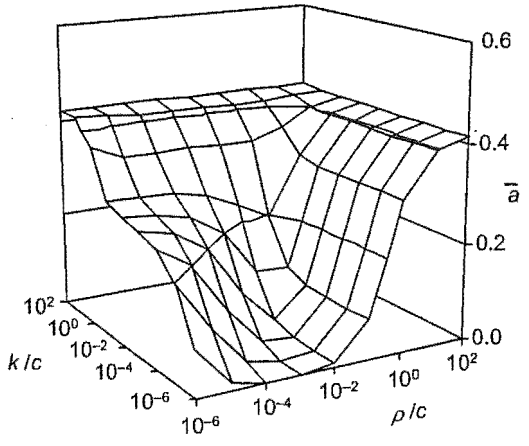

Figure 4.16. $\overline{a}$ calculated from model $\overline{n}$ data generated for a range of both ρ/c and k/c values using the Smith-Ewart model with propagation of re-entrant radicals, and using a radius dependent value for k (where $k \propto 1/r_s^2$).

Having identified the effect of a radius dependent exit rate coefficient on $\overline{a}$, it remains to re-fit the experimental data using this new variation of the Smith-Ewart model. The fitting procedure used here is the same as that described earlier except that in this case the adjustable parameters are ρ and the value of the exit rate coefficient *at the start of the steady-state period*, k_0, which is used to calculate k as a function of Interval II conversion, according to $k = k_0(r_s^0/r_s)^2$. The results of this re-fitting of the experimental data are also presented in Figure 4.17.

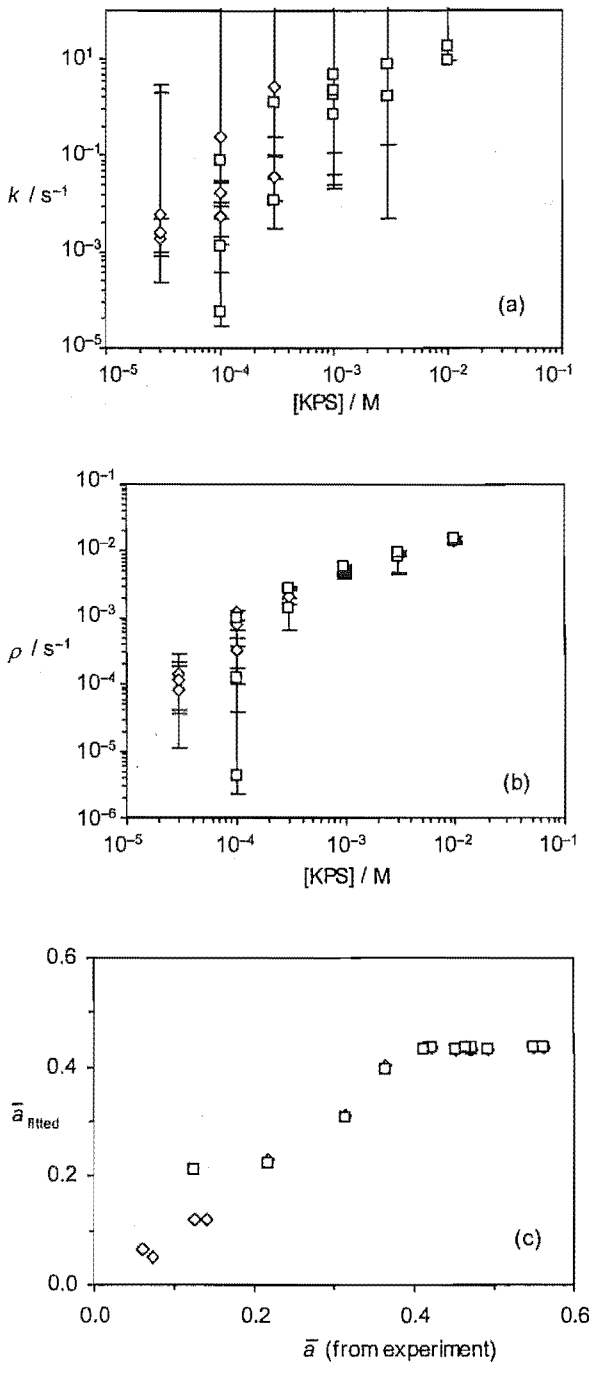

Figure 4.17. Results of least-squares fitting of the Smith-Ewart model to experimental data assuming re-entry followed by propagation, and with either radius independent k (diamonds) or radius dependent k (squares); **(a)** values of k and **(b)** values of ρ as functions of initiator concentration (with uncertainties corresponding to a 95% joint confidence interval); **(c)** values of $\bar{a}$ from fitted data plotted against experimental $\bar{a}$.

As is evident from Figures 4.17 (a) – (c), data fitting efforts are unable to furnish precise values of ρ, k (or k_0) and $\bar{a}$ for every experiment, and some explanation for this is now given. Firstly, for the case where k is assumed to be independent of radius the fitting of data from

experiments with [KPS] $\geq 10^{-3}$ M is found to be insensitive to the value of k; *i.e.*, here $\overline{n}$ (and hence $\overline{a}$) is determined only by the values of ρ and c. This reflects the accuracy of the pseudo-bulk model under these conditions. Secondly, for the alternative case, where k takes a $1/r_s^2$ dependence, the situation is similar, however in most cases a "best fit" value for k_0 may be isolated – albeit with an extremely large associated uncertainty. Finally, also for the case with $k \sim 1/r_s^2$, no "best fit" is obtained in data fitting for experiments with [KPS] = 0.03 mM (the lowest [KPS] used). Here, the effect of a radius dependent k causes the value of $\overline{a}$ from modelling to be well above that from experiment, guaranteeing a comparatively poor fit. The values of both ρ and k_0 are also relatively low and termination is therefore rapid and non-rate-determining; *i.e.*, the zero-one kinetic limit is reached. Under these conditions a marginal improvement in the (poor) fit to experimental data can always be achieved by further decreasing the values of ρ and k_0 in concert; hence the sum of squared residuals from fitting may never be truly minimised.

Notwithstanding the specific data fitting limitations discussed above, the results obtained from fitting with a radius independent k are generally very similar to those obtained using a radius dependent k value. The most significant finding here is the ability of the Smith-Ewart model to account for values of $\overline{a} < 0.42$ in at least some cases through the effects of compartmentalisation, as shown in Figure 4.17 (c). However, it would be misleading to suggest that this explanation is free of any inconsistencies. In particular it is noted that the value of k (or k_0 in the case of radius dependent k) generated from data fitting is seen to vary from experiment to experiment, spanning several orders of magnitude, and in all cases is also subject to considerable uncertainty. Theory provides no basis for explaining such a dramatic effect on the rate coefficient for exit simply from varying the initiator concentration. Seeking to improve on this situation, a slightly different modelling approach is next employed.

Re-entry followed by re-exit

As stated earlier, it is assumed (based on estimates of reaction rates for the present system) that aqueous-phase termination of exited radicals is negligible, and that all exited radicals rapidly encounter and re-enter a latex particle. The model of the previous section also assumed complete propagation of all re-entrant radicals, *i.e.*, that $k_p^1[M]_p \gg k_{dM}$ (see earlier discussion). However, as has been the case elsewhere in this work, it is sensible to consider the alternative limit of $k_{dM} \gg k_p^1[M]_p$ (if only to acknowledge the uncertainty in the value of k_p^1

– *e.g.*, see Figure 4.10). In this limit we assume that the rate of desorption for monomeric radicals is sufficiently high that, upon re-entry into a particle, a monomeric radical will rapidly re-exit that particle again before it is able to undergo any propagation steps. In this way, any radical formed by transfer to monomer will continue to move back and forth between particle and aqueous phases until it eventually enters a particle in which the rate of termination is sufficiently high that radical annihilation prevails.

An immediate kinetic implication of the situation described above is that the contribution to the entry rate coefficient from the flux of re-entering radicals is now zero (since re-entry now generates no *propagating* radicals). Therefore ρ_{total} must be re-defined simply as:

$$\rho_{\text{total}} = \rho \tag{4.56}$$

In the zero-one limit of ρ/c, $k/c \ll 1$ the situation described above then leads to a slightly different time-evolution for $\bar{n}$. Substituting equation (4.56) into equation (4.54) gives:

$$\frac{\mathrm{d}\bar{n}}{\mathrm{d}t} = \rho(1-2\bar{n}) - k\bar{n} \tag{4.57}$$

Here the exit loss term is only first-order in $\bar{n}$, since any monomeric radical produced from transfer will continue to undergo re-entry and re-exit until it finally re-enters an occupied (N_1) particle and terminates with a propagating radical. This corresponds to the so-called zero-one "Limit 2b" of Chapter 1. Additionally, since it is assumed that $k_{\text{dM}} \gg k_{\text{p}}^1[\text{M}]_{\text{p}}$ here, one might expect the exit rate coefficient to take the value $k = 2k_{\text{tr}}[\text{M}]_{\text{p}}$ (akin to equation (4.25), but larger by a factor of two since in this case every chain transfer to monomer reaction leads to loss of two propagating radicals). On this basis we henceforth assume the value of k to be radius independent.

Clearly, equation (4.57) embodies a qualitatively different zero-one kinetic limit to that of the previous section. With this limit as an alternative starting point it is therefore of interest to determine the effect that varying the degree of compartmentalisation has in this case. This may be achieved by removing the zero-one closure condition and hence obtaining an applicable form of the Smith-Ewart equation, analogous to that used in the previous section. With the value of ρ_{total} set equal to ρ as in this case, it is seen that the appropriate form of the Smith-Ewart equation is in fact exactly as it was originally written in equation (4.50), although the physical reason for this is different: every exited radical is now lost as a result of

rapid intra-particle termination (as opposed to aqueous-phase termination). However, one should not push this physical representation too far, as clearly it is only strictly valid for zero-one conditions and not for conditions where there are multiple free radicals per particle. In essence the following kinetic modelling is therefore best regarded as Smith-Ewart modelling with $\alpha = 0$.

As before, we start by solving this equation in conjunction with equation (4.51) using the same "standard" parameter values as for Figures (4.15) and (4.16) to give $\overline{n}$ data from which model values of $\overline{a}$ may be calculated. The results obtained in this case are presented in Figure 4.18. As might be expected, it is evident that assuming a different fate for re-entrant radicals has very little effect on the acceleration under conditions where exit is a relatively insignificant kinetic event, *i.e.*, when $k \ll \rho$, c the results are identical to those of Figures (4.15) and (4.16). However, under all conditions where exit becomes the dominant mode of radical loss the acceleration is seen to take the limiting value of $\overline{a} = 0$ – reflecting the radius independence of k, which goes hand-in-hand with the idea of transfer-controlled exit, as discussed above.

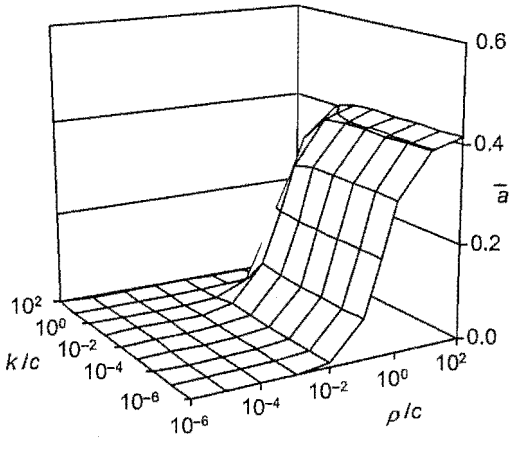

Figure 4.18. $\overline{a}$ calculated from model $\overline{n}$ data generated for a range of both ρ/c and k/c values using the Smith-Ewart model with radical re-entry followed by re-exit.

Clearly, the calculated values of $\overline{a}$ displayed in Figure 4.18 suggest the potential for this particular modelling approach to reproduce the experimental variation in $\overline{a}$ with ρ (and [KPS]). We therefore proceed with fitting experimental data using this variation of the Smith-Ewart model. Once again, the fitting procedure freely adjusts the values of ρ and k to give

calculated Interval II $\bar{n}$ data that are in closest accord with experimental $\bar{n}$ data. Results from data fitting for each experiment are shown in Figure 4.19.

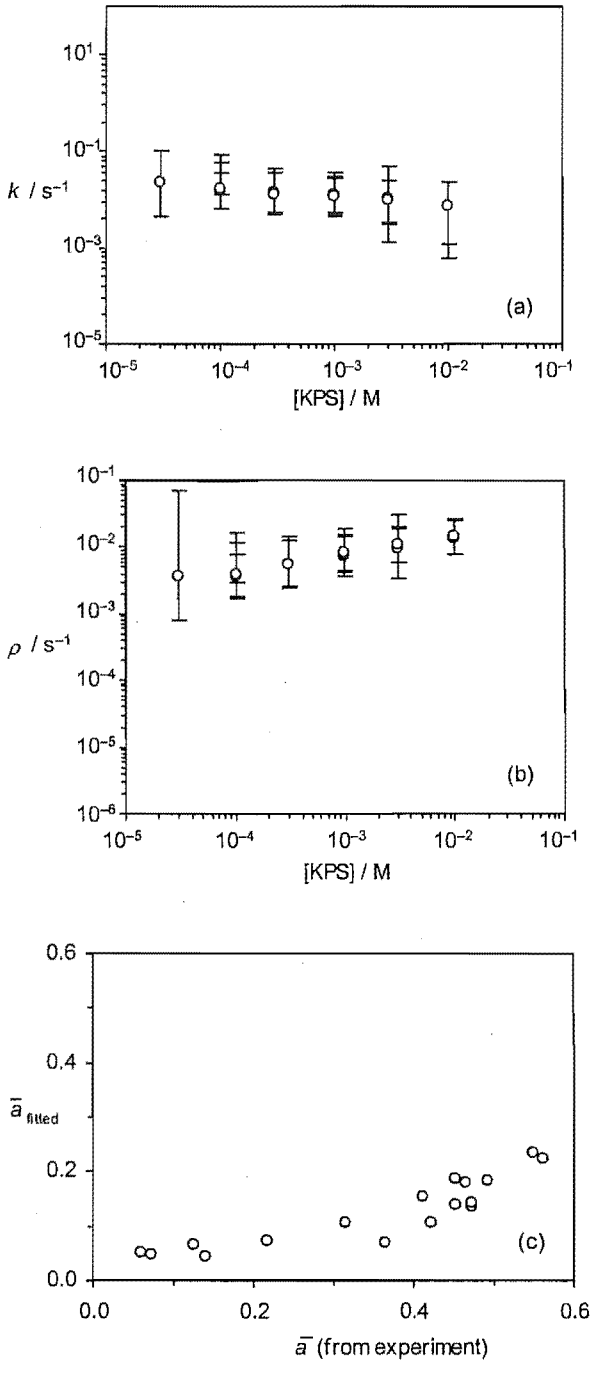

Figure 4.19. Results of least-squares fitting of the Smith-Ewart model to experimental data assuming re-entry followed by re-exit and radius independent k; **(a)** values of k and **(b)** values of ρ as functions of initiator concentration (with uncertainties corresponding to a 95% joint confidence interval); **(c)** values of $\bar{a}$ from fitted data plotted against experimental $\bar{a}$.

In contrast to the data fitting in the previous section, best fit values for ρ and k are obtained for experiments over the full range of [KPS] in this case (note that this does not mean that in all cases a good fit to the experimental data was obtained, just that the limits of the joint confidence were well defined). It is evident from Figure 4.19 (a) that the fitted values of k show no significant variation with changing [KPS]. However, in all cases the value of k is about an order of magnitude less than the theoretical value of $k = 2k_{tr}[M]_p \approx 0.51$ (based on the values $k_{tr} = 3.7 \times 10^{-2}$ M^{-1} s^{-1} and $[M]_p = 6.9$ M, used throughout this work). Perhaps most significantly, in Figure 4.19 (c) it is seen that the agreement between experimental and fitted values of $\bar{a}$ is relatively good for the lowest accelerations but deteriorates markedly for experiments with higher $\bar{a}$ (reflecting poor data fits at high $\bar{a}$). This is quite different to the data fitting of the previous section which gave considerably better accord for experiments wherein the measured acceleration was highest. This last observation indicates that the radius independence of k significantly affects the acceleration calculated from fitted data even for experiments with highest [KPS], *i.e.*, exit remains a significant mode of radical loss in modelled data under all conditions of interest here.

The above observation highlights the fundamental difference between the variant of the Smith-Ewart model used here and that of the previous section. In the present case, with $k_{dM} \gg k_p^1[M]_p$, all exited radicals are supposed to ultimately undergo termination inside a latex particle with a propagating radical. Therefore every exit event results in the loss of two propagating radicals and, as seen in Figure 4.19 above, exit remains a significant radical loss process over a broad range of conditions. In fact, the assumption that exit claims two propagating radicals represents an upper bound for the extent of radical loss *via* exit. Indeed, it should be noted that even if this assumption is accurate under zero-one conditions (where termination is assumed to be pseudo-instantaneous) this is no guarantee of its accuracy under other conditions where the rate of termination may be substantially slower. Equivalently, the lower bound for exit loss is given by the founding assumption for the Smith-Ewart modelling of the previous section: that $k_p^1[M]_p \gg k_{dM}$, and every exited radical undergoes re-entry followed by subsequent propagation. In this case, exit is only a significant radical loss mechanism under zero-one conditions; under other conditions exit results in no net loss of radicals whatsoever.

Of course, it is difficult to identify one of the above limiting assumptions as being strictly applicable. For example, given the uncertainty in k_p^1, it may well be the case that $k_p^1[M]_p \approx$

k_{dM}, and hence that re-entry involves a combination of propagation and re-exit. Furthermore, the precise kinetic circumstances (and appropriate assumptions) may vary from one experiment to another along with the magnitudes of ρ, k, c and $\bar{n}$. However, while definitive resolution of these matters may not be found here, the results of data fitting above are by no means worthless. We acknowledge above that the assumption of re-entry followed by re-exit and eventual intra-particle termination may overestimate the extent of radical loss *via* exit. Accordingly, any fitted value of ρ obtained using the Smith-Ewart model with this assumption must constitute an approximate upper bound for the radical entry rate coefficient in a given experiment. Similarly the assumption of complete propagation of re-entrant radicals may underestimate the extent of exit loss, and hence any fitted value of ρ obtained using this assumption must constitute an approximate lower bound for this quantity.

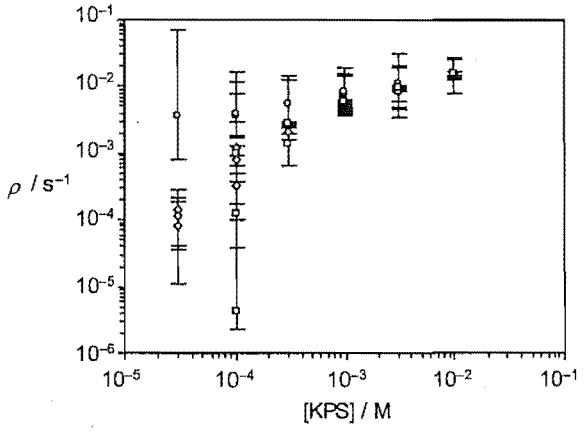

Figure 4.20. ρ values obtained from least-squares fitting of the Smith-Ewart model to experimental data assuming re-entry followed by propagation and radius independent k (diamonds), re-entry followed by propagation with radius dependent k (squares), and $\alpha = 0$ with radius independent k (circles); uncertainties correspond to a 95% confidence interval.

Combining the three sets of ρ data obtained from fitting using variations of the Smith-Ewart model, as in Figure 4.20, thus provides the most useful means for estimating the "true" value of ρ in this case. Clearly, the upper and lower bound values of ρ obtained from fitting of experimental data for low [KPS] span a broad range (in the case of [KPS] = 0.03 mM no precise lower bound could be identified – see earlier). However, this observation is not surprising when it is considered that at low [KPS] the value of ρ is lowest and therefore most sensitive to the assumed fate of exited radicals. Accordingly, as the value of ρ increases with increasing [KPS] the effects of exit and re-entry become less significant, and at highest [KPS]

the upper and lower bound values for ρ are seen to converge, because termination dominates the radical loss kinetics.

Summarising the results obtained in this section using variations of the Smith-Ewart model, it has been established that the effects of radical compartmentalisation can at least semi-quantitatively explain the variation observed in experimental measurements of the Interval II acceleration. As in earlier sections, it was found that the determination of unique values for entry and exit rate coefficients was complicated by the sensitivity of these quantities to the assumed fate of exited monomeric radicals. While significant improvement of this situation can come only with a more detailed understanding of the exit and re-entry kinetics of this system, careful consideration of various limiting assumptions has enabled useful estimates to be made for the values of these rate parameters.

Finally, it is noted that a fundamental limitation common to all the variants of the Smith-Ewart kinetic model used throughout this section is the absence of a microscopic treatment of the processes of exit and re-entry. An obvious avenue for future work is therefore to extend the kinetic framework of equation (4.50) to incorporate the population balances of monomeric radicals generated inside the latex particles by transfer to monomer, as well as exited monomeric radicals in the aqueous phase, and all initiator-derived aqueous-phase radicals. The details of formulating a kinetic treatment of this sort will be expounded in Chapter 8.

4.6.5 Summary: Best Estimates for $\langle k_t \rangle$, ρ_{spont}, ρ_{init} and f_{entry}

Based on the results of the preceding sections we now compile best estimates for the values of various key rate parameters in the Interval II emulsion polymerisation of MMA at 50°C.

As discussed earlier, the values of $\langle k_t \rangle$ and ρ_{spont} may be determined with confidence by fitting the integrated form of the pseudo-bulk equation to data from γ-relaxation experiments. Thus, the values $\langle k_t \rangle = (1.9 \pm 0.1) \times 10^4$ M^{-1} s^{-1} and $\rho_{spont} = (1.5 \pm 0.1) \times 10^{-4}$ s^{-1} were obtained. It has been postulated that the value of ρ_{spont} may in fact be subject to a particle volume dependence (which may affect the Interval II acceleration in some cases), however in the absence of a detailed mechanistic understanding of spontaneous polymerisation for this system we assume that this is not the case. It is also noted that the value of $\langle k_t \rangle$ is likely to be responsive to changes in the precise radical chain length distribution. Modelling with chain length dependence has revealed a small effect on $\langle k_t \rangle$ from changes in particle volume,

however in practical terms this effect is likely to be smaller in magnitude than the uncertainty associated with experimental measurements. The effect of a change in ρ on the radical distribution and hence $\langle k_t \rangle$ should also be considered. However, it will be shown in the following chapter that this effect is also relatively minor; the present system appears to be close to the so-called transfer limit for termination, where the radical chain length distribution is largely determined by the chain transfer reaction. It is therefore concluded that the value of $\langle k_t \rangle$ quoted above is appropriate for all experimental conditions in the present work.

We now turn to the kinetic parameters pertaining directly to entry of initiator-derived radicals: ρ_{init} and f_{entry}. Given values of ρ obtained from experiment, the value of ρ_{init} may be obtained *via* equation (4.9), and values of f_{entry} subsequently calculated according to equation (4.7). The question then remains as to which set of ρ data to use. The original estimates, ρ_0, obtained using the pseudo-bulk equation with $\alpha = 1$, and the values of $\bar{n}$ and c at the start of the steady-state period for each experiment, were brought into question by the discrepancy between the (constant) value of $\bar{a}$ predicted by the pseudo-bulk model and the values of $\bar{a}$ measured experimentally. This discrepancy was lessened in several cases by use of the pseudo-bulk model with $\alpha \leq 1$. However, the lack of any microscopic model for α sheds uncertainty on the values of ρ obtained through the use of this parameter. Next a modelling-only study was undertaken to ascertain the effect of chain length dependent termination on the value of $\bar{a}$. Based on the finding that the acceleration was generally very similar to that obtained assuming chain length independent termination it is concluded that no substantial improvement in the accuracy of ρ values from experiments here will be gained by fitting data with a chain length dependent model. Finally, the effects of compartmentalisation on the value of $\bar{a}$ were examined through the use of the Smith-Ewart equation. Here the agreement with experimental $\bar{a}$ values was improved significantly in cases. However, the treatment was restricted to two different limiting forms of the model for exit – dependent on the value assumed for k_p^1 – resulting in upper and lower bound estimates for ρ, which spanned a broad range in some cases. Further, no model to explain the entire data set was found.

Table 4.9. Results obtained from kinetic experiments using chemical initiator (KPS), with ρ calculated from equation (4.22), and averaged over entire steady-state period; ρ_{init} and f_{entry} calculated from equations (4.7) and (4.9).

Run	[KPS] / 10^{-3} M	ρ / 10^{-4} s^{-1}	ρ_{init} / 10^{-4} s^{-1}	f_{entry}
C54	0.030	4.9	3.4	0.35
C61	0.030	6.5	5.0	0.52
C101	0.030	7.0	5.4	0.58
C52	0.10	13	11	0.36
C68	0.10	11	9.7	0.31
C102	0.10	14	13	0.39
C69	0.30	28	27	0.28
C62	0.30	30	28	0.30
C73	1.0	50	49	0.15
C67	1.0	52	51	0.16
C66	1.0	55	53	0.17
C50	1.0	61	59	0.19
C72	3.0	94	92	0.097
C55	3.0	90	88	0.093
C70	3.0	98	97	0.10
C56	9.9	146	144	0.046
C58	9.9	159	158	0.050

It is therefore concluded that while the kinetic effects above may partially explain the experimental Interval II acceleration data, none of these effects quantitatively accounts for the observed variation in $\bar{a}$. Given this lack of a definitive explanation, the departure of $\bar{a}$ from the pseudo-bulk value may best be treated as a small but significant unresolved problem at the present time. The most appropriate estimate of ρ for each experiment is therefore deemed to be the mean value of ρ over the steady-state period of Interval II as calculated using equation

(4.22) (*i.e.*, the pseudo-bulk equation with $\alpha = 1$), with any variation in ρ providing an indication of the experimental error associated with this value. This approach furnishes the values of ρ presented for each experiment in Table 4.9.

These values of ρ obtained are also shown in Figure 4.21, together with the values obtained using the Smith-Ewart model earlier. The averaged results from pseudo-bulk fitting are seen to fall approximately mid-way between the upper and lower limiting values from the Smith-Ewart method at low initiator concentrations, with all results converging towards high initiator concentration. This justifies the approach of using the $\alpha = 1$, pseudo-bulk values of ρ as best estimates.

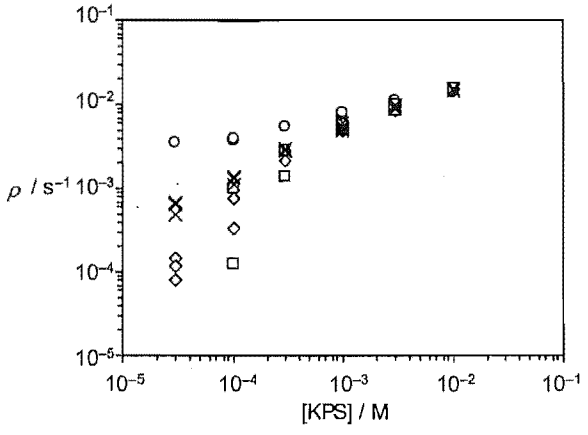

Figure 4.21. ρ obtained from experiment using the pseudo-bulk equation and averaged over entire steady-state period (crosses); values presented as a function of initiator concentration, together with results from Smith-Ewart fitting with re-entry followed by propagation and radius independent k (diamonds), re-entry followed by propagation with radius dependent k (squares), and $\alpha = 0$ with radius independent k (circles).

Values for ρ_{init} and f_{entry} may then be calculated in each case from ρ according to equations (4.7) and (4.9), and using the value of ρ_{spont} quoted above. The resulting best estimates of these parameters for each experiment are presented in Table 4.9, with f_{entry} values also presented graphically in Figure 4.22.

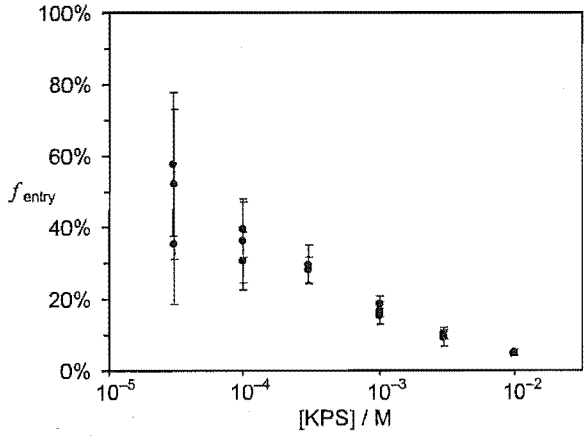

Figure 4.22. f_{entry} as a function of initiator concentration, obtained from experiment using the pseudo-bulk equation along with uncertainties arising from the variation in ρ during the steady-state period.

It is apparent that the values of f_{entry} as calculated above for MMA at 50°C are generally much less than 100%. This suggests that a substantial fraction of the radicals derived from initiator are claimed by aqueous-phase termination reactions before they are able to undergo sufficient propagation to form an entering species. Notably, these results are in line with those reported by Ballard *et al.*,[1] who estimated f_{entry} to be somewhere in the range of 20 – 50% under similar conditions. It is also evident from Figure 4.22 that, despite considerable uncertainty in the value of f_{entry} at low [KPS], there is a systematic decrease in entry efficiency with increasing initiator concentration, with only a small fraction of the total radical flux undergoing entry when [KPS] = 10 mM. Very importantly, this finding is model-independent, because ρ values are model-independent at high [KPS] (see Figure 4.21). The reason for this is that radical loss must be dominated by termination at high [KPS], with exit and re-entry only being perturbations to explain fine trends (*e.g.*, possible variations in $\bar{a}$ from its theoretical value) in the data.

4.6.6 Modelling Entry

The values of f_{entry} obtained from experimental rate data are now interpreted in terms of the entry model of Maxwell *et al.* As in Chapter 3, model values for f_{entry} are calculated from numerical solutions of the population balance equations for initiator-derived aqueous-phase radicals, shown earlier as equations (4.37) – (4.39). This approach is favoured over the use of equation (4.6) due to the inaccuracy of the analytic solution under conditions of high entry efficiency (see Chapter 1).

The values used for aqueous-phase rate parameters (fk_d, $k_{p,w}$, $k_{t,w}$) in model calculations here are as stated previously in the text, and the value of $N_c = 4.3 \times 10^{16}$ dm^{-3} corresponds to that for chemically initiated experiments. z is treated as an adjustable parameter and its value varied over the range 1 to 20.

Modelled f_{entry} results are plotted as functions of initiator concentration in Figure 4.23, along with the values obtained from experiment above. It is seen that increasing initiator concentration leads to a decrease in entry efficiency due to an increase in the total concentration of aqueous radicals, and hence also the rate of termination (except in the limit of $z = 1$ where f_{entry} is 100% for all [KPS]). Furthermore, it is seen that increasing the number of propagation steps required for entry by having a higher value for z results in longer residence times for radicals in the aqueous phase and hence a higher incidence of aqueous-phase termination (lower f_{entry}).

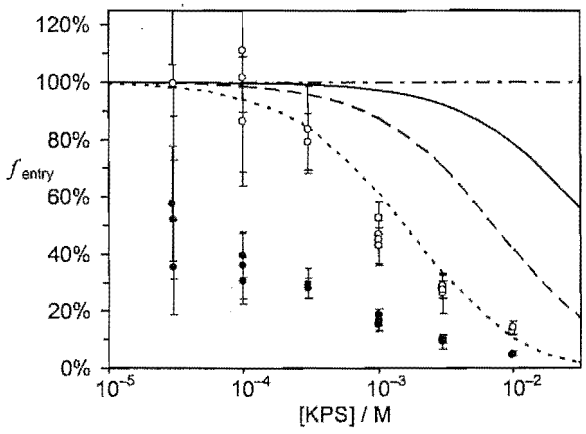

Figure 4.23. f_{entry} as a function of initiator concentration, obtained from experiment using the pseudo-bulk equation (filled circles) presented together with scaled experimental values (empty circles, see text for explanation), and modelled results obtained using the Maxwell-Morrison model with $z = 1$ (— – — –), $z = 5$ (————), $z = 10$ (— — —), and $z = 20$ (– – – –).

From Figure 4.23 it is apparent that the decrease observed in experimental f_{entry} values is consistent with the trend in modelled data for the case of $z \gg 1$ and suggests that, due to significant termination of initiator-derived radicals in the aqueous phase, the value of f_{entry} is highly sensitive to the concentration of added initiator. What is more difficult to reconcile is the fact that, regardless of the value of z used in modelling, entry is inevitably seen to be approximately 100% efficient for calculations with [KPS] ~ 10^{-5} – 10^{-4} M, whereas this is certainly not the case for experimental data. This brings to mind that experimental f_{entry}

values for such conditions are subject to the greatest uncertainty in ρ_{init} (associated with the unexplained variation in Interval II acceleration). For example, an explanation here is that ρ_{init} values are higher at low [KPS], for example the $\alpha = 0$ values of Figure 4.21 (the circles). In fact these would give f_{entry} above 100%, dropping to below 10% at high [KPS]. However this would lead to the problem (see following discussion) of an enormous z value, much greater than 20. Hence this is an unsatisfactory suggestion.

Another suggestion is that entry is significantly impeded by some sort of repulsive interaction between the negatively charged entering radicals and the surface-bound initiator fragments and surfactant molecules (also negatively charged) occupying the particle surface. Such an effect would not be accounted for in the Maxwell-Morrison model. However, the work of Chapter 3, employing different radical-particle charge combinations, suggests that any such charge-charge interactions have a negligible effect on the rate of entry.

Referring to equation (4.7) it is seen that the only remaining sources for error in f_{entry} are the values of N_c and fk_d. Contemplating the potential for error in either of these quantities, it is noted that N_c is affected chiefly by uncertainty in the measured particle size, and that the value of fk_d is known to be sensitive to the precise experimental conditions.[16] Indeed, the effect of aqueous MMA on the value of fk_d in an emulsion system remains an interesting area for experimental investigation. Importantly, an error in either N_c or fk_d will have an equal effect on the value of f_{entry} obtained from each experiment. Thus, one approach which may aid the interpretation of our results is to scale all experimental entry efficiency data by some constant scaling factor, such that $f_{entry} \approx 100\%$ for [KPS] ~ 10^{-5} – 10^{-4} M (as should be the case). It is emphasised that this scaling relies on the supposition that the discrepancy in f_{entry} at low [KPS] is explained entirely by an underlying error in the value of N_c and/or fk_d used (and is therefore not purely arbitrary). So long as this assumption is correct the accuracy of our interpretation of the experimental data will not be compromised. However, in the event that some other unknown source of error is responsible, this scaling may cloud the picture, rather than clarify it.

The scaled experimental f_{entry} results are also displayed in Figure 4.23 and reveal a significant improvement in the agreement with data generated using the Maxwell-Morrison model. The scaled data appear to be fitted reasonably well by the model using a value of $z = 20$. Of course, it must be reiterated that this inferred value for z is subject to the caveats relating to

the scaling applied. It is noted, however, that the unscaled experimental results are certainly suggestive of a value for z at least as high as $z = 20$.

In their original work,[9] Maxwell *et al.* presented a thermodynamic approach for estimating the value of z for a given monomer based on its water solubility. In Chapter 3 this approach was shown to be consistent with experimental data from styrene emulsion polymerisations using both persulfate and amidinium initiators. In the case of a persulfate initiator the expression for z is as follows,

$$z = 1 + \mathrm{int}\left\{\frac{-23\ \mathrm{kJ\ mol^{-1}}}{RT\ \ln([\mathrm{M}]_w/\mathrm{mol\ dm^{-3}})}\right\} \tag{4.58}$$

where the integer function "int" reduces to the next lowest integer value.

Here the value of –23 kJ mol^{-1} was estimated by Maxwell *et al.* as the value of the hydrophobic free energy of adsorption, ΔG_{hyd}, required to render a polar SO_4^- group (from initiator) surface-active. The denominator in equation 4.58 approximates the value of ΔG_{hyd} for a single monomer unit on the basis of the monomer's water-solubility as $RT\ \ln\{[\mathrm{M}]_w/(\mathrm{mol\ dm^{-3}})\}$. The essence of this approach is thus to assume an equal free energy contribution from each monomer unit, assumed to be the same as that for an isolated monomer unit, and to identify the value of z as the minimum number of monomer units for which the cumulative value of ΔG_{hyd} exceeds –23 kJ mol^{-1} (in absolute magnitude). This approach is illustrated graphically in Figure 4.24.

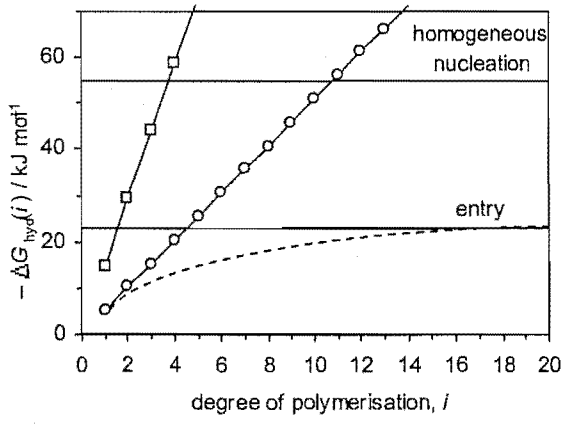

Figure 4.24. Free energy of adsorption for persulfate-derived oligomers calculated using group-additivity approach of Maxwell *et al.*; calculated values for styrene (squares) and MMA (circles) compared with solid lines

indicating (estimated) free energy thresholds required for entry (–23 kJ mol^{-1}) and homogeneous nucleation (–55 kJ mol^{-1}); dashed line illustrates a possible departure from group-additivity.

Figure 4.24 shows the way in which the estimated free energy contribution per monomer unit varies with monomer water-solubility. Thus for styrene, with comparatively low-water solubility, two monomer units are sufficient to make entry of a sulfate-ended oligomer thermodynamically favourable, while for the more water-soluble monomer MMA addition of five units is required for entry. Additionally, Figure 4.24 shows the free energy threshold value of –55 kJ mol^{-1} which Maxwell *et al.* postulated is required for an oligomeric species to form a new particle *via* homogeneous nucleation. For a persulfate-derived styrene oligomer this value is attained after addition of four monomer units, while for MMA 11 units must be added.

Thus from Figure 4.24, or equally using the Interval II value of $[M]_w = 0.15$ M in equation (4.58), the thermodynamic approach of Maxwell *et al.* predicts a value of $z = 5$ for MMA at 50°C. This model value is considerably lower than the value of $z \approx 20$ inferred from experiment above. Importantly, Figure 4.23 further shows that such a difference is non-negligible in terms of kinetic data for entry: a value of $z = 5$ should give rise to f_{entry} values close to 100% over the entire range of [KPS] of interest – quite a different trend to the strong decrease in f_{entry} with increasing [KPS] which was observed experimentally.

It is therefore of critical interest to seek out possible explanations for the discrepancy between the trend in experimental f_{entry} values and that predicted by the Maxwell-Morrison model (*i.e.*, $z = 5$, and hence f_{entry} close to 100%).

Firstly, one may consider the possibility of an error in the raw conversion-time data obtained experimentally by dilatometry. A fundamental problem of this sort seems unlikely given that the apparatus and approach used in this work have been shown to furnish results consistent with those obtained by other workers using different apparatus, *viz.* the results of Hawkett *et al.* for styrene[42] and those of Ballard for MMA.[1] Nevertheless, the validity of any underlying assumptions of the method should be considered. Most notable amongst these is the assumption in dilatometry of ideal mixing of monomer and polymer inside swollen latex particles. It is possible that significant non-ideality of mixing could give rise to error in the values of $\hat{x}$ calculated from the measured volume contraction.[43] However, it is noted that for experiments carried out in Interval II (as in this work) any such error will be systematic,

affecting all values of $\hat{x}$ – and hence also the measured rates – equally. Thus this effect cannot explain the observed difference in the *trend* of f_{entry} and $\bar{a}$ values.

Assuming that the raw experimental data are accurate, one may next question the validity of the methods of kinetic analysis used to extract the values of various rate parameters, including those related to entry: ρ, ρ_{init} and f_{entry}. In the present case these analysis methods draw on established kinetic frameworks for emulsion polymerisation, including the model of Smith and Ewart[10] and the pseudo-bulk model.[1,11] Admittedly, the data analysis is unable to account for some important features of the experimental data (*e.g.*, the observed variation of $\bar{a}$ with initiator concentration), indicating that these models do not represent a complete kinetic treatment. However, it would be unjustified to suggest that the results of this one study are sufficient to refute the well established models named above, as supported by a large body of literature.

Assuming that the means used to obtain values for f_{entry} from experiment are indeed sound, the spotlight is shifted onto the Maxwell-Morrison entry model. Following this line of thought there are four possible sources of error:

(1) The simplest explanation is that the thermodynamic estimate of $z = 5$ is indeed correct, and the difference in f_{entry} values is the result of an error in the parameters used to generate the predictions of Figure 4.23. Examining equations (4.37) and (4.38), it is clear that an overestimate for $[IM^{\bullet}_{z-1}]$, and hence f_{entry}, must arise from an error in the values assumed for $k_{p,w}$ and $k_{t,w}$. The value used here for $k_{t,w}$ of 3.7×10^9 M^{-1} s^{-1} is that suggested by Maxwell *et al.*[9] based on a range of literature data for reactions of small aqueous radical species. This value also agrees well with the diffusion-limit value of $k_{t,w} \approx 4\pi\sigma p_{spin} D_w N_A \approx 3 \times 10^9$ M^{-1} s^{-1}, calculated for aqueous-phase termination of monomeric MMA radicals using the Smoluchowski equation (4.29) with $\sigma = 1$ nm (approximating molecular dimensions), $p_{spin} = 0.25$ and $D_w = 1.7 \times 10^{-9}$ m^2 s^{-1}. Given that diffusion of monomeric radicals is likely to be faster than that of longer oligomers, this value represents an upper bound for $k_{t,w}$ in the present instance. It is found that agreement between experiment and modelled results for $z = 5$ requires the significantly higher value of $k_{t,w} \approx 10^{11}$ M^{-1} s^{-1}, hence an error in this parameter value seems unlikely to be the explanation here. Similarly, it is difficult to explain the discrepancy solely in terms of the value of $k_{p,w}$, since the value required for agreement with modelled results using $z = 5$ is $k_{p,w} \approx 100$ M^{-1} s^{-1} – approximately 80% less than the value

used here. Given that the value for $k_{p,w}$ is currently approximated by that measured for bulk polymerisations it is not unreasonable to suggest some effect from changing to a more polar solvent (water). However, while some slight (approximately 10%) reductions in k_p have been reported for MMA in solution[44] it would appear that in more cases an elevated value of k_p for MMA has been seen in the presence of relatively polar solvents.[45,46]

In light of the above, it is difficult to attribute the discrepancy between experimental f_{entry} data and modelled values for $z = 5$ simply to errors in the presumed values for $k_{p,w}$ and/or $k_{t,w}$.

(2) Secondly, it is possible that the thermodynamic reasoning which predicts formation of a surface-active species at $z = 5$ is sound, but that the Maxwell-Morrison kinetic treatment is somehow incomplete (*e.g.*, due to the omission of some additional rate-determining steps). One suggestion is that the Maxwell-Morrison model's correlation of entry with radical surface-activity may not hold true in all cases. Importantly, Maxwell *et al.* noted that even for a surface-active z-mer entry is not likely to occur upon the radical's first encounter with a latex particle. Indeed, a consideration of the relative rates of propagation, termination and desorption (given in Appendix B of reference[9]) showed that a z-mer is likely to encounter ~ 100 particles before finally undergoing entry. One must therefore distinguish *adsorption* of a radical onto a particle's surface (which may be followed by desorption back into the aqueous-phase) from true, irreversible *entry*. Here entry is assumed to occur when an adsorbed z-mer undergoes a single propagation event, forming a radical of length $(z + 1)$ which is regarded as totally water-insoluble and unable to desorb. In the case of the only other monomer for which a value of z has been identified, styrene, it is likely that this assumption is quite accurate due to the fact that this monomer is highly water insoluble. However, in the case of MMA, with its considerably greater water solubility, it is conceivable that a single added monomer unit (or perhaps even several) is insufficient to preclude any subsequent desorption of the $(z + 1)$-mer formed. In this event it might be possible for radicals to return to the aqueous phase, being exposed to termination for considerably longer, and growing beyond the length nominally prescribed for entry. Hence, while the thermodynamic value of z from equation (4.58) remains an accurate estimate for the attainment of *surface-activity*, it is perhaps only a lower bound for *entry*. Admittedly, this theory is unlikely to provide the full explanation for the low values of f_{entry} observed experimentally, because it would require that desorption rather than entry kept occurring for $IM_i^\bullet$ radicals from $i = 5$ to $i = 20$, which seems unlikely. However, it may at least be a contributing factor.

At this point it is additionally noted that the Maxwell-Morrison kinetic treatment assumes that only initiator-derived radicals partake in the aqueous-phase reactions leading to entry, *i.e.*, the presence of aqueous radicals arising from either exit or the unidentified source of spontaneously-generated radicals is neglected. It is realised that, should such radicals be present in sufficient concentration, acknowledging the possibility of termination with initiator-derived radicals could substantially reduce the modelled values of f_{entry} from those given in Figure 4.23. Investigation of this effect on modelled results reveals that in order to obtain agreement between experiment and modelled data with $z = 5$ the concentration of such supplementary radicals must be of order 10 – 100 times greater than that of *all* initiator-derived radicals. This explanation is therefore regarded as highly unlikely under the present conditions.

(3) Thirdly, it is possible that the modelled f_{entry} data in Figure 4.23 are indeed accurate, and the value of z is actually significantly greater than the thermodynamic prediction of $z = 5$. We therefore seek to explain why the thermodynamic approach of Maxwell *et al.* might underestimate the value of z. One possible explanation is hydrolysis of the ester group in MMA monomer units (either before or after their incorporation into an oligomer chain) to form methacrylic acid. In their analysis of aqueous species formed during emulsion polymerisation using mass spectrometry, Thomson *et al.* give evidence for the inclusion of up to two methacrylic acid units in aqueous oligomers. The presence of one or more relatively polar (or even charge-carrying, depending on pH conditions) methacrylic acid groups would serve to increase the water solubility of a growing oligomer, thus requiring the addition of a greater number of hydrophobic MMA units and lengthening the aqueous-phase residence time prior to entry. This effect might well be enough to cause the observed increase in the value of z; however, it will be shown experimentally in Chapter 5 that the possibility of monomer hydrolysis prior to entry seems unlikely.

Another explanation is based on the assumption in the Maxwell-Morrison model of group-additivity for successive monomer addition steps. Specifically, in equation (4.58) and Figure 4.24 it is assumed that every added monomer unit makes an equal contribution to the thermodynamic quantity governing the overall surface-activity of a growing radical in the aqueous phase: ΔG_{hyd}, the free energy change associated with transferring a growing radical from a hydrophilic to a hydrophobic environment. This contribution is estimated from the monomer's water solubility, *i.e.*, for the case of a monomer unit completely surrounded by

water. Again, for styrene systems, where only one or two monomer units are added, this approach is likely to be reasonable. However, for MMA radicals, where the number of added monomer units is significantly higher, the local environment experienced by a given monomer unit will be highly dependent on its position in a radical chain and thus the assumption of group-additivity may be questioned. While monomer units at the end of a radical chain will be largely surrounded by water, those near the centre will be shielded from the aqueous environment by neighbouring monomer units, possibly leading to a smaller free energy change for such monomer units upon adsorption. The departure from group-additivity arising from a diminishment in monomeric free energy contributions with increasing degree of polymerisation is illustrated schematically (as a dashed line) for comparison in Figure 4.24. Also, worth considering is the possibility for changes in chain conformation with increasing degree of polymerisation. Given that chain lengths in the range of 5 – 20 are anticipated it is not inconceivable that at some point linear chains may give way to coiled-chain conformations, *i.e.*, the effect ultimately leading to homogeneous nucleation. In this event it is even more feasible to expect non-additivity for free energy contributions since monomer units near the centre of a coiled chain are likely to be almost totally shielded from the aqueous surrounds. Under such extreme conditions it is postulated that entry may no longer be considered simply as a surfactant adsorption phenomenon, but may perhaps be better thought of as a coagulative process, similar to that undergone by precursor particles during particle formation[12] (not that the actual nature of the entry step is important in the Maxwell-Morrison model).

(4) The final possibility is that the Maxwell-Morrison model for entry is wrong. If this is the case, it is a remarkable coincidence that it does work so well for such a large body of data from styrene emulsion systems. Also, all other models must in fact build on the basic aqueous-phase kinetics of the Maxwell-Morrison model, *i.e.*, they will have the same problems with the MMA data. Shortly it will be shown that in fact other models do not fare any better; quite the opposite in fact.

In summary, whether one or all of the above effects is responsible for the value of $z \approx 20$ inferred from kinetic experiments, it appears that the simple entry model of Maxwell *et al.* does not provide a comprehensive account for entry in the case of MMA at 50°C. What is clear, however, is that the monomer type has a significant impact on the entry process. Kinetic results presented previously for styrene/persulfate systems have revealed a value of z

= 2. From the present study it is apparent that the trend in f_{entry} values measured for the MMA/persulfate system are consistent only with a considerably higher value of z. This is in line with the prediction by Maxwell *et al.* that z should increase with increasing monomer water solubility, however the effect appears to be somewhat greater than expected. It is felt that the most likely explanation for this is (3) given above.

It is tantalising that the variation of f_{entry} with [KPS] is in fact much the same for MMA as for styrene (see Chapter 3).

4.6.7 Comparison with Other Entry Models

Finally, given the possibility identified above that the Maxwell-Morrison entry model does not fully account for the experimental data obtained in this chapter it is prudent to consider whether any additional explanation may be obtained from any of the other models postulated for entry.

The key feature of the entry data obtained from experiment is the strong decrease observed in f_{entry} with increasing initiator concentration. Given the rapid rates of diffusion for small radicals, and the fact that seed latex particles of the same size were employed for all experiments, it is difficult to conceive of how a diffusion-controlled entry model[47-49] offers any explanation for the data. Additionally, the surfactant coverage for particles was the same in all experiments, thus the large variation in f_{entry} with initiator concentration may not be rationalised in terms of a model where surfactant displacement is the key step for entry.[50] A model for entry which may bear some relevance here, however, is that which treats entry as a an interaction involving colloidal radical and particle species.[51,52] While this model was discounted for the styrene systems of Chapter 3, where entry is by very small (certainly non-colloidal) radicals, it is possible that entry in the MMA/persulfate system involves much larger radicals which may well be colloidal in nature, as intimated in the previous section. A useful strategy for verification of this possibility would be a series of experiments wherein the ionic strength in the aqueous-phase is varied significantly (by addition of an inert salt). Increasing the ionic strength should enhance the rate of colloidal entry by disrupting the electrical double-layer surrounding reacting colloidal species.

4.7 Conclusions

Kinetic data have been obtained from emulsion polymerisations of MMA employing chemical initiator (persulfate), γ-radiolysis, and also in the absence of any added initiator. γ-relaxation data were fitted using the pseudo-bulk model (assuming complete re-entry of exited radicals) and the values of $\langle k_t \rangle$ and ρ_{spont} were in line with those observed previously for a similar system.[1]

Chemically initiated experiments exhibited a non-constant rate of polymerisation during Interval II, wherein the value of $\bar{n}$ was seen to gradually increase with conversion. The magnitude of this "acceleration" effect was found to vary with initiator concentration and hence was not fully described by the pseudo-bulk model (which predicts constant acceleration for all experiments). A variety of alternative theories were applied to attempt to explain the observed acceleration results. Of these, the most likely explanations appear to be a volume dependence of ρ_{spont} (usually assumed to be constant), and the effect of radical compartmentalisation (into distinct latex particles) under conditions of low radical flux. It is also important to note that all theory presented in this work is general, *i.e.*, not restricted to MMA emulsion systems, and may therefore be considered for use in kinetic investigations involving other monomers.

Values of f_{entry} obtained as a function of initiator concentration were subject to considerable uncertainty arising from the acceleration effect described above. Furthermore, low values of f_{entry} at low initiator concentration suggest either an overestimate for the radical flux based on the literature value of fk_d, or an underestimate of the particle concentration arising from uncertainty in the measured particle size. The variation in f_{entry} with changing initiator concentration indicates that the value of z may be as high as $z = 20$. However, this estimate is subject to considerable uncertainty from the sources discussed above.

The value of z inferred from kinetic experiments for the MMA/persulfate system is considerably higher than that observed previously for styrene/persulfate, where $z = 2$. This is in line with the Maxwell-Morrison theory which suggests (on thermodynamic grounds) that z should increase with increasing monomer water solubility, predicting a value of $z = 5$ for persulfate/MMA, and hence also that f_{entry} should be approximately 100% under all experimental conditions of the present study. The observed trend in f_{entry} data and the value of $z \approx 20$ thus inferred suggest that the influence of monomer solubility on entry is considerably

greater than the model predicts. The most plausible explanations for this appear to be the incorporation of hydrolysed MMA units (*i.e.*, methacrylic acid groups) into entering radicals, and the non-additivity of the contributions from each monomer unit to the free energy of adsorption for a growing oligomer chain. The explanation may also lie in the underlying assumption of the model that entry is immediate for a surface-active radical; while z may identify the critical chain length for surface-activity, it may be only a lower bound to that required for entry.

4.8 References

(1) Ballard, M. J.; Napper, D. H.; Gilbert, R. G. *J. Polym. Sci., Polym. Chem. Edn.* **1984**, *22*, 3225.

(2) Lane, W. H. *Ind. Eng. Chem.* **1946**, *18*, 295.

(3) Wang, S.-H.; Poehlein, G. W. *J. Appl. Polym. Sci.* **1994**, *51*, 593.

(4) Thomson, B.; Wang, Z.; Paine, A.; Lajoie, G.; Rudin, A. *J. Polym. Sci. Part A - Polymer Chem.* **1995**, *33*, 2297.

(5) Marestin, C.; Guyot, A.; Claverie, J. *Macromolecules* **1998**, *31*, 1686.

(6) Leemans, L.; Jerome, R.; Teyssie, P. *Macromolecules* **1998**, *31*, 5565.

(7) Zammit, M. D.; Davis, T. P.; Haddleton, D. M. *Macromolecules* **1996**, *29*, 492.

(8) Zammit, M. D.; Davis, T. P.; Haddleton, D. M.; Suddaby, K. G. *Macromolecules* **1997**, *30*, 1915.

(9) Maxwell, I. A.; Morrison, B. R.; Napper, D. H.; Gilbert, R. G. *Macromolecules* **1991**, *24*, 1629.

(10) Smith, W. V.; Ewart, R. H. *J. Chem. Phys.* **1948**, *16*, 592.

(11) Ballard, M. J.; Gilbert, R. G.; Napper, D. H. *J. Polym. Sci., Polym. Letters Edn.* **1981**, *19*, 533.

(12) Gilbert, R. G. *Emulsion Polymerization: A Mechanistic Approach*; Academic: London, 1995.

(13) Halnan, L. F.; Napper, D. H.; Gilbert, R. G. *J. Chem. Soc. Faraday Trans. 1* **1984**, *80*, 2851.

(14) Eastmond, G. C. *Makromolekulare Chemie, Macromolecular Symposia* **1987**, *10-11*, 71.

(15) Beuermann, S.; Buback, M.; Gilbert, R. G.; Hutchinson, R. A.; Klumperman, B.; Olaj, F. O.; Russell, G. T.; Schweer, J. *Macromol. Chem. Phys.* **1997**, *198*, 1545.

(16) Behrman, E. J.; Edwards, J. O. *Rev. Inorg. Chem.* **1980**, *2*, 179.

(17) De Bruyn, H.; Gilbert, R. G. *Polymer* **2001**, *42*, 7999.

(18) Russell, G. T.; Gilbert, R. G.; Napper, D. H. *Macromolecules* **1992**, *25*, 2459.

(19) Russell, G. T.; Gilbert, R. G.; Napper, D. H. *Macromolecules* **1993**, *26*, 3538.

(20) Morton, M.; Kaizerman, S.; Altier, M. W. *J. Colloid Sci.* **1954**, *9*, 300.

(21) Ugelstad, J.; Hansen, F. K. *Rubber Chem. Technol.* **1976**, *49*, 536.

(22) Harada, M.; Nomura, M.; Eguchi, W.; Nagata, S. *J. Chem. Eng. Japan* **1971**, *4*, 54.

(23) Casey, B. S.; Morrison, B. R.; Maxwell, I. A.; Gilbert, R. G.; Napper, D. H. *J. Polym. Sci. A: Polym. Chem.* **1994**, *32*, 605.

(24) Morrison, B. R.; Casey, B. S.; Lacík, I.; Leslie, G. L.; Sangster, D. F.; Gilbert, R. G.; Napper, D. H. *J. Polym. Sci. A: Polym. Chem.* **1994**, *32*, 631.

(25) Wilke, C. R.; Chang, P. *A.I.Ch.E. J.* **1955**, *1*, 264.

(26) Heuts, J. P. A.; Radom, L.; Gilbert, R. G. *Macromolecules* **1995**, *28*, 8771.

(27) Moad, G.; Rizzardo, E.; Solomon, D. H.; Beckwith, A. L. J. *Polym. Bull.* **1992**, *29*, 647.

(28) Gridnev, A. A.; Ittel, S. D. *Macromolecules* **1996**, *29*, 5864.

(29) Ballard, M. J., 1983, Ph.D. Thesis, University of Sydney.

(30) Stickler, M.; Meyerhoff, G. *Makromol. Chem.* **1978**, *179*, 2729.

(31) Willemse, R. X. E.; Staal, B. B. P.; van Herk, A. M.; Pierik, S. C. J.; Klumperman, B. *Macromolecules* **2003**, *36*, 9797.

(32) Griffiths, M. C.; Strauch, J.; Monteiro, M. J.; Gilbert, R. G. *Macromolecules* **1998**, *31*, 7835.

(33) Russell, G. T. *Macromol. Theory Simul.* **1994**, *3*, 439.

(34) Strauch, J.; McdDonald, J.; Chapman, B. E.; Kuchel, P. W.; Hawkett, B. S.; Roberts, G. E.; Tonge, M. P.; Gilbert, R. G. *J. Polym. Sci. A Polym. Chem. Ed.* **2003**, *41*, 2491.

(35) Russell, G. T.; Napper, D. H.; Gilbert, R. G. *Macromolecules* **1988**, *21*, 2133.

(36) de Gennes, P.-G. *Scaling Concepts in Polymer Physics*; Cornell University: Ithaca NY, 1979.

(37) Russell, G. T., 1990, Ph.D. Thesis, University of Sydney.

(38) Dainton, F. S.; James, D. G. L. *J. Polym. Sci.* **1959**, *39*, 299.

(39) Dainton, F. G.; Eaton, R. S. *J. Polym. Sci.* **1959**, *39*, 313.

(40) Clay, P. A.; Gilbert, R. G. *Macromolecules* **1995**, *28*, 552.

(41) van Herk, A. M. *J. Chem. Ed.* **1995**, *72*, 138.

(42) Hawkett, B. S.; Napper, D. H.; Gilbert, R. G. *J. Chem. Soc. Faraday Trans. 1* **1980**, *76*, 1323.

(43) Panke, D.; Wunderlich, W. *Die Makromolekulare Chemie* **1973**, *167*, 351.

(44) Olaj, O. F.; Schnoll-Bitai, I. *Mon. Chem.* **1999**, *130*, 731.

(45) Beuermann, S. *Prog. Polym. Sci.* **2002**, *27*, 191.

(46) Beuermann, S. *Macromolecules* **2004**, *37*, 1037.

(47) Vanderhoff, J. W., in *Vinyl Polymerization*; Ham, G., Ed.; Marcel Dekker: New York, 1969; Vol. 7 part 2.

(48) Fitch, R. M.; Tsai, C. H., in *Polymer Colloids*; Fitch, R. M., Ed.; Plenum: New York, 1971, p 73.

(49) Hansen, F. K.; Ugelstad, J., in *Emulsion Polymerization*; Piirma, I., Ed.; Academic: New York, 1982.

(50) Yeliseyeva, V. I., in *Emulsion Polymerization*; Piirma, I., Ed.; Academic: New York, 1982.

(51) Ottewill, R. O., in *Emulsion Polymerization*; Piirma, I., Ed.; Academic: New York, 1982.

(52) Penboss, I. A.; Gilbert, R. G.; Napper, D. H. *J. Chem. Soc. Faraday Trans. 1* **1986**, *82*, 2247.

5. Aqueous-Phase Oligomers in the Emulsion Polymerisation of Methyl Methacrylate

5.1 Introduction

The results of kinetic investigations presented in Chapter 4 for the persulfate/MMA system at 50°C suggest that, at least under conditions of moderate to high initiator concentration ([KPS] $> 1 \times 10^{-4}$ M), a significant proportion of initiator-derived radicals undergo termination in the aqueous-phase to form oligomeric "dead" chains of various lengths. Interpreting this kinetic data in terms of the Maxwell-Morrison model for entry,[1] a value for the critical degree of polymerisation for entering radicals of order $z \approx 20$ was inferred. The precise chain length distribution of oligomeric dead chains generated in the aqueous phase will be strongly dependent on the value of z for the system, thus analysis of this distribution is viewed as a promising means for verifying the value of z inferred already from kinetic data alone. This chapter details various approaches used to characterise the aqueous dead chain distribution for persulfate/MMA systems at 50°C.

5.2 Modelling Aqueous-Phase Oligomers in Emulsion Polymerisation

We begin with the realisation that a prediction for the aqueous dead chain distribution may be made based on the Maxwell-Morrison aqueous-phase kinetic scheme. This scheme, presented and discussed in detail in previous chapters, gives rise to the following set of rate equations for aqueous radical concentrations:

$$\frac{d[IM_1^\bullet]}{dt} = 2fk_d[I] - k_{p,w}[M]_w[IM_1^\bullet] - 2k_{t,w}[T_w^\bullet][IM_1^\bullet] \tag{5.1}$$

$$\frac{d[IM_i^\bullet]}{dt} = k_{p,w}[M]_w\left([IM_{i-1}^\bullet] - [IM_i^\bullet]\right) - 2k_{t,w}[T_w^\bullet][IM_i^\bullet], \quad 1 < i < z \tag{5.2}$$

Applying the steady-state approximation then gives:

$$[\mathrm{IM}_1^\bullet] = \frac{2fk_d[\mathrm{I}]}{k_{p,w}[\mathrm{M}]_w + 2k_{t,w}[\mathrm{T}_w^\bullet]} \tag{5.3}$$

$$[\mathrm{IM}_i^\bullet] = \frac{k_{p,w}[\mathrm{M}]_w[\mathrm{IM}_{i-1}^\bullet]}{k_{p,w}[\mathrm{M}]_w + 2k_{t,w}[\mathrm{T}_w^\bullet]}, \quad 1 < i < z \tag{5.4}$$

The total concentration of aqueous-phase radicals $[\mathrm{T}_w^\bullet]$ is then calculated as:

$$[\mathrm{T}_w^\bullet] = \sum_{i=1}^{z-1} [\mathrm{IM}_i^\bullet] \tag{5.5}$$

where equation (5.5) ignores the typically small contribution from exited radicals as well as from $\mathrm{I}^\bullet$ and $\mathrm{IM}_z^\bullet$ radicals, the concentrations of which are vanishingly small in the Maxwell-Morrison model.

Using D_i to denote an aqueous-phase dead chain containing i monomer units, and recognising that termination may occur by either of two modes, disproportionation or combination, the following time evolution is given for $[\mathrm{D}_i]$.

$$\frac{d[\mathrm{D}_i]}{dt} = 2\lambda k_{t,w}[\mathrm{IM}_i^\bullet][\mathrm{T}_w^\bullet] + (1-\lambda)k_{t,w}\sum_{j=1}^{i-1}[\mathrm{IM}_j^\bullet][\mathrm{IM}_{i-j}^\bullet], \quad 1 \le i \le (2z-2) \tag{5.6}$$

Note that chains of degree of polymerisation up to $(2z - 2)$ can be formed, even though $[\mathrm{IM}_i^\bullet] = 0$ for $i \ge z$. Here λ is the fraction of termination occurring by disproportionation, and the factor of two in the first term accounts for the fact that each disproportionation reaction produces two dead chains, whereas combination forms only one. The aqueous dead chain populations may thus be obtained directly from the aqueous radical concentrations, calculated according to equations (5.3) – (5.5). Finally, the obtained for $d[\mathrm{D}_i]/dt$ are normalised in the usual way:

$$\sum_{i=1}^{2z-2}\frac{d[\mathrm{D}_i]}{dt} = 1 \tag{5.7}$$

Of course, $d[\mathrm{D}_i]/dt$ is the instantaneous distribution, but for a steady-state system, as is considered here, it is also the cumulative chain length distribution for aqueous dead chains.

The above approach was used to model the aqueous dead chain distribution for the present system under a range of conditions. Here a value of $\lambda = 1$ was employed, in line with the

findings of Zammit *et al.* that termination occurs predominantly by disproportionation in MMA systems.[2,3] This means that the sum in equation (5.7) is evaluated only up to $i = z - 1$. Calculations were carried out using both the thermodynamic estimate[1] of $z = 5$ and the value of $z = 20$ obtained from experiment, and three initiator concentrations were considered, spanning the range used experimentally. Equations (5.3) – (5.5) were solved iteratively in the usual way, and normalised $d[D_i]/dt$ then generated. The resulting distributions are presented in Figure 5.1.

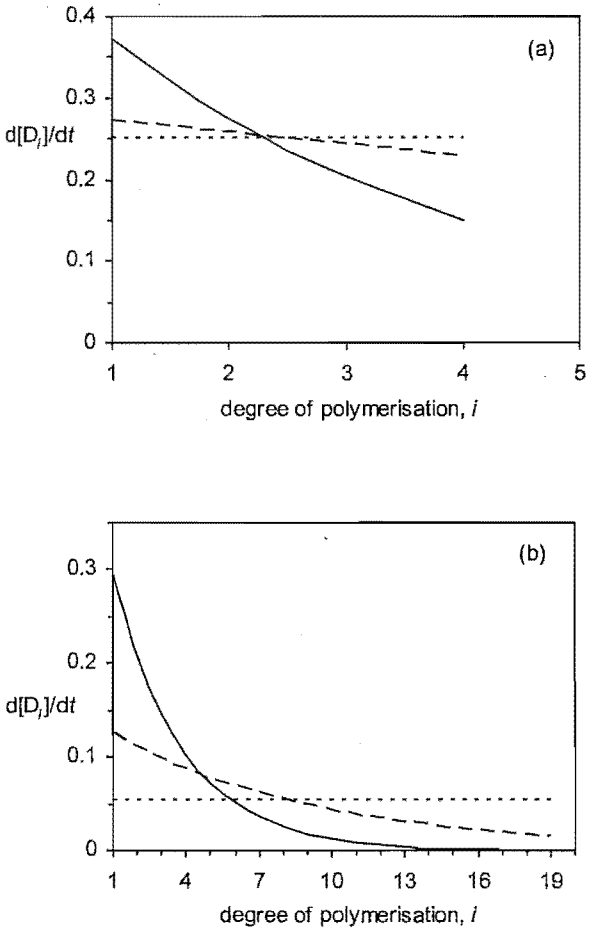

Figure 5.1. Aqueous dead chain populations calculated for MMA at 50°C according to the Maxwell-Morrison entry model, with [KPS] = 100 mM (————), 10 mM (—— —— ——), and 0.01 mM (– – – –); (**a**) for $z = 5$; (**b**) for $z = 20$.

The observed variation in the dead chain distribution with initiator concentration is explained as follows. At [KPS] = 0.01 mM the calculated entry efficiency is approximately 100%, thus the flat dead chain distribution reflects the negligible loss of aqueous radicals as they propagate towards length z. At higher initiator concentration where there is significant termination of growing radicals, the concentration of radicals, and hence also that of dead

chains formed, decreases exponentially with increasing chain length. It is also noted that the normalised distributions of Figure 5.1 do not reflect the considerable increase in *total* dead chains formed with increasing initiator concentration.

The value of z provides a cut-off point for the dead chain distribution, with the longest dead chains formed (by disproportionation) being of length $(z - 1)$. However, while changing z from 5 to 20 extends the distribution to greater chain lengths, the shape of the distribution is seen to remain unchanged.

At this stage it is pointed out that the above formulation for $d[D_i]/dt$ ignores the possibility of dead chain formation by chain transfer to monomer. This omission is strictly required for consistency with the Maxwell-Morrison entry scheme used throughout this work; reactions (4.1) – (4.5) of Chapter 4 assume negligible transfer to monomer. However, the accuracy of this assumption was checked *via* incorporating transfer to monomer into the model above and using a value of $k_{tr} = 3.7 \times 10^{-2}$ M^{-1} s^{-1}.[4] Indeed, this check revealed no significant change in any of the aqueous-phase radical or dead chain populations. In this case the assumption of no transfer is valid due to the relatively low rate coefficient for transfer to monomer. In the event of a much higher value for k_{tr} (*e.g.*, in the presence of an added chain transfer agent[5]) consideration of this reaction may become necessary. However, it is further noted that in MMA systems, where termination is *via* disproportionation, the *shape* of the dead chain distribution will not be affected since transfer also gives rise to the same exponential-like distribution of dead chains.

Additionally, it is worth noting that the number average degree of polymerisation, DP_n, for each of these exponential chain length distributions is considerably less than the maximum chain length of $(z - 1)$. Here DP_n may be calculated simply as the first moment of the normalised dead chain distribution. In the low initiator concentration limit ($f_{entry} \approx 100\%$), where the distribution is perfectly flat, the maximum value of $DP_n = z/2$ is obtained (for 100% disproportionation). As the steepness of the exponential distribution increases with increasing initiator concentration, the value of DP_n must be even lower. This is illustrated by the distributions shown in Figure 5.1 with [KPS] = 100 mM where, for the case of $z = 5$, the value $DP_n = 2.1$ is calculated, and for the case for $z = 20$, $DP_n = 3.3$.

5.3 Experimental Analysis of Aqueous-Phase Oligomers

The above results from modelling of aqueous MMA dead chain distributions using the Maxwell-Morrison approach may now be compared with experimental data obtained for the persulfate/MMA system at 50°C.

5.3.1 Mass Spectrometry

In recent years mass spectrometry (MS) has emerged as a powerful tool for polymer characterisation. As outlined in Chapter 4, variants of this technique, including both electrospray ionisation (ESI) and matrix-assisted laser desorption/ionization time-of-flight (MALDI-TOF), have been successfully applied to the analysis of oligomeric aqueous species.[6-10] Of particular relevance here are the investigations of Thomson *et al.*[9] into the aqueous species generated during the emulsion polymerisation of MMA with persulfate initiator (*i.e.*, the same system as used in the present work). These workers analysed the aqueous phase of their reacted latexes by MALDI-TOF MS (after removal of latex particles by centrifugation) and found a clear distribution of signals corresponding to MMA oligomers ranging in length from 2 to 14 monomer units. This is immediately suggestive of a value for z significantly greater than the thermodynamic estimate of $z = 5$ by Maxwell *et al.* Additionally, Thomson *et al.* comment that the most surface-active oligomers (*i.e.*, those of highest degree of polymerisation) are probably underrepresented in the observed results, suggesting that these species may well be partitioned between the aqueous and particle phases (adsorbed to the particle surface) and thus partially removed by the centrifugation process. Also of significance is the absence of any MS signals arising from oligomers containing two sulfate groups, the products of termination by combination. This is in agreement with the results of Zammit *et al.*[2,3] and the assumption used in the earlier modelling work that all termination is *via* disproportionation.

It should be noted that Thomson *et al.* conducted experiments at a temperature of 80°C – somewhat higher than the 50°C used here – and furthermore that Thomson *et al.* carried out *ab initio* emulsion polymerisations, whereas those of the present work employed seed latex particles. However, these differences are unlikely to be the source of any significant discrepancy in the dead chain distributions, since the value of z is thought to be relatively insensitive to a temperature change of this magnitude,[1] and the vast majority of dead chains in

an *ab initio* system will be formed after particle formation has ceased (*i.e.*, under identical conditions to a seeded experiment).

Also of note are results obtained by Lamb *et al.*[11] from ESI MS analysis of the aqueous species formed in MMA emulsion polymerisations at 50°C employing a continuous feed of an aqueous redox initiator which gives rise to oligomeric radicals with a sulfite terminal group (thought to be the primary amongst many possibilities). This system is likely to have a value of z very similar to that with persulfate initiator. In this case it is apparent that aqueous dead chains are formed incorporating one sulfite group and up to ~ 10 MMA units, once again consistent with a value for z significantly greater than 5.

In light of the above results, considerable efforts were made to obtain mass spectrometric data for the oligomeric species generated under the conditions of the present study. A range of the product latexes obtained from the chemically initiated seeded MMA kinetic experiments at 50°C conducted in Chapter 4 were centrifuged at 15000 rpm to remove latex particles and the resultant aqueous-phase solution was analysed by ESI MS.

ESI mass spectra were recorded from a Micromass LCT TOF mass spectrometer, with a probe voltage of 3200 V and temperature of 150°C, and a source temperature of 80°C. Direct injection used 10 μL of a 10 μg mL^{-1} solution and the carrier solvent was 50% acetonitrile-50% water at a flow rate of 20 μL min^{-1}. Mass spectrometry was kindly carried out by Bruce Clark and Marie Squire at the University of Canterbury's Department of Chemistry.

In all cases the only MS signals evident were those due to salt species derived from initiator (KPS) and/or surfactant (AMA-80) (depending on the relative amounts of each added), *e.g.* see Figure 5.2.

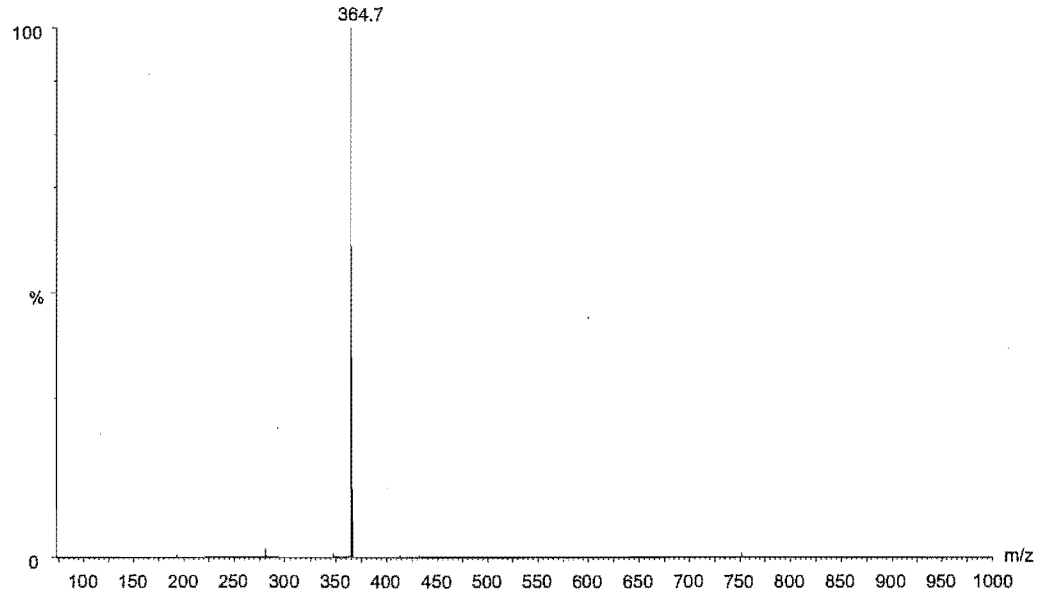

Figure 5.2. Electrospray ionisation mass spectrum obtained in negative ion mode from analysis of the aqueous phase of a seeded MMA emulsion polymerisation at 50°C under typical experimental conditions (run C102 from Chapter 4) with [KPS] = 0.1 mM; the main signal corresponds to negative ion from Aerosol MA-80 surfactant (sodium di(1,3-dimethylbutyl)sulfosuccinate).

These results suggest that the total concentration of dead chains formed during the course of a *typical* seeded polymerisation here is too low, relative to those of other aqueous species present, to provide any appreciable MS signal. This situation was found not to be improved by pre-concentration of the aqueous solution for ESI MS analysis. However, under the relatively extreme polymerisation conditions of [KPS] = 36 mM, with double the usual initial charge of monomer (so as to significantly increase the total number of dead chains formed during the experiment) and no added surfactant, ESI MS analysis of the aqueous phase revealed a small series of signals with a separation of m/z = 100 (where m/z is the mass-to-charge ratio measured by the mass spectrometer), corresponding to MMA oligomers of length 1 to 6 monomer units. The results are presented in Figure 5.3, where the signal at, *e.g.*, m/z = 397 is due to a singly-charged oligomer consisting of a sulfate group (m/z = 96), three monomer units (each contributing m/z = 100), and a hydrogen atom (abstracted during disproportionation, m/z = 1). The signal at m/z = 231 is due to residual initiator (KPS). Interestingly, the only oligomeric species observed appear to be those containing an abstracted hydrogen atom; the other disproportionation product, from which hydrogen was abstracted (and thus with m/z less by 2) is apparently absent. While no explanation for this finding is offered here, it is noted that the results of all other MS analyses are consistent, *i.e.*, in no study are both disproportionation products observed to be present, let alone in equal

numbers. However, it is emphasised that the end-group identification provides confidence that the observed species are disproportionation products, not oligomers generated by combination.

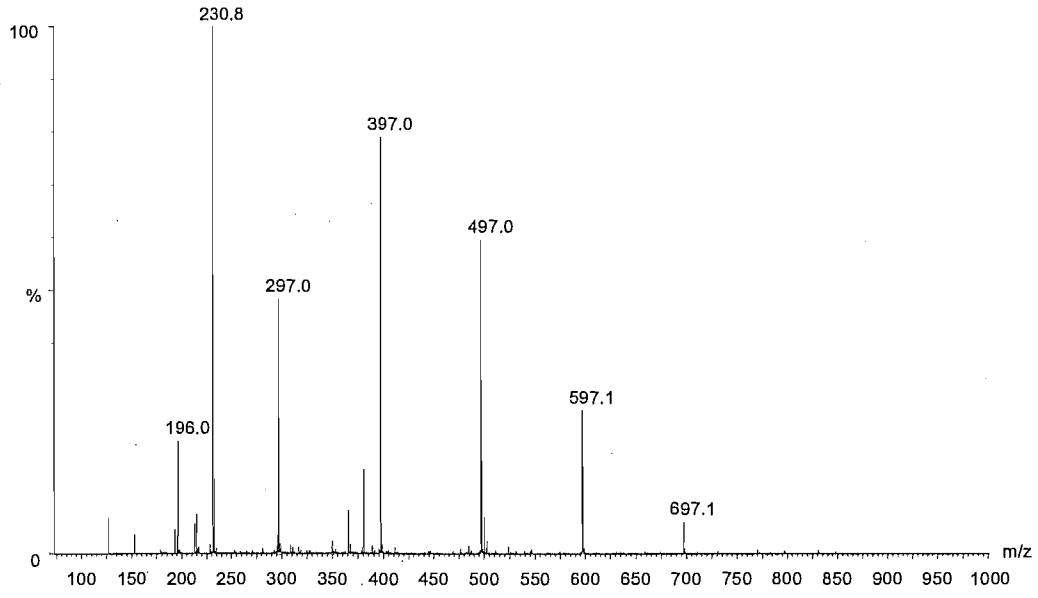

Figure 5.3. Electrospray ionisation mass spectrum obtained in negative ion mode from analysis of the aqueous phase of a seeded MMA emulsion polymerisation at 50°C with [KPS] = 36 mM, no added surfactant, and double the usual initial charge of monomer.

On the basis of these results it is suggested that the comparatively high quality experimental results obtained by Thomson *et al.* and Lamb *et al.* may be explained by their having conditions of significantly greater radical flux (*i.e.*, persulfate at 80°C, or a high feed rate for redox initiator) – perhaps in conjunction with a larger amount of added monomer – than those used in the seeded kinetic experiments of this study. It is also noted that under the atypical experimental conditions required to obtain the MS results of Figure 5.3 the combination of high initiator concentration/ionic strength, no added surfactant, and large amount of added monomer (leading to a high polymer content) gave rise to extensive coagulation of the latex particles during the course of the polymerisation. The resulting uncertainty in the particle concentration, N_c, meant that no reliable kinetic data could be obtained from this particular experiment.

In Figure 5.3 it is evident that the relatively small signals corresponding to monomeric and dimeric species do not follow the exponential trend predicted for the distribution of MMA oligomers from modelling. However, given that these shortest oligomers are likely to be

considerably more volatile than their longer counterparts, it is conceivable that a significant fraction of each escapes from solution at some stage prior to ESI MS analysis.

Finally, it is of interest to compare the remainder of the oligomeric distribution to the results obtained from modelling earlier. In Figure 5.4 are presented the modelled results for $z = 20$, together with the relative distribution from ESI MS (estimated from the heights of the peaks), which has been scaled to give approximate agreement with model values for 3-mers and 4-mers. It is important to note here that ESI MS signals may not be assumed to provide a quantitative comparison of oligomer concentrations; this approach is only intended to provide a general estimate of the distribution.

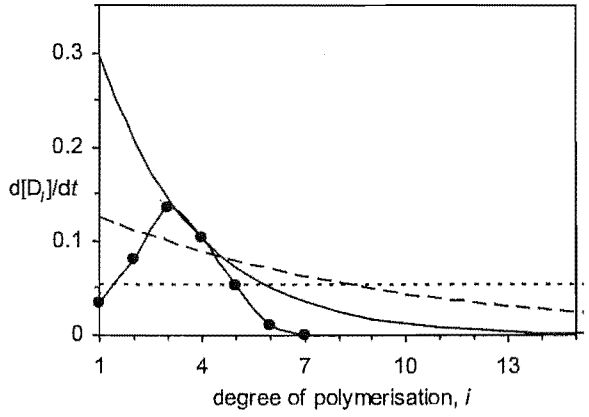

Figure 5.4. Aqueous dead chain populations for MMA at 50°C; estimated from ESI MS data (circles); calculated according to the Maxwell-Morrison entry model with $z = 20$, [KPS] = 100 mM (————), 10 mM (— – — ——), and 0.01 mM (– – – –).

Given the experimental conditions of [KPS] = 36 mM, the ESI MS distribution should lie somewhere between the modelled distributions for [KPS] of 10 mM and 100 mM. Clearly the experimental data show an unexpectedly rapid decrease in the dead chain concentration with increasing chain length. This may well be explained by an insensitivity of the ESI MS technique to the longest oligomer chains; while there may be a significant concentration of singly-charged 7-mers and longer oligomers in solution, they may not "fly" as readily in the spectrometer and thus not be accurately quantified. Of course, the results obtained from this particular experiment do not rule out the alternative explanation that z is in fact significantly lower than 20, *viz.* $z = 7$ (corresponding to the longest oligomer seen here). On its own, this result would be a triumph for the thermodynamic rationalisation of z given by Maxwell *et al.*;[1] however, there is the problem that kinetic experiments and both other MS studies suggest $z \gg$

7. Also, it should be mentioned that solving equations (5.3) – (5.5) with $z = 7$ does not give $d[D_i]/dt$ which show better quantitative agreement with the experimental distribution.

In summary, the MS results obtained by other workers for aqueous-phase oligomeric species formed in MMA emulsion systems are certainly indicative of a value for z significantly greater than the value of $z = 5$ predicted by the Maxwell-Morrison model, and therefore consistent with the kinetic data of the present study. While the MS data obtained here from a seeded kinetic experiment at 50°C are also consistent with the value of z from kinetic experiments, it is not possible to rule out the possibility of a lower value for z on the basis of this experiment alone.

5.3.2 Aqueous-Phase Gel Permeation Chromatography

The aqueous samples extracted from seeded polymerisations were also analysed using aqueous-phase gel-permeation chromatography (GPC). For this work, the GPC instrument was configured with the following components: system controller (SCL-10Avp, Shimadzu), automated sample injector (SIL-10ADvp, Shimadzu), pump operating in high pressure mode (LC-10ATvp, Shimadzu) with the solution passing through a degasser (DGU-14A, Shimadzu), column (Ultra Hydrogel 120, Waters) in a column heater (CTO-10ACvp, Shimadzu), static light scattering detector (DAWN EOS, Wyatt Technology) and a refractive index detector (Optilab DSP Interferometric Refractometer, Wyatt Technology). ASTRA (Version 4.90.07, Wyatt Technology) data collection and processing software was used. GPC analyses were kindly carried out by Hollie Zondanos and Herbert Chiou at the University of Sydney's Key Centre for Polymer Colloids.

The static light scattering detector is capable of furnishing absolute molecular weight data for a polymer sample provided that the way in which refractive index changes with polymer concentration, quantified by the value dn/dc, is known.[12] Reported values of dn/dc for poly(MMA) in tetrahydrofuran are generally around 0.08 mL g^{-1};[13] however this value is likely to be sensitive to the nature of the solvent used and, in the case of oligomeric species, may well be influenced by the presence of a polar/charged end-group. Therefore, in the absence of a specific literature value of dn/dc for poly(MMA) oligomers in aqueous solution, a value in the range of 0.04 – 0.12 mL g^{-1} was estimated based on variations in reported dn/dc values with solvent polarity for different polymers.

Figure 5.5 presents the molecular weight distributions from GPC for the same aqueous sample used to obtain the ESI MS results in Figure 5.3. Data are presented in the form of $W(\log_{10}M)$ – sometimes referred to as the "GPC distribution" (see the following chapter for a detailed discussion of various forms of the molecular weight distribution). It is evident that GPC analysis employing a light scattering detector gives a peak molecular weight in the region of $10^5 - 10^6$, corresponding to aqueous "oligomers" of degree of polymerisation $10^3 - 10^4$ (since the molecular weight of a MMA monomer unit is 100 g mol^{-1}). Moreover, the measured distribution is seen to be relatively insensitive to the value of dn/dc over the small range employed here. The suggestion of oligomers of such high molecular weights remaining soluble in the aqueous phase is unprecedented and appears highly unlikely; thus it seems reasonable to question the accuracy of the aqueous GPC results of Figure 5.5.

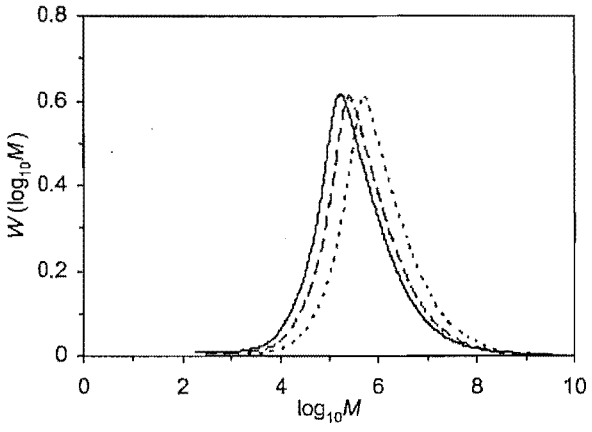

Figure 5.5. Normalised molecular weight distributions obtained using aqueous-phase GPC with light scattering detection for analysis of the aqueous phase of a seeded MMA emulsion polymerisation at 50°C with [KPS] = 36 mM, no added surfactant, and double the usual initial charge of monomer; data processed with dn/dc = 0.12 mL g^{-1} (————), 0.08 mL g^{-1} (— — —), or 0.04 mL g^{-1} (– – – – –).

These doubts are compounded by the GPC results obtained for the aqueous-phase sample from a typical seeded kinetic experiment (run C102 from Chapter 4), presented in Figure 5.6. The sample used in this case was that which gave rise to the ESI mass spectrum in Figure 5.2, dominated by the presence of Aerosol MA-80 surfactant. The broad GPC signal centred at molecular weight ~ $10^4 - 10^5$ in Figure 5.6 is thought to be due to surfactant, with the smaller peak at molecular weight ~ $10^7 - 10^8$ arising from aqueous oligomers. Given that Aerosol MA-80 contains ester functionality and carries a negatively charged sulphite group, the position of the surfactant peak is thought to provide a useful point of reference for poly(MMA) oligomer molecular weights. The molecular weight of Aerosol MA-80 is known

to be 388 g mol^{-1} (including the weights of both surfactant anion and sodium counter-ion); thus it seems likely that the absolute molecular weight measurements inferred from light-scattering measurements are in error by a factor of 100 or so. Applying this reasoning to the GPC results of Figure 5.5 suggests that aqueous oligomers are in fact of degree of polymerisation 10 – 100, which is possible. However, applying this reasoning to what is thought to be the aqueous oligomer peak in Figure 5.6 gives chain lengths of 10^5 – 10^6 monomer units, which is still completely unrealistic. If nothing else, this indicates the inconsistency of aqueous-phase GPC results.

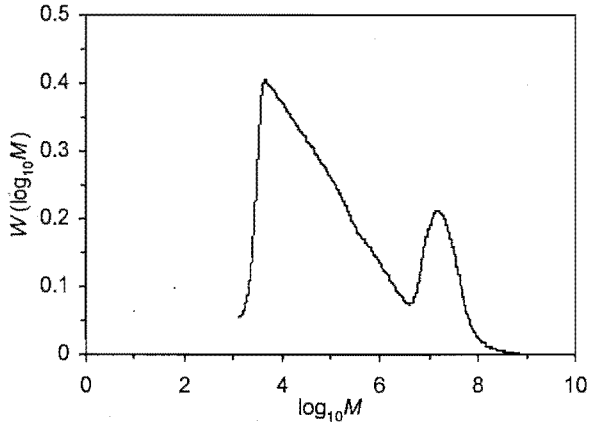

Figure 5.6. Normalised molecular weight distribution obtained using aqueous-phase GPC with light scattering detection for analysis of the aqueous phase of a typical seeded MMA experiment (run C102 from Chapter 4) at 50°C with [KPS] = 0.1 mM; data processed with dn/dc = 0.08 mL g^{-1}.

In light of the questionable GPC results obtained using light scattering detection, an alternative strategy was to re-process these results, this time with molecular weight calibration provided by comparison with molecular weight standards (*i.e.*, without the use of static light scattering data). In the absence of oligomeric poly(MMA) standards, an approximate calibration curve was constructed using water-soluble oligo-glucose and pullulan (polymaltotriose) polysaccharide standards (G-7: 1140 g mol^{-1}, P-5: 5900 g mol^{-1}, P-10: 11800 g mol^{-1}). The re-processed results from Figures 5.5 and 5.6 are presented together in Figure 5.7.

The results obtained from GPC calibrated with molecular weight standards are significantly different to those presented earlier. Here the sample obtained from the experiment with high amounts of added initiator and monomer, and no added surfactant, exhibits a peak molecular weight of ~ 10^4, corresponding to oligomeric species of degree of polymerisation ~ 100.

Similarly, for the sample obtained from a typical kinetic run (C102 from Chapter 4) the small GPC signal attributed to oligomer is also centred at molecular weight ~ 10^4. While such molecular weights still appear remarkably high for aqueous oligomers, they are certainly more physically realistic than the earlier results from light scattering. It is also pleasing that the peaks due to oligomers are now in agreement.

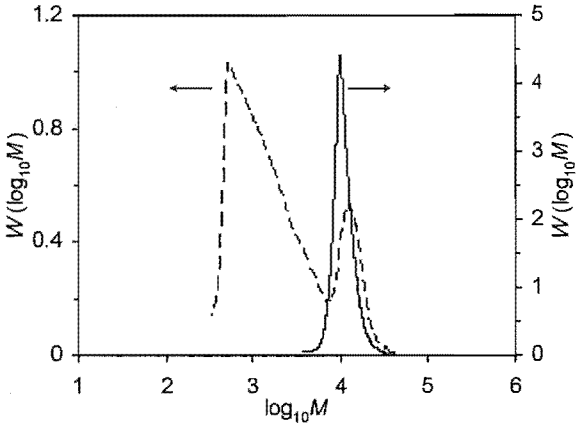

Figure 5.7. Normalised molecular weight distributions obtained using aqueous-phase GPC calibrated using polysaccharide molecular weight standards for analysis of the aqueous phase of a seeded MMA emulsion polymerisations at 50°C; results for typical seeded kinetic run with [KPS] = 0.1 mM (— — —); results with [KPS] = 36 mM, no added surfactant, and double the usual initial charge of monomer (————).

In this case it is also noted that the broad peak due to surfactant is centred at molecular weight of ~ 10^3. Comparing this result to the known surfactant molecular weight of 388 g mol^{-1} suggests that the calibration used here may still be in error by a factor of 2 – 3. The possibility for such an error is not inconceivable given that the polysaccharide molecular weight standards used are chemically dissimilar to poly(MMA) and no effort has been made to take into account possible differences in intrinsic viscosity, *i.e.*, Figure 5.7 gives GPC results for poly(MMA) oligomers only in terms of their equivalent polysaccharide molecular weight. Any difference in intrinsic viscosity could, in principle, be factored out using the so-called universal calibration procedure; however, this method would require knowledge of the Mark-Houwink parameters for sulfate-ended poly(MMA) oligomers in water and is therefore not possible at present. In fact, it must be questioned whether GPC of the present oligomer systems is at all reliable, as the sulfate end-groups must introduce enthalpic interactions as oligomers pass through a GPC column, which certainly renders universal calibration uncertain (it assumes entropic interactions only). This suggests that useful GPC analysis is probably only feasible if sulfate-ended oligomer standards are available for direct calibration.

In general one would have to say that aqueous-phase GPC is notoriously difficult, as is oligomeric GPC. Here we combine both lots of difficulties. While in principle aqueous-phase GPC should yield the answers sought here, it must be questioned whether, in practice, any reliable results can be obtained as the state of the "art" currently stands.

5.4 Hydrolysis of MMA Ester Functionality

In Chapter 4 the possibility of MMA monomer hydrolysis to form a more water soluble methacrylic acid (MAA) species, and subsequent incorporation of such MAA units into oligomeric radicals, was postulated as an explanation for the high value of z inferred from kinetic experiments. It is therefore of interest to consider experimental means for verifying the presence of MAA units in aqueous oligomers.

5.4.1 Mass spectrometry

As mentioned in Chapter 4, some tangible support for the possibility of incorporation of hydrolysed MMA units into aqueous oligomers may be found in the mass spectrometry data of Thomson *et al.*[9] These workers identified signals in measured MALDI-TOF spectra consistent with series of oligomeric species containing one or two MAA units, and noted that the basic conditions provided by the ammonium persulfate initiator used may help to promote such reactions. Similarly, the ESI MS data presented by Lamb[11] show several sets of peaks offset from one another by a consistent spacing of m/z = 14, a value which corresponds exactly to the change in mass accompanying the replacement of an ester OCH3 group by OH. That said, it is difficult to rationalise the exact molecular weights of these peaks.

5.4.2 FTIR Spectroscopy

A widely used method for analysing the composition of polymer molecules is Fourier transform infrared (FTIR) spectroscopy. In the present work it was hoped that identifying particular FTIR spectral features unique to either poly(MMA) or poly(MAA) would permit the relative numbers of MMA and MAA monomeric units present in the aqueous oligomers to be quantified from measured spectra. The following experiments were kindly conducted by Shane Seabrook at the University of Sydney.

FTIR spectra were measured from a Bruker IFS66v FTIR spectrometer utilising a Diffuse Reflectance (DRIFT) accessory. All spectra were obtained under vacuum (to minimise interference from carbon dioxide) from 64 scans at 4 cm^{-1} resolution. Spectral data were collected and processed using OPUS software (Version 3.0.1, Bruker).

Samples of aqueous-phase oligomers for FTIR analysis were prepared by drying of aqueous-phase samples under a flow of nitrogen to leave a solid residue. In addition reference spectra were obtained from solid samples of poly(MMA) (Perspex™), poly(MAA) (prepared as part of this work by aqueous solution polymerisation and dried under vacuum), and potassium persulfate (crystals).

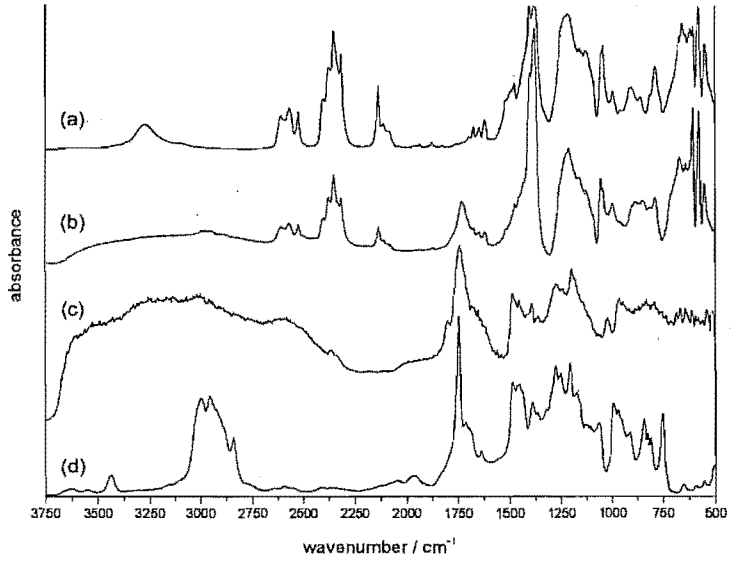

Figure 5.8. FTIR spectra measured for solid samples of **(a)** potassium persulfate, **(b)** dried aqueous-phase residue from seeded emulsion polymerisation of MMA at 50°C (same sample as used to obtain mass spectrum in Figure 5.3), **(c)** poly(methacrylic acid) and **(d)** poly(methyl methacrylate).

Unfortunately, the results obtained from FTIR analysis were inconclusive. In all cases the FTIR spectrum of the aqueous-phase residue isolated from seeded experiments was found to be dominated by spectral bands attributed to potassium persulfate, as is evident from comparison of spectra (a) and (b) in Figure 5.8. The only feature of the sample spectrum clearly attributable to either poly(MMA) or poly(MAA) was the band at approximately 1750 cm^{-1}, which arises from a stretching mode of the carbonyl group. Given that this spectral band is common to both poly(MMA) and poly(MAA) no useful discernment may be made as to the composition of the aqueous oligomers, although if forced one might opine that there is

some evidence for the presence of MAA residues (the broad shoulder of the polymerisation sample in Figure 5.8 (b) perhaps intimates MAA).

5.4.3 A Model System for MMA Hydrolysis

While the results of mass spectrometry work by Thomson *et al.*[14] and Lamb[11] described earlier represent strong evidence for the presence of MAA units in dead oligomers isolated at the end of an emulsion polymerisation, it is important to realise that they provide no indication as to when hydrolysis of the MMA ester functionality occurs. Clearly, hydrolysis may befall MMA monomer molecules prior to radical addition, but it is also possible that the ester functionality may be hydrolysed after incorporation of monomer into an aqueous oligomeric species. In the latter case hydrolysis may either occur during the growth of an oligomeric radical or after aqueous-phase termination of such radicals (*i.e.*, hydrolysis of dead oligomer). Clearly, ester hydrolysis occurring subsequent to termination will have no effect on the water solubility of entering radicals and thus cannot explain the high value of z inferred from kinetic experiments. Additionally, given the relatively short lifetime of individual radicals in the aqueous phase it seems improbable that hydrolysis will occur during this period. It is therefore thought that the only route for ester hydrolysis which may significantly affect the value of z is that involving MMA monomer prior to aqueous-phase radical addition.

An estimate for the ester hydrolysis equilibrium constant, K_{hydr}, for MMA may be obtained from literature data available for other small organic esters. Equilibrium constants measured[15-18] for methyl formate, ethyl formate, propyl formate and ethyl acetate suggest a value of approximately $K_{hydr} = 0.3$ (where the standard states for ester, water, acid and alcohol are defined as 1 mol dm^{-3}). Under dilute aqueous solution conditions this corresponds to a molar ratio of acid to ester in the range of 2 – 6. Thus it seems possible that at equilibrium a significant fraction of aqueous-phase MMA monomer could be hydrolysed to MAA. However, it should also be noted that in some of the studies cited above it took several days for equilibrium hydrolysis conditions to be attained, indicating that the rate of the hydrolysis reaction itself may in fact be very slow.

A further literature result of interest here is the observation by Tauer *et al.*[19] of a small increase in conductivity measured in a dilute aqueous solution of MMA monomer during a one hour thermal equilibration period at 70°C prior to the commencement of emulsion polymerisation. These authors ascribed this change in conductivity to the hydrolysis of MMA

to MAA. However, this conclusion is questionable given the possible sensitivity of such conductivity measurements to, *e.g.*, changes in temperature and the presence (and possible reaction) of impurities in the emulsion.

In view of the above results a simple model system was designed to investigate the possibility of monomer hydrolysis under reaction conditions similar to those used in MMA kinetic experiments. Here 5 g of MMA and ~ 55 g water (Milli-Q) were added to a 60 cm^3 dilatometer vessel which was then sealed using a glass stopper and stirred overnight at room temperature. The mixture was then emulsified by vigorous stirring and heated to 60°C for 30 min before heating at 50°C for a further 150 min at 50°C. This heating/stirring regime was analogous to that employed during the swelling, degassing and early polymerisation periods of a typical kinetic run. An aqueous-phase sample was carefully extracted from the emulsion (using a separating funnel) and the relative amounts of dissolved MMA and MAA determined by high-performance liquid chromatography (HPLC) as described below. Importantly, no effort was made to remove dissolved oxygen in this experiment and the absence of any turbidity in the reaction mixture, even after extended heating, indicated that the presence of oxygen was sufficient to prevent any spontaneous polymerisation from occurring.

HPLC was carried out on a Dionex instrument: P680 HPLC pump, ASI 100 automated sample injector, Phenomenex Prodigy C18 (5 μm, 250 x 4.6 mm) reverse phase column, TCC 100 column heater, UVD 340U diode array detecting at a wavelength of 210 nm. The mobile phase (eluent) solvent system consisted of varying proportions of acetonitrile (HPLC grade) and water (Milli-Q) at a flow rate of 1 mL min^{-1}. The eluent composition varied with time as follows: started with 10% acetonitrile and maintained isocratic for 2 min; linear gradient to 75% acetonitrile over 12 min; isocratic at 75% acetonitrile for 10 min; linear gradient to 100% acetonitrile over 2 min; isocratic at 100% acetonitrile 4 min; linear gradient to 10% acetonitrile over 2 min; isocratic at 10% acetonitrile (to re-equilibrate) for 8 min.

In this way, the most polar components of the subject sample, which interact most weakly with the non-polar stationary-phase elute at the earliest times when the eluent is a relatively polar solvent (*i.e.*, mainly water). At later elution times the eluent becomes sufficiently non-polar (due to the increasing proportion of acetonitrile) that the most non-polar components of the sample are eluted.

The use of HPLC to determine the relative amounts of MMA and MAA present in aqueous solution is illustrated in Figure 5.9. Here a dilute aqueous standard solution containing approximately equal amounts of dissolved MMA (concentration 3.1 mg mL^{-1}) and MAA (concentration 3.3 mg mL^{-1}) monomers was freshly prepared and analysed by HPLC. MAA was obtained from Aldrich and used here without further purification. Due to its greater polarity, MAA was observed to have a shorter elution time, 9 minutes, than MMA, which eluted after 13 minutes. It is noted that the third HPLC signal observed at elution time of 34 min in Figure 5.9 is an artifact arising from the rapid change in the composition of the carrier solvent near the end of the analysis. Importantly, the integrals of the HPLC signals corresponding to dissolved MMA and MAA were seen to very accurately reflect the relative molar amounts of the two monomers, indicating that this method is suitable for quantitative determination of the presence of any MAA formed by hydrolysis of MMA.

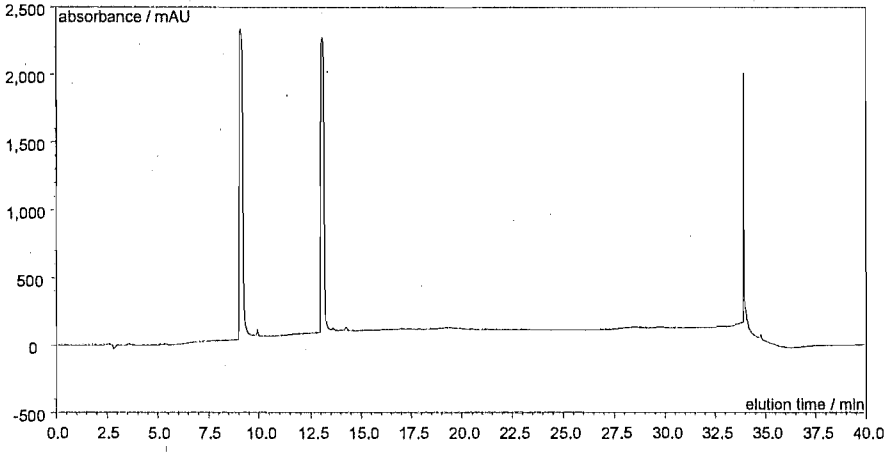

Figure 5.9. HPLC chromatogram measured from 210 nm UV detector for a mixture of MMA and MAA in dilute aqueous solution at approximately equal concentrations of ~ 3 mg mL^{-1}.

Next, the sample obtained from the model system for hydrolysis described earlier was subjected to HPLC analysis, with results as shown in Figure 5.10. While the signal at elution time of 13 min due to dissolved MMA monomer is clearly visible, there is only the slightest evidence of a signal at elution time of 9 min arising from the presence of MAA. Thus it would appear that any hydrolysis of MMA occurring under the conditions of the model emulsion system used here is negligible.

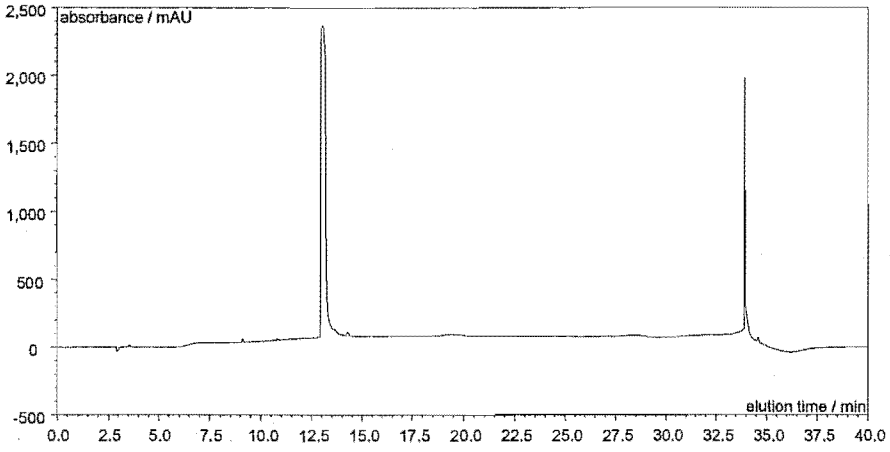

Figure 5.10. HPLC chromatogram measured from 210 nm UV detector for the aqueous sample extracted from an emulsion of 5 g MMA in 55 g water after heating at 60°C for 30 min and at 50°C for a further 150 min.

Additionally, the model emulsion system was subjected to prolonged heating at 50°C over a further period of 24 hours. Even in this case, the HPLC chromatogram obtained from analysis of an extracted sample of the aqueous phase showed no discernible differences to that in Figure 5.10.

As a cross check, the aqueous samples extracted at each stage were also analysed by ^{1}H NMR. This work was kindly performed by Martin Lee at the University of Canterbury on a Varian UNITY INOVA-500 spectrometer. In this case, the relative integrals of the NMR signals due to the two methyl groups of MMA (one attached to the vinyl double bond, the other in the methyl ester group) should ordinarily be equal. Thus the occurrence of any significant monomer hydrolysis would be revealed by an appreciable change in these relative integrals, as the methyl ester group would be removed by hydrolysis while the methyl group attached to the vinyl double bond would remain unchanged. For all extracted samples (*i.e.*, even after prolonged heating) the integrals of the ^{1}H NMR signals due to these two methyl groups remained approximately equal to each other, thus confirming the HPLC findings of negligible hydrolysis.

Given the above results obtained at 50°C, it was also of interest to investigate the possibility of MMA ester hydrolysis under the conditions employed by Tauer *et al.*,[19] in order to verify the postulate of those authors. In this case a dilute solution of MMA in water (~ 13 mg mL^{-1}) was emulsified in a dilatometer vessel and heated at 70°C for 90 min. Once again analysis of the aqueous solution after heat treatment revealed an HPLC trace identical to that of Figure 5.1, indicating that even under these harsher experimental conditions, negligible hydrolysis of

MMA occurs. Thus the small change in observed in measured conductivity by Tauer *et al.* must be attributable to some effect other than monomer hydrolysis (*e.g.*, temperature change or impurities).

5.5 Conclusions

The aim of this section of work was to characterise the aqueous-phase oligomers formed in the persulfate/MMA emulsion system in order to rationalise the value of z inferred from the kinetic experiments of the previous chapter. While none of the techniques employed here has provided definitive characterisation, it is useful to consider the relative merits of these methods in light of the results obtained.

The mass spectrometric characterisation of oligomers formed under the experimental conditions of the present work was difficult, apparently due to the low total concentration of these species formed. The limited data obtained are consistent with the value of $z = 20$ inferred from kinetics in Chapter 4, however further experiments are required to rule out the possibility of a lower z value. The use of mass spectrometry methods in conjunction with modelling of the oligomeric dead chain distribution using the Maxwell-Morrison entry scheme represents a useful cross-check for the entry results obtained from kinetic experiments. It is also notable that the mass spectrometry data obtained by Thomson *et al.*[9] and Lamb *et al.*[11] for aqueous oligomers from MMA systems constitute strong evidence in support of a value of z at least as high as 10 – 15. Overall, mass spectrometry is likely, in principle, to provide the most comprehensive information for oligomer characterisation (permitting resolution of individual oligomer molecular weights, and identification of end-groups and changes in the functionality of monomeric units); however, in practical terms, it seems that these advantages have yet to be fully developed.

Aqueous-phase GPC analysis did not appear to be subject to the same problems as mass spectrometry regarding detection of oligomeric species present in low concentration, with an appreciable signal arising from oligomer even in the presence of excess surfactant (Figure 5.7). However, in the absence of any reliable means for calibrating the raw GPC results obtained (at present), it is clear that the inferred molecular weight data are highly suspect (*e.g.*, the suggestion of aqueous oligomers of degree of polymerisation $10^5 - 10^6$).

It was hoped that FTIR spectroscopy would provide a means for accurately quantifying the extent to which the aqueous oligomers were composed of MAA monomer units – formed by ester hydrolysis of MMA monomer. However, spectra obtained for oligomer samples were dominated by the presence of residual KPS initiator, making any such quantification impossible. Accurate FTIR analysis of MMA/MAA composition may be possible for oligomeric samples generated in emulsion polymerisations using a different initiator which is not an FTIR interferent. Such results are of limited worth, however, in the present context where the specific aim is to determine whether the nature of the oligomeric species formed from persulfate/MMA is consistent with the value of z inferred from kinetic experiments. Additionally, it is suggested that FTIR analysis of polymeric MMA/MAA content should be accompanied by studies of well-defined reference systems (*e.g.*, copolymers of known composition).

HPLC was shown to yield the most definitive results regarding the extent of MMA monomer hydrolysis in the aqueous phase of an emulsion polymerisation, revealing that for a simple model system consisting of an emulsion of monomer and water, negligible hydrolysis occurs even after extended periods of heating at 50°C or 70°C. These results have important implications for the interpretation of the kinetic results of Chapter 4, suggesting that the unexpectedly high value of $z = 20$ inferred for persulfate/MMA is unlikely to be attributable to the incorporation of relatively water-soluble MAA units into aqueous oligomeric radicals. On the basis of these results the best explanation for the high value of z appears to be a departure from the group-additivity model used by Maxwell *et al.*[1] to estimate the free energy of adsorption for a growing oligomer chain (which predicts $z = 5$ for this system).

It should of course be considered that ester hydrolysis in the persulfate/MMA *polymerisation* system may involve species that were absent from the simple model system used here, such as surfactant and initiator. With regard to the former, these model experiments may easily be repeated with varying amounts of added surfactant in order to identify any effect on the incidence of monomer hydrolysis. KPS initiator may be speculated to have some effect on the hydrolysis of MMA, either by way of radical reactions or by some direct reaction of persulfate. However, in the case of radical-monomer reactions it is noted that radical addition is likely to occur rapidly[20,21] and even if this were not the case, literature data for reactions involving radicals and carboxylic esters indicate that abstraction of a hydrogen atom is the next most likely outcome.[22-24] In any event, the effect of initiator on monomer hydrolysis

could also be examined by addition of KPS to the model system. Although in this case, HPLC analysis may be complicated by the formation of oligomeric species and latex particles. One option here is to remove any latex particles from extracted aqueous samples by centrifugation and/or filtration and then analyse the recovered samples by HPLC in the usual way. An alternative approach would be to conduct these experiments using methyl isobutyrate in place of MMA monomer. This saturated analogue of MMA is likely to be susceptible to ester hydrolysis (to form isobutyric acid) under similar conditions to the monomer, with the advantage that the analysis will not be complicated by polymerisation.

5.6 References

(1) Maxwell, I. A.; Morrison, B. R.; Napper, D. H.; Gilbert, R. G. *Macromolecules* **1991**, *24*, 1629.

(2) Zammit, M. D.; Davis, T. P.; Haddleton, D. M. *Macromolecules* **1996**, *29*, 492.

(3) Zammit, M. D.; Davis, T. P.; Haddleton, D. M.; Suddaby, K. G. *Macromolecules* **1997**, *30*, 1915.

(4) Ballard, M. J., 1983, Ph.D. Thesis, University of Sydney.

(5) Maxwell, I. A.; Morrison, B. R.; Napper, D. H.; Gilbert, R. G. *Makromol. Chem.* **1992**, *193*, 303.

(6) Wang, S.-T.; Poehlein, G. W. *J. Appl. Polym. Sci.* **1993**, *50*, 2173.

(7) Wang, S.-H.; Poehlein, G. W. *J. Appl. Polym. Sci.* **1994**, *51*, 593.

(8) Kshirsagar, R. S.; Poehlein, G. W. *J. Appl. Polymer Sci.* **1994**, *54*, 909.

(9) Thomson, B.; Wang, Z.; Paine, A.; Lajoie, G.; Rudin, A. *J. Polym. Sci. Part A - Polymer Chem.* **1995**, *33*, 2297.

(10) De Bruyn, H.; Gilbert, R. G. *Polymer* **2001**, *42*, 7999.

(11) Lamb, D. J., 2003, Ph.D. Thesis, University of Sydney.

(12) Trathnigg, B., in *Encyclopedia of Analytical Chemistry*; Meyers, R. A., Ed.; John Wiley & Sons Ltd: Chichester, 2000.

(13) Brandrup, J.; Immergut, E. H.; Grulke, E. A. *Polymer Handbook*; 4th ed.; Brandrup, J.; Immergut, E. H.; Grulke, E. A., Ed.; John Wiley & Sons: New York, 1999.

(14) Thomson, B.; Suddaby, K.; Rudin, A.; Lajoie, G. *European Polymer J.* **1996**, *32*, 239.

(15) Jones, W. J.; Lapworth, A. *J. Chem. Soc., Abstracts* **1911**, *99*, 1427.

(16) Williams, R. J.; Gabriel, A.; Andrews, R. C. *J. Am. Chem. Soc.* **1928**, *50*, 1267.

(17) Schultz, R. F. *J. Am. Chem. Soc.* **1939**, *61*, 1443.

(18) Jencks, W. P.; Gilchrist, M. *J. Am. Chem. Soc.* **1964**, *86*, 4651.

(19) Tauer, K.; Padtberg, K.; Dessy, C. *ACS Symp. Ser.* **2002**, *801*, 93.

(20) Kolthoff, I. M.; Meehan, E. J.; Carr, E. M. *J. Am. Chem. Soc.* **1953**, *75*, 1439.

(21) Sangster, D. F.; Davison, A. *J. Polym. Sci., Polym. Symp.* **1975**, *49*, 191.

(22) Smith, P.; Pearson, J. T.; Wood, P. B.; Smith, T. C. *J. Chem. Phys.* **1965**, *43*.

(23) Gilbert, B. C.; Norman, R. O. C.; Placucci, G.; Sealy, R. C. *J. Chem. Soc., Perkin Trans. 2: Physical Organic Chemistry (1972-1999)* **1975**, 885.

(24) Bennett, J. E.; Gilbert, B. C.; Lawrence, S.; Whitwood, A. C.; Holmes, A. J. *J. Chem. Soc., Perkin Trans. 2: Physical Organic Chemistry* **1996**, 1789.

6. Chain Stopping Reactions in the Emulsion Polymerisation of Methyl Methacrylate

6.1 Introduction

The importance of the second-order rate coefficients for transfer to monomer and termination, k_{tr} and $\langle k_t \rangle$ respectively, in emulsion polymerisation kinetics should be plainly evident from the content of the preceding chapters of this thesis. Not only does the value of k_{tr} have significant implications regarding the nature of the radical chain length distribution (thereby also affecting the chain length dependent value of $\langle k_t \rangle$), but it is also the only means by which monomeric radicals may be produced inside a latex particle and is thus crucial to determining the rate of radical loss from a particle *via* exit. $\langle k_t \rangle$, in turn, determines the rate for the only other process leading to radical loss inside a particle. Furthermore, both k_{tr} and $\langle k_t \rangle$ are responsible for determining the exact distribution of non-growing, or "dead", polymer chains formed inside a particle.

The kinetic investigations of Chapter 3 dealt with an emulsion polymerisation system (styrene at 50°C) wherein exit, and hence transfer, was rate-determining, with intra-particle termination being rapid on this timescale; the significant simplifications associated with "zero-one" kinetics were thus taken advantage of. In Chapter 4 it was discussed how, in some systems, both exit and intra-particle termination may be rate-determining. Subsequently it was also shown, using the emulsion polymerisation of methyl methacrylate (MMA) as an example, that under certain conditions exit is almost certainly non-rate-determining. Here one may confidently assume that radical loss from a particle is by termination only and make use of the simplifications offered by the "pseudo-bulk" model.

In this chapter we look in more detail at the process of termination in emulsion polymerisation. In order that this process may be investigated *via* kinetic experiments we once again choose to examine the emulsion polymerisation of MMA, wherein termination kinetics are directly rate-determining and may therefore be quantified. Additional information will be procured from examination of the molecular weight distribution of

polymer formed in this emulsion system. Along the way it will be seen that in many cases the value of $\langle k_t \rangle$ is inextricably linked to the value of k_{tr}. Thus a concurrent aim of this chapter is to determine a value for the rate coefficient for transfer to monomer in this system. Naturally, the results obtained here may be considered complementary to those of Chapter 4, and, indeed, we will draw on some of the experimental results from that chapter in addition to the new data obtained here.

6.2 Background Information

6.2.1 Measured Values for $\langle k_t \rangle$

The only literature data available for $\langle k_t \rangle$ in the emulsion polymerisation of MMA are those reported by Ballard *et al.*,[1] who utilised the same γ-relaxation technique as here to obtain values of $\langle k_t \rangle$ from seeded polymerisations (with seed particles of unswollen radius ~ 75 nm) over a range of weight fraction of polymer, w_p. Of most relevance to the present study was their finding that $\langle k_t \rangle = (3.8 \pm 1.0) \times 10^4$ M^{-1} s^{-1} during Interval II polymerisation at 50°C. Importantly, at the time of that work the current understanding of chain length dependent termination had not yet been developed and the associated effects on $\langle k_t \rangle$ were therefore not considered. However the possible influence of this phenomenon was alluded to.

More recently Clay *et al.*[2] put forward an alternative method for measuring $\langle k_t \rangle$ from analyses of molecular weight distributions for emulsion systems where the pseudo-bulk approximation is applicable. This method was applied to large particle seeded emulsion polymerisations of styrene and the results showed reasonable agreement with $\langle k_t \rangle$ data obtained from kinetic measurements using the γ-relaxation technique.[3] However, this approach has yet to be used for measuring $\langle k_t \rangle$ in other emulsion polymerisation systems.

6.2.2 Measured Values for k_{tr}

As will be discussed in detail later in this chapter, the above methodology based on molecular weight distributions may also be used to determine the value of the rate coefficient for chain transfer in a polymerisation system. Specifically, this method yields a value for k_{tr}/k_p (the so-called "transfer constant") with k_{tr} then being isolated using an appropriate value for the propagation rate coefficient (*e.g.*, one obtained from pulsed-laser polymerisation

experiments). Moreover, variants of this technique can be used to measure k_{tr}/k_p in bulk systems and in emulsion systems that obey either zero-one or pseudo-bulk kinetics, and it has therefore been applied to a number of systems,[2,4-6] including those with added chain transfer agent.[7-10] Of greatest interest here are the findings of Ballard[4] concerning the transfer to monomer rate coefficient in MMA emulsion polymerisations. Here the values $k_{tr}/k_p = 5.7 \times 10^{-5}$ and $k_{tr}/k_p = 8.5 \times 10^{-5}$ were obtained at 50°C and 60°C respectively. Although these results relied on the assumption that essentially all dead polymer chains are formed by transfer to monomer, it is noted that the results of the present study will be seen to be supportive of this assumption.

Interestingly, the values nominally measured for the rate coefficient for transfer to monomer in MMA emulsions by Ballard are seen to be significantly higher than the analogous values determined by Stickler and Meyerhoff, using essentially the well-known Mayo method,[11] for a highly-purified MMA bulk system:[12] $k_{tr}/k_p = 1.1 \times 10^{-5}$ at 50°C, and $k_{tr}/k_p = 1.4 \times 10^{-5}$ at 60°C (amongst values from 0°C to 140°C). This discrepancy (which is difficult to ascribe solely to experimental uncertainty in both values, *e.g.*, from GPC errors) has previously been attributed to the presence of "adventitious impurities" (*e.g.*, surfactant-derived species) giving rise to additional transfer reactions in the emulsion system. However, it is noted that Kukulj *et al.*[6] have recently also conducted bulk polymerisations of MMA and used both the methodology described above as well as the Mayo method to determine values of $k_{tr}/k_p = 5.2 \times 10^{-5}$ and $k_{tr}/k_p = 7.7 \times 10^{-5}$ respectively at 50°C. Thus it would appear that the presence of adventitious impurities is not restricted to emulsion polymerisations, and hence that the value for the rate coefficient for transfer to monomer (perhaps more precisely termed "the rate coefficient for transfer in the absence of any added chain transfer agent") may well be sensitive to the specific conditions in a given experiment, *e.g.*, the extent of monomer purification, of reactor cleaning, *etc.*[12]

6.2.3 Chain Length Dependent Termination

As a final background note we briefly recall the definition for the chain length dependent (CLD) value of the intra-particle termination rate coefficient which was utilised in Chapter 4 and is also assumed throughout this chapter. The definition used here is the same as that of Russell *et al.*,[13] whereby the overall ("macroscopic") rate coefficient for termination in a pseudo-bulk system, $\langle k_t \rangle$, obtained for example from a γ-relaxation experiment, is a weighted

sum of the microscopic termination rate coefficients, $k_t^{i,j}$, pertaining to the reaction of two radicals of degree of polymerisation i and j respectively, as shown in equation (6.1).

$$\langle k_t \rangle = \sum_{i=1}^{\infty} \sum_{j=1}^{\infty} k_t^{i,j} \frac{n_i}{\bar{n}} \frac{n_j}{\bar{n}} \tag{6.1}$$

The particular weighting for each $k_t^{i,j}$ value is determined by the values of n_i and n_j, the average number of radicals of degree of polymerisation i and j respectively, per particle, with the sum over all n_i being equal to the average number of radicals per particle, $\bar{n}$.

$$\bar{n} = \sum_{i=1}^{\infty} n_i \tag{6.2}$$

Finally, the values of $k_t^{i,j}$ are assigned some sort of chain length dependence, for example the "diffusion mean" value given in equation (6.3) (and derived from the Smolochowski equation in Chapter 4), where $k_t^{1,1}$ is the rate coefficient for mutual termination of monomeric radicals and e is a scaling exponent specifying the strength of the chain length dependence of $k_t^{i,j}$.

$$k_t^{i,j} = \tfrac{1}{2} k_t^{1,1} \left(i^{-e} + j^{-e} \right) \tag{6.3}$$

6.3 Experimental Details

6.3.1 Kinetic Experiments

Full details of the synthesis and characterisation of the seed latex MMA06 used in all seeded MMA emulsion polymerisations were given in the previous chapter. Also given in Chapter 4 were the experimental procedure and conditions used in seeded MMA kinetic experiments (initiated chemically, spontaneously, or by γ-radiolysis) at 50°C. The same techniques were employed in the present work to carry out further γ-relaxation experiments at the higher temperatures of 60, 70 and 80°C (runs G36, G38 and G35 respectively). Thus it was necessary to determine values for $[M]_p^{sat}$ and $[M]_w^{sat}$ at each of these temperatures. $[M]_p^{sat}$ was measured in each case using the "static swelling" method described in Chapter 1 and elsewhere,[1,14,15] with results as shown in Table 6.1. $[M]_w^{sat}$ was measured using a variation of the static swelling method, developed as part of this work, wherein no seed latex particles or

surfactant are added. A dilatometer vessel was therefore charged with water (degassed to prevent bubble formation during the measurement) and 0.01 g of hydroquinone, as well as sufficient monomer to saturate the aqueous solution and provide a small (~ 1 g) excess. After stirring the mixture for 30 minutes at the specified temperature the excess monomer was allowed to separate from the aqueous solution for 15 minutes. A narrow capillary tube (of known bore diameter) was then attached to the dilatometer vessel and the separated monomer displaced into the capillary by addition of a small amount of water. The length of monomer in the capillary was precisely measured using a dilatometry "tracker" (see Chapter 2) and the exact mass of excess monomer calculated using d_M = 0.936 g cm^{-3}, the MMA density at 20°C[16] (the temperature at the capillary). The value of $[M]_w^{sat}$ was then easily calculated as follows:

$$[M]_w^{sat} = \frac{m_{M,total} - m_{M,excess}}{M_0 V_w} \tag{6.4}$$

where $m_{M,total}$ is the total mass of added monomer, $m_{M,excess}$ the mass of excess monomer measured, M_0 the molar mass of monomer, and V_w the volume of the aqueous phase of the emulsion (calculated from the known volumes of added monomer and polymer, taking into account the variation of densities with temperature). The values obtained in this way were found to be in good agreement with literature data for $[M]_w^{sat}$ in the range of 40 – 90°C,[1,17] with $[M]_w^{sat}$ increasing linearly with temperature over this range as shown in Figure 6.1. The values of $[M]_w^{sat}$ used in all subsequent kinetic analyses were obtained from a linear fit to all data and are presented in Table 6.1.

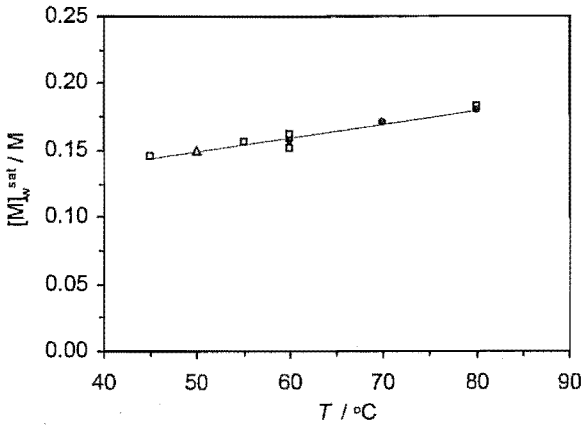

Figure 6.1. $[M]_w^{sat}$ measured for MMA as a function of temperature; values from present study (filled circles) together with literature values from Ballard *et al.*[1] (empty triangle) and Getzen *et al.*[17] (empty squares) and linear fit to all values (line).

It was also necessary to measure the temperature dependence of $d_{M,w}$ (the density of aqueous monomer), for which only limited literature data are available.[1] First, the value $d_{M,w}$ was measured at 40°C (*via* dilatometry) from the observed volume contraction upon dissolving a known mass of MMA in water.[4] This value was then used as a reference point for determining the variation of $d_{M,w}$ with temperature using the following procedure (developed in this work). A standard solution of monomer in water (~ 0.12 M) was prepared, adding a small amount of hydroquinone to prevent any polymerisation. The solution was degassed and heated through the range 40 – 80°C, monitoring the volume expansion dilatometrically. The temperature profile of $d_{M,w}$ was then be obtained by subtracting the known volume expansion due to water,[18] leading to the results of Figure 6.2. The value of $d_{M,w}$ was seen to decrease linearly over this temperature range and the fitted results used in kinetic analyses are given in Table 6.1. The 50°C value found here, 0.981 g cm^{-3}, (also used for all data analyses in Chapter 4) compares well with the Ballard *et al.*[1] value at 50°C, 0.978 g cm^{-3}.

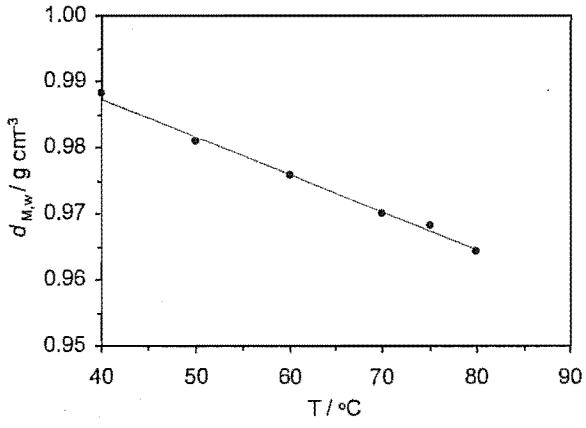

Figure 6.2. $d_{M,w}$ measured for MMA as a function of temperature (circles), along with linear fit (line).

Of course there is considerable uncertainty associated with the results obtained here for $d_{M,w}$ as a function of temperature, since the measured volume expansion is dominated by that due to water. However, given the small fraction of monomer in the aqueous phase of an emulsion polymerisation, any error in $d_{M,w}$ is likely to have a small effect on the rate data obtained during Interval III (and no effect at all in Interval II).

Table 6.1. Temperature dependent solubility and density values for MMA measured experimentally for use in analysis of kinetic data.

T / °C	50	60	70	80
$[M]_p^{sat}$ / M	6.92	6.73	6.75	6.57
$[M]_w^{sat}$ / M	0.150	0.161	0.171	0.182
$d_{M,w}$ / g cm^{-3}	0.981	0.976	0.970	0.964
w_p (Interval II)†	0.296	0.310	0.297	0.311

† calculated from $[M]_p^{sat}$, d_M and d_p (see reference[14])

6.3.2 Molecular Weight Analyses

Molecular weight distributions were measured for the seed latex polymer and the polymer from latexes produced in four seeded kinetic experiments with potassium persulfate as chemical initiator (runs C68, C69, C72 and C73 from Chapter 4). The seeded runs were monitored by dilatometry and stopped at the end of Interval II, rapidly quenched with hydroquinone, and cooled in an ice bath. Final conversion was checked by gravimetry, to make absolutely sure that all "new" (*i.e.*, non-seed) polymer was indeed formed under Interval II conditions. Molecular weight distributions were determined using gel-permeation chromatography (GPC), kindly performed by Dr. Chris Ferguson at the University of Sydney's Key Centre for Polymer Colloids. Samples were prepared by dissolving the dried polymer in tetrahydrofuran at 0.1% by weight. Analyses were carried out using a Shimadzu system fitted with a series of 3 HT6E Waters columns and a refractive index detector. The molecular weight distribution was determined with Polymer Laboratories Cirrus™ software. A calibration curve was constructed using a combination of low polydispersity poly(MMA) (Polymer Standards Service, molecular weight range 505 – 2.5×10^6 g mol^{-1}) and polystyrene (Polymer Laboratories, molecular weight range 5000 – 1.0×10^7 g mol^{-1}) standards, the latter of which were required to cater for the high molecular weight of polymer produced in the present study. The universal calibration procedure was employed for the polystyrene standards, using the following Mark-Houwink parameters: $K = 14.1 \times 10^{-3}$ mL g^{-1}, $\alpha = 0.7$ for polystyrene; $K = 12.8 \times 10^{-3}$ mL g^{-1}, $\alpha = 0.69$ for poly(MMA).

6.4 Results and Discussion

The γ-relaxation kinetic data were analysed using the approach described in detail in Chapter 4, the key equations for which are now briefly revisited.

Analysis of the volume contraction measured using dilatometry yields data for conversion of monomer into polymer, $\hat{x}$ (in grams). The overall rate of polymerisation, obtained as the time-derivative of $\hat{x}$, may be related to the average number of radicals per particle, $\bar{n}$, according to equation (6.5).

$$\frac{d\hat{x}}{dt} = \frac{k_p [M]_p M_0 N_c V_w}{N_A} \bar{n} \qquad (6.5)$$

In the present case we must also specify temperature dependent values for the intra-particle densities of monomer and polymer, d_M and d_p respectively, and the rate coefficients for propagation, k_p, and transfer to monomer, k_{tr}. Here we adopt the following literature expressions for MMA:

$$d_M = \frac{1}{1.025934 + 0.001494(T/°C)} \tag{6.6}$$

$$d_p = \frac{d_M}{0.767089 + 0.000516(T/°C)} \tag{6.7}$$

$$k_p = 10^{6.427}\ M^{-1}\ s^{-1} \exp\left(\frac{-22.36\ kJ\ mol^{-1}}{RT}\right) \tag{6.8}$$

$$\log_{10}\left(\frac{k_{tr}}{k_p}\right) = -1.13 - \frac{23.8\ kJ\ mol^{-1}}{2.303\ RT} \tag{6.9}$$

The density values are those appropriate for solutions of polymer in monomer, reported from the findings of an IUPAC working party on free radical polymerisation.[19] The expression for k_p constitutes benchmark data for the range –1 to 90°C and arises from the work of another IUPAC working party.[20] The temperature variation of k_{tr}/k_p is that measured by Stickler and Meyerhoff[12] over the range 0 – 140°C.

The time evolution of $\bar{n}$ has been shown to be well described by equations (6.10) and (6.11) (*i.e.*, the pseudo-bulk equation assuming complete re-entry of exited radicals) for the case of a γ-relaxation, where the aqueous radical flux is very low.[1]

$$\frac{d\bar{n}}{dt} = \rho - 2c\bar{n}^2 \tag{6.10}$$

$$c = \frac{\langle k_t \rangle}{N_A V_s} \tag{6.11}$$

Integration of equations (6.5) and (6.10) gives the following expression for $\hat{x}$ as a function of time.

$$\hat{x} = \frac{k_p [M]_p M_0 N_c V_w}{2 N_A c} \left[\ln\left|Q \exp(\delta t) + \exp(-\delta t)\right| - \ln\left|Q + 1\right| \right] \tag{6.12}$$

where $Q = \frac{\bar{n}_f + \bar{n}_i}{\bar{n}_f - \bar{n}_i}$, $\delta = 2\,c\,\bar{n}_f$ and $\bar{n}_f = \left(\frac{\rho}{2\,c}\right)^{\frac{1}{2}}$. In the case of a γ-relaxation $\bar{n}_i$ and $\bar{n}_f$ are the "in-source" and "out-of-source" steady-state values of $\bar{n}$ respectively, and $\rho = \rho_{spont}$ the rate coefficient for entry of "spontaneously-generated" radicals.

It should be recognised that the above kinetic formulation assumes constant c over a relaxation period. Referring to equation (6.11), this entails (1) constant V_s, and (2) constant $\langle k_t \rangle$. Of course there will be some volume change, but it can be assumed to be negligible for the small conversion change of a relaxation. As for the value of $\langle k_t \rangle$, for it to be constant over the course of a given γ-relaxation is an assumption that is seemingly at odds with one of the precepts of this work: that $\langle k_t \rangle$ is sensitive to the precise chain length distribution of growing radicals. However, for reasons that will shortly be made clear, it turns out that this assumption is actually not too deleterious in the present setting. Furthermore, it is important to clarify that while the above treatment may neglect the effects of CLD termination within a given γ-relaxation experiment, the variation of $\langle k_t \rangle$ with temperature – of foremost interest in this section – is not restricted in any way. Hence the effects of changes in the radical chain length distribution will certainly be manifested in the measured temperature variation of $\langle k_t \rangle$.

It is also noted that in some cases the period of the γ-relaxation experiment encroached somewhat into Interval III. However, the resulting decrease in $[M]_p$ [assumed to be constant in integrating equation (6.5) to obtain (6.12)] during such relaxations is a relatively minor source of error and unlikely to significantly impact the results of data fitting.

Equation (6.12) was fitted to the experimental conversion-time from each γ-relaxation experiment by non-linear regression, with c and ρ_{spont} as adjustable parameters and using the temperature dependent parameter values listed above. From c equation (6.11) gives $\langle k_t \rangle$. The values for $\langle k_t \rangle$, c and ρ_{spont} obtained at each temperature are presented in Table 6.2.

The 50°C values of Table 6.2 are in acceptable but not perfect agreement with those measured in Interval II by Ballard *et al.*:[1,4] $\langle k_t \rangle = (3.8 \pm 1.0) \times 10^{-4}$ M^{-1} s^{-1} and $\rho_{spont} = (2.5 \pm 2.0) \times 10^{-4}$ s^{-1}. In fact, the value of $\langle k_t \rangle$ here differs from that of Ballard *et al.* only by a factor of about 1.5, which is a very small difference given the usual spread noted in literature values for $\langle k_t \rangle$.[21] Moreover, it is noted that the data of Ballard *et al.* were subject to quite a lot of scatter and

that theirs were pioneering days – the greater precision and accuracy of the present experimental apparatus is evident, for example, in the $\bar{a}$ values of Chapter 4 in comparison with those of Ballard *et al.*

Table 6.2. Results obtained from fitting of kinetic data for γ-relaxation of MMA over a range of temperatures.

T / °C	50‡	60*	70*	80*
$\langle k_t \rangle^{\dagger}$ / M^{-1} s^{-1}	1.9×10^4	2.6×10^4	3.6×10^4	4.6×10^4
c / s^{-1}	2.4×10^{-2}	3.5×10^{-2}	4.4×10^{-2}	5.9×10^{-2}
ρ_{spont} / s^{-1}	1.5×10^{-4}	2.6×10^{-4}	2.5×10^{-4}	4.7×10^{-4}

† Values of $\langle k_t \rangle$ calculated according to equation (6.11) using fitted values of c and initial swollen particle volume, $V_s^0 = 1.3 \times 10^{-18}$ dm^{-3} (approximately the same for all experiments)

‡ 50°C is average of duplicate experiments

* Relative errors assumed to be as for 50°C values (see Table 4.3 of Chapter 4)

The values of $\langle k_t \rangle$ and ρ_{spont} were next used to construct the Arrhenius plots shown in Figures (6.3) and (6.4). In the case of $\langle k_t \rangle$ the data were found to be well fitted by the following expression:

$$\langle k_t \rangle = 10^{8.88 \pm 0.03} \text{ M}^{-1} \text{ s}^{-1} \exp\left[\frac{-(28 \pm 3) \text{ kJ mol}^{-1}}{RT}\right] \qquad (6.13)$$

The data for ρ_{spont} showed considerably more scatter but were fitted approximately by the expression,

$$\rho_{spont} = 10^{1.2 \pm 0.1} \text{ M}^{-1} \text{ s}^{-1} \exp\left[\frac{-(31 \pm 11) \text{ kJ mol}^{-1}}{RT}\right] \qquad (6.14)$$

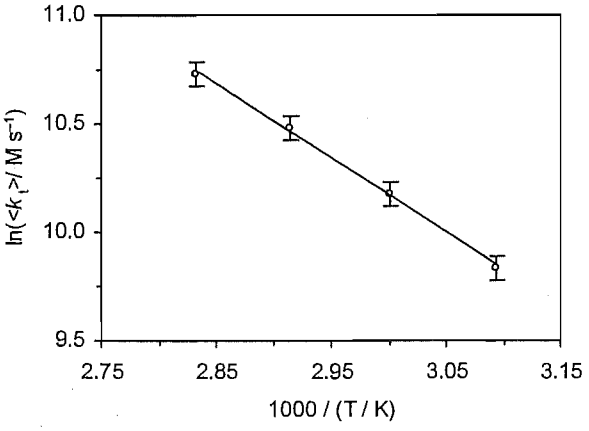

Figure 6.3. Temperature dependence of $\langle k_t \rangle$ obtained for MMA from γ-relaxation experiments.

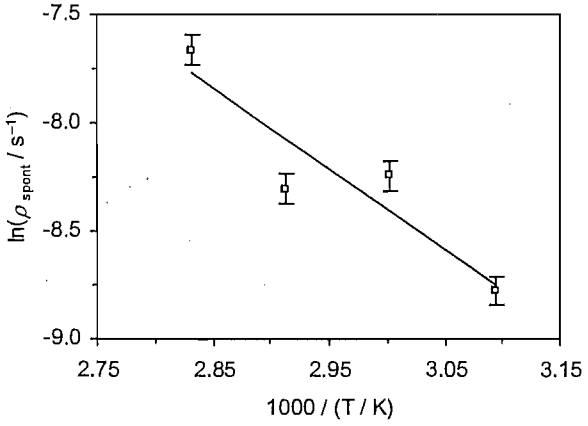

Figure 6.4. Temperature dependence of ρ_{spont} obtained for MMA from γ-relaxation experiments.

In interpreting the activation energy for $\langle k_t \rangle$ determined above, the first inclination may be to suppose that the value of E_a should simply reflect the fact that termination reactions are diffusion-controlled, *i.e.*, that $E_a(\langle k_t \rangle) \approx E_a(D)$, where D is an appropriate diffusion coefficient. A value for $E_a(D)$ in polymerising systems may be obtained from measured diffusion coefficient data. In this case, literature values[22] for toluene diffusion through a polystyrene matrix, which give $E_a(D) = 12.8$ kJ mol^{-1} at weight fraction of polymer $w_p = 0.3$, are thought to provide one estimate for the present study. Notably, this value falls within the broader range of values obtained from more recent work on diffusion of butyl methacrylate (BMA) and MMA through poly(butyl methacrylate) and poly(MMA) polymer matrixes, respectively, where $E_a(D) \sim 12 - 18$ kJ mol^{-1} was reported for $w_p = 0.30$.

The value of $E_a(\langle k_t \rangle)$ measured from Figure 6.3 is therefore considerably greater than that due simply to small molecule diffusion. This usefully demonstrates the fact that $E_a(\langle k_t \rangle)$ is significantly affected by the effects of chain length dependence. Indeed, this matter has been addressed in detail by Russell,[23] who showed that $E_a(\langle k_t \rangle)$ is a rather complex quantity whose value depends critically on the precise nature of the polymerising system of interest (*e.g.*, the type and concentration of initiator and monomer). We thus attempt to interpret the measured value of $E_a(\langle k_t \rangle)$ for the present system in terms of the effects of chain length dependent termination. Here we draw on related work[24,25] to that of Russell, which derives convenient analytic solutions for the value of $\langle k_t \rangle$ under different limiting conditions. These results were originally derived in the context of bulk or solution polymerisation systems, but may equally be applied to the case of a pseudo-bulk emulsion system (with complete re-entry), as is used here.

For the case of a polymerising system in the limit where chain stopping is totally by termination and the value of $k_t^{i,j}$ is assumed to take the so-called "geometric mean" value of $k_t^{i,j} = k_t^{1,1}(ij)^{-e/2}$, the following result may be shown to hold.[24]

$$\langle k_t \rangle = k_t^{1,1}\left[\Gamma\left(\frac{2}{2-e}\right)\right]^{-2}\left[\frac{\sqrt{2R_{init}\,k_t^{1,1}}}{k_p[M]_p}\left(\frac{2}{2-e}\right)\right]^{2e/(2-e)} \tag{6.15}$$

Here Γ is the gamma function and R_{init} is the rate of generation of initiating radicals in the polymerising system; hence, in the present case of an emulsion system in the out-of-source stage of a γ-relaxation, $R_{init} = \rho_{spont}/(N_A V_s)$.

From Equation (6.15), the complex dependence of $\langle k_t \rangle$ on a range of experimental conditions becomes clear. But more importantly, this equation represents a convenient means for estimating the value for $E_a(\langle k_t \rangle)$ without the need for extensive (and computationally demanding) simulation of the complete radical chain length distribution. Assuming e, and $[M]_p$ and V_s (which enters into R_{init}) to be constant with temperature, $E_a(\langle k_t \rangle)$ is therefore related to the activation energies for initiation, propagation and mutual termination of monomeric radicals as shown below.

$$E_a(\langle k_t \rangle) = E_a(k_t^{1,1}) + \frac{2e}{2-e}\left[\tfrac{1}{2}E_a(R_{init}) + \tfrac{1}{2}E_a(k_t^{1,1}) - E_a(k_p)\right] \tag{6.16}$$

If we ally monomeric radical termination with the process of monomer diffusion we may assume that $E_a(k_t^{1,1}) = E_a(D) = 12.8$ kJ mol^{-1} from above, and furthermore that the termination scaling exponent, e, is approximated by that measured for oligomeric diffusion: $e = 1.26$ at $w_p = 0.30$.[26,27] Obviously $E_a(k_p)$ from equation (6.8) is used. It then remains only to specify a value for $E_a(R_{init})$, or in this case $E_a(\rho_{spont})$. Here we adopt three different values in order to gain greater insight from calculations: (a) 0 kJ mol^{-1}, corresponding to a temperature independent value of ρ_{spont}; (b) 135.1 kJ mol^{-1}, the activation energy for decomposition of persulfate initiator; and (c) 31 kJ mol^{-1}, the value obtained from experiment in Figure 6.4. The extreme values of (a) and (b) are thought to represent acceptable physical limits for $E_a(\rho_{spont})$; these cases yield values of $E_a(\langle k_t \rangle) = -41.4$ kJ mol^{-1} (where $\langle k_t \rangle$ is actually predicted to decrease with rising temperature) and 188.7 kJ mol^{-1} respectively, according to equation (6.16). These results show how sensitive $E_a(\langle k_t \rangle)$ is to factors other than just diffusion E_a. Neither of these values is in good agreement with the value of $E_a(\langle k_t \rangle) = 31$ kJ mol^{-1} from experiment, however it would seem that the relatively low value for $E_a(\rho_{spont})$ provides the closest accord. Thus, it is not surprising that when the measured value of $E_a(\rho_{spont})$ is used in case (c) the predicted value of $E_a(\langle k_t \rangle) = 11.4$ kJ mol^{-1} is much closer to that obtained from experiment. However, it is noted that the physical origin for the experimentally measured activation energy for ρ_{spont} remains to be established. Purely coincidentally, this calculated $E_a(\langle k_t \rangle)$ is very close in value to $E_a(k_t^{1,1})$; this coincidence should not be taken as meaning that the $E_a(\langle k_t \rangle)$ arises solely from variation of $k_t^{1,1}$.

We now consider the alternative kinetic limit to that above, *i.e.*, where chain transfer to monomer is the dominant chain stopping event. In this case, if one assumes the "diffusion mean" value of $k_t^{i,j}$, given earlier as equation (6.3), a different analytic form may be derived for $\langle k_t \rangle$:[25]

$$\langle k_t \rangle = k_t^{1,1} \Gamma(1-e) \left(\frac{k_{tr}}{k_p} \right)^e \tag{6.17}$$

Note that this equation formally holds only for $e < 1$, however it seems reasonable to use it for discussion and semi-quantitative purposes even for $e > 1$. Assuming again that e is

temperature independent, the activation energy for $\langle k_t \rangle$ is now related (more simply) to those for $k_t^{1,1}$, k_{tr} and k_p:

$$E_a(\langle k_t \rangle) = E_a(k_t^{1,1}) + e\left[E_a(k_{tr}) - E_a(k_p)\right] \tag{6.18}$$

Note that the same expression for $E_a(\langle k_t \rangle)$ is also obtained with the geometric mean value for $k_t^{i,j}$.[25] Combining the value of $E_a(k_{tr}/k_p) = 23.8$ kJ mol^{-1} from equation (6.9) with the value of $E_a(k_p) = 22.36$ kJ mol^{-1} from equation (6.8) gives $E_a(k_{tr}) = 46.2$ kJ mol^{-1}. Using these values in equation (6.18) furnishes a value of $E_a(\langle k_t \rangle) = 42.8$ kJ mol^{-1} – somewhat greater than that obtained from γ-relaxation experiments.

At this point it is acknowledged that equations (6.15) – (6.18) are derived assuming steady-state polymerisation and making the "long chain approximation" (*i.e.*, that $\rho \ll k_p[M]_p$). Furthermore, these analytic forms are based on the geometric mean model for $k_t^{i,j}$ which may not necessarily apply. However, in the present context, where we seek merely to establish estimates for the value of $E_a(\langle k_t \rangle)$, it is unlikely that the error arising from these assumptions will have any profound effect on the inferences made. Additionally, the computational simplicity offered by this approach should not be hastily disregarded.

While the value of $E_a(\langle k_t \rangle) = 31$ kJ mol^{-1} obtained from γ-relaxation experiments at first sight looks improbably large, in fact it has been shown to be reasonable. Although it is not reproduced precisely by the simple limiting calculations presented here, it is seen to lie nicely between the value of $E_a(\langle k_t \rangle) = 11.4$ obtained for the termination limit [in the most physically reasonable case (c)], and that for the transfer limit of $E_a(\langle k_t \rangle) = 42.8$ kJ mol^{-1}. Hence, at this stage we cannot rule out either termination or transfer as significant chain stopping mechanisms. However, from subsequent results in this chapter it will emerge that transfer dominates at 50°C, and hence it should also dominate at 60 – 80°C, as it becomes more favoured as temperature increases. If one assumes that $E_a(\langle k_t \rangle) = 31$ kJ mol^{-1} is indeed a transfer-controlled value, then equation (6.18) gives $E_a(k_t^{1,1}) = 1.01$ kJ mol^{-1} (using e = 1.26 and $E_a(k_{tr}) = 46.2$ kJ mol^{-1}), or $e = 0.765$ (using $E_a(k_t^{1,1}) = E_a(D) = 12.8$ kJ mol^{-1} and $E_a(k_{tr}) = 46.2$ kJ mol^{-1}), or $E_a(k_{tr}) = 36.8$ kJ mol^{-1} (using $E_a(k_t^{1,1}) = 12.8$ kJ mol^{-1} and $e = 1.26$). Although this $E_a(k_t^{1,1})$ is unreasonable, the values of e and $E_a(k_{tr})$ are quite reasonable given

the uncertainties to which they are hostage. One must also acknowledge experimental error in $\langle k_t \rangle$ and that equation (6.17) strictly only holds for $e < 1$.

Another point which must be discussed is that there is some small variation of w_p with temperature for these measurements (see Table 6.1). Because both $k_t^{1,1}$ and e vary with w_p,[26,27] this introduces variation of $\langle k_t \rangle$ above and beyond the factors implicit in the above (where it is assumed that w_p is constant). And one should also not forget that e has been measured to vary with temperature.[28]

It is difficult to elucidate any more detailed information on the nature of chain stopping in MMA emulsion systems from this data alone (that remains the task for the rest of this chapter), nevertheless it is significant that the approximate calculations carried out here serve to explain the values of $\langle k_t \rangle$ obtained from γ-relaxation experiments and, moreover, provide additional corroboration of our kinetic understanding of this system: the temperature variation of $\langle k_t \rangle$ is certainly consistent with that expected for a pseudo-bulk emulsion system wherein termination is chain length dependent. This will now be investigated more rigorously.

6.4.1 Modelling of CLD Termination in the Emulsion Polymerisation of MMA at 50 °C

In this section we endeavour to elicit more detailed information on chain stopping in MMA emulsion systems by examining kinetic data from both γ-relaxation and chemically (KPS) initiated polymerisations at 50°C. It will be recalled that in Chapter 4 this approach was used in a modelling-only study of chemically initiated polymerisations. In that case the kinetic feature of most interest was the rate of increase in $\bar{n}$ during Interval II – the so-called acceleration, $\bar{a}$ – and it was shown that including CLD termination had a negligible effect on the value of $\bar{a}$ (under usual conditions). This is because the change in the radial chain length distribution during Interval II is minimal. Of course these findings do not preclude a significant change in $\langle k_t \rangle$ from experiment to experiment with changing [KPS]. We therefore now use the CLD termination modelling methodology of the previous chapter to fit experimental data from γ-relaxation and chemically initiated runs, and determine the variation of $\langle k_t \rangle$ with ρ (and hence [KPS]). As intimated in the analytic solutions above, equations (6.15) and (6.17), in the case where chain stopping occurs mainly by termination $\langle k_t \rangle$ will show an appreciable dependence on ρ due to the effect on the radical chain length distribution

from changing the flux of short initiating radicals into the particles. Whereas, in the transfer limit the chain length distribution, and hence also the value of $\langle k_t \rangle$, will be completely independent of ρ.

Data fitting for γ-relaxation at 50°C

Initially, simulated conversion-time data are fitted to those obtained from γ-relaxation experiment G32 at 50°C. As in previous work, fitting of conversion data is preferred over fitting of $\bar{n}$ data which is somewhat "noisier" as a result of numerical differentiation. Briefly, the simulated data consist of numerical solutions of equations (6.5) and (6.19) – (6.21), in conjunction with equations (6.1), (6.2) and (6.22).[13,29] We assume the diffusion mean value for $k_t^{i,j}$ shown earlier in equation (6.3). It is also assumed that entry is by monomeric radicals (noting that even if entry is in fact by longer radicals – *e.g.*, as was found for chemically initiated experiments in the previous chapter – this assumption does not introduce significant error because of the transfer-dominated nature of the radical chain length distribution), and, in light of the aqueous reaction rate calculations of the previous chapter, that there is complete re-entry of exited radicals. A more detailed description of the simulation method may be found in Chapter 4.

$$\frac{dn_1}{dt} = \rho + k_{tr}[M]_p \sum_{j=2}^{\infty} n_j - k_p^1[M]_p n_1 - 2n_1 \sum_{j=1}^{\infty} c^{1,j} n_j \qquad (6.19)$$

$$\frac{dn_2}{dt} = k_p^1[M]_p n_1 - k_p[M]_p n_2 - k_{tr}[M]_p n_2 - 2n_2 \sum_{j=1}^{\infty} c^{2,j} n_j \qquad (6.20)$$

$$\frac{dn_i}{dt} = k_p[M]_p(n_{i-1} - n_i) - k_{tr}[M]_p n_i - 2n_i \sum_{j=1}^{\infty} c^{i,j} n_j, \quad i > 2 \qquad (6.21)$$

$$c^{i,j} = \frac{k_t^{i,j}}{N_A V_s} \qquad (6.22)$$

As in the earlier work, we assume the following parameter values for MMA at 50°C: $k_p^1 = 15$ k_p,[14,30-33] $e = 1.26$ (at $w_p = 0.30$)[26,27] and $a = 6.9$ Å.[34] In order to allow for the uncertainty in the value of the rate coefficient for transfer to monomer in MMA emulsion polymerisations separate simulations were carried out using two different values: the value reported by

Ballard[4] of $k_{tr} = 5.7 \times 10^{-5}$ $k_p = 3.7 \times 10^{-2}$ M^{-1} s^{-1}, and also that reported by Stickler and Meyerhoff[12] of $k_{tr} = 1.1 \times 10^{-5}$ $k_p = 7.0 \times 10^{-3}$ M^{-1} s^{-1} [where $k_p = 649$ M^{-1} s^{-1} is the IUPAC recommended value from equation (6.8)]. Additionally, separate simulations were carried out with and without a contribution to $k_t^{i,j}$ from reaction diffusion[34] in order to determine the importance of this contribution.

In each of the four different simulations prescribed above, the value of $k_t^{1,1}$ in equation (6.3) is treated as an adjustable parameter – note: it is the only one – and varied until a satisfactory fit to the experimental conversion-time data is achieved. Such a fit is exemplified by Figure 6.5 and the full results of this fitting procedure are presented in Table 6.3.

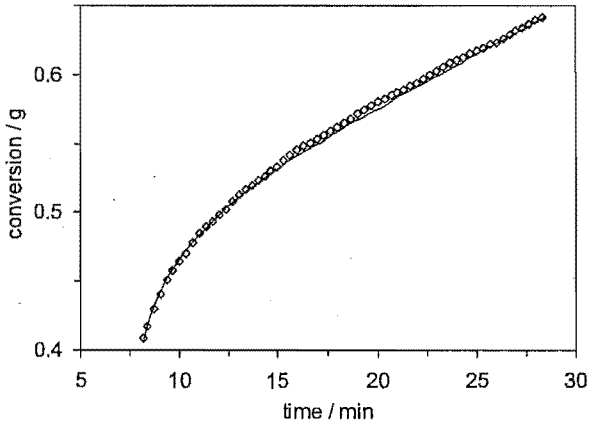

Figure 6.5. Data fitting for γ-relaxation experiment G32 using $k_{tr} = 5.7 \times 10^{-5}$ k_p (Ballard) and the pseudo-bulk model with CLD termination (including reaction diffusion); simulated conversion data (line) and experimental data (diamonds) presented as functions of time.

The value of $k_t^{1,1}$ obtained from γ-relaxation data fitting is seen to be significantly affected by the magnitude of k_{tr}, with a five-fold increase in k_{tr} leading to a decrease in the fitted $k_t^{1,1}$ of a similar magnitude. This confirms that transfer is a significant chain-stopping event in the system, *i.e.*, the system is not "termination-controlled" under these conditions. It is also evident that the impact of reaction diffusion is relatively small, causing only a slight change in the fitted value of $k_t^{1,1}$.

Table 6.3. Results of 50°C γ-relaxation data fitting using pseudo-bulk model with CLD termination: the effect of reaction diffusion.

reaction diffusion	k_{tr} / M^{-1} s^{-1}	ρ_{spont} / s^{-1}	$k_t^{1,1}$ / M^{-1} s^{-1}
included	5.7×10^{-5} k_p (Ballard)	1.5×10^{-4}	9.80×10^7
excluded	5.7×10^{-5} k_p (Ballard)	1.5×10^{-4}	1.05×10^8
included	1.1×10^{-5} k_p (Stickler and Meyerhoff)	1.5×10^{-4}	5.05×10^8
excluded	1.1×10^{-5} k_p (Stickler and Meyerhoff)	1.5×10^{-4}	5.50×10^8

In fact the importance of k_{tr}/k_p in determining $\langle k_t \rangle$ is made beautifully evident by equation (6.17): for a lower k_{tr}/k_p, a higher $k_t^{1,1}$ will be needed to reproduce a given $\langle k_t \rangle$. The present simulations clearly show this. Because of the uncertainty in k_{tr}/k_p, all modelling will be carried out with both values, regarding the Ballard value as a (likely) upper bound for the real value and the Stickler and Meyerhoff value as a (likely) lower bound. Indeed the value obtained from molecular weight distributions in this work, presented later in this chapter, is found to lie between the two literature values. However, this measured value of k_{tr}/k_p will not be used in the present modelling, because it is clear that this value would simply give fitted parameter values between those obtained with the "limiting" values used here.

Next, we investigate the influence that the assumed scaling law for $k_t^{i,j}$ has on the results obtained from data fitting. The results presented above were obtained using a single exponent (e = 1.26) to describe how $k_t^{i,j}$ scales with chain length in the CLD termination model. In Chapter 4 another approach was suggested wherein the scaling exponent is allowed to vary with both w_p and radical chain length. While the first of these allowances is redundant in the present Interval II setting where w_p is constant, the second does warrant investigation here. This may be achieved by specifying a "crossover chain length", X_c, at which the scaling law changes. For the purposes of modelling here we will identify X_c as the minimum chain length for which motion is by reptation, governed by a scaling exponent of e = 2.00[35] which gives a more rapid decrease in diffusion coefficients with chain length. For chains of length X_c and below we assume that motion is by diffusion with the lower value of e = 1.26 as before.

According to this definition the previous calculations with $e = 1.26$, independent of chain length, correspond to a value of $X_c = \infty$. We next adopt a value of $X_c = 10$ (retaining the scaling exponent of $e = 1.26$ for chains of length less than 10), in line with the data of Griffiths *et al.*,[26] who measured e only up to $i = 10$, and as an interesting extension we finally consider the extreme case of $X_c = 1$ where the value of $e = 2.00$ is applied over all chain lengths. While this case is physically unrealistic (since the movement of very short oligomeric chains is unlikely to be restricted to reptation), it does provide a useful estimate of the upper bound for $k_t^{1,1}$. Probably the value $X_c = 10$ is most realistic (no definitive information is available on this), as the measured scaling law for oligomeric diffusion cannot realistically extend to infinite chain lengths.

Table 6.4. Results of 50°C γ-relaxation data fitting using pseudo-bulk model with CLD termination: the effect of a CLD scaling law for diffusion coefficients

X_c	k_{tr} / M^{-1} s^{-1}	ρ_{spont} / s^{-1}	$k_t^{1,1}$ / M^{-1} s^{-1}
∞	5.7×10^{-5} k_p (Ballard)	1.5×10^{-4}	9.80×10^{7}
10	5.7×10^{-5} k_p (Ballard)	1.5×10^{-4}	1.58×10^{8}
1	5.7×10^{-5} k_p (Ballard)	1.5×10^{-4}	4.30×10^{8}
∞	1.1×10^{-5} k_p (Stickler and Meyerhoff)	1.5×10^{-4}	5.05×10^{8}
10	1.1×10^{-5} k_p (Stickler and Meyerhoff)	1.5×10^{-4}	8.50×10^{8}
1	1.1×10^{-5} k_p (Stickler and Meyerhoff)	1.5×10^{-4}	2.30×10^{9}

The results of re-fitting the γ-relaxation data with the above modifications are shown in Table 6.4. As is to be expected, varying the diffusion scaling laws governing $k_t^{i,j}$ has a significant effect on the value of $k_t^{1,1}$ obtained from experimental data fitting. Specifically, as X_c is changed from ∞ to 1 (*i.e.*, the strongest chain length dependence is applied) there is an approximately four-fold increase in the value of $k_t^{1,1}$ required to fit the γ-relaxation data. Again, equation (6.17) makes this beautifully clear: as e is increased, the value of $k_t^{1,1}$ that gives a particular value of $\langle k_t \rangle$ must also increase. It is also evident that applying the stronger

chain length dependence only to decameric and longer chains (as is more reasonable based on experimental evidence) results in a non-negligible increase in the fitted value of $k_t^{1,1}$.

The purpose of the above data fitting exercises was to clearly demonstrate that the nature of the chain length dependence applied to $k_t^{i,j}$ is of considerable importance in modelling experimental data. In the remainder of the modelling work presented this chapter it is assumed that the value of $k_t^{i,j}$ for all chain lengths may be described by a single scaling law: that of equation (6.3) with $e = 1.26$. This assumption is made for the sake of clarity and consistency in comparing the data presented, however it is not meant to suggest that this simple treatment is of any greater merit than others also described above.

A priori calculation of $k_t^{1,1}$

Before proceeding we consider the value of $k_t^{1,1}$ predicted under the assumption of diffusion controlled termination by the Smoluchowski equation, which provides a useful reference for interpreting the values of $k_t^{1,1}$ obtained from fitting of experimental data above. This value may be calculated according to the expression,

$$k_t^{1,1} = 2\pi\sigma p_{spin}(D_M + D_M)N_A \qquad (6.23)$$

The variables in equation (6.23) are defined as follows, with best estimates for the present MMA system in brackets: σ = interaction radius for radical-radical reaction (3.0 Å[36]), p_{spin} = probability of radical reaction based on spin alignments (0.25[36]), and D_M is the diffusion coefficient for a monomer molecule in a latex particle, used to approximate that of a chemically similar monomeric radical (1.12×10^{-9} m^2 s^{-1}[26]). Of these D_M is known with the most confidence, as it has been measured, while p_{spin} and σ are "best guesses" (although both should be quite close to the given values). The value of $k_t^{1,1}$ given by equation (6.23) is then 6.4×10^8 M^{-1} s^{-1} – certainly within the range of $k_t^{1,1}$ values obtained from fitting of γ-relaxation data above (see Tables 6.3 and 6.4). Actually, given that $X_c = 10$ is thought to be the most reliable estimate and that it is later found that k_{tr}/k_p measured for the present system is intermediate between the Stickler-Meyerhoff and Ballard values, it is no exaggeration to suggest that the most likely value of $k_t^{1,1}$ here is within the range $1.58 - 8.50 \times 10^8$ M^{-1} s^{-1}, *i.e.*, in spectacular agreement with the *a priori* prediction for $k_t^{1,1}$. Not only does the good

agreement found here quantitatively support the notion that the Smoluchowski equation provides a good foundation for modelling termination kinetics in the present system, it also means that, to good approximation, the values of $\langle k_t \rangle$ required to fit experimental kinetic data for γ-relaxation and chemically initiated polymerisations may be predicted entirely from first principles based on the model for chain length dependent termination used here.

Data fitting for chemically initiated experiments at 50°C

Simulated conversion-time data were next fitted to data obtained from Interval II of chemically initiated experiments. The details of all kinetic runs analysed in this section have already been given in the preceding chapter, therefore these experiments will be referred to here only by their labels (*e.g.*, run "C50"). The procedure here was to use the value of $k_t^{1,1}$ as determined from fitting of 50°C γ-relaxation data above and to treat ρ as the only adjustable parameter. Once again separate simulations were carried out for each of the two k_{tr} values used above:

(a) Modelling with $k_{tr} = 5.7 \times 10^{-5}\ k_p$ (Ballard)

A key result from Chapter 4 was the finding that the pseudo-bulk model, assuming complete re-entry of exited radicals and either CLI or CLD termination, precisely predicts the evolution of $\overline{n}$ during Interval II only for experiments with [KPS] ~ 10^{-3} M. This was illustrated by the variation with initiator concentration of the experimentally measured acceleration, contrary to the pseudo-bulk model's prediction of a constant value of $\overline{a}$ = 0.42. Accordingly, in the present context of fitting experimental conversion-time data using the pseudo-bulk model with CLD termination, it was found that an exact fit was only obtained for the same conditions of intermediate initiator concentration. This is well exemplified by the fit for [KPS] = 10^{-3} M (run C50) shown in Figure 6.6.

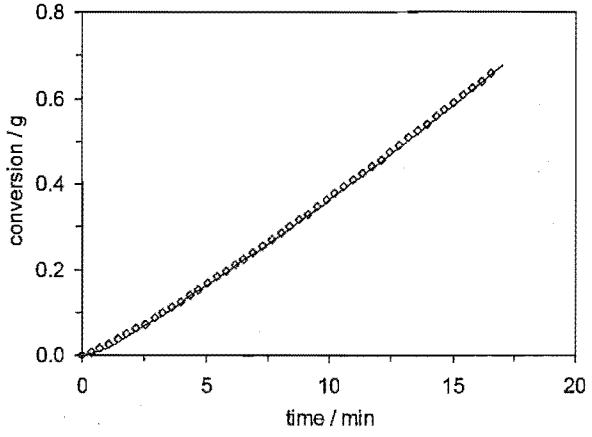

Figure 6.6. Data fitting for chemically initiated experiment with [KPS] = 10^{-3} M using $k_{tr} = 5.7 \times 10^{-5}\ k_p$ (Ballard) and the pseudo-bulk model with CLD termination (including reaction diffusion); simulated conversion data (line) and experimental data (diamonds) presented as functions of time.

Notably, simulations reproduce the experimental conversion data not only during the steady-state period, but also during the approach to steady-state. This is an important observation in view of speculation, based on the theory,[37] that the approach to steady-state for chemically initiated MMA polymerisations is likely to be significantly affected by the retardative effect of residual dissolved oxygen. Any such effect appears to be negligible in the present experiments, although it is noted that the de-oxygenation procedures used in this work, while not onerous, were an improvement on those usually used for emulsion polymerisation (see Chapter 2). The fact that the approach to steady-state is so perfectly described is a result which re-opens the door to using this transient period as a way to deduce values of rate coefficients.

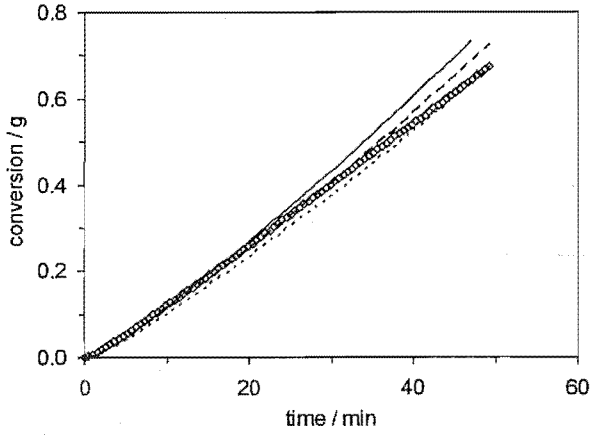

Figure 6.7. Data fitting for chemically initiated experiment with [KPS] = 3×10^{-5} M using $k_{tr} = 5.7 \times 10^{-5}\ k_p$ (Ballard) and the pseudo-bulk model with CLD termination (including reaction diffusion); experimental conversion data (diamonds), and simulated conversion data for $\rho = 7 \times 10^{-4}$ s^{-1} (————), $\rho = 8 \times 10^{-4}$ s^{-1} (— — —) and $\rho = 9 \times 10^{-4}$ s^{-1} (– – – – –), presented as functions of time.

The fit to experimental conversion data afforded by the CLD pseudo-bulk model was found to become less satisfactory as initiator concentration deviated from the intermediate region of [KPS] ~ 10^{-3} M. This is illustrated for [KPS] = 3×10^{-5} M (run C61) in Figure 6.7, where the experimental data are not precisely fitted by any of the range of ρ values tried (reflecting that the acceleration is less, in this case, than pseudo-bulk kinetics with $\alpha = 1$ can describe). Bearing in mind this deterioration in fitting quality, the CLD pseudo-bulk model was found to adequately simulate data over the initiator concentration range 10^{-4} M ≤ [KPS] ≤ 3×10^{-3} M (*i.e.*, excluding the highest and lowest initiator concentrations, where significant variation in the experimental acceleration is most apparent). The results obtained from CLD pseudo-bulk fitting for a series of experiments spanning this range of conditions are presented in Table 6.5. Also presented for comparison are the best estimates for ρ obtained in Chapter 4 using the pseudo-bulk model with CLI termination.

Table 6.5. Results of data fitting for 50°C chemically initiated runs using $k_t^{1,1} = 9.80 \times 10^7$ M^{-1} s^{-1} and $k_{tr} = 5.7 \times 10^{-5}\ k_p$ (Ballard) in the pseudo-bulk model with CLD termination (including reaction diffusion).

run	[KPS] / M	ρ / s^{-1} with CLI $\langle k_t \rangle$†	ρ / s^{-1} with CLD $\langle k_t \rangle$	$\langle k_t \rangle$ / M^{-1} s^{-1}
C52	1×10^{-4}	1.29×10^{-3}	1.40×10^{-3}	1.94×10^4
C62	3×10^{-4}	2.98×10^{-3}	3.30×10^{-3}	1.96×10^4
C50	1×10^{-3}	6.09×10^{-3}	6.50×10^{-3}	1.98×10^4
C55	3×10^{-3}	8.95×10^{-3}	9.80×10^{-3}	2.00×10^4

† from Table 4.9 of Chapter 4, obtained using $\langle k_t \rangle = 1.92 \times 10^4$ M^{-1} s^{-1}.

The value of ρ obtained from fitting with CLD termination in this section is seen in all cases to be slightly greater than that from the CLI fitting of Chapter 4. This difference reflects a slight enhancement in the value of $<k_t>$ in the case of the CLD model. Firstly, this reflects that the present modelling does not make the steady-state assumption, whereas the CLI modelling did. Secondly, it reflects that CLD modelling allows $\langle k_t \rangle$ to vary with ρ. In this respect, the most notable result in Table 6.5 is the fact that a change in ρ of approximately an order of magnitude gives rise to only a very small increase (~ 3%) in the chain length dependent value of $\langle k_t \rangle$. As outlined earlier, such insensitivity of $\langle k_t \rangle$ to changing ρ indicates that the chain length distribution is close to being transfer controlled – the limit of which is characterised by the value of $\langle k_t \rangle$ being invariant with ρ. This result illustrates an important feature of the chain length dependent termination model: under conditions where transfer is the prevailing radical loss mechanism, kinetic data may be modelled with acceptable accuracy using a chain length *independent* value of $\langle k_t \rangle$ (which, it is stressed, is not to say that $k_t^{i,j}$ is chain length independent, but just that $\langle k_t \rangle$ does not change significantly as a result of varying ρ). Hence the analysis of γ-relaxation (carried out earlier) assuming constant $\langle k_t \rangle$ for a given relaxation is likely to be valid for this particular system, and, indeed, for any other transfer controlled system.

(b) Modelling with $k_{tr} = 1.1 \times 10^{-5}\ k_p$ (Stickler and Meyerhoff)

The fitting of Interval II conversion data from chemically initiated experiments was next repeated using the value for k_{tr} reported by Stickler and Meyerhoff[12] The analysis here is of particular interest in view of the results presented in part (a) above as the Stickler and Meyerhoff value is thought to represent a lower bound for k_{tr}, hence modelled results here should exhibit the strongest possible effects of the chain length dependence of termination.

Once again, the simulated data gave a perfect fit to experiment in the region of 1×10^{-4} M $\leq$ [KPS] $\leq 3 \times 10^{-3}$ M (with ρ as the only adjustable parameter), but failed to satisfactorily fit the data for the highest and lowest initiator concentrations. The results obtained from CLD pseudo-bulk fitting in this case are presented in Table 6.6.

Table 6.6. Results of data fitting for 50°C chemically initiated runs using $k_t^{1,1} = 5.05 \times 10^8$ M^{-1} s^{-1} and $k_{tr} = 1.1 \times 10^{-5}\ k_p$ (Stickler and Meyerhoff) in the pseudo-bulk model with CLD termination (including reaction diffusion).

run	[KPS] / M	ρ / s^{-1} with CLI $\langle k_t \rangle$†	ρ / s^{-1} with CLD $\langle k_t \rangle$	$\langle k_t \rangle$ / M^{-1} s^{-1}
C52	1×10^{-4}	1.29×10^{-3}	1.55×10^{-3}	2.14×10^4
C62	3×10^{-4}	2.98×10^{-3}	3.80×10^{-3}	2.27×10^4
C50	1×10^{-3}	6.09×10^{-3}	7.90×10^{-3}	2.44×10^4
C55	3×10^{-3}	8.95×10^{-3}	1.25×10^{-2}	2.58×10^4

† from Table 4.9 of Chapter 4, obtained using $\langle k_t \rangle = 1.92 \times 10^4$ M^{-1} s^{-1}.

As was the case in part (a), the value of ρ obtained from CLD modelling is seen in all cases to be slightly greater than that from CLI modelling for the same reasons. The more marked discrepancy between the CLI and CLD fitted ρ values observed in this case reflects the greater sensitivity of the chain length dependent $\langle k_t \rangle$ value to the value of ρ under these conditions – further from the limit of transfer control than in part (a). This means that the

same $k_t^{i,j}$ values that reproduced the γ-relaxation now give rise to a higher $\langle k_t \rangle$, because ρ is higher. Because of this higher $\langle k_t \rangle$ (compare Tables 6.5 and 6.6), the value of ρ is forced to be higher. In this case an increase in ρ of almost an order of magnitude is accompanied by a 20% increase in $\langle k_t \rangle$.

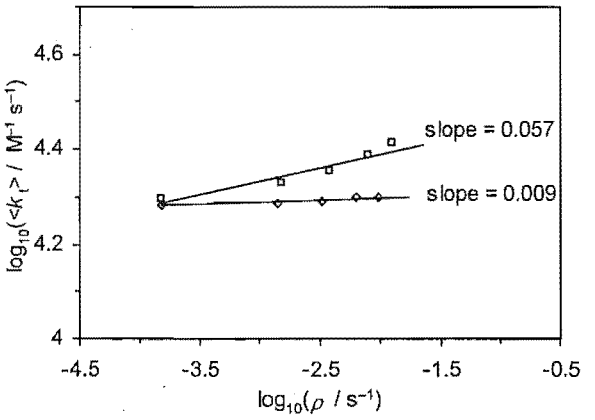

Figure 6.8. Chain length dependent values of $\langle k_t \rangle$ obtained from modelling of 50°C γ-relaxation and chemically initiated experiments at intermediate [KPS]; $\log_{10}(\langle k_t \rangle / M^{-1} s^{-1})$ is presented as a function of $\log_{10}(\rho / s^{-1})$ for both values of k_{tr} used: $k_{tr} = 5.7 \times 10^{-5} k_p$ due to Ballard (diamonds), and $k_{tr} = 1.1 \times 10^{-5} k_p$ due to Stickler and Meyerhoff (squares); slope of best-fit line is as indicated in each case.

The values of $\langle k_t \rangle$ obtained from data fitting for γ-relaxation and chemically initiated experiments using the CLD pseudo-bulk model in parts (a) and (b) above are presented in Figure 6.8. In each case the variation of $\log_{10}(\langle k_t \rangle / M^{-1} s^{-1})$ with $\log_{10}(\rho / s^{-1})$ is approximated by a linear best fit. The slope of each best fit line is seen to be close to zero, with values of 0.057 and 0.09 obtained from the results with $k_{tr} = 5.7 \times 10^{-5} k_p$ (Ballard) and $k_{tr} = 1.1 \times 10^{-5} k_p$ (Stickler and Meyerhoff) respectively. This is consistent with the system being close to the transfer limit for either value of k_{tr} used here. In order to obtain more quantitative verification that this is the case we refer back to equations (6.15) and (6.17) – the analytic solutions for $\langle k_t \rangle$ in the termination and transfer limits (respectively) employed earlier in this chapter. The absence of R_{init} [where $R_{init} = \rho/(N_A V_s)$, for emulsion polymerisations obeying pseudo-bulk kinetics] in equation (6.17) trivially predicts a slope of zero for a plot of

$\log_{10}(\langle k_t \rangle / M^{-1} s^{-1})$ versus $\log_{10}(\rho / s^{-1})$ in the transfer limit. In the case of the termination limit, equation (6.15) predicts $\log_{10}(\langle k_t \rangle / M^{-1} s^{-1}) \propto \log_{10}(\rho / s^{-1}) \times e/(2 - e)$. Thus, using the value of $e = 1.26$ employed here for Interval II polymerisations,[26,27] a plot of $\log_{10}(\langle k_t \rangle / M^{-1} s^{-1})$ versus $\log_{10}(\rho / s^{-1})$ should then have a slope of approximately 1.70 in the termination limit. Of course this estimate is subject to several assumptions invoked in the derivation of equation (6.15), *viz.*, the steady-state and long-chain approximations, as well as the assumptions of a geometric mean model for $k_t^{i,j}$ and that the scaling exponent, e, for diffusion may be applied to the values of $k_t^{i,j}$. However, even given some uncertainty in the slope of a $\log_{10}(\langle k_t \rangle / M^{-1} s^{-1})$ versus $\log_{10}(\rho / s^{-1})$ plot predicted from equation (6.15), it is clear that the low slopes measured from the fitted values of $\langle k_t \rangle$ are indicative of this system being close to the transfer limit under the range of experimental conditions of interest here.

In conclusion, two important points are stressed: (1) CLD termination only introduces an uncertainty into ρ values which is much smaller than other uncertainties (see Chapter 4); in other words, the modelling here endorses the values of ρ in Chapter 4. (2) The one set of $k_t^{i,j}$ values reproduces, without adjustment, both chemically initiated kinetics (including the approach to steady-state) and γ-relaxation kinetics. Further, all values of $k_t^{i,j}$ are consistent with best *a priori* prediction. This is a remarkable result.

6.4.2 Molecular Weight Distributions in the Emulsion Polymerisation of MMA at 50 °C

The results of the previous sections suggest that the MMA system under investigation is well described using the pseudo-bulk model with complete re-entry and chain length dependent termination for conditions of [KPS] ~ 1 mM. Furthermore, fitting of kinetic data strongly suggests that the system should be close to the limit of transfer control, where all chain stopping is the result of transfer to monomer reactions (as opposed to bimolecular termination). We therefore next seek to verify these inferences by a different means: the analysis of polymer molecular weight distributions.

The molecular weight distribution (MWD) constitutes a record of the dead polymer chains formed during a given period of polymerisation, and careful interpretation of the form of the MWD can yield values of kinetic rate parameters for comparison with those obtained earlier from kinetic experiments. The methodology used is that due to Clay *et al.*,[2,38] introduced

briefly in section 6.2. This approach relies on the key assumptions that termination reactions are chain length dependent (an underlying belief throughout this work), and moreover that termination reactions are predominantly between a short radical and a long radical (so-called "short-long" termination, which has been suggested previously[3,13,29,39]). It is further assumed that the polymerising system is in a steady-state and that the "long-chain approximation" holds (and as such the radical chain length distribution can be treated as a continuous distribution). Under these circumstances the following analytic solution is found to be applicable for describing the form of the molecular weight distribution of dead polymer at high molecular weight:

$$\lim_{M\to\infty} P(M) = \exp\left(-\frac{k_{tr}[\mathrm{M}]_p + \langle k_t\rangle[\mathrm{R}^\bullet]}{k_p[\mathrm{M}]_p}\frac{M}{M_0}\right) \tag{6.24}$$

Here $P(M)$ denotes the *instantaneous* number molecular weight distribution – the rate of formation of dead chains at a given time – such that

$$P(M) = \frac{\mathrm{d}\bar{P}(M)}{\mathrm{d}t} \tag{6.25}$$

where $\bar{P}(M)$ is the cumulative molecular weight distribution of dead chains over time (affected by time-variations in the polymerising system, *e.g.* changes in $\bar{n}$ and w_p). Notably, equation (6.24) holds for the long chain region of the MWD regardless of which modes of chain stopping are operative: chain transfer by a long radical produces a dead chain of the corresponding length, and termination of a long radical by either disproportionation or combination also yields a dead chain of approximately the same length due to the assumption of short-long termination. This analytic form applies equally to bulk and solution systems, as well as to the present case of a pseudo-bulk emulsion system, where the total radical concentration, $[\mathrm{R}^\bullet]$, is given by $[\mathrm{R}^\bullet] = \bar{n}/(N_A V_s)$.

Equation (6.24) suggests plotting $\ln P(M)$ versus M at high molecular weight. We will use a dimensionless parameter, Λ, defined as follows:

$$\Lambda = \lim_{M\to\infty}\left[-M_0\frac{\mathrm{d}\ln P(M)}{\mathrm{d}M}\right]$$
$$= \frac{k_{tr}}{k_p} + \frac{\langle k_t\rangle\,\bar{n}}{k_p[\mathrm{M}]_p N_A V_s}$$
$$= \frac{k_{tr}}{k_p} + \frac{\rho}{2R_{pol}} \qquad (6.26)$$

where $R_{pol} = k_p[\mathrm{M}]_p\bar{n}$ is the rate of polymerisation per particle (note the unusual definition) and $\rho = 2\langle k_t\rangle\bar{n}^2/(N_A V_s)$ according to the steady-state solution of equation (6.10). Equation (6.26) therefore provides a useful means for directly relating the slope of a $\ln P(M)$ plot at high molecular weight to the values of various kinetic parameters for the polymerisation. Most notably in the present context, it is seen [from the first form of equation (6.26)] that under conditions of transfer control, where $k_{tr}[\mathrm{M}]_p \gg \langle k_t\rangle\,\bar{n}/(N_A V_s)$, the value of Λ becomes constant and equal to k_{tr}/k_p. Hence one application of this method has been to conduct a series of experiments in which the initiator concentration was decreased until a constant value of $\Lambda = k_{tr}/k_p$ was found.[6] The expectation that the present system is close to the transfer control limit (and hence $\Lambda \approx k_{tr}/k_p$) may therefore be tested in a similar way.

The second form of equation (6.26) has additionally been used to isolate values for both k_{tr} and $\langle k_t\rangle$.[2] In this case instantaneous MWDs were obtained for a given experiment over changing w_p and R_{pol}. The resulting values of Λ were plotted against $1/(2R_{pol})$ to give a line with slope ρ and intercept k_{tr}/k_p, and the value of ρ then used to calculate $\langle k_t\rangle = \rho N_A V_s/(2\bar{n}^2)$ [again from equation (6.10)] at each w_p. Of course this procedure assumes that ρ is constant with w_p, which is actually contrary to Maxwell-Morrison entry theory. Nevertheless the values of $\langle k_t\rangle$ so obtained were found to agree reasonably well with data for the same system obtained from γ-relaxation experiments. Considering the first form of equation (6.26), an initial impression may be that a similar procedure could be used to yield values of $\langle k_t\rangle$ in the present system: values of Λ obtained from experiments with different initiator concentrations being plotted as a linear function of $\bar{n}$, yielding $\langle k_t\rangle$ from the slope and k_{tr} by extrapolation to $\bar{n} = 0$. However, this approach is flawed in that it assumes a constant value for $\langle k_t\rangle$ with changing initiator concentration, which is certainly not assured while termination is chain length dependent. In practice, however, the extent of the change in $\langle k_t\rangle$ with initiator

concentration may or may not be sufficient to preclude the use of this approach (depending on the nature of the chain length dependence) – this will be an interesting area for investigation.

Obtaining $P(M)$ and Λ from experiment

It is important to understand that equations (6.24) and (6.26) apply only to the *instantaneous* number MWD for the system. However, in practice, experimental techniques such as GPC determine the *cumulative* MWD, $\overline{P}(M)$, for all polymer produced during a finite period of polymerisation and direct application of these equations therefore entails some uncertainty. One way of circumventing this problem is to analyse the cumulative MWD obtained from polymerisation over a narrow range of conversion.[6,8-10] But in the present case of seeded emulsion polymerisations this simple approach is complicated by the fact that the MWD obtained includes polymer from seed particles as well as the new polymer obtained during the seeded run. The method used here is to separately determine the MWD of the seed polymer and subtract this contribution from the MWD for the total polymer obtained from a seeded run based on the relative amounts of seed and new polymer (known from dilatometry/gravimetry measurements). The resulting "pseudo-instantaneous" MWD is that due only to new polymer formed at 50°C during Interval II.

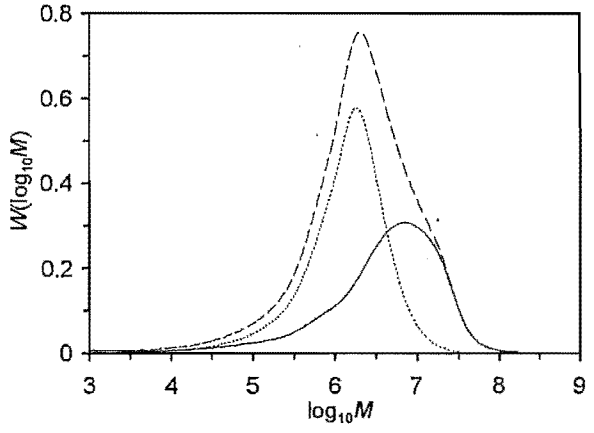

Figure 6.9. MWDs determined for a seeded emulsion polymerisation of MMA at 50°C with [KPS] = 3×10^{-4} M (run C69); cumulative MWD for total polymer from seeded run (— — —), cumulative MWD of seed (latex MMA06) polymer (– – – – –) and pseudo-instantaneous MWD of new Interval II polymer (————), all presented in the form of $W(\log_{10}M)$.

MWDs were obtained in this way for each of the four chemically initiated Interval II kinetic runs C68, C69, C72 and C73 from Chapter 4 carried out with [KPS] between 1×10^{-4} and $3 \times$

10^{-3} M. Typical results are shown in Figure 6.9 in the form of the weight distribution $W(\log_{10}M)$ versus $\log_{10}M$. A brief description of how this distribution is obtained from raw GPC data is now given.

GPC yields as its output the weight of polymer, W, eluting for a given increment of elution volume, V, normalised such that,

$$\int_0^\infty W(V)\mathrm{d}V = 1 \tag{6.27}$$

A calibration curve (constructed using molecular weight standards) defines the relationship between elution volume and molecular weight: $\log_{10}M = g(V)$. Hence, $g'(V) = \mathrm{d}\log_{10}M/\mathrm{d}V$ and equation (6.27) becomes:

$$\int_\infty^{-\infty} \frac{W(V)}{g'(V)}\,\mathrm{d}\log_{10}M = 1 \tag{6.28}$$

where the new limits of integration reflect the fact that as $V \rightarrow 0$, $\log_{10}M \rightarrow \infty$, and as $V \rightarrow \infty$, $\log_{10}M \rightarrow -\infty$. Therefore the normalised weight distribution may finally be expressed as a function of molecular weight (as $\log_{10}M$) instead of elution volume:

$$\int_{-\infty}^{\infty} W(\log_{10}M)\,\mathrm{d}\log_{10}M = 1 \tag{6.29}$$

where $W(\log_{10}M) = -W(V)/g'(V)$. It is seen that in the case of a linear calibration curve [*i.e.*, a constant value for $g'(V)$], $W(\log_{10}M) \sim W(V)$, and hence $W(\log_{10}M)$ is sometimes referred to as the "GPC distribution".

It remains to convert the $W(\log_{10}M)$ weight MWD to the number MWD form of $P(M)$ in equation (6.26). We first change the domain of the distribution from $\log_{10}M$ to M, using the relation: $\mathrm{d}\log_{10}M = \mathrm{d}\ln M/\mathrm{d}\ln 10 = \mathrm{d}M/(M\ln 10)$. Substituting into equation (6.29) and adjusting the limits of integration accordingly gives:

$$\int_0^\infty \frac{W(\log_{10}M)}{M\ln 10}\,\mathrm{d}M = \int_0^\infty W(M)\,\mathrm{d}M = 1 \tag{6.30}$$

where $W(M) = W(\log_{10}M)/(M\ln 10)$ denotes the familiar form of the normalised weight MWD. Finally, the number MWD is given from the relationship between the total *weight* of chains of molecular weight M and the total *number* of chains of molecular weight M, as shown in equation (6.31) and noting that the $P(M)$ distribution so obtained must be normalised independently.

$$P(M) = \frac{W(M)}{M} \tag{6.31}$$

The normalised $P(M)$ distribution for new polymer, obtained as above from the $W(\log_{10}M)$ distribution in Figure 6.9, is presented as a plot of $\ln P(M)$ versus M in Figure 6.10. An interesting feature of the distributions in both these Figures is the relatively high molecular weight of polymer formed in this system. While it is generally the case that an emulsion system yields polymer of higher molecular weight than the equivalent bulk system, due to the suppression of termination that accompanies radical compartmentalisation (*e.g.*, in a zero-one emulsion system),[14] the lack of compartmentalisation in the pseudo-bulk system used here should lead to a frequency of termination and thus polymer molecular weights similar to those in a bulk system. The explanation for the high molecular weights measured here is therefore transfer control, as will be seen. It is also interesting that the seed polymer is of considerably lower molecular weight (see Figure 6.9). This must reflect the higher reaction temperature (60°C then 80°C, see Chapter 4), giving a higher k_{tr}/k_p (remember that only a small fraction of the seed will stem from Interval II conditions, otherwise transfer should prevail as the chain stopping mechanism).

We next seek to fit the $\ln P(M)$ data obtained from experiment to obtain values of Λ for each experiment. As is evident from Figure 6.10 the plot of $\ln P(M)$ is seen to be not strictly linear, even at relatively high molecular weights. This is not too alarming given that previous studies have revealed significant non-linearity in some cases,[2,6] although it is noted that highly linear distributions have been obtained from experiments with added chain transfer agent.[10] This observed non-linearity may be the result of errors introduced by the GPC baseline subtraction,[40] in the isolation of the new polymer MWD from the seed MWD, or the effects of GPC column broadening of the distribution (investigated below). Consideration of such issues has led to the recommendation that the most accurate value for Λ may be obtained by fitting of the region of the $\ln P(M)$ distribution corresponding to the peak region of the associated $W(\log_{10}M)$ distribution,[2,10,40] and that fitting of the highest molecular weight region

may in fact be more prone to error. In view of this recommendation it was decided to obtain two values of Λ for each experiment, denoted Λ_{peak} and Λ_{high}, by fitting both the peak and high molecular weight regions respectively. Here it should be clarified that the "high molecular weight region" corresponds to the highest molecular weight region in which there is still an *appreciable* amount of polymer measured (beyond which point error from baseline subtraction becomes increasingly unavoidable), and is determined for each MWD from the form of the $W(\log_{10}M)$ plot. For example, in the case of the pseudo-instantaneous $W(\log_{10}M)$ distribution for new polymer in Figure 6.9, the high molecular weight region is taken as $\log_{10}M = 7.5 - 7.8$.

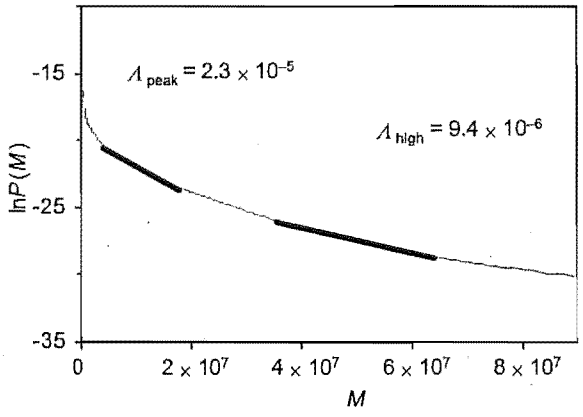

Figure 6.10. Plot of $\ln P(M)$ for pseudo-instantaneous number MWD obtained for a seeded emulsion polymerisation of MMA at 50°C with [KPS] = 3×10^{-4} M (run C69); slope of plot, Λ, measured from peak (Λ_{peak}) and high molecular weight (Λ_{high}) regions as indicated.

The fitting of Λ_{peak} and Λ_{high} is illustrated in Figure 6.10 and the values obtained for each experiment are presented in Figure 6.11. Also presented for comparison are the values of $\Lambda = k_{tr}/k_p$ predicted by equation (6.26) in the transfer limit using the values reported for MMA at 50°C by Ballard and by Stickler and Meyerhoff.

As expected from the observed non-linearity in the $\ln P(M)$ plots there is a significant difference between the values of Λ obtained from the two different regions of the distributions. It is also seen that while all Λ_{peak} results lie above the value for Λ calculated for the transfer limit using the Stickler and Meyerhoff literature value for k_{tr}/k_p, two of the Λ_{high} results lie below this value. Given that the literature figure for Λ represents a lower bound (due to the highly purified conditions used) it seems implausible that any experimental result

for Λ from the present system could fall below this value, even in the transfer limit. Although this discrepancy is possibly due simply to experimental scatter, the results appear to be consistent with the suggestion that Λ_{high} is more prone to error than Λ_{peak}. Moreover, it is noted that the value of Λ_{high} is in all cases taken from a region of the ln$P(M)$ distribution slightly above the molecular weight of the highest molecular weight standard (~ 10^7) used to construct the GPC calibration curve, which is likely to also be a significant source of error. Hence (in line with others[2,10,40]) we adopt the values of Λ_{peak} as best estimates.

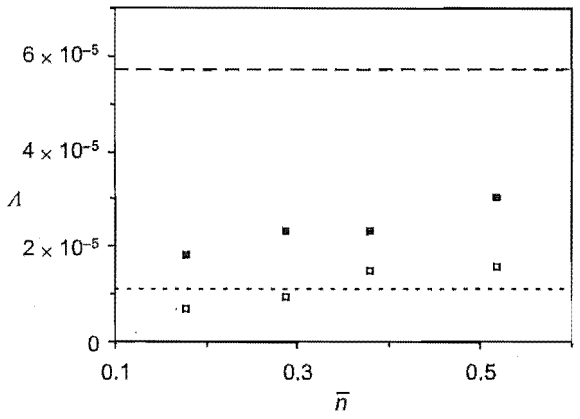

Figure 6.11. Values of Λ for chemically initiated seeded emulsion polymerisations of MMA at 50°C over a range of initiator concentrations, presented as a function of $\overline{n}$: Λ_{peak} (filled squares), Λ_{high} (empty squares), and predicted values assuming transfer control ($\Lambda = k_{tr}/k_p$) with $k_{tr} = 5.7 \times 10^{-5}\ k_p$ due to Ballard (— — —) and $k_{tr} = 1.1 \times 10^{-5}\ k_p$ due to Stickler and Meyerhoff (– – – – –).

Clearly there is seen to be only a slight variation in Λ_{peak} (and in Λ_{high} for that matter) with changing initiator concentration over the range [KPS] = $1 \times 10^{-4} - 3 \times 10^{-3}$ M, indicating qualitatively that chain transfer to monomer is indeed the predominant chain stopping reaction in this system. At this point it is of interest to test the allegedly flawed procedure described earlier for obtaining values of both k_{tr} and $\langle k_t \rangle$. A linear fit to the values of Λ_{peak} plotted as a function of $\overline{n}$ in Figure 6.11 reveals a slope of 3.4×10^{-5} and intercept of 1.2×10^{-5}, and hence the values $\langle k_t \rangle = 1.7 \times 10^5$ M^{-1} s^{-1} and $k_{tr} = 8.0 \times 10^{-3}$ M^{-1} s^{-1} from equation (6.26). Although this value of k_{tr}/k_p is remarkably close to the Stickler-Meyerhoff value, the value for $\langle k_t \rangle$ is seen to be approximately an order of magnitude greater than that obtained independently from relaxation experiments at 50°C ($\langle k_t \rangle = 1.9 \times 10^4$ M^{-1} s^{-1}). While it is difficult to judge whether this large discrepancy is the result of the chain length dependence of termination or simply

due to scatter in the experimental values of Λ_{peak}, it seems clear that this approach is of limited merit in the present case.

In view of the above results, the most sensible approach would appear to be to assume transfer controlled conditions and thus obtain an estimate for k_{tr} from each experiment using the corresponding limit of equation (6.26): $\Lambda_{peak} = k_{tr}/k_p$. Combining these estimates gives a final mean value for the rate coefficient for transfer to monomer at 50°C of $k_{tr}/k_p = (2.4 \pm 0.7) \times 10^{-5}$ – approximately twice that reported by Stickler and Meyerhoff[12] for the equivalent bulk system, and approximately half that reported by Ballard[4] for emulsion. This should be taken as the best value of k_{tr}/k_p from this work. It is not known whether its closer agreement with the Stickler-Meyerhoff value is due to elimination of "adventitious impurities" compared with Ballard's system, or to improvements in GPC over the 20 years since Ballard conducted his investigation.

At this juncture it is acknowledged that there has been considerable discussion in the literature[2,6-10,40] of the similarities and differences (not to mention the relative advantages and disadvantages) between the $\ln P(M)$ slope methodology used above and the more traditional Mayo method for determining k_{tr} and $\langle k_t \rangle$.[11] It is therefore of interest to complement the above analysis with the approach of Mayo, which centres on the following well-known equation:

$$\frac{1}{DP_n} = \frac{k_{tr}}{k_p} + \frac{(1+\lambda)\langle k_t \rangle R_{pol}}{k_p^2 [M]_p^2 N_A V_s} \qquad (6.32)$$

where DP_n = number average degree of polymerisation, λ = fraction of termination occurring by disproportionation (with $\lambda \approx 1$ assumed here for MMA, based on experimental findings[41,42]), and once again $R_{pol} = k_p[M]_p\bar{n}$. The similarity between these two methods is immediately evident upon comparison of equations (6.26) and (6.32), and in practical terms the Mayo approach is identical to that used above. Once again, in principle a plot of $1/DP_n$ versus $R_{pol}/(N_A V_s)$ may be used to infer a value of $\langle k_t \rangle$. However, this value is only accurate in the event that $\langle k_t \rangle$ does not change, a fact which may limit the accuracy of this approach given that a change in DP_n reflects a change in the overall radical distribution and hence $\langle k_t \rangle$ *cannot* remain constant under the provisos of chain length dependent termination. However, similar to the earlier approach, the value of $1/DP_n$ is seen to converge to k_{tr}/k_p in the transfer limit.

Thus it may still be possible to obtain accurate values for k_{tr}/k_p under transfer controlled conditions.

Values of $1/DP_n$ may be most simply obtained for experimental $P(M)$ distributions from the number average molecular weight, M_n, as $DP_n = M_n/M_0$. However, recognising that the value of M_n is considerably more sensitive to GPC uncertainties than the weight average molecular weight, M_w,[40] we here assume (as have others[10,43]) a value for the polymer polydispersity index of $M_w/M_n = 2$, from which is derived the preferred relation of $DP_n = M_w/(2M_0)$. It is pointed out that since a polymer polydispersity index of 2 is characteristic of MWDs for dead chains formed by transfer or termination by disproportionation, the above assumption is likely to be a good one for MMA systems irrespective of whether transfer controlled conditions hold.

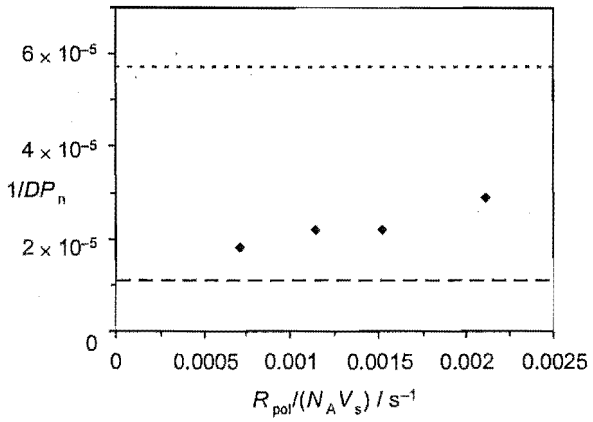

Figure 6.12. Values of $1/DP_n$ for chemically initiated seeded emulsion polymerisations of MMA at 50°C over a range of initiator concentrations, presented as a function of $R_{pol}/(N_A V_s)$: experimental data (filled diamonds), and predicted values assuming transfer control ($1/DP_n = k_{tr}/k_p$) with $k_{tr} = 5.7 \times 10^{-5}\ k_p$ due to Ballard (— — —) and $k_{tr} = 1.1 \times 10^{-5}\ k_p$ due to Stickler and Meyerhoff (– – – – –).

The values obtained for $1/DP_n$ are plotted against $R_{pol}/(N_A V_s)$ in Figure 6.12 and comparison with Figure 6.11 reveals a similar trend to the values of Λ_{peak} from the previous method, but not the values of Λ_{high} – providing further support for the recommended approach in the $\ln P(M)$ slope method discussed earlier. The values obtained from the slope (7.5×10^{-3} s) and intercept (1.3×10^{-5}) of a linear fit to these data were then $\langle k_t \rangle = 7.5 \times 10^4$ M^{-1} s^{-1} and $k_{tr} = 8.2 \times 10^{-3}$ M^{-1} s^{-1}. While the value of $\langle k_t \rangle$ is still considerably larger than that obtained from γ-

relaxation experiments, it is nevertheless closer than that obtained using Λ_{peak} values. Both approaches give the same estimate of k_{tr}.

Once again a better approach may be to assume that the system is in the transfer limit and hence that $1/DP_n = k_{tr}/k_p$. In this case the combined results from all four experiments give rise to a mean value for the transfer to monomer rate coefficient at 50°C of $k_{tr}/k_p = (2.3 \pm 0.6) \times 10^{-5}$, in good agreement with the value obtained using the $\ln P(M)$ slope methodology.

One may debate which method – Mayo or Λ – is easier to use, but here it has once again[10] been shown that conceptually they are the same and that they give essentially identical results.

Based on the results obtained using both methods above it is apparent that analysis of MWDs is in agreement with the predictions made based on fitting of kinetic data using the pseudo-bulk model with CLD termination that the present system, MMA at 50°C, is close to the transfer limit and that the rate coefficient for transfer to monomer in this system is $k_{tr} = (2.4 \pm 0.7) \times 10^{-5}$ $k_p = (1.5 \pm 0.4) \times 10^{-2}$ M^{-1} s^{-1}. It must be stressed that this conclusion is not from the variation of MWD parameters, which is actually greater than expected, but from the fact that these parameters are so low in value that they must be transfer determined.

Modelling of MWDs and Λ

Up until this point, modelling efforts have focussed only on predicting or fitting the intra-particle radical populations (*i.e.*, $\bar{n}$, n_1, n_2,...). Of course, the models used may be extended relatively easily to predict values for the molecular weight distribution of dead chains in the system and, indeed, this was the approach used by Clay *et al.*[38] in their original derivation of the model used for fitting experimental MWDs in the previous section. We therefore next attempt to account for the experimentally determined dead chain MWDs in terms of simulated MWDs, using the pseudo-bulk model with chain length dependent termination.

The approach here begins with the radical balance equations (6.19) – (6.21) presented earlier in section 6.4.1. The steady-state approximation is applied and these equations solved numerically using the "truncated coarse-graining method"[13,29] to give a complete set of intra-particle radical populations, n_i, over all chain lengths i. From these radical populations it is possible to directly (non-iteratively) calculate the steady-state rate of formation, *i.e.*, the instantaneous distribution, of dead chains using the following equation:

$$P_i = \frac{d\bar{P}_i}{dt} = k_{tr}[M]_p n_i + 2\, n_i \sum_{j=1}^{\infty} \lambda\, c^{i,j} n_j + \sum_{j=1}^{i-1} (1-\lambda) c^{i,j} n_j\, n_{i-j} \qquad (6.33)$$

where the first, second and third terms represent the contributions from transfer, disproportionation and combination respectively. Note that in equation (6.33) P_i represents a slightly different form of the dead chain number distribution than has been used above. Here P_i denotes the instantaneous number *chain length distribution* (and $\bar{P}_i$ the associated cumulative distribution) of dead chains of degree of polymerisation i produced per particle, and is used instead of the number *molecular weight distribution* $P(M)$ for notational consistency with the earlier radical balance equations. However $P_i \sim P(M)$, so the two are the same distribution (if P_i is normalised, then $P(M) = P_i/M_0$ is also normalised, where M_0 is the molar mass of monomer).

Simulated MWDs were therefore calculated under conditions corresponding to each of the four chemically initiated Interval II kinetic runs (C68, C69, C72 and C73) for which experimental MWDs were obtained in the previous section. These conditions (MMA at 50°C) are summarised in Table 6.7.

Here we adopt the value of $k_{tr} = 1.5 \times 10^{-2}$ M^{-1} s^{-1} determined for the present system from analysis of experimental MWDs above (using both the $\ln P(M)$ slope and Mayo methods).

The values of ρ used were those obtained from experiment in Chapter 4. It was also assumed that entry is by monomeric radicals, although it is noted that calculations carried out with entry by radicals of length 20 monomer units (the value inferred for this system in Chapter 4) revealed negligible change in the MWD due to the predominance of transfer. As previously in the current chapter, we also assume that entry-derived monomeric radicals behave identically to monomeric radicals produced by transfer to monomer, and that all exited monomeric radicals will re-enter a latex particle.

Table 6.7. Details of MWD simulations using the pseudo-bulk model with chain length dependent termination and complete re-entry of exited radicals.

Simulation parameter	Value
r_u / nm	42
N_c / dm^{-3}	4.3×10^{16}
$[M]_p$ / M	6.9
V_s / dm^{-3}	1.3×10^{-18}
w_p	0.30
k_p / M^{-1} s^{-1}	649
k_p^1 / k_p	15
k_{tr} / M^{-1} s^{-1}	1.5×10^{-2}
σ / Å	1.2
p_{spin}	0.25
D_M / m^2 s^{-1}	1.12×10^{-9}
e	1.26
ρ / s^{-1}	$1.1 \times 10^{-3} - 9.4 \times 10^{-3}$

In these simulations the physically reasonable diffusion-mean model was used to calculate $k_t^{i,j}$ values, with a single scaling exponent e covering all chain lengths [see equation (6.3)]. $k_t^{1,1}$ was calculated according to equation (6.23) with σ, p_{spin} and D_M as given in Table 6.7. It is noted that the value of σ used here was significantly smaller than the literature value of $\sigma =$ 3.0 Å used in section 6.4.1. It was found that using literature values[23,26] for σ, p_{spin} and D_M resulted in a $k_t^{1,1}$ that gave a value of $\langle k_t \rangle$ a factor of 2 – 3 times greater than that measured from γ-relaxation experiments, which is consistent with the $X_c = 10$ values of Table 6.4, for which a relatively low $k_t^{1,1}$ was found to reproduce the γ-relaxation data. To obtain such a low value of $k_t^{1,1}$ in simulations, σ was decreased, giving consistency with experimental results.

However this is not meant to imply that the lowered value of σ rigorously accounts for this discrepancy in $\langle k_t \rangle$; the difference may well be due to uncertainties in any of the parameters used to calculate $k_t^{1,1}$, or (more likely) related to the particular chain length dependence chosen for the termination model here. An illustration of the latter effect is provided by the earlier results in Tables (6.3) and (6.4). Whatever the explanation, it is important to note that while the values of $\langle k_t \rangle$ and $\overline{n}$ were affected by changing σ from 1.2 to 3.0 Å, this caused no significant change in the simulated MWDs – a consequence of the system being close to the transfer limit. Thus in the present context, where our chief interest is in comparing the form of MWDs, this difference is of relatively minor import. In fact it was found (work not presented) that the classical Schulz-Flory model for MWDs, which of course assumes chain length independent termination, generated MWDs essentially indistinguishable from those of the sophisticated calculations presented here. So all the results which follow should not be thought of as having anything to do with CLD termination.

Presented in Figures 6.13 (a) – (d) are the $W(\log_{10}M)$ weight distributions obtained from each simulation together with that from experiment under the same conditions. It is apparent that the present simulation methodology of using experimentally determined values for ρ and k_{tr}, in conjunction with chain length dependent termination rate coefficients calculated *a priori*, generates $W(\log_{10}M)$ distributions that reproduce experimentally measured distributions with some success (and it is stressed that the identical parameter values simultaneously reproduce the kinetics). However, while there is reasonable accord between the peak of the experimental and simulated MWD in most cases, it is clear that the overall shape of the experimental distribution is always significantly different to that from simulation. Of course, there is likely to be some effect on the shape of the distribution from GPC baseline subtraction and/or the subtraction of seed polymer in each case. Most clearly evident, though, is fact that the experimental $W(\log_{10}M)$ distributions are broadened significantly from their simulated counterparts.

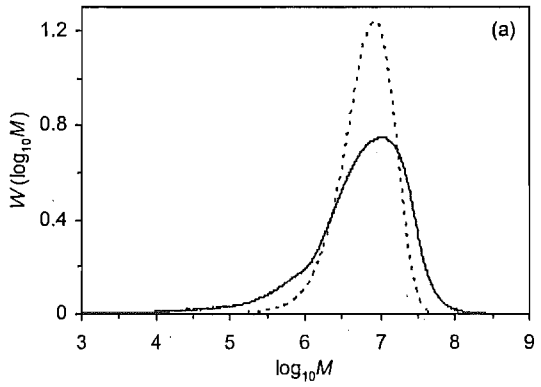
(a)
$W(\log_{10}M)$
$\log_{10}M$

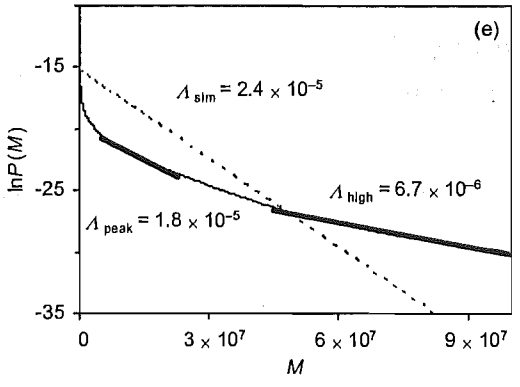
(e)
$\Lambda_{slm} = 2.4 \times 10^{-5}$
$\Lambda_{high} = 6.7 \times 10^{-6}$
$\Lambda_{peak} = 1.8 \times 10^{-5}$
$\ln P(M)$
M

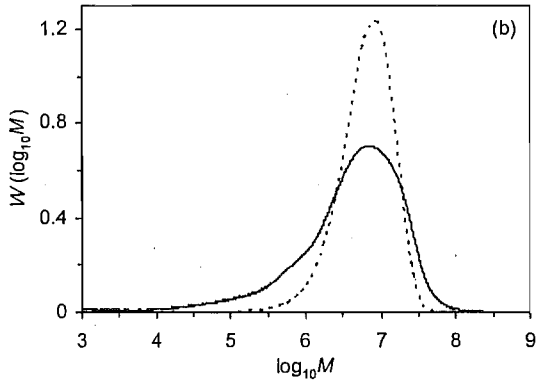
(b)
$W(\log_{10}M)$
$\log_{10}M$

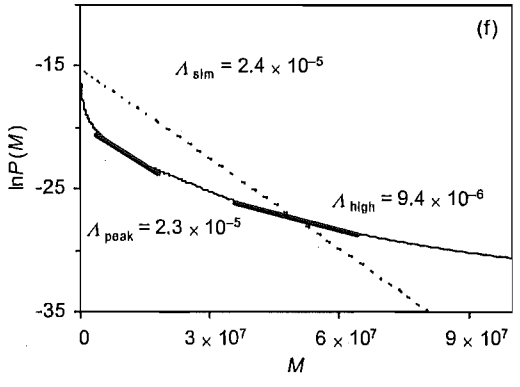
(f)
$\Lambda_{slm} = 2.4 \times 10^{-5}$
$\Lambda_{high} = 9.4 \times 10^{-6}$
$\Lambda_{peak} = 2.3 \times 10^{-5}$
$\ln P(M)$
M

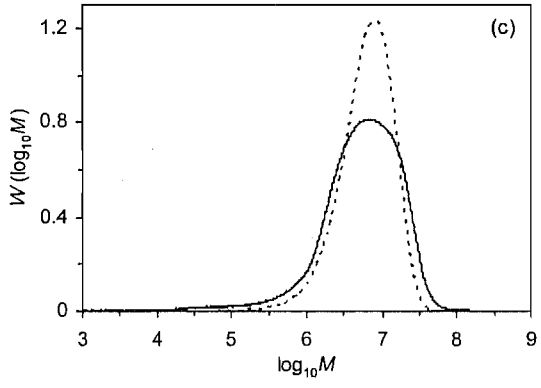
(c)
$W(\log_{10}M)$
$\log_{10}M$

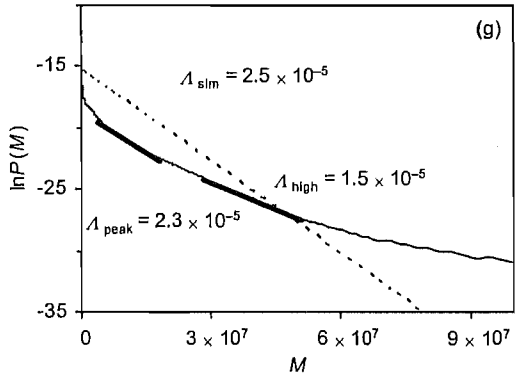
(g)
$\Lambda_{slm} = 2.5 \times 10^{-5}$
$\Lambda_{high} = 1.5 \times 10^{-5}$
$\Lambda_{peak} = 2.3 \times 10^{-5}$
$\ln P(M)$
M

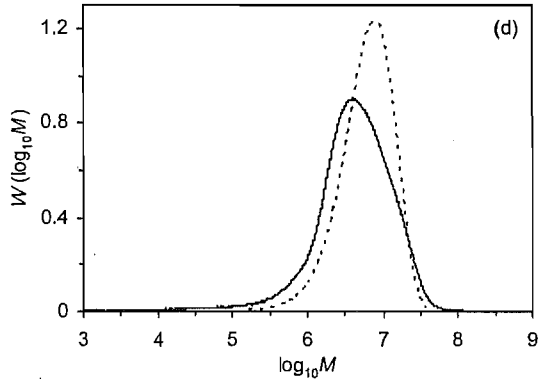
(d)
$W(\log_{10}M)$
$\log_{10}M$

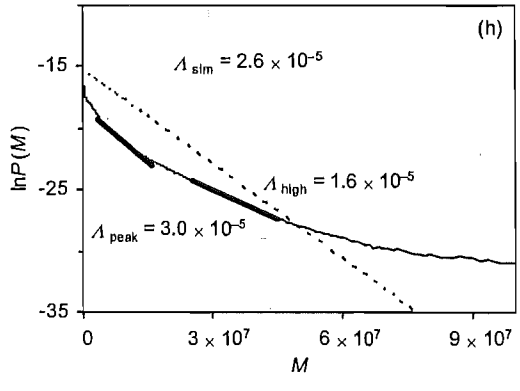
(h)
$\Lambda_{slm} = 2.6 \times 10^{-5}$
$\Lambda_{high} = 1.6 \times 10^{-5}$
$\Lambda_{peak} = 3.0 \times 10^{-5}$
$\ln P(M)$
M

Figure 6.13. Normalised experimental (solid lines) and simulated (dashed lines) MWDs for chemically initiated seeded emulsion polymerisations of MMA at 50°C over a range of initiator concentrations: [KPS] = 1×10^{-4} M **(a,e)** (run C68), 3×10^{-4} M **(b,f)** (run C69), 1×10^{-3} M **(c,g)** (run C73), 3×10^{-3} M **(d,h)** (run C72); regions of experimental $\ln P(M)$ plots where Λ_{peak} and Λ_{high} fitted indicated by bold lines.

The corresponding number distribution plots of $\ln P(M)$ are presented in Figures 6.13 (e) – (h). Here the value of Λ calculated for simulated data is given in each case as Λ_{sim}, and in the case of experimental plots the linear regions over which values for Λ_{peak} and Λ_{high} are fitted are indicated by bold lines. Notably, despite the significant differences evident between experimental and simulated $W(\log_{10}M)$ distributions, in each case the value of Λ_{peak} remains in remarkable agreement with the value of Λ_{sim}. However, the slope of the fit at high molecular weight is considerably flatter and in all cases Λ_{high} is significantly less than Λ_{sim}. The results obtained here are supportive of the findings and recommendations of other workers,[2,10,40] advocating that Λ_{peak} gives the most accurate estimate of the "true" Λ value for an experimentally measured MWD.

These simulations – in that they properly include both transfer and CLD termination – indicate that the difference between the experimental and simulated $W(\log_{10}M)$ distributions must be due to GPC column broadening. It is of interest to find some means of incorporating such effects into the results from MWD simulations and, indeed, to determine whether GPC broadening alone may account for the variation in the value of Λ observed in different molecular weight regions.

Modelling the effects of GPC column broadening on MWDs and the value of Λ

As a polymer sample is passed through a GPC instrument its concentration profile is bound to undergo some band broadening. This is often referred to as "GPC column broadening" (although the broadening effect is not restricted to the columns and may also occur elsewhere in the instrument) and the effect on the GPC chromatogram is generally approximated mathematically by a Gaussian functional form. Thus, for a monodisperse polymer sample the broadened GPC trace may be represented as:

$$G(V) = \frac{1}{\sigma_V\sqrt{2\pi}} \exp\left[\frac{-(V-V_0)^2}{2\sigma_V^2}\right] \qquad (6.34)$$

where V is elution volume, V_0 is the elution volume for the monodisperse sample if there were no broadening, and σ_V is the standard deviation of the Gaussian function.

In the more usual case of a GPC trace obtained from a polydisperse polymer sample covering a range of elution volumes, the Gaussian function above must be modified to include a second elution volume variable, y, as follows:

$$G(V-y) = \frac{1}{\sigma_V\sqrt{2\pi}}\exp\left[\frac{-(V-y)^2}{2\sigma_V^2}\right] \tag{6.35}$$

so that $G(V-y)$ describes the Gaussian function associated with the polymer eluting at any given elution volume, y. Thus we may treat the trace from a polydisperse polymer sample as an accumulation of monodisperse GPC traces, each broadened by the same Gaussian function, with the sum of these individual elements giving the broadened GPC trace for the entire sample. The effect of this Gaussian broadening on the GPC trace is expressed mathematically using Tung's equation:

$$f(V) = \int_{V=-\infty}^{\infty} G(V-y)\, W(y)\, \mathrm{d}y \tag{6.36}$$

where $W(V)$ is the "true" unbroadened polymer GPC trace [using the notation of equation (6.27)] and $f(V)$ is the actual (broadened) chromatogram measured by GPC.

Several mathematical procedures have been reported for isolating the true polymer GPC trace, $W(y)$, in equation (6.36) by deconvolution of the measured chromatogram.[44] However, here we adopt the alternative, simpler approach of Buback *et al.*[45] whereby a modelled (*i.e.*, unbroadened) MWD may be convoluted according to the Gaussian functional form of column broadening above in order to simulate a broadened MWD obtained from GPC.

Since the simulations of the previous section generated only MWDs, equations (6.35) and (6.36) must first be transformed from functions of volume elution to functions of molecular weight. Combining equations (6.27) and (6.28) and assuming that the GPC calibration curve, $g(V)$, is linear (which is often true to good approximation) gives for the true (unbroadened) MWD:

$$\log_{10}M = g(y) = a - by \tag{6.37}$$

$$y = \frac{a - \log_{10}M}{b} \tag{6.38}$$

$$\mathrm{d}\log_{10}M = -b\,\mathrm{d}y \tag{6.39}$$

$$W(y) = -g'(y)\,W(\log_{10}M) = b\,W(\log_{10}M) \tag{6.40}$$

And, similarly, for the broadened MWD:

$$\log_{10}M' = g(V) = a - bV \tag{6.41}$$

$$V = \frac{a - \log_{10}M'}{b} \tag{6.42}$$

$$\mathrm{d}\log_{10}M' = -b\,\mathrm{d}V \tag{6.43}$$

$$f(V) = -g'(V)\,W(\log_{10}M') = b\,W(\log_{10}M') \tag{6.44}$$

Here the elution volume variables V and y have been transformed to molecular weight variables $\log_{10}M'$ and $\log_{10}M$. The broadened and unbroadened molecular weight distributions are denoted $W(\log_{10}M')$ and $W(\log_{10}M)$ respectively, and are the transformations of the corresponding GPC traces $f(V)$ and $W(y)$.

Substituting for V and y in the Gaussian form of equation (6.35) and combining this with equations (6.39), (6.40) and (6.44) gives the following transformation of Tung's equation:

$$b\,W(\log_{10}M') = \int_{\log_{10}M=\infty}^{-\infty} \frac{1}{\sigma_V\sqrt{2\pi}} \exp\left[\frac{-(\log_{10}M' - \log_{10}M)^2}{2b^2\sigma_V^2}\right] b\,W(\log_{10}M)\left[-\frac{\mathrm{d}\log_{10}M}{b}\right]$$

$$W(\log_{10}M') = \int_{\log_{10}M=0}^{\infty} \frac{1}{b\sigma_V\sqrt{2\pi}} \exp\left[\frac{-(\log_{10}M' - \log_{10}M)^2}{2b^2\sigma_V^2}\right] W(\log_{10}M)\,\mathrm{d}\log_{10}M \tag{6.45}$$

Here the new integration limits result from the fact that $\log_{10}M \to \infty$ as $V \to -\infty$ (and *vice versa*) and that $\int_{\log_{10}M=0}^{\infty} \approx \int_{\log_{10}M=-\infty}^{\infty} = -\int_{\log_{10}M=\infty}^{-\infty}$, since there is a negligible contribution from chains with $\log_{10}M < 0$ (*i.e.*, $M < 1$).

Equation (6.45) therefore represents a simple means for applying broadening to simulated MWDs, with the degree of broadening dictated by the two parameter values b and σ_V. We therefore next seek estimates for these parameters that are appropriate for the GPC work carried out in the present study. As defined in equation (6.37), b is obtained from the slope of the GPC calibration curve. In the present case a non-linear calibration curve was used and the slope was found to vary over $b = 0.3 - 0.65$ mL^{-1} for the range of elution volumes spanned by polymer. An estimate for the standard deviation of the Gaussian function may be obtained from the GPC traces of the low polydispersity molecular weight standards used in the GPC calibration. In this case the five highest molecular weight standards (which span the relevant range of elution volumes) were fitted using the Gaussian function of equation (6.34) and a mean value of $\sigma_V = (0.4 \pm 0.1)$ mL was obtained. It is noted that this procedure assumes the molecular weight standards to be perfectly monodisperse with Gaussian GPC traces arising solely from column broadening. In reality such standards will have some degree of polydispersity and the value of σ_V given above may therefore be regarded as an upper bound. Based on these estimates it is reasonable to expect the effect of column broadening on the experimental GPC distributions presented in the previous section to be simulated by a value of $\sigma_V b$ in the range of $0.12 - 0.26$. A "normal" value of $\sigma_V b$ is reported as being of order 0.1, not inconsistent with the experimental estimates here. That these estimates are a little high may be related to the high polymer molecular weights involved in this work and the possibility that more polydisperse (high) molecular weight standards were therefore used here.

The Gaussian broadening procedure described above was applied to the simulated MWDs obtained in the previous section using both the highest and lowest values estimated for $\sigma_V b$ in the present system. The effect of various degrees of broadening on the simulated $W(\log_{10}M)$ distribution is illustrated in Figure 6.14. Here it is seen that the simulated MWD with $\sigma_V b = 0.12$ is only slightly different to the unbroadened distribution ($\sigma_V b = 0$), however broadening of $\sigma_V b = 0.26$ (the highest value estimated for the present GPC analysis) results in a simulated MWD that resembles the experimental distribution far more closely. In this case it was also found that broadening of $\sigma_V b = 0.45$ (somewhat outside the predicted range) resulted in a simulated $W(\log_{10}M)$ distribution that best reproduced that from experiment.

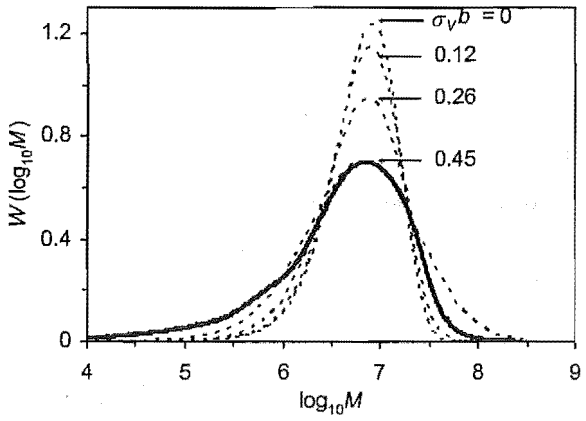

Figure 6.14. The effect of Gaussian broadening on simulated instantaneous $W(\log_{10}M)$ distributions for a seeded emulsion polymerisation of MMA at 50°C with [KPS] = 3×10^{-4} M; MWDs simulated (dashed lines) with increasing broadening applied using values of $\sigma_V\, b$ = 0, 0.12, 0.26 and 0.45 as indicated; experimental MWD (solid line) for [KPS] = 3×10^{-4} M (run C69) determined by GPC also presented.

The $W(\log_{10}M)$ and $\ln P(M)$ distributions obtained from experiments and simulations (with broadening) under all four sets of conditions are finally presented in Figure 6.15. In light of the results in Figure 6.14 the maximum estimated value of $\sigma_V\, b$ = 0.26 was used for broadening of all simulated MWDs. It is evident that this degree of broadening is sufficient for simulated $W(\log_{10}M)$ distributions to approximately reproduce experimental $W(\log_{10}M)$ distributions in all cases [Figures 6.15 (a) – (d)], with particularly good agreement observed for the distributions obtained at highest initiator concentrations. In all cases the broadening procedure led to a considerable improvement over the unbroadened results [*cf.* Figures 6.13 (a) – (d)].

Of perhaps even greater significance is the observed effect of broadening on the shapes of the $\ln P(M)$ plots, and hence on the values of Λ measured for different molecular weight regions. In Figures 6.15 (e) – (h) values of Λ are measured from linear fits to the simulated $\ln P(M)$ plots over the same "peak" and "high" molecular weight regions as in the experimental distributions. These values, denoted $\Lambda_{sim,p}$ and $\Lambda_{sim,h}$ respectively, are seen to be in remarkably good agreement with the corresponding experimental values in all cases – a marked improvement over the results obtained from the unbroadened simulations in Figures 6.13 (e) – (h).

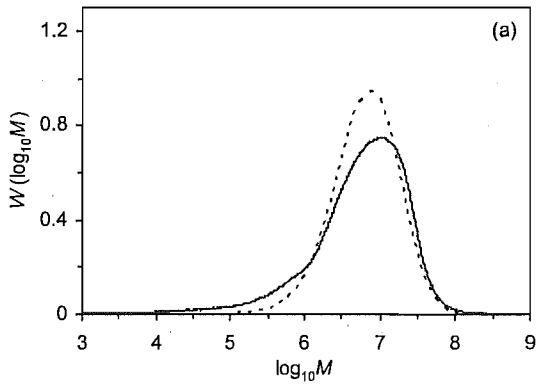
(a)
1.2
0.8
0.4
0
3
4
5
6
7
8
9
$W(\log_{10}M)$
$\log_{10}M$

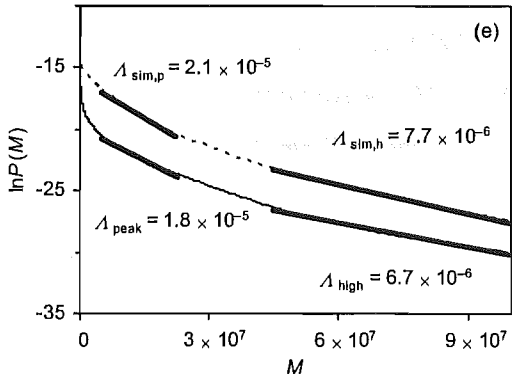
(e)
$\Lambda_{sim,p} = 2.1 \times 10^{-5}$
$\Lambda_{sim,h} = 7.7 \times 10^{-6}$
$\Lambda_{peak} = 1.8 \times 10^{-5}$
$\Lambda_{high} = 6.7 \times 10^{-6}$
-15
-25
-35
$\ln P(M)$
0
3×10^7
6×10^7
9×10^7
M

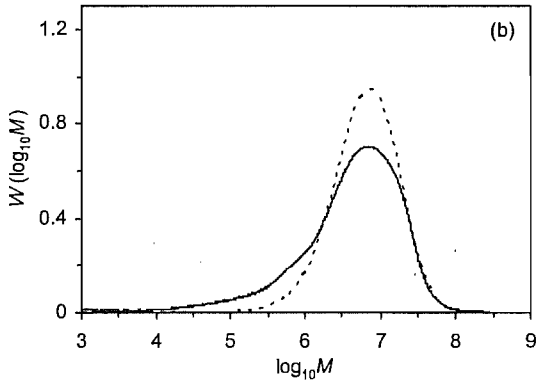
(b)
1.2
0.8
0.4
0
3
4
5
6
7
8
9
$W(\log_{10}M)$
$\log_{10}M$

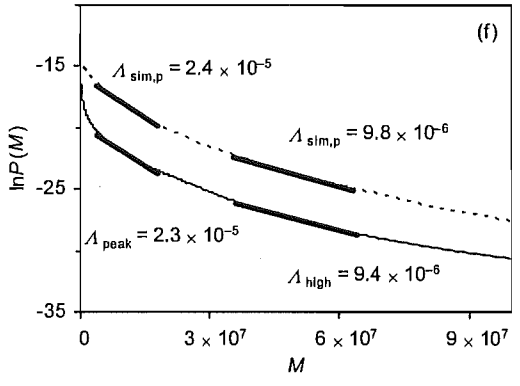
(f)
$\Lambda_{sim,p} = 2.4 \times 10^{-5}$
$\Lambda_{sim,p} = 9.8 \times 10^{-6}$
$\Lambda_{peak} = 2.3 \times 10^{-5}$
$\Lambda_{high} = 9.4 \times 10^{-6}$
-15
-25
-35
$\ln P(M)$
0
3×10^7
6×10^7
9×10^7
M

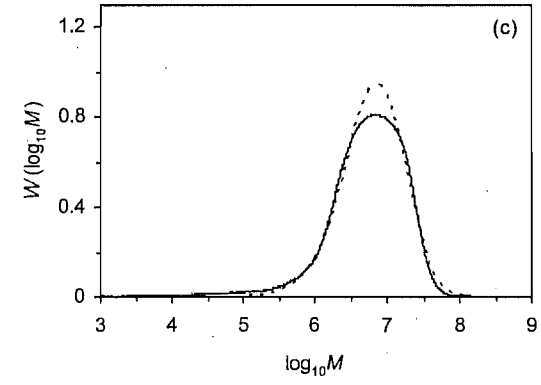
(c)
1.2
0.8
0.4
0
3
4
5
6
7
8
9
$W(\log_{10}M)$
$\log_{10}M$

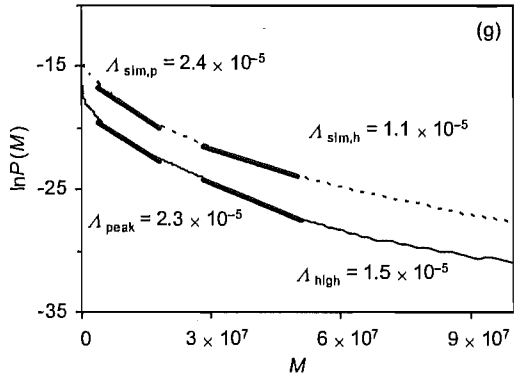
(g)
$\Lambda_{sim,p} = 2.4 \times 10^{-5}$
$\Lambda_{sim,h} = 1.1 \times 10^{-5}$
$\Lambda_{peak} = 2.3 \times 10^{-5}$
$\Lambda_{high} = 1.5 \times 10^{-5}$
-15
-25
-35
$\ln P(M)$
0
3×10^7
6×10^7
9×10^7
M

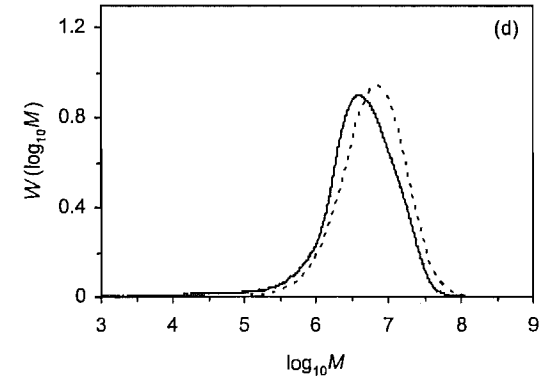
(d)
1.2
0.8
0.4
0
3
4
5
6
7
8
9
$W(\log_{10}M)$
$\log_{10}M$

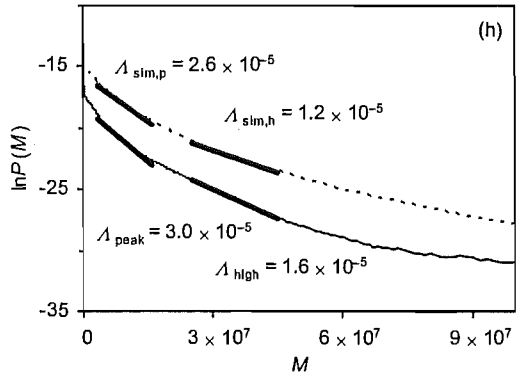
(h)
$\Lambda_{sim,p} = 2.6 \times 10^{-5}$
$\Lambda_{sim,h} = 1.2 \times 10^{-5}$
$\Lambda_{peak} = 3.0 \times 10^{-5}$
$\Lambda_{high} = 1.6 \times 10^{-5}$
-15
-25
-35
$\ln P(M)$
0
3×10^7
6×10^7
9×10^7
M

Figure 6.15. The effect of Gaussian broadening ($\sigma_Y b = 0.26$) on simulated instantaneous MWDs for chemically initiated seeded emulsion polymerisations of MMA at 50°C; experimental (solid lines) and simulated (dashed lines) MWDs for a range of initiator concentrations: [KPS] = 1×10^{-4} M **(a,e)** (run C68), 3×10^{-4} M **(b,f)** (run C69), 1×10^{-3} M **(c,g)** (run C73), 3×10^{-3} M **(d,h)** (run C72); regions of ln$P(M)$ plots where Λ_{peak}, $\Lambda_{sim,p}$, Λ_{high} and $\Lambda_{sim,h}$ fitted indicated by bold lines.

Finally, it is worth noting that comparison of the simulated ln$P(M)$ distributions in Figures 6.13 (e) – (h) with the simulated distributions of Figures 6.15 (e) – (h) shows that broadening has very little effect on the value of Λ measured in the vicinity of the peak molecular weight. This makes intuitive sense, as broadening must affect the edges much more than the centre of a MWD. Thus, even if there are other factors that significantly affect the shape of experimental MWDs measured by GPC, the approach of measuring Λ in the peak region is advisable purely on the grounds that it has been seen here to minimise the effects of column broadening on the measured value.

That said, it is clear that GPC broadening also distorts the value of Λ_{peak}. In fact this leads to another very important conclusion. While the Λ_{sim} values of Figures 6.13 (e) – (h) increase only marginally as ρ is increased, reflecting the small value of $\langle k_t \rangle$, the $\Lambda_{sim,p}$ values of Figures 6.15 (e) – (h) show a stronger increase. Thus if one plotted the $\Lambda_{sim,p}$ values as in Figure 6.11, one would deduce an erroneously high $\langle k_t \rangle$. This explains the erroneously high $\langle k_t \rangle$ that was found from Figure 6.11, and shows that while the Λ method is in principle a good one for determining $\langle k_t \rangle$, in practice it is hostage to unavoidable errors that have a significant effect. It should also be noted that this conclusion has been reached by a perfectly valid theory *versus* theory comparison that is free of any experimental errors that may introduce ambiguity.

Based on the results obtained here from modelling of MWDs it is apparent that the discrepancy between modelled and experimental distributions may well be accounted for solely in terms of the effects of GPC column broadening. While these results certainly do not rule out the possibility that the GPC baseline subtraction and the extraction of the seed polymer MWD (among other things) may significantly affect the form of the pseudo-instantaneous MWD obtained from GPC analysis, it is nevertheless encouraging that the relatively simple modelling methodology used here (including the means for estimating the expected degree of broadening based on GPC calibration data) is able to provide an accurate account of the results. Of course, it remains an interesting area for future work to see whether

this modelling approach reproduces experimental MWDs obtained from other polymerisation systems with similar success.

6.5 Conclusions

The work of this chapter employed a strategy of analysis of both kinetic data and molecular weight distributions to investigate the chain stopping reactions of termination and transfer to monomer in seeded emulsion polymerisations of MMA at 50°C. Both approaches are strongly suggestive that this system is close to the transfer limit, where chain stopping (*i.e.*, dead chain formation) is dominated by transfer to monomer.

Analysis of γ-relaxation kinetic data from experiments over a range of temperatures (50 – 80°C) furnished activation energies for the overall termination rate coefficient, $\langle k_t \rangle$, and the rate coefficient for entry of spontaneously-generated radicals, ρ_{spont}. Analytic expressions for $\langle k_t \rangle$ were shown to provide a computationally efficient means for confirming that the value of $E_a(\langle k_t \rangle)$ from experiment lies within the range expected for chain length dependent termination. It is also noted that values of $E_a(\rho_{spont})$ obtained from such experiments may constitute useful data for elucidating the mechanism of spontaneous emulsion polymerisation.

Fitting of Interval II kinetic data using a pseudo-bulk model with chain length dependent termination revealed that the fitted value of $\langle k_t \rangle$ is relatively invariant with changing initiator concentration, and that this system is therefore close to the transfer limit. Importantly, it was seen that this inference is unaffected by varying the value of k_{tr} used in model calculations over the significant range spanned by literature values.[4,12] It was also significant to note that the chain length dependent termination rate coefficients required for fitting of kinetic data are found to agree well with those calculated totally *a priori* using the Smoluchowski equation.

Independent verification that the system is transfer controlled was been provided by the analysis of measured molecular weight distributions. Here it was found, using the method of Clay *et al.*,[2] that the slope of the $\ln P(M)$ distribution taken in the region of peak molecular weight was approximately constant with changing initiator concentration and yielded a value of $k_{tr}/k_p = (2.4 \pm 0.7) \times 10^{-5}$ – in excellent agreement with the value obtained from the same MWDs using the Mayo equation. However, it is noted that while both these methods appear

to be valuable means for measuring k_{tr}, they gave a value of $\langle k_t \rangle$ which was inconsistent with the kinetic results and is probably an artefact of MWD broadening.

The lack of linearity in the ln$P(M)$ plot led to a different (and erroneously low) value for Λ from the slope at high molecular weight. This experimental finding seems to support the recommendation of several workers[2,10,40] that the most accurate estimate for Λ is that obtained from the peak region of the MWD. This issue has been further explored in the current chapter through modelling of full MWDs using the pseudo-bulk model with chain length dependent termination. While simulated MWDs were seen to approximately reproduce those from experiment (a result that is of considerable note in itself), it was found that applying a degree of Gaussian broadening comparable to that affecting experimental data resulted in a substantial improvement in the agreement. Most notably, the variation of Λ with molecular weight in simulated ln$P(M)$ plots with broadening applied was seen to very closely mimic the variation in Λ observed experimentally. Thus, it seems possible from these results that the non-linearity observed in experimental ln$P(M)$ plots may be accounted for largely by the effect of GPC column broadening – at least over the molecular weight range in which there is an appreciable amount of polymer.

6.6 References

(1) Ballard, M. J.; Napper, D. H.; Gilbert, R. G. *J. Polym. Sci., Polym. Chem. Edn.* **1984**, *22*, 3225.

(2) Clay, P. A.; Christie, D. I.; Gilbert, R. G., in *Advances in Free-Radical Polymerization*; Matyjaszewski, K., Ed.; A.C.S.: Washington D.C., 1998; Vol. 685, p 104.

(3) Adams, M. E.; Russell, G. T.; Casey, B. S.; Gilbert, R. G.; Napper, D. H.; Sangster, D. F. *Macromolecules* **1990**, *23*, 4624.

(4) Ballard, M. J., 1983, Ph.D. Thesis, University of Sydney.

(5) Whang, B. C. Y.; Ballard, M. J.; Napper, D. H.; Gilbert, R. G. *Aust. J. Chem.* **1991**, *44*, 1133.

(6) Kukulj, D.; Davis, T. P.; Gilbert, R. G. *Macromolecules* **1998**, *31*, 994.

(7) Heuts, J. P. A.; Clay, P. A.; Christie, D. I.; Piton, M. C.; Hutovic, J.; Kable, S. H.; Gilbert, R. G. *Progress in Pacific Polymer Science; Proceedings* **1994**, *3*, 203.

(8) Christie, D. I.; Gilbert, R. G. *Macromol. Chem. Phys.* **1996**, *197*, 403.

(9) Christie, D. I.; Gilbert, R. G. *Macromol. Chem. Phys.* **1997**, *198*, 663.

(10) Heuts, J. P. A.; Davis, T. P.; Russell, G. T. *Macromolecules* **1999**, *32*, 6019.

(11) Mayo, F. R. *J. Am. Chem. Soc.* **1943**, *65*, 2324.

(12) Stickler, M.; Meyerhoff, G. *Makromol. Chem.* **1978**, *179*, 2729.

(13) Russell, G. T.; Gilbert, R. G.; Napper, D. H. *Macromolecules* **1992**, *25*, 2459.

(14) Gilbert, R. G. *Emulsion Polymerization: A Mechanistic Approach*; Academic: London, 1995.

(15) Halnan, L. F.; Napper, D. H.; Gilbert, R. G. *J. Chem. Soc. Faraday Trans. 1* **1984**, *80*, 2851.

(16) Brandrup, J.; Immergut, E. H.; Grulke, E. A. *Polymer Handbook*; 4th ed.; Brandrup, J.; Immergut, E. H.; Grulke, E. A., Ed.; John Wiley & Sons: New York, 1999.

(17) Getzen, F.; Hefter, G.; Maczynski, A.; Editors *Esters with Water Part 1: Esters 2-C to 6-C*; Pergamon, Oxford, UK, 1992; Vol. 49.

(18) Lide, D. R. *CRC Handbook of Chemistry and Physics*; 82nd ed.; Lide, D. R., Ed.; CRC Press, 2001.

(19) Eastmond, G. C. *Makromolekulare Chemie, Macromolecular Symposia* **1987**, *10-11*, 71.

(20) Buback, M.; Gilbert, R. G.; Hutchinson, R. A.; Klumperman, B.; Kuchta, F.-D.; Manders, B. G.; O'Driscoll, K. F.; Russell, G. T.; Schweer, J. *Macromol. Chem. Phys.* **1995**, *196*, 3267.

(21) Buback, M.; Egorov, M.; Gilbert, R. G.; Kaminsky, V.; Olaj, O. F.; Russell, G. T.; Vana, P.; Zifferer, G. *Macromol. Chem. Phys.* **2002**, *203*, 2570.

(22) Pickup, S.; Blum, F. D. *Macromolecules* **1989**, *22*, 3961.

(23) Russell, G. T. *Macromol. Theory Simul.* **1995**, *4*, 549.

(24) Smith, G. B.; Russell, G. T.; Heuts, J. P. A. *Macromol. Theory & Simulations* **2003**, *12*, 299.

(25) van Berkel, K. Y. "B.Sc.(Hons) Report," University of Canterbury, 1999.

(26) Griffiths, M. C.; Strauch, J.; Monteiro, M. J.; Gilbert, R. G. *Macromolecules* **1998**, *31*, 7835.

(27) Strauch, J.; McdDonald, J.; Chapman, B. E.; Kuchel, P. W.; Hawkett, B. S.; Roberts, G. E.; Tonge, M. P.; Gilbert, R. G. *J. Polym. Sci. A Polym. Chem. Ed.* **2003**, *41*, 2491.

(28) Olaj, O. F.; Vana, P. *Journal of Polymer Science, Part A: Polymer Chemistry* **2000**, *38*, 697.

(29) Russell, G. T.; Gilbert, R. G.; Napper, D. H. *Macromolecules* **1993**, *26*, 3538.

(30) Heuts, J. P. A.; Radom, L.; Gilbert, R. G. *Macromolecules* **1995**, *28*, 8771.

(31) Moad, G.; Rizzardo, E.; Solomon, D. H.; Beckwith, A. L. J. *Polym. Bull.* **1992**, *29*, 647.

(32) Gridnev, A. A.; Ittel, S. D. *Macromolecules* **1996**, *29*, 5864.

(33) Willemse, R. X. E.; Staal, B. B. P.; van Herk, A. M.; Pierik, S. C. J.; Klumperman, B. *Macromolecules* **2003**, *36*, 9797.

(34) Russell, G. T.; Napper, D. H.; Gilbert, R. G. *Macromolecules* **1988**, *21*, 2133.

(35) de Gennes, P.-G. *Scaling Concepts in Polymer Physics*; Cornell University: Ithaca NY, 1979.

(36) Russell, G. T. *Macromol. Theory Simulations* **1995**, *4*, 497.

(37) De Bruyn, H.; Hawkett, B. S.; Gilbert, R. G. *Polymer* **2000**, *41*, 8633.

(38) Clay, P. A.; Gilbert, R. G. *Macromolecules* **1995**, *28*, 552.

(39) Scheren, P. A. G. M.; Russell, G. T.; Sangster, D. F.; Gilbert, R. G.; German, A. L. *Macromolecules* **1995**, *28*, 3637.

(40) Moad, G.; Moad, C. L. *Macromolecules* **1996**, *29*, 7727.

(41) Zammit, M. D.; Davis, T. P.; Haddleton, D. M. *Macromolecules* **1996**, *29*, 492.

(42) Zammit, M. D.; Davis, T. P.; Haddleton, D. M.; Suddaby, K. G. *Macromolecules* **1997**, *30*, 1915.

(43) Kukulj, D.; Davis, T. P. *Macromolecules* **1998**, *31*, 5668.

(44) Sadao, M.; Barth, H. G. *Size Exclusion Chromatography*; Springer: Berlin Heidelberg, 1999.

(45) Buback, M.; Busch, M.; Lämmel, R. A. *Macromol. Theory Simul.* **1996**, *5*, 845.

7. Spontaneous Emulsion Polymerisation: Observations and Mechanistic Inferences

7.1 Introduction

The occurrence of polymerisation in the absence of any deliberately applied source of free radicals, referred to as "spontaneous polymerisation" or "thermal polymerisation", has been known for some time to occur in a range of different free radical polymerisation systems.[1-9] It is therefore a somewhat surprising realisation that the precise kinetics and mechanism of this process remain poorly understood to the present day.

In the context of the kinetic investigations of this thesis, it has been seen that this phenomenon is of unavoidable import. In Chapter 3 it was first acknowledged that the rate of formation of propagating radicals inside a latex particle corresponding to "spontaneous" generation is measurable for typical styrene emulsion polymerisation systems, and hence that the overall rate coefficient for entry should, correctly, include a contribution, denoted ρ_{spont}, from this mystery source. Indeed, it was seen in kinetic experiments with low initiator concentration that the value of ρ_{init} (and thus also entry efficiency, f_{entry}) is always highly sensitive to the value stipulated for ρ_{spont}, and that in the case of a high value for ρ_{spont} the accuracy of values measured for other rate coefficients, such as that for exit, may also be significantly affected. Moreover, it was discovered that the value of ρ_{spont} may vary dramatically depending on the chemical composition of the system. In Chapter 4 it was found that the value of ρ_{spont} is of similar importance in obtaining values of f_{entry} for methyl methacrylate (MMA) emulsion systems. Furthermore, it was seen that the nature of the possible evolution of ρ_{spont} with conversion during Interval II of polymerisation is of considerable interest in terms of establishing the accuracy of different kinetic models for MMA systems.

The purpose of this chapter is to compile and compare all values obtained in this thesis for the rate coefficient describing entry of "spontaneously-generated" radicals throughout the course of this project. While this data set is surely insufficient to yield definitive mechanistic

answers – such was never a focus of this work – it is hoped that adding the present results to the limited literature data available will provide some new insights, and a basis for more detailed investigations of spontaneous emulsion polymerisation.

7.2 Summary of Experimental Results

In Tables 7.1 and 7.2 are presented the experimental details and kinetic results for all spontaneous polymerisation experiments carried out as part of this work. In some cases the results are average values obtained from repeated experiments under identical conditions where good reproducibility was observed. Experiments investigating spontaneous polymerisation have traditionally been avoided because of their tedious nature due to slow rates. However the development of automated dilatometry for this work has eliminated this problem, explaining the large number of results. In short, it is now possible to investigate the kinetics of spontaneous polymerisations as readily as for experiments with added initiator.

All experiments were seeded emulsion polymerisations carried out according to the methods detailed in Chapters 3 and 4; "gamma" indicates results obtained from fitting of "out-of-source" γ-relaxation data, while "spont" denotes results inferred from the steady-state value of $\bar{n}$ in Interval II of a polymerisation carried out in the absence of any added initiator (using independently determined values for exit and termination rate coefficients), and "gamma/spont" indicates results obtained from combined fitting of both steady-state and γ-relaxation data.

In the case of styrene, kinetic results were analysed using the well-established "zero-one" kinetic approximation, described in detail in Chapters 1 and 3. For MMA systems the results are those obtained using the pseudo-bulk model with α=1. Recalling from Chapter 4 that this model predicts an increase in the steady-state value of $\bar{n}$ during Interval II, the constant value of $\bar{n}$ observed in spontaneous polymerisations of MMA may or may not be accounted for by a gradual decrease in the value of ρ_{spont}. In the case of experiments labelled "spont" in Table 7.2 we therefore present only the values of ρ_{spont} measured at the start of the steady-state period, recognising the possibility that this value could vary with conversion.

Table 7.1. Experimental details and results for all spontaneous emulsion polymerisations of styrene.

result label	experiment	seed latex	T /°C	r_s /nm	$[M]_p$ / M	N_c / 10^{17} dm^{-3}	$\bar{n}_{spont}$	ρ_{spont} / 10^{-4} s^{-1}
S1	gamma/spont	AN01	50	45	5.4	0.75	0.063	1.1
S2	gamma/spont	AN01	50	45	5.4	1.6	0.070	1.3
S3	spont	ANH05	50	45	5.4	0.75	0.065	1.1
S4	gamma	CAT02	50	49	6.1	3.0	0.22	19
S5	spont	CAT02	50	49	6.1	1.0	0.29	40
S6	gamma	CATH03	50	46	5.7	2.2	0.059	0.41
S7	spont	CATH03	50	46	5.7	1.0	0.036	0.25
S8	gamma	AN04	50	49	5.3	2.4	0.108	1.5

Table 7.2. Experimental details and results for all spontaneous emulsion polymerisations of MMA.

result label	experiment	seed latex	T / °C	r_s / nm	$[M]_p$ / M	N_c / 10^{17} dm^{-3}	$\bar{n}_{spont}$	ρ_{spont} / 10^{-4} s^{-1}
M1	gamma	MMA06	50	80	6.9	1.0	0.074	1.5
M2	spont	MMA06	50	68	6.9	0.43	0.081	3.0
M3	gamma	MMA06	60	81	6.7	1.1	0.082	2.6
M4	gamma	MMA06	70	82	6.8	1.1	0.069	2.5
M5	spont	MMA06	70	68	6.8	0.43	0.088	6.8
M6	gamma	MMA06	80	82	6.6	1.0	0.084	4.7
M7	spont	MMAH07	50	82	6.9	0.43	0.058	2.1

While most of the experimental results in Tables 7.1 and 7.2 have appeared (in some form) in Chapters 3 and 4 of this thesis, three experiments which are discussed only in the present chapter are the those labelled S3, M5 and M7 in Table 7.2. M5 is a seeded emulsion polymerisation of MMA with no added initiator at 70°C, which was carried using an identical

procedure to that described for seeded polymerisations of MMA at 50°C in Chapter 4, but at elevated temperature. M7 is a seeded MMA polymerisation at 50°C also using the same procedure as in Chapter 4, but only after heat-treatment of the poly(MMA) seed latex MMA06 under argon at 90°C for four days. The heat-treated latex is denoted MMAH07. Similarly, S3 gives results from a seeded styrene polymerisation at 50°C using the procedure of Chapter 3 after heat-treatment of polystyrene seed latex AN01 at 90°C for four days under argon. This heat-treated latex is labelled ANH05.

7.3 Existing Mechanisms for Spontaneous Free Radical Polymerisation

Historically, spontaneous free radical polymerisation has been investigated relatively extensively for a range of bulk and solution systems, and various reaction mechanisms accounting for the formation of polymerising radicals have been postulated (*e.g.*, see the reviews of Pryor and Lasswell,[3] and Moad and Solomon[10]).

7.3.1 Styrene Systems

In the case of styrene bulk and solution systems the most widely accepted (and experimentally validated) mechanism for spontaneous polymerisation is that due to Mayo.[11] The distinguishing feature of this mechanism is the Diels-Alder reaction of two styrene molecules, illustrated in Scheme 7.1, to form the dimeric adduct denoted AH. This adduct, which has a labile hydrogen atom as shown, then reacts with a third styrene molecule in a molecule-assisted homolysis (which might be considered to be like a transfer reaction) to yield a styryl radical and a 1-phenyl-1,2,3,9-tetrahydronaphthalene radical, which are both thought to initiate polymerisation. The driving force for this radical-forming homolysis reaction is the aromaticisation of the 1-phenyl-1,2,3,9-tetrahydronaphthalene species.

A kinetic scheme and simulated results for spontaneous polymerisation, based on the mechanism of Scheme 7.1, were presented by Pryor *et al.*[3,12] Drawing on this work, Hui and Hamielec applied the same kinetic model to experimentally measured data for conversion and polymer molecular weight in styrene spontaneous polymerisation systems,[2] identifying kinetic limits in which the rate of "spontaneous initiation" is either second-order or third-order in monomer concentration. The essence of their kinetic treatment is now presented.

Scheme 7.1. Mechanism for spontaneous styrene polymerisation due to Mayo

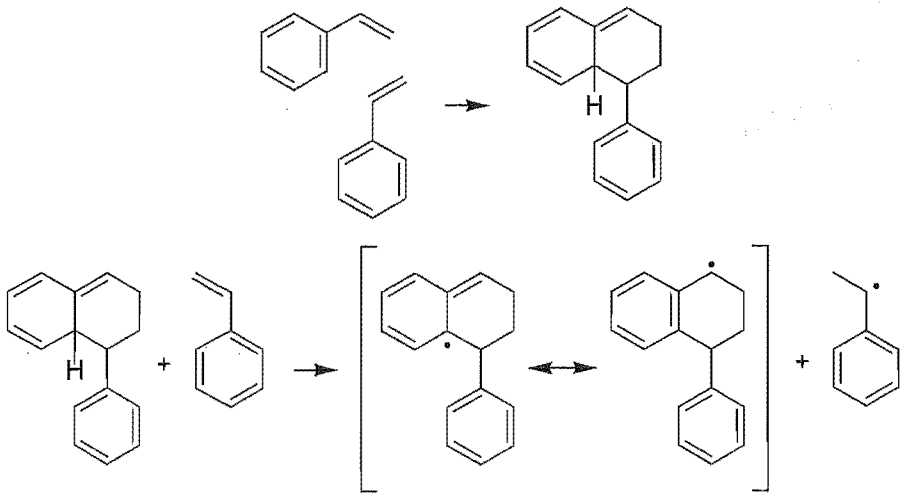

The Diels-Alder dimerisation of styrene may be regarded as the equilibrium shown in reaction (7.1), where M is a monomer molecule and k_1 and k_{-1} are the rate coefficients for forward (addition) and reverse (fragmentation) reactions respectively. MH$^\bullet$ and A$^\bullet$ are the styryl and adduct radicals formed by the homolysis reaction (7.2), with rate coefficient k_i.

$$M + M \underset{k_{-1}}{\overset{k_1}{\rightleftharpoons}} AH \tag{7.1}$$

$$AH + M \xrightarrow{k_i} MH^\bullet + A^\bullet \tag{7.2}$$

Assuming that both radicals formed go on to initiate polymerisation the rate of spontaneous initiation is given by:

$$R_{init} = 2\,k_i[M][AH] \tag{7.3}$$

From reactions (7.1) and (7.2) the following rate equation for [AH] is obtained:

$$\frac{d[AH]}{dt} = k_1[M]^2 - k_{-1}[AH] - k_i\,[M][AH] \tag{7.4}$$

which gives the steady-state concentration of AH as,

$$[AH] = \frac{k_1[M]^2}{k_{-1} + k_i\,[M]} \tag{7.5}$$

Now, if we assume $k_i[M] \gg k_{-1}$, so that AH, once formed, reacts rapidly with monomer, the following limiting form for R_{init} is obtained:

$$R_{init} = 2\,k_i[M]\frac{k_1[M]^2}{k_i[M]} = 2\,k_1[M]^2 \qquad (7.6)$$

where the rate of spontaneous initiation is clearly second-order in monomer concentration. Clearly this limit is that of the Diels-Alder dimerisation being rate-determining.

Alternatively, if $k_{-1} \gg k_i[M]$, which corresponds to the homolysis reaction being the rate-determining step for initiation, then R_{init} is third-order in monomer concentration:

$$R_{init} = 2\,k_i[M]\frac{k_1[M]^2}{k_{-1}} = \frac{2\,k_i\,k_1}{k_{-1}}[M]^3 = 2\,\bar{k}_i\,[M]^3 \qquad (7.7)$$

where $\bar{k}_i = \dfrac{k_i\,k_1}{k_{-1}}$.

Hui and Hamielec[2] used both equations (7.6) and (7.7) to fit their experimental data from bulk styrene systems over the temperature range 100 – 200°C. They obtained

$$k_1 / \mathrm{M^{-1}\,s^{-1}} = 1.015 \times 10^6 \exp\left(\frac{-113.1\ \mathrm{kJ\ mol^{-1}}}{RT}\right) \qquad (7.8)$$

$$\bar{k}_i / \mathrm{M^{-2}\,s^{-1}} = 2.19 \times 10^5 \exp\left(\frac{-114.8\ \mathrm{kJ\ mol^{-1}}}{RT}\right) \qquad (7.9)$$

Both models gave acceptable and approximately equally good fits to the data, although possibly the third-order model was slightly better, and indeed it is the model which is generally accepted as being more physically likely.

From the above equations the value of R_{init} pertaining to spontaneous polymerisation may be estimated, at least for styrene bulk systems.

7.3.2 MMA Systems

In comparison to styrene, considerably less is known about the mechanism for spontaneous polymerisation in MMA polymerisation systems. While measurable and reproducible rates of

spontaneous polymerisation have been reported for this monomer,[3,4,13] the rate in this case is considerably slower than that observed in styrene systems, as will shortly be seen.

While it is possible that spontaneous generation of radicals in MMA systems could arise through a Diels-Alder dimerisation mechanism similar to that of styrene (see reaction (a) in Scheme 7.2), this is thought to be unlikely given the absence of aromatic stabilisation in this case.[3] The mechanism that is generally preferred, on the basis of experimental results,[10,14,15] involves the reaction of two MMA monomer molecules to form a 1,4-biradical (illustrated in reaction (b) of Scheme 7.2), purported to initiate polymerisation. It is noted that this would give rise to unusual free radical polymerisation kinetics, *e.g.*, chain stopping obviously is complicated by having polymerising biradicals.

Scheme 7.2. Possible reactions involved in spontaneous polymerisation of MMA; **(a)** Diels-Alder dimerisation; **(b)** 1,4-biradical formation

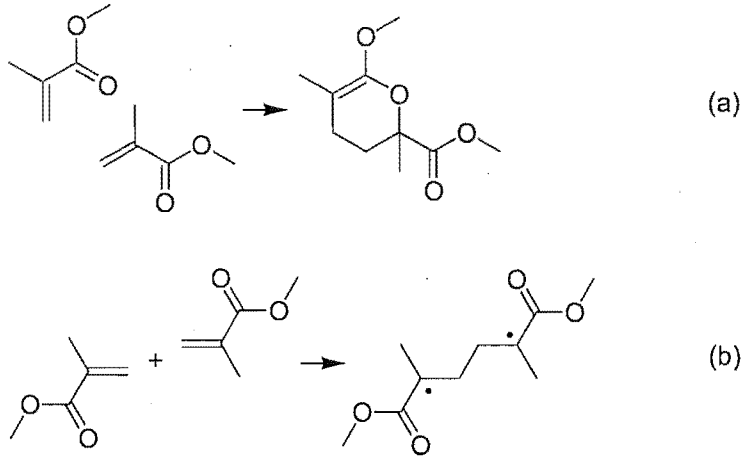

Note that one might anticipate a second-order rate law in [MMA] for reaction (b).

Whatever the mechanism for this process, Stickler and Meyerhoff have measured the rate of spontaneous polymerisation in low conversion bulk MMA systems over the temperature range 0 – 140°C.[4] Here the rate of spontaneous initiation was found to vary with temperature according to the following expressions:

$$\log_{10} R_{\text{init},0} = \frac{\ln R_{\text{init},0}}{2.303} = 0.73 - \frac{108.5 \text{ kJ mol}^{-1}}{2.303\, RT} \tag{7.10}$$

$$R_{\text{init}} = R_{\text{init},0} + 3.71 \times 10^{-17} \text{ M s}^{-1} \tag{7.11}$$

where $R_{init,0}$ is the value of R_{init} measured for a system shielded from natural ionizing radiation, while R_{init} is the value for an unshielded system.

It is of interest at this point to compare the values of R_{init} predicted for styrene and MMA bulk systems under comparable conditions using equations (7.6) – (7.11) above. Here we note that the results of Stickler and Meyerhoff for bulk MMA systems reveal nothing of the dependence of R_{init} on monomer concentration. Thus, it should be appreciated that (strictly speaking) the value of R_{init} in equation (7.11) may be assumed to hold only for bulk monomer (the types of system that were studied) at a given temperature. Assuming low conversion conditions, this concentration may be approximated as [M] = d_M/M_0, where M_0 is the molecular weight of monomer and d_M is the monomer density, reported for MMA by Stickler and Meyerhoff as:

$$d_M / \text{g cm}^{-3} = 0.9659 - 1.2129 \times 10^{-3} (T / °\text{C}) + 1.6816 \times 10^{-6} (T / °\text{C})^2 - 1.0164 \times 10^{-8} (T / °\text{C})^3 \quad (7.12)$$

Similarly the temperature dependence of the monomer concentration in a low conversion bulk styrene system may be obtained from the monomer density quoted by Hui and Hamielec, which is that measured by Patnode and Scheiber:[16]

$$d_M / \text{g cm}^{-3} = 0.924 - 0.918 \times 10^{-3} (T / °\text{C}) \quad (7.13)$$

Equations (7.6) – (7.13) were used to calculate R_{init} for bulk styrene and MMA systems over a range of temperatures; the results of these calculations are presented in Figure 7.1. Here the values of R_{init} calculated for styrene using either the second- or third-order mechanism at any given temperature are indistinguishable (however the variations with conversion will be quite different at a given temperature). This is a consequence of equations (7.8) and (7.9) being obtained from fitting of the same experimental data (although data over a range of conversion was fitted, presumably it was the low-conversion data that dominated the fitted R_{init}). In the case of MMA the effect on R_{init} of shielding the system from natural radiation is seen to become significant at temperatures below 60°C. Overall, it is clear that the rate of spontaneous initiation in a styrene bulk system is several orders of magnitude higher than the rate in an equivalent MMA bulk system. Above 60°C, this difference is about 6 orders of magnitude.

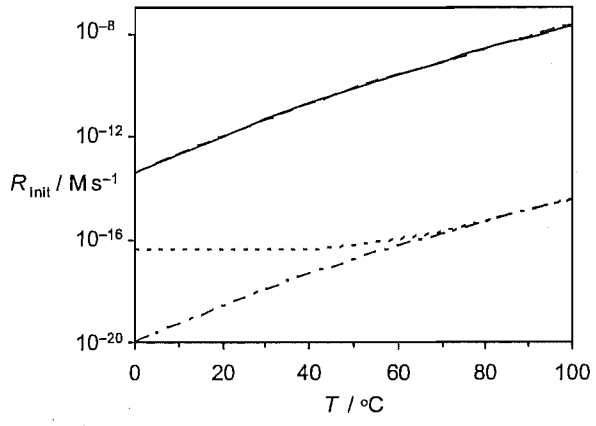

Figure 7.1. Rate of spontaneous radical generation in bulk polymerisation systems; styrene, assuming a mechanism that is either second-order (————) or third-order (— — —) in monomer; MMA, shielded from natural ionising radiation (– – – –) or unshielded (– —— –).

7.3.3 Temperature Variation of ρ_{spont} for MMA

In view of Figure 7.1, this is an appropriate juncture to discuss some results from Chapter 6 and Table 7.2: the variation of ρ_{spont} with temperature for MMA as measured in γ-relaxation experiments (for reasons soon to become clear, we consider only experiments with the same $N_c = 1 \times 10^{17}$ dm^{-3}). These were shown in Chapter 6 to give $E_a(\rho_{spont}) = 31$ kJ mol^{-1}. At first glance this suggests a transfer reaction, *e.g.*, $E_a(k_{tr}) = 46$ kJ mol^{-1} for transfer to monomer in MMA systems,[4] or $E_a(k_{tr}) = 22$ kJ mol^{-1} for transfer to dodecanethiol in MMA systems;[17] it could also suggest a propagation reaction, *e.g.*, $E_a(k_p) = 22$ for MMA. This brings to mind reaction (7.2), which (even if for styrene rather than MMA) bears obvious similarities to both transfer and propagation. But then it is noted that the Mayo scheme is a complex mechanism, and thus it will not necessarily have an activation energy corresponding to any single reaction step. Indeed, equation (7.7) shows that $E_a(\bar{k}_i) = E_a(k_i) + E_a(k_1) - E_a(k_{-1})$ for the third-order mechanism. That said, for the second-order mechanism there does exist a simple correspondence: equation (7.6) shows that in this event $E_a(k_1)$ is the activation energy. Whatever the case, equations (7.8) and (7.9) show a measured activation energy of 113 – 115 kJ mol^{-1}, well in excess of $E_a(\rho_{spont})$ for MMA measured here. This immediately suggests that a different and more facile chemical process must generate radicals in MMA emulsion polymerisation than in styrene bulk systems. That this is also the case for MMA emulsion *versus* MMA bulk systems is shown by equation (7.10), which reveals that $E_a(R_{init,0}) = 109$ kJ mol^{-1} for MMA bulk polymerisation. In fact, the near identical temperature dependences of

spontaneous initiation in MMA and styrene bulk systems is evident from Figure 7.1. It would be remarkable if this were just a coincidence, and suggests a common mechanism for spontaneous radical generation in both bulk systems. Equally, the much lower value of $E_a(\rho_{spont})$ for MMA strongly suggests a different mechanism, a conclusion which will soon be confirmed by showing that the rates of initiation are much higher in emulsion than in bulk.

7.4 Mechanistic Inferences for Spontaneous Emulsion Polymerisation

The mechanisms for spontaneous radical generation in seeded emulsion systems are potentially far more complex than those described above for bulk systems. Given that there are three different phases: latex particle, monomer droplet, aqueous – all containing monomer – the possibility of spontaneous initiation in all phases must be considered. Indeed, Christie *et al.*[9] have suggested that spontaneous radical generation occurs in all phases, based on their experimental results for seeded emulsion polymerisations of styrene and chlorobutadiene. Furthermore, it is necessary to consider the possibility of a mechanism involving other species present in a seeded emulsion system, such as aqueous phase species (*e.g.*, buffer) and particle surface species (*e.g.*, surfactant).

One may therefore choose to define the overall value of ρ_{spont} in terms of contributions from all possible sources:

$$\rho_{spont} = \rho_{sp,bulk} + \rho_{sp,w} + \rho_{sp,other} \qquad (7.14)$$

Here $\rho_{sp,bulk}$ is the component of ρ_{spont} arising from radical-generating reactions of monomer in the interior of latex particles and/or monomer droplets (both environments akin to a bulk polymerisation system), $\rho_{sp,w}$ is the contribution from radical-generating reactions of aqueous monomer, and $\rho_{sp,other}$ is the component due to spontaneous radical generation in any phase that does not arise directly from monomeric reactions, including, for example, radicals produced by any reactive peroxidic functionalities present.[9,18] Really one should write $\rho_{sp,other} = \rho_{sp,other,bulk} + \rho_{sp,other,w} + \rho_{sp,other,surface}$ as will be seen. We now consider the kinetics and mechanisms of each of these modes of spontaneous radical generation in more detail. Note that $\rho_{sp,bulk}$ must be a contribution, as the droplet and latex particle interiors are chemically equivalent to bulk systems – it is just a case of whether this contribution is a significant portion of the overall spontaneous initiation rate.

7.4.1 Bulk Mechanism for Spontaneous Emulsion Polymerisation

If it is assumed firstly that the value of $\rho_{sp,bulk}$ arises from spontaneous radical generation inside a latex particle, which proceeds *via* the same mechanism as in a bulk system, we may calculate a value for $\rho_{sp,bulk}$ using the kinetic results of section 7.3, according to the following expression:

$$\rho_{sp,bulk}(\text{particles}) = \tfrac{4}{3}\pi r_s^3 R_{init} N_A \qquad (7.15)$$

For simplicity we assume here that the intra-particle monomer concentration is the same as that in a bulk system at zero conversion and may therefore be calculated from equations (7.12) and (7.13) as $[M]_p = d_M/M_0$. We also adopt the largest value of r_s from each of Tables (7.1) and (7.2) in calculations. Clearly, both of these assumptions will result in overestimation of $\rho_{sp,bulk}$(particles), because $[M]_p$ is actually lower in an Interval II system, and the actual r_s can only be smaller. Because of the assumption of bulk $[M]_p$, both equations (7.6) and (7.7) give the same result (see Figure 7.1), so it does not matter which is chosen. However this would not be the case if the lower $[M]_p$ of Interval II was used.

Values of $\rho_{sp,bulk}$(particles) calculated according to equation (7.15) are presented in Table 7.3. Comparison of the calculated values with the experimentally measured values of ρ_{spont} (also presented) for MMA systems reveals in every case that even the overestimate for $\rho_{sp,bulk}$(particles) calculated here is many orders of magnitude too low to account for observed rates of spontaneous radical generation in emulsion.

Table 7.3. Calculations for spontaneous initiation originating in latex particle and monomer droplet phases.

result label	T / °C	ρ_{spont} / s^{-1}	$\rho_{sp,bulk}$ (particles) / s^{-1}	$R_{pol,expt}$ / 10^{-4} g s^{-1}	$R_{pol,bulk}$ (monomer droplets) / 10^{-4} g s^{-1}
S1	50	1.1×10^{-4}	2.3×10^{-5}	6.4×10^{-5}	7.0×10^{-7}
S2	50	1.3×10^{-4}	2.3×10^{-5}	1.4×10^{-4}	7.0×10^{-7}
S3	50	1.1×10^{-4}	2.3×10^{-5}	6.6×10^{-5}	7.0×10^{-7}
S4	50	1.9×10^{-3}	2.3×10^{-5}	4.2×10^{-4}	7.0×10^{-7}
S5	50	4.0×10^{-3}	2.3×10^{-5}	4.4×10^{-4}	7.0×10^{-7}
S6	50	4.1×10^{-5}	2.3×10^{-5}	8.0×10^{-5}	7.0×10^{-7}
S7	50	2.5×10^{-5}	2.3×10^{-5}	5.0×10^{-5}	7.0×10^{-7}
S8	50	1.5×10^{-4}	2.3×10^{-5}	1.4×10^{-4}	7.0×10^{-7}
M1	50	1.5×10^{-4}	7.3×10^{-11}	1.3×10^{-4}	2.9×10^{-9}
M2	50	3.0×10^{-4}	7.3×10^{-11}	1.4×10^{-4}	2.9×10^{-9}
M3	60	2.6×10^{-4}	1.2×10^{-10}	1.4×10^{-4}	4.5×10^{-9}
M4	70	2.5×10^{-4}	2.8×10^{-10}	1.2×10^{-4}	7.9×10^{-9}
M5	70	6.8×10^{-4}	2.8×10^{-10}	1.4×10^{-4}	7.9×10^{-9}
M6	80	4.7×10^{-4}	7.1×10^{-10}	1.4×10^{-4}	1.5×10^{-8}
M7	50	2.1×10^{-4}	7.3×10^{-11}	1.0×10^{-4}	2.9×10^{-9}

In the case of styrene the calculated values of $\rho_{sp,bulk}$(particles) are seen to be high enough to suggest that the measured ρ_{spont} data may be partially accounted for by intra-particle spontaneous initiation, at least for seed latexes AN01, ANH05, CATH03 and AN04. However, it is important to note that these styrene systems are thought to be zero-one. Thus, the two radicals formed inside a particle by the bulk mechanism suggested here would generally be expected to undergo rapid termination with one another. The only possible exception to this would be if the monomeric styryl radical was able to escape from the particle

before termination had occurred (the dimeric radical would be too hydrophobic to escape). The probability for escape, P_{exit}, may be estimated from the following expression:

$$P_{exit} = \frac{k_{dM}}{k_{dM} + k_p^1[M]_p + c^{MM}} \tag{7.16}$$

where k_{dM}, k_p^1 and c^{MM} are, respectively, the relative rates of desorption, propagation and mutual termination for a monomeric radical. As will be seen in Chapter 8, these rates may be roughly approximated (for styrene systems with particles of the present size) as: $k_{dM} = 2 \times 10^3$ s^{-1}, $k_p^1[M]_p = 6 \times 10^3$ s^{-1} and $c^{MM} = 5 \times 10^3$ s^{-1}, leading to value of $P_{exit} \approx 15\%$. The true value of $\rho_{sp,bulk}$(particles) for styrene is therefore likely to be at least an order of magnitude less than calculated here, because ~ 85% of initiation events will lead to rapid termination, and thus no polymerisation.

Thus, while it appears that spontaneous intra-particle radical generation may not be ruled out completely for styrene systems, clearly this cannot be the dominant mechanism for spontaneous initiation.

Another possibility is that spontaneous polymerisation occurs mainly inside the monomer droplets *via* the bulk mechanism. In this event it is difficult to relate the value of R_{init} directly to the measured value of ρ_{spont}; however a useful comparison may be made between the observed overall rate of polymerisation, R_{pol}, and the theoretical rate for a bulk polymerisation given by the following familiar classical kinetic equation:

$$R_{pol} / M\ s^{-1} = -\frac{d[M]}{dt} = k_p\,[M]\left(\frac{R_{init}}{2k_t}\right)^{\frac{1}{2}} \tag{7.17}$$

The additional values required to calculate R_{pol} for a bulk styrene system are given by Hui and Hamielec as[2] [note that their k_t expression has been halved to allow for the factor of 2 included in equation (7.17)]:

$$k_p / M^{-1}\ s^{-1} = = 1.051 \times 10^7 \exp\left(\frac{-3557}{T/K}\right) \tag{7.18}$$

$$2k_t / M^{-1}\ s^{-1} = = 1.255 \times 10^9 \exp\left(\frac{-844}{T/K}\right) \tag{7.19}$$

And the values for MMA given by Stickler and Meyerhoff are:[4]

$$\log_{10}\left(\frac{k_p^{\,2} / \mathrm{M^{-1}\,s^{-1}}}{2k_t}\right) = 3.45 - \frac{1810}{T/\mathrm{K}} \qquad (7.20)$$

Once again we assume for simplicity the zero conversion bulk value for [M] in the monomer droplets. We also estimate the total volume of monomer droplets to be 5 cm^3, which constitutes an upper bound to the true value for any of the experimental systems used in this work. Using equations (7.17) – (7.20) together with the earlier equations pertaining to R_{init} leads to the calculated values of $R_{pol,bulk}$(monomer droplets), in g s^{-1}, presented in Table 7.3. Also presented are the experimentally observed polymerisation rates, $R_{pol,expt}$. It is important to understand that droplet kinetics, being bulk-like (hence the equations for bulk k_t), are different to emulsion kinetics, and thus the ρ comparisons are different to the R_{pol} comparisons.

It is evident that the calculated bulk rate is generally several orders of magnitude less than that observed experimentally, even given the generous estimate of total monomer volume employed here. Thus, by inference, it seems unlikely that the value of ρ_{spont} in seeded styrene and MMA emulsion systems contains any significant component due to spontaneous radical generation inside monomer droplets. Aside from this kinetic argument there is the phenomenological one that spontaneous emulsion polymerisations are *emulsion*, and not suspension, polymerisations, *i.e.*, they produce latex particles, not beads.

The possibility that monomer droplets are a locus for spontaneous polymerisation may be further refuted when it is considered that, were this the case, the decrease in the total volume of droplets during Interval II should be accompanied by a linear decrease in the observed value of ρ_{spont} with conversion. While the results of Chapter 4 for MMA may be viewed as qualitatively consistent with this theory ($\bar{a} \approx 0$ implies a decreasing ρ_{spont}), no such decrease in ρ_{spont} was observed in styrene experiments.

Also of considerable significance here are the results of Lacík *et al.*[19] who found that addition of the radical scavenger Fremy's salt (potassium nitrosodisulfonate) during the course of a seeded γ-relaxation experiment for styrene, under zero-one conditions, resulted in total (and reproducible) suppression of spontaneous polymerisation (*i.e.*, $\rho_{spont} = 0$) during the out-of-source period, whereas $\rho_{spont} > 0$ was measured in the absence of Fremy's salt. Fremy's salt is

soluble in water, but insoluble in monomer-rich environments[9] and will therefore not hinder intra-particle or intra-droplet polymerisation. Total suppression of ρ_{spont} was observed for γ-relaxations conducted in both Interval II and III of polymerisation and therefore provides conclusive evidence that spontaneous polymerisation inside latex particles or monomer droplets is negligible, at least for this zero-one system. Note that the hypothesis of rapid exit cannot challenge this, for even if P_{exit} is close to 1 (unlikely) for monomeric radicals, meaning they will desorb and terminate with Fremy's salt, there will still be a dimeric radical left behind to initiate polymerisation, making the observation of zero polymerisation impossible to explain. So the results of Lacík *et al.* can only be explained by spontaneous radical generation in these systems being in the aqueous phase or at the particle surface, to which Fremy's salt will have access.

It is noted that Christie *et al.* have claimed[9] that spontaneous polymerisation inside styrene monomer droplets is significant, based on an experiment where droplet conditions were simulated by an Interval III polymerisation under (large particle – unswollen radius 130 nm) "pseudo-bulk" conditions. In this experiment the presence of Fremy's salt reportedly led to "diminished but still significant spontaneous radical generation". This they interpreted as meaning that radicals are generated both in the aqueous phase and in the particles, with the latex contribution presumably not being seen in the experiments of Lacík *et al.* because they were zero-one with $P_{exit} \approx 0$ (*i.e.*, all intra-particle spontaneous radicals terminate rapidly with each other before exit can occur). However, this interpretation is open to question, not least all in that Lacík *et al.* also observed that Fremy's salt stopped spontaneous polymerisation even in Interval II, *i.e.*, when radicals could form in large monomer droplets, and thus avoid rapid termination. The interpretation of Christie *et al.* is also unlikely given the improbability of spontaneous polymerisation inside monomer droplets based on the calculations of the present section. It is therefore suggested that the effect observed by Christie *et al.* may be the result of incomplete inhibition by Fremy's salt. As detailed by Lacík *et al.*,[19] Fremy's salt is highly reactive and careful measures are necessary in order to obtain reliable kinetic results with this reagent. Indeed, careful attempts to use Fremy's salt during the course of this project to investigate the kinetics of aqueous-phase initiator decomposition (described in Chapter 3) yielded no usable results. Here Fremy's salt was added at the start of reaction either as a freshly prepared solution or in solid form (as recommended by Lacík *et al.*); however no reliable inhibition effect was observed. In view of these facts, it is difficult to

accept the single experimental result of Christie *et al.* as definitive proof of spontaneous initiation inside large particles, and therefore also monomer droplets.

7.4.2 Aqueous-Phase Mechanism for Spontaneous Emulsion Polymerisation

The results of Lacík *et al.* cited in the previous section represent strong evidence for spontaneous emulsion polymerisation originating in the aqueous phase or on the particle surface; the presence of an aqueous-phase radical scavenger completely inhibits spontaneous polymerisation. Of these two possibilities, the aqueous-phase one is supported by results obtained by Hawkett for styrene emulsion systems.[20] Here the value of ρ_{spont} was measured for a series of seeded spontaneous polymerisations carried out using three different latexes, each with a different N_c: 4.9×10^{16} dm^{-3}, 1.0×10^{17} dm^{-3}, 2.6×10^{17} dm^{-3}. It was found that the product of ρ_{spont} and N_c was approximately the same ($\sim 1.3 \times 10^{13}$ s^{-1} dm^{-3}) in each case, consistent with the flux of spontaneously-generated radicals originating in the aqueous phase and thus being independent of the concentration of latex particles present. On the other hand, surface-phase initiation, which should lead to ρ_{spont} being independent of N_c, is not consistent with these results.

Values of $\rho_{spont}N_c$ obtained from the present study are presented in Table 7.4. While the variation of ρ_{spont} with N_c was not examined specifically in this work it is nevertheless possible to gain some insight from comparison of results from γ-relaxation with those from the equivalent steady-state experiment (typically carried out with a lower particle concentration). Notably, this comparison assumes that the rate of spontaneous polymerisation is unaffected by intermittent exposure to γ-radiation (if it is, then that makes spontaneous polymerisation in emulsion even more difficult to understand). In the cases of seed latexes MMA06 (results M1/M2) and CAT02 (results S4/S5) at 50°C the value of $\rho_{spont}N_c$ is seen to be reasonably constant with changing N_c, and similarly for MMA06 at 70°C (results M4/M5). However, for CATH03 at 50°C (results S6/S7) the value of $\rho_{spont}N_c$ is seen to vary with changing N_c by up to a factor of about 3.5. Similarly, for AN01 at 50°C (results S1/S2), doubling the particle concentration results in a significant increase in $\rho_{spont}N_c$. Thus the results of the present study alone provide insufficient grounds to clearly confirm or refute an aqueous source of spontaneous initiation. Further experiments measuring how ρ_{spont} varies with N_c are ongoing.

Table 7.4. Calculations for spontaneous initiation originating in the aqueous phase.

result label	experiment	seed latex	T / °C	N_c / 10^{17} dm^{-3}	$\rho_{spont}N_c$ / 10^{13} dm^{-3} s^{-1}
S1	gamma/spont	AN01	50	0.75	0.81
S2	gamma/spont	AN01	50	1.6	2.1
S3	spont	ANH05	50	0.75	0.84
S4	gamma	CAT02	50	3.0	58
S5	spont	CAT02	50	1.0	40
S6	gamma	CATH03	50	2.2	0.91
S7	spont	CATH03	50	1.0	0.25
S8	gamma	AN04	50	2.4	3.6
M1	gamma	MMA06	50	1.0	1.6
M2	spont	MMA06	50	0.43	1.3
M3	gamma	MMA06	60	1.1	2.8
M4	gamma	MMA06	70	1.1	2.6
M5	spont	MMA06	70	0.43	2.9
M6	gamma	MMA06	80	1.0	4.9
M7	spont	MMAH07	50	0.43	0.92

Nevertheless a somewhat cohesive picture does start to emerge from the above results. For MMA one has $\rho_{spont}N_c \approx$ constant, suggesting that $\rho_{spont} \approx \rho_{sp,w}$ [in the terms of equation (7.14)], *i.e.*, that radicals arise in the aqueous phase. The fact that heat treating latex MMA06 causes only slight reduction in ρ_{spont} (compare M2 and M7) is consistent with this, *i.e.*, that the origin of most spontaneous radicals is not associated with the seed latex.

For CAT02 one also observes $\rho_{spont}N_c \approx$ constant, again suggesting aqueous-phase origin. However, the vast reduction of ρ_{spont} upon heat treatment of this latex (compare S5 and S7)

shows that for CAT02 experiments one must have $\rho_{spont} \approx \rho_{sp,other}$, where the source of the "other" radicals is the latex. A possible origin of these "other" radicals will soon be discussed. An important background point to make clear here is that in kinetic experiments, seed particles are added in the form of seed *latex*, *i.e.*, including both particles *and* aqueous phase. So the aqueous phase in a seeded kinetic run consists of both added "pure" water and water from the seed latex. It should therefore be considered that both the seed latex particles and the seed latex aqueous phase could contain sources contributing to $\rho_{sp,other}$. Moreover, any such contributions to $\rho_{sp,other}$ from either particles or seed latex aqueous phase should scale as $\rho_{sp,other} \propto N_c$, since varying N_c between experiments means varying the amount of added seed *latex* (*i.e.*, particles and aqueous phase). In view of the above there is no obvious explanation as to why $\rho_{spont}N_c \approx$ constant for CAT02, nor is it possible to identify either the seed latex *particles* or seed latex *aqueous phase* as the source. An obvious experimental approach which might shed some light here would be to conduct a series of CAT02 seeded experiments all with the same N_c, but where the ratio of added seed latex particles to added seed latex aqueous phase is varied (*e.g.*, by removal of some seed particles *via* centrifugation). A constant value of ρ_{spont} would suggest the particles (specifically their surfaces) as a likely source, while a variation in ρ_{spont} could be consistent with spontaneous initiation arising from the added seed latex aqueous phase.

Whatever the explanation for ρ_{spont} in seed CAT02, heat treatment eliminates this source and for CATH03 one observes $\rho_{spont} \approx$ constant (see results S6 and S7), suggesting perhaps that $\rho_{spont} \approx \rho_{sp,bulk}$, *i.e.*, radical generation is indeed by the Mayo mechanism in the particles as Table 7.3 confirms is feasible for these experiments.

Finally, there are styrene experiments S1, S2 and S3, with anionic latex AN01 and its heat treated form ANH05. These also show $\rho_{spont} \approx$ constant, independent of N_c. However, ρ_{spont} here is about a factor of 3 higher than for CATH03, suggesting $\rho_{spont} \approx \rho_{sp,bulk} + \rho_{sp,other}$, where $\rho_{sp,other} \propto N_c$, and so is probably associated with either the seed latex aqueous phase or the particle surface. Note that this is consistent with the Fremy's salt results of Lacík *et al.*[19] The fact that there is no change in ρ_{spont} between experiments S1 and S3 shows that the species giving rise to $\rho_{sp,other}$ in AN01 is not removed by heat treatment. It remains only to explain why Hawkett[20] observed $\rho_{spont} \propto 1/N_c$ for anionic latexes – different to here. One can only

suggest that there are different origins associated with $\rho_{sp,other}$, and that they are latex dependent (*e.g.*, different buffers, different surfactants, different impurities, *etc.*). It is quite possible that by preparing his latex differently, Hawkett shifted the primary locus of radical generation to the aqueous phase. In the present cationic latexes there are also "other" sources of radicals, but it seems that these can be exhausted by heat treatment prior to an experiment.

The simplest mechanistic explanation for aqueous-phase spontaneous radical generation is reaction involving the small but appreciable amount of aqueous monomer according to the mechanisms described earlier for bulk systems. Since N_c is the number concentration of latex particles per unit volume of aqueous phase, an upper bound for $\rho_{sp,w}$ may therefore be estimated from the rate of aqueous spontaneous initiation as follows (by assuming that all radicals undergo entry):

$$\rho_{sp,w} = \frac{R_{init} N_A}{N_c} \tag{7.21}$$

where R_{init} is once again furnished by equations (7.6) – (7.11). Importantly, a pair of radicals generated by the aqueous-phase reaction of monomer are likely to rapidly diffuse away from each other; thus the rate of geminate recombination of such radicals will be very low in this instance (*cf.* the high rate of recombination expected for radicals generated inside a zero-one particle).

For styrene at 50°C, $[M]_w = 4.3 \times 10^{-3}$ M,[21] and assuming the second-order mechanism for spontaneous initiation gives $R_{init} = 2.0 \times 10^{-17}$ M^{-1} s^{-1}, while the third-order mechanism gives a lower value of $R_{init} = 9.6 \times 10^{-21}$ M^{-1} s^{-1}. While there is good reason to suspect that the third-order mechanism may hold not just in general but under conditions of low monomer concentration in particular [see denominator of equation (7.5)]), we may nevertheless take the second-order value of R_{init} as an upper bound. Similarly, we adopt the lowest value for N_c = 7.5×10^{16} dm^{-3} used in the styrene systems of Table 7.4 to obtain an upper bound for $\rho_{sp,w}$ of 1.6×10^{-10} s^{-1}.

In the case of MMA the highest value of $\rho_{sp,w}$ will be obtained at 80°C, where $[M]_w = 0.18$ M (from Chapter 6). While the results of Stickler and Meyerhoff provide only the rate of spontaneous initiation in bulk MMA systems, in the absence of any other information it is reasonable to expect that this rate will be either second- [see Scheme 7.2 (b)] or third-order in

monomer concentration. Thus, scaling the bulk value of R_{init} by $([M]_w/[M]_{bulk})^2$ and $([M]_w/[M]_{bulk})^3$ gives $R_{init} = 2.2 \times 10^{-19}$ M^{-1} s^{-1} and $R_{init} = 4.6 \times 10^{-21}$ M^{-1} s^{-1} respectively at 80°C. Again, adopting the second-order value of R_{init} and the lowest value of N_c for MMA systems in Table 7.4 we obtain an upper bound value of $\rho_{sp,w} = 3.1 \times 10^{-12}$ s^{-1}. Note that the calculated $\rho_{sp,w}$ values for MMA and styrene here are much closer together than the R_{init} values calculated earlier because $[M]_w$ is considerably higher for MMA than for styrene.

Comparison with the experimental ρ_{spont} data reveals that for styrene the calculated value of $\rho_{sp,w}$ is of order 10^5 times less than the lowest experimental value, and in the case of MMA this discrepancy is even greater ($\sim 10^7$). However, it is interesting to note, for the case of styrene, that the rates of Diels-Alder reactions have been widely reported to be enhanced dramatically in aqueous environments.[22-25] This effect is generally attributed to hydrophobic interactions between the diene and dienophile, as well as the effects of hydrogen bonding on the Diels-Alder transition state.[26,27] Given that rate enhancements of up to $10^3 - 10^4$ times have been observed, it is conceivable that the value of ρ_{spont} measured experimentally for some styrene systems here could be accounted for by the Diels-Alder radical generation mechanism with a significant rate enhancement in the aqueous phase. This postulate is not directly applicable to the MMA systems studied here, since a non-Diels-Alder mechanism is suspected in this case. However, the possibility of a rate enhancement for any bimolecular reaction involving MMA molecules in aqueous solution, along similar lines to the styrene case, must also be considered.

Finally, additional substantiation of a significant aqueous source of spontaneous initiation may be provided by the observation of "secondary nucleation" of latex particles in some experiments. In the case of spontaneous polymerisation, the likely absence of charge-carrying entering species means that less colloidal stability is imparted to growing latex particles than in the case of experiments with added initiator (*e.g.*, persulfate). Given the long time scales of spontaneous polymerisations (up to two or three days in some cases), it was therefore not uncommon to observed significant "shear-induced" coagulation of latex particles on the stirring bar inside the dilatometer vessel. In some cases this coagulation was accompanied by the observation of new (*i.e.*, non-seed) particle formation upon inspection by transmission electron microscopy, where the larger seed particles are easily distinguished from much smaller particles formed during the course of seeded polymerisation. Importantly, this new

particle formation is thought to occur late in the polymerisation and therefore will not affect the steady-state value of $\overline{n}_{spont}$ measured earlier in Interval II. This is supported by the absence of any new particle formation or coagulation in the case of γ-relaxation experiments which are carried out over relatively shorter time scales (*i.e.*, a few hours at most).

The occurrence of secondary nucleation at any stage of a spontaneous polymerisation represents further evidence for spontaneous radicals being generated in the aqueous phase.

7.4.3 Supplementary Mechanisms for Spontaneous Emulsion Polymerisation

Finally, we consider the potential for spontaneous polymerisation arising from mechanisms other than simple bulk and aqueous-phase reactions of monomer. While aqueous-phase spontaneous radical generation appears to be generally consistent with observed experimental results, this mechanism cannot fully account for all measured values of ρ_{spont}. Most notable is the high value of ρ_{spont} obtained in the case of the cationic polystyrene seed latex CAT02. A detailed discussion of a mechanism thought to explain this result is has already been presented in Chapter 3; a brief summary is now provided.

Dissolved oxygen, present at the commencement of the polystyrene seed latex synthesis (~ 10^{-3} M), is likely to react with radicals to form polymeric peroxide species, predominantly located in the aqueous phase. Thermal decomposition of such peroxidic species is unlikely to be significant; however it is thought that amine species formed from reactions of the initiator, 2,2′-azobis-(2-methylpropionamidine) dihydrochloride (or V-50), may give rise to accelerated peroxide decomposition to yield initiating radicals. As seen in Tables (7.1) and (7.2) this mechanism is consistent with the low values of $\overline{n}_{spont}$ (and hence ρ_{spont}) observed for all other seed latexes; although the polymeric peroxide species will be formed in all cases, only latex CAT02 has amine species present to induce their decomposition. It was found that the value of ρ_{spont} measured in seeded experiments was considerably lower after seed latex CAT02 had been subjected to extended heat-treatment (90°C for 4 days). This was presumed to indicate that the peroxide species had been largely decomposed.

Interestingly, it is further noted that for seed latex CAT02, the inhibition period observed in spontaneous seeded polymerisations was several hours in length – comparable to that typically observed for polystyrene seed latex AN01, which has an order of magnitude lower value of ρ_{spont}. If the value of ρ_{spont} for both latexes was due to aqueous-phase chemistry, then

for CAT02, with its high flux of spontaneously-generated radicals, one would expect a significant reduction in inhibition time. The fact that this does not occur shows that the matter is not so simple. One immediate suggestion is that for CAT02 there is a relatively low flux of spontaneously-generated radicals whose entry efficiency is very high (*e.g.*, an adsorbed peroxide species on the particle surface), whereas for AN01 there is also a low flux but a low entry efficiency. However this is problematic firstly in that for spontaneously-generated radicals there is no reason for entry efficiencies to be low, as they are for KPS in this system (see Chapter 3). Further problems are that, as has been discussed, the variation of ρ_{spont} with N_c in fact suggests surface-phase initiation for AN01 and aqueous-phase initiation for CAT02, the opposite of what the inhibition times in concert with ρ_{spont} imply. While it is interesting to note this observation, it is probably best to regard inhibition times as difficult to interpret. For example, CAT02 could contain in-situ generated inhibitor (from latex preparation) where AN01 does not: both latexes were prepared differently.

The mechanism suggested for spontaneous polymerisation in seed latex CAT02 lends weight to the long held suspicion that peroxides may play an important part in spontaneous polymerisation.[9,18] Christie *et al.* reported that the rate of spontaneous polymerisation in a chlorobutadiene emulsion system was considerably higher than that for styrene. Furthermore, they showed for the case of a seeded spontaneous polymerisation of chlorobutadiene that the addition of Fe^{2+} ions – known to react with peroxides to form radicals[10] – results in an appreciable rate acceleration. Notably, the results of Christie *et al.* were all obtained using polystyrene seed latexes, prepared using methods similar to those of the present work. The effect of Fe^{2+} addition therefore appears consistent with the formation of peroxides postulated earlier. Indeed, it is perhaps also possible that the high rate of spontaneous polymerisation measured for chlorobutadiene may be explained by induced peroxide decomposition involving some species present in the chlorobutadiene system.

Attempts were made to identify whether a low rate of peroxide decomposition could contribute to the value of ρ_{spont} for other seed latexes in the present study. Samples of latexes AN01 and MMA06 were subjected to the same heat-treatment procedure as for CAT02. As shown by results S3 and M7 of Tables (7.1) and (7.2), this resulted in no significant change in the measured value of ρ_{spont} in either case. It is therefore possible that peroxide-derived radicals make no contribution to ρ_{spont} in these systems. However, given that neither of these

seed latexes contains any amine species, it may be that heat-treatment in the absence of a decomposition catalyst is far less effective at destroying peroxidic species.

In another experiment, a solution of $FeSO_4$ was added at the start of a seeded spontaneous polymerisation using seed latex AN01 to give $[Fe^{2+}] = 1 \times 10^{-4}$ M. It was expected that the presence of peroxides might give rise to an enhancement in $\overline{n}_{spont}$, but instead the extremely low value of $\overline{n}_{spont} = 0.0064$ was measured (*cf.* $\overline{n} = 0.06 - 0.07$ in the absence of Fe^{2+}). Furthermore, no appreciable inhibition time was observed in this case. Assuming that the addition of Fe^{2+} does not give rise to any retardation, one possible explanation for this unusual result is that the Fe^{2+} rapidly destroys any peroxides present and that the rate of spontaneous polymerisation measured here is that arising only from the bulk and aqueous radical generation mechanisms described earlier in this chapter.

In view of the above result, a similar spontaneous polymerisation was carried out using seed latex AN01, involving the addition of 1×10^{-4} M tetraethylenepentamine (TEPA) at the start of the reaction. It was hoped that TEPA would generate radicals at a slower rate than Fe^{2+} through redox reaction with any peroxides present.[28] However, as above, the rate of spontaneous polymerisation was observed to be significantly diminished in the presence of TEPA, with a measured value of $\overline{n}_{spont} = 0.0049$. Once again, a possible explanation is that the addition of TEPA removes peroxides that would otherwise yield initiating radicals. Notably, the value of $\overline{n}_{spont}$ observed here is very similar to that measured with added Fe^{2+}.

7.5 Conclusions and Future Work

In closing this chapter it is clear that the task of elucidating the precise kinetics and mechanism of spontaneous emulsion polymerisation is a challenging one, and is yet far from completion. Indeed, if nothing else, the results obtained here provide some notion of the complexity of this process and its sensitivity to the exact composition and history of a given emulsion polymerisation system. The multi-phase nature of emulsion systems, with radicals being able to move across phases, makes it very difficult to reach unambiguous conclusions about the locus of spontaneous radical generation, especially when the nature of the radicals (*i.e.*, their phase-transfer tendencies) is unknown.

Nevertheless, combining the present results with a range of literature data has permitted some insight into the workings of spontaneous emulsion polymerisation. It has been shown that

application of the kinetic models derived for spontaneous bulk polymerisation (assuming that spontaneous radical generation involves only monomeric reactions) represents a useful starting point. The results obtained suggest that spontaneous initiation inside latex particles and monomer droplets is unlikely to be sufficient to account for observed rates of emulsion polymerisation. A more likely prospect is that significant spontaneous generation of radicals occurs *via* reactions of aqueous monomer. This suggestion is supported by a range of experimental results from the literature, the most notable of which is the observation of complete suppression of spontaneous polymerisation in the presence of an aqueous-phase radical scavenger.

It seems probable that the rate of spontaneous radical generation in emulsion systems is also significantly supplemented by other mechanisms, in particular, those involving peroxidic species present in the seed latex. Such species may be located in the aqueous phase or on the particle surface and their decomposition to form radicals will be significantly influenced by other chemical species present in the system.

In fact, a reasonably comprehensive picture of spontaneous initiation in emulsion systems has started to emerge, although it is not possible to explain all observations (*e.g.*, inhibition times and results with added Fe^{2+} and TEPA remain a mystery).

Finally, it is evident that there is broad scope for future research into spontaneous emulsion polymerisation. Some obvious areas for investigation arising from the work of this chapter are listed below:

- In order to more clearly establish the likelihood of an aqueous source of spontaneous radicals it is of interest to determine values of $\rho_{spont}N_c$ over a wide range of seed particle concentrations, and for a range of different seed latexes.

- Given the postulate of polymeric peroxides present in seed latexes, variation of the amount of dissolved oxygen present during seed synthesis should significantly affect the rate of spontaneous seeded polymerisation.

- The precise effects of seed latex heat-treatment on the value of ρ_{spont} should be determined by varying the heating period. The effect of heat-treatment in the presence of added reagents such as Fe^{2+} and amines should also be examined.

- Where spontaneous radical generation is thought to be aqueous phase in origin, experiments should be carried out in which seed latex particles are used after separation from their aqueous phase, or alternatively where the ratio of seed latex particles to seed latex aqueous phase is altered (*e.g.*, by removal of some seed particles *via* centrifugation). This would establish if it is non-monomeric species from the aqueous phase of the seed latex that are giving rise to spontaneous initiation, or whether the mechanism only involves monomer, *i.e.*, is bulk-like but occurring in the aqueous phase.

- Radical generation due to non-monomeric aqueous-phase species could also be investigated by extraction of a sample of the seed latex aqueous phase followed by analysis using electron spin resonance (ESR) spectroscopy or radical trapping techniques.

7.6 References

(1) Mayo, F. R. *J. Am. Chem. Soc.* **1968**, *90*, 1289.

(2) Hui, A. W.; Hamielec, A. E. *J. App. Polym. Sci.* **1972**, *16*, 749.

(3) Pryor, W. A.; Lasswell, L. D. *Adv. Free Radical Chem.* **1975**, *5*, 27.

(4) Stickler, M.; Meyerhoff, G. *Makromol. Chem.* **1978**, *179*, 2729.

(5) Hawkett, B. S.; Napper, D. H.; Gilbert, R. G. *J. Chem. Soc. Faraday Trans. 1* **1980**, *76*, 1323.

(6) Lansdowne, S. W.; Gilbert, R. G.; Napper, D. H.; Sangster, D. F. *J. Chem. Soc. Faraday Trans. 1* **1980**, *76*, 1344.

(7) Ballard, M. J.; Napper, D. H.; Gilbert, R. G. *J. Polym. Sci., Polym. Chem. Edn.* **1984**, *22*, 3225.

(8) Adams, M. E.; Russell, G. T.; Casey, B. S.; Gilbert, R. G.; Napper, D. H.; Sangster, D. F. *Macromolecules* **1990**, *23*, 4624.

(9) Christie, D. I.; Gilbert, R. G.; Congalidis, J. P.; Richards, J. R.; McMinn, J. H. *Macromolecules* **2001**, *34*, 5158.

(10) Moad, G.; Solomon, D. H. *The Chemistry of Free Radical Polymerization*; Pergamon: Oxford, 1995.

(11) Mayo, F. R. *Polym. Prepr., Am. Chem. Soc., Div. Polym. Chem.* **1961**, *2*, 55.

(12) Pryor, W. A.; Coco, J. H. *Macromolecules* **1970**, *3*, 500.

(13) Walling, C.; Briggs, E. R. *J. Am. Chem. Soc.* **1946**, *68*, 1141.

(14) Lingnau, J.; Stickler, M.; Meyerhoff, G. *Eur. Polym. J.* **1980**, *16*, 785.

(15) Lingnau, J.; Meyerhoff, G. *Macromolecules* **1984**, *17*, 941.

(16) Patnode, W. P.; Scheiber, W. J. *J. Am. Chem. Soc.* **1939**, *61*, 3449.

(17) Hutchinson, R. A.; Paquet, D. A., Jr.; McMinn, J. H. *Macromolecules* **1995**, *28*, 5655.

(18) Gilbert, R. G. *Emulsion Polymerization: A Mechanistic Approach*; Academic: London, 1995.

(19) Lacík, I.; Casey, B. S.; Sangster, D. F.; Gilbert, R. G.; Napper, D. H. *Macromolecules* **1992**, *25*, 4065.

(20) Hawkett, B. S., 1980, Ph.D. Thesis, University of Sydney.

(21) Lane, W. H. *Ind. Eng. Chem.* **1946**, *18*, 295.

(22) Rideout, D. C.; Breslow, R. *J. Am. Chem. Soc.* **1980**, *102*, 7816.

(23) Pindur, U.; Lutz, G.; Otto, C. *Chem. Rev.* **1993**, *93*, 741.

(24) Pai, C. K.; Smith, M. B. *J. Org. Chem.* **1995**, *60*, 3731.

(25) Kumar, A.; Volume 101, N. J. *Chem. Rev.* **2001**, *101*, 1.

(26) Furlani, T. R.; Gao, J. *J. Org. Chem.* **1996**, *61*, 5492.

(27) Meijer, A.; Otto, S.; Engberts, J. B. F. N. *J. Org. Chem.* **1998**, *63*, 8989.

(28) Lamb, D.; Anstey, J. F.; Fellows, C. M.; Monteiro, J. M.; Gilbert, R. G. *Biomacromolecules* **2001**, *2*, 518.

8. Extension of the Smith-Ewart Model for Emulsion Polymerisation Kinetics

8.1 Introduction

Over half a century ago Smith and Ewart[1] presented their pioneering work on the kinetics of emulsion polymerisation. While many important discoveries have been made in this field in the intervening period, it is to the credit of those authors that the fundamental concepts of their work remain undisputed to this day: namely, that the radical concentration inside the latex particles is determined (at least in a conventional emulsion polymerisation system) by the kinetics of radical entry, exit and intra-particle termination.

These principles were originally formalised mathematically by Smith and Ewart in a set of equations given by the following generic form (introduced in Chapter 1 of this thesis):

$$\frac{dN_n}{dt} = \rho N_{n-1} - [\rho + nk + n(n-1)c]N_n + (n+1)kN_{n+1} + (n+2)(n+1)cN_{n+2} \qquad (8.1)$$

where N_n is the fraction of latex particles containing n radicals, and ρ, k and c denote pseudo-first-order rate coefficients for entry, exit and intra-particle termination respectively. The average number of radicals per latex particle, $\bar{n}$, may then be defined as the first moment of the distribution of particle populations, N_n, as follows:

$$\bar{n} = \sum_{n=1}^{\infty} nN_n \qquad (8.2)$$

Given that $\bar{n}$ is readily obtained from the experimentally measured rate of an emulsion polymerisation, as shown in Chapter 1, the Smith-Ewart kinetic treatment provides a method for relating observable rate data to the fundamental physical and chemical processes taking place in the system.

However, this original treatment is not without its limitations. Firstly, as is clear from equation (8.1), Smith and Ewart assumed that all intra-particle radicals undergo exit at the

same rate, governed by the rate coefficient k. This assumption is certainly erroneous, given the low water solubility of large polymer molecules consisting of hundreds or thousands of hydrophobic monomer units, and exit is now understood[2-6] to be the result of chain transfer to monomer which yields a small radical, far more likely to escape into the aqueous phase. Secondly, the Smith-Ewart treatment assumes that the fate of all exited radicals is simply to undergo aqueous-phase termination. Of course, this neglects the possibility that such radicals may encounter and re-enter another latex particle, and that the flux of such re-entering radicals should therefore be added to that of initiator-derived radicals, ρ. Finally, the value of the first-order termination rate coefficient, c, in equation (8.1) is assumed to be independent of chain length. However, it is now understood that termination reactions are diffusion-controlled, with rate dependent on the chain lengths of the reacting radicals, and hence that the value of c may be sensitive to the precise radical chain length distribution in a given particle.

Perhaps surprisingly, despite sustained interest in the field of emulsion polymerisation kinetics, in the last fifty years the above issues have been addressed to only a limited extent in the context of the Smith-Ewart equations. Ugelstad *et al.*[3] recognised that exited radicals are not necessarily doomed to aqueous-phase termination, suggesting that ρ in equation (8.1) be replaced by an overall flux of entering and re-entering radicals of the form:

$$\rho_{total} = \rho + \alpha k\bar{n} \tag{8.3}$$

Here $k\bar{n}$ is the flux of exiting radicals and α the so-called "fate parameter", representing the fraction of exited radicals that undergo re-entry, and taking a value between the limits of $\alpha = 1$ (complete re-entry) and $\alpha = 0$ (complete aqueous-phase termination of exited radicals – either by "homo-termination" with other exited radicals, or by "hetero-termination" with initiator-derived radicals in a system with low entry efficiency). This original approach was extended by Whang *et al.*[7] in recognition of the possibility that exited radicals may also undergo hetero-termination with initiator-derived radicals which would otherwise have entered a latex particle. In this case the effect of exit is to reduce the flux of entering radicals below the value of ρ, hence a new lower limiting value of $\alpha = -1$ was introduced for the case of complete hetero-termination of this type for exited radicals. This approach was also employed by Ballard *et al.*[8] who elected to substitute a model-based value for k in equation (8.1) (recognising that exit is by monomeric radicals and assuming that the rate of exit is

identical to the rate of transfer to monomer in the particles) and used an iterative method to solve the coupled equations (8.1) – (8.3). While the incorporation of a fate parameter for exited radicals represented a significant conceptual improvement to the original Smith-Ewart model, this was by no means a definitive solution, since α encapsulates the combined effect of a variety of kinetic events (*e.g.*, adsorption, desorption, aqueous-phase radical reactions) without any means of relating its value to specific microscopic rate coefficients. Also, except in the cases of $\alpha = 1$ or -1, this parameter must itself be a dependent on the aqueous-phase radical concentration, and hence on $\bar{n}$, however the model conveys nothing as to the nature of this dependence.

Other solutions to the above limitations have been formulated in the context of approximations to the full Smith-Ewart equations. As explained in detail in Chapters 1 and 4 of this thesis, the "pseudo-bulk" model is found to be an accurate approximation to the Smith-Ewart equations under steady-state conditions where $\rho > c$ and/or $k > c$. Here the compartmentalisation of radicals into distinct reaction loci may be neglected and the emulsion system may be treated similarly to a bulk system. Using this approximation, Adams *et al.*[9] and Russell *et al.*[10] formulated kinetic models incorporating chain length dependent termination schemes. The approach of Adams *et al.* was to categorise radicals of various chain lengths as being either "short" or "long", defining a specific chain length at which the changeover from short to long occurs. In this way, termination involving two short radicals is distinguishable from termination involving a short and a long radical and termination between two long radicals. The model of Russell *et al.* went further to individually consider the population of radicals for each chain length (or at least for a narrow group of chain lengths – an approximation known as "coarse-graining") and thus distinguished termination involving every different pair of radical chain lengths. This model was used extensively in Chapters 4 and 6 and the reader is thus referred to those parts of this thesis for more detailed discussion.

Another approximation to the Smith Ewart equation is that which holds under conditions of $c \gg \rho, k$. Here the rate of intra-particle termination is sufficiently fast that two radicals may not occupy a given latex particle for any significant length of time without undergoing termination. Radical entry into an occupied particle results in "pseudo-instantaneous" termination and any given particle may only ever contain zero or one radical (on the timescale of entry and exit). Under such conditions full Smith-Ewart kinetics are accurately approximated by considering just the population balance equations for N_0- and N_1-type

particles (as shown in Chapter 4). This approach, known as the "zero-one" approximation, gives rise to considerably simpler mathematical solutions than the full set of equations. Using the zero-one approximation, Casey, Morrison *et al.*[4,5] formulated a kinetic model which constitutes the most thorough treatment of the kinetics of exit and re-entry presently available. This model includes a detailed account of all reactions involving monomeric radicals: their formation *via* transfer to monomer, the intra-particle reactions competing with exit, and the aqueous-phase reactions of exited radicals. This approach is seen to be far superior to the earlier fate parameter (α) approach in that here the kinetics of exit and re-entry are described entirely in terms of microscopic rate parameters, values for many of which are known or may be predicted with confidence. However, it is noted that the zero-one approximation restricts the use of the Casey-Morrison model to systems wherein $c \gg \rho, k$ and so $N_2, N_3, N_4, \ldots \approx 0$.

In view of the preceding discussion, the aims of the present work may now be clearly stated. Here we seek to bridge the gap that exists between the most kinetically complete form of the general Smith-Ewart model (*i.e.*, that incorporating α for re-entry[7,8]) and the most complete form of the zero-one model (*i.e.*, the Casey-Morrison model) by formulating an extended form of the Smith-Ewart model which includes all reactions of monomeric radicals and also allows for the case of $c \leq \rho, k$ (*i.e.*, where there may be more than a single radical in a given latex particle). This will provide a means for modelling emulsion polymerisation kinetics, based entirely on well-defined microscopic rate parameters, under a significantly wider range of conditions than is presently possible, and will obviate the use of the fate parameter, α. Importantly, it will also be shown that existing kinetic models (the Casey-Morrison zero-one model, the conventional Smith-Ewart model, and the pseudo-bulk model) may be obtained as limiting cases of this more general treatment.

It should be made clear that this work will not incorporate the kinetics of chain length dependent termination. In the setting of the Smith-Ewart equations, a chain length dependent termination scheme requires not only a knowledge of the number of radicals per latex particle, but also of the precise chain length distribution for the radicals in each particle. The significant increase in the number and complexity of differential equations required for such kinetic modelling presents a computational challenge that is presently suspected to be intractable.

8.2 Model Development

In this section we present the complete reaction scheme for the new model outlined above, which shall henceforth be referred to as the "extended Smith-Ewart model". The various reactions of each species involved are considered and the underlying assumptions of the model clearly specified. Finally, on the basis of this scheme the full set of rate equations required for kinetic modelling is formulated.

8.2.1 Reactions Pertaining to Intra-Particle Free Radicals

Central to this new model is the inclusion of the reactions of monomeric radicals, in both latex particle and aqueous phases, because it is these species that exit and re-enter. It is thus necessary to consider the population distributions of two different types of latex particles: those containing only polymeric radicals, and those containing up to one transfer-derived monomeric radical, whilst also containing any number of polymeric radicals. Here we distinguish these types of latex particles using nomenclature similar to that of the Casey-Morrison model, with N_n denoting the fraction of all particles containing n polymeric radicals (for $n \geq 0$), and N_n^{M} denoting the fraction containing one monomeric radical and $(n - 1)$ polymeric radicals (for $n \geq 1$). The following normalisation is then applied to the particle populations:

$$N_0 + \sum_{n=1}^{\infty} \left(N_n + N_n^{\mathrm{M}} \right) = 1 \tag{8.4}$$

The reaction scheme for all reactions impacting the populations of intra-particle radicals in the model is given below.

Entry of oligomeric radicals into latex particles is described by:

$$N_n \xrightarrow{\rho_{\mathrm{L}}} N_{n+1} \tag{8.5}$$

$$N_n^{\mathrm{M}} \xrightarrow{\rho_{\mathrm{L}}} N_{n+1}^{\mathrm{M}} \tag{8.6}$$

where ρ_{L} = pseudo-first-order entry rate coefficient for oligomeric (*i.e.*, non-monomeric) radicals.

Chain transfer to monomer is given by:

$$N_n \xrightarrow{nk_{tr}[M]_p} N_n^M \tag{8.7}$$

$$N_n^M \xrightarrow{(n-1)k_{tr}[M]_p} N_{n-2} \tag{8.8}$$

where k_{tr} = rate coefficient for transfer to monomer and $[M]_p$ = intra-particle monomer concentration. Equation (8.8) assumes pseudo-instantaneous termination of the two monomeric radicals.

Propagation of a monomeric radical in an N_n^M-type particle is:

$$N_n^M \xrightarrow{k_p^1[M]_p} N_n \tag{8.9}$$

where k_p^1 = intra-particle propagation rate coefficient for monomeric radical.

Desorption of a monomeric radical from an N_n^M-type particle is described by:

$$N_n^M \xrightarrow{k_{dM}} N_{n-1} + M_w^\bullet \tag{8.10}$$

where k_{dM} = desorption rate coefficient for monomer, used to approximate that for a monomeric radical.

Re-entry of an exited monomeric radical is:

$$N_n \xrightarrow{\rho_M} N_{n+1}^M \tag{8.11}$$

$$N_n^M \xrightarrow{\rho_M} N_{n-1} \tag{8.12}$$

where ρ_M = pseudo-first-order rate coefficient for re-entry. Again, equation (8.12) assumes pseudo-instantaneous termination of the two monomeric radicals.

Intra-particle termination is described in one of two ways. Termination of two polymeric radicals in an N_n-type particle is given by:

$$N_n \xrightarrow{n(n-1)c^{LL}} N_{n-2} \tag{8.13}$$

Here c^{LL} is the pseudo-first-order rate coefficient for intra-particle termination involving two polymeric radicals, defined as: $c^{LL} = k_t^{LL}/(N_A V_s)$, where k_t^{LL} is the second-order termination rate coefficient for the same process. Importantly, k_t^{LL} and c^{LL} are assumed to apply to termination of any pair of polymeric radicals, regardless of their chain lengths.

Termination of one polymeric and one monomeric radical in an N_n^M-type particle is then given by:

$$N_n^M \xrightarrow{(n-1)c^{ML}} N_{n-2} \tag{8.14}$$

Analogously to above, c^{ML} is the pseudo-first-order rate coefficient for intra-particle termination involving one monomeric and one polymeric radical, defined as: $c^{ML} = k_t^{ML}/(N_A V_s)$, where k_t^{ML} is the second-order termination rate coefficient for the same process. In this case k_t^{ML} and c^{ML} are assumed to apply to termination of a monomeric radical with a polymeric radical of any chain length.

It is noted that although the reactions involving c^{LL} and c^{ML} are written in a consistent manner, this results in a difference in the way that k_t^{LL} and k_t^{ML} are defined. A detailed explanation of the definition of termination rate coefficients is given in Appendix A.1.

Here it is assumed that termination of two polymeric radicals in an N_n^M-type particle will not occur before some other reaction involving the monomeric radical that is also present. This assumption is based on the high mobility and fast rates of reactions expected for monomeric radicals;[11-16] at the very least it is expected that monomeric-polymeric radical termination should precede polymeric-polymeric radical termination in an N_n^M-type particle. In practice, when k_t^{LL} is low one must have $k_t^{LL} \ll k_t^{ML}$, so the assumption is valid, and when k_t^{LL} is high, *i.e.*, $k_t^{LL} \geq k_t^{ML}$, it is likely that zero-one conditions will hold (as shown later in this work), in which event $N_n^M \approx 0$ for $n \geq 3$ (the only N_n^M-type particles in which LL-termination can occur).

We also choose not to entertain the possibility that particles may contain more than one monomeric radical, again based on the rapid reaction rates expected for monomeric radicals. We therefore impose the closure condition that formation of a second monomeric radical through transfer or re-entry of a monomeric radical from the aqueous-phase into a particle already containing one monomeric radical both result in pseudo-instantaneous termination of the monomeric radical pair. As will be seen from model calculations the relative concentration of particles containing one monomeric radical is generally very low. Thus it is unlikely that neglecting the far lower concentration of particles containing more than one monomeric radical will significantly compromise the accuracy of the model.

Finally, it is noted that intra-particle propagation of a polymeric radical (with rate coefficient k_p) is omitted from the above reaction scheme, *i.e.*, the reactions:

$$N_n \xrightarrow{k_p[M]_p} N_n \tag{8.15}$$

$$N_n^M \xrightarrow{k_p[M]_p} N_n^M \tag{8.16}$$

While this process affects the chain length of a given radical, it clearly does not change the number of radicals in any particle and may therefore be omitted in the present setting.

8.2.2 Reactions Pertaining to Exited Monomeric Free Radicals

We next consider the reaction scheme for monomeric radicals in the aqueous phase, denoted $M_w^\bullet$.

Desorption from N_n^M-type latex particles is as already shown in reaction (8.10), while re-entry of a monomeric radical into a latex particle has also been described in reactions (8.11) and (8.12), and is related to the aqueous concentration of monomeric radicals through the following definition of ρ_M:

$$\rho_M = k_{re} \frac{V_w}{V_r} [M_w^\bullet] \tag{8.17}$$

Here k_{re} is the second-order rate coefficient for re-entry of monomeric radicals and V_w/V_r is a volume correction accounting for the fact that the latex particles occupy a non-negligible portion of the total reaction volume (see Chapter 4).

Aqueous-phase termination is given by:

$$M_w^\bullet + T_w^\bullet \xrightarrow{2k_{t,w}} \text{inert products} \tag{8.18}$$

where $T_w^\bullet$ denotes any aqueous-phase radical species and $k_{t,w}$ the termination rate coefficient for aqueous radicals.

Aqueous-phase propagation is described by:

$$M_w^\bullet + M \xrightarrow{k_{p,w}^M} M_{2,w}^\bullet \tag{8.19}$$

$$M_{2,w}^\bullet \xrightarrow{\rho_{di}} \text{entry} \quad \text{(rapid)} \tag{8.20}$$

where M is a monomer molecule. Here it is assumed that aqueous-phase propagation of an exited radical, with rate coefficient $k_{p,w}^M$, produces a dimeric radical, $M_{2,w}^\bullet$, that rapidly undergoes re-entry into a particle. This assumption is intended to reflect the fact that exit-derived radicals contain no initiator end-group and their water-solubility is therefore expected to decrease dramatically with addition to monomer.[4] The pseudo-first-order rate coefficient for dimeric re-entry, ρ_{di}, is thus directly related to the rate of propagation of exited radicals as follows:

$$\rho_{di} = k_{p,w}^M [M]_w [M_w^\bullet] \frac{N_A}{N_c} \tag{8.21}$$

where $[M]_w$ and N_c are respectively the aqueous-phase concentrations of monomer and latex particles. Because dimeric radicals are highly hydrophobic, they will make a contribution to ρ_L.

8.2.3 Reactions Pertaining to Initiator-Derived and Spontaneously-Generated Free Radicals

Here we assume the Maxwell-Morrison model for entry of initiator-derived radicals,[17] which was shown to provide an accurate account for entry in various styrene and methyl methacrylate systems in Chapters 3 and 4 of this thesis. The kinetic scheme associated with that model is thus briefly revisited.

$$\text{initiator} \xrightarrow{fk_d} 2\,\text{I}^\bullet \tag{8.22}$$

$$\text{I}^\bullet + \text{M} \xrightarrow{k_{p\text{I,w}}} \text{IM}_1^\bullet \quad \text{(rapid)} \tag{8.23}$$

$$\text{IM}_i^\bullet + \text{M} \xrightarrow{k_{p,w}} \text{IM}_{i+1}^\bullet, \quad 1 \le i < z \tag{8.24}$$

$$\text{IM}_i^\bullet + \text{T}_w^\bullet \xrightarrow{2k_{t,w}} \text{inert products}, \quad 1 \le i < z \tag{8.25}$$

$$\text{IM}_z^\bullet \xrightarrow{\rho_{init}} \text{entry} \quad \text{(rapid)} \tag{8.26}$$

Here $\text{I}^\bullet$ is a primary free-radical produced by initiation, illustrated by the thermal decomposition of initiator with overall rate coefficient fk_d, $\text{IM}_i^\bullet$ is an aqueous-phase radical derived from initiator and containing i monomer units, $\text{IM}_z^\bullet$ is a surface-active radical (containing z monomer units) bound to undergo rapid entry, and reaction (8.23) is assumed to be extremely fast and thus non-rate-determining.[18-20] The pseudo-first-order rate coefficient for entry of initiator-radicals, ρ_{init}, is then directly related to the rate of propagation of $\text{IM}_{z-1}^\bullet$ radicals as follows:

$$\rho_{init} = k_{p,w}\,[\text{M}]_w\,[\text{IM}_{z-1}^\bullet]\,\frac{N_A}{N_c} \tag{8.27}$$

At this point we must also consider the contribution to entry from so-called "spontaneously-generated" radicals, *i.e.*, entry arising in the absence of any added initiator, which shall be denoted ρ_{spont}. While the value of ρ_{spont} is readily measured from experiment and a number of possible theories exist for its origin – as shown in Chapter 7 – there is at present no definitive mechanistic explanation for this phenomenon. Thus, for now at least, ρ_{spont} will be regarded as a flux of non-monomeric (*i.e.*, oligomeric) entering radicals that do not interact with any aqueous-phase radicals.

It is thus possible to define the pseudo-first-order rate coefficient for entry of all oligomeric radicals, ρ_L, [used in reactions (8.5) and (8.6)] as follows:

$$\rho_L = \rho_{init} + \rho_{spont} + \rho_{di} \tag{8.28}$$

8.2.4 *Formulated Rate Equations*

From reactions (8.5) – (8.14) the following rate equations are formulated for the two qualitatively different types of latex particles considered in this model:

$$\frac{dN_n}{dt} = \rho_L N_{n-1} - \left[\rho_L + \rho_M + n\,k_{tr}[M]_p + n(n-1)c^{LL}\right] N_n + (n+2)(n+1)c^{LL} N_{n+2} + k_p^1 [M]_p N_n^M + \left[\rho_M + k_{dM}\right] N_{n+1}^M + \left[k_{tr}[M]_p + c^{ML}\right](n+1) N_{n+2}^M \quad (8.29)$$

$$\frac{dN_n^M}{dt} = \rho_M N_{n-1} + n\,k_{tr}[M]_p N_n + \rho_L N_{n-1}^M - \left[\rho_L + \rho_M + k_{dM} + (n-1)k_{tr}[M]_p + k_p^1[M]_p + (n-1)c^{ML}\right] N_n^M \quad (8.30)$$

From reactions (8.17) – (8.21), together with earlier reactions (8.10) – (8.12), the rate equation obtained for aqueous monomeric radicals is:

$$\frac{d[M_w^\bullet]}{dt} = k_{dM}\frac{N_c}{N_A}\sum_{i=1}^{\infty} N_n^M - k_{p,w}^M [M]_w [M_w^\bullet] - 2k_{t,w}[T_w^\bullet][M_w^\bullet] - k_{re}\frac{N_c}{N_A}\frac{V_w}{V_r}[M_w^\bullet] \quad (8.31)$$

Reactions (8.22) – (8.26) give rise to the following rate equations for initiator-derived radicals:

$$\frac{d[IM_1^\bullet]}{dt} = 2fk_d[I] - k_{p,w}[M]_w[IM_1^\bullet] - 2k_{t,w}[T_w^\bullet][IM_1^\bullet] \quad (8.32)$$

$$\frac{d[IM_i^\bullet]}{dt} = k_{p,w}[M]_w\left([IM_{i-1}^\bullet] - [IM_i^\bullet]\right) - 2k_{t,w}[T_w^\bullet][IM_i^\bullet], \quad 1 < i < z \quad (8.33)$$

here [I] denotes the aqueous-phase concentration of initiator. The total concentration of aqueous-phase radicals may then be defined as the sum of all radicals derived from initiator and exit to give:

$$[T_w^\bullet] = [M_w^\bullet] + [M_{2,w}^\bullet] + [I^\bullet] + \sum_{i=1}^{z}[IM_i^\bullet] \approx [M_w^\bullet] + \sum_{i=1}^{z-1}[IM_i^\bullet] \quad (8.34)$$

where the concentrations of $M_{2,w}^\bullet$, $I^\bullet$ and $IM_z^\bullet$ are assumed to be vanishingly small due to their rapid rates of reaction.

Finally, $\bar{n}$ must be redefined in terms of both the N_n and N_n^M particle populations as follows:

$$\bar{n} = \sum_{n=1}^{\infty} n\left(N_n + N_n^{\mathrm{M}}\right) \tag{8.35}$$

8.3 Numerical Solutions

Equations (8.29) – (8.35) together with the definitions for entry rate coefficients in equations (8.17), (8.21), (8.27) and (8.28) comprise the complete set of equations required for kinetic modelling. These equations may now be solved numerically to give values for all radical and particle populations and hence a value of $\bar{n}$ for the system. Here we present a method for obtaining steady-state solutions to the above equations. This approach is consistent with the work of this thesis being mainly concerned with particle growth kinetics in Interval II of emulsion polymerisation, under which conditions the steady-state approximation generally holds. However, this is not to suggest that modelling of polymerisation under non-steady-state conditions is never of interest, important examples of this being polymerisation with an intermittent source of initiation (*e.g.*, γ-relaxation), and polymerisation at high weight fraction of polymer (w_p) where the gel effect is operative. Under these conditions it may be necessary to use alternative numerical methods to those given here in order to obtain time-dependent solutions to the rate equations presented above. Specifically, numerical solution of at least equation (8.29) would be required, with the following steady-state solutions possibly still being valid even under conditions such that $\bar{n}$ changes rapidly.

Applying the steady-state approximation to rate equations (8.29) – (8.33) yields the following steady-state populations:

$$N_n = \frac{\rho_{\mathrm{L}} N_{n-1} + (n+2)(n+1)c^{\mathrm{LL}} N_{n+2} + k_{\mathrm{p}}^1[\mathrm{M}]_{\mathrm{p}} N_n^{\mathrm{M}} + \left[\rho_{\mathrm{M}} + k_{\mathrm{dM}}\right] N_{n+1}^{\mathrm{M}} + \left[k_{\mathrm{tr}}[\mathrm{M}]_{\mathrm{p}} + c^{\mathrm{ML}}\right](n+1) N_{n+2}^{\mathrm{M}}}{\rho_{\mathrm{L}} + \rho_{\mathrm{M}} + n k_{\mathrm{tr}}[\mathrm{M}]_{\mathrm{p}} + n(n-1)c^{\mathrm{LL}}},$$

$$n \geq 0 \tag{8.36}$$

$$N_n^{\mathrm{M}} = \frac{\rho_{\mathrm{M}} N_{n-1} + n\, k_{\mathrm{tr}}[\mathrm{M}]_{\mathrm{p}} N_n + \rho_{\mathrm{L}} N_{n-1}^{\mathrm{M}}}{\rho_{\mathrm{L}} + \rho_{\mathrm{M}} + k_{\mathrm{dM}} + (n-1)\, k_{\mathrm{tr}}[\mathrm{M}]_{\mathrm{p}} + k_{\mathrm{p}}^1[\mathrm{M}]_{\mathrm{p}} + (n-1)\, c^{\mathrm{ML}}}, \quad n \geq 1 \tag{8.37}$$

$$[\mathrm{M}_{\mathrm{w}}^{\bullet}] = \frac{k_{\mathrm{dM}} \dfrac{N_{\mathrm{c}}}{N_{\mathrm{A}}} \displaystyle\sum_{i=1}^{\infty} N_n^{\mathrm{M}}}{k_{\mathrm{p,w}}^{\mathrm{M}}[\mathrm{M}]_{\mathrm{w}} + 2\, k_{\mathrm{t,w}}[\mathrm{T}_{\mathrm{w}}^{\bullet}] + k_{\mathrm{re}} \dfrac{N_{\mathrm{c}}}{N_{\mathrm{A}}} \dfrac{V_{\mathrm{w}}}{V_{\mathrm{r}}}} \tag{8.38}$$

$$[\mathrm{IM}_1^\bullet] = \frac{2fk_\mathrm{d}[\mathrm{I}]}{k_{\mathrm{p,w}}[\mathrm{M}]_\mathrm{w} + 2k_{\mathrm{t,w}}[\mathrm{T}_\mathrm{w}^\bullet]} \tag{8.39}$$

$$[\mathrm{IM}_i^\bullet] = \frac{k_{\mathrm{p,w}}[\mathrm{M}]_\mathrm{w}[\mathrm{IM}_{i-1}^\bullet]}{k_{\mathrm{p,w}}[\mathrm{M}]_\mathrm{w} + 2k_{\mathrm{t,w}}[\mathrm{T}_\mathrm{w}^\bullet]} = [\mathrm{IM}_1^\bullet]\left(\frac{k_{\mathrm{p,w}}[\mathrm{M}]_\mathrm{w}}{k_{\mathrm{p,w}}[\mathrm{M}]_\mathrm{w} + 2k_{\mathrm{t,w}}[\mathrm{T}_\mathrm{w}^\bullet]}\right)^{i-1} \quad 1 < i < z) \tag{8.40}$$

8.3.1 Truncation of Calculation

For the sake of computational efficiency it is desirable to reduce the infinite set of equations (8.36) and (8.37) to the minimum number required to obtain an accurate solution. To this end, we adopt a truncation procedure similar to that used by Ballard *et al.*[21] in finding steady-state solutions of the Smith-Ewart equations. This approach relies on the fact that in the limit of large n the values of N_n and N_n^M become very small, making a negligible contribution to the value of $\bar{n}$. Thus, we specify a truncation value of $n = m$ such that $N_n = N_n^\mathrm{M} = 0$ is assumed for all $n > m$. Under any given set of conditions the truncation value m may be increased to the point where this approximation becomes accurate. Additional closure conditions must also be applied to the particle populations at the truncation limit. Specifically, we assume that radical entry (or re-entry) into either an N_m or N_m^M particle results in instantaneous termination to give an N_{m-1} particle:

$$N_m^\mathrm{M} \xrightarrow{\rho_\mathrm{L}} N_{m-1} \tag{8.41}$$

$$N_m \xrightarrow{\rho_\mathrm{L}} N_{m-1} \tag{8.42}$$

$$N_m \xrightarrow{\rho_\mathrm{M}} N_{m-1} \tag{8.43}$$

As a result of this truncation procedure, the steady-state populations of N_m and N_{m-1} are given by the following modified forms of equation (8.36):

$$N_{m-1} = \frac{\rho_\mathrm{L}N_{m-2} + k_\mathrm{p}^1[\mathrm{M}]_\mathrm{p}N_{m-1}^\mathrm{M} + [\rho_\mathrm{L} + \rho_\mathrm{M}]N_m + [\rho_\mathrm{L} + \rho_\mathrm{M} + k_\mathrm{dM}]N_m^\mathrm{M}}{\rho_\mathrm{L} + \rho_\mathrm{M} + (m-1)k_\mathrm{tr}[\mathrm{M}]_\mathrm{p} + (m-1)(m-2)c^\mathrm{LL}} \tag{8.44}$$

$$N_m = \frac{\rho_\mathrm{L}N_{m-1} + k_\mathrm{p}^1[\mathrm{M}]_\mathrm{p}N_m^\mathrm{M}}{\rho_\mathrm{L} + \rho_\mathrm{M} + m\,k_\mathrm{tr}[\mathrm{M}]_\mathrm{p} + m\,(m-1)\,c^\mathrm{LL}} \tag{8.45}$$

Although the truncation procedure also changes the result of oligomeric entry into N_m^M particles [which now gives an N_{m-1} particle according to equation (8.41)], the steady-state equation for N_m^M is unchanged from the general form of equation (8.37).

It is noted that the general set of equations presented in this section applies to a system wherein the maximum number of radicals per particle (either polymeric or monomeric) is $m \geq 3$. Truncation with either of $m = 1$ or $m = 2$ constitutes a special case, as detailed in the following section.

A detailed description of the computational method used to obtain full numerical solutions to the Extended Smith-Ewart model is provided in Appendix A.6. Briefly, we begin with a rough approximation for all radical and particle populations and an iterative routine is used to calculate improved values from the coupled steady-state equations (8.36) – (8.45) until self-consistency is achieved. This process is then repeated with the truncation number of radicals per particle, m, being successively increased until there is negligible change in the value of $\bar{n}$ (typically, a relative change in $\bar{n}$ of less than ~ 10^{-8} is specified).

8.4 Special Cases of the Extended Smith-Ewart Model

8.4.1 Truncation with m = 1: a "Zero-One" Model

In the limit of $m = 1$ (only one radical – either monomeric or polymeric – per particle) the general set of rate equations reduces to the three equations shown below, together with the full set of equations for aqueous-phase radicals, $M_w^\bullet$, $IM_1^\bullet$ and $IM_i^\bullet$, in the same form as given previously (and therefore omitted here). As is evident from the absence of any termination rate coefficients, intra-particle termination is assumed to occur rapidly upon radical entry into an occupied particle.

$$\frac{dN_0}{dt} = -\left[\rho_L + \rho_M\right] N_0 + \left[\rho_L + \rho_M\right] N_1 + \left[\rho_L + \rho_M + k_{dM}\right] N_1^M \tag{8.46}$$

$$\frac{dN_1}{dt} = \rho_L N_0 - \left[\rho_L + \rho_M + k_{tr}\,[M]_p\right] N_1 + k_p^1\,[M]_p\, N_1^M \tag{8.47}$$

$$\frac{dN_1^M}{dt} = \rho_M N_0 + k_{tr}\,[M]_p\, N_1 - \left[\rho_L + \rho_M + k_{dM} + k_p^1\,[M]_p\right] N_1^M \tag{8.48}$$

This truncated model will only be an accurate approximation to the general extended Smith-Ewart model under conditions of low $\bar{n}$. However, finding numerical solutions to the set of zero-one rate equations is a considerably simpler computational task than in the general case.

Importantly, this limiting form of the general equations is almost identical to the zero-one model formulated by Casey *et al.*[4] Those authors have presented a thorough discussion of their equations and the limits to which they lead. The only discrepancy between the two models is the inclusion of the propagation term in equation (8.31) of the present model. Casey *et al.* specifically excluded aqueous-phase propagation of exited radicals from their model, however this may be a significant kinetic process for monomers with appreciable water-solubility (*e.g.*, MMA). The model represented by the above set of rate equations will henceforth be referred to as the "extended zero-one model".

8.4.2 Truncation with m = 2: a "Zero-One-Two" Model

In the other special case of truncation with $m = 2$ we obtain a so-called "zero-one-two" model with the general equations reducing to the set of five equations shown below. The idea of this model is to retain zero-one character but at the same time allow for some non-instantaneous termination.[22]

$$\frac{dN_0}{dt} = -\left[\rho_L + \rho_M\right] N_0 + 2\, c^{LL} N_2 + \left[\rho_M + k_{dM}\right] N_1^M + \left[k_{tr}\,[M]_p + c^{ML}\right] N_2^M \tag{8.49}$$

$$\frac{dN_1}{dt} = \rho_L N_0 - \left[\rho_L + \rho_M + k_{tr}\,[M]_p\right] N_1 + \left[\rho_L + \rho_M\right] N_2 + k_p^1\,[M]_p\, N_1^M + \left[\rho_L + \rho_M + k_{dM}\right] N_2^M \tag{8.50}$$

$$\frac{dN_2}{dt} = \rho_L N_1 - \left[\rho_L + \rho_M + 2\, k_{tr}\,[M]_p + 2\, c^{LL}\right] N_2 + k_p^1\,[M]_p\, N_2^M \tag{8.51}$$

$$\frac{dN_1^M}{dt} = \rho_M N_0 + k_{tr}\,[M]_p N_1 - \left[\rho_L + \rho_M + k_{dM} + k_p^1\,[M]_p\right] N_1^M \tag{8.52}$$

$$\frac{dN_2^M}{dt} = \rho_M N_1 + 2\, k_{tr}\,[M]_p\, N_2 + \rho_L N_1^M - \left[\rho_L + \rho_M + k_{dM} + k_{tr}\,[M]_p + k_p^1\,[M]_p + c^{ML}\right] N_2^M \tag{8.53}$$

Once again, a reduction in the number of rate equations here offers computational advantages over the general ($m \geq 3$) case. However, the zero-one-two model will also only be a good approximation under conditions of relatively low $\bar{n}$.

Ultimately, the accuracy of the zero-one and zero-one-two models derived here may only be established for a given system by comparison with calculations using the general form of the extended Smith-Ewart model. This will be shown in due course.

8.5 Application of Extended Smith-Ewart Model to Styrene Systems

We now examine the kinetic modelling methodology developed over the preceding sections by applying it to exemplary emulsion polymerisation systems. Firstly, we look at the Interval II seeded polymerisation of styrene at 50°C using potassium persulfate as initiator – a well-studied system for which literature values of many required rate parameters are available.

8.5.1 Comparison of Extended Smith-Ewart and Zero-One Models

For some time the Interval II emulsion polymerisation of styrene using small particles (*e.g.* those of $r_s = 44$ nm, as used in modelling here) has been thought to be accurately described by a zero-one kinetic scheme.[6] This supposition originated with the observation of a plateau at $\bar{n} = 0.5$ in kinetic experiments with high initiator concentration conducted by Hawkett *et al.*[23] (consistent with the zero-one model when the rate of entry greatly exceeds the rate of exit), and was subsequently rationalised by Casey *et al.*[4] on the basis of a detailed comparison of estimated rate parameters. Central to the zero-one approximation is the assumption that two radicals occupying a given particle will undergo termination before radical entry or exit can occur – termination is "pseudo-instantaneous". Given that the extended Smith-Ewart model developed here allows for a particle to be occupied by more than one radical, this new model presents a means for testing the accuracy of the zero-one approximation under a given set of experimental conditions. As a first step we now apply this methodology to the styrene/persulfate system.

Table 8.1. Standard simulation parameter values used for extended Smith-Ewart modelling of styrene emulsion polymerisations at 50°C.

Simulation parameter	Value
m_p^0 / g	0.85
m_M^{tot} / g	5.0
r_s / nm	44
N_c / dm^{-3}	1.3×10^{17}
V_r / dm^3	0.06
$[M]_p$ / M	5.8
$[M]_w$ / M	4.3×10^{-3}
k_{dM} / s^{-1}	1.7×10^3
fk_d / s^{-1}	1.1×10^{-6}
z	2
ρ_{spont} / s^{-1}	0
k_{tr} / M^{-1} s^{-1}	9.3×10^{-3}
k_p / M^{-1} s^{-1}	258
k_p^1 / k_p	4
k_t^{ML} / M^{-1} s^{-1}	6×10^8
k_t^{LL} / M^{-1} s^{-1}	300
$k_{re,coll}$ / M^{-1} s^{-1}	5×10^{11}
$k_{re} / k_{re,coll}$	1
$k_{p,w}$ / M^{-1} s^{-1}	258
$k_{p,w}^M / k_{p,w}$	4
$k_{t,w}$ / M^{-1} s^{-1}	3.7×10^9

A "standard" set of parameter values used for all styrene/persulfate model calculations here – except where variations are otherwise specified – is given in Table 8.1. Here m_p^0 and m_M^{tot} are the initial masses of polymer and monomer respectively and r_s is the swollen particle radius. The value for $[M]_p$ is an average of the values measured experimentally in Chapter 3 of this thesis and that of Hawkett *et al.*[23] and $[M]_w$ is as measured by Lane.[24] The rate coefficient for persulfate decomposition is taken from Behrman and Edwards,[25] and the value of z for styrene/persulfate is that predicted by the Maxwell-Morrison entry model[17] and verified experimentally in Chapter 3. For simplicity we ignore the entering flux of spontaneously-generated radicals here, assuming $\rho_{spont} = 0$, although this contribution may be trivially included if it is accurately known for a given system. The value of k_{tr} is that from the k_{tr}/k_p reported by Tobolsky and Offenbach,[26] while k_p is from an IUPAC working party[27] and the value of k_p^1 is that inferred from fitting of exit rate data.[5] We assume the values of the monomeric and long chain propagation rate coefficients for aqueous radicals to be the same as their intra-particle equivalents, and use the value of $k_{t,w}$ adopted by Maxwell *et al.*[17]

k_{dM} is calculated according to equation (8.54) from the literature,[3,6] and which is derived in Appendix A.5.

$$k_{dM} = \frac{3D_w[M]_w}{r_s^2[M]_p} \tag{8.54}$$

Here the value of the diffusion coefficient for monomer in water, $D_w = 1.5 \times 10^{-9}$ m^2 s^{-1}, is taken from Wilke and Chang.[28]

We next assume that re-entry of monomeric radicals and intra-particle termination between a monomeric and a non-monomeric radical are both diffusion-controlled processes, and hence estimate values for k_{re} and k_t^{ML} using the Smoluchowski equation.

$$k_{re,coll} = 4\pi D_w r_s N_A \tag{8.55}$$

Equation (8.55) assumes that encounter between an aqueous monomeric radical and a latex particle results in a successful re-entry event, giving a value for $k_{re,coll}$ of order 5×10^{11} M^{-1} s^{-1}.

k_t^{ML} is defined as described in Appendix A.1 to give:

$$k_t^{ML} = 4\pi\sigma p_{spin} D_{ML} N_A \tag{8.56}$$

Here we assume literature values[29] for the interaction radius, $\sigma = 3$ Å, and the probability of radical-radical reaction based on spin alignments, $p_{spin} = 0.25$. The mutual diffusion coefficient for monomeric and non-monomeric radicals inside a particle may be taken as the sum of the diffusion coefficients for each of the two species, $D_{ML} = D_M + D_L$. We then make the approximation that $D_M \gg D_L$, and hence that $D_{ML} \approx D_M$; *i.e.*, we assume that the rate of "ML-termination" is dictated solely by diffusion of the monomeric radical. Adopting a value of $D_M \approx 10^{-9}$ m^2 s^{-1} (in line with experimental measurements[16]), equation (8.56) then yields a value for k_t^{ML} of approximately 6×10^8 M^{-1} s^{-1}. Since the value of D_L will actually be an average diffusion coefficient for all non-monomeric radicals (from dimeric up to longest chain lengths), the approximation of $D_{ML} \approx D_M$ will result in a slight underestimate of the value of k_t^{ML}. However, given that $D_L \leq D_M$ an upper bound for D_{ML} must be $D_{MM} = 2D_M$. Hence it is safe to assume that the true value of k_t^{ML} will be, at most, a factor of two greater than the value calculated above.

The calculated value for k_t^{ML} may be compared with the results of Chapter 6, where values of $k_t^{1,1}$ were obtained from fitting of γ-relaxation data. Given the assumption above that ML-termination involves a highly mobile monomeric radical and a relatively immobile longer chain radical, and taking into account the different definitions used for the termination rate coefficients k_t^{ML} and $k_t^{1,1}$ (discussed in Appendix A.1), we can approximate here that $k_t^{ML} \approx k_t^{1,1}$, giving k_t^{ML} in the range of $10^8 - 10^9$ M^{-1} s^{-1}. Thus, the calculated value of k_t^{ML} agrees with experimental inferences.

It remains only to specify a value for the rate coefficient for termination involving two non-monomeric radicals, k_t^{LL}. Once again, assuming a diffusion-controlled termination model the value of k_t^{LL} may be estimated as follows (as described in Appendix A.1):

$$k_t^{LL} = 2\pi\sigma p_{spin} D_{LL} N_A \tag{8.57}$$

where D_{LL} is the average mutual diffusion coefficient for any two non-monomeric radicals. The value of D_{LL} is not straightforward to estimate given the wide range of chain lengths of non-monomeric radicals typically present. As a first approximation we may consider the

limiting case of two long radical chains inside a particle. At a weight fraction of polymer typical for Interval II of a seeded polymerisation ($w_p \approx 0.3$) the translational diffusion of such chains may be negligible compared to the motion of the radical sites by "reaction diffusion",[30] giving:

$$D_{LL} = 2\,D_L = 2\,\frac{k_p[M]_p a^2}{6} = \tfrac{1}{3}\,k_p[M]_p a^2 \qquad (8.58)$$

where a is the root-mean-square end-to-end distance per square root of the number of monomer units in a polymer chain. Using a literature value of $a \approx 7$ Å,[29,30] and further assuming that the slow encounter of long chains gives rise to $p_{spin} \approx 1$, equations (8.57) and (8.58) predict a value of k_t^{LL} of order 300 M^{-1} s^{-1} in the reaction diffusion limit. This value will clearly be a lower bound for the value of k_t^{LL} given that "LL-termination" actually involves all non-monomeric radicals, from long chains down to short oligomers.

In Figures 8.1 and 8.2 are presented values of $\bar{n}$ calculated using the extended Smith-Ewart model with parameter values as in Table 8.1 (except where otherwise stated) over a range of initiator concentrations. Also presented are the values of $\bar{n}$ calculated under identical conditions using the extended zero-one model of section 8.4.1. Importantly, it was found that calculations using the Casey-Maxwell zero-one model[4] were in exact agreement with those from the "extended zero-one model" under the present conditions.

The plateau at $\bar{n} = 0.5$ predicted by the zero-one model at high initiator concentration (and thus high entry rate) is clearly evident in Figure 8.2. However, it is also clear that the results obtained from the extended Smith-Ewart model, using the standard parameter set of Table 8.1 (with $k_{tr} = 9.3 \times 10^{-3}$ M^{-1} s^{-1} and $k_t^{ML} = 6 \times 10^8$ M^{-1} s^{-1}), agree with the zero-one model only when $\bar{n}$ is very low (*i.e.*, at low initiator concentration), and, moreover, that no $\bar{n} = 0.5$ plateau is observed at high initiator concentration. This would seem to indicate that the zero-one model's assumption of pseudo-instantaneous termination does not hold under all conditions for this system.

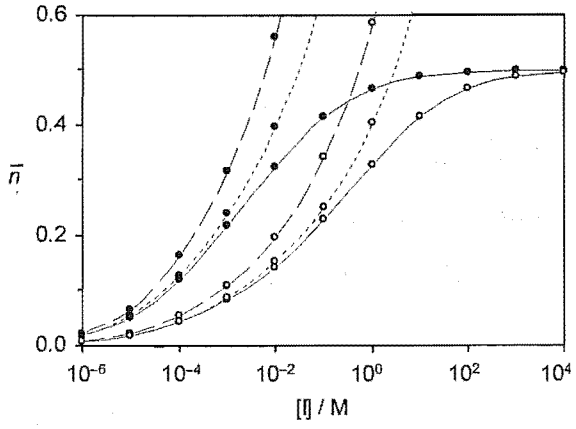

Figure 8.1. Steady-state $\bar{n}$ as a function of initiator concentration for Interval II seeded emulsion polymerisation of styrene at 50°C; calculations for $k_{tr} = 9.3 \times 10^{-3}$ M^{-1} s^{-1} (filled circles) and $k_{tr} = 9.3 \times 10^{-2}$ M^{-1} s^{-1} (empty circles) using the extended zero-one model (—●————●— and —o————o—), and using the extended Smith-Ewart model with $k_t^{ML} = 6 \times 10^8$ M^{-1} s^{-1} (—●—— ——●— and —o—— ——o—) or $k_t^{ML} = 6 \times 10^9$ M^{-1} s^{-1} (—●— – – —●— and —o— – – – —o—).

Given the means used to estimate some of the parameter values for modelling here, it is reasonable to suspect that uncertainty in one or more of these values may offer some explanation for the discrepancy between the results of the general and zero-one models. Of most interest are the parameters related to intra-particle termination: k_t^{ML}, k_t^{LL} and k_{tr}.

In their treatment of the zero-one model Casey *et al.*[4] reasoned that bimolecular termination inside a latex particle will be pseudo-instantaneous provided that the following conditions are met:

- termination involving a monomeric radical and a non-monomeric radical is more rapid than desorption or propagation of a monomeric radical; *i.e.*, $c^{ML} > k_{dM}$, $k_p^1 [M]_p$
- chain transfer to monomer inside a latex particle is more rapid than entry of non-monomeric radicals; *i.e.*, $k_{tr}[M]_p > \rho_L$

Under these circumstances, if two radicals occupy the same particle and one is monomeric, ML-termination will rapidly ensue. Alternatively, if both radicals are non-monomeric, one

will undergo transfer to monomer and subsequent ML-termination will occur before a third radical is able to enter the particle.

Calculations by Casey *et al.* demonstrated that the first of the above conditions should be met for styrene systems with particles of swollen radius less than ~ 100 nm. However, it is noted that those calculations used an earlier model to estimate a value for k_t^{ML} (and hence of c^{ML}) an order of magnitude higher than that used in the present work (because they assumed $p_{spin} = 1$ and σ about a factor of 2 too high). Furthermore, the treatment of Casey *et al.* did not take into account the enhancement of k_p for monomeric radicals ($k_p^1 \approx 4k_p$ for styrene[5]). Using the parameter values of Table 8.1 one finds that for the present system it is actually the case that $c^{ML} \approx k_p^1[M]_p$. In order to establish whether this explains the observed discrepancy between the general and zero-one models the calculations are therefore repeated with an order of magnitude increase in the value of k_t^{ML} (giving $c^{ML} > k_p^1[M]_p$). The data presented in Figure 8.2 show that this change significantly extends the range of conditions over which general and zero-one models agree, however the results still diverge towards high initiator concentration, and there is no evidence of a plateau in the value of $\bar{n}$ from the general model.

Turning next to the second condition imposed above, Casey *et al.* also recommended that the zero-one model is only accurate when $\rho_L < k_{tr}[M]_p$. Thus, an increase in the value of k_{tr} may improve the agreement between the general and zero-one models at higher initiator concentrations. Based on reported results for transfer to monomer in styrene systems[26,31,32] it seems reasonable to expect some degree of uncertainty in k_{tr} (at least a factor of two or three). The sensitivity of the modelled results to the likely uncertainty in k_{tr} may therefore be determined from calculations conducted using the parameter values of Table 8.1 but with an order of magnitude increase in the value of k_{tr}. In Figure 8.2 it is seen that this change results in agreement between the general and zero-one models over a significantly broader range of initiator concentrations, and that this effect is further enhanced by a simultaneous increase in the value of k_t^{ML}. It should be noted, however, that accompanying the increase in k_{tr} is a general decrease in the modelled value of $\bar{n}$. So while the agreement between the two models extends to higher initiator concentration, the range of $\bar{n}$ values over which the zero-one approximation holds is the same irrespective of the value of k_{tr}. Further, even with the order of magnitude increases in both k_t^{ML} and k_{tr}, an $\bar{n} = 0.5$ plateau is still not observed with the extended Smith-Ewart model.

At this stage it is pointed out that the practicable range of initiator concentrations used in seeded emulsion polymerisations will usually not exceed 1×10^{-1} M. On the basis of the results in Figure 8.2 it seems that in order for the zero-one approximation to be accurate over this range of initiator concentration the values of k_t^{ML} and k_{tr} must be at least an order of magnitude higher than the best estimates presented in Table 8.1. Furthermore, it appears that even assuming these improbably high parameter values the zero-one approximation will not be valid for the styrene/persulfate system when $\bar{n}$ is greater than 0.3. Hence no plateau at $\bar{n} = 0.5$ should be observed for this system.

Importantly, the approach of Casey *et al.* assumes that pseudo-instantaneous termination is provided solely by way of ML-termination. Thus, the two requirements listed earlier ($c^{ML} > k_{dM}$, $k_p^1[M]_p$ and $k_{tr}[M]_p > \rho_L$) identify conditions where the zero-one approximation is accurate, without needing to take account of the possibility of LL-termination. However, the value of k_t^{LL} may well be significant in determining whether or not a system is zero-one.

As described earlier, the value of k_t^{LL} quoted in Table 8.1 is a lower bound value corresponding to long chains whose motion is by reaction-diffusion only. Recognising that k_t^{LL} governs mutual termination of all non-monomeric radicals – many of which will not be restricted to reaction-diffusion – a preferable estimate for k_t^{LL} would be some sort of average over all (non-monomeric) chain lengths. Such an estimate may be obtained *a priori* from a detailed model for chain length dependent termination, such as that used in Chapters 4 and 6. However a simpler approach is to estimate k_t^{LL} from the (chain length averaged) values of $\langle k_t \rangle$ measured from γ-relaxation experiments. Measurements of $\langle k_t \rangle$ for large-particle pseudo-bulk styrene systems by Adams *et al.*,[9] Scheren *et al.*[33] and Clay *et al.*[31] suggest a value of order $\langle k_t \rangle = 1 \times 10^6$ M^{-1} s^{-1} for the Interval II conditions ($w_p \approx 0.3$) modelled here. It is noted that the value of $\langle k_t \rangle$ measured from γ-relaxation will include a contribution from termination of monomeric radicals (which should strictly be excluded from the value of k_t^{LL} sought here), therefore this value must constitute an upper bound to the true value of k_t^{LL}.

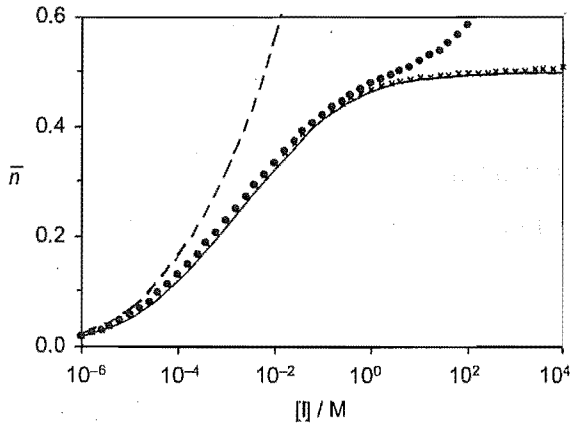

Figure 8.2. Steady-state $\bar{n}$ as a function of initiator concentration for Interval II seeded emulsion polymerisation of styrene at 50°C; calculations for $k_{tr} = 9.3 \times 10^{-3}$ M^{-1} s^{-1} using the extended zero-one model (————), and using the extended Smith-Ewart model with $k_t^{LL} = 3 \times 10^2$ M^{-1} s^{-1} (— — —), $k_t^{LL} = 1 \times 10^6$ M^{-1} s^{-1} (• • • •), or $k_t^{LL} = 1 \times 10^8$ M^{-1} s^{-1} (× × × ×).

In Figure 8.2 are presented results from model calculations using the original parameter values of Table 8.1, but with k_t^{LL} spanning several orders of magnitude. It is evident that when the rate coefficient for LL-termination is increased in line with the estimate from γ-relaxation data, the general and zero-one models are in good agreement for modelling with initiator concentration up to at least 10 M. Significantly, these results are obtained without any change to the original best estimates for k_t^{ML} and k_{tr} from Table 8.1. However, it should also be noted that in order to observe an appreciable plateau at $\bar{n} = 0.5$ a value of $k_t^{LL} = 1 \times 10^8$ M^{-1} s^{-1} is required – well outside the estimated range.

On the basis of the extended Smith-Ewart modelling results above, it therefore seems likely that the zero-one model will provide an accurate account of the kinetics over the range of practicable conditions for the styrene/persulfate system. Importantly, this modelling reveals that under conditions of high initiator concentration, where $\bar{n} > 0.3$, the zero-one assumption of pseudo-instantaneous termination is not guaranteed by ML-termination alone (a requirement of the Casey *et al.* approach). However, termination between non-monomeric radicals is likely to be sufficiently rapid for the zero-one approximation to remain accurate. Finally, the calculations here suggest that the plateau at $\bar{n} = 0.5$ given by the zero-one model may well not be attained under realistic experimental conditions for styrene emulsion systems.

One might therefore wonder if Hawkett *et al.*[23] really observed such a plateau. If they did it would suggest that k_t^{LL} is higher in these systems than can currently be explained.

It is interesting to note that the results of Figure 8.2 obtained with $k_t^{LL} = 1 \times 10^6$ M^{-1} s^{-1} indicate that the plateau at $\bar{n} = 0.5$ may also be approached from higher $\bar{n}$. This trend in $\bar{n}$ appears to be similar to that observed by Lamb *et al.* in a system using a redox initiator.[34] In such systems a high flux of radicals from redox initiator makes it possible to obtain values of $\bar{n}$ in excess of 0.5.

At this point it is also relevant to mention a useful alternative approach for assessing whether or not a system will be zero-one in nature, proposed by Maeder and Gilbert.[35] This approach determines the probability of termination for two radicals propagating inside a latex particle and how this probability varies with changing radical chain length.

8.5.2 Comparison of Extended Zero-One and Casey-Morrison Zero-One Models

As remarked above, it was found in all calculations for the styrene/persulfate system of the previous section that the results obtained using the extended zero-one model (derived from the extended Smith-Ewart model using a truncation number of radicals $m = 1$) were identical to the results obtained using the zero-one model of Casey *et al.*[4] The only difference between these two models is the added allowance for propagation of exited monomeric radicals (followed by rapid entry of the dimeric radical species produced) in the extended zero-one model. The observed agreement may therefore be attributed to the very low water solubility of styrene, which gives rise to a negligible probability of aqueous-phase propagation occurring before either re-entry into a latex particle or termination with an aqueous radical species.

It is therefore of interest to establish the conditions under which aqueous-phase propagation of exited radicals is kinetically significant. A consideration of aqueous-phase reaction rates for exited radicals [using equations (4.49) of Chapter 4] reveals that monomeric radical re-entry is by far the most probable fate for this system, so long as this process is assumed to be diffusion-limited, with $k_{re} = k_{re,coll}$ from equation (8.55). Thus no difference will be observed between the two models unless the probability of re-entry is reduced. Figure 8.3 presents the results obtained from calculations using both the extended zero-one model and the Casey-Morrison zero-one model using the parameter values from Table 8.1 but varying the value of

$k_{re}/k_{re,coll}$. No significant difference in the results from the two models is observed until the value of $k_{re}/k_{re,coll}$ is reduced to the order of 10^{-5}, at which point the effect of aqueous-phase termination of exited radicals becomes significant, causing a decrease in $\bar{n}$. Under these conditions the extended zero-one model is seen to give consistently higher values of $\bar{n}$ than the Casey-Morrison model due to the ability of exited radicals to undergo propagation and subsequent re-entry as dimeric radicals, and thus escape aqueous-phase termination. However, while $k_{re,coll}$ is an upper bound for k_{re}, it is highly unlikely that the real value will be anything like 5 orders of magnitude less, because that would imply a barrier to re-entry of order 31 kJ mol^{-1} [calculated using $10^{-5} = \exp(-E_a/RT)$ at 50°C], which is difficult to rationalise given current understanding of emulsion polymerisation.

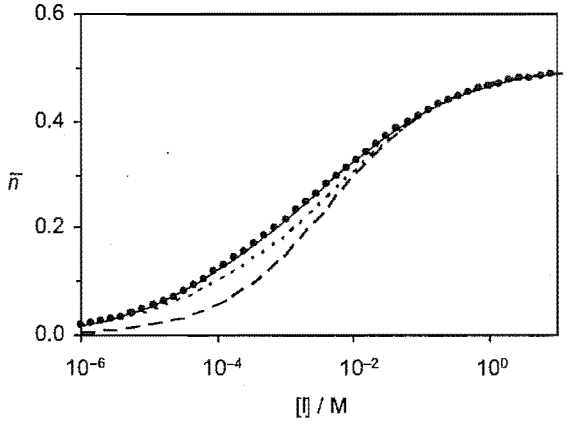

Figure 8.3. Steady-state $\bar{n}$ as a function of initiator concentration for Interval II seeded emulsion polymerisation of styrene at 50°C; calculations using the Casey-Morrison zero-one model with $k_{re}/k_{re,coll} = 1$ (• • • •) and $k_{re}/k_{re,coll} = 1 \times 10^{-5}$ (— — —), and using the extended zero-one model with $k_{re}/k_{re,coll} = 1$ (————) and $k_{re}/k_{re,coll} = 1 \times 10^{-5}$ (– – – –).

The difference between results obtained from the two zero-one models examined here will clearly be of greatest magnitude under conditions of high aqueous monomer concentration. Thus, it is not surprising that little difference is observed in modelling using standard parameters for styrene (a relatively water-insoluble monomer). In order to determine the effect of greater monomer solubility, further calculations were carried out using the standard parameter values for styrene at 50°C from Table 8.1, but with the value of $[M]_w$ increased by two orders of magnitude to 0.43 M. This value is representative (to within an order of magnitude) of the water solubility of other commonly used emulsion polymerisation monomers such as methyl methacrylate, methyl acrylate and vinyl acetate.

Results of calculations with a higher aqueous monomer concentration are shown in Figure 8.4. Firstly, it should be noted that at low initiator concentration, [I] < 1 × 10^{-2} M, the $\bar{n}$ values in Figure 8.4 are lower than those of Figure 8.3, whereas for [I] > 1 × 10^{-2} M the reverse is true. This may be explained by the fact that increasing $[M]_w$ affects the value of $\bar{n}$ in two ways: (1) by increasing the entry efficiency, and hence the value of ρ_{init}, and (2) by increasing the value of k_{dM}, as monomeric radicals are now more hydrophilic and thus desorb more readily. At low initiator concentration, entry efficiency is high, even with $[M]_w$ = 4.3 × 10^{-3} M (Figure 8.3), thus as $[M]_w$ is increased to 0.43 M (Figure 8.4) there is little change in ρ, and the increase in k_{dM} gives rise to a lower value of $\bar{n}$. However, at high initiator concentration the increase in $[M]_w$ causes a significant increase in entry efficiency and ρ – sufficient to overcome the opposing increase in k_{dM}, and to give higher values of $\bar{n}$ in Figure 8.4 than in Figure 8.3.

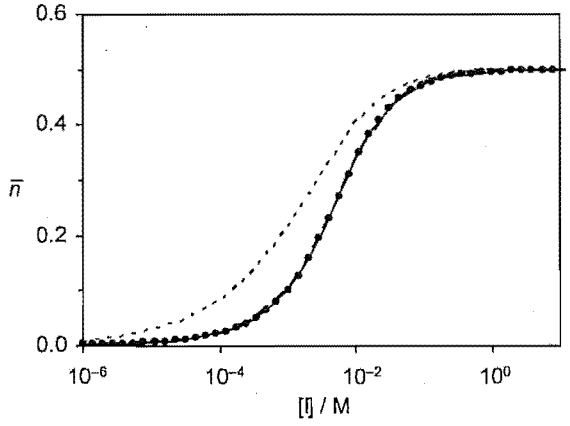

Figure 8.4. Modelled $\bar{n}$ as a function of initiator concentration for Interval II seeded emulsion polymerisation of styrene at 50°C with $[M]_w$ = 0.43 M; calculations using the Casey-Morrison zero-one model with $k_{re}/k_{re,coll}$ = 1 (• • • •) and $k_{re}/k_{re,coll}$ = 1 × 10^{-3} (– – – –) (indistinguishable results), and using the extended zero-one model with $k_{re}/k_{re,coll}$ = 1 (————) and $k_{re}/k_{re,coll}$ = 1 × 10^{-3} (– – – –).

From Figure 8.4 it is evident once again that, even for a relatively water-soluble monomer, identical results are obtained from both the Casey-Maxwell and extended zero-one models so long as re-entry of monomeric radical is assumed to be diffusion-controlled. Notably, however, the modelled results here are seen to be more sensitive to the value of $k_{re}/k_{re,coll}$ than in previous calculations, with a decrease to the order of $k_{re}/k_{re,coll}$ = 10^{-3} being sufficient to yield a significant discrepancy between the results from the two models. Under these

conditions the $\bar{n}$ data from the Casey-Morrison model remains indistinguishable from that obtained with $k_{re}/k_{re,coll}$ = 1, however the extended Smith-Ewart model is seen to give consistently higher values of $\bar{n}$. This result reflects the fact that with a high aqueous monomer concentration the probability of propagation of exited radicals is substantially higher than that of aqueous termination. Furthermore, setting $k_{re}/k_{re,coll} = 10^{-3}$ in this case means that re-entry occurs predominantly *via* aqueous-phase propagation to form a dimeric entering species which is assumed to re-enter a latex particle irreversibly, undergoing termination if that particle is occupied and otherwise forming a propagating radical chain. This type of re-entry is kinetically distinct from straightforward re-entry of a monomeric radical in that a monomeric radical that re-enters an unoccupied latex particle is capable of immediately re-exiting that particle, thus providing a new opportunity for radical loss through termination in the aqueous-phase termination or re-entry into an occupied particle. Hence the value of $\bar{n}$ is increased as dimeric re-entry prevails over monomeric re-entry.

In summary, it appears that under usual emulsion polymerisation conditions for the styrene/persulfate system the extended zero-one model shows good agreement with the Casey-Morrison zero-one model. The high probability for diffusion-controlled re-entry of exited monomeric radicals ensures that aqueous-phase propagation of these species is kinetically insignificant. It is possible that in the event of some barrier to re-entry the difference between the two models could become significant. However, it is seen that even in the case of a monomer of relatively high water solubility a significant decrease in the rate of monomeric radical re-entry is required. It should also be noted that in the case of a highly water soluble monomer the zero-one approximation itself may well be inadmissible (as demonstrated in the following section).

8.6 Application of Extended Smith-Ewart Model to Methyl Methacrylate Systems

Methyl methacrylate (MMA) is another commonly used emulsion polymerisation monomer that is well-suited to model studies in that the required rate parameter values are largely available in the literature. This section applies the extended Smith-Ewart model to the emulsion polymerisation of MMA at 50°C, using persulfate as initiator, with the objective of determining the conditions where existing modelling methodologies provide accurate and meaningful results, and where (if at all) the extended Smith-Ewart treatment offers distinct advantages.

Table 8.2. Standard simulation parameter values used for extended Smith-Ewart modelling of MMA emulsion polymerisations at 50°C.

Simulation parameter	Value
m_p^0 / g	0.85
m_M^{tot} / g	5.0
r_s / nm	68
N_c / dm^{-3}	4.1×10^{16}
V_r / dm^3	0.06
$[M]_p$ / M	6.9
$[M]_w$ / M	0.15
k_{dM} / s^{-1}	2.4×10^4
fk_d / s^{-1}	1.1×10^{-6}
z	5
ρ_{spont} / s^{-1}	0
k_{tr} / M^{-1} s^{-1}	1.5×10^{-2}
k_p / M^{-1} s^{-1}	649
k_p^1 / k_p	15
k_t^{ML} / M^{-1} s^{-1}	6×10^8
k_t^{LL} / M^{-1} s^{-1}	300
$k_{re,coll}$ / M^{-1} s^{-1}	9×10^{11}
$k_{re} / k_{re,coll}$	1
$k_{p,w}$ / M^{-1} s^{-1}	649
$k_{p,w}^M / k_{p,w}$	15
$k_{t,w}$ / M^{-1} s^{-1}	3.7×10^9

Once again, we assemble in Table 8.2 a standard set of parameter values which shall be employed for all MMA/persulfate model calculations here, except where otherwise stated.

For convenience, the values of r_s, m_p^0, m_M^{tot} and $[M]_p$ closely approximate those of the MMA emulsion system used for the experimental investigations of Chapters 4, 5 and 6. $[M]_w$ is as measured by Ballard *et al.*,[8] and the value of k_{tr} obtained from experiment in Chapter 6 is used here. The value of z is that predicted for MMA/persulfate by the Maxwell-Morrison entry model.[17] While it should be noted that the results of Chapter 4 suggest that z is actually somewhat higher than the model predicts, such a difference will not significantly affect the inferences made here (basically, it only affects the value of ρ_L, not the *nature* of the kinetics). k_p is as recommended by an IUPAC working party,[36] and the value of k_p^1 is the upper bound inferred from experimental studies.[5,14,15] Once again, the values of aqueous-phase propagation rate coefficients are assumed to be the same as those for intra-particle propagation. Equations (8.54) and (8.55) are used to calculate values for k_{dM} and $k_{re,coll}$, assuming a value of $D_w = 1.7 \times 10^{-9}$ m^2 s^{-1} for MMA,[28] and initially k_t^{ML} and k_t^{LL} are assigned the same estimates as given in Table 8.1 earlier. Values of all remaining (monomer-non-specific) parameters are the same as those employed in the previous section.

8.6.1 Comparison of Extended Smith-Ewart Model with Existing Models

The zero-one approximation

As discussed in Chapter 4 the emulsion polymerisation kinetics of MMA are generally thought to be poorly approximated by the zero-one model. The extended Smith-Ewart model offers a useful means for confirming whether or not this is the case. We therefore begin by carrying out calculations using both the extended Smith-Ewart model and the extended zero-one model, employing the standard parameter values in Table 8.2. It is noted that (as intimated in the previous section) identical results are obtained from the extended zero-one model and the Casey-Morrison model, even in the case of a monomer of appreciable water-solubility such as MMA, so long as the rate of re-entry of monomeric exited radicals is assumed to be diffusion-controlled.

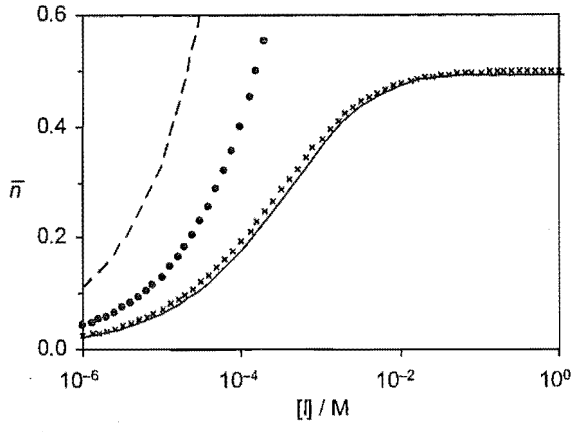

Figure 8.5. Steady-state $\bar{n}$ as a function of initiator concentration for Interval II seeded emulsion polymerisation of MMA at 50°C; calculations using the extended zero-one model (————), and using the extended Smith-Ewart model with $k_t^{LL} = 3 \times 10^2$ M^{-1} s^{-1} (— — —), $k_t^{LL} = 1 \times 10^4$ M^{-1} s^{-1} (• • • •), or $k_t^{LL} = 1 \times 10^8$ M^{-1} s^{-1} (× × × ×).

As shown in Figure 8.1, when the standard parameter values are used there is a significant discrepancy between the results of the general and zero-one models. However, in view of earlier results it is necessary to consider that the value of k_t^{LL} may be significantly greater than the reaction-diffusion value of Table 8.2. As before, an upper bound for k_t^{LL} may be estimated from the value of $\langle k_t \rangle$ measured by γ-relaxation. In Chapter 6 a value for $\langle k_t \rangle$ of approximately 2×10^4 M^{-1} s^{-1} was determined for an MMA emulsion system in Interval II ($w_p \approx 0.3$), in good agreement with the value of 3.8×10^4 M^{-1} s^{-1} reported by Ballard *et al.*[8] Notably, both these values are significantly less than the value of $\langle k_t \rangle \approx 1 \times 10^6$ M^{-1} s^{-1} for styrene systems quoted in the previous section. The explanation for this is most likely the difference in the radical chain length distributions for the styrene and MMA systems, as evidenced by the measured pseudo-instantaneous molecular weight distributions of dead chains. For styrene, reference[31] indicates that this distribution is centred around molecular weight of $10^5 - 10^6$, whereas for MMA the distribution is centred at molecular weight of ~ 10^7 (see the measured distributions of Chapter 6). Higher populations of slowly-diffusing long chains will lead to a lower (chain length dependent) value of $\langle k_t \rangle$ in the MMA system. That said, it would be fair to say that the precise reasons for $\langle k_t \rangle$ being different in MMA and styrene are still not understood.

Comparison of Figures 8.5 and 8.2 leads to an important conclusion: that MMA must be more pseudo-bulk in behaviour where styrene is more zero-one because of slower termination

kinetics rather than faster entry and exit. In other words, if k_t^{LL} were as high for MMA as it appears to be for styrene, then there is every reason to suspect that MMA would also be zero-one-like in behaviour.

Further calculations reveal that full accord between the general and zero-one models (including the characteristic plateau at $\bar{n} = 0.5$) is only obtained when the unusually high value of $k_t^{LL} = 10^8$ M^{-1} s^{-1} is used (exactly as found for styrene – see Figure 8.2).

The "traditional" Smith-Ewart model

An alternative approach to modelling MMA emulsion polymerisation kinetics is to solve the full set of Smith-Ewart equations arising from equation (8.1). An efficient means for doing this, which incorporates the elementary treatment of re-entry given in equation (8.3), is the "recursive-closure" method of Ballard *et al.*[21] In order to avoid confusion, this method will henceforth be referred to as the "traditional (Smith-Ewart) model", distinguishing it from the "extended (Smith-Ewart) model" developed as part of the present work. Modelling using the traditional approach requires specification of the parameter values of ρ, k, c and α – unlike the extended model where these values are effectively calculated *a priori* (indeed, that is the raison d'être for the extended model). It is therefore of interest to determine whether the results obtained from the extended model may be reproduced by the traditional model using meaningful values for the four parameters listed above.

Reference calculations are first carried out using the extended model with the parameter values of Table 8.2, but varying the value of k_t^{LL} to span the range of conditions over which the kinetics were seen to change significantly in Figure 8.5. Results are presented in Figures 8.6 and 8.7 for calculations employing two different initiator concentrations, [I] = 10^{-6} M and 10^{-1} M respectively, which roughly span the range of initiator concentrations that may be used in practice.

We next seek to estimate values for ρ, k, c and α in the traditional Smith-Ewart model that may accurately simulate the conditions specified in Table 8.2. The value of ρ is likely to be well approximated by the value of ρ_{init} calculated from the extended model, given that ρ_{spont} is assumed to be zero here. Similarly, the value of c may be approximated by the value of c^{LL}

from the extended model, bearing in mind that this value excludes the contribution from termination of monomeric radicals and will thus be a slight underestimate for c.

Since the extended model furnishes no simple estimate for the exit rate coefficient, k, this parameter must be estimated from theory. The simplest approach is to assume that every monomeric radical formed by chain transfer to monomer inside a particle undergoes exit, and hence that the value of k is equal to the rate of transfer:

$$k = k_{tr}[M]_p \tag{8.59}$$

Using the parameter values of Table 8.2, k is then calculated as 1.0×10^{-1} s^{-1}.

A more sophisticated expression for k was derived in Chapter 1 by assuming that monomeric radicals produced inside a particle will either desorb into the aqueous phase or propagate to form a macro-radical that is incapable of desorption, with the rate-determining step for desorption being aqueous diffusion of monomer away from the particle surface. The rate coefficient for exit is then:

$$k = k_{tr}[M]_p \frac{k_{dM}}{k_{dM} + k_p^1[M]_p} \tag{8.60}$$

Combining this expression with equation (8.54) for k_{dM}, and assuming the value $D_w = 1.7 \times 10^{-9}$ m^2 s^{-1} for MMA[28] leads to a second estimate for k of 2.7×10^{-2} s^{-1}. This should be regarded as a best estimate, but because it has used a high value of k_p^1, the value from equation (8.59) can also be used as a likely upper bound.

As alluded to earlier, the fate parameter, α, incorporated in the traditional Smith-Ewart model may appear deceptively simple but it is, in fact, a complex kinetic parameter that is difficult to estimate a value for, based on the prescribed polymerisation conditions. The approach adopted here will be to consider only the values of α that have the clearest physical interpretations: $\alpha = 1$, corresponding to complete re-entry of exited radicals; $\alpha = 0$, for complete aqueous-phase homo-termination of exited radicals, *or* hetero-termination with initiator-derived radicals under circumstances where the value of ρ is not affected by exit (*e.g.*, when the entry efficiency is low); and $\alpha = -1$ when hetero-termination of every exited radical results in destruction of an initiator-derived radical otherwise bound to undergo entry.

Results from calculations using the traditional Smith-Ewart model with the values of ρ, k, c and α specified above are presented together with the results obtained from the extended model in Figures 8.6 and 8.7. It is immediately evident that the traditional model with $\alpha = 1$ provides the closest general agreement with the extended model under all conditions. Comparison of Figures 8.6 (a) and (b) reveals that (at low initiator concentration) the value of $k = 2.7 \times 10^{-1}$ s^{-1} gives rise to close agreement between the two models for all $k_t^{LL} > 3 \times 10^3$ M^{-1} s^{-1}, whereas in the case of $k = 1.0 \times 10^{-1}$ s^{-1} the range of agreement is restricted only to the region of $k_t^{LL} \approx 3 \times 10^3$ M^{-1} s^{-1}. This is in accord with $k = 2.7 \times 10^{-1}$ s^{-1} being the estimate that best corresponds with the extended Smith-Ewart input parameter values. Interestingly, the difference in k appears to be significant for the traditional model despite the fact that $\alpha = 1$ stipulates complete re-entry of exited radicals. The explanation lies in the effect of compartmentalisation on the system, as is now explained.

Under conditions of $c \gg \rho$, k, in the traditional Smith-Ewart model, the rate at which radicals are circulated amongst different latex particles is relatively slow; radicals are "compartmentalised" into different reaction loci. In this setting termination occurs rapidly upon radical entry into an occupied particle and hence the rate of radical loss inside the particles is controlled solely by the rates of entry and exit (*i.e.*, the zero-one limit is reached). In Figure 8.6 the onset of compartmentalisation is evident in the region of $k_t^{LL} \sim 10^4 - 10^5$ M^{-1} s^{-1}. As k_t^{LL} increases beyond this region (*i.e.*, towards $c \gg k$, ρ) $\bar{n}$ is seen to become insensitive to changing k_t^{LL}, converging to a constant value determined by the relative values of ρ and k. Therefore decreasing the value of k from 1.0×10^{-1} s^{-1} in Figure 8.6 (a) to 2.7×10^{-2} s^{-1} in Figure 8.6 (b) results not only in compartmentalisation occurring at a lower value of k_t^{LL}, but also in convergence to a higher limiting value of $\bar{n}$ due to the lower rate of radical loss by exit in the compartmentalised system.

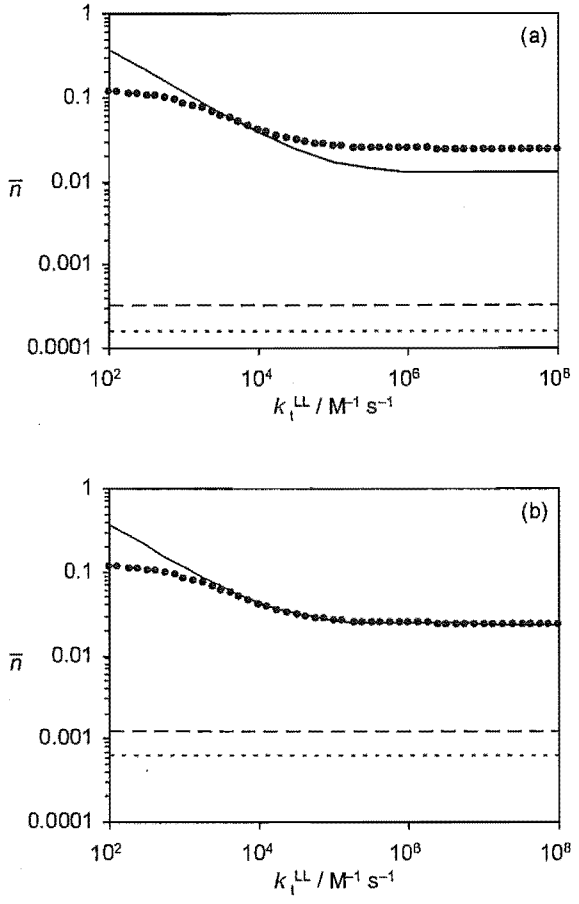

Figure 8.6. Logarithmic plots of steady-state $\bar{n}$ as a function of k_t^{LL} for Interval II seeded emulsion polymerisation of MMA at 50°C with [I] = 10^{-6} M; calculations using the "extended" Smith-Ewart model (• • • •) (same in both plots), and for **(a)** $k = 1.0 \times 10^{-1}$ s^{-1} and **(b)** $k = 2.7 \times 10^{-2}$ s^{-1}, using the "traditional" (see text) Smith-Ewart model with $\rho = 3.3 \times 10^{-5}$ s^{-1} and $\alpha = 1$ (————), $\alpha = 0$ (— — —), or $\alpha = -1$ (– – – –).

It is noted that in Figure 8.7 the results of the traditional model with $\alpha = 1$ are unaffected by the same change in k responsible for the effect described above, despite the fact that the effect of compartmentalisation on $\bar{n}$ is clearly observed for $k_t^{LL} > 10^6$ M^{-1} s^{-1}.

In this case, high initiator concentration gives rise to $\rho \gg k$ and, under compartmentalised conditions, all particles rapidly gain and lose radicals through entry, resulting in a limiting value of $\bar{n} = 0.5$. Since $\rho \gg k$ applies for both $k = 1.0 \times 10^{-1}$ s^{-1} and 2.7×10^{-2} s^{-1} at high initiator concentration, the same compartmentalised value of $\bar{n} = 0.5$ is attained in both cases.

Also significant in comparing the results of the traditional model in Figures 8.6 and 8.7 is the observation that changing α has less effect on the value of $\bar{n}$ at high initiator concentration. This is because as the entering flux of initiator-derived radicals increases with initiator

concentration, the relative flux of exiting radicals becomes relatively small, and thus the fate of those exited radicals is of less consequence.

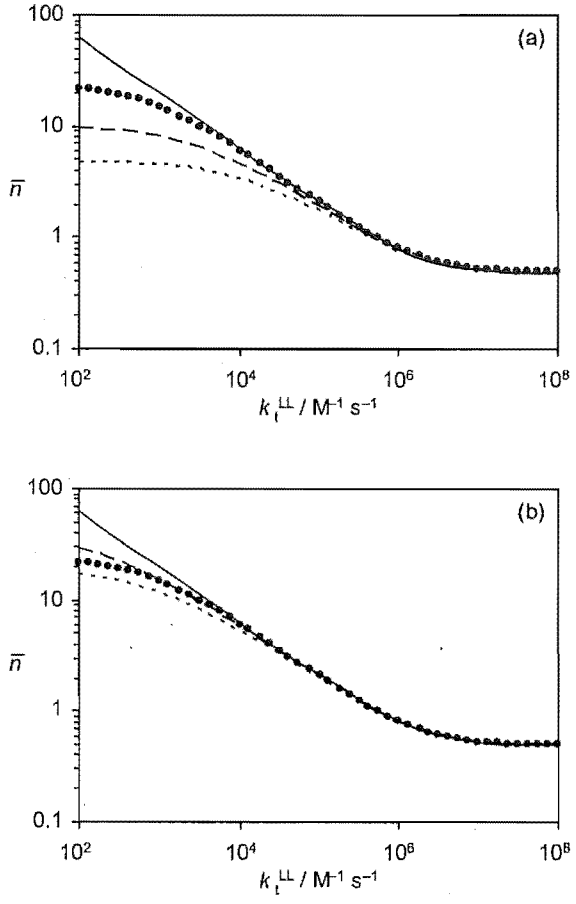

Figure 8.7. Logarithmic plots of steady-state $\bar{n}$ as a function of k_t^{LL} for Interval II seeded emulsion polymerisation of MMA at 50°C with [I] = 10^{-1} M; calculations using the "extended" Smith-Ewart model (• • • •) (same in both plots), and for **(a)** $k = 1.0 \times 10^{-1}$ s^{-1} and **(b)** $k = 2.7 \times 10^{-2}$ s^{-1}, using the "traditional" (see text) Smith-Ewart model with $\rho = 9.9 \times 10^{-1}$ s^{-1} and $\alpha = 1$ (————), $\alpha = 0$ (— — —), or $\alpha = -1$ (– – – –).

In both Figures 8.6 and 8.7 the value of $\bar{n}$ obtained for $k_t^{LL} < 3 \times 10^3$ M^{-1} s^{-1} using the extended Smith-Ewart model is seen to fall below that of the traditional Smith-Ewart model with $\alpha = 1$, indicative of an additional radical loss mechanism in the extended model. Given the rapid rate of re-entry of monomeric radicals evidenced in the previous section and in Chapter 4, it is unlikely that this radical loss is by aqueous-phase termination of exited radicals. The explanation is therefore thought to be the effect of intra-particle termination between monomeric radicals and non-monomeric radicals.

In the present system the probability of ML-termination appears low, with Table 8.2 giving the rates of propagation, desorption and ML-termination per monomeric radical as: $k_p^1[M]_p$ = 6.7×10^4 s^{-1}, $k_{dM} = 2.4 \times 10^4$ s^{-1} and $c^{ML} = 7.6 \times 10^2$ s^{-1}. Thus it is most likely that a monomeric radical will propagate to form a macro-radical which may then undergo LL-termination. However, as k_t^{LL} decreases the rate of LL-termination eventually becomes sufficiently slow that the dominant mode for radical loss inside a particle is transfer to monomer followed by ML-termination.

As is evident from Figures 8.6 and 8.7, under conditions where ML-termination is significant it is possible to reproduce the results of the extended model by using the traditional model with a non-integer value for α. However, it is also clear that the value of α required will vary depending on the values of other parameters (*e.g.*, [I], k and k_t^{LL}), and, most importantly, there is no obvious relationship between these parameters and the value of α.

The pseudo-bulk approximation

Another useful approximation to the traditional Smith-Ewart model that is applicable under very different conditions to the zero-one model is the pseudo-bulk model. A brief derivation of this model is the following, described by Ballard *et al.*[21]

Here we assume that the particle populations are normalised such that:

$$\sum_{n=1}^{\infty} N_n = 1 \tag{8.61}$$

Multiplying equation (8.1) by the number of radicals, n, and summing over all $n \geq 1$ gives:

$$\sum_{n=1}^{\infty} n \frac{dN_n}{dt} = \sum_{n=1}^{\infty} n \left\{ \rho N_{n-1} - [\rho + nk + n(n-1)c]N_n + (n+1)kN_{n+1} + (n+2)(n+1)cN_{n+2} \right\}$$

$$= \sum_{n=1}^{\infty} \rho [nN_{n-1} - nN_n] - k[n^2 N_n - (n+1)nN_{n+1}] - c[n^2(n-1)N_n - (n+2)(n+1)nN_{n+2}]$$

$$= \rho \sum_{n=1}^{\infty} N_n - k \sum_{n=1}^{\infty} nN_n - 2c \sum_{n=1}^{\infty} [n^2 N_n - nN_n]$$

$$\frac{d\bar{n}}{dt} = \rho - k\bar{n} - 2c\left(\overline{n^2} - \bar{n}\right) \tag{8.62}$$

where $\bar{n}$ is defined as in equation (8.2) and $\overline{n^2}$ denotes the second moment of the particle populations. Finally, we invoke the closure relation $\overline{n^2} - \bar{n} = \bar{n}^2$ (which is accurate if the N_n populations follow a Poisson distribution[6]), and replace ρ by the value of ρ_{total} in equation (8.3) to give the following single evolution equation for $\bar{n}$:

$$\frac{d\bar{n}}{dt} = \rho - (1-\alpha)k\bar{n} - 2c\bar{n}^2 \tag{8.63}$$

The above equation is referred to as the pseudo-bulk equation, in recognition of its similarity to the evolution equation for total radical concentration in a bulk polymerisation system (the difference being the existence of an additional first-order radical loss term in the present case). The steady-state solution of equation (8.63) has been shown[8,21] to accurately reproduce the steady-state value of $\bar{n}$ obtained from the full Smith-Ewart equations [equation (8.1)] under conditions of $\rho \gg c$ and/or $k \gg c$ – where the effects of radical compartmentalisation (neglected through the assumption of a Poisson distribution for N_n[6]) are insignificant.

Thus, where the pseudo-bulk approximation is valid, this approach offers the considerable advantage that an accurate value for $\bar{n}$ may be obtained from the solution of a single differential equation. In this section we seek to identify conditions for which the results of the extended Smith-Ewart model are acceptably approximated using the simple pseudo-bulk method.

Here we begin with the same reference calculations as in the previous section, using the extended Smith-Ewart model with the parameter values in Table 8.2 and varying the value of k_t^{LL} over the range $10^2 - 10^8$ M^{-1} s^{-1}. The estimates of ρ, k, c and α used in the pseudo-bulk model are also taken from the previous section, with ρ and c approximated by ρ_{init} and c^{LL} from the extended Smith-Ewart model. The value of $k = 2.7 \times 10^{-2}$ s^{-1} from equation (8.60) is assumed and calculations are carried out using the integer values of $\alpha = 1$, 0 and –1.

The results obtained from the two models using [I] = 10^{-6} M and 10^{-1} M are compared in Figures 8.8 (a) and (b). Given that the pseudo-bulk model is known to accurately approximate the traditional Smith-Ewart model for $\rho \gg c$ or $k \gg c$, it is not surprising that the

results obtained using the pseudo-bulk model at low k_t^{LL} are identical to those of Figures 8.6 (b) and 8.7 (b). As k_t^{LL} increases however, the effects of compartmentalisation become significant and the discrepancy between the pseudo-bulk and extended Smith-Ewart model widens. Thus, at high initiator concentration the pseudo-bulk model with $\alpha = 1$ is accurate only over the range $k_t^{LL} = 3 \times 10^3 - 3 \times 10^5$ M^{-1} s^{-1}, and at low initiator concentration this range narrows to $3 \times 10^3 - 3 \times 10^4$ M^{-1} s^{-1}. Also noteworthy is the fact that at high initiator concentration, with k_t^{LL} in the range stated above, the accuracy of the pseudo-bulk model is not significantly affected by the value chosen value for α.

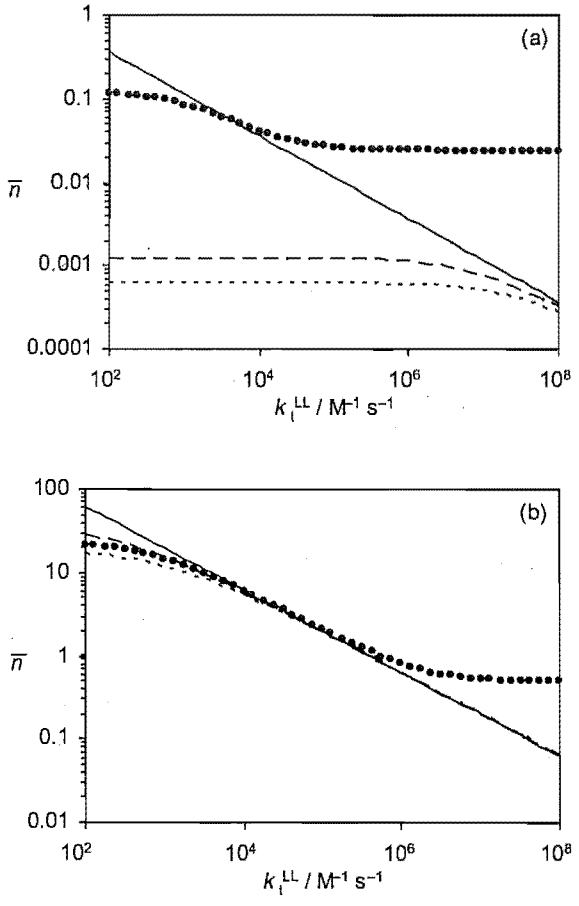

Figure 8.8. Logarithmic plots of steady-state $\bar{n}$ as a function of k_t^{LL} for Interval II seeded emulsion polymerisation of MMA at 50°C with **(a)** [I] = 10^{-6} M and **(b)** [I] = 10^{-1} M; calculations using the pseudo-bulk model with $k = 2.7 \times 10^{-2}$ s^{-1} and $\alpha = 1$ (————), $\alpha = 0$ (— — —), or $\alpha = -1$ (– – – –); and calculations using the extended Smith-Ewart model (• • • •). For pseudo-bulk model, $\rho = 3.3 \times 10^{-5}$ s^{-1} **(a)** and 9.9×10^{-1} s^{-1} **(b)** used.

Finally, the pseudo-bulk model suffers the same limitation as the traditional Smith-Ewart model in the region of $k_t^{LL} < 3 \times 10^3$ M^{-1} s^{-1} in that the values of $\bar{n}$ calculated using the extended Smith-Ewart model over this range cannot be reproduced using a single value for α, nor is there any obvious way of relating the required change in α to the changes in [I] and k_t^{LL}.

Summary and Implications

In closing this section it is instructive to summarise the observed relationships between the extended Smith-Ewart model developed here and various existing kinetic models, and to identify the specific merits of each model. While this is done in the context of the emulsion polymerisation of MMA at 50°C, it is emphasised that this exercise may similarly be carried out for any system.

In Figure 8.9 are presented the results obtained from the extended Smith-Ewart model and the extended zero-one model, using the parameter values from Table 8.2 with varying k_t^{LL}. Also presented are the results from the traditional Smith-Ewart model and the pseudo-bulk model derived therefrom, using parameter values of $\rho = \rho_{init}$, $k = 2.7 \times 10^{-2}$ s^{-1}, $c = c^{LL}$, and $\alpha = 1$.

As discussed above, the results of both the traditional and extended Smith-Ewart models are well approximated by the zero-one model when the rate of intra-particle termination of non-monomeric radicals is high. Under these conditions the system becomes highly compartmentalised and, as such, the pseudo-bulk approximation is invalid.

From Figure 8.9 there is seen to be a region of "intermediate" k_t^{LL} wherein the zero-one approximation becomes increasingly inaccurate: $k_t^{LL} < 3 \times 10^5$ M^{-1} s^{-1} in the case of low initiator concentration, and $k_t^{LL} < 1 \times 10^7$ M^{-1} s^{-1} for high initiator concentration. Under these conditions the effects of compartmentalisation remain non-negligible, however the assumption of pseudo-instantaneous termination is no longer strictly valid. Here an accurate value for $\bar{n}$ may only be obtained using either the traditional or extended Smith-Ewart models.

As k_t^{LL} decreases below the "intermediate" range described above, the effects of compartmentalisation become insignificant and the pseudo-bulk model agrees exactly with both the traditional and extended Smith-Ewart models. The range of k_t^{LL} over which this agreement holds is seen to depend on the value of [I].

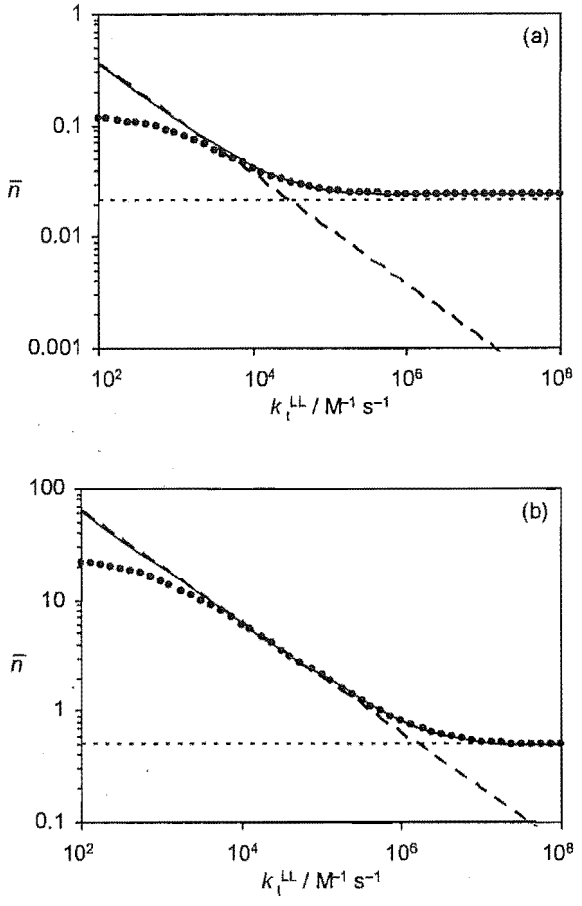

Figure 8.9. Logarithmic plots of steady-state $\bar{n}$ as a function of k_t^{LL} for Interval II seeded emulsion polymerisation of MMA at 50°C with **(a)** [I] = 10^{-6} M and **(b)** [I] = 10^{-1} M; calculations using the traditional Smith-Ewart model (————) and the pseudo-bulk model (— — —) with $k = 2.7 \times 10^{-2}$ s^{-1} and $\alpha = 1$; calculations using the extended zero-one model (– – – –); and calculations using the extended Smith-Ewart model (• • • •). For traditional Smith-Ewart and pseudo-bulk models, $\rho = 3.3 \times 10^{-5}$ s^{-1} **(a)** and 9.9×10^{-1} s^{-1} **(b)** used.

Finally, when mutual termination of non-monomeric radicals is extremely slow (for instance if motion of these radicals is restricted largely to reaction diffusion), ML-termination becomes important. Under these conditions the overall rate of radical loss (and hence $\bar{n}$) is sensitive to the values of [I] and k_t^{LL} in a way that is not accounted for using existing models. The traditional Smith-Ewart and pseudo-bulk models are able to reproduce the value of $\bar{n}$ by allowing for variation in the value of α. While a purely modelling outlook allows α to vary, the physical interpretation it gives here is wrong, for $\alpha < 1$ is meant to represent aqueous-phase radical loss, but what is actually happening here is that some of the monomeric radicals formed by transfer are lost before they are able to re-initiate chain growth. Moreover, while it

is clear that changing [I] and k_t^{LL} affects the value of α, it is impossible to draw any mechanistic inferences from such observations.

Thus, the foremost advantage of the extended Smith-Ewart model (at least in the context of MMA at 50°C) would appear to be the ability to model systems where k_t^{LL} is very low, using only well-defined rate parameters. In the case of all other conditions, one (or more) of the existing models is likely to provide equally accurate results while being less computationally demanding. In particular, under conditions where the zero-one or pseudo-bulk models are accurate, the mathematical simplicity offered by these approximate methods makes them preferable over either the traditional or extended Smith-Ewart model. For conditions where only the Smith-Ewart models are accurate, one might argue that the traditional model is preferable as it involves fewer rate parameters and a non-iterative solution method. However, the added computational demands of the extended Smith-Ewart model should be weighed up against the fact that this is an *a priori* approach, drawing only on meaningful rate parameters and avoiding the need to specify any value for α (integer or otherwise). In fact even where the zero-one and pseudo-bulk models are accurate, this is the advantage of the extended Smith-Ewart model: it uses bona fide rate parameters, whereas ρ, k and α are not parameters corresponding to a single microscopic process.

As a final note, it would be remiss not to relate the findings of this section to the analyses of experimental results obtained from the MMA/persulfate system at 50°C presented in chapters 4, 5 and 6. Specifically, it is of interest to determine whether re-fitting of experimental data using the extended Smith-Ewart model developed here would be likely to give results that are at variance with those already obtained using existing methods.

As stated earlier, the "standard" parameter values given in Table 8.2 were chosen to correspond to the conditions used in the experiments of the earlier chapters, thus the results of the present section should be comparable to good approximation. The value of $\langle k_t \rangle$ for this system was determined from γ-relaxation experiment to be approximately 2×10^4 M^{-1} s^{-1} (with a small amount of variation depending on whether termination kinetics are assumed to be chain length dependent or independent). Thus, on the same grounds as earlier, we may approximate the value of k_t^{LL} to be of a similar magnitude. Inspection of Figure 8.9 reveals that under such conditions the results of the extended Smith-Ewart equation will be very similar to the results obtained using either the pseudo-bulk model or the traditional Smith-

Ewart model with a value of $\alpha = 1$. Since both these approaches were included in the data analyses of the earlier chapters it may be concluded that the results of re-fitting of the experimental data using the extended Smith-Ewart model would be consistent with the results already presented.

8.6.2 The "Acceleration" During Interval II

In Chapter 4 a great deal of effort was devoted to attempting to model – using various approaches – not only the overall magnitude of $\bar{n}$ measured experimentally, but also its evolution with conversion during Interval II, for MMA at 50°C. Recalling that none of the approaches used there provided a complete explanation for this aspect of the experimental data, it is of interest to examine the Interval II evolution of $\bar{n}$ as predicted using the extended Smith-Ewart model.

As in Chapter 4 the evolution of $\bar{n}$ during the steady-state period of Interval II is quantified using a linear fit to the data as a function of conversion, $\hat{x}$ (in grams). The value of the "acceleration" parameter, $\bar{a}$, is then defined as follows:

$$\bar{a} = \frac{\dfrac{d\bar{n}}{d\hat{x}} m_p^0}{\bar{n}_0} \tag{8.64}$$

where $d\bar{n}/d\hat{x}$ is the slope of such a fit, and $\bar{n}_0$ and m_p^0 are, respectively, the value of $\bar{n}$ and mass of polymer at the at the start of the steady-state period (for a more detailed description of how $\bar{a}$ is obtained, see Chapter 4).

Initially, we calculate $\bar{n}$ as a function of Interval II (steady-state) conversion over the range $0 \leq \hat{x} \leq 0.7$ g, using the parameter values of Table 8.2 (consistent with the experimental conditions), and the estimate of $k_t^{LL} \approx \langle k_t \rangle = 2 \times 10^4$ M^{-1} s^{-1} obtained from γ-relaxation data. Both c^{LL} and c^{ML} are varied with $\hat{x}$ according to $c = k_t/(N_A V_s)$, while k_{dM} varies according to equation (8.54), and k_{re} varies according to equation (8.55). The modelled $\bar{n}$ data are then least-squares fitted to a straight line and $\bar{a}$ calculated according to equation (8.64). The values of $\bar{a}$ obtained are presented as a function of initiator concentration in Figure 8.10, together with the values measured experimentally in Chapter 4.

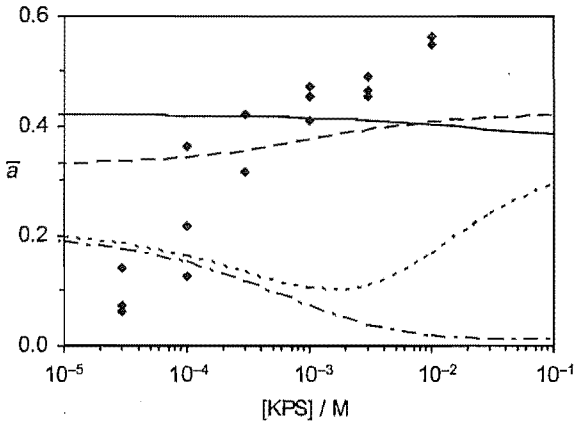

Figure 8.10. $\bar{a}$ as a function of initiator (KPS) concentration from chemically initiated emulsion polymerisations of MMA at 50°C. Experimental data from Chapter 4 (filled diamonds) are shown along with values calculated using the extended Smith-Ewart model with $k_t^{LL} = 1 \times 10^2$ M^{-1} s^{-1} (————), 2×10^4 M^{-1} s^{-1} (— — —), 1×10^6 M^{-1} s^{-1} (– – – –), and 1×10^8 M^{-1} s^{-1} (– —— –).

It is evident that, using best estimates for the rate parameters for MMA at 50°C, the trend in $\bar{a}$ as calculated by the extended Smith-Ewart model is at least qualitatively consistent with the experimental trend of rising $\bar{a}$ with increasing initiator concentration. This is in line with the suggestion in Chapter 4 that the effects of compartmentalisation are significant at low initiator concentration. However, it is clear that the extended Smith-Ewart model does not provide a substantially better account of the observed acceleration than the modelling approaches used previously. Indeed, this is not surprising in light of the preceding section which demonstrated that, for the present system, the pseudo-bulk and traditional Smith-Ewart models are likely to give very similar results to the extended model.

In order to gain broader insight into modelling of the Interval II acceleration using the extended Smith-Ewart model, results are also presented in Figure 8.10 for $\bar{a}$ calculated using a range of different values for k_t^{LL}. These data are intended to provide an overview of the type of results that may be obtained under a range of different polymerisation conditions – beyond just those of the MMA system – and reveal rather complex trends, a brief discussion of which is now given.

Assuming that the rate at which radicals are supplied to latex particles by entry is independent of particle radius (as is implicit in the Maxwell-Morrison entry model), the change in $\bar{n}$ with

conversion during the steady-state period of Interval II may then be directly related to the particle radius-dependence of the radical loss processes that are operative in the system.

In the case of the results with $k_t^{LL} = 1 \times 10^2$ M^{-1} s^{-1} in Figure 8.10, the rates of radical entry and exit are relatively fast and the effects of radical compartmentalisation disappear. Under these conditions radical loss by intra-particle termination is prevalent, thus the acceleration reflects the inverse dependence of both c^{LL} and c^{ML} on particle volume, characterised by a value of $\overline{a} \approx 0.42$ (*cf.* the value of $\overline{a}$ given by the pseudo-bulk and traditional Smith-Ewart models when $\rho > c$ or $k > c$, in Chapter 4).

In the other extreme of $k_t^{LL} = 1 \times 10^8$ M^{-1} s^{-1} the rate of intra-particle termination is rapid and, as such, radical loss in the particles results from exit as well as radical entry into an occupied particle. At low initiator concentration the rate of entry is low and the value of $\overline{a} \approx 0.2$ corresponds to exit loss. Since the overall rate of exit is related to the rates for desorption, propagation and termination of monomeric radicals, the particle radius-dependence of this process is complex, arising from contributions from k_{dM} (α $1/r_s^2$), c^{ML} (α $1/r_s^3$), and k_p^1 (independent of r_s). As initiator concentration increases the rate of entry rises and this radius independent process becomes the dominant form of radical loss, with $\overline{a}$ tending towards zero.

At "intermediate" values of k_t^{LL} the trend in $\overline{a}$ reflects some combination of the cases described above. For $k_t^{LL} = 2 \times 10^4$ M^{-1} s^{-1} the rate of entry at low initiator concentration is sufficiently slow that radical compartmentalisation causes some decrease in the value of $\overline{a}$ below the uncompartmentalised value of $\overline{a} \approx 0.42$. In the case of $k_t^{LL} = 1 \times 10^6$ M^{-1} s^{-1} an unusual trend is observed with $\overline{a}$ passing through a minimum at intermediate initiator concentration. Here the value of $\overline{a}$ at lowest initiator concentration, $\overline{a} \approx 0.2$, corresponds to the situation with exit as the dominant form of radical loss in a compartmentalised system, and increasing the initiator concentration initially causes some decrease in $\overline{a}$ as (radius-independent) entry becomes a significant loss mechanism. However, in this particular case, at high initiator concentration the high rate of entry lessens the effects of compartmentalisation and an appreciable acceleration ($\overline{a} \approx 0.3$) is still observed. Of passing note is that the increase in $\overline{a}$ at high [KPS] with $k_t^{LL} = 1 \times 10^6$ M^{-1} s^{-1} (not unreasonable) matches the experimental increase, and that these are the only *a priori* calculations of this work to show anything like

this. However it is in no way clear how these calculations could represent what is going on in reality.

As is evident from the above discussion, the extended Smith-Ewart model gives rise to complex predictions for the acceleration during Interval II of polymerisation, due to the range of mechanisms which contribute to this phenomenon. Careful measurement of $\overline{a}$ (shown to be possible Chapter 4) over a range of experimental conditions, combined with the mechanistic inferences available through extended Smith-Ewart modelling, may represent a useful means for future interpretation of kinetic data from emulsion polymerisation systems.

8.7 Application of Extended Smith-Ewart Model to Butyl Methacrylate Systems

As a final example we consider the emulsion polymerisation of butyl methacrylate (BMA) at 50°C with persulfate as initiator. This system is not as well-studied as either of the previous systems and it is therefore intended that the model predictions obtained here may be used as a guide for future work.

In their examination of BMA emulsion polymerisation kinetics Halnan *et al.*[37] carried out Interval II seeded emulsion polymerisations at 50°C over the range of initiator (persulfate) concentrations $1 \times 10^{-5} - 1 \times 10^{-3}$ M, reporting values of $\overline{n} = 0.18 - 0.71$. Concluding that the zero-one model is inappropriate for this system (because of $\overline{n} > 0.5$), these workers employed a modified version of the traditional Smith-Ewart kinetic model to obtain values of $\rho_{init} = 8 \times 10^{-4} - 1.6 \times 10^{-2}$ s^{-1}, $\rho_{spont} = 2 \times 10^{-4}$ s^{-1}, $k = 7 \times 10^{-3}$ s^{-1}, $c = 2.5 \times 10^{-2}$ s^{-1}, and $\alpha = 0.5 - 1$ from data fitting.

It is noted that, in the absence of a precise value for k_p, Halnan *et al.* inferred a value of k_p = 600 M^{-1} s^{-1} from kinetic experiments. Recently, a more definitive value of k_p = 756 M^{-1} s^{-1} has been measured by an IUPAC working party[38] using the well-established PLP-SEC (pulsed-laser polymerisation with size-exclusion chromatography) method. Interestingly, this more accurate value of k_p means that the experimental $\overline{n}$ data quoted above must actually be reduced by a factor of 600/756, *i.e.*, the upper limit is close to 0.5. This means these systems may have been closer to zero-one in nature than was thought.

Table 8.3. Standard simulation parameter values used for extended Smith-Ewart modelling of BMA emulsion polymerisations at 50°C.

Simulation parameter	Value
m_p^0 / g	2.2
m_M^{tot} / g	6.5
r_s / nm	54
N_c / dm^{-3}	7.6×10^{16}
V_r / dm^3	0.12
$[M]_p$ / M	3.75
$[M]_w$ / M	2.5×10^{-3}
k_{dM} / s^{-1}	8.7×10^{2}
fk_d / s^{-1}	1.1×10^{-6}
z	2
ρ_{spont} / s^{-1}	2×10^{-4}
k_{tr} / M^{-1} s^{-1}	4.1×10^{-2}
k_p / M^{-1} s^{-1}	756
k_p^1 / k_p	15
k_t^{ML} / M^{-1} s^{-1}	2.8×10^{8}
$k_{re,coll}$ / M^{-1} s^{-1}	6×10^{11}
$k_{re} / k_{re,coll}$	1
$k_{p,w}$ / M^{-1} s^{-1}	756
$k_{p,w}^M / k_{p,w}$	15
$k_{t,w}$ / M^{-1} s^{-1}	3.7×10^{9}

The set of parameter values that best approximates the 50°C BMA/persulfate system of Halnan *et al.* is listed in Table 8.3. The value of fk_d is that used previously for persulfate at 50°C,[25] and z is calculated from the Maxwell-Morrison entry model. The value of k_p is the IUPAC working party value[38] mentioned above, and k_p^1 is the maximum value inferred from experimental studies.[5,14,15] Aqueous-phase propagation rate coefficients are assumed to take the same values as their intra-particle equivalents, and the value of $k_{t,w}$ is that quoted by Maxwell *et al.*[17] All other parameter values are estimated as closely as possible from the information provided for the system of Halnan *et al.*[37,39]

An upper bound for k_t^{LL} in Interval II ($w_p = 0.43$) of order 1×10^4 M^{-1} s^{-1} may be estimated (as previously) from the value of $\langle k_t \rangle = cN_A V_s$ reported by Halnan *et al.* Assuming that the diffusion coefficient for a BMA monomeric radical, D_M, is approximated by that of a BMA monomer molecule, an estimate of $D_M = 4.9 \times 10^{-10}$ m^2 s^{-1} may be inferred from experimental diffusion data.[16] Using this value, equation (8.56) then estimates k_t^{ML} as 2.8×10^8 M^{-1} s^{-1}.

Results are presented in Figure 8.11 from calculations using both the extended and traditional Smith-Ewart models, as well as the zero-one model, and the pseudo-bulk model with $\alpha = 1$. The parameter values for BMA at 50°C from Table 8.3 are used, together with the value of k_t^{ML} estimated above, and with initiator concentration spanning the range covered experimentally by Halnan *et al.* The results of Figure 8.11 exhibit the same general trends observed for MMA systems in the previous section. At high k_t^{LL} the extended Smith-Ewart model is well approximated by the zero-one model. As k_t^{LL} decreases, conditions are obtained where the only existing model that provides good agreement is the traditional Smith-Ewart model; however, as k_t^{LL} decreases further and compartmentalisation effects become negligible the pseudo-bulk approximation is also seen to be valid. At lowest k_t^{LL} ML-termination becomes important and the results of the extended Smith-Ewart model may only be accounted for by varying the value of α used in the traditional models. Considering the value of $k_t^{LL} = 1 \times 10^4$ M^{-1} s^{-1} that has been estimated for the present BMA system, it is apparent from Figure 8.11 that the zero-one approximation may well be a reasonable approximation for Interval II kinetics (certainly at low initiator concentration).

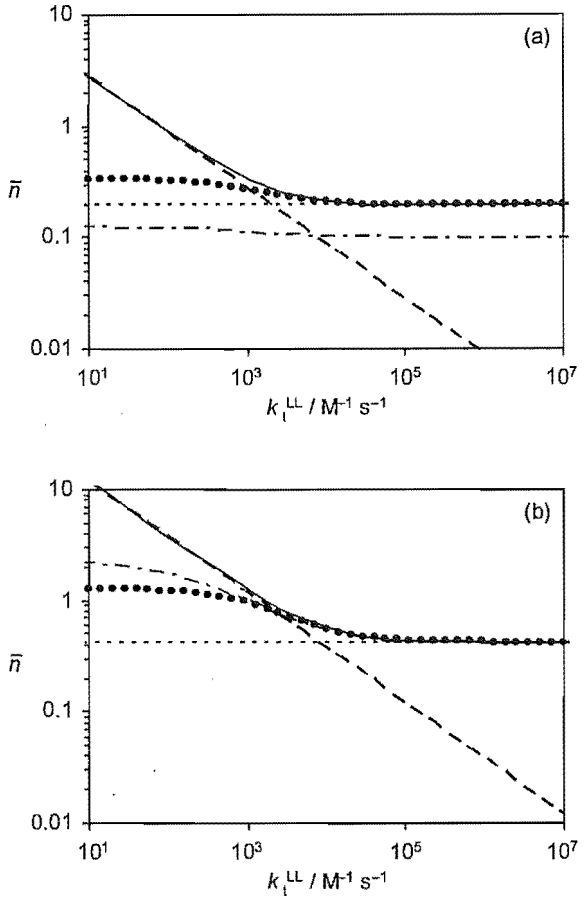

Figure 8.11. Logarithmic plots of steady-state $\bar{n}$ as a function of k_t^{LL} for Interval II seeded emulsion polymerisation of BMA at 50°C with **(a)** [I] = 10^{-5} M and **(b)** [I] = 10^{-3} M; calculations for $k = 3.0 \times 10^{-3}$ s^{-1} using the traditional Smith-Ewart model with $\alpha = 1$ (————) or $\alpha = 0$ (– ——– –), and using the pseudo-bulk model with $\alpha = 1$ (— — —); calculations using the extended zero-one model (– – – –); and calculations using the extended Smith-Ewart model (• • • •). For traditional Smith-Ewart and pseudo-bulk models, ρ = 3.7×10^{-4} s^{-1} **(a)** and 6.7×10^{-3} s^{-1} **(b)** used.

It is interesting to note that Halnan *et al.* also conducted γ-relaxation experiments using the same BMA system at 50°C but in Interval III, with weight fraction of polymer, $w_p = 0.60$ – considerably higher than $w_p = 0.43$ during Interval II for this system (and for other systems, *e.g.*, $w_p = 0.35$ for styrene and $w_p = 0.30$ for MMA in Interval II). Under these conditions the rate of radical diffusion will be slowed considerably, and hence the values of k_t^{ML} and k_t^{LL} reduced. In this case Halnan *et al.* obtained a value of $c = 3.3 \times 10^{-3}$ s^{-1} from data fitting, corresponding to a value of $\langle k_t \rangle$ of order 1×10^3 M^{-1} s^{-1}. Using this value as an estimate for k_t^{LL}, Figure 8.11 would appear to indicate that ML-termination may become significant in Interval III. To further investigate this, calculations are carried out to simulate the BMA

system in Interval III of polymerisation. Here the parameter values of Table 8.3 are once again used but with a lower value of $k_t^{ML} = 2.2 \times 10^8$ M^{-1} s^{-1} [reflecting the effect of increased w_p on the value of D_M in equation (8.56)[16]] and with conversion allowed to increase into Interval III until $w_p = 0.60$ is reached. Results are presented in Figure 8.12.

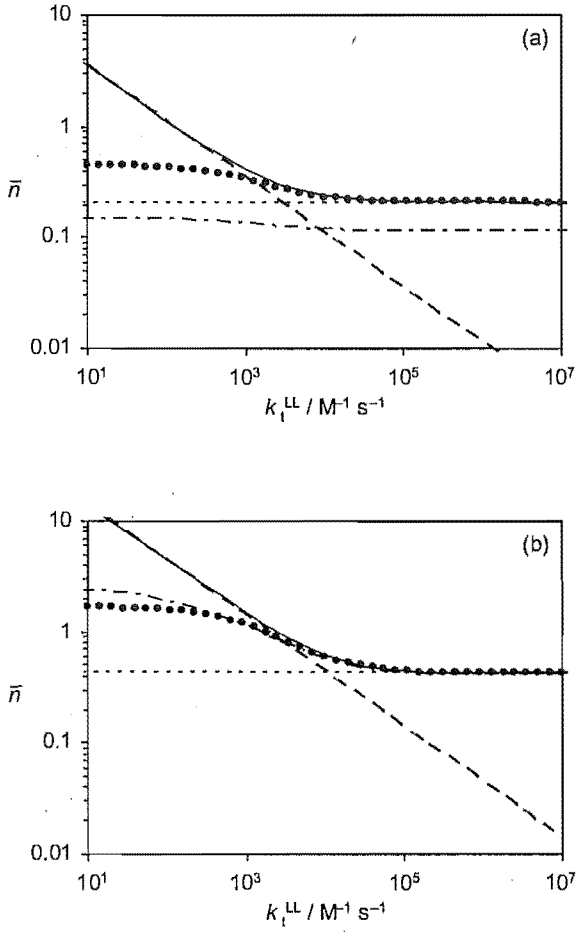

Figure 8.12. Logarithmic plots of steady-state $\bar{n}$ as a function of k_t^{LL} for Interval III seeded emulsion polymerisation of BMA at 50°C with $w_p = 0.60$; **(a)** [I] = 10^{-5} M and **(b)** [I] = 10^{-3} M; calculations for $k = 2.5 \times 10^{-3}$ s^{-1} using the traditional Smith-Ewart model with $\alpha = 1$ (————) or $\alpha = 0$ (– —— –), and using the pseudo-bulk model with $\alpha = 1$ (— — —); calculations using the extended zero-one model (– – – –); and calculations using the extended Smith-Ewart model (• • • •). For traditional Smith-Ewart and pseudo-bulk models, $\rho = 3.7 \times 10^{-4}$ s^{-1} **(a)** and 5.9×10^{-3} s^{-1} **(b)** used.

The values of $\bar{n}$ in Figure 8.12 are seen to be generally higher than those of Figure 8.11, due to the increased particle volume, and hence reduced values of c^{ML} and c^{LL}, at $w_p = 0.60$ (compared with $w_p = 0.43$). As anticipated, assuming the Halnan *et al.* value of $k_t^{LL} = 1 \times 10^3$ M^{-1} s^{-1} under these conditions, the zero-one model is seen to no longer be an acceptable

approximation and the effects of ML-termination on the value of $\bar{n}$ is evident. In the case of low initiator concentration, the traditional Smith-Ewart and pseudo-bulk models must employ a value of α somewhat less than one. At high initiator concentration the value of $\bar{n}$ is seen to be less sensitive to changes in α, thus an even lower value of α will be required under these conditions. In physical terms, this decrease in α with increasing initiator concentration may be qualitatively interpreted as reflecting the increasing probability of monomeric radical loss by ML-termination accompanying the increase in $\bar{n}$. However, as has been discussed previously, the value of α itself provides no meaningful quantitative account of this effect. Of further note, the observation of $\alpha < 1$ by Halnan *et al.* was interpreted as signifying loss of exited radicals by termination in the aqueous-phase. However, as established earlier in this chapter (and in Chapter 4), the rate of re-entry is far too rapid for any significant aqueous termination to occur. Thus it is also clear that the mechanistic interpretation of α (and any change in this value) is dangerously ambiguous. In view of this it would be interesting to re-model the Halnan *et al.* BMA data using the extended Smith-Ewart model. The approach would be to see if $\bar{n}$ as a function of initiator concentration could be reproduced through variation of a single parameter value, treating all others as known. The most obvious such parameter value would be k_t^{LL}, the inferred value of which could then be compared with that from the γ-relaxation experiments of Halnan *et al.* (which actually must be in error due to the incorrect k_p used in deducing it).

The greatest significance of the results obtained here for BMA systems is that they illustrate the effect that changing w_p has on the accuracy of different kinetic modelling approaches. In this case, the comparatively high value of $w_p = 0.60$ during Interval III leads to significantly lower values of both k_t^{LL} and k_t^{ML} than for Interval II ($w_p = 0.43$), and as a result the effects of ML-termination must be taken into account. Under these conditions, the interpretation of results using existing models, with varying α, is unsatisfactory and the extended Smith-Ewart model offers distinct advantages. This effect is likely to be of general importance for systems wherein the value of w_p is high, and (as seen here) will be of particular relevance in modelling of emulsion polymerisation kinetics through the course of Interval III, where the value of w_p steadily increases.

8.8 The "Extended Pseudo-Bulk Model"

A possible impediment to the implementation of the extended Smith-Ewart model, as it has been described thus far, is the requirement for iterative solution of a large number of differential equations. It has been shown that in the event of a relatively high value for k_t^{LL} the set of equations required to give accurate results may be reduced to a far more manageable size using the zero-one approximation. Moreover, in their work Casey *et al.* provided a means for further condensing the zero-one model, resulting in a single overall rate equation (in terms of $\overline{n}$) for which useful analytic solutions may be found.[4] Given the near identical nature of the Casey-Morrison zero-one model and the extended zero-one model of the present work, the same treatment may be employed to derive similar solutions for the extended zero-one model. For a detailed description of this approach the reader is referred to the original work of Casey *et al.*[4]

In the general case of the traditional Smith-Ewart model it has also been shown that the full set of equations may be combined to give a single evolution equation for $\overline{n}$ – the pseudo-bulk equation – the solution of which accurately approximates the exact (iterative) solution under conditions of $\rho > c$ or $k > c$, and is comparatively trivial to compute. Analogously, it is thought that the derivation of a pseudo-bulk-type approximation to the general case of the extended Smith-Ewart model may provide a useful alternative to the full numerical solution method used up until this point.

With $\overline{n}$ defined as in equation (8.35), and rate equations (8.29) and (8.30) describing the N_n and N_n^M particle populations, the following overall rate equation may be obtained for $\overline{n}$:

$$\frac{d\overline{n}}{dt} = \rho_L + \rho_M - 2\,c^{LL}\,\overline{n}^2 - \left(\frac{\rho_M + k_{tr}\,[M]_p\,\overline{n}}{k_{dM} + k_p^1\,[M]_p + c^{ML}}\right)\left(k_{dM} + 2\,c^{ML}\,\overline{n}\right) \qquad (8.65)$$

Full details of the derivation leading to equation (8.65) – henceforth referred to as the "extended pseudo-bulk equation" – are provided in Appendix A.7, including the specification of all assumptions invoked.

Also derived in Appendix A.7 are the following expressions for the entry rate coefficients appearing in equation (8.65):

$$\rho_{init} = \frac{2fk_d[I]N_A}{N_c}\left(\frac{k_{p,w}[M]_w}{k_{p,w}[M]_w + 2k_{t,w}[T_w^\bullet]}\right)^{z-1} \tag{8.66}$$

$$\rho_{di} = \frac{k_{p,w}^M[M]_w k_{dM}}{k_{re}N_cV_w/N_AV_r + 2k_{t,w}[T_w^\bullet] + k_{p,w}^M[M]_w}\left(\frac{\rho_M + k_{tr}[M]_p\bar{n}}{k_{dM} + k_p^1[M]_p + c^{ML}}\right) \tag{8.67}$$

$$\rho_M = \frac{k_{tr}[M]_p\bar{n}}{\left(1 + \frac{k_p^1[M]_p + c^{ML}}{k_{dM}}\right)\left(1 + \frac{2k_{t,w}[T_w^\bullet] + k_{p,w}^M[M]_w}{k_{re}N_cV_w/N_AV_r}\right) - 1} \tag{8.68}$$

Equations (8.65) – (8.68), together with the definition of ρ_L in equation (8.28), comprise the minimum set of equations required to obtain approximate solutions to the full extended Smith-Ewart model. These equations may now be solved analytically if some simple means is found for estimating the total aqueous radical concentration, $[T_w^\bullet]$. Assuming that aqueous radicals are generated only by initiator (*i.e.*, that the relative concentration of exited-derived radicals is negligibly low) and are lost by entry and aqueous termination leads to the following steady-state expression for $[T_w^\bullet]$:

$$[T_w^\bullet] = \left(\frac{2fk_d[I] - k_p[M]_w[IM_{z-1}^\bullet]}{2k_{t,w}}\right)^{\frac{1}{2}} \tag{8.69}$$

Maxwell *et al.*[17] proposed that in the limit of "negligible entry", where $2fk_d[I] \gg k_p[M]_w[IM_{z-1}^\bullet]$ in equation (8.69), the value of $[T_w^\bullet]$ may therefore be estimated as:

$$[T_w^\bullet] = \left(\frac{fk_d[I]}{k_{t,w}}\right)^{\frac{1}{2}} \tag{8.70}$$

This will be a reasonable approximation for $[T_w^\bullet]$ in systems with low entry efficiency, such as styrene with high aqueous radical flux (see Chapter 3). It is noted that an alternative estimate for $[T_w^\bullet]$ may be obtained by assuming the opposite limit of "negligible termination". Under such conditions $k_p[M]_w \gg 2k_{t,w}[T_w^\bullet]$, thus, from equations (8.39) and (8.40), $[IM_i^\bullet] \approx [IM_1^\bullet] \approx 2fk_d[I]/(k_p[M]_w)$, and the value of $[T_w^\bullet]$ may be estimated as:

$$[T_w^\bullet] = \sum_{i=1}^{z-1}[IM_i^\bullet] = (z-1)\frac{2fk_d[I]}{k_p[M]_w} \tag{8.71}$$

It is noted that a value for $[T_w^\bullet]$ could also be obtained from iterative solution of the steady-state aqueous radical equations (8.39) and (8.40), as has been carried out in earlier chapters in this thesis. However, in this case the iterative method is rejected in favour of the (mathematically simpler) analytic approach described here, the accuracy of which is now demonstrated.

Obtaining a steady-state value for $\bar{n}$ now amounts to setting the left-hand side of equation (8.65) to zero and solving the resulting quadratic equation, incorporating the values given for other parameters in equations (8.66) – (8.71). The accuracy of this approximate solution may then be checked against the full numerical solution obtained using earlier methods.

For example purposes we once again turn to the Interval II emulsion polymerisation of MMA at 50°C using persulfate as initiator. Figures 8.13 (a) – (c) present values of steady-state $\bar{n}$ obtained from calculations employing the extended pseudo-bulk model with the parameter values from Table 8.2, and varying k_t^{LL} over the same range as in previous calculations. Results are shown for a series of different initiator concentrations and with $[T_w^\bullet]$ calculated assuming both the negligible entry and negligible termination limits. Also presented for comparison are the results obtained under identical conditions for the extended Smith-Ewart model using the exact numerical method, and also values of $\bar{n}$ calculated using the traditional pseudo-bulk model, assuming a value of $\alpha = 1$.

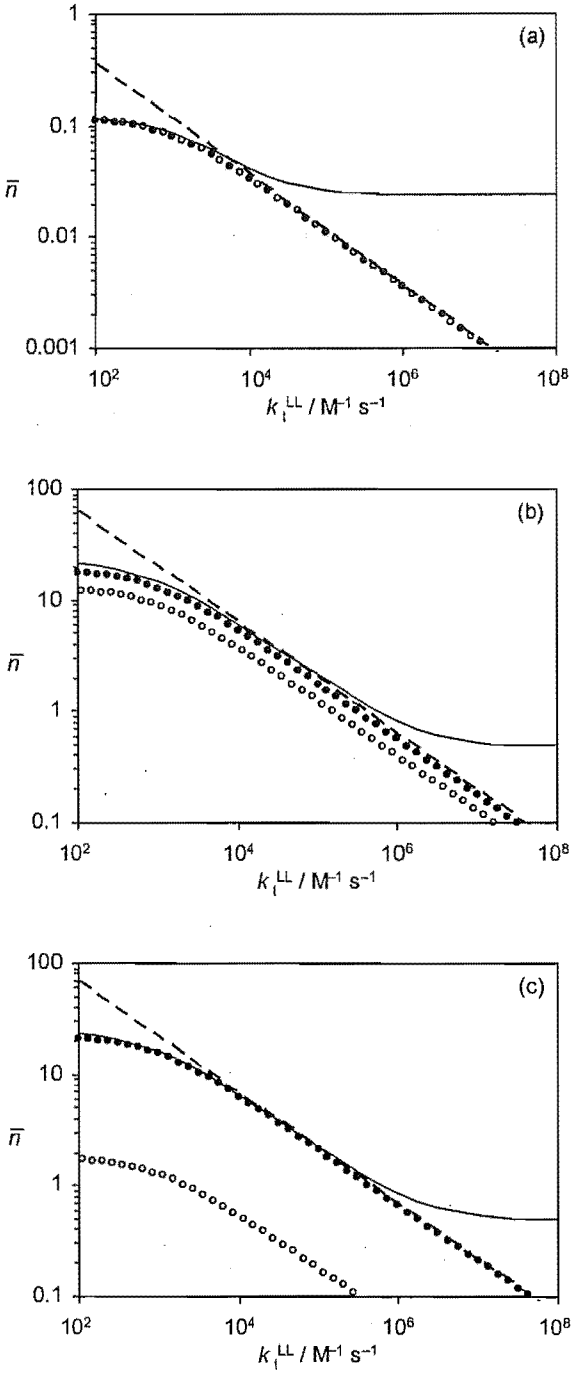

Figure 8.13. Logarithmic plots of steady-state $\bar{n}$ as a function of k_t^{LL} for Interval II seeded emulsion polymerisation of MMA at 50°C with **(a)** [I] = 10^{-6} M (giving $\rho_{init} = 3.3 \times 10^{-5}$ s^{-1}), **(b)** [I] = 10^{-1} M (giving $\rho_{init} = 9.9 \times 10^{-1}$ s^{-1}), and **(c)** [I] = 1 M (giving $\rho_{init} = 1.2$ s^{-1}); values obtained from exact solutions to the extended Smith-Ewart model (————), the (traditional) pseudo-bulk model (— — —) with $\rho = \rho_{init}$, $k = 2.7 \times 10^{-2}$ s^{-1} and $\alpha = 1$, and from the extended pseudo-bulk model assuming either negligible entry (• • • •) or negligible termination (o o o o) of aqueous-phase radicals.

From Figure 8.13 it is apparent that the extended pseudo-bulk model is able to approximately reproduce the results of the exact extended Smith-Ewart model when the value of k_t^{LL} is relatively low. This is exactly analogous to the agreement between the traditional pseudo-bulk and Smith-Ewart models observed when $\rho > c$ or $k > c$ (see earlier sections of this chapter or references[21] and[40] for example) and indicates the conditions under which the closure relation of $\overline{n^2} - \bar{n} = \bar{n}^2$ holds true. Physically this corresponds to the region where the effects of radical compartmentalisation are negligible in the present system. As the value of k_t^{LL} rises and compartmentalisation becomes important, the results of the extended pseudo-bulk model are no longer accurate and – for the present system – are seen to converge with the results of the traditional pseudo-bulk model with $\alpha = 1$. The value of k_t^{LL} at which the extended pseudo-bulk model first fails to be accurate is seen to vary with initiator concentration (from $k_t^{LL} = 1 \times 10^4$ M^{-1} s^{-1} for [I] = 1×10^{-6} M, to $k_t^{LL} = 1 \times 10^6$ M^{-1} s^{-1} for [I] = 1 M) consistent with the fact that as the rate of entry increases with increasing [I] a higher k_t^{LL} is required to give rise to appreciable compartmentalisation in the system.

It is important to note that the extended pseudo-bulk model is seen to accurately reproduce the exact value of $\bar{n}$ from the extended Smith-Ewart model in the region of low k_t^{LL}, *i.e.*, under conditions where ML-termination is significant. This finding is of considerable significance given that it has been established that none of the existing kinetic models provides satisfactory accord in this region (since they do not consider ML-termination).

In addition to the error arising from the closure relation/compartmentalisation above, it is evident in Figure 8.13 that the choice of approximation used for [$T_w^\bullet$] can lead to significant inaccuracy in the extended pseudo-bulk model. In assuming that one of the modes for aqueous radical loss is negligible, both equations (8.70) and (8.71) must produce overestimates for the value of [$T_w^\bullet$]. A sensible approach is therefore to calculate [$T_w^\bullet$] using both approaches and simply use whichever value is lowest (*i.e.*, least overestimated). Additionally, calculating the value for entry efficiency as $f_{entry} = \rho_{init} N_c / (2fk_d[I]N_A)$ should reveal that the best estimate for [$T_w^\bullet$] is given by equation (8.70) when f_{entry} is close to zero, and equation (8.71) when $f_{entry} \approx 100\%$.

Figure 8.14 illustrates the error associated with the above estimates for $[T_w^\bullet]$ for various initiator concentrations. The results displayed here clearly account for the accuracy of the $\bar{n}$ values obtained using the negligible entry approximation for $[T_w^\bullet]$ with [I] = 1 M, presented in Figure 8.13 (c). In this case the overestimate of $[T_w^\bullet]$ given by the negligible termination approximation leads to erroneously low values of $\bar{n}$.

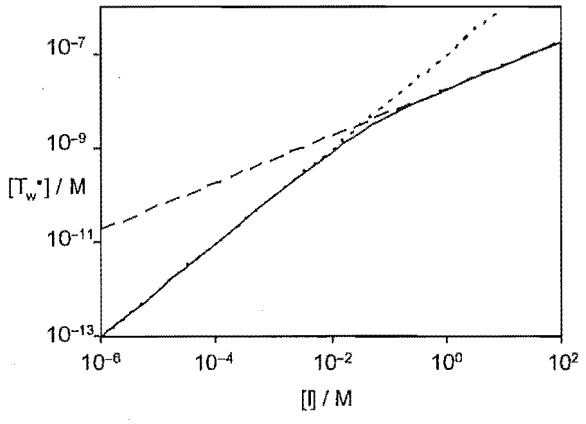

Figure 8.14. $[T_w^\bullet]$ as a function of initiator concentration for Interval II seeded emulsion polymerisation of MMA at 50°C with $k_t^{LL} = 1 \times 10^4$ M^{-1} s^{-1}; exact values obtained from numerical solutions of the extended Smith-Ewart model (————), and approximate values assuming either negligible entry (— — —) or negligible termination (– – – –) of aqueous-phase radicals.

It is also apparent from Figure 8.14 that there will be a region of "intermediate" initiator concentration where neither approximation for $[T_w^\bullet]$ is strictly accurate; here the entry efficiency will be non-negligible but significantly less than 100%. Under such conditions both approximations will slightly underestimate the value of $\bar{n}$, as illustrated for the case of [I] = 1×10^{-1} M in Figure 8.13 (b).

Finally, at low initiator concentration, where $f_{entry} \approx 100\%$, Figure 8.14 shows that the value of $[T_w^\bullet]$ predicted using the negligible entry approximation may be in error by more than an order of magnitude. Interestingly, however, in Figure 8.13 (a) it is seen that both approximations for $[T_w^\bullet]$ result in values of $\bar{n}$ in good agreement with the exact solution. The explanation here is that at low initiator concentration $[T_w^\bullet]$ is so low, and thus the occurrence of aqueous termination so unlikely, that even the seemingly significant overestimate of $[T_w^\bullet]$ given by the negligible entry approximation causes very little error in the value of $\bar{n}$.

Therefore, the range of conditions over which the negligible termination approximation is significantly more accurate than the negligible entry approximation is in fact relatively small. This is demonstrated for conditions of $k_t^{LL} = 1 \times 10^4$ M^{-1} s^{-1} in Figure 8.15, where it is observed that the assumption of negligible termination only provides a substantial advantage in the region of [I] = $1 \times 10^{-3} - 1 \times 10^{-2}$ M. It is also noted that the increasing error associated with both approximations as [I] falls below 1×10^{-4} M arises from increasing compartmentalisation in the system when the rate of entry is reduced.

It is paradoxical that in a system in which f_{entry} values are generally high, it is actually the "negligible entry" limit which gives the best results overall.

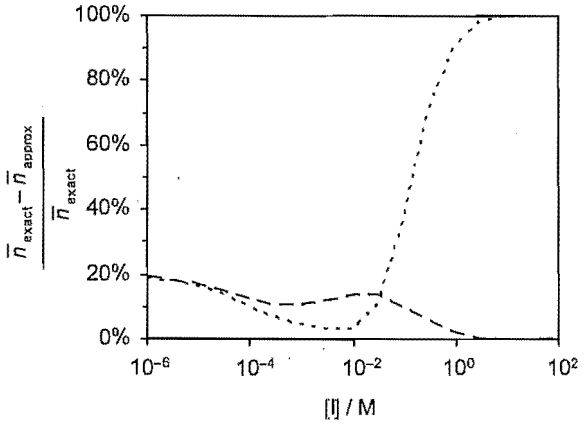

Figure 8.15. Error in value of $\bar{n}$ calculated over a range of initiator concentrations for $k_t^{LL} = 1 \times 10^4$ M^{-1} s^{-1}, using the extended pseudo-bulk model assuming either negligible entry (— — —) or negligible termination (– – – –) of aqueous-phase radicals; error calculated as $(\bar{n}_{exact} - \bar{n}_{approx})/\bar{n}_{exact}$ where $\bar{n}_{exact}$ corresponds to extended Smith-Ewart model and $\bar{n}_{approx}$ to extended pseudo-bulk model.

8.8.1 Limiting Cases of the Extended Pseudo-Bulk Model

Casey *et al.*[4] showed for the zero-one model that, by considering the possible fates for exited monomeric radicals, a number of different limiting forms for the general set of equations may be identified. This gives rise to a small set of simplified kinetic equations (each corresponding to a different assumed fate) that are mathematically easier to solve and intuitively easier to relate to the important physical processes. Judicious use of these limiting forms represents the most accessible means for implementing the zero-one kinetic model.

The identification of similar limiting forms of the extended Smith-Ewart model is obviously an area of considerable interest. However, the final result in this case is likely to be somewhat more complex than for the zero-one model given that here we must consider three possible fates for monomeric radicals inside a latex particle, *viz.*, propagation, termination and desorption, as well as three possible aqueous-phase fates: propagation, termination and re-entry. A full consideration of each of these fates is undertaken in Appendix A.7, resulting in the formulation of a set of seven distinct limiting kinetic equations. While this is a comparatively large set of equations, it is nevertheless possible that these simplified forms may provide a useful alternative to the general form of the extended pseudo-bulk model presented in the previous section. This is an interesting topic for further investigation.

8.8.2 Chain Length Dependent Termination

As stated earlier in this chapter, the incorporation of chain length dependent termination kinetics into the extended Smith-Ewart model is thought to give rise to a set of kinetic equations that is too extensive to be solved using present methods. However, the much simpler set of equations comprising the extended pseudo-bulk model may well be amenable to the inclusion of chain length dependent termination.

It is suggested that a similar approach to that used by Russell *et al.*[10] in the context of the traditional pseudo-bulk model could be used here, defining $\overline{n}$ as the first moment of the intra-particle radical chain length distribution:

$$\overline{n} = \sum_{i=1}^{\infty} n_i \tag{8.72}$$

where n_i is the fraction of radicals that are of degree of polymerisation i.

If $k_t^{i,j}$ is defined as the chain length dependent microscopic rate coefficient for intra-particle termination involving a pair of radicals of degrees of polymerisation i and j respectively, values for k_t^{ML} and k_t^{LL} may then be defined as summations of the $k_t^{i,j}$ values, weighted according to the specific distribution of n_i populations:

$$k_t^{ML} = 2 \sum_{i=2}^{\infty} k_t^{1,i} \frac{n_1}{\overline{n}} \frac{n_i}{\overline{n}} \tag{8.73}$$

$$k_t^{LL} = \sum_{i=2}^{\infty}\sum_{j=2}^{\infty} k_t^{i,j} \frac{n_i}{\overline{n}} \frac{n_j}{\overline{n}} \tag{8.74}$$

where the factor of two appearing in equation (8.73) is consistent with the definition of k_t^{ML} in Appendix A.1.

The incorporation of chain length dependent termination into the extended pseudo-bulk model also represents an interesting area for future work, although it is noted that in essence such modelling has already been carried out as part of this work (section 4.6.3).

8.9 Conclusions

This chapter has detailed the formulation of a new kinetic model which extends the founding kinetic equations for emulsion polymerisation formulated by Smith and Ewart[1] to include radical chain transfer to monomer reactions within a latex particle, and subsequent reactions involving the monomeric radicals so formed. A relatively simple numerical method may be used to obtain steady-state solutions to the full set of rate equations, yielding values for all relevant radical and particle populations. Importantly, this methodology is based on input values of only well-defined rate parameters, thus requiring no preconceived mechanistic assumptions.

This extended Smith-Ewart model has been applied to a number of exemplary emulsion polymerisation systems and in all cases the results obtained were critically compared with those procured using existing kinetic models.

In the case of the styrene/persulfate system at 50°C, results obtained using the new model confirm that the zero-one approximation which is often applied to this system is likely to be valid under typical experimental conditions. However, this work also revealed that the provision of pseudo-instantaneous termination, central to the zero-one model, is not guaranteed solely by termination involving a monomeric radical (ML-termination), as has previously been suggested,[4] and requires a sufficiently rapid rate for mutual termination of non-monomeric radicals (LL-termination). Furthermore, it appears unlikely that the plateau in $\overline{n}$ values at 0.5 predicted by the zero-one model at high initiator concentration may be observed under realistic experimental conditions.

For the MMA/persulfate system at 50°C it is also found that existing methods provide accurate results under typical experimental conditions. In this case the extended Smith-Ewart model agrees well with both the traditional Smith-Ewart and pseudo-bulk models when a value of $\alpha = 1$ is assumed. Importantly, these results are supportive of the methods used for analysis of experimental data from this system in Chapters 4 and 6.

In view of the comparative computational simplicity offered by existing modelling methodologies there is an obvious argument for favouring these approaches over the extended Smith-Ewart model wherever they are of commensurate accuracy. However, even in these cases it should be considered that (1) the extended model is free of any mechanistic assumptions, *e.g.*, the effects of radical compartmentalisation are always accounted for, and the fate of exited radicals is effectively determined *a priori*; (2) this new model is based entirely on meaningful rate parameters – as opposed to less well-defined quantities such as α, ρ and k – thus permitting more detailed mechanistic interpretations than current models; and (3) by explicitly calculating the values of a wide range of individual rate parameters, the extended model automatically accounts for the effect of changes in, *e.g.*, $[M]_p$, $[M]_w$, $[I]$, $[T_w^\bullet]$ and r_s on the various rates of radical entry, exit and termination in the system. Given that the computational demands for obtaining steady-state solutions as described here are relatively modest by current standards, with calculations easily carried out on a personal computer, the above reasons alone are probably sufficient grounds to advocate indiscriminate use of the extended Smith-Ewart model (at least under conditions where the neglect the chain length dependent termination is not ruinous). In particular point (2) above is important.

Notwithstanding the above recommendation, it has also been found that the extended Smith-Ewart model offers a distinct advantage over existing models for systems where LL-termination is relatively slow and ML-termination thus becomes important. The Interval III emulsion polymerisation of BMA appears to provide an example of such a system; here a high value of w_p provides for reductions in both k_t^{LL} and k_t^{ML} (as compared with their Interval II values). It is anticipated that the extended model may offer similar advantages for other systems in which w_p is high, and it remains of interest to carry out modelling of styrene and MMA emulsion systems under Interval III conditions using this new approach.

Finally, the extended Smith-Ewart model has been condensed into a single (approximate) overall rate equation for $\bar{n}$ – the "extended pseudo-bulk equation" – and a method given for

obtaining analytic solutions to this equation. This simple approach alleviates the computational difficulties associated with exact numerical solutions and has been shown to accurately reproduce the exact results over a wide range of conditions.

8.10 References

(1) Smith, W. V.; Ewart, R. H. *J. Chem. Phys.* **1948**, *16*, 592.

(2) Nomura, M.; Harada, M.; Nakagawara, K.; Eguchi, W.; Nagata, S. *J. Chem. Eng. Japan* **1970**, *4*, 160.

(3) Ugelstad, J.; Hansen, F. K. *Rubber Chem. Technol.* **1976**, *49*, 536.

(4) Casey, B. S.; Morrison, B. R.; Maxwell, I. A.; Gilbert, R. G.; Napper, D. H. *J. Polym. Sci. A: Polym. Chem.* **1994**, *32*, 605.

(5) Morrison, B. R.; Casey, B. S.; Lacík, I.; Leslie, G. L.; Sangster, D. F.; Gilbert, R. G.; Napper, D. H. *J. Polym. Sci. A: Polym. Chem.* **1994**, *32*, 631.

(6) Gilbert, R. G. *Emulsion Polymerization: A Mechanistic Approach*; Academic: London, 1995.

(7) Whang, B. C. Y.; Napper, D. H.; Ballard, M. J.; Gilbert, R. G.; Lichti, G. *J. Chem. Soc. Faraday Trans. 1* **1982**, *78*, 1117.

(8) Ballard, M. J.; Napper, D. H.; Gilbert, R. G. *J. Polym. Sci., Polym. Chem. Edn.* **1984**, *22*, 3225.

(9) Adams, M. E.; Russell, G. T.; Casey, B. S.; Gilbert, R. G.; Napper, D. H.; Sangster, D. F. *Macromolecules* **1990**, *23*, 4624.

(10) Russell, G. T.; Gilbert, R. G.; Napper, D. H. *Macromolecules* **1992**, *25*, 2459.

(11) Dainton, F. G.; Eaton, R. S. *J. Polym. Sci.* **1959**, *39*, 313.

(12) Dainton, F. S.; James, D. G. L. *J. Polym. Sci.* **1959**, *39*, 299.

(13) Sangster, D. F.; Davison, A. *J. Polym. Sci., Polym. Symp.* **1975**, *49*, 191.

(14) Moad, G.; Rizzardo, E.; Solomon, D. H.; Beckwith, A. L. J. *Polym. Bull.* **1992**, *29*, 647.

(15) Gridnev, A. A.; Ittel, S. D. *Macromolecules* **1996**, *29*, 5864.

(16) Griffiths, M. C.; Strauch, J.; Monteiro, M. J.; Gilbert, R. G. *Macromolecules* **1998**, *31*, 7835.

(17) Maxwell, I. A.; Morrison, B. R.; Napper, D. H.; Gilbert, R. G. *Macromolecules* **1991**, *24*, 1629.

(18) McAskill, N. A.; Sangster, D. F. *Aust. J. Chem.* **1979**, *32*, 2611.

(19) McAskill, N. A.; Sangster, D. F. *Aust. J. Chem.* **1984**, *37*, 2137.

(20) Maruthamuthu, P. *Makromol. Chem., Rapid. Commun.* **1980**, *1*, 23.

(21) Ballard, M. J.; Gilbert, R. G.; Napper, D. H. *J. Polym. Sci., Polym. Letters Edn.* **1981**, *19*, 533.

(22) Lichti, G.; Gilbert, R. G.; Napper, D. H. *J. Polym. Sci. A.* **1980**, *18*, 1297.

(23) Hawkett, B. S.; Napper, D. H.; Gilbert, R. G. *J. Chem. Soc. Faraday Trans. 1* **1980**, *76*, 1323.

(24) Lane, W. H. *Ind. Eng. Chem.* **1946**, *18*, 295.

(25) Behrman, E. J.; Edwards, J. O. *Rev. Inorg. Chem.* **1980**, *2*, 179.

(26) Tobolsky, A. V.; Offenbach, J. *J. Polym. Sci.* **1955**, *16*, 311.

(27) Buback, M.; Gilbert, R. G.; Hutchinson, R. A.; Klumperman, B.; Kuchta, F.-D.; Manders, B. G.; O'Driscoll, K. F.; Russell, G. T.; Schweer, J. *Macromol. Chem. Phys.* **1995**, *196*, 3267.

(28) Wilke, C. R.; Chang, P. *A.I.Ch.E. J.* **1955**, *1*, 264.

(29) Russell, G. T. *Macromol. Theory Simulations* **1995**, *4*, 497.

(30) Russell, G. T.; Napper, D. H.; Gilbert, R. G. *Macromolecules* **1988**, *21*, 2133.

(31) Clay, P. A.; Christie, D. I.; Gilbert, R. G., in *Advances in Free-Radical Polymerization*; Matyjaszewski, K., Ed.; A.C.S.: Washington D.C., 1998; Vol. 685, p 104.

(32) Kukulj, D.; Davis, T. P.; Gilbert, R. G. *Macromolecules* **1998**, *31*, 994.

(33) Scheren, P. A. G. M.; Russell, G. T.; Sangster, D. F.; Gilbert, R. G.; German, A. L. *Macromolecules* **1995**, *28*, 3637.

(34) Lamb, D. J., 2003, Ph.D. Thesis, University of Sydney.

(35) Maeder, S.; Gilbert, R. G. *Macromolecules* **1998**, *31*, 4410.

(36) Beuermann, S.; Buback, M.; Gilbert, R. G.; Hutchinson, R. A.; Klumperman, B.; Olaj, F. O.; Russell, G. T.; Schweer, J. *Macromol. Chem. Phys.* **1997**, *198*, 1545.

(37) Halnan, L. F.; Napper, D. H.; Gilbert, R. G. *J. Chem. Soc. Faraday Trans. 1* **1984**, *80*, 2851.

(38) Beuermann, S.; Buback, M.; Davis, T. P.; Gilbert, R. G.; Hutchinson, R. A.; Kajiwara, A.; Klumperman, B.; Russell, G. T. *Macromol. Chem. Phys.* **2000**, *201*, 1355.

(39) Halnan, L. F., 1983, B.Sc.(Hons) Thesis, University of Sydney.

(40) Ballard, M. J.; Gilbert, R. G.; Napper, D. H.; Pomery , P. J.; O'Donnell, J. H. *Macromolecules* **1984**, *17*, 504.

9. Towards Improved Models for Entry

9.1 Introduction

As Appendix A.8 shows, the model of Maxwell *et al.* represents an elegant and relatively simple kinetic treatment for the entry process. Indeed, this is probably a major reason for the model being reasonably well accepted in the period since its inception. However, as the depth of understanding and breadth of experimental endeavour in the field of emulsion polymerisation have increased, the Maxwell-Morrison model has become the subject of some scrutiny, and, as with any model, its limitations have inevitably started to become apparent. This chapter discusses the areas in which the Maxwell-Morrison model is thought to provide an incomplete account for observed results described in various literature works and through the course of this thesis. New kinetic approaches are proposed which may facilitate more accurate modelling of the entry process, and which are intended to provide a starting point for future investigations in this area.

9.2 Incorporating Aqueous Reactions of Spontaneously-Generated Radicals

In Chapters 3 and 4 it was shown that the rate of radical entry attributed to "spontaneous" radical generation may be of considerable significance in polymerisations initiated by either γ-radiolytic or chemical means. In the latter case it was evident that the rate coefficient for entry of initiator-derived radicals, ρ_{init}, (and hence also the entry efficiency, f_{entry}) is highly sensitive to that assumed for spontaneous entry, ρ_{spont}, at low initiator concentration. This is because ρ_{init} is inferred from the experimentally measured value of ρ (for total entry from all sources), according to equation (9.1), and so ρ_{spont} becomes a large fraction of ρ at low initiator concentration.

$$\rho = \rho_{init} + \rho_{spont} \tag{9.1}$$

In Chapter 7 it was further suggested that the aqueous phase is likely to be a significant locus for spontaneous radical generation, *via* reactions of aqueous monomer and/or reactions involving other species present (*e.g.*, aqueous peroxidic species). It is notable then, that the

Maxwell-Morrison entry model considers only reactions involving aqueous radicals derived from added (chemical) initiator, ignoring the possibility of termination with spontaneously-generated radicals. An alternative modelling approach which accounts for such interaction is described by Scheme 9.1.

Scheme 9.1. Extension of the Maxwell-Morrison entry model to incorporate aqueous-phase kinetics of spontaneously-generated radicals.

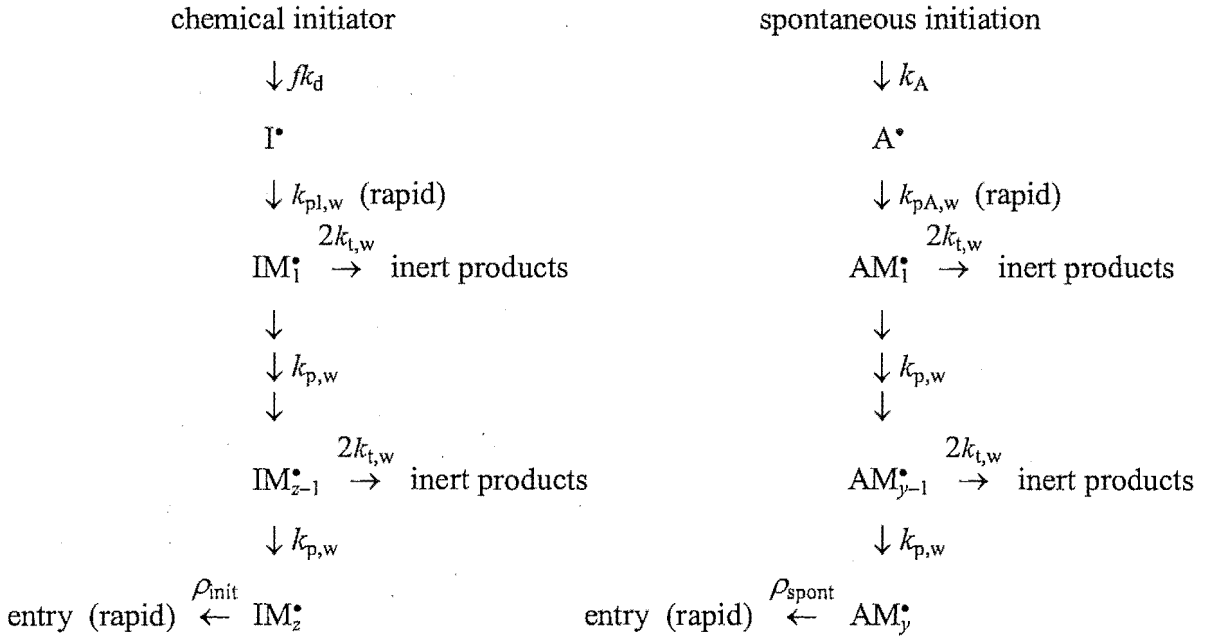

The left-hand-side of Scheme 9.1 presents the full set of aqueous-phase reactions for initiator-derived radicals according to the Maxwell-Morrison entry model, along with the relevant rate coefficients (as defined elsewhere in this thesis) in each case. The right-hand-side gives an analogous reaction scheme for spontaneously-generated radicals, assuming (for simplicity) that these are generated solely in the aqueous phase and undergo the same reactions as initiator-derived radicals. The as yet poorly understood mechanism for spontaneous initiation is assumed to be governed by some rate coefficient k_A, estimates for which may possibly be obtained using the approaches of Chapter 7. Spontaneously-generated radicals, denoted A•, are supposed to rapidly propagate to form $AM_1^\bullet$ radicals which may then undergo further propagation to eventually form a surface-active entering radical of degree of polymerisation y, provided that termination does not occur first. The length of entrant radicals created by spontaneous initiation is not assumed to be the same as that for initiator-derived radicals (z).

It is timely at this point to mention the work of Christie *et al.*[1] who have also developed a new kinetic treatment for spontaneous polymerisation. The key feature of this work was the

allowance made for significant spontaneous radical generation occurring inside the latex particles (in addition to any arising in the aqueous phase), and these authors developed extended versions of the zero-one and pseudo-bulk model which account for the effect of such radical generation on the polymerisation kinetics and molecular weight distribution [note that this treatment has not been employed in the present work, since the incidence of intra-particle spontaneous radical generation is thought to be negligibly low in the systems used here (see Chapter 7)]. It should be noted however that the Christie *et al.* treatment does not allow for the interactions between spontaneous and initiator-derived radicals in the aqueous phase (as in Scheme 9.1 above) and, as such, the model developed here may be regarded as complementary to that of Christie *et al.* Importantly, the present model for aqueous radical kinetics is general and independent of any particular assumptions made regarding intra-particle kinetics (*e.g.*, those of the zero-one or pseudo-bulk models).

The set of rate equations arising from Scheme 9.1 is as follows:

$$\frac{d[IM_1^\bullet]}{dt} = 2fk_d[I] - k_{p,w}[M]_w[IM_1^\bullet] - 2k_{t,w}[T_w^\bullet][IM_1^\bullet] \tag{9.2}$$

$$\frac{d[IM_i^\bullet]}{dt} = k_{p,w}[M]_w\left([IM_{i-1}^\bullet] - [IM_i^\bullet]\right) - 2k_{t,w}[T_w^\bullet][IM_i^\bullet], \quad 1 \le i < z \tag{9.3}$$

$$\frac{d[IM_z^\bullet]}{dt} = k_{p,w}[M]_w[IM_{z-1}^\bullet] - \rho_{init}\frac{N_c}{N_A} \tag{9.4}$$

$$\frac{d[AM_1^\bullet]}{dt} = k_A[A] - k_{p,w}[M]_w[AM_1^\bullet] - 2k_{t,w}[T_w^\bullet][AM_1^\bullet] \tag{9.5}$$

$$\frac{d[AM_i^\bullet]}{dt} = k_{p,w}[M]_w\left([AM_{i-1}^\bullet] - [AM_i^\bullet]\right) - 2k_{t,w}[T_w^\bullet][AM_i^\bullet], \quad 1 \le i < y \tag{9.6}$$

$$\frac{d[AM_y^\bullet]}{dt} = k_{p,w}[M]_w[AM_{y-1}^\bullet] - \rho_{spont}\frac{N_c}{N_A} \tag{9.7}$$

where $k_A[A]$ represents the aqueous flux of spontaneously-generated radicals (assumed, for simplicity, to be given by a first-order reaction of some species denoted A), $AM_i^\bullet$ represents a radical of chain length i derived from spontaneous-initiation, and $k_{pA,w}$ is the rate coefficient for the first propagation step, assumed to be rapid. Notably, it is assumed here that for a given monomer the rate coefficients for aqueous propagation and termination of

spontaneously-generated oligomeric radicals are the same as those for initiator-derived radicals; however this assumption may be trivially removed. Of course, spontaneous radical generation is probably not a first-order process (see Chapter 7), and besides, the nature of species "A" is unknown – indeed it quite possibly varies from system to system, even for the one monomer (again, see Chapter 7). Thus $k_A[A]$ should be thought of as the rate of spontaneous radical generation here, not as tying spontaneous radical generation to a particular reaction order.

The essence of this model is the allowance for termination involving both initiator-derived and spontaneously-generated radicals. Thus, the total concentration of aqueous radicals is now defined as:

$$[T_w^\bullet] = \sum_{i=1}^{z-1} [IM_i^\bullet] + \sum_{i=1}^{y-1} [AM_i^\bullet] \tag{9.8}$$

Steady-state solutions of equations (9.2) – (9.8) may be obtained using the same numerical methods described for the original Maxwell-Morrison model in Chapter 1. The rate coefficients for radical entry are then also obtained by applying the steady-state approximation to equations (9.4) and (9.7):

$$\rho_{init} = k_{p,w}[M]_w[IM_{z-1}^\bullet]\frac{N_A}{N_c} \tag{9.9}$$

$$\rho_{spont} = k_{p,w}[M]_w[AM_{y-1}^\bullet]\frac{N_A}{N_c} \tag{9.10}$$

Illustrative results from the new model are presented in Figures 9.1 and 9.2 for the seeded emulsion polymerisation of styrene at 50°C with persulfate as initiator. Here we adopt values of $fk_d = 1.1 \times 10^{-6}$ s^{-1},[2] $k_{p,w} = k_p = 2.6 \times 10^2$ M^{-1} s^{-1},[3] $[M]_w = 4.3 \times 10^{-3}$ M,[4] $k_{t,w} = 3.5 \times 10^9$ M^{-1} s^{-1},[5] $N_c = 1 \times 10^{17}$ dm^{-3}, and $z = 2$ (see reference[5] and Chapter 3 of this thesis). Also displayed are a set of calculated values of ρ obtained using the Maxwell-Morrison model and the conventional approach of assuming a constant value for ρ_{spont} in equation (9.1). In this case a typical value for ρ_{spont} (see Chapter 7) of 1×10^{-4} s^{-1} is used. It is noted that this conventional approach may be emulated by the new model using a value of $y = 1$, in which case it is assumed that all spontaneously-generated radicals undergo entry and thus a constant value is given for $\rho_{spont} = k_A[A]N_A/N_c$.

In Figure 9.1 are presented values of ρ calculated over the relevant range for experimental investigations using a range of values for the flux of spontaneously-generated radicals. Here it is assumed that $y = z = 2$; *i.e.*, entrant radicals derived from chemical and spontaneous initiation are of the same chain length. As is to be expected, increasing the flux of spontaneously-generated radicals has a significant effect on the value of ρ at low initiator concentration. Clearly, the conventional approach is reasonably well approximated by the new model with $y = 2$ and $k_A[A]$ of order 1×10^{-11} M s^{-1}. As $k_A[A]$ increases to 1×10^{-9} M s^{-1}, entry of spontaneously-generated radicals is seen to dominate over initiator-derived radicals even at relatively high initiator concentrations. While such a high flux of spontaneous radicals is certainly not representative of typical emulsion systems, this may be an accurate account of entry in systems such as that using the cationic styrene seed latex CAT02 of Chapter 3, for such high ρ_{spont} were found, as well as evidence suggesting that these radicals originate in the aqueous phase (see Chapter 7). The reason for the plateaux in ρ values in Figure 9.1 is that $k_A[A] \gg 2fk_d[I]$ and is independent of [I], and one is in the "propagation limit" (see Appendix A.8).

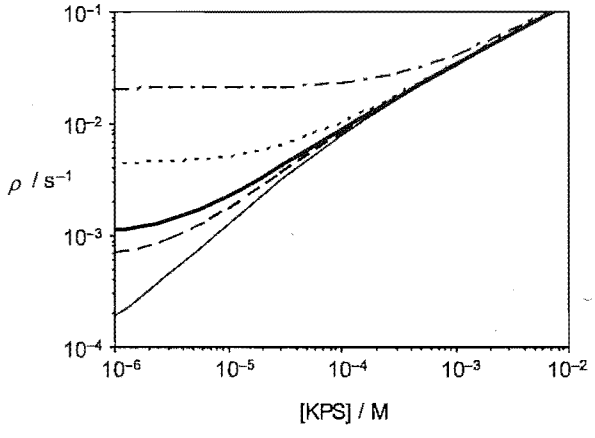

Figure 9.1. ρ as a function of initiator concentration; calculated using Maxwell-Morrison model and a constant value of $\rho_{spont} = 1 \times 10^{-4}$ s^{-1} (————); calculated using model of Scheme 9.1 with $y = 2$ and spontaneously-generated radical flux of $k_A[A] = 1 \times 10^{-12}$ M s^{-1} (————), 1×10^{-11} M s^{-1} (— — —), 1×10^{-10} M s^{-1} (– – – –) and 1×10^{-9} M s^{-1} (– —— –).

It is also found, not surprisingly, that the value of ρ obtained using the new model is highly sensitive to the value assumed for y. In Figure 9.2 are presented results calculated using the original Maxwell-Morrison model and assuming $\rho_{spont} = 0$ s^{-1} in equation (9.1) (such that $\rho =$

ρ_{init}). Also shown are ρ values obtained from the new model assuming a spontaneous radical flux of $k_A[A] = 1 \times 10^{-10}$ M s^{-1}. When a value of $y \leq 3$ is used in the new model the rate coefficient for entry is seen to be significantly enhanced by the contribution from spontaneously-generated radicals over a wide range of initiator concentrations. As the value of y increases, so does the residence time of spontaneous radicals in the aqueous phase; greater incidence of termination leads to a significant decrease in the modelled value of ρ. Under some conditions the presence of spontaneous radicals is even seen to cause the value of ρ to fall below that calculated in the absence of spontaneous initiation (because of extra radical loss due to termination; again, see Appendix A.8 for an explanation of this counter-intuitive behaviour, *i.e.*, how an increase in radical flux can result in a decrease in ρ).

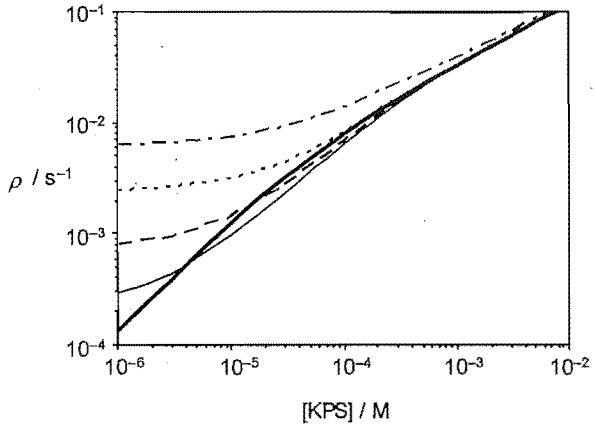

Figure 9.2. ρ as a function of initiator concentration; calculated using Maxwell-Morrison model and value of $\rho_{spont} = 0$ s^{-1} (————); calculated using model of Scheme 9.1 with spontaneously-generated radical flux of $k_A[A] = 1 \times 10^{-10}$ M s^{-1}, and $y = 1$ (– —— –), 3 (– – – –), 5 (— — —), or 7 (————).

It should be noted, however, that the mechanistic inferences of Chapter 7 suggest that spontaneously-generated radicals may well be derived from monomeric, dimeric or oligomeric species. Thus, in the case of styrene systems, a low value of $y \approx 1$ might be expected – given that $y = 2$ would be consistent with a radical species as water-soluble as $SO_4^{\bullet-}$. On the other hand, the incorporation of peroxidic functionality (thought to be involved in spontaneous radical generation under some circumstances, see Chapter 7) would raise the value of y.

In view of the results obtained here it seems unlikely that interactions between initiator-derived and spontaneously-generated radicals in the aqueous phase will be of great

significance under usual emulsion polymerisation conditions. However, the model presented here may provide useful insights into modelling systems wherein the rate of spontaneous initiation is uncommonly high, such as chlorobutadiene.[1] It is noted that Verdurmen *et al.*[6] observed ρ independent of [I] in butadiene systems and interpreted this as evidence of $z = 3$ (see Appendix A.8 for the explanation). However, the calculations of the present work make it clear that such results can also be explained by dominant spontaneous polymerisation. Given the importance of such initiation in chlorobutadiene,[1] it is not unreasonable to suggest that it is also important in butadiene. This suggestion warrants investigation at least in the form of closer scrutiny of the butadiene data.

Finally, it is explained that in the context of this thesis the particular motivation for this section of work was the observation of a plateau in the value of ρ at low initiator concentration in the styrene V-50/AN01 system of Chapter 3. Specifically, the value of ρ at the lowest initiator concentration used, [V-50] = 3×10^{-6} M, was found to be the same as that of ρ_{spont}. In this case it was found that the model of Scheme 9.1 was able to account for the trend in experimental ρ using a high flux of spontaneous radicals, $k_A[A] = 1 \times 10^{-10}$ M s^{-1}, with a high critical degree of polymerisation for entry, $y = 6$. While it was pleasing that the model provided some sort of explanation here, as remarked above, conditions such as these do not seem physically realistic for typical emulsion systems.

9.3 Incorporating Adsorption, Desorption and Entry for Oligomers of Different Chain Lengths

The central assumption of the Maxwell-Morrison model is the stipulation that the only aqueous radical species capable of undergoing entry into a latex particle are initiator-derived radicals of degree of polymerisation z. It is recognised that this is an oversimplification of reality: entry must actually occur over a (possibly narrow) range of chain lengths, with some radicals entering before the addition of z monomer units and some radicals growing to length greater than z before undergoing entry. In effect, z may therefore be thought of as some sort of average chain length for entry. While this approach offers considerable simplicity, a more complete model would allow for entry by a range of oligomeric radical species.

A further supposition of the Maxwell-Morrison model is that entry of z-meric radicals is rapid and non-rate-determining. As noted in Chapter 1, Morrison *et al.* have used "competitive

growth" experiments (incorporating a bimodal seed latex) to show that the relative rates of entry vary with particle radius approximately as expected for a diffusion-controlled process.[7-9] Coen *et al.* have also provided evidence that in a system with electrostatically stabilised latex particles this diffusion-controlled entry step is indeed non-rate-determining.[10] However it is noted that the same may not be assumed for entry into *electrosterically* stabilised particles (*i.e.*, particles with charge-carrying polymeric species adsorbed or grafted to their surface, which impart colloidal stability through a combination of electrostatic and steric repulsion between particles), as is now discussed.

Leemans *et al.* observed changes in the rate of *ab initio* emulsion polymerisations of MMA when different block polyelectrolytes were used as adsorbed electrosteric stabilisers.[11] These workers have proposed that charge interactions between block polyelectrolyte surfactant and entrant radicals give rise to differences in the rate of radical entry in such systems. While the significance of such charge interactions to entry would appear to be refuted by the results in Chapter 3 of this thesis, it is conceivable that the rate of diffusion-controlled entry may be significantly affected by the steric hindrance to entry provided by the polyelectrolyte stabiliser. However, it should be noted that Leemans *et al.* compared only overall polymerisation rate data, conveying no knowledge of the actual rates of particle entry and exit (and termination for that matter). Thus it seems impossible to unambiguously attribute the observed rate disparities to an entry effect; these could equally be the result of some influence of polyelectrolyte stabiliser on the rate of radical exit from the particles. Moreover, it should be recognised that differences in the rates of initiator decomposition and particle formation in these *ab initio* polymerisations might further complicate the interpretation of these results.

More definitive kinetic data for entry in electrosterically stabilised systems has been presented by Coen *et al.*[10] and Vorwerg *et al.*[12] who studied the effects of poly(acrylic acid) stabiliser copolymerised onto the surface of polystyrene particles used in seeded emulsion polymerisations of styrene. Here the rates of both radical entry and exit were isolated and both were found to be to be significantly diminished in the presence of extensive coverage by electrosteric stabiliser. This was thought to reflect slowed diffusion of entering/exiting radicals near the particle surface due to interaction with electrosteric stabiliser.

Given the Maxwell-Morrison model's assumption that the entry step is non-rate-determining, any observed reduction in the entry rate due to electrosteric stabilisers may only be accommodated by an increase in the value inferred for z – an approach that is physically

misleading given that, in reality, a species should become capable of entry at the same length whether or not such stabilisers are present. Thus, a further improvement would be to specifically account for the rate of adsorption of aqueous oligomers onto latex particles. If such stabilisers represent a barrier to entry, then effectively a radical gets blocked from entering, even though in terms of hydrophobicity it is ready to enter. During this additional "waiting time" the radical may propagate further or terminate, thus reducing the rate of entry and giving longer entering species, which of course would represent a kinetic rather than thermodynamic effect.

One approach to modelling entry that incorporates both the extensions described above – *i.e.*, radical diffusion/adsorption considerations and the possibility of entrant radicals spanning a range of oligomeric chain lengths – is proposed in Scheme 9.2.

Scheme 9.2. Extension of the Maxwell-Morrison entry model to incorporate the possibility of adsorption, desorption and entry of oligomeric radicals of all chain lengths.

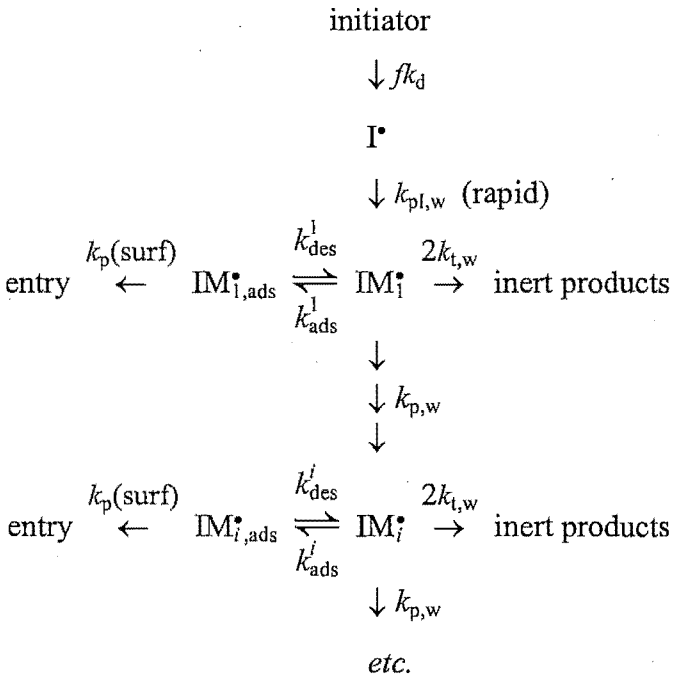

In a sense this is a return to the "HUFT" theory,[13,14] which also allows for entry by oligomeric radicals of all lengths. What is new here are the adsorption-desorption kinetics. Here it is assumed (based on experimental evidence[15-17]) that the first propagation step is rapid and non-rate-determining. Oligomeric radicals are assumed to partition themselves between the aqueous phase and particle surface according to an adsorption-desorption equilibrium, where k^i_{ads} and k^i_{des} are the second-order rate coefficient for adsorption and the first-order rate

coefficient for desorption of an i-meric radical, respectively. $IM_i^\bullet$ denotes an aqueous radical of degree of polymerisation i, and $IM_{i,ads}^\bullet$ is the adduct formed by adsorption of an $IM_i^\bullet$ radical onto a particle's surface, *i.e.*, $IM_{i,ads}^\bullet$ represents a *single* particle with a *single* i-meric radical adsorbed. This approach therefore implicitly assumes that the aqueous concentration of $IM_{i,ads}^\bullet$ adducts is less than the total aqueous particle concentration – *i.e.*, $[IM_{i,ads}^\bullet] < N_c/N_A$ – and that (on average) any particle will never contain more than one adsorbed radical. The validity of this assumption may be roughly assessed as follows. Using a persulfate-initiated system at 50°C as an example, we assume a maximum initiator concentration of [KPS] = 0.01 M (the highest [KPS] used in any experiments in this thesis) and approximate the total steady-state concentration of aqueous radicals as $[T_w^\bullet] = \sqrt{fk_d[KPS]/k_{t,w}}$ (a reasonable approximation when entry efficiency is low). Assuming values of $fk_d = 1.1 \times 10^{-6}$ s^{-1} and $k_{t,w} = 3.7 \times 10^9$ M^{-1} s^{-1}, as in earlier chapters, gives $[T_w^\bullet] = 1.7 \times 10^{-9}$ M. Taking a realistic lower bound value for N_c of 1×10^{15} dm^{-3} and assuming that *all* aqueous radicals are in fact adsorbed onto particles then gives the average number of adsorbed radicals per particle as $[T_w^\bullet]N_A/N_c \approx 1$. Of course the above approach will considerably overestimate the number of adsorbed radicals per particle, thus the earlier assumption of $[IM_{i,ads}^\bullet] < N_c/N_A$ is valid.

From Scheme 9.2 it is possible to formulate the following population balance equations for all oligomeric radicals and radical-particle adducts:

$$\frac{d[IM_1^\bullet]}{dt} = 2fk_d[I] + k_{des}^1[IM_{1,ads}^\bullet] - k_{ads}^1\frac{N_c}{N_A}[IM_1^\bullet] - k_{p,w}[M]_w[IM_1^\bullet] - 2k_{t,w}[T_w^\bullet][IM_1^\bullet] \qquad (9.11)$$

$$\frac{d[IM_i^\bullet]}{dt} = k_{p,w}[M]_w[IM_{i-1}^\bullet] + k_{des}^i[IM_{i,ads}^\bullet] - k_{ads}^i\frac{N_c}{N_A}[IM_i^\bullet] - k_{p,w}[M]_w[IM_i^\bullet] - 2k_{t,w}[T_w^\bullet][IM_i^\bullet], \quad 1 < i \qquad (9.12)$$

$$\frac{d[IM_{i,ads}^\bullet]}{dt} = k_{ads}^i\frac{N_c}{N_A}[IM_i^\bullet] - k_{des}^i[IM_{i,ads}^\bullet] - k_{p,w}(surf)[M]_w(surf)[IM_{i,ads}^\bullet], \quad 1 \le i \qquad (9.13)$$

It is important to note that all concentrations and rate coefficients used in equations (9.11) – (9.13) are defined *per unit volume of the aqueous phase*. While this approach may seem non-intuitive – *e.g.*, it might seem more logical to consider the *surface concentration* of adsorbed species – it affords considerable kinetic simplicity, obviating the need to re-define rate coefficients in terms of, *e.g.*, unit particle surface area. Thus $[IM_{i,ads}^\bullet]$ is defined as the

concentration of particles containing a single adsorbed i-meric radical, *per unit volume of aqueous phase*, and the average number of adsorbed radicals per particle may be calculated (if necessary) simply as $\sum_{i=1}^{\infty}[\mathrm{IM}^{\bullet}_{i,\mathrm{ads}}]N_\mathrm{A}/N_\mathrm{c}$.

Also, there is assumed to be no interaction between oligomeric radicals adsorbed onto the particle surface and any propagating radicals that may be resident in the particle interior; adsorption and desorption of oligomeric radicals occur independently of the presence or absence of intra-particle radicals.

The rate of propagation for adsorbed radicals depends on the propagation rate coefficient and monomer concentration in the vicinity of the particle surface, denoted $k_{\mathrm{p,w}}(\mathrm{surf})$ and $[\mathrm{M}]_\mathrm{w}(\mathrm{surf})$ respectively, and defined per unit volume of aqueous phase. Here it is assumed that $k_{\mathrm{p,w}}(\mathrm{surf}) = k_{\mathrm{p,w}} = k_\mathrm{p}$ (*i.e.*, the bulk value), and it is sensible to suppose that the monomer concentration at the particle surface will be significantly greater than that in the aqueous phase, while not exceeding the intra-particle value, *i.e.*, $[\mathrm{M}]_\mathrm{w} < [\mathrm{M}]_\mathrm{w}(\mathrm{surf}) \leq [\mathrm{M}]_\mathrm{p}$. A simple approach is to assume that, to reasonable approximation, $[\mathrm{M}]_\mathrm{w}(\mathrm{surf}) = [\mathrm{M}]_\mathrm{p}$.

Thus, the only rate coefficients in equations (9.11) – (9.13) that remain unfamiliar are those for adsorption and desorption, k^i_{ads} and k^i_{des}. Based on the findings of Morrison *et al.*[7-9] we assume adsorption to be diffusion-controlled, and therefore described by the Smoluchowski equation, with a barrier to entry:

$$k^i_{\mathrm{ads}} = 4\pi D^i_\mathrm{w} r_\mathrm{s} N_\mathrm{A} \exp(-E_{\mathrm{a,ads}}/RT) \qquad (9.14)$$

where D^i_w is the diffusion coefficient for an i-meric initiator-derived radical in water and r_s is the swollen particle radius. Here $E_{\mathrm{a,ads}}$ is the activation energy for adsorption, which may for example be significant if electrosteric stabiliser is present. Values for D^i_w may then be estimated by assuming that the aqueous diffusion coefficient for a 1-meric radical derived from initiator is well-approximated by that for a monomer molecule (denoted D_w) and using the empirical scaling law for diffusion coefficients reported by Griffiths *et al.*[18,19], which together yield:

$$D^i_\mathrm{w} = D_\mathrm{w} i^{-0.664} \qquad (9.15)$$

Recognising that in a seeded polymerisation with no secondary nucleation N_c remains constant, it is convenient to define the pseudo-first-order rate coefficient for adsorption of an i-meric aqueous radical as:

$$k^i_{ads}(\text{pfo}) = k^i_{ads}N_c/N_A = 4\pi D^i_w r_s N_c \exp(-E_{a,ads}/RT) \tag{9.16}$$

Importantly, the inclusion of the adsorption activation energy in equations (9.14) and (9.16) provides a means for specifically accounting for the effects of electrosterically stabilised particles. It should be noted that the treatment used here for the barrier to entry is only an approximate one, and that a more exact treatment could be derived using Kramer's equation or from DLVO theory. It should also be considered that the effective value of D^i_w might be affected by the presence of electrosteric stabiliser in that the rate of diffusion of aqueous radicals may be slowed significantly as they near the particle surface.

Assuming that equilibrium conditions hold, the first-order rate coefficients for radical adsorption and desorption will be related by the adsorption-desorption equilibrium constant, $K^i_{a\text{-}d}$.

$$K^i_{a\text{-}d} = \frac{k^i_{ads}(\text{pfo})}{k^i_{des}} = \frac{[\text{IM}^\bullet_{i,ads}]}{[\text{IM}^\bullet_i]} \tag{9.17}$$

where the standard states for both $\text{IM}^\bullet_i$ (aqueous oligomeric radicals) and $\text{IM}^\bullet_{i,ads}$ (particles containing an adsorbed oligomeric radical) are defined simply as 1 mol per dm^3 of the aqueous phase. Thus the value of k^i_{des} will be available through equation (9.17), given a value for $K^i_{a\text{-}d}$. Ideally, this equilibrium constant could be measured experimentally for the relevant systems. Alternatively, a value of $K^i_{a\text{-}d}$ may be obtained from the hydrophobic free energy of adsorption for an i-meric radical, ΔG^i_{hyd}:

$$K^i_{a\text{-}d} = \exp\left(\frac{-\Delta G^i_{hyd}}{RT}\right) \tag{9.18}$$

Of course ΔG^i_{hyd} should not be very much affected by electrosteric stabiliser, thus as well as k^i_{ads}, k^i_{des} must be lowered in such cases [see equation (9.17)]. It has indeed been found that exit rates are lowered in such systems.[10,12] These effects are thus kinetic, not thermodynamic, in origin: the free energy change associated with a radical transferring between aqueous and

surface phases is still the same, but a barrier exists making the rates of transfer slower. The above approach bears some similarity to that proposed by Casey *et al.*[8] However, it is noted that the treatment of those authors was aimed only at establishing a method for *a priori* prediction of the value of z in the Maxwell-Morrison entry model, whereas the aim of the present exercise is to propose a means for advancing beyond the "z-mer entry" restriction.

Unfortunately (as also remarked by Casey *et al.*) no definitive experimental data yet exist for the values of either $K^i_{\text{a-d}}$ or ΔG^i_{hyd} pertaining to the oligomeric radicals of interest here. Until such data become available it is thus useful to consider any methods proposed for estimating this quantity.

ΔG^i_{hyd} may be approximated for oligomeric radicals derived from persulfate using the group-additive approach originally proposed by Maxwell *et al.*,[5] who estimated (from surfactant micellisation data) the free energy change required to render a polar SO_4^- group surface-active as ~ 23 kJ mol^{-1}. In addition they suggested that the hydrophobic free energy for a monomer molecule may be estimated from its water-solubility, $[M]^{\text{sat}}_{\text{w}}$, as: $RT \ln([M]^{\text{sat}}_{\text{w}}/\text{mol dm}^{-3})$. Thus the overall value of ΔG^i_{hyd} for a persulfate-derived radical may be roughly approximated from these contributions as ΔG^i_{hyd} / kJ mol^{-1} = 23 + $iRT \ln([M]^{\text{sat}}_{\text{w}}/\text{mol dm}^{-3})$, although it should be noted that this approach implicitly assumes that the standard states adopted in obtaining this estimate are the same as those defined earlier. More recently, Dong and Sundberg[20] have presented a more elaborate group-additive approach for estimating ΔG^i_{hyd}, which uses a so-called "lattice model" to describe the conformations of adsorbed radical chains at the particle surface. This model is also applicable to oligomers formed in copolymerisations, but once again is limited to persulfate-derived radicals. Alternatively, it is possible that estimates for ΔG^i_{hyd} may be obtained from semi-empirical quantum mechanical modelling methods, such as those used by Cummins and Gready to calculate the solvation free energies for a range of ionised molecules in water.[21] However, it is emphasised that when employing any approximate value for ΔG^i_{hyd} obtained from model calculations, careful consideration must be given to the standard states adopted.

In the event that a value of ΔG^i_{hyd} is available, or is estimated using one of the above approaches, calculation of k^i_{ads}(pfo) and k^i_{des} *via* equations (9.16) – (9.18) then enables the

concentrations of all radicals and radical-particle adducts to be obtained from the steady-state solutions of equations (9.11) – (9.13):

$$[\mathrm{IM}_1^\bullet] = \frac{2fk_\mathrm{d}[\mathrm{I}] + k_\mathrm{des}^1[\mathrm{IM}_{1,\mathrm{ads}}^\bullet]}{k_\mathrm{ads}^1(\mathrm{pfo})[\mathrm{IM}_1^\bullet] + k_{\mathrm{p,w}}[\mathrm{M}]_\mathrm{w} + 2k_{\mathrm{t,w}}[\mathrm{T}_\mathrm{w}^\bullet]} \tag{9.19}$$

$$[\mathrm{IM}_i^\bullet] = \frac{k_{\mathrm{p,w}}[\mathrm{M}]_\mathrm{w}[\mathrm{IM}_{i-1}^\bullet] + k_\mathrm{des}^i[\mathrm{IM}_{i,\mathrm{ads}}^\bullet]}{k_\mathrm{ads}^i(\mathrm{pfo}) + k_{\mathrm{p,w}}[\mathrm{M}]_\mathrm{w} + 2k_{\mathrm{t,w}}[\mathrm{T}_\mathrm{w}^\bullet]}, \quad 1 < i \tag{9.20}$$

$$[\mathrm{IM}_{i,\mathrm{ads}}^\bullet] = \frac{k_\mathrm{ads}^i(\mathrm{pfo})[\mathrm{IM}_i^\bullet]}{k_\mathrm{des}^i + k_\mathrm{p}[\mathrm{M}]_\mathrm{p}}, \quad 1 \le i \tag{9.21}$$

The essence of the entry model of Scheme 9.2 is that an adsorbed oligomeric radical is not deemed to have *entered* a particle, and thus become an *intra-particle* radical, until it has undergone propagation at the particle surface. The model assumes that after this first propagation step the probability of further propagation into the particle interior is overwhelming and there is no chance of desorption occurring beyond this point. Importantly, it is also only at this point that any interaction with other intra-particle radicals may first occur. This entry criterion is similar to that of the original Maxwell-Morrison model; however the present case considers entry of all radicals – not just z-mers. Therefore, it is possible to define the pseudo-first-order rate coefficient for entry of initiator-derived radicals in this case as follows:

$$\rho_\mathrm{init} = k_\mathrm{p}[\mathrm{M}]_\mathrm{p}\frac{N_\mathrm{A}}{N_\mathrm{c}}\sum_{i=1}^{\infty}[\mathrm{IM}_{i,\mathrm{ads}}^\bullet] \tag{9.22}$$

Clearly, the contribution to entry from radicals of a given chain length will be determined by the concentration of these radicals adsorbed at the particle surface as given by equation (9.21). For i-meric radicals with $k_\mathrm{ads}^i(\mathrm{pfo}) \ll k_\mathrm{des}^i$, the value of $[\mathrm{IM}_{i,\mathrm{ads}}^\bullet]$ will be very low and the contribution to entry negligible. As i increases so will the contribution to entry; however, eventually a point will be reached where $k_\mathrm{ads}^i(\mathrm{pfo}) \gg k_\mathrm{des}^i$ and the concentration of $\mathrm{IM}_i^\bullet$ radicals in the aqueous phase is very low. The contribution to entry from radicals of these longest chain lengths will also be negligible. Thus, it will be possible to identify the specific range of oligomeric chain lengths responsible for entry in a given system.

Importantly, the Maxwell-Morrison model for entry comes out of the present model given the following limiting conditions:

(1) $k^{i}_{ads}(\text{pfo}) = 0$ for $i < z$. This gives $[\text{IM}^{\bullet}_{i,ads}] = 0$ for $i < z$ [see equation (9.21)].

(2) $k^{z}_{des} = 0$. This gives $[\text{IM}^{\bullet}_{z,ads}] = \dfrac{k^{z}_{ads}(\text{pfo})[\text{IM}^{\bullet}_{z}]}{k_p[\text{M}]_p}$ [see equation (9.21)].

(3) $k^{z}_{ads}(\text{pfo}) \gg k_{p,w}[\text{M}]_w,\ 2k_{t,w}[\text{T}^{\bullet}_w]$. This gives $k^{z}_{ads}(\text{pfo})[\text{IM}^{\bullet}_{z}] = k_{p,w}[\text{M}]_w[\text{IM}^{\bullet}_{z-1}]$ [see equation (9.20)].

Substituting these three results into equation (9.22) gives $\rho_{init} = k_p[\text{M}]_p[\text{IM}^{\bullet}_{z-1}]N_A/N_c$, *i.e.*, the Maxwell-Morrison result. The physical meaning for the above three assumptions is clear, and thus it is evident how they are equivalent to the Maxwell-Morrison model.

9.4 Incorporating Desorption of Oligomeric Radicals after Propagation at the Particle Surface

The above model is actually only a first step in terms of formulating a rigorous model for entry. Fundamentally, this approach is marred by its (greatly simplifying) assumption of irreversible entry following propagation of an adsorbed i-mer. In reality the $(i+1)$-mer formed by propagation must have a smaller, but finite, probability of desorption; thus the assumption of irreversible entry invoked above will result in an over-estimate of the true rate of entry.

A better (but more complex) approach is thought to be that outlined in Scheme 9.3, where the possibility for desorption following propagation of an adsorbed radical is acknowledged.

Scheme 9.3. Extension of the Maxwell-Morrison entry model incorporating adsorption-desorption equilibrium and allowing for desorption of absorbed radicals after propagation at the particle surface.

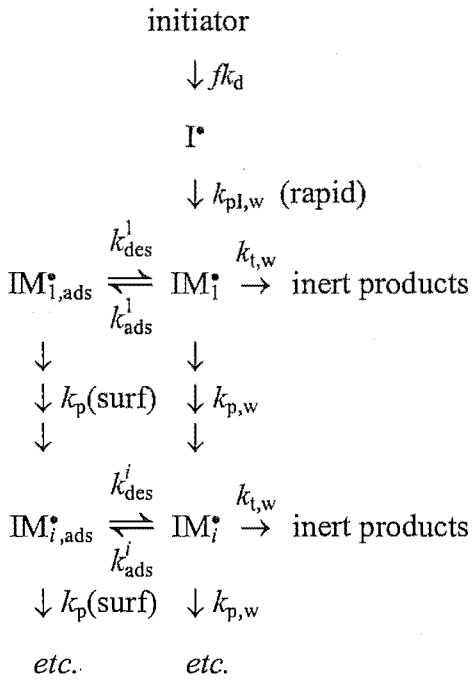

Once again population balance equations may be easily formulated if rate parameters are defined per unit volume of the aqueous phase. In this case the equations pertaining to aqueous oligomeric radicals are the same as given in equations (9.11) and (9.12), and that for radical-particle adducts is as follows:

$$\frac{d[IM^{\bullet}_{i,ads}]}{dt} = k^i_{ads}\frac{N_c}{N_A}[IM^{\bullet}_i] + k_{p,w}(surf)[M]_w(surf)[IM^{\bullet}_{i-1,ads}] - k^i_{des}[IM^{\bullet}_{i,ads}] - k_{p,w}(surf)[M]_w(surf)[IM^{\bullet}_{i,ads}], \quad 1 \le i \quad (9.23)$$

While it is relatively straightforward to solve these rate equations to obtain the concentrations of all aqueous radicals and radical-particle adducts, this approach clearly raises a number of kinetic complications. Foremost among these is the fact that the model does not stipulate the point at which an oligomeric radical is deemed to have *entered* a particle. Thus it is impossible to relate the kinetics of Scheme 9.3 to the rate of formation of *intra-particle* radicals.

In practice, k^i_{des} will decrease with increasing degree of polymerisation such that, for some value of i, k^i_{des} will become sufficiently low that desorption of i-mers from the particles is negligible; oligomers of this degree of polymerisation may be thought of as having

irreversibly *entered* a latex particle. Thus, one possible approach is to define the rate of entry as the rate of formation of oligomers of this specific degree of polymerisation. However, the assumption of a single chain length for entrant radicals is clearly reminiscent of the *z*-mer entry approach of Maxwell *et al.*, and conflicts with one of the fundamental aims of this section of work.

An alternative approach is to assume that all adsorbed oligomeric radicals effectively behave as *intra-particle* radicals during their residence time at the particle surface. In this case, "entry" may be considered as a reversible occurrence (at least for short oligomers) and it is no longer possible to define a simple overall rate coefficient for this process (*i.e.*, ρ_{init}). In addition, for this approach Scheme 9.3 and equations (9.11), (9.12), and (9.23) must be extended to include the kinetics of intra-particle reactions (*e.g.*, termination, transfer) for adsorbed radicals. This extension requires careful consideration of the definition of rate parameters used, since $[\text{IM}^{\bullet}_{i,\text{ads}}]$ has thus far been defined *per unit volume of the aqueous phase*, whereas adsorbed radicals must now be treated as intra-particle species, which are typically defined on a *per particle* basis. It is also necessary to consider the accuracy of assuming that adsorbed radicals undergo the same reactions as other intra-particle radicals – for example, whether an oligomeric radical residing briefly at the particle surface really undergoes termination or transfer at a comparable rate to a long polymeric species whose radical site is buried deep in the particle interior. Finally, in treating all adsorbed radicals as intra-particle radicals, it becomes necessary to somehow include their contribution to the average number of radicals per particle, $\bar{n}$.

For the above reasons the model of section 9.2 actually seems, in hindsight, to be a more physically reasonable model, for it contains the idea that a surface-phase propagation event compels an adsorbed radical to remain permanently particle-bound. In principle, it seems inconsistent to say that an $\text{IM}^{\bullet}_{i-1,\text{ads}}$ radical which propagates has irreversibly entered, while an $\text{IM}^{\bullet}_{i,\text{ads}}$ radical may desorb. However, this is only unreasonable from a strictly thermodynamic viewpoint, whereas entry is a kinetic phenomenon.

9.5 Conclusions

In concluding this chapter it is emphasised that the model development presented herein is by no means purported to constitute rigorous new theory for the kinetics of entry. Rather, it is

hoped that the speculative approach adopted here has provided a range of new ideas for future modelling of entry. It is evident that the formalisation of many of these ideas into a comprehensive theory will be subject to a number of non-trivial kinetic challenges, most notably concerning the precise definition of various kinetic and thermodynamic parameters pertaining to radical adsorption and desorption. Furthermore, it is clear that the effectiveness of more elaborate modelling methods is dependent on the acquisition of new experimental data for radical adsorption and desorption processes. It is stressed that a rigorous account of these processes is the key to progressing beyond the limitations of the existing model for entry. At the same time, the above should not be mistaken as suggesting that the Maxwell-Morrison model is a poor model for entry.

9.6 References

(1) Christie, D. I.; Gilbert, R. G.; Congalidis, J. P.; Richards, J. R.; McMinn, J. H. *Macromolecules* **2001**, *34*, 5158.

(2) Behrman, E. J.; Edwards, J. O. *Rev. Inorg. Chem.* **1980**, *2*, 179.

(3) Buback, M.; Gilbert, R. G.; Hutchinson, R. A.; Klumperman, B.; Kuchta, F.-D.; Manders, B. G.; O'Driscoll, K. F.; Russell, G. T.; Schweer, J. *Macromol. Chem. Phys.* **1995**, *196*, 3267.

(4) Lane, W. H. *Ind. Eng. Chem.* **1946**, *18*, 295.

(5) Maxwell, I. A.; Morrison, B. R.; Napper, D. H.; Gilbert, R. G. *Macromolecules* **1991**, *24*, 1629.

(6) Verdurmen, E. M.; Geurts, J. M.; Vertsegen, J. M.; Maxwell, I. A.; German, A. L. *Macromolecules* **1993**, *26*, 6289.

(7) Morrison, B. R.; Maxwell, I. A.; Gilbert, R. G.; Napper, D. H., in *ACS Symp. Series - Polymer Latexes - Preparation, Characterization and Applications*; Daniels, E. S., Sudol, E. D. and El-Aasser, M., Ed.; American Chemical Society: Washington D.C., 1992; Vol. 492, p 28.

(8) Casey, B. S.; Morrison, B. R.; Gilbert, R. G. *Prog. Polym. Sci.* **1993**, *18*, 1041.

(9) Gilbert, R. G. *Emulsion Polymerization: A Mechanistic Approach*; Academic: London, 1995.

(10) Coen, E.; Lyons, R. A.; Gilbert, R. G. *Macromolecules* **1996**, *29*, 5128.

(11) Leemans, L.; Jerome, R.; Teyssie, P. *Macromolecules* **1998**, *31*, 5565.

(12) Vorwerg, L.; Gilbert, R. G. *Macromolecules* **2000**, *33*, 6693.

(13) Hansen, F. K.; Ugelstad, J., in *Emulsion Polymerization*; Piirma, I., Ed.; Academic: New York, 1982.

(14) Fitch, R. M.; Tsai, C. H., in *Polymer Colloids*; Fitch, R. M., Ed.; Plenum: New York, 1971, p 73.

(15) McAskill, N. A.; Sangster, D. F. *Aust. J. Chem.* **1979**, *32*, 2611.

(16) McAskill, N. A.; Sangster, D. F. *Aust. J. Chem.* **1984**, *37*, 2137.

(17) Maruthamuthu, P. *Makromol. Chem., Rapid. Commun.* **1980**, *1*, 23.

(18) Griffiths, M. C.; Strauch, J.; Monteiro, M. J.; Gilbert, R. G. *Macromolecules* **1998**, *31*, 7835.

(19) Strauch, J.; McdDonald, J.; Chapman, B. E.; Kuchel, P. W.; Hawkett, B. S.; Roberts, G. E.; Tonge, M. P.; Gilbert, R. G. *J. Polym. Sci. A Polym. Chem. Ed.* **2003**, *41*, 2491.

(20) Dong, Y.; Sundberg, D. C. *Macromolecules* **2002**, *35*, 8185.

(21) Cummins, P. L.; Gready, J. E. *J. Comput. Chem.* **1997**, *18*, 1496.

10. Conclusion

The Abstract of this thesis presented a very brief overview of the main themes of this research project. Additionally, each chapter has put forward detailed conclusions specific to the work covered therein. An attempt is now made to take stock of results from the wide range of investigations undertaken as part of this study, drawing attention to the most significant findings and explaining, in a global sense, how the various sections of work are related.

Given that this project set out with the aim of a systematic study of entry in emulsion polymerisation, the work ultimately presented in this thesis may appear to have deviated from this path at various stages (although, it is thought, not without good reason). Nevertheless, it is important to recognise that a number of significant kinetic and mechanistic inferences for entry have duly emerged.

Kinetic experiments using zero-one styrene systems at 50°C (Chapter 3) have revealed that when persulfate is used as initiator, the radical entry efficiency, f_{entry}, is unaffected by changing the particle surface charge from positive to negative. Thus any radical-particle charge interactions must not affect the kinetics of entry. Not only did these results refute a number of historical models for entry, they were found to be well explained by the Maxwell-Morrison entry model, both qualitatively – since this model asserts that the particle surface charge should have no effect on entry kinetics – and quantitatively – in terms of the good agreement between trends in experimental data and modelled entry efficiencies for $z = 2$.

Extending this study to examine the effect of changing the initiator from negatively-charged persulfate to positively-charged V-50, it was found that the kinetics of entry are, however, sensitive to the nature of the initiating radical. Given that radical-particle charge interactions could be ruled out (based on the results above), this effect was deduced to arise from the relative hydrophobicity of the initiating radicals. It was postulated that V-50-derived radicals are more hydrophobic than KPS-derived radicals, and thus must add fewer styrene monomer units to form an entering species, *i.e.*, giving rise to a value of $z = 1$. Kinetically, this should mean virtually no aqueous-phase termination and generally high f_{entry} for V-50 compared with KPS. Such was certainly found to be the case for entry into cationically-charged latex particles, however the results were less clear-cut for the anionic latex (possibly the result of

adsorption of initiator onto the particle surface). Nevertheless, a comparison of trends in experimental and modelled entry efficiencies is consistent with the above postulate for V-50 radical entry.

At this point it should be remarked that the good accord between the Maxwell-Morrison model and experimental entry data described above is encouraging news for the model, and while these effects were observed in styrene emulsion systems, there is every reason to expect that changes in particle surface charge and initiator will have similar impacts in other systems.

In addition to the nature of initiator and latex particles, the nature of monomer, and more specifically monomer water-solubility, was identified as a key factor in the kinetics of entry. Thus experiments to elucidate the effect of increased monomer water solubility on entry were carried out using MMA (instead of styrene) at 50°C with persulfate as initiator (Chapter 4).

In this case it was found to be no straightforward matter to elicit accurate entry rate data from experimental kinetic measurements. Notably, the greater precision afforded by the experimental methods of this work revealed important kinetic effects that had not been identified in earlier work on this system. One such effect was the decrease in the Interval II acceleration, $\overline{a}$, with decreasing initiator concentration. A range of existing kinetic methodologies, including the Smith-Ewart equations and the pseudo-bulk model (with and without chain length dependent termination kinetics) were applied to attempt to account for this variation in $\overline{a}$, and while it is thought that both radical compartmentalisation and the nature of spontaneous polymerisation in this system may be partly responsible, none of the existing kinetic frameworks was able to provide a satisfactory explanation. Importantly, while the unexplained variation in $\overline{a}$ resulted in significant uncertainty in the value of f_{entry} at low initiator concentration, it was nevertheless possible to garner reasonable estimates for this quantity, and more importantly to identify a systematic decrease in f_{entry} with increasing initiator concentration. Interpretation of this trend in terms of the Maxwell-Morrison entry model suggested a value of at least $z \approx 20$ for this system – significantly greater than that (z = 5) predicted from the simple thermodynamic model of Maxwell *et al.*

Attempts were made to verify the value of z inferred from kinetics (for MMA/persulfate) by isolating the oligomeric species formed in the aqueous phase of these emulsion systems and analysing them by electrospray mass spectrometry (MS) and aqueous-phase GPC (Chapter 5). It was noted that literature data for MS of aqueous oligomers from similar systems has

provided strong evidence for a value of z of at least 10 – 15. Obtaining MS data for the present system was found to be difficult, and ultimately this technique evidenced only oligomeric species of length up to 6 monomer units. Obviously, this is consistent with a low value of $z \approx 7$, however an important *caveat* here is that while the presence of a MS signal confirms the presence of a species, the opposite is not necessarily true. On the other hand, aqueous GPC suggested oligomeric species of length $10^2 - 10^6$ (depending on the calibration used). Of these two methods, the results from aqueous GPC must be viewed as the more suspicious, with highest order estimates undoubtedly arising from calibration error; however it is clear that both these techniques, as they are currently practiced, are not yet suitable for extracting an accurate estimate of z from aqueous oligomer populations.

In seeking to rationalise the value of $z \approx 20$ obtained from MMA/persulfate kinetics, the most credible explanations appeared to be either incorporation of relatively water-soluble methacrylic acid units (formed by MMA ester hydrolysis) into oligomeric radicals prior to entry, or a departure from the group-additive nature assumed for the free energy of monomer units in a radical chain. The first of these explanations was refuted by studies using a model emulsion system wherein no significant monomer hydrolysis occurred, even after extended periods of heating. Thus the favoured explanation here was that the free energy of a monomer unit incorporated into an aqueous oligomeric MMA radical is significantly different to that of an individual aqueous monomer molecule, and thus that the assumption of additive free energy contributions used by Maxwell *et al.* in formulating their thermodynamic estimate of $z = 5$, must underestimate the number of MMA monomer addition steps required to form an entering radical. Of course, this hypothesis must be reconciled with the fact that the thermodynamic estimate of $z = 2$ for styrene/persulfate was borne out by kinetic experiments. Here it was suggested that the group-additivity assumption is valid for very short oligomers, where all monomer units are exposed to their aqueous surroundings, but worsens for longer oligomers where some monomer units are partially shielded from the aqueous phase by other monomer units (possibly due to coiling of the radical chain).

Finally, in considering the results for MMA entry in terms of the theory of Maxwell *et al.*, two important points are noted. Firstly, it should not be overlooked that the value of z inferred here is completely consistent with the fundamental tenets of the Maxwell-Morrison model with regard to the influence of monomer on entry; *i.e.*, comparing the values of z for MMA and styrene with persulfate as initiator, $z = 20$ and 2 respectively, it is clear that the

more water soluble a monomer is, the greater the number of added monomer units required to form an entering species. Secondly, while the above results bring into question the accuracy of the *thermodynamic* approach proposed by Maxwell *et al.* for directly estimating z, the results here do not refute their *kinetic* model which provides a good account for the observed trend in experimental entry data.

It is contended that the results from the study of entry described above, while not exhaustive, certainly reveal the most significant effects on entry kinetics arising from the nature of the initiator, monomer and particle surface charge used in emulsion polymerisation. Furthermore, these effects are seen to be reasonably well accounted for by the provisions of the Maxwell-Morrison kinetic model. Of course, some natural courses for consolidation and extension of the results obtained here are readily identified. It is of interest to carry out seeded polymerisations of MMA using V-50 as initiator instead of persulfate. The observation of higher entry efficiencies with V-50 would provide useful verification of the postulate that V-50-derived radicals are more hydrophobic than those from KPS, and thus give rise to a lower z value. Additionally, to complete the systematic variations used here, a cationically-stabilised MMA seed latex could be synthesised and used in seeded experiments to determine whether entry kinetics in these systems are also independent of particle surface charge (in line with styrene systems and the principles of the Maxwell-Morrison model). Also, having examined entry for monomers of moderate (MMA) and low (styrene) water-solubility, an enticing prospect for future kinetic investigations is a system with a highly water-insoluble monomer such as dodecyl methacrylate (DMA). $[M]_w^{sat}$ for DMA at 50°C is in the range of 10^{-5} – 10^{-4} M, and the rate of aqueous-phase propagation, and hence also that of entry, is likely to be extremely low and highly sensitive to initiator concentration for this system (see the "termination limit" described in Appendix A.8). In practice, ρ values for such an insoluble monomer may be too low to be measured with accuracy. Thus one solution may be to incorporate a cyclodextrin in the emulsion system. It is anticipated that this would raise the effective aqueous-phase concentration of DMA, resulting in higher, accurately-measurable entry rates from which a value for z may be inferred for this monomer.

It should be recognised that the systems elected for study in this work may be regarded as typical model systems for emulsion polymerisation – employing commonly used initiator, monomer and latex particle types – and, as such, the demonstrated applicability of the relatively simple kinetic model of Maxwell *et al.* to these systems is of considerable import.

However, looking further afield, there will certainly be systems for which this model does not provide an accurate description of entry kinetics (*e.g.*, systems employing steric or electrosteric stabilisers). In the simplest instances, it may be the case that the Maxwell-Morrison model is able to account for a given kinetic effect (*e.g.*, a barrier to entry) simply through adjustment of the value of z. Thus the model would still provide a functional means for modelling entry, but one with diminished physical meaning. In other cases it may well prove impossible to account for kinetic data using this model. In recognition of this, approaches for improving the kinetic model for entry were proposed (see Chapter 9), with these efforts focussing on the incorporation of radical adsorption-desorption kinetics and the allowance for entry by radicals of different chain lengths. Even from this preliminary work it was evident that the development of a more rigorous model for entry brings with it considerable new levels of kinetic complexity (thus highlighting the elegance of the Maxwell-Morrison model) and, moreover, hinges on estimates of kinetic and thermodynamic parameters that are largely unavailable at present. It is hoped that the ideas proposed here will provide a useful starting point for future kinetic work in this area.

An important point with regard to kinetic modelling of entry is that the effectiveness of model discrimination is always limited by the accuracy with which ρ can be measured from experiment. The approach of the present study was to extract the value of ρ from the observed rate of polymerisation – an approach which requires a detailed consideration of the rates of other radical processes, such as termination, exit and re-entry. In the case of zero-one systems, the kinetic methodology is well established, enabling the value of ρ to be measured with some confidence for these systems (Chapter 3). However, the same may not be said for non-zero-one systems, as evidenced by the extensive (and not wholly satisfactory) efforts to model MMA data using existing methods (Chapter 4). As a result, the quest for accurate entry rate data has naturally motivated a number of investigations into the wider kinetic framework of emulsion polymerisation which are now discussed.

The kinetics of chain stopping reactions for MMA systems were investigated through measurement of both the polymerisation rate and the molecular weight distribution of polymer formed (Chapter 6). Results here revealed that for MMA emulsion systems at 50°C, the radical chain length distribution is dominated by transfer to monomer reactions, and that, as a result, the chain length dependence of termination does not have any pronounced effect on $\bar{n}$, thus condoning the assumption of chain length independent termination used in some

data analyses for this system. It was also found that current models for termination in emulsion systems provided a remarkably good account for both types of experimental data, *a priori*, using the same set of "best estimate" parameter values; this is a strong endorsement for the current understanding of termination kinetics.

A particular shortcoming of the traditional non-zero-one kinetic treatments used here was the way in which the kinetics of radical exit and re-entry were treated, requiring the use of poorly defined rate parameters such as k and α, which (in some way) encapsulate the kinetics of a number of different chemical and physical processes. While fitting of experimental data allowed such parameter values to be determined, these generally amounted to just that: fitting parameters that provided no mechanistic insight. In an effort to relieve this unsatisfactory situation an extended version of the Smith-Ewart kinetic model was developed (Chapter 8) which regarded exit and re-entry entirely in terms of their constituent elementary processes. This model was shown to agree with existing models (including the zero-one model) under various limiting conditions, but even in these cases it retained the advantage of incorporating only well-defined (*i.e.*, microscopic) rate parameters. Importantly, using current best estimates for all parameter values, this model confirmed the accuracy of the values of ρ obtained earlier for both styrene and MMA by existing methods. However, despite its obvious kinetic improvements, this new model was unable to provide any better account for the most perplexing kinetic feature of MMA systems: the variation of $\overline{a}$ with initiator concentration. Given the highly general nature of the model developed here, it is anticipated that it should be applicable over a far wider range of emulsion polymerisation systems and conditions than the few exemplary cases examined so far, thus providing considerable scope for future work in this area.

Finally, some attention was devoted to the kinetics spontaneous emulsion polymerisation in the systems studied here (Chapter 7) – since the value of ρ_{spont} was found to be especially influential on the values of ρ_{init} (and hence f_{entry}) at low initiator concentration, and its time-evolution was cited as a possible explanation for the observed variation in $\overline{a}$ for MMA systems. Although ρ_{spont} values were readily measured for the various systems used, their interpretation was not at all straightforward. Indeed, it was apparent that small differences in the composition and history of different emulsion systems gave rise to significant variations in the mechanism for spontaneous radical generation. While no definitive mechanism was identified, the main sources of spontaneous radicals appear likely to be located at the surface

of seed latex particles and in the aqueous phase (possibly derived from the seed latex aqueous phase). Most importantly, the results of this work have shown that ρ_{spont} can be readily and accurately measured using current experimental methods, and, as such, systematic studies should certainly be undertaken to further elucidate the mechanism of spontaneous emulsion polymerisation and its ramifications for the interpretation of kinetic data.

In closing, it is ventured that the work presented in this thesis has brought to light some new understanding of the factors influencing entry in emulsion polymerisation, in line with the principal aim of these endeavours. Hopefully also emerging from this work is some notion of the inextricable links that exist between various facets of emulsion polymerisation kinetics, with advancement in one area inevitably stimulating progress in others. Thus, the pursuit of an improved understanding of entry will go hand-in-hand with the collective development of emulsion polymerisation kinetics. Much remains to be uncovered; it is hoped that this work has served to affirm existing courses of investigation, as well as to encourage some new ones.

Appendices

A.1 Definition of Termination Rate Coefficients

Fundamental to any piece of kinetic work is the unambiguous definition of the rate coefficients used. Only when such is provided may the reader confidently compare the results obtained with those from other work, where the rate coefficients may or may not be defined in a consistent manner. While this may seem a trivial issue in general (given that obvious intuitive definitions have been widely adopted for most of the rate coefficients of concern in polymerisation systems), it is of particular importance with regard to the kinetics of termination. Thus, this Appendix is intended to provide the reader with clear and explicit definitions for the termination rate coefficients used throughout this thesis.

A.1.1 Definition of Termination Rate Coefficients in Radical Population Balance Equations

We first consider termination kinetics as they pertain to radical balance equations. Consistent with the general approach of this thesis we assume termination to be a diffusion-limited process (due to the rapidity of radical-radical chemical reactions) and thus use the Smoluchowski equation[1] as a kinetic starting point. This equation describes the rate of collisional encounter between two different diffusing species, here denoted R_i and R_j (labels which, in the present setting, may be associated with radicals of degree of polymerisation i and j), as $4\pi D_{ij}(r_i + r_j)N_A[R_i][R_j]$, where D_{ij} is the mutual diffusion coefficient for the two species, r_i and r_j are their respective radii (assuming approximately spherical dimensions), and N_A is Avagadro's constant. In the context of termination we replace $(r_i + r_j)$ by the interaction radius, σ, which in actuality may or may not be simply equal to the sum of the radii. We also take account of the fact that termination requires the pairing of electrons in a singlet rather than a triplet state, and thus the probability that any given collision results in termination is given by the factor $0.25 \leq p_{spin} \leq 1$. Consequently, the rate of occurrence of diffusive termination reactions as derived from the Smoluchowski equation may finally be written as: $4\pi\sigma p_{spin} D_{ij} N_A[R_i][R_j]$.

Considering the radical "homo-termination" reaction, where $i = j$ and species R_i and R_j are identical, the number of reactive radical pairs is given simply by the number of combinations of R_i radicals. If n_i is the number of R_i radicals (such that $n_i = [R_i]N_A V$, where V is the relevant reaction volume) then the number of such combinations is given by $\frac{1}{2} n_i(n_i - 1) \approx \frac{1}{2} n_i^2$, assuming that $n_i \gg 1$. Accordingly, the rate of occurrence of homo-termination reactions is then $2\pi\sigma p_{spin} D_{ii}[R_i][R_i]$. And since each such bimolecular reaction results in the loss of two radicals of length i, the rate of disappearance of these species is given by:

$$-\left.\frac{d[R_i]}{dt}\right|_{\text{homo-termination}} = 4\pi\sigma p_{spin} D_{ii} N_A [R_i][R_i] \qquad (A.1)$$

Following the IUPAC recommendation, we stipulate the following form for the rate equation for homo-termination of radicals of length i:

$$-\left.\frac{d[R_i]}{dt}\right|_{\text{homo-termination}} = 2\, k_t^{i,i}[R_i]^2 \qquad (A.2)$$

Comparison of equations (A.1) and (A.2) then dictates that the diffusion-limited rate coefficient for homo-termination is defined as:

$$k_t^{i,i} = 2\pi\sigma p_{spin} D_{ii} N_A \qquad (A.3)$$

If we next consider the case of "hetero-termination" involving two radicals of length i and j, the rate of disappearance of both radicals is in this case equal to the rate of occurrence of hetero-termination. Thus from the Smoluchowski equation,

$$-\left.\frac{d[R_i]}{dt}\right|_{\text{hetero-termination}} = -\left.\frac{d[R_j]}{dt}\right|_{\text{hetero-termination}} = 4\pi\sigma p_{spin} D_{ij} N_A [R_i][R_j] \qquad (A.4)$$

Importantly, at this point we choose to depart from IUPAC recommendation and define the rate equation for hetero-termination in a similar manner to that for homo-termination above (*i.e.*, including a factor of two as shown):

$$-\left.\frac{d[R_i]}{dt}\right|_{\text{hetero-termination}} = -\left.\frac{d[R_j]}{dt}\right|_{\text{hetero-termination}} = 2\, k_t^{i,j}[R_i][R_j] \qquad (A.5)$$

Comparison of equations (A.4) and (A.5) then specifies the diffusion-limited rate coefficient for hetero-termination as:

$$k_t^{i,j} = 2\pi\sigma p_{spin} D_{ij} N_A \qquad (A.6)$$

While this approach may seem counter-intuitive (*i.e.*, a factor of two appearing in the rate equation for a reaction that consumes only one of a given type of radical), the advantage gained here is that the same mathematical form may be used for all termination terms, homo- or hetero-, appearing in radical balance equations, and for evaluating all termination rate coefficients *via* the Smoluchowski equation.

It is noted that the definitions for homo- and hetero-termination rate coefficients derived above are applied consistently throughout this thesis to all termination terms involving the following combinations of radical populations and termination rate coefficients.

- The aqueous-phase radical concentrations $[IM_i^\bullet]$, $[M_w^\bullet]$ and $[T_w^\bullet]$, with termination rate coefficient $k_{t,w}$
- The intra-particle radical populations n_i, with termination rate coefficients $c^{i,j} = k_t^{i,j}/(N_A V_s)$
- The intra-particle radical population $\bar{n}$, with termination rate coefficients c (in the case of the "Smith-Ewart" or "pseudo-bulk" models) or c^{LL} (in the case of the "extended Smith-Ewart" model)

The only exception to the definitions derived here occurs in the case of termination terms involving $\bar{n}$ with the termination rate coefficient c^{ML} in the case of the "extended pseudo-bulk" model. The reason for an exception in this case is made clear in the next section of this Appendix.

A.1.2 Definition of Termination Rate Coefficients in Latex Particle Population Balance Equations

In a similar way to above, we next consider termination kinetics in the context of latex particle population balances, with a view to clarifying the definitions of termination rate coefficients in this setting as well.

In the first instance we consider the evolution equation for an N_n particle (*i.e.*, one containing n radicals) from the Smith-Ewart model:

$$\frac{dN_n}{dt} = \rho N_{n-1} - [\rho + nk + n(n-1)c]N_n + (n+1)kN_{n+1} + (n+2)(n+1)cN_{n+2} \qquad (A.7)$$

where $c = \langle k_t \rangle / (N_A V_s)$ and $\langle k_t \rangle$ is the termination rate coefficient for the system, averaged over all chain lengths. Here the rate expression for loss of an N_n particle by termination is:

$$-\left.\frac{dN_n}{dt}\right|_{\text{termination}} = n(n-1)\,c\,N_n = n(n-1)\frac{\langle k_t \rangle}{N_A V_s} N_n \qquad (A.8)$$

Given that every occurrence of termination causes the loss of one N_n particle, the rate of loss may be calculated directly from the Smoluchowski equation. For particles containing n identical radicals [and thus $\frac{1}{2}n(n-1)$ distinct combinations] this gives:

$$-\left.\frac{dN_n}{dt}\right|_{\text{termination}} = \frac{4\pi\sigma p_{\text{spin}}\langle D \rangle}{V_s}\frac{n(n-1)}{2}N_n = \frac{2\pi\sigma p_{\text{spin}}\langle D \rangle}{V_s} n(n-1)\,N_n \qquad (A.9)$$

where $\langle D \rangle$ is an average diffusion coefficient for the system and V_s is introduced to give units consistent with equation (A.8) above. Comparison of equations (A.8) and (A.9) then defines $\langle k_t \rangle$ as:

$$\langle k_t \rangle = 2\pi\sigma p_{\text{spin}}\langle D \rangle N_A \qquad (A.10)$$

Notably, this definition for $\langle k_t \rangle$ is consistent with those from the previous section where a factor of two appeared in the termination term. This results from the presence of $n(n-1)$ in equation (A.8) which "double-counts" the number of distinct combinations of n radicals. Importantly, this is also the origin of the factor of two that ultimately appears in the termination term of the pseudo-bulk equation (see derivation of this equation in Section 0).

We next consider the evolution equations from the extended Smith-Ewart model for particles containing n radicals:

$$\frac{dN_n}{dt} = \rho_L N_{n-1} - \left[\rho_L + \rho_M + n\,k_{tr}[M]_p + n(n-1)\,c^{LL}\right] N_n + (n+2)(n+1)\,c^{LL} N_{n+2}$$
$$+ k_p^1 [M]_p N_n^M + \left[\rho_M + k_{dM}\right] N_{n+1}^M + \left[k_{tr}[M]_p + c^{ML}\right](n+1)\,N_{n+2}^M \qquad (A.11)$$

$$\frac{dN_n^M}{dt} = \rho_M N_{n-1} + n\, k_{tr}\,[M]_p\, N_n + \rho_L N_{n-1}^M - \left[\rho_L + \rho_M + k_{dM} + (n-1)\, k_{tr}\,[M]_p + k_p^1\,[M]_p + (n-1)\, c^{ML}\right] N_n^M \quad (A.12)$$

where $c^{LL} = k_t^{LL}/(N_A V_s)$ for termination of two polymeric radicals, and $c^{ML} = k_t^{ML}/(N_A V_s)$ for termination of one monomeric and one polymeric radical.

The rate expression for loss of an N_n particle by "LL termination" is:

$$-\left.\frac{dN_n}{dt}\right|_{\text{LL termination}} = n(n-1)\, c^{LL} N_n = n(n-1)\frac{k_t^{LL}}{N_A V_s} N_n \quad (A.13)$$

Clearly, this is analogous to the previous example, and leads to the following definition for k_t^{LL}:

$$k_t^{LL} = 2\pi\sigma p_{spin} D_{LL} N_A \quad (A.14)$$

where D_{LL} is the mutual diffusion coefficient for polymeric radicals.

Finally, we consider the rate expression for loss of an N_n^M particle by "ML termination":

$$-\left.\frac{dN_n^M}{dt}\right|_{\text{ML termination}} = (n-1)\, c^{ML} N_n = (n-1)\frac{k_t^{ML}}{N_A V_s} N_n^M \quad (A.15)$$

In this case of a particle containing one monomeric and $(n-1)$ polymeric radicals the Smoluchowski equation gives:

$$-\left.\frac{dN_n}{dt}\right|_{\text{ML termination}} = \frac{4\pi\sigma p_{spin} D_{ML}}{V_s}(n-1)\, N_n \quad (A.16)$$

where D_{ML} is the mutual diffusion coefficient for a monomeric and a polymeric radical. Thus, k_t^{ML} is defined as:

$$k_t^{ML} = 4\pi\sigma p_{spin} D_{ML} N_A \quad (A.17)$$

So it is clear that the definitions of the termination rate coefficients $\langle k_t \rangle$ and k_t^{LL} as they pertain to latex particle population balance equations are consistent with the definitions specified for

radical balances in the previous section. However, the definition for k_t^{ML} differs by a factor of two as a result of the ML termination terms in the extended Smith-Ewart model being written in a way that is consistent with the LL termination terms.

The definition of k_t^{ML} could be made to match that of other k_t values simply by writing all ML termination terms with an added factor of two. However, in this case the preferred approach is to maintain consistency in the particle evolution equations, and thus k_t^{ML} remains defined as in equation (A.17). Therefore it is emphasised that throughout this thesis k_t^{ML} is the only rate coefficient for hetero-termination that is defined in the manner recommended for *hetero-termination* by IUPAC (*i.e.*, without a factor of two). All other second-order termination rate coefficients, whether they be related to hetero- *or* homo-termination, are defined in the manner recommended by IUPAC for *homo-temination* (*i.e.*, including a factor of two).

A.2 The Kinetic Effects of Secondary Nucleation in Seeded Emulsion Polymerisation

Seeded emulsion polymerisation offers the advantages of a pre-determined latex particle size distribution (PSD) and number concentration, N_c, both of which permit accurate kinetic information to be obtained from a given system. The formation of new particles, of unknown size and concentration, during a seeded experiment introduces uncertainty to the data obtained. The extent to which this so-called secondary nucleation occurs may be estimated using techniques such as capillary hydrodynamic fractionation (CHDF) or transmission electron microscopy (TEM). In the case of TEM (used here), the secondary or "new" (*i.e.*, non-seed) particles are visible as a second population that is appreciably smaller in diameter than the seed particles.

This Appendix presents the results of a modelling study aimed at determining the extent of secondary nucleation that is sufficient to introduce significant error to kinetic results. These results were used as a basis for judging whether or not the incidence of any secondary nucleation observed for a seeded kinetic experiment was sufficient to render experimental data unusable.

The model employed here is that developed by Coen *et al.* and described in detail elsewhere.[2] Briefly, this model monitors the precise size distribution of latex particle populations throughout the course of a simulated polymerisation (beginning, in the case of a seeded

system, with the PSD of the seed latex). Correspondingly, changes in the values of all particle-size dependent rate parameters, *e.g.*, rate coefficients for entry and exit, are specifically accounted for. Also taken into account are the concentrations of all initiator-derived and exit-derived radicals in the aqueous-phase, and their dependences on various rate parameters and the nature of the PSD.

For the purposes of illustration we consider the polymerisation conditions applicable to the KPS/AN01 system of Chapter 3: Interval II polymerisation of styrene at 50°C using anionically stabilised polystyrene seed latex particles of number-average unswollen diameter 64 nm, and a particle polydispersity index (*i.e.*, ratio of weight-average to number-average diameter) of 1.02. A potassium persulfate (KPS) initiator concentration of 1 mM was adopted for the present simulations (although it is noted that the inferences made here were found to apply for the entire range of experimentally practicable initiator concentrations) and the value of N_c for seed particles was specified as $N_{c,seed} = 7.5 \times 10^{16}$ dm^{-3}. The values taken for all other kinetic parameters were those given for styrene at 50°C in Chapter 3.

The purpose of this study was to investigate the effect on particle growth kinetics of a bimodal PSD. Hence initial simulations were carried out in the absence of any secondary nucleation (in practical terms this meant carrying out calculations with aqueous surfactant below the critical micelle concentration, as well as specifying an artificially high value for the critical chain length for homogenous nucleation, *e.g.*, $j_{crit} = 100$). The seed PSD was approximated by a Gaussian distribution centred at unswollen diameter 64 nm with a standard deviation of 4 nm (corresponding to the polydispersity quoted above). After a short approach period $\bar{n}$ attained a steady-state value of $\bar{n}_{SS} = 0.27$. The seed latex PSD was then altered to incorporate a second population of particles (as illustrated in Figure A.2.1), representative of particles formed by secondary nucleation, and the corresponding value of $\bar{n}_{SS}$ was obtained from simulation. For simplicity, the secondary particle PSD was assumed to have the same standard deviation as the seed particle PSD.

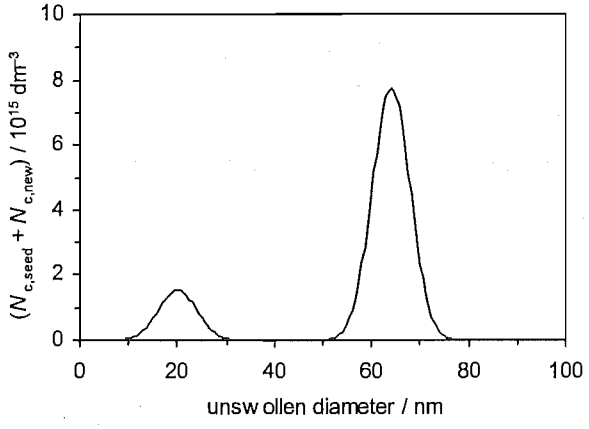

Figure A.2.1. Bimodal latex PSD consisting of (Gaussian) seed particle population with number-average unswollen diameter 64 nm, standard deviation 4 nm and number concentration $N_{c,seed} = 7.5 \times 10^{16}$ dm^{-3}, and "new" particle population with diameter 20 nm, standard deviation 4 nm and number concentration $N_{c,new} = 1.5 \times 10^{16}$ dm^{-3}.

This modelling approach was applied over a range of different sizes and relative concentrations for the secondary particles. Note that $\overline{n}_{SS}$ is now the average across the entire particle population, not just the nominal "seed" particles. The effects of secondary particle formation on the value of $\overline{n}_{SS}$ are presented in Figure A.2.2. It is seen that so long as the ratio of new to seed particles is below about 0.1 the value of $\overline{n}_{SS}$ is approximately unchanged from the value of $\overline{n}_{SS} = 0.27$ obtained in the absence of secondary nucleation. However, for $N_{c,new}/N_{c,seed} > 0.1$ the value of $\overline{n}_{SS}$ is seen to decrease significantly. This decline in $\overline{n}_{SS}$ is partly explained by the enhanced rate of radical loss *via* exit in new particles that are smaller than the seed particles; the exit rate coefficient, k, scales as $1/r_s^2$, as shown in equation (3.17) of Chapter 3. Accordingly, the greatest reduction in $\overline{n}_{SS}$ is observed in the case of smallest new particle diameter (10 nm). However, clearly this is not the full explanation here since a decrease in $\overline{n}_{SS}$ is also observed in the case where the new particles are assumed to be of equal diameter to the seed particles (64 nm). This is explained by the fact that increasing the number of new particles leads to a decrease in the rate of entry calculated for each individual particle as the same flux of entering radicals (dictated solely by aqueous-phase radical reactions) must now be shared over a greater *total* number of particles. Thus the overall rate coefficient for entry, ρ, decreases, and so must $\overline{n}_{SS}$.

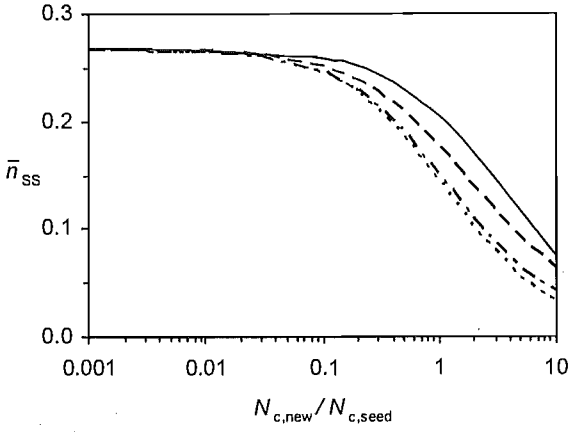

Figure A.2.2. Results obtained from full PSD kinetic modelling of secondary nucleation in the seeded emulsion polymerisation of styrene at 50°C with [KPS] = 1 mM and $N_{c,seed} = 7.5 \times 10^{16}$ dm^{-3}. Values of $\bar{n}_{SS}$ presented for a range of different relative concentrations of "new" particles, and with average new particle diameter of 64 nm (————), 40 nm (— — —), 20 nm (– —— –), or 10 nm (– – – –).

Now, it is important to note that experimentally $\bar{n}$ is not measured directly but is extracted from the overall rate of polymerisation assuming that the value of N_c for the system is simply equal to $N_{c,seed}$. Thus any effect that changes the measured *rate* will in turn affect the value of $\bar{n}$ inferred. In fact, secondary nucleation has two opposing effects on the rate. Clearly, the decrease in $\bar{n}$ seen above will cause a decrease in rate, but also associated with secondary particle formation is an increase in the overall value of N_c which will increase the rate of polymerisation. The overall kinetic effect of secondary nucleation therefore depends on which of these two opposing effects is strongest. This may be determined by calculating the product of overall N_c (= $N_{c,seed}$ + $N_{c,new}$) and $\bar{n}$ under various conditions. This quantity represents the total concentration of intra-particle radicals and is directly proportional to the overall rate of polymerisation.

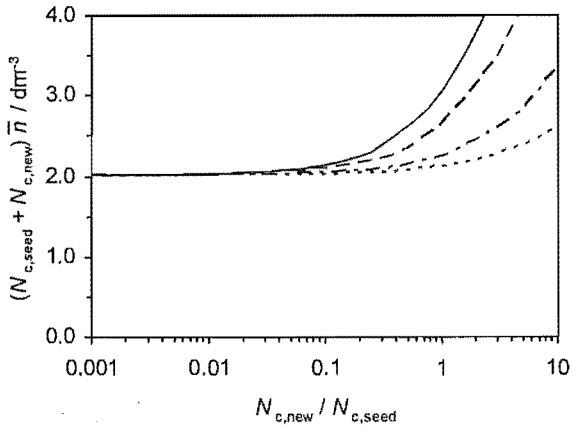

Figure A.2.3. Values of total intra-particle radical number concentration (proportional to the rate of polymerisation) obtained from full PSD kinetic modelling of secondary nucleation in the seeded emulsion polymerisation of styrene at 50°C with [KPS] = 1 mM, $N_{c,seed}$ = 7.5 × 10^{16} dm^{-3}, and different relative concentrations of "new" particles of average diameter 64 nm (————), 40 nm (— — —), 20 nm (– —— –), or 10 nm (– – – –).

Results for the present system are shown in Figure A.2.3. While the relative concentration of new particles is negligible, the value of $(N_{c,seed} + N_{c,new})\bar{n}$, and hence rate, remains constant. However, as the number of new particles rises the rate is inevitably seen to increase. Clearly the effect on the polymerisation rate of increasing overall N_c outweighs the opposing effect of decreasing $\bar{n}$. Notably, the size of the new particles is also of significance: as particle diameter increases, a relatively lower number of new particles is required to effect a given increase in rate. Thus the effect of secondary nucleation on rate is also likely to vary with conversion as the new particles grow in size.

In the context of the experimental investigations of this thesis the results of full PSD modelling presented above suggest that the occurrence of secondary nucleation will have negligible effect on the value of $\bar{n}$ (and subsequent kinetic analyses) so long as the ratio of new particles to seed particles is of order 0.1 or less. As this ratio becomes greater the increase in the observed rate of polymerisation will lead to an erroneously high value of $\bar{n}$. However, even when the ratio of new to seed particles is ~ 0.3 the error in $\bar{n}$ is unlikely to be ruinous, with an error of less than 20% observed for the extreme case where new particles are equal in size to seed particles.

A.3 Kinetic Data Obtained from Chemically Initiated Seeded Emulsion Polymerisations of Styrene in Chapter 3

Table A.3.1. Kinetic data obtained from polymerisation system KPS/AN01 at 50°C, $N_c = 7.5 \times 10^{16}$ dm^{-3}.

[KPS] / 10^{-3} M	$\bar{n}_{SS}$	ρ_{init} / 10^{-4} s^{-1}	f_{entry}
5.0	0.39	164	0.21
1.5	0.34	83	0.35
1.5†	0.34	82	0.34
0.50	0.30	53	0.67
0.15	0.23	21	0.88
0.030	0.14	5.4	1.09

† Experiment carried out using seed latex AN04 (with assistance of Sam Currie). Data analysed using k value for seed latex AN01 since similarity in $\bar{n}$ at same initiator concentration indicates that k is actually comparable for both anionic latexes (despite being measured as about 50% less for AN04 see Table 3.3); preference for AN01 k value is based on the greater number of γ-relaxations performed and better agreement with theoretical value for this latex.

Table A.3.2. Kinetic data obtained from polymerisation system V-50/CATH03 at 50°C, $N_c = 1.0 \times 10^{17}$ dm^{-3}.

[V-50] / 10^{-3} M	$\bar{n}_{SS}$	ρ_{init} / 10^{-4} s^{-1}	f_{entry}
0.32	0.40	144	0.79
0.11	0.33	57	0.87
0.10	0.34	64	1.09
0.030	0.22	14	0.81
0.011	0.14	4.6	0.73
0.0032	0.09	1.3	0.70

Table A.3.3. Kinetic data obtained from polymerisation system KPS/CATH03 at 50°C, $N_c = 1.0 \times 10^{17}$ dm^{-3}.

[KPS] / 10^{-3} M	$\bar{n}_{SS}$	ρ_{init} / 10^{-4} s^{-1}	f_{entry}
1.5	0.28	31	0.17
0.50	0.29	33	0.56
0.15	0.23	17	0.93
0.050	0.16	6.8	1.13
0.015	0.15	5.8	3.18

Table A.3.4. Kinetic data obtained from polymerisation system V-50/AN01 at 50°C.

$N_c = 7.5 \times 10^{16}$ dm^{-3}				$N_c = 1.6 \times 10^{17}$ dm^{-3}			
[V-50] / 10^{-3} M	$\bar{n}_{SS}$	ρ_{init} / 10^{-4} s^{-1}	f_{entry}	[V-50] / 10^{-3} M	$\bar{n}_{SS}$	ρ_{init} / 10^{-4} s^{-1}	f_{entry}
1.0	0.34	86	0.11	1.0	0.36	104	0.27
	0.33	80	0.099		0.36	104	0.25
	0.33	77	0.094		0.35	101	0.25
					0.35	98	0.24
0.30	0.34	88	0.36	0.30	0.29	48	0.40
	0.34	83	0.34				
	0.33	77	0.32				
0.10	0.24	25	0.31	0.10	0.20	15	0.37
	0.23	24	0.29			14	0.35
0.030	0.15	6.5	0.29	0.030	0.12	3.1	0.26
	0.14	5.0	0.21				
	0.13	4.6	0.19				
0.013	0.11	2.4	0.25				
0.0040	0.063	0.0002	0.0001				

A.4 Derivation of an Approximate Theoretical Value for the "Acceleration"

An approximate theoretical value for the acceleration, $\bar{a}$, during the steady-state period of Interval II polymerisation was first derived by Ballard *et al.*[3] using the following approach. It is noted that the explicit definitions of the quantities used in the present derivation, provided in Section 4.4 and Figure 4.1 of Chapter 4, clarify some small ambiguities in the derivation of Ballard *et al.* (specifically with regard to the definitions of m_p^0 and $\bar{n}_0$).

The unswollen volume, V_u, of a latex particle may be described at any time during the steady-state period in terms of the mass of polymer and conversion (in grams).

$$V_u = \frac{m_p^{seed} + \hat{x}}{d_p} = \frac{m_p^0 + \hat{x} - \hat{x}_0}{d_p} \approx \frac{m_p^0}{d_p}\left(1 + \frac{\hat{x} - \hat{x}_0}{m_p^0}\right) \qquad \text{(A.18)}$$

where m_p^{seed} is the mass of seed polymer initially added, d_p is the density of polymer, $\hat{x}$ is conversion (in grams), and $\hat{x}_0$ and m_p^0 are, respectively, the conversion and the mass of monomer at the start of the steady-state period (thus $m_p^0 = m_p^{seed} + \hat{x}_0$). Of course it is clear from equation (A.18) that the choice of the starting reference state is arbitrary, *e.g.*, one could make $\hat{x}_0$ and m_p^0 the values at $t = 0$. However then the value of $\bar{n}_0$ below is that which the system would have had if it were in a steady-state at $t = 0$, and this can only be obtained by extrapolation of the (pseudo-)linear region of $\bar{n}(\hat{x})$ back to $t = 0$. The advantage of the choice of $\hat{x}_0$ and m_p^0 as here is that it corresponds to an experimental value of $\bar{n}_0$. Note that the $(\hat{x} - \hat{x}_0)$ term appearing in equation (A.18) and elsewhere corresponds to the mass of monomer converted into polymer *only* during the steady-state period; thus at the start of this period $\hat{x} = \hat{x}_0$ and $(\hat{x} - \hat{x}_0) = 0$.

The volume of a latex particle swollen with monomer may then be expressed as follows:

$$V_s = \frac{d_M}{d_M - [M]_p M_0} V_u = \frac{d_M}{d_M - [M]_p M_0} \frac{m_p^0}{d_p} \left(1 + \frac{\hat{x} - \hat{x}_0}{m_p^0}\right) = V_s^0 \left(1 + \frac{\hat{x} - \hat{x}_0}{m_p^0}\right) \qquad \text{(A.19)}$$

where $V_s^0 = \frac{d_M}{d_M - [M]_p M_0} \frac{m_p^0}{d_p}$ is the swollen volume at the start of the steady-state period.

Substitution of equation (A.19) above into equation (4.13) from Chapter 4 gives the following *exact* form for the dependence of $\bar{n}$ on conversion.

$$\bar{n} = \left(\frac{\rho N_A V_s^0}{2 \langle k_t \rangle}\right)^{\frac{1}{2}} \left(1 + \frac{\hat{x} - \hat{x}_0}{m_p^0}\right)^{\frac{1}{2}} = \bar{n}_0 \left(1 + \frac{\hat{x} - \hat{x}_0}{m_p^0}\right)^{\frac{1}{2}} \qquad \text{(A.20)}$$

where $\bar{n}_0 = \left(\frac{\rho N_A V_s^0}{2 \langle k_t \rangle}\right)^{\frac{1}{2}}$ is the value of $\bar{n}$ at the start of the steady-state period.

Approximating equation (A.20) using a Taylor series in $(\hat{x} - \hat{x}_0)$ gives:

$$\bar{n} = \bar{n}_0 + \frac{\bar{n}_0}{2 m_p^0} (\hat{x} - \hat{x}_0) - \frac{\bar{n}_0}{8 m_p^{0\,2}} (\hat{x} - \hat{x}_0)^2 + \frac{\bar{n}_0}{16 m_p^{0\,3}} (\hat{x} - \hat{x}_0)^3 + \ldots \qquad \text{(A.21)}$$

Ballard et al. elected to truncate this Taylor series to first-order in $(\hat{x} - \hat{x}_0)$.

$$\overline{n} = \overline{n}_0 + \frac{\overline{n}_0}{2\, m_p^0}(\hat{x} - \hat{x}_0) \tag{A.22}$$

As is clear from equation (A.22) this approximation is effectively a linearisation of $\overline{n}$ as a function of conversion during the steady-state period. Hence the first-order coefficient of $(\hat{x} - \hat{x}_0)$ corresponds to the average value of $d\overline{n}/d\hat{x}$. Substituting this value into equation (4.15) from Chapter 4 gives the following value for the acceleration, $\overline{a}$.

$$\overline{a} = \frac{\dfrac{d\overline{n}}{d\hat{x}}\, m_p^0}{\overline{n}_0} = \frac{\left(\dfrac{\overline{n}_0}{2\, m_p^0}\right) m_p^0}{\overline{n}_0} = \frac{1}{2} \tag{A.23}$$

It is noted that this value of $\overline{a} = 0.5$ is an approximate result whose accuracy depends on the accuracy of the Taylor series truncation used in its derivation. It is easy to see from equation (A.21) that the *exact* variation of $\overline{n}$ with $(\hat{x} - \hat{x}_0)$ is (1) non-linear with slope decreasing as $\hat{x}$ increases, and (2) of lower slope than given by equation (A.22), as shown in the exact calculations of Chapter 4. In fact, to second-order one has

$$\frac{d\overline{n}}{d(\hat{x} - \hat{x}_0)} = \frac{\overline{n}}{m_p^0}\left[\frac{1}{2} - \frac{2\,(\hat{x} - \hat{x}_0)}{8\, m_p^0}\right] \tag{A.24}$$

If one considers a conversion range of 0 – 0.7 g, and therefore uses $(\hat{x} - \hat{x}_0) = 0.35$ g in equation (A.24), as well as $m_p^0 = 0.85$ g, all as used in Chapter 4, one obtains $\overline{a} = 0.40$ (very close to the exact value of $\overline{a} = 0.42$ in Chapter 4). Moreover, this equation also shows that $\overline{a}$ depends on $\hat{x}$ and m_p^0, but is independent of ρ and c. All of the above conclusions are consistent with what has been found from exact calculations in Chapter 4.

It is emphasised that the theoretical results of this thesis for $\overline{a}$ – above, as well as in Chapter 4 – clearly demonstrate the inaccuracy, under typical emulsion conditions, of the value of $\overline{a} = 0.5$ given by the first-order Taylor series truncation. Importantly, the accuracy of this approximation was only questioned in light of the precise values for $\overline{a}$ obtained from experiment in Chapter 4 (several of which fell below 0.5); earlier experimental measurements of $\overline{a}$ by Ballard *et al.* lacked this level of precision.

A.5 Derivation of the Rate Coefficient for Desorption of Monomer

The following derivation of the first-order rate coefficient for desorption of monomer from a latex particle into the aqueous phase, k_{dM}, was originally put forward by Ugelstad and Hansen[4] and has since been presented elsewhere.[5]

Here it is assumed that diffusion of monomer within the interior of a latex particle is rapid and the rate-determining step for desorption is diffusion of monomer away from the particle surface into the aqueous medium. This assumption is likely to be accurate under Interval II conditions of a typical emulsion polymerisation, although it is noted that under conditions of high weight-percent polymer, and hence high viscosity inside a latex particle (such as late in Interval III of polymerisation), monomer diffusion may be slowed significantly. In this event an alternative derivation which takes full account of intra-particle diffusion may be required.[6]

With aqueous-phase diffusion as the sole rate-limiting step the desorption process can be viewed simply as the reverse of monomer adsorption from the aqueous phase onto a latex particle. The rate coefficient for this adsorption, k_{ads}, may be described by the Smoluchowski equation as,

$$k_{ads} = 4\pi D_w N_A r_s \tag{A.25}$$

where N_A is Avagadro's constant and r_s the radius of a monomer-swollen latex particle. Equation (A.25) approximates the aqueous diffusion coefficient for a monomeric radical as being the same as for monomer, D_w, and reasonably assumes, for mutual aqueous diffusion of a particle and a monomeric radical, that $D_{part} + D_w \approx D_w$, where D_{part} is the aqueous diffusion coefficient for a particle. Further, it is assumed that $r_s + r_M \approx r_s$, where r_M is the radius of an aqueous monomeric radical. The latter two of these assumptions follow from a particle being much more massive than a monomeric radical.

The partitioning of monomer between particle and aqueous phases is thus determined by the equilibrium established by opposing adsorption and desorption processes:

$$M_w + \text{particle} \underset{k_{dM}}{\overset{k_{ads}}{\rightleftharpoons}} (\text{M–particle}) \tag{A.26}$$

The rate of change in the concentration of aqueous monomer may then be considered in terms of the contributions from adsorption and desorption.

$$\frac{d[M]_w}{dt} = k_{ads}[M]_w\frac{N_c}{N_A} - k_{dM}[M]_p V_s N_c \qquad (A.27)$$

Here $[M]_w$ and $[M]_p$ are the concentration of monomer in the aqueous and particle phase respectively, N_c is the aqueous-phase particle number concentration and V_s is the swollen particle volume. Finally it is noted that at steady state $d[M]_w/dt = 0$. Applying this condition to equation (A.27) and making use of equation (A.25), as well as the fact that $V_s = \frac{4}{3}\pi r_s^3$, leads to the following simplified expression for k_{dM}.

$$k_{dM} = \frac{4\pi D_w N_A r_s [M]_w \frac{N_c}{N_A}}{\frac{4}{3}\pi r_s^3 [M]_p N_c} = \frac{3D_w[M]_w}{r_s^2[M]_p} \qquad (A.28)$$

It is noted that the value of k_{dM} derived here from a monomer *molecule* is commonly used to approximate the desorption rate coefficient for a monomeric *radical* in view of the fact that these species are chemically very similar. The assumption of fast intra-particle diffusion is implicit in the above in that it is assumed that species are readily available for desorption at the particle surface.

A.6 Computational Method for Obtaining Steady-State Solutions of the "Extended Smith-Ewart Model"

A.6.1 Background Information

Ballard *et al.*[7] showed that, by truncating the number of radicals per particle at some appropriate point, the steady-state form of the original Smith-Ewart equations could be presented as a fully recursive set of equations. Thus, by specifying the value of the truncation population, N_m (following the nomenclature of Chapter 8 of this thesis), the steady-state values for all other populations, N_n for $0 \leq n < m$, could easily be calculated by non-iterative means. Initial attempts to derive a similar fully recursive set of steady-state equations for the extended Smith-Ewart model of Chapter 8 showed that such is not possible in this case.

However, it was found that a useful starting approximation for the latex particle populations could be obtained efficiently using an *approximate* recursive method, as described shortly.

Another solution approach that was tried here was to treat the set of differential rate equations (8.29) – (8.33) from Chapter 8 as a vector-valued function which acts on a solution vector consisting of all radical and particle populations in the model. Solving the differential equations in the steady-state amounts to a root-finding problem in many dimensions, and it was thus hoped that the well-known Newton-Raphson method would be a suitable means for solution. This method relies on solving a matrix equation involving the Jacobian matrix derived from the set of rate equations. Unfortunately, in all cases the Jacobian matrix obtained from the extended Smith-Ewart model was found to be ill-conditioned, preventing the solution of this matrix equation. However, it is noted that in the mathematically simpler case of the original Smith-Ewart model, the Newton-Raphson method was able to provide accurate steady-state solutions, although not with any significant gain in speed or accuracy over the recursive method of Ballard *et al.*

A computational approach that was finally found to provide steady-state solutions for the extended Smith-Ewart model was the relatively simple iterative method described in detail below.

A.6.2 Starting Approximations

We commence the calculation by specifying the current truncation value for the number of radicals per particle, m, starting with the minimum value for the general extended Smith-Ewart model of $m = 3$.

Initially it is assumed that the aqueous-phase concentration of exited radicals, $[M_w^\bullet]$, is zero and hence that ρ_M and ρ_{di} are also zero, according to equations (8.17) and (8.21) from Chapter 8. Next preliminary estimates for the aqueous concentrations of initiator-derived radicals are calculated according to equations (8.39) and (8.40), subject to the starting assumption that the total aqueous radical concentration, $[T_w^\bullet]$, is zero. An initial estimate for ρ_{init} is then obtained from equation (8.27) and leads to the starting value of $\rho_L = \rho_{init} + \rho_{spont}$.

We next calculate starting values for the latex particle populations using a recursively-defined set of equations which are close approximations to the exact steady-state equations.

Rearranging equation (8.29) of Chapter 8 it is seen that N_n may be expressed in the steady-state as follows:

$$N_n = \frac{1}{\rho_L}\left\{ \left[\rho_L + \rho_M + (n+1)k_{tr}[M]_p + (n+1)nc^{LL}\right]N_{n+1} - (n+3)(n+2)c^{LL}N_{n+3} \right.$$
$$\left. - k_p^1[M]_p N_{n+1}^M - \left[\rho_M + k_{dM}\right]N_{n+2}^M - \left[k_{tr}[M]_p + c^{ML}\right](n+2)N_{n+3}^M \right\} \qquad (A.29)$$

Applying the truncation from Chapter 8 that $N_n = N_n^M = 0$ for $n > m$, gives the following expressions:

$$N_{m-2} = \frac{1}{\rho_L}\left\{ \left[\rho_L + \rho_M + (m-1)k_{tr}[M]_p + (m-1)(m-2)c^{LL}\right]N_{m-1} \right.$$
$$\left. - k_p^1[M]_p N_{m-1}^M - \left[\rho_L + \rho_M\right]N_m - \left[\rho_L + \rho_M + k_{dM}\right]N_m^M \right\} \qquad (A.30)$$

$$N_{m-1} = \frac{1}{\rho_L}\left\{ \left[\rho_L + \rho_M + mk_{tr}[M]_p + m(m-1)c^{LL}\right]N_m - k_p^1[M]_p N_m^M \right\} \qquad (A.31)$$

Finally, we assume that an N_n^M particle may only be formed by transfer to monomer inside an N_n particle, so that equation (8.37) from Chapter 8 reduces to the following approximate form:

$$N_n^M = \frac{n\, k_{tr}\, [M]_p\, N_n}{\rho_L + \rho_M + k_{dM} + (n-1)\, k_{tr}\, [M]_p + k_p^1\, [M]_p + (n-1)\, c^{ML}} \qquad (A.32)$$

A reasonable starting approximation for all latex particle populations may now be calculated from the above equations, without the need for iteration. N_m is set to some arbitrary value (typically $N_m = 1$) and N_m^M is first calculated using equation (A.32), then N_{m-1} from equation (A.31), N_{m-1}^M from equation (A.32), and so on down to N_0.

From the initial particle populations a starting value for $\bar{n}$ may be calculated according to equation (8.35) from Chapter 8, and finally estimates for $[M_w^\bullet]$, ρ_M and ρ_{di} may be calculated from equations (8.38), (8.17) and (8.21).

A.6.3 Iterative Routine

Having specified initial estimates for all radical and particle populations the first iterative step begins with calculating an updated value for $[T_w^\bullet]$ according to equation (8.34). This value is used to recalculate the values of all initiator-derived radicals [equations (8.39) and (8.40)] which in turn gives rise to new values for ρ_{init} and ρ_L [equations (8.27) and (8.28)].

Improved values for the particle populations are then calculated using the *exact* steady-state equations (8.36), (8.37), (8.45), (8.44) from Chapter 8. These values are then used to recalculate the values of $\bar{n}$, $[M_w^\bullet]$, ρ_M and ρ_{di} [equations (8.35), (8.38), (8.17) and (8.21)].

At this point all radical and particle populations have been updated and we therefore begin the next iterative step, repeating the calculations for all species (starting with $[T_w^\bullet]$) employing the latest set of values. This iterative process is repeated until self-consistent values are obtained for all populations.

Having obtained a converged solution for the current truncation limit, the value of m is then incremented and the entire computation repeated, beginning with new starting approximations for all populations. This process is continued until increasing the value of m is found to have a negligible effect on the calculated value of $\bar{n}$. The criterion used for "negligible effect" was typically that $\left|(\bar{n}_{m+1} - \bar{n}_m)/\bar{n}_{m+1}\right| < 10^{-8}$.

A.7 Derivation of the Extended Pseudo-Bulk Model

Beginning with the definition of $\bar{n}$ in equation (8.35) of Chapter 8, and rate equations (8.29) and (8.30) for N_n and N_n^M, the time-evolution of $\bar{n}$ may be constructed as follows:

$$\frac{d\bar{n}}{dt} = \sum_{n=1}^{\infty} n \left\{ \frac{dN_n}{dt} + \frac{dN_n^M}{dt} \right\}$$

$$= \sum_{n=1}^{\infty} n \left\{ \rho_L \left[N_{n-1} - N_n + N_{n-1}^M - N_n^M \right] + \rho_M \left[N_{n-1} - N_n - N_n^M + N_{n+1}^M \right] \right.$$

$$\left. + k_{tr} [M]_p \left[n N_n - n N_n + (n+1) N_{n+2}^M - (n-1) N_n^M \right] + k_{dM} \left[N_{n+1}^M - N_n^M \right] \right.$$

$$+ k_p^1 [M]_p \left[N_n^M - N_n^M\right] + c^{ML} \left[(n+1) N_{n+2}^M - (n-1) N_n^M\right]$$

$$+ c^{LL} \left[(n+2)(n+1) N_{n+2} - n(n-1) N_n\right] \Bigg\}$$

$$= \rho_L + \rho_M \left[\sum_{n=1}^{\infty} N_n - \sum_{n=1}^{\infty} N_n^M\right] - k_{dM} \sum_{n=1}^{\infty} N_n^M$$

$$- 2 \left[k_{tr} [M]_p + c^{ML}\right] \sum_{n=1}^{\infty} (n-1) N_n^M - 2 c^{LL} \sum_{n=1}^{\infty} (n^2 - n) N_n \qquad \text{(A.33)}$$

We next invoke the following assumptions:

$$\rho_M N_{n-1},\ n k_{tr} [M]_p N_n \gg \rho_L N_{n-1}^M$$

$$k_{dM},\ k_p^1 [M]_p,\ (n-1) c^{ML} \gg \rho_L,\ \rho_M,\ (n-1) k_{tr} [M]_p$$

the first of which is reasonable given that the populations of N_n-type particles are considerably larger than those of N_n^M-type particles, and the second of which is based on the rapid rates of reaction for monomeric radicals. Applying these assumptions to the steady-state expression for N_n^M given in equation (8.37) of Chapter 8 gives:

$$N_n^M = \frac{\rho_M N_{n-1} + n k_{tr} [M]_p N_n}{k_{dM} + k_p^1 [M]_p + (n-1) c^{ML}}$$

$$= \frac{\rho_M N_{n-1} + n k_{tr} [M]_p N_n - (n-2) c^{ML} N_n^M}{k_{dM} + k_p^1 [M]_p + c^{ML}} \qquad \text{(A.34)}$$

Summing over all N_n^M populations we obtain the following two useful results:

$$\sum_{n=1}^{\infty} N_n^M = \frac{\rho_M \sum_{n=1}^{\infty} N_n + k_{tr} [M]_p \sum_{n=1}^{\infty} n N_n}{k_{dM} + k_p^1 [M]_p + c^{ML}} \qquad \text{(A.35)}$$

$$\sum_{n=1}^{\infty} (n-1) N_n^M = \frac{\rho_M \sum_{n=1}^{\infty} n N_n + k_{tr} [M]_p \sum_{n=1}^{\infty} (n^2 - n) N_n}{k_{dM} + k_p^1 [M]_p + c^{ML}} \qquad \text{(A.36)}$$

with equations (A.35) and (A.36) being subject to the following two assumptions (once again based on the very small populations of particles containing monomeric radicals):

$$\rho_M \sum_{n=1}^{\infty} N_n,\ k_{tr}\,[M]_p \sum_{n=1}^{\infty} n\,N_n \gg c^{ML} \sum_{n=1}^{\infty} (n-2)\,N_n^M$$

$$\rho_M \sum_{n=1}^{\infty} n\,N_n,\ k_{tr}\,[M]_p \sum_{n=1}^{\infty} (n^2-n)\,N_n \gg c^{ML} \sum_{n=1}^{\infty} (n-2)\,(n-1)\,N_n^M$$

Substituting equations (A.35) and (A.36) into the overall expression (A.33), and assuming that $c^{ML} \gg k_{tr}[M]_p$ (consistent with earlier), gives:

$$\frac{d\bar{n}}{dt} = \rho_L + \rho_M \left[\sum_{n=1}^{\infty} N_n - \sum_{n=1}^{\infty} N_n^M\right] - 2\,c^{LL} \sum_{n=1}^{\infty} (n^2-n)\,N_n$$

$$- k_{dM}\left[\frac{\rho_M \sum_{n=1}^{\infty} N_n + k_{tr}\,[M]_p \sum_{n=1}^{\infty} n\,N_n}{k_{dM} + k_p^1\,[M]_p + c^{ML}}\right] - 2\,c^{ML}\left[\frac{\rho_M \sum_{n=1}^{\infty} n\,N_n + k_{tr}\,[M]_p \sum_{n=1}^{\infty} (n^2-n)\,N_n}{k_{dM} + k_p^1\,[M]_p + c^{ML}}\right]$$

(A.37)

We next make the approximations that

$$\sum_{n=1}^{\infty} N_n^M \ll \sum_{n=1}^{\infty} N_n \approx 1$$

$$\sum_{n=1}^{\infty} n\,N_n^M \ll \sum_{n=1}^{\infty} n\,N_n \approx \bar{n}$$

Finally, we apply the same closure relation used in the original pseudo-bulk model:[7]

$$\sum_{n=1}^{\infty} (n^2-n)\,N_n \approx \left(\sum_{n=1}^{\infty} n\,N_n\right)^2 = \bar{n}^2$$

which leads to the following overall equation for the time evolution of $\bar{n}$:

$$\frac{d\bar{n}}{dt} = \rho_L + \rho_M - 2\,c^{LL}\,\bar{n}^2 - \left(\frac{\rho_M + k_{tr}\,[M]_p\,\bar{n}}{k_{dM} + k_p^1\,[M]_p + c^{ML}}\right)\left(k_{dM} + 2\,c^{ML}\,\bar{n}\right) \qquad \text{(A.38)}$$

Additionally, the various entry rate coefficients appearing in equation (A.38) are defined as in equations (8.17), (8.21), (8.27) and (8.28) of Chapter 8. Substituting the steady-state concentrations of $M_w^\bullet$ and $IM_z^\bullet$ as given in equations (8.38) and (8.40), and the expression for $\sum_{n=1}^{\infty} N_n^M$ in equation (A.35) gives (after some algebra):

$$\rho_{init} = \frac{2fk_d[I]N_A}{N_c}\left(\frac{k_{p,w}[M]_w}{k_{p,w}[M]_w + 2k_{t,w}[T_w^\bullet]}\right)^{z-1} \tag{A.39}$$

$$\rho_M = \frac{k_{tr}[M]_p \bar{n}}{\left(1 + \frac{k_p^1[M]_p + c^{ML}}{k_{dM}}\right)\left(1 + \frac{2k_{t,w}[T_w^\bullet] + k_{p,w}^M[M]_w}{k_{re}N_cV_w/N_AV_r}\right) - 1} \tag{A.40}$$

$$\rho_{di} = \frac{k_{p,w}^M[M]_w k_{dM}}{k_{re}N_cV_w/N_AV_r + 2k_{t,w}[T_w^\bullet] + k_{p,w}^M[M]_w}\left(\frac{\rho_M + k_{tr}[M]_p\bar{n}}{k_{dM} + k_p^1[M]_p + c^{ML}}\right) \tag{A.41}$$

A.7.1 Limiting Cases of the Extended Pseudo-Bulk Model

Various limiting forms of the extended pseudo-bulk model may now be derived if one assumes a given fate for monomeric radicals produced by transfer to monomer inside a latex particle. Here we employ a similar approach to that used by Casey *et al.* for the zero-one model[8] and also, to avoid confusion, adopt a naming system that is consistent with the work of those authors.

Limit 1: Complete aqueous-phase termination of exited radicals

Here we assume that $2k_{t,w}[T_w^\bullet] \gg k_{re}N_cV_w/(N_AV_r)$, $k_{p,w}^M[M]_w$, and hence that ρ_L, $k_{tr}[M]_p\bar{n} \gg \rho_M$ and $\rho_{init} \gg \rho_{di}$, so that any exited monomeric radicals are bound to undergo termination in the aqueous-phase.

- ***Limit 1a: Intra-particle propagation dominant***

If it is further assumed that $k_p^1[M]_p \gg k_{dM}$, c^{ML}, and hence the predominant fate for a monomeric radical inside a latex particle is propagation to form a macro-radical, equations (A.38) – (A.41) reduce to:

$$\frac{d\bar{n}}{dt} = \rho_{init} + \rho_{spont} - 2\,c^{LL}\,\bar{n}^2 - k_{tr}\,[M]_p\,\bar{n}\left(\frac{k_{dM} + 2\,c^{ML}\,\bar{n}}{k_p^1\,[M]_p}\right) \qquad (A.42)$$

- ***Limit 1b: Desorption dominant***

If desorption is assumed as the dominant fate for a monomeric radical inside a particle, then $k_{dM} \gg k_p^1[M]_p$, c^{ML} and equations (A.38) – (A.41) reduce to:

$$\frac{d\bar{n}}{dt} = \rho_{init} + \rho_{spont} - 2\,c^{LL}\,\bar{n}^2 - k_{tr}\,[M]_p\,\bar{n}\left(1 + \frac{2\,c^{ML}\,\bar{n}}{k_{dM}}\right) \qquad (A.43)$$

- ***Limit 1c: Intra-particle termination dominant***

If ML-termination is the dominant fate for a monomeric radical inside a particle, then $c^{ML} \gg k_p^1[M]_p$, k_{dM} and equations (A.38) – (A.41) reduce to:

$$\frac{d\bar{n}}{dt} = \rho_{init} + \rho_{spont} - 2\,c^{LL}\,\bar{n}^2 - 2\,k_{tr}\,[M]_p\,\bar{n}^2\left(1 + \frac{k_{dM}}{2\,c^{ML}\,\bar{n}}\right) \qquad (A.44)$$

Limit 2: Complete re-entry of exited radicals

Here we assume that $k_{re}N_cV_w/(N_AV_r) \gg 2k_{t,w}[T_w^\bullet]$, $k_{p,w}^M[M]_w$, and hence that $\rho_M = \dfrac{k_{dM}\,k_{tr}\,[M]_p\,\bar{n}}{k_p^1\,[M]_p + c^{ML}}$ and $\rho_{init} \gg \rho_{di}$, so that any exited monomeric radicals are bound to undergo re-entry into a latex particle.

- ***Limit 2a: Intra-particle propagation dominant***

If it is further assumed that propagation is the principal fate for a monomeric radical inside a particle, then $k_p^1[M]_p \gg k_{dM}$, c^{ML} and equations (A.38) – (A.41) reduce to:

$$\frac{d\bar{n}}{dt} = \rho_{init} + \rho_{spont} - 2\,c^{LL}\,\bar{n}^2 - \frac{2\,c^{ML}\,k_{tr}\,[M]_p\,\bar{n}^2}{k_p^1\,[M]_p} \qquad (A.45)$$

- ***Limit 2b: Desorption dominant***

If desorption of monomeric radicals prevails, then $k_{dM} \gg k_p^1[M]_p$, c^{ML} and equations (A.38) – (A.41) reduce to:

$$\frac{d\bar{n}}{dt} = \rho_{init} + \rho_{spont} - 2\,c^{LL}\,\bar{n}^2 - \frac{2\,c^{ML}\,k_{tr}\,[M]_p\,\bar{n}^2}{k_p^1\,[M]_p + c^{ML}} \qquad (A.46)$$

- ***Limit 2c: Intra-particle termination dominant***

If the most probable fate for a monomeric radical inside a particle is ML-termination, then $c^{ML} \gg k_p^1[M]_p$, k_{dM} and equations (A.38) – (A.41) reduce to:

$$\frac{d\bar{n}}{dt} = \rho_{init} + \rho_{spont} - 2\,c^{LL}\,\bar{n}^2 - 2\,k_{tr}\,[M]_p\,\bar{n}^2 \qquad (A.47)$$

Limit 3: Complete propagation of exited radicals

Here we assume that $k_{p,w}^M[M]_w \gg 2k_{t,w}[T_w^\bullet]$, $k_{re}N_cV_w/(N_AV_r)$, and hence that ρ_L, $k_{tr}[M]_p\,\bar{n} \gg \rho_M$ and $\rho_{di} = \dfrac{k_{dM}\,k_{tr}\,[M]_p\,\bar{n}}{k_{dM} + k_p^1\,[M]_p + c^{ML}}$, so that any exited monomeric radicals are bound to undergo aqueous-phase propagation to form a dimeric radical that undergoes pseudo-instantaneous entry into a latex particle.

- ***Limit 3a: Intra-particle propagation dominant***

If propagation is the most likely fate for a monomeric radical inside a particle, then $k_p^1[M]_p \gg k_{dM}$, c^{ML} and equations (A.38) – (A.41) reduce to:

$$\frac{d\bar{n}}{dt} = \rho_{init} + \rho_{spont} - 2\,c^{LL}\,\bar{n}^2 - \frac{2\,c^{ML}\,k_{tr}\,[M]_p\,\bar{n}^2}{k_p^1\,[M]_p} \qquad (A.48)$$

- ***Limit 3b: Desorption dominant***

If desorption of monomeric radicals is the dominant fate, then $k_{dM} \gg k_p^1[M]_p$, c^{ML} and equations (A.38) – (A.41) reduce to:

$$\frac{d\bar{n}}{dt} = \rho_{init} + \rho_{spont} - 2\,c^{LL}\,\bar{n}^2 - \frac{2\,c^{ML}\,k_{tr}\,[M]_p\,\bar{n}^2}{k_{dM}} \qquad (A.49)$$

- ***Limit 3c: Intra-particle termination dominant***

If ML-termination is most prevalent, then $c^{ML} \gg k_p^1[M]_p$, k_{dM} and equations (A.38) – (A.41) reduce to:

$$\frac{d\overline{n}}{dt} = \rho_{init} + \rho_{spont} - 2\,c^{LL}\,\overline{n}^2 - 2\,k_{tr}\,[M]_p\,\overline{n}^2 \qquad (A.50)$$

A.8 Explaining Trends in Modelled Entry Data

The aim of this section of work is to explain why the value of ρ_{init} as calculated using the Maxwell-Morrison entry model[9] may either increase or decrease as a function of initiator concentration, [I], depending on the value of z used.

One form of the Maxwell-Morrison analytic expression for ρ_{init} is

$$\rho_{init} = \frac{2fk_d[I]N_A}{N_c}\left\{\frac{k_{p,w}[M]_w}{k_{p,w}[M]_w + 2k_{t,w}[T_w^\bullet]}\right\}^{z-1} \qquad (A.51)$$

The dependence of ρ_{init} on [I] in equation (A.51) is clearly through the value of [I] itself, and also through the total aqueous-phase radical concentration, $[T_w^\bullet]$ (which is related to the flux of initiating radicals, and hence also to [I]).

This explanation centres on the consideration of the two possible fates for an aqueous-phase radical of degree of polymerisation less than z (*i.e.*, non-entering radicals). Such radicals may undergo either propagation or termination with another aqueous radical. An important quantity is thus the "propagation probability", P_{prop}, the ratio of the propagation rate (per radical) to the sum of the propagation and termination rates.

$$P_{prop} = \frac{k_{p,w}[M]_w}{k_{p,w}[M]_w + 2k_{t,w}[T_w^\bullet]} \qquad (A.52)$$

This ratio is seen to be crucial to the calculation of ρ_{init} *via* equation (A.51).

Two limiting cases of equation (A.52) with respect to [I] may be considered. At "low" [I], and hence low $[T_w^\bullet]$, $k_{p,w}[M]_w \gg 2k_{t,w}[T_w^\bullet]$ and the value of P_{prop} is approximately unity and insensitive to [I].

$$P_{\text{prop}} = \frac{k_{\text{p,w}}[\text{M}]_{\text{w}}}{k_{\text{p,w}}[\text{M}]_{\text{w}} + 2k_{\text{t,w}}[\text{T}^{\bullet}_{\text{w}}]} \approx \frac{k_{\text{p,w}}[\text{M}]_{\text{w}}}{k_{\text{p,w}}[\text{M}]_{\text{w}}} = 1 \qquad \text{(A.53)}$$

The physical explanation here is that at low $[\text{T}^{\bullet}_{\text{w}}]$ the rate of aqueous-phase termination is very low and virtually all radicals undergo propagation rather than termination.

In the other extreme of high [I], and hence high $[\text{T}^{\bullet}_{\text{w}}]$, $2k_{\text{t,w}}[\text{T}^{\bullet}_{\text{w}}] \gg k_{\text{p,w}}[\text{M}]_{\text{w}}$ and the value of P_{prop} takes its other limiting value.

$$P_{\text{prop}} = \frac{k_{\text{p,w}}[\text{M}]_{\text{w}}}{k_{\text{p,w}}[\text{M}]_{\text{w}} + 2k_{\text{t,w}}[\text{T}^{\bullet}_{\text{w}}]} \approx \frac{k_{\text{p,w}}[\text{M}]_{\text{w}}}{2k_{\text{t,w}}[\text{T}^{\bullet}_{\text{w}}]} \qquad \text{(A.54)}$$

Here, the high rate of aqueous-phase termination means that only a very small number of aqueous-phase radicals undergo propagation rather than terminating. Also, the value of P_{prop} remains sensitive to the value of $[\text{T}^{\bullet}_{\text{w}}]$, and therefore also dependent on [I].

Let us now consider how P_{prop} affects the value of ρ_{init} in Equation (A.51). In the first limiting case of $P_{\text{prop}} \approx 1$, the expression for ρ_{init} is simplified greatly.

$$\rho_{\text{init}} \approx \frac{2fk_{\text{d}}[\text{I}]N_{\text{A}}}{N_{\text{c}}} \{1\}^{z-1} = \frac{2k_{\text{d}}[\text{I}]N_{\text{A}}}{N_{\text{c}}} \qquad \text{(A.55)}$$

Equation (A.55) reflects the fact that at low $[\text{T}^{\bullet}_{\text{w}}]$ (*i.e.*, low [I]), the flux of entering radicals is approximately the same as the radical flux from initiator. Thus ρ_{init} shows a simple first-order dependence on [I] at "low" [I]. One might refer to this situation as ρ_{init} being in the "propagation limit", *i.e.*, the dominant mechanism for radical loss from the aqueous phase is by *entry* of z-meric radicals.

Next we must consider how P_{prop} affects the value of ρ_{init} in the other limiting case of high [I] (and $[\text{T}^{\bullet}_{\text{w}}]$). Substituting equation (A.54) into equation (A.51) gives,

$$\rho_{\text{init}} \approx \frac{2fk_{\text{d}}[\text{I}]N_{\text{A}}}{N_{\text{c}}} \left\{\frac{k_{\text{p,w}}[\text{M}]_{\text{w}}}{2k_{\text{t,w}}[\text{T}^{\bullet}_{\text{w}}]}\right\}^{z-1} \qquad \text{(A.56)}$$

In this case we may refer to ρ_{init} as being in the "termination limit", where the dominant mechanism for radical loss from the aqueous phase is simply termination with another

aqueous radical. Here we see that at high [I] the dependence of ρ_{init} on [I] is slightly more complicated due to the dependence on $[T_w^\bullet]$.

In order to clarify the dependence of ρ_{init} on [I] let us make the assumption that all aqueous-phase radical loss occurs *via* termination (clearly a value assumption at high $[T_w^\bullet]$). Given that initiation is the sole source of radicals, the population balance differential equation for $[T_w^\bullet]$ is simply

$$\frac{d[T_w^\bullet]}{dt} \approx 2fk_d[I] - 2k_{t,w}[T_w^\bullet]^2 \tag{A.57}$$

Applying the steady-state approximation to equation (A.57) gives

$$2fk_d[I] - 2k_{t,w}[T_w^\bullet]^2 = 0$$

$$[T_w^\bullet] = \left(\frac{fk_d[I]}{k_{t,w}}\right)^{\frac{1}{2}} \tag{A.58}$$

Now, substituting this value for $[T_w^\bullet]$ into equation (A.56) allows us to more clearly identify the dependence of ρ_{init} on [I] in the "termination limit".

$$\begin{aligned}
\rho_{init} &= \frac{2fk_d[I]N_A}{N_c}\left\{\frac{k_{p,w}[M]_w}{2k_{t,w}\left(\frac{fk_d[I]}{k_{t,w}}\right)^{\frac{1}{2}}}\right\}^{z-1} \\
&= \frac{2fk_d[I]N_A}{N_c}\left\{\frac{k_{p,w}C_w}{2k_{t,w}^{1/2}(fk_d)^{1/2}[I]^{1/2}}\right\}^{z-1} \\
&= \frac{2k_d[I]N_A}{N_c}\left\{\frac{k_{p,w}[M]_w}{2k_{t,w}^{1/2}(fk_d)^{1/2}}\right\}^{z-1}[I]^{\left(\frac{1-z}{2}\right)} \\
&= \frac{2fk_dN_A}{N_c}\left\{\frac{k_{p,w}[M]_w}{2k_{t,w}^{1/2}(fk_d)^{1/2}}\right\}^{z-1}[I]\times[I]^{\left(\frac{1-z}{2}\right)} \\
&= \frac{2fk_dN_A}{N_c}\left\{\frac{k_{p,w}C_w}{2k_{t,w}^{1/2}(fk_d)^{1/2}}\right\}^{z-1}[I]^{\left(\frac{3-z}{2}\right)}
\end{aligned} \tag{A.59}$$

Thus in the "termination limit" the dependence of ρ_{init} on [I] will have an exponential dependence on [I] that is critically influenced by the value of z. Furthermore, it is evident that

for $z < 3$, ρ_{init} will be an *increasing* function of [I], while for $z = 3$, ρ_{init} will be *constant* with [I], and for $z > 3$, ρ_{init} will *decrease* with increasing [I].

The above result that for z greater than 3 at high [I], the addition of further initiator will in fact result in a *decrease* in the rate coefficient for entry, may at first seem counter-intuitive. However, if we consider this in light of our understanding that under these conditions entry is in the "termination limit" (where virtually all radicals terminate before they are able to attain the critical chain length for entry), then it follows that the increase in $[T_w^\bullet]$ accompanying any increase in [I] will result in an increase in the overall rate of radical termination. Now, whether or not this increase in termination rate will, in turn, mean a decrease in the entry rate coefficient depends on the value of z. Clearly, the higher the value of z, the longer a growing radical must reside in the aqueous phase, and the more likely it is to undergo termination. Thus, the impact of a higher rate of termination on entry will scale with the value of z. Equation (A.59) shows that increasing z from 1 to 3 is sufficient to nullify any augmentative effect that increasing [I] might have on the rate of entry.

We have now considered the two limiting cases of equation (A.52), and how applying them to equation (A.51) gives ρ_{init} in the "propagation limit" at low [I], with $\rho_{init} \propto [I]$, or alternatively in the "termination limit" at high [I], with $\rho_{init} \propto [I]^{(3-z)/2}$. These two limiting cases for ρ_{init} are clearly illustrated in Figure A.8.1 below.

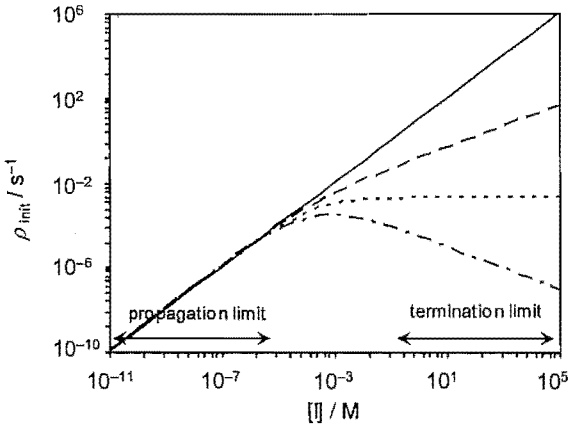

Figure A.8.1. ρ_{init} calculated as a function of initiator concentration using the analytic form of the Maxwell-Morrison entry model for styrene at 50°C with persulfate as initiator.

It is important to note that the precise definition of "low" and "high" [I] has been avoided as this will vary considerably from system to system, depending on the values of k_d, $k_{p,w}$, $k_{t,w}$ and $[M]_w$.

Thus far we have not considered the value of ρ_{init} in the region of "intermediate" [I]. In this region, as [I] increases, the value of P_{prop} decreases according to equation (A.52) from approximately unity to its low "termination limit" value. The value of ρ_{init} varies accordingly with [I], however being in neither of the two limits discussed above, the dependence of ρ_{init} on [I] is not as simple as before; here, the effects of both propagation *and* termination are significant. It is for this reason that the region of "intermediate" initiator concentration is of most interest for model discrimination in the study of entry. It is important to note that in the case of persulfate-initiated styrene polymerisations at 50°C, illustrated in Figure A.8.1, the situation is rather fortuitous in that the region of "intermediate" [I] corresponds well to the range of [I] that is experimentally accessible, *viz.* [KPS] ~ 10^{-6} – 10^{-2} M. Thus the styrene/persulfate system at 50°C is somewhat of an ideal system for investigating the kinetics of entry.

The above explanation regarding the Maxwell-Morrison entry model was formulated *independently* as part of the work of this thesis and employed as a tool for identifying relevant systems for the study of entry in emulsion polymerisation (see Chapter 10). However, it should be noted that it was subsequently discovered that this explanation has already, in essence, been presented by Verdurmen *et al.*[10]

A.9 References

(1) Smoluchowski, M. v. *Physik. Z.* **1916**, *17*, 557.

(2) Coen, E. M.; Gilbert, R. G., in *Polymeric Dispersions. Principles and Applications*; Asua, J. M., Ed.; Kluwer Academic: Dordrecht, 1997; Vol. NATO Advanced Studies Institute, p 67.

(3) Ballard, M. J.; Napper, D. H.; Gilbert, R. G. *J. Polym. Sci., Polym. Chem. Edn.* **1984**, *22*, 3225.

(4) Ugelstad, J.; Hansen, F. K. *Rubber Chem. Technol.* **1976**, *49*, 536.

(5) Gilbert, R. G. *Emulsion Polymerization: A Mechanistic Approach*; Academic: London, 1995.

(6) Harada, M.; Nomura, M.; Eguchi, W.; Nagata, S. *J. Chem. Eng. Japan* **1971**, *4*, 54.

(7) Ballard, M. J.; Gilbert, R. G.; Napper, D. H. *J. Polym. Sci., Polym. Letters Edn.* **1981**, *19*, 533.

(8) Casey, B. S.; Morrison, B. R.; Maxwell, I. A.; Gilbert, R. G.; Napper, D. H. *J. Polym. Sci. A: Polym. Chem.* **1994**, *32*, 605.

(9) Maxwell, I. A.; Morrison, B. R.; Napper, D. H.; Gilbert, R. G. *Macromolecules* **1991**, *24*, 1629.

(10) Verdurmen, E. M.; Geurts, J. M.; Vertsegen, J. M.; Maxwell, I. A.; German, A. L. *Macromolecules* **1993**, *26*, 6289.

Glossary of Symbols and Abbreviations

a	root-mean-square end-to-end distance per square root of the number of monomer units in a polymer chain
a	intercept of linear GPC calibration curve
$\overline{a}$	"acceleration" quantifying the change in $\overline{n}$ during Interval II steady-state period
A	generic aqueous-phase species giving rise to spontaneously-generated radicals
AH	dimeric adduct formed by Diels-Alder reaction of two styrene molecules
$AM_i^\bullet$	aqueous-phase radical of degree of polymerisation i derived from spontaneous initiation by aqueous species A
A–X	generic chain transfer agent
$A^\bullet$	generic radical species used variously to represent species produced by either chain transfer to species A–X (Chapter 1), homolysis of the dimeric adduct AH formed by Diels-Alder reaction of two styrene molecules (Chapter 7), or spontaneous initiation by some aqueous species A (Chapter 9)
AMA-80	Aerosol MA-80 (a surfactant)
b	slope of linear GPC calibration curve
c	pseudo-first-order rate coefficient for intra-particle termination
$c^{i,j}$	pseudo-first-order rate coefficient for intra-particle termination involving a pair of radicals with degrees of polymerisation i and j
c^{LL}	pseudo-first-order rate coefficient for intra-particle termination involving two non-monomeric radicals
c^{ML}	pseudo-first-order rate coefficient for intra-particle termination involving one monomeric and one non-monomeric radical
c^{MM}	pseudo-first-order rate coefficient for intra-particle termination involving two monomeric radicals
CHDF	capillary hydrodynamic fractionation
CLD	chain length dependent
CLI	chain length independent
d_M	density of monomer
$d_{M,w}$	density of monomer in aqueous solution
dn/dc	linear dependence of refractive index on polymer concentration for a light scattering detector

d_p	density of polymer
D_l	diffusion coefficient for a monomeric radical inside a latex particle
D_i	diffusion coefficient for a radical of degree of polymerisation i inside a latex particle
D_{ij}	mutual diffusion coefficient for a pair of radicals of degrees of polymerisation i and j inside a latex particle
D_L	average diffusion coefficient for non-monomeric radicals inside a latex particle
D_{LL}	mutual diffusion coefficient for two non-monomeric radicals inside a latex particle
D_M	diffusion coefficient for a monomeric radical inside a latex particle
D_{ML}	mutual diffusion coefficient for a monomeric and a non-monomeric radical inside a latex particle
D_{part}	diffusion coefficient for a latex particle in water
DP_n	number average degree of polymerisation for a distribution of dead polymer chains
D_{rd}	diffusion coefficient for radical motion by "reaction diffusion"
DTAB	dodecyl trimethyl ammonium bromide
D_w	diffusion coefficient for a monomer molecule in water
D_w^i	diffusion coefficient for an oligomer of degree of polymerisation i in water
e	scaling exponent for chain length dependent diffusion coefficients
E_a	activation energy
ESI	electrospray ionisation (an ionisation method used in mass spectrometry)
f	"initiator efficiency" describing the fraction of initiator molecules which yield primary radicals through thermal decomposition
f_{entry}	"entry efficiency" describing the fraction of primary radicals which eventually make their way into the interior of a latex particle
f_{entry}^0	entry efficiency calculated for the start of the Interval II steady-state period
ΔG_{hyd}	hydrophobic free energy of adsorption
ΔG_{hyd}^i	hydrophobic free energy of adsorption specific to a radical of degree of polymerisation i
GPC	gel-permeation chromatography
Δh_{dil}	change in meniscus height measured during a dilatometry experiment
HPLC	high-performance liquid chromatography
HPPS	High Performance Particle Sizer (Malvern)

i	index used to denote the degree of polymerisation, or "chain length", in monomer units of a growing radical or dead polymer chain
[I]	concentration of initiator in the aqueous phase
$IM_i^\bullet$	initiator-derived aqueous-phase radical of degree of polymerisation i
$IM_{i,ads}^\bullet$	radical-particle adduct species formed by adsorption of an initiator-derived radical of degree of polymerisation i to the surface of a latex particle
JCI	joint confidence interval
k	pseudo-first-order rate coefficient for radical exit from a latex particle
k_0	rate coefficient for exit at the start of the Interval II steady-state period
k_1	rate coefficient for Diels-Alder dimerisation of two styrene molecules
k_{-1}	rate coefficient for fragmentation of dimeric adduct formed by Diels-Alder reaction of two styrene molecules
k_{ads}^i	second-order rate coefficient for adsorption of a radical of degree of polymerisation i
k_{ads}^i(pfo)	pseudo-first-order rate coefficient for adsorption of a radical of degree of polymerisation i
k_d	rate coefficient for thermal decomposition of initiator
k_{des}^i	rate coefficient for desorption of a radical of degree of polymerisation i
k_{di}	rate coefficient for entry of an aqueous-phase dimeric radical (derived from exit) into a latex particle
k_{dM}	rate coefficient for desorption of a monomer molecule from a latex particle
k_i	rate coefficient for reaction between styrene monomer molecule and dimeric adduct formed by Diels-Alder reaction of two styrene molecules
k_p	rate coefficient for intra-particle propagation
k_p^1	rate coefficient for intra-particle propagation of a monomeric radical
$k_{p,w}$	rate coefficient for aqueous-phase propagation
$k_{p,w}^M$	rate coefficient for aqueous-phase propagation of a monomeric radical derived from exit
$k_{p,w}$(surf)	rate coefficient for propagation of a radical adsorbed at the particle surface
k_{re}	rate coefficient for re-entry of an aqueous-phase monomeric radical (derived from exit) into a latex particle
$k_{re,coll}$	rate coefficient for re-entry of an aqueous-phase monomeric radical (derived from exit) into a latex particle, assuming that re-entry is diffusion-controlled
k_t	second-order rate coefficient for bimolecular termination

$\langle k_t \rangle$	macroscopic rate coefficient for intra-particle termination averaged over all chain lengths
k_{theor}	value of pseudo-first-order rate coefficient for exit calculated from theory
$k_t^{i,j}$	rate coefficient for intra-particle termination involving a pair of radicals with degrees of polymerisation i and j
k_t^{LL}	rate coefficient for intra-particle termination involving two non-monomeric radicals
k_t^{ML}	rate coefficient for intra-particle termination involving one monomeric and one non-monomeric radical
$k_{t,w}$	rate coefficient for termination involving two aqueous-phase radicals
k_{tr}	rate coefficient for radical chain transfer to monomer
K	parameter used in the Mark-Houwink equation describing the relationship between molecular weight and intrinsic viscosity for a polymer molecule
$K_{a\text{-}d}^{i}$	equilibrium constant for adsorption and desorption of an aqueous-phase radical of degree of polymerisation i
K_{hydr}	equilibrium constant for ester hydrolysis
KPS	potassium persulfate
l_{Hg}	measured length of mercury bead for calibration of glass capillary tube used in dilatometry
m_M^{excess}	mass of excess monomer not contained in swollen particles or aqueous phase
m_M^{p}	total mass of monomer inside all swollen latex particles
m_M^{tot}	total mass of monomer added to reactor at start of experiment
m_M^{w}	total mass of monomer dissolved in the aqueous phase
$m_{M,init}^{w}$	total mass of aqueous-phase monomer at start of experiment
m_p^0	mass of polymer at the start of the Interval II steady-state period
m_p^{seed}	total mass of polymer in seed latex particles at start of experiment
M	molecular weight of dead polymer chains
M_0	molar mass of monomer
MALDI-TOF	matrix-assisted laser desorption/ionisation time of flight (an ionisation method used in mass spectrometry)
$M^{\bullet}$	monomeric radical formed inside a latex particle by transfer to monomer
$M_w^{\bullet}$	aqueous-phase monomeric radical (derived from exit)
$M_{2,w}^{\bullet}$	aqueous-phase dimeric radical (derived from exit)
MMA	methyl methacrylate

$[M]$	generic monomer concentration in a polymerising system
$[M]_{bulk}$	monomer concentration in a bulk system at zero conversion
$[M]_p$	concentration of monomer in the particle phase
$[M]_p^{sat}$	concentration of monomer in the monomer-saturated particle phase
MS	mass spectrometry
$[M]_w$	concentration of monomer in the aqueous phase
$[M]_w^{sat}$	concentration of monomer in a saturated aqueous solution of monomer
$[M]_w(surf)$	concentration of monomer at the particle surface
MWD	molecular weight distribution
m/z	mass-to-charge ratio measured by mass spectrometry
n	index used to describe the number of radicals occupying a latex particle
n_i	fraction of total intra-particle radicals that are of degree of polymerisation i
$\overline{n}$	average number of radicals per latex particle in an emulsion polymerisation
$\overline{n}_0$	value of $\overline{n}$ at the start of the Interval II steady-state period
$\overline{n}_i$	initial steady-state value of $\overline{n}$ attained prior to a γ-insertion or γ-relaxation
$\overline{n}_f$	final steady-state value of $\overline{n}$ attained following to a γ-insertion or γ-relaxation
n_M^0	concentration of monomer initially present per unit volume of aqueous phase
$\overline{n}_{SS}$	average number of radicals per latex particle during a steady-state period of emulsion polymerisation
n_{term}	number of radicals claimed by termination with a single inhibitor molecule
N_A	Avagadro's constant
N_c	number concentration of latex particles per unit volume of aqueous phase
$N_{c,new}$	number concentration of "new" latex particles (formed by secondary nucleation in a seeded polymerisation) per unit volume of aqueous phase
$N_{c,seed}$	number concentration of seed latex particles per unit volume of aqueous phase
N_n	number fraction of all latex particles containing n radicals (in the case of the Extended Smith-Ewart model this nomenclature further specifies particles containing only polymeric radicals)
N_n^M	number fraction of all latex particles containing n radicals, of which one is monomeric and all others are polymeric
p_{spin}	probability that a radical-radical encounter will result in termination, based on spin alignments
PCS	photon correlation spectroscopy

P_{exit}	probability of exit for a monomeric radical inside a latex particle
$P(M)$	instantaneous number molecular weight distribution of dead polymer chains
$\overline{P}(M)$	cumulative number molecular weight distribution of dead polymer chains
P_i	instantaneous number chain length distribution of dead polymer chains
$\overline{P}_i$	cumulative number chain length distribution of dead polymer chains
PSD	particle size distribution
r_{cap}	radius of glass capillary tube used in dilatometry
r_M	radius of a monomeric radical in the aqueous phase
r_u	radius of an unswollen latex particle
r_s	radius of a latex particle swollen with monomer
r_s^0	swollen radius of a latex particle at the start of the Interval II steady-state period
R	the gas constant
$[R^\bullet]$	total concentration of radicals
R_i	radical of degree of polymerisation i
R_{init}	generic rate of generation of initiating radicals in a polymerising system (*e.g.*, in bulk systems with a thermally decomposing initiator giving rise to two initiating radicals $R_{init} = 2fk_d[I]$, or in a "pseudo-bulk" emulsion system $R_{init} = \rho N_c/N_A$)
$R_{init,0}$	rate of initiation for a spontaneous polymerisation of MMA carried out in a system that is shielded from natural ionising radiation
$R_{p,w}$	per radical rate of aqueous-phase propagation for monomeric radicals derived from exit
R_{pol}	the overall rate (in M^{-1} s^{-1}) of polymerisation
R_{re}	per radical rate of re-entry into a latex particle for monomeric radicals derived from exit
$R_{t,w}$	per radical rate of aqueous-phase termination for monomeric radicals derived from exit
t	time
t_{inhib}	inhibition time at the start of polymerisation
T	temperature
TEM	transmission electron microscopy
$T_w^\bullet$	any aqueous-phase radical species
V	elution volume for gel-permeation chromatography

ΔV_{dil}	volume contraction measured during a dilatometry experiment
V_{Hg}	measured volume of mercury bead for calibration of glass capillary tube used in dilatometry
V_r	total volume of reaction medium in an emulsion polymerisation
V_s	volume of a latex particle swollen with monomer
V_s^0	volume of a swollen latex particle at the start of the Interval II steady-state period
V_u	volume of an unswollen latex particle
V_w	volume of aqueous phase in an emulsion polymerisation
$W(\log_{10}M)$	weight molecular weight distribution of dead polymer chains expressed as a function of the logarithm of polymer molecular weight
$W(M)$	weight molecular weight distribution of dead polymer chains expressed as a function of polymer molecular weight
x	fraction of monomer converted into polymer during polymerisation
$\hat{x}$	mass of monomer converted into polymer during polymerisation
$\hat{x}_0$	mass of monomer converted into polymer at the start of the Interval II steady-state period
x_{trans}	fractional conversion corresponding to transition from Interval II to Interval III of polymerisation
y	critical degree of polymerisation for formation of a surface-active radical derived from aqueous spontaneous initiation and bound to undergo entry into a latex particle
z	critical degree of polymerisation for formation of a surface-active initiator-derived radical bound to undergo entry into a latex particle
α	"fate parameter" for radicals undergoing exit from a latex particle
α	parameter used in the Mark-Houwink equation describing the relationship between molecular weight and intrinsic viscosity for a polymer molecule
λ	fraction of termination occurring by disproportionation (as opposed to combination)
Λ	slope of a plot of $\ln P(M)$ against M
Λ_{high}	slope of a plot of $\ln P(M)$ against M taken in the high molecular weight region of a molecular weight distribution
Λ_{peak}	slope of a plot of $\ln P(M)$ against M taken in the peak region of a molecular weight distribution
Λ_{sim}	slope of a simulated plot of $\ln P(M)$ against M

$\Lambda_{sim,h}$ slope of a simulated plot of $\ln P(M)$ against M taken in the high molecular weight region

$\Lambda_{sim,p}$ slope of a simulated plot of $\ln P(M)$ against M taken in the peak molecular weight region

ρ pseudo-first-order rate coefficient for radical entry into a latex particle

ρ_0 rate coefficient for entry calculated at the start of the Interval II steady-state period

$\rho_{100\%}$ pseudo-first-order rate coefficient for entry of initiator-derived radicals into a latex particle, corresponding to complete entry of all primary radicals generated from initiator

ρ_{init} pseudo-first-order rate coefficient for entry of initiator-derived radicals into a latex particle

ρ_{init}^{0} pseudo-first-order rate coefficient for entry of initiator-derived radicals calculated at the start of the Interval II steady-state period

ρ_L pseudo-first-order rate coefficient for entry of all non-monomeric radicals into a latex particle

ρ_M pseudo-first-order rate coefficient for re-entry of an aqueous-phase monomeric radical (derived from exit) into a latex particle

ρ_{spont} pseudo-first-order rate coefficient for entry of spontaneously-generated radicals into a latex particle

ρ_{spont}^{0} rate coefficient for entry of spontaneously-generated radicals at the start of the Interval II steady-state period

$\rho_{sp,bulk}$ component of ρ_{spont} arising from radical-generating reactions of monomer in the bulk-like interior of latex particles and/or monomer droplets

$\rho_{sp,w}$ component of ρ_{spont} arising from radical-generating reactions of aqueous monomer

$\rho_{sp,other}$ component of ρ_{spont} due to spontaneous radical generation in any phase that does not arise directly from monomeric reactions (*e.g.*, radicals derived from reactive peroxidic functionalities)

ρ_{total} pseudo-first order rate coefficient for entry of radicals from all sources (*i.e.*, initiator-derived, exit-derived and spontaneously-generated) into a latex particle

σ interaction radius for radical-radical reaction

σ_V standard deviation (width at $1/\sqrt{e}$ height) of the Gaussian gel-permeation chromatogram for a narrow polydispersity standard